# The Chemistry of Tantalum and Niobium Fluoride Compounds

Anatoly Agulyansky

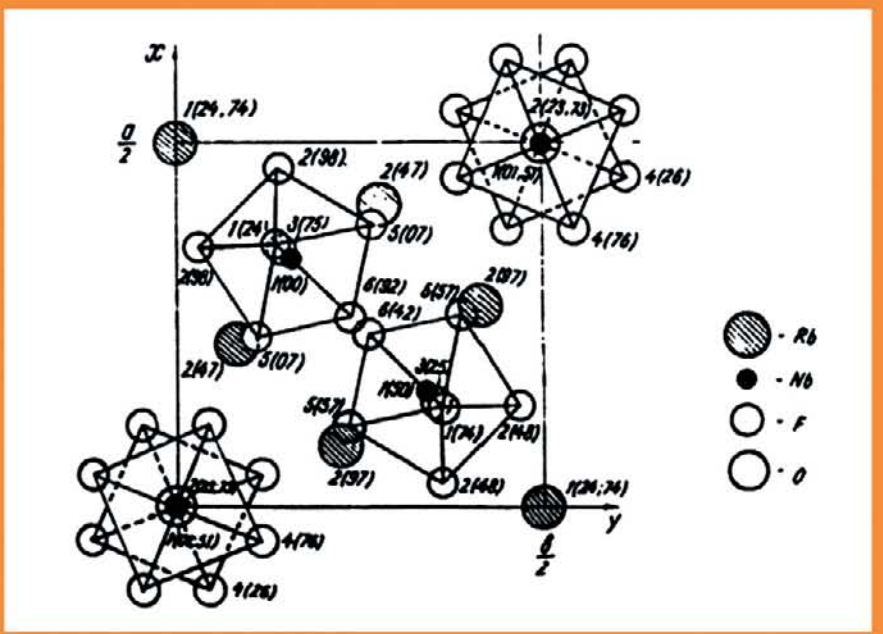

# THE CHEMISTRY OF TANTALUM AND NIOBIUM FLUORIDE COMPOUNDS

This Page Intentionally Left Blank

# THE CHEMISTRY OF TANTALUM AND NIOBIUM FLUORIDE COMPOUNDS

Anatoly AGULYANSKY

*Fluortech Ltd.*
*6 Duhefate Street*
*P.O. Box 2130*
*Lehavim*
*Israel 85338*

ELSEVIER

2004

Amsterdam – Boston – Heidelberg – London – New York – Oxford – Paris
San Diego – San Francisco – Singapore – Sydney – Tokyo

**ELSEVIER B.V.**
**Sara Burgerhartstraat 25**
**P.O. Box 211, 1000 AE**
**Amsterdam, The Netherlands**

ELSEVIER Inc.
525 B Street
Suite 1900, San Diego
CA 92101-4495, USA

ELSEVIER Ltd.
The Boulevard
Langford Lane, Kidlington,
Oxford OX5 1GB, UK

ELSEVIER Ltd.
84 Theobalds Road
London WC1X 8RR
UK



First edition 2004

Library of Congress Cataloging in Publication Data
A catalog record is available from the Library of Congress.

British Library Cataloguing in Publication Data
A catalogue record is available from the British Library.

ISBN: 0-444-51604-2

♾ The paper used in this publication meets the requirements of ANSI/NISO Z39.48-1992 (Permanence of Paper).
Printed in The Netherlands.

Dedicated to the
memory of my father

This Page Intentionally Left Blank

# Preface

Although the elements tantalum and niobium were discovered more than 200 years ago in the form of oxides, the true beginning of the chemistry of tantalum and niobium was the discovery and investigation of complex fluorotantalates and fluoroniobates of alkali metals. Application of complex fluoride compounds enabled the separation of tantalum and niobium and in fact initiated the development of the industrial production of the metals and their compounds.

Modern refining technology uses tantalum and niobium fluoride compounds, and includes fluorination of raw material, separation and purification of tantalum and niobium by liquid–liquid extraction from such fluoride solutions. Preparation of additional products and by-products is also related to the treatment of fluoride solutions: oxide production is based on the hydrolysis of tantalum and niobium fluorides into hydroxides; production of potassium fluorotantalate (K - salt) requires the precipitation of fine crystals and finishing avoiding hydrolysis. Tantalum metal production is related to the chemistry of fluoride melts and is performed by sodium reduction of fluoride melts. Thus, the refining technology of tantalum and niobium involves work with tantalum and niobium fluoride compounds in solid, dissolved and molten states.

This monograph compiles the latest research on the chemistry of complex fluorides and oxyfluorides of tantalum and niobium, and covers synthesis and fluorination processes, crystal structure peculiarities and crystal chemical classification, as well as the behavior of complex ions in fluorine solutions and melts.

The monograph will be useful for tantalum and niobium producers, for researchers studying the chemistry of fluorides, and for teachers and students at chemistry and metallurgy departments.

I would like to take this opportunity to thank my colleagues, with whom I have had the pleasure to work. I would like to extend my gratitude to the brilliant professionals at the Institute of Chemistry at the Kola Science Center of the Russian Academy of Sciences (Apatity, Russia), Institute of Common and Inorganic Chemistry of the Ukraine Academy of Science (Kiev, Ukraine), Karpov Institute of Physical Chemistry (Moscow, Russia), Institute of Chemistry of Nitrogen (Moscow, Russia), Technion – Israel Institute of Technology (Haifa, Israel), Chemistry of Solids Laboratory of CNRS (Bordeaux, France), Tan Ceramics Ltd. (Migdal Haemek, Israel).

I also wish to thank my family: my wife Dr. Ludmila Agulyansky and my sons Michael and Alex, whose constant encouragement enabled me to write and complete this monograph.

Anatoly Agulyansky, Lehavim, Israel

# CONTENTS

This Page Intentionally Left Blank

# 1.

# INTRODUCTION

## 1.1. General information on the applications of tantalum and niobium

Our life would never be as advanced and comfortable as it is if not for the applications of tantalum and niobium. These materials' unique properties ensure their increasing usage in electronic, optic, mechanical, aerospace, nuclear and other modern applications.

Tantalum and niobium are used widely, in the form of metals and alloys, in the process industry, vacuum techniques, chemical machinery, surgical devices, and the automotive industry [1-4]. Niobium additives are used to stabilize and improve modern stainless steels [5, 6], and super alloys containing tantalum and niobium are successfully applied in gas turbine engines and in the aerospace industry [7-9]. Intermediate metal compounds based on niobium, such as $Nb_3Sn$, $Nb_3Ge$, $Nb_3Al$ and others, which display superconductivity at relatively high temperatures, are widely used in special applications [1, 10, 11]. Niobium-titanium alloys are used for superconducting magnets in magnetic resonance imaging equipment (MRI) used for the detection of abnormalities in soft tissue.

Tantalum and niobium are added, in the form of carbides, to cemented carbide compositions used in the production of cutting tools. Pure oxides are widely used in the optical industry as additives and deposits, and in organic synthesis processes as catalysts and promoters [12, 13]. Binary and more complex oxide compounds based on tantalum and niobium form a huge family of ferroelectric materials that have high Curie temperatures, high dielectric permittivity, and piezoelectric, pyroelectric and non-linear optical properties [14-17]. Compounds of this class are used in the production of energy transformers, quantum electronics, piezoelectrics, acoustics, and so on. Two of

these compounds are highly important - lithium tantalate, $LiTaO_3$, and lithium niobate, $LiNbO_3$. These compounds are produced in the form of single crystal wafers and are used in the manufacture of optoelectronic and acoustoelectronic devices and infrared sensors [15, 18].

The major consumer of tantalum is the capacitor production industry. About 60% of the total amount of tantalum currently produced is in the form of fine, agglomerated high purity powder of capacitor grade. Tantalum capacitors have high volumetric efficiency and reliability. A basic description of tantalum capacitor technology is presented in overview [19].

Tantalum production has increased steadily and strongly since 1993. An optimistic forecast regarding the strongly increasing demand for tantalum capacitors caused excessive demand for tantalum powder in 2000, when the overproduction of capacitors led to a sharp shortage in tantalum powder. It is still difficult to predict when the electronics industry will return to balanced condition.

Table 1 presents the distribution of tantalum and niobium processor shipments for 1999, 2000 and 2001. The values presented in Table 1 were estimated based on graphs given by Mosheim in a comprehensive statistical analysis [20]. Breakdown of the total worldwide amount of tantalum and niobium used in 2000 in main applications is given in Figs.1 and 2, respectively.

*Table 1. Distribution of tantalum and niobium shipments (in million lbs)*

| | 1999 | 2000 | 2001 |
|---|---|---|---|
| Total tantalum processors shipments | **3.8** | **4.9** | **3.4** |
| Capacitor-grade powder | 2.25 | 3.00 | 1.6 |
| Ingots | 0.315 | 0.258 | 0.310 |
| Chemicals, including oxides | 0.25 | 0.325 | 0.38 |
| Carbide | 0.28 | 0.38 | 0.48 |
| Mill products | 0.57 | 0.72 | 0.48 |
| Others | 0.1 | 0.2 | 0.15 |
| | | | |
| Total niobium processors shipments | **51** | **53** | **57** |
| Ferro-niobium | 45 | 45 | 49 |
| Chemicals and vacuum grade | 5 | 6.4 | 6.8 |
| Mill products | 0.33 | 0.48 | 0.62 |
| Alloys (NbZr, NbTi, NbCu) | 1.0 | 1.2 | 0.7 |

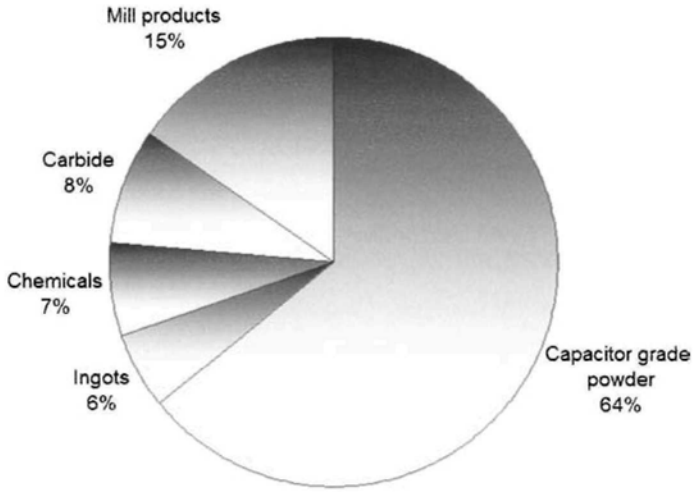


*Fig. 1. Breakdown of tantalum shipments by main products – year 2000.*

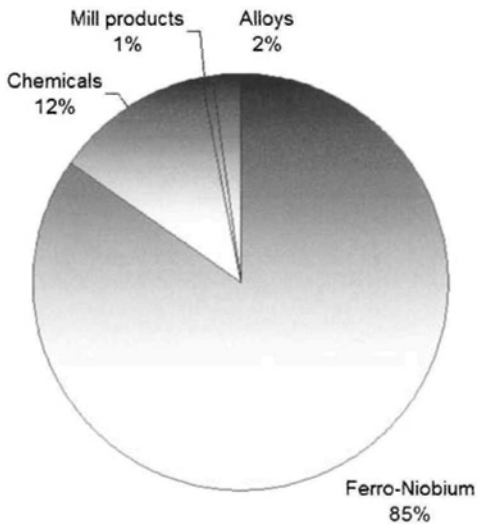


*Fig. 2. Breakdown of niobium shipments by main products – year 2000.*

## 1.2.Tantalum and niobium raw materials

Niobium and tantalum are rare elements. The content of niobium and of tantalum in the Earth's crust is $1\times10^{-3}$ and $2\times10^{-4}$ wt. %, respectively [21]. Niobium and tantalum are encountered in nature together, mostly in the form of oxides that are derived from orthoniobic (orthotantalic), metaniobic (metatantalic) and pyroniobic (pyrotantalic) acids. The main minerals are listed in Table 2, which reveals that the most important source of tantalum and niobium is tantalite-columbite, $(Fe,Mn)(Nb,Ta)_2O_6$.

Deposits of niobium-tantalum ores are found in Australia, Brazil, Canada, China, Malaysia, Namibia, Nigeria, Russia, Rwanda, Spain, Thailand, Zaire, and Zimbabwe. A more detailed analysis of worldwide tantalum mineral raw material supply can be found in Linden's comprehensive overview [22, 23].
The niobium–tantalum weight ratio in North American pyrochlores is 100–150:1, while in Russian ores the ratio varies between 8:1 and 1:20 [21].

*Table 2. Composition of main tantalum–niobium-containing minerals [21,24]*

| Mineral | Composition | $Ta_2O_5$,wt. % | $Nb_2O_5$, wt. % |
|---|---|---|---|
| Columbite | $(Fe, Mn)(Nb, Ta)_2O_6$ | 5 - 30 | 55 – 78 |
| Tantalite | $(Fe, Mn)(Nb, Ta)_2O_6$ | 42 - 84 | 2 – 40 |
| Pyrochlore | $(Ce,Ca,Y)_2(Nb,Ta)_2O_6(OH,F)$ | 0 - 6 | 37 – 66 |
| Microlite | $(Na,Ca)_2Ta_2O_6(O,OH,F)$ | 68 - 77 | 0 – 7 |
| Loparite | $(Ce,Na,Ca)_2(Ti,Nb)_2O_6$ | 0.5 – 3 | 5 - 20 |
| Euxenite | $(Y,Ca,Ce,U,Th)(Nb,Ta,Ti)_2O_6$ | 0 - 47 | 4 – 47 |
| Ilmenorutile | $(Ti,Nb,Fe)_3O_6$ | 0 - 36 | 20 – 43 |
| Simpsonite | $Al_4(Ta,Nb)_3O_{13}(OH)$ | 60 -80 | 0.3 – 6 |
| Thoreaulite | $SnTa_2O_6$ | 73 - 77 | - |
| Strueverite | $(Ti,Ta,Fe^{3+})_3O_6$ | 6 - 13 | 9 – 14 |
| Fergusonite | $(Re^{3+},Nb,Ta)O_4$ | 4 - 43 | 14 – 46 |
| Sumarskite | $(Fe,Ca,U,Y,Ce)_2(Nb,Ta)_2O_6$ | 15 - 30 | 40 – 55 |
| Tapiolite | $(Fe,Mn)(Nb,Ta,Ti)_2O_6$ | 40 - 85 | 8 - 15 |

Additional sources of the elements are tin slag and scrap. For instance, cassiterite deposits, in Australia, Brazil, Thailand and some other countries, contain a significant amount of tantalum. The bulk of this tantalum is collected in the slag and processed separately. Recycling of various tantalum-bearing scrap is also a very important source for tantalum production. These scrap materials include powder surplus from sintering operations, scrap from mill products, rejected and used capacitors, scrapped cutting tools and furnace hardware.

## 1.3. Refining processes

Niobium was discovered in 1801 by an English chemist named Hatchett [25]. One year later, a Swedish chemist, Ekeberg, announced his discovery of tantalum [26]. Both tantalum and niobium were discovered in the form of oxides. It took about 65 years until an effective method for the separation of tantalum and niobium was found by Marignac, in 1866 [27]. According to this method, a mixture of niobic and tantalic acid slurries is dissolved using anhydrous hydrofluoric acid (HF). A stoichiometric quantity of potassium fluoride is added to the solution, yielding slightly soluble potassium fluorotantalate, $K_2TaF_7$, which precipitates from the solution. Niobium, on the other hand, forms potassium oxyfluoroniobate, $K_2NbOF_5 \cdot H_2O$, whose solubility is sufficiently high and remains dissolved. Solubility of potassium fluorotantalate in a ~1% HF solution is about 10-12 times less than that of potassium oxyfluoroniobate. Potassium fluorotantalate precipitates in the form of fine needles that can be separated from the mother solution by means of filtration, washed and dried. This method of fractional crystallization was assumed as the basis for industrial production and was used until the middle of the 20th century, when liquid–liquid extraction processes replaced fractional crystallization [28].

The discovery of the process for the separation of tantalum and niobium using fluorination marked, in fact, the beginning of the development of the chemistry and technology of tantalum and niobium in general, and initiated the development of complex fluoride compound chemistry in particular.

Two main methods exist for the production of tantalum and niobium from the mineral raw material. The first method is based on the chlorination of raw material, followed by separation and purification by distillation of tantalum and niobium in the form of pentachlorides, $TaCl_5$ and $NbCl_5$ [24, 29]. Boiling points of tantalum and niobium pentachlorides (236°C and 248°C, respectively) are relatively low and are far enough apart to enable separation by distillation.

Two types of chlorination processes are used for the different kinds of raw material. The first process is a reductive process by which oxide-type raw materials in the form of ores or concentrates are chlorinated. The essence of this process is the interaction with chlorine gas in the presence of coal or other related material.

Chlorination of ferroalloys (ferroniobium-tantalum) is a more economical and simple alternative [30]. The process is performed on a sodium chloride melt that contains iron trichloride, $FeCl_3$. Chlorine is passed through the melt yielding $NaFeCl_4$, which interacts as a chlorination agent with the Fe-Nb-Ta alloy. Chlorination of ferroalloys allows for the production of pure tantalum and niobium pentachlorides, which are used further in the production of high purity oxides and other products.

The performance of different types of chlorination processes is discussed comprehensively in overview [31]. It should be mentioned that carbon tetrachloride can also be applied successfully in the chlorination of rare refractory metal oxides, including tantalum oxide.

The second method of tantalum and niobium production is related historically to Marignac's process of tantalum and niobium separation, in the form of complex fluoride compounds, and is based on the fluorination of raw material. The modern production process consists of slightly different steps, as described below.

Raw material is digested at a high temperature, under intensive stirring, using a mixture of highly concentrated hydrofluoric acid, HF, and sulfuric acid, $H_2SO_4$. It is also reported that the digestion can be carried out successfully using only HF acid [32]. The purpose of the digestion is to dissolve the tantalum and niobium as complex fluoride acids. It is obvious that all other impurities that form soluble fluoride compounds are also dissolved. The insoluble residual part of the slurry, which usually contains fluorides of alkaline earth and rare earth elements, is separated from the solution by filtration. After adjustment of its acidity by the addition of sulfuric acid, the filtrated solution is processed using liquid–liquid extraction. The process of liquid–liquid extraction was developed by Ames Laboratory together with the US Bureau of Mines and has been implemented since 1957 [33] as an alternative to Marignac's fractional crystallization method. Use of liquid–liquid extraction provides better separation of tantalum and niobium and allowed for the development of the production of high-purity materials.

The liquid–liquid (solvent) extraction is based on the extraction of various ions into either an organic or aqueous phase according to the complex ion structure. The structure of the complex ions generally depends on the solution parameters and, first and foremost, on the acidity of the aqueous solution. At

high levels of acidity, tantalum and niobium ions extract from the aqueous phase into the organic phase. At the same time, most of the impurities remain in the aqueous solution. Lower levels of acidity lead to the stripping of tantalum and niobium ions from the organic solution into the aqueous phase. The separation of tantalum and niobium is carried out utilizing the fact that niobium requires a higher level of acidity of the aqueous solution to pass into the organic phase and a lower level of acidity to be stripped into the aqueous solution, compared to tantalum.

Using highly acidic initial solutions originating from the digestion of the raw material, conventional technology includes collective extraction of tantalum and niobium into the organic phase, followed by scrubbing and the separation of tantalum and niobium during the stripping step. Numerous solvents can be used in the liquid–liquid extraction of tantalum and niobium, but the most frequently used extractants are methyl isobutyl ketone (MIBK), which is the most popular extractant, tributyl phosphate (TBP), cyclohexanone and fatty alcohols (such as 2-octanol) [34].

The products of the solvent extraction process are tantalum strip solution, niobium strip solution and raffinate – liquid wastes containing impurities and residual acids.

Niobium hydroxide precipitates from the niobium-containing strip solution following treatment with ammonia solution. After washing, drying and calcinations, niobium hydroxide is converted into niobium oxide. Tantalum oxide is produced in the same way, using a tantalum-containing strip solution. Hydroxide precipitation and washing actually bring about the defluorination of the dissolved complex fluoride compounds to form oxide compounds by means of hydrolysis.

Another application of tantalum strip solution is in the precipitation of potassium fluorotantalate, $K_2TaF_7$, which is used as a precursor in the production of tantalum powder by sodium reduction of melts.

Very impure tantalum powder was first prepared in 1825 by Berzelius, who reduced $K_2TaF_7$ using metallic potassium. About 40 years later, Rose produced a purer tantalum powder from $Na_2TaF_7$ using sodium as the reducing agent. Until this day, the most applicable method of tantalum powder preparation is based on sodium reduction of melts containing potassium fluorotantalate or K-salt, as it is called commercially. An alternative method of tantalum production is the electrolysis of alkali metal halide melts that contain $K_2TaF_7$ and periodic additions of tantalum oxide, $Ta_2O_5$. The electrochemical reduction process was used, mainly in the US, for a long period of time, starting in 1922, for the production of tantalum metal [35-37].

In the second part of the 20th century, the tantalum capacitor industry became a major consumer of tantalum powder. Electrochemically produced tantalum powder, which is characterized by an inconsistent dendrite structure, does not meet the requirements of the tantalum capacitor industry and thus has never been used for this purpose. This is the reason that current production of tantalum powder is performed by sodium reduction of potassium fluorotantalate from molten systems that also contain alkali metal halides. The development of electronics that require smaller sizes and higher capacitances drove the tantalum powder industry to the production of purer and finer powder providing a higher specific charge – CV per gram. This trend initiated the vigorous and rapid development of a sodium reduction process.

The intensive increase in capacitor production has initiated the development of novel processes for the production of tantalum and niobium capacitor-grade powders, and the successful development of a new method, based on the reduction of tantalum or niobium oxide using magnesium vapors, was recently announced [38].

Nevertheless, tantalum and niobium refining technology was, and remains, a part of fluorine chemistry, since its main processes are related to the chemistry of tantalum and niobium fluorides in solid, dissolved and molten states.

## 1.4. Material science aspects

The physical and chemical properties of any material are closely related to the type of its chemical bonds. Oxygen atoms form partially covalent bonds with metals that account for the unique thermal stability of oxide compounds and for typically high temperatures of electric and magnetic structure ordering, high refractive indexes, but also for relatively narrow spectral ranges of transparency.

As opposed to the oxides, fluoride compounds are characterized by the formation of mostly ionic bonds. This peculiarity is related to fluorine's high electronegativity.

Despite the relatively short history of the chemistry of fluoride compounds, several thousands of binary and ternary fluoride compounds have been described, and their systematization is well developed [39 – 41]. Significant progress was achieved in the study of the crystal chemistry of fluoride compounds thanks to the ionic character of their chemical bonds and corresponding simplicity of their crystal structure. The structure of these kinds of compounds is defined primarily by the geometry and the energy of mainly

electrostatic interactions. From this point of view, fluoride compounds are a truly unique subject for the investigation of correlations between the composition of compounds and their crystal structure.

On the other hand, fluorine's high electronegativity and its ability to form mostly ionic chemical bonds, provide materials with several useful properties. First, compared to oxides, fluoride compounds have a wide forbidden zone and as a result, have low electroconductivity. In addition, fluorides are characterized by a high transparency in a wide optical range that allows for their application in the manufacturing of electro-optical devices that operate in the UV region [42, 43].

At the same time, the relatively low energy and ionic character of the chemical bonds between metal and fluorine cause some difficulties in the application of fluoride compounds. First, fluorides typically have a tendency towards thermolysis and hygroscopicity. In addition, fluoride compounds usually display relatively low temperatures of electrostatic and magnetic ordering.

Oxygen and fluorine ions have very similar ionic radii. This steric similarity ensures relatively easy substitution of the oxygen in the compounds, by fluorine ions. Such substitution opens up huge possibilities for the synthesis of oxyfluoride compounds with desired crystal structure and properties.

Fluorine–oxygen substitution, yielding oxyfluoride compounds, can be performed without changing the initial oxide crystal structure, provided the changes in the anionic sublattice are compensated by appropriate substitutions in the cationic sublattice. In these particular cases, the properties of the compounds will change due to variations in the character of the chemical bonds. On the other hand, fluorine–oxygen substitution can also cause cardinal changes in the initial crystal structure. Hence, compounds with desired structures and specific properties can be obtained only through controlled fluorine–oxygen substitution.

Investigation of the ferroelectric properties of oxyfluoride compounds is also a relatively new but fast-developing area in solid state chemistry [44-46].

Since niobates and tantalates belong to the octahedral ferroelectric family, fluorine–oxygen substitution has a particular importance in managing ferroelectric properties. Thus, the variation in the Curie temperature of such compounds with the fluorine–oxygen substitution rate depends strongly on the crystalline network, the ferroelectric type and the mutual orientation of the spontaneous polarization vector, metal displacement direction and covalent bond orientation [47]. Hence, complex tantalum and niobium fluoride compounds seem to have potential also as new materials for modern electronic and optical applications.

In summary, investigations in the area of the chemistry of tantalum and niobium fluoride compounds will advance tantalum-niobium metallurgy and promote the development of new materials for modern applications.

# 2.

# SYNTHESIS OF TANTALUM AND NIOBIUM FLUORIDE COMPOUNDS

The variety of fluoride compounds that exist and the wide spectrum of their preparation methods are related to the properties of fluorine, and above all to fluorine's high electronegativity. Low dissociation energy of the fluorine molecule, $F_2$, relatively high energies of bond formation found in most fluoride compounds, as well as fluorine's strong oxidizing ability lead, in some cases, to spontaneous fluorination.

Another peculiarity of the synthesis of fluoride compounds is their relatively low thermal stability and tendency to undergo hydrolysis and pyrolysis. These features are very common in the case of rare metal fluoride compounds [48]. Thus, special conditions are required for the successful processing of fluoride compounds: special preparation of initial reagents, dry atmosphere, vacuum conditions, and so on. In addition, the high corrosivity of fluorides, especially those of polyvalent metals, precludes the use of any equipment made of glass or quartz and requires the use of special materials. Successful processing, therefore, requires the construction of special installations, containing vacuum–inert gas systems and containers made of Teflon, platinum, gold, graphite, glassy carbon and other suitable materials with special properties [49, 50].

The synthesis of tantalum and niobium fluoride compounds is, above all, related to the fluorination of metals or oxides. Table 3 presents a thermodynamic analysis of fluorination processes at ambient temperature as performed by Rakov [51, 52]. It is obvious that the fluorination of both metals and oxides of niobium and tantalum can take place even at low temperatures, whereas fluorination using ammonium fluoride and ammonium hydrofluoride can be performed only at higher temperatures.

*Table 3. Changes in Gibbs's potential for niobium and tantalum fluorination (after Rakov [51, 52]).*

| Fluorination process | ΔG, Kcal/mol, 298 K | |
|---|---|---|
| | Me = Nb | Me = Ta |
| $Me + 5HF = MeF_5 + 2.5H_2$ | -333 | -423 |
| $Me + 2.5NH_4HF_2 = MeF_5 + 2.5H_2 + 2.5NH_3$ | -199 | -209 |
| $Me + 5NH_4F = MeF_5 + 2.5H_2 + 5NH_3$ | -38 | -130 |
| $Me_2O_5 + 10\,HF = 2MeF_5 + 5H_2O$ | -63.6 | -81.6 |
| $Me_2O_5 + 5NH_4HF_2 = 2MeF_5 + 5H_2O + 5NH_3$ | 150 | 132 |
| $Me_2O_5 + 10NH_4F = 2MeF_5 + 5H_2O + 10NH_3$ | 231 | 213 |

Synthesis of fluoride compounds is performed in various media, such as aqueous solutions, non-aqueous systems and heterogeneous interactions.

## 2.1. Aqueous solutions

Precipitation of fluoride compounds from solutions of hydrofluoric acid, HF, is performed by the addition of certain soluble compounds to solutions containing niobium or tantalum. Initial solutions can be prepared by dissolving metals or oxides of tantalum or niobium in HF solution. Naturally, a higher concentration of HF leads to a higher dissolution rate, but it is recommended to use a commercial 40–48% HF acid. A 70% HF solution is also available, but it is usually heavily contaminated by $H_2SiF_6$ and other impurities, and the handling of such solutions is extremely dangerous.

Beakers and other related equipment made of polyethylene, polypropylene, Teflon or glassy carbon are usually used in the preparation of such solutions.

Both tantalum and niobium dissolve in HF, but relatively slowly at first. The interaction is shown schematically in Equation (1), Me = Ta or Nb:

$$Me^{solid} + 6\,HF = HMeF_6 + 2.5\,H_2^{gas} + \Delta Q \qquad (1)$$

In some cases, a small amount of nitric acid, $HNO_3$, or hydrogen peroxide, $H_2O_2$, is added to the solution in order to accelerate the dissolution of the metal. Heating the solution increases dissolution rates as well. Taking into

account the exothermal character of the interaction (1), the digestion of tantalum and niobium metals must be performed very gently to avoid uncontrollable process rates and overheating and boiling of the solution.

Tantalum and niobium oxides dissolve very slowly in HF solutions. Thus, it is recommended to use a high concentration of HF or a mixture of HF and $H_2SO_4$ at a temperature of about 70–90°C. The best precursors for the preparation of fluoride solutions are hydroxides. Both tantalum hydroxide, $Ta_2O_5 \cdot nH_2O$, and niobium hydroxide, $Nb_2O_5 \cdot nH_2O$, dissolve well, even in diluted HF solutions.

The dissolution of oxides and hydroxides can be presented schematically as follows:

$$Me_2O_5 + 12\,HF = 2\,HMeF_6 + 10\,H_2O; \quad (2)$$

$$Me_2O_5 \cdot nH_2O + 12\,HF = 2\,HMeF_6 + (10 + n)\,H_2O; \quad (3)$$

Where Me = Ta or Nb.

Using metallic precursors, HF solutions with higher concentrations of tantalum or niobium can be achieved. It is possible to prepare solutions that have maximum concentrations of about 1000 g/l tantalum oxide and about 600 g/l niobium oxide ($Me_2O_5$).

Synthesis of the compounds from such HF solutions is performed by adding soluble fluoride compounds to the tantalum or niobium solution or by re-crystallization of prepared fluoride compounds from water or HF solutions of different concentrations. In the first case, the composition of the compounds obtained depends on the ratio between Ta/Nb and the added metal and on the initial concentration of the HF used, whereas in the second case, it depends only on the HF concentration.

Tananaev and Savchenko performed detailed investigations of the solubility of potassium fluorotantalate, $K_2TaF_7$, [53] and potassium fluoroniobate, $K_2NbF_7$, [54] in HF solutions. The solubility isotherm (25°C) of $K_2TaF_7$ displays two distinct crystallization fields (Fig. 3). Potassium heptafluorotantalate, $K_2TaF_7$, precipitates from HF solutions up to a concentration of about 42%. This concentration corresponds to a potassium fluorotantalate point of maximum solubility. HF solutions of higher concentration provide precipitation of potassium hexafluorotantalate, $KTaF_6$. This fact can be accounted for by several of mechanisms. One such explanation is that at high HF concentrations, the fluorotantalate ion interacts with HF yielding hydrofluoride ion, $HF_2^-$.

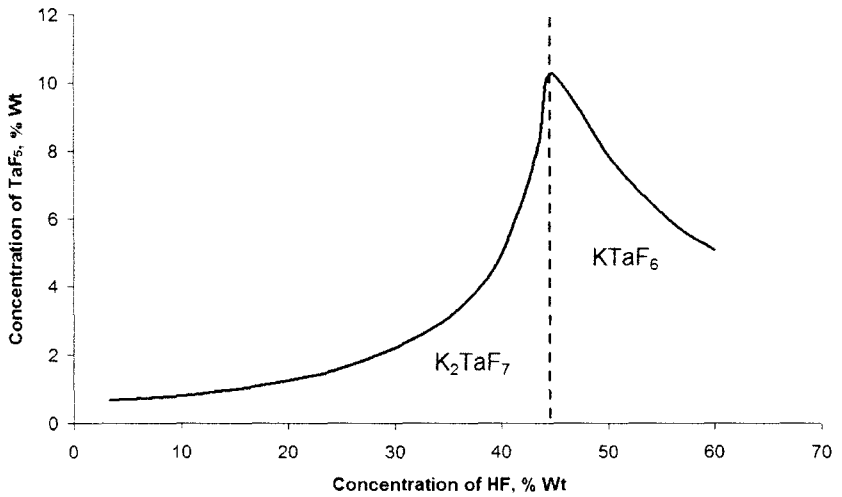


*Fig. 3. Potassium fluorotantalate, $K_2TaF_7$, solubility in HF solutions at 25°C Reproduced from [53], G. S. Savchenko, I. V. Tananaev, Zh. Prikl. Khim 20 (1947) 385, Copyright 1947, with permission of "Nauka" (Russian Academy of Sciences) publishing.*

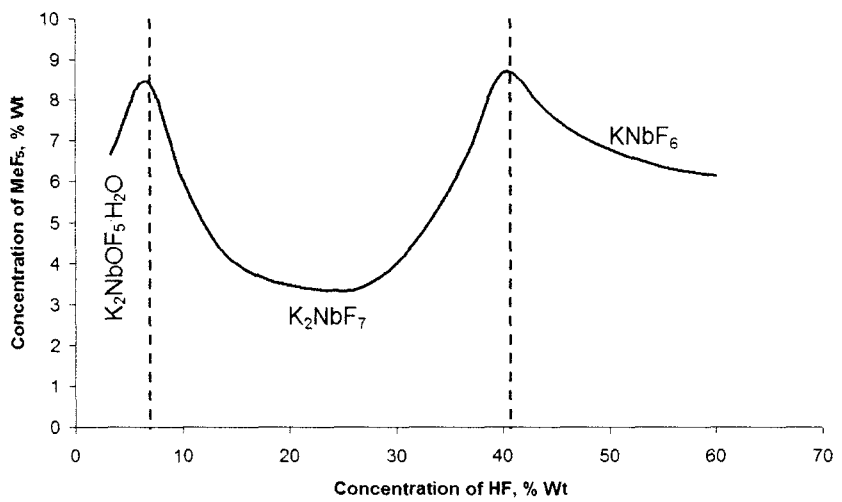


*Fig. 4. Solubility of potassium fluoroniobate, $K_2NbF_7$, in HF solutions at 25°C Reproduced from [54], G. S. Savchenko, I. V. Tananaev, Zh. Prikl. Khim.19 (1946) 1093, Copyright 1946, with permission of "Nauka" (Russian Academy of Sciences) publishing.*

Schematically, the reaction can be given in molecular terms, as follows:

$$K_2TaF_7 + HF = KTaF_6 + KHF_2 \quad (4)$$

Another mechanism is expressed in terms of Lewis acidity. According to this approach, highly acidic compounds are more stable in highly acidic media.

Fig. 4 presents the solubility isotherm (25°C) of potassium fluoroniobate in HF solutions [54]. Crystallization fields of three different compounds are evident: At HF concentrations lower than 7%, crystal hydrate $K_2NbOF_5 \cdot H_2O$ is formed. At HF concentrations between 7% and 40%, the precipitation of $K_2NbF_7$ occurs. Further concentration of HF leads to the formation of potassium hexaflouroniobate, $KNbF_6$. As can be seen, the solubility of niobium-containing compounds is significantly higher than that of tantalum-containing compounds. This was the main basis for the fractional precipitation method for the separation of tantalum and niobium.

The concept of Lewis acidity enables one to analyze and better understand the composition of the compounds that can be precipitated from different solutions using different additives, taking the acidity of the additives into account as well.

Balke [55] obtained ammonium octafluorotantalate, $(NH_4)_3TaF_8$, and octafluoroniobate, $(NH_4)_3NbF_8$, by increasing the concentration of an HF solution containing tantalum or niobium by adding an excessive amount of ammonium fluoride, $NH_4F$. Similarly, ammonium heptafluorotantalate, $(NH_4)_2TaF_7$, was prepared by adding $NH_4F$ to a solution of tantalum hydroxide in saturated HF until the appearance of a white precipitate [56]. However, re-crystallization of $(NH_4)_2TaF_7$ from a 60% HF solution and from water resulted in the precipitation of $NH_4TaF_6$ [57] and $(NH_4)_3TaF_8$ [29], respectively.

Adding $NH_4F$ or $NH_4OH$ alternately to solutions containing tantalum or niobium and hydrofluoric acid (F:Me = 5) resulted in the formation of the following compounds: $(NH_4)_3Nb_2O_2F_9$, $(NH_4)_2NbOF_5$, $(NH_4)_3TaOF_6$, $(NH_4)_3Ta_2O_3F_7$ [57].

Balke [55] obtained crystal hydrate of lithium hexafluorotantalate, $LiTaF_6 \cdot H_2O$, by evaporating a solution prepared by the dissolution of $Ta_2O_5$ and $Li_2CO_3$ in HF. Crystal hydrate of sodium heptafluorotantalate, $Na_2TaF_7 \cdot H_2O$, was prepared in the same way [56], while re-crystallization of $Na_2TaF_7 \cdot H_2O$ from water yielded sodium octafluorotantalate, $Na_3TaF_8$ [29].

By diluting HF by means of multiple additions of water, followed by the evaporation of a solution initially prepared by the dissolution of NaF and $Nb_2O_5$ in HF, Stomberg [58] obtained $Na_3NbOF_6$ in the form of small single crystals that were suitable for X-ray structure investigations.

Potassium-containing tantalum and niobium fluoride compounds can be precipitated from HF solutions as described previously (see Fig. 3 and 4). Ritchie and Mitra [59] described the synthesis of $K_2TaF_7$ in an HF solution, based on the following interaction (5), using $TaCl_5$ as a precursor:

$$5\,HF + 2\,KF + TaCl_5 = K_2TaF_7 + 5\,HCl \qquad (5)$$

Hydrolysis of $K_2TaF_7$ in an alcohol solution containing KOH yielded potassium oxyfluorotantalate, $K_4Ta_2F_{12}O$ [59].

Crystals of $Rb_2TaF_7$ were prepared from relatively diluted solutions of HF, while re-crystallization of rubidium heptafluorotantalate, $Rb_2TaF_7$, using a 33% HF solution resulted in the precipitation of rubidium hexafluorotantalate, $RbTaF_6$ [56]. Under the same conditions, niobium-containing solutions yielded rubidium oxyfluoroniobate, $Rb_2NbOF_5$ [29].

$CsNbF_6$ can be prepared from a 35% HF solution, while $CsTaF_6$ can be precipitated from more diluted solutions [29].

An interaction between $NbF_5$ and CsF (molar ratio 1: 4-10) in aqueous solution yields $Cs_2NbOF_5$ [56].

Systematic investigations of the compounds that can be precipitated by adding alkali metals fluorides to HF solutions containing tantalum or niobium are discussed in [60, 61]. Compositions of the precipitated compounds and of their corresponding mother solutions are given in Table 4.

Two kinds of tantalum-containing initial solutions were chosen according to their ionic complex structure. The first one contained mostly $TaF_6^-$ ions (Ta:F = 1:18) while the second was characterized predominantly by $TaF_7^{2-}$ ions (Ta:F = 1:6.5). The ionic composition of the solutions was determined by Raman spectroscopy.

Three kinds of niobium-containing initial solutions were used, with different Nb:F ratios: 1:9, 1:18 and 1:6. The first two initial solutions contained mostly $NbF_6^-$ ions, whereas the third was composed primarily of $NbOF_5^{2-}$ ions. Table 5 presents the composition of the compounds that were precipitated following the addition of certain alkali fluorides to the initial solutions.

Table 6 summarizes the main compounds that can be prepared by adding alkali metal fluorides to fluorine solutions that contain niobium or tantalum.

An increase in the Me:F ratio leads to an increase in the acidity of the initial solution, whereas the acidity of alkali metals increases according to their molecular weight, from Li to Cs. Therefore the additives of fluorides of alkali metals having higher atomic weight provide formation of complex fluorides with lower coordination number of tantalum or niobium.

*Table 4. Compounds precipitated from tantalum-containing solutions Reproduced from [61], D. V. Tsikaeva, A. I. Agulyansky, Y. I. Balabanov, V. Y. Kuznetsov, V. T. Kalinnikov, Zh. Neorg. Khim. 34 (1989) 3046, Copyright 1989, with permission of "Nauka" (Russian Academy of Sciences) publishing.*

| Additive | M:Ta | Residual, M/l | Main phase | Impurities |
|---|---|---|---|---|
| ***Initial solution: Ta – 1.24 M/l, F – 22.11 M/l*** | | | | |
| $Li_2CO_3$ | 1:1 | Ta – 1.14; Li – 0.16 | $LiHF_2$ | $LiTaF_6$ |
| NaF | 1:1 | Ta – 1.15; Na – 1.03 | $Na_2TaF_7$ | $NaHF_2$ |
| | 2:1 | Ta – 0.60; Na – 1.19 | $Na_2TaF_7$ | $NaHF_2$ |
| | 3:1 | Ta – 0.54; Na – 1.13 | $Na_2TaF_7$, $NaHF_2$ | $Na_2TaF_7 \cdot H_2O$ |
| KF | 1:1 | Ta – 0.67; K – 0.21 | $K_2TaF_7$ | |
| RbF | 1:1 | Ta – 0.34; Rb – 0.43 | $RbTaF_6$ | |
| CsF | 1:1 | Ta – 0.24; Cs – 0.14 | $CsTaF_6$ | |
| ***Initial solution: Ta – 1.02 M/l; F – 6.63 M/l*** | | | | |
| $Li_2CO_3$ | 1:1 | Ta – 0.93; Li – 1.02 | LiF | |
| NaF | 1:1 | Ta – 0.74; Na – 0.64 | $Na_3TaF_8$ | $Na_2TaF_7 \cdot H_2O$ |
| KF | 1:1 | Ta – 0.37; K – 0.02 | $K_2TaF_7$ | |
| RbF | 1:1 | Ta – 0.40; Rb – 0.05 | $Rb_2TaF_7$ | |
| | 2:1 | Ta – 0.004; Rb – 0.05 | $Rb_2TaF_7$ | |
| CsF | 1:1 | Ta – 1.16; Cs – 0.22 | $CsTaF_6$ | |
| | 2:1 | Ta – 0.10; Cs – 0.47 | $Cs_2TaF_7$ | |

*Table 5. Compounds precipitated from niobium-containing solutions Reproduced from [61], D. V. Tsikaeva, A. I. Agulyansky, Y. I. Balabanov, V. Y. Kuznetsov, V. T. Kalinnikov, Zh. Neorg. Khim. 34 (1989) 3046, Copyright 1989, with permission of "Nauka" (Russian Academy of Sciences) publishing.*

| Additive | M:Nb | Residual, M/l | Main phase | Impurities |
|---|---|---|---|---|
| ***Initial solution: Nb – 3.20 M/l, F – 27.10 M/l*** | | | | |
| NaF | 1:1 | Nb – 2.63; Na – 0.98 | $Na_2NbOF_5$ | NaF |
| | 2:1 | Nb – 1.63; Na – 1.23 | $NaHF_2$ | $Na_2NbOF_5$ |
| KF | 1:1 | Nb – 1.52; K – 0.18 | $K_5Nb_3OF_{18}$ | 5%$K_2NbF_7$ |
| | 1:2 | Nb – 0.33; K – 0.30 | $K_2NbF_7$ | 10%$K_5Nb_3OF_{18}$ |
| RbF | 1:2 | Nb – 1.81; Rb – 0.06 | $RbNbOF_4$ | |
| | 1:1 | Nb – 0.49; Rb – 0.17 | $RbNbOF_4$ | $RbNbF_6$ |
| | 2:1 | Nb – 0.08; Rb – 1.12 | $Rb_5Nb_3OF_{18}$ | $Rb_2NbOF_5$ |
| CsF | 1:1 | Nb – 0.40; Cs – 0.06 | $CsNbF_6$ | |
| ***Initial solution: Nb – 1.54 M/l; F – 27.90 M/l*** | | | | |
| $Li_2CO_3$ | 1:1 | Nb – 1.11; Li – 0.10 | $LiHF_2$; LiF | $LiNbOF_4$ |
| LiF | 1:1 | Nb – 1.54; Li – 0.10 | $LiNbOF_4$ | LiF |
| NaF | 1:1 | Nb – 1.51; Na – 1.39 | No precipitate | |
| KF | 1:1 | Nb – 0.99; K – 0.39 | $K_2NbF_7$ | $K_5Nb_3OF_{18}$ |
| RbF | 1:1 | Nb – 0.41; Rb – 0.24 | $RbNbF_6$ | $RbNbOF_4$ |
| CsF | 1:1 | Nb – 0.23; Cs – 0.09 | $CsNbF_6$ | $Cs_5Nb_3O_3F_{14}$ |
| ***Initial solution: Nb – 1.75 M/l; F – 10.66 M/l*** | | | | |
| LiF | 1:1 | Nb – 1.64; Li – 0.29 | 50% $LiNbOF_4$ | 50% LiF |
| NaF | 1:1 | Nb – 1.53; Na – 1.42 | $NaHF_2$ | |
| KF | 1:1 | Nb – 1.02; K – 0.45 | $K_5Nb_3OF_{18}$ | |
| RbF | 1:1 | Nb – 0.89; Rb – 0.19 | $Rb_5Nb_3O_3F_{14}$ | $RbNbOF_4$ |
| CsF | 1:1 | Nb – 1.02; Cs – 0.20 | $Cs_5Nb_3O_3F_{14}$ | |

*Table 6. Main compounds precipitated from Nb- and Ta-containing solutions*

| Me: F | Li | Na | K | Rb | Cs |
|---|---|---|---|---|---|
| | | | ***Niobium-containing solutions*** | | |
| 1:6 | $LiNbOF_4$ | | $K_5Nb_3OF_{18}$ | $Rb_5Nb_3O_3F_{14}$ | $Cs_5Nb_3O_3F_{14}$ |
| 1:9 | $LiNbOF_4$ | $Na_2NbOF_5$ | $K_5Nb_3OF_{18}$ | $RbNbOF_4$ | $CsNbF_6$ |
| 1:18 | $LiNbOF_4$ | | $K_2NbF_7$ | $RbNbF_6$ | $CsNbF_6$ |
| | | | ***Tantalum-containing solutions*** | | |
| 1:6.5 | | $Na_3TaF_8$ | $K_2TaF_7$ | $Rb_2TaF_7$ | $CsTaF_6$ |
| 1:18 | $LiTaF_6$ | $Na_2TaF_7$ | $K_2TaF_7$ | $RbTaF_6$ | $CsTaF_6$ |

Attempts to obtain fluoride compounds of niobium and tantalum with alkali earth and some transitional metals were made as early as one hundred years ago, but synthesis and identification methods were described only at later times.

Davidovich et al. [62, 63] investigated the compositions of precipitates obtained from HF solutions by the addition of carbonates and fluorides of bivalent metals. The initial solutions were prepared by dissolution of either tantalum or niobium oxides in HF solutions. Addition of alkali earth metals to the niobium- or tantalum-containing fluoride solutions yielded the following crystal hydrates: $MgNbOF_5 \cdot 4H_2O$, $CaNbOF_5 \cdot 2H_2O$, $Sr_3(NbOF_6)_2 \cdot 3H_2O$, $Ba_3(NbOF_6)_2 \cdot 3H_2O$ and $SrTaF_7 \cdot 2H_2O$ [62].

The addition of equivalent amounts of bivalent metal carbonates to a solution with a Nb(Ta):F ratio of 1:40 yielded the following compounds: $MNbOF_5 \cdot 4H_2O$ (where M = Mn, Cu, Cd), $MNbOF_5 \cdot 6H_2O$ (where M = Co, Ni, Zn), $MTaF_7 \cdot 6H_2O$ (where M = Mn, Co, Ni, Zn, Cd) and $CuTaF_7 \cdot 4H_2O$ [63].

No available data was found on the precipitation from fluoride solutions of niobium and tantalum fluoride compounds containing tri- and tetravalent metals.

The results available on the synthesis of niobium and tantalum fluoride compounds from aqueous solutions are in good correlation with the concept of

Lewis acidity. Niobium (V) and tantalum (V) can be considered hard acids due to their relatively high charge and small size [64]. Fluoride, therefore, forms the complexes $NbOF_5^{2-}$-$NbF_6^-$ and $TaF_7^{2-}$-$TaF_6^-$, representing Lewis bases whose acidity decreases with the increase in the coordination number of tantalum and niobium. The interaction between the complex ions and the alkali metal cations, whose acidity decreases with the increase in their atomic mass, shifts the equilibrium in toward the base. The higher the acidity of the cation, the stronger the shift in equilibrium.

Effective precipitators are relatively weak acids, such as $Co^{2+}$, $Ni^{2+}$, $Cu^{2+}$, $Zn^{2+}$ etc. Such precipitators were ranked by Pirson to form a contiguous group of cations [65]. However, in order to synthesize compounds of either $M^{II}(TaF_6)_2$ or $M^{II}(NbF_6)_2$ type, it is necessary either to use cations with a higher acidity or anhydrous hydrogen fluoride, HF [64].

It should be mentioned here that in relatively low concentrations of HF, and all other conditions being equal, tantalum-containing solutions yield heptafluorotantalates, $M_nTaF_7$, while niobium-containing solutions yield monooxyfluoroniobates, $M_nNbOF_5$. This phenomenon is due to the greater tendency of niobium complex ions to undergo hydrolysis as compared to that of tantalum complex ions.. Thus, using $^{19}F$ NMR, it was found that the anion trans-$NbOF_4 \cdot H_2O^-$ has a molar ratio of F:Nb$\leq$5 following the addition of triethylamine. Following basic hydrolysis, a further increase in alkalinity leads to the formation of $NbOF_5^{2-}$ complex [66]. Transformation of the complex ion structure can be explained to be the result of the effects of two opposing processes, namely, the bonding of protons associated with fluorine and hydrolysis [66]. The Nb=O bond also has a higher covalence compared with the Ta=O bond [67]. This particular feature of aqueous niobium-containing systems enables the formation of oxyfluoride complexes providing a wider spectrum of compounds that can be precipitated from such solutions, compared with similar tantalum-containing systems. Table 7 presents a list of compounds that can be prepared from HF solutions along with their refractive indexes [61].

$M_5Nb_3OF_{18}$ type compounds are of particular interest because of their intermediate position between pure fluoroniobates, $MNbF_6$ or $M_2NbF_7$ and monooxyfluoroniobates, $M_2NbOF_5$. The structure and properties of these compounds will be discussed later.

The compound $(NH_4)_5Nb_3OF_{18}$ can be prepared by adding ammonium fluoride, $NH_4F$, to a solution containing Nb (3.20 M/l) and F (27.10 M/l). The solubility isotherm (25°) of this compound is presented in Fig. 5. The minimum point on the solubility isotherm approximately corresponds to the stoichiometrical ammonium–niobium ratio of the compound $(NH_4)_5Nb_3OF_{18}$.

*Table 7. Niobium-containing compounds prepared from HF solutions. Reproduced from [61], D. V. Tsikaeva, A. I. Agulyansky, Y. I. Balabanov, V. Y. Kuznetsov, V. T. Kalinnikov, Zh. Neorg. Khim. 34 (1989) 3046, Copyright 1989, with permission of "Nauka" (Russian Academy of Sciences) publishing.*

| Compound | Refractive Indexes | |
|---|---|---|
| | $N_p$ | $N_q$ |
| $(NH_4)_5Nb_3OF_{18}$ | 1.462 | 1.498 |
| $LiNbOF_4$ | 1.482 | 1.672 |
| $Na_2NbOF_5$ | | 1.457 |
| $K_5Nb_3OF_{18}$ | 1.441 | 1.500 |
| $K_2NbF_7$ | 1.435 | 1.445 |
| $Rb_5Nb_3O_3F_{14}$ | 1.431 | 1.463 |
| $RbNbF_6$ | 1.444 | 1.453 |
| $RbNbOF_4$ | 1.453 | 1.642 |
| $Rb_5Nb_3OF_{18}$ | 1.452 | 1.498 |
| $CsNbF_6$ | 1.450 | 1.479 |
| $Cs_5Nb_3O_3F_{14}$ | 1.459 | 1.485 |

The addition of ammonium fluoride leads to the precipitation of ammonium hydrofluoride, $NH_4HF_2$.

$Rb_5Nb_3OF_{18}$ is precipitated and re-crystallized from 20-30% HF solutions (Fig. 6). Lower concentrations of HF yield $Rb_5Nb_3O_3F_{14}$, while $RbNbF_6$ precipitates at concentrations over 35%.

Single crystals of $Rb_5Nb_3OF_{18}$ can be grown successfully by dissolving the prepared compound in a 20-30% HF solution at increased temperature and subsequent slow cooling of the solution down to room temperature. The solubility of $Rb_5Nb_3OF_{18}$ in 20% HF solution versus the temperature of the solution is given in Fig. 7.

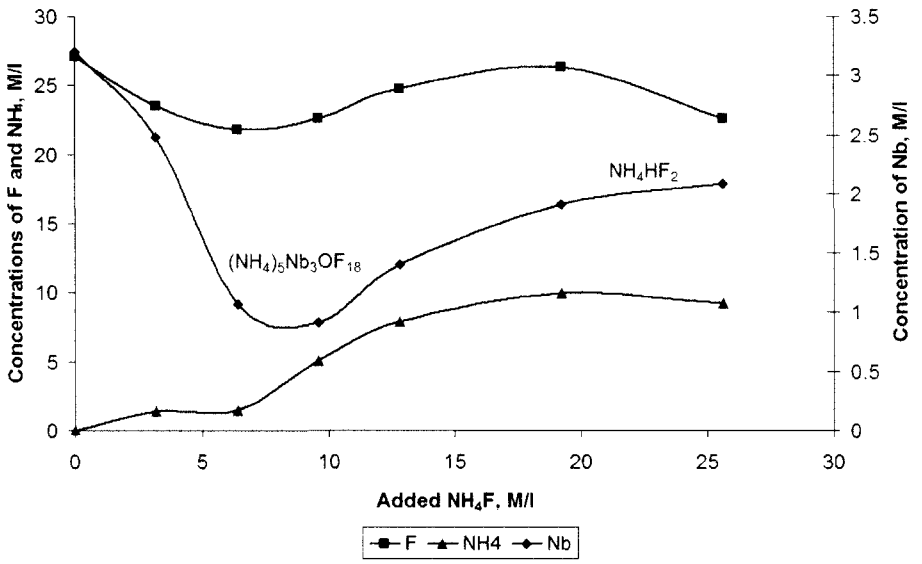


*Fig. 5. Concentration of $NH_4$, F, and Nb versus the amount of $NH_4F$ added to a solution initially containing 3.20 M/l Nb and 27.10 M/l F (after Tsikaeva et al. [60, 61]).*

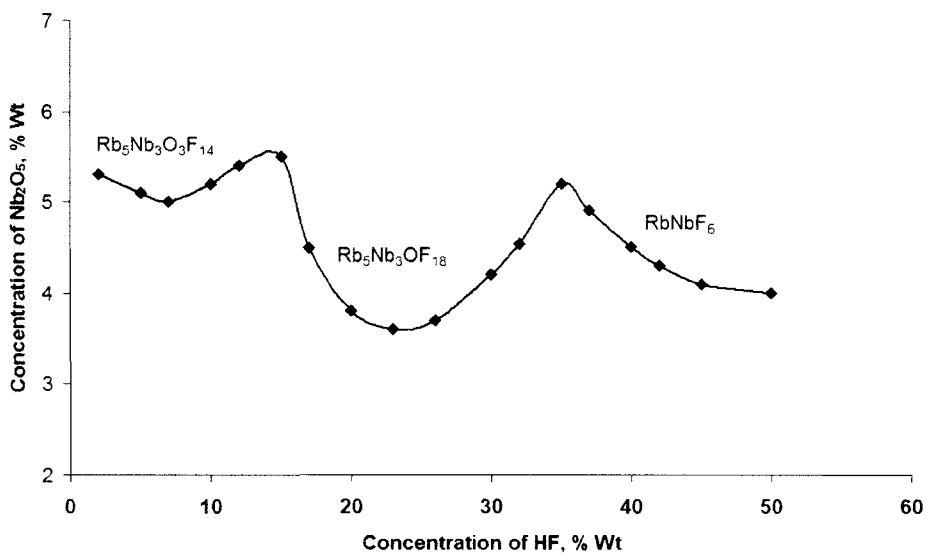


*Fig. 6.Crystallization field and solubility (45°C) of $Rb_5Nb_3OF_{18}$ in HF solutions (after Tsikaeva et al. [60, 61]).*

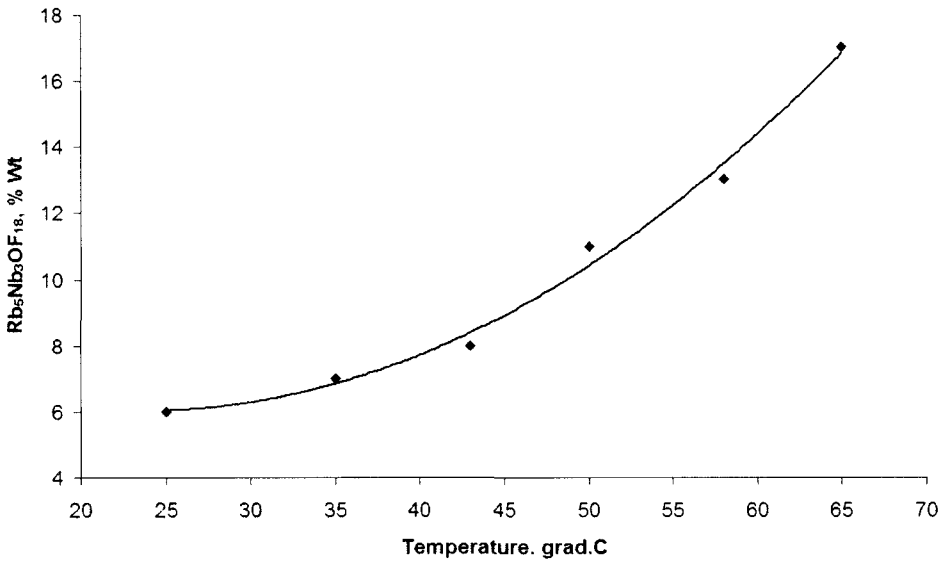


*Fig. 7. Solubility of $Rb_5Nb_3OF_{18}$ in 20% wt HF versus solution temperature (after Tsikaeva et al. [60, 61]).*

## 2.2. Non-aqueous solutions

In the absence of water molecules in the system, similar compositions of fluoride complexes of tantalum and niobium are expected. An analysis of the $^{19}F$ and $^{93}Nb$ NMR spectra of solutions based on anhydrous hydrogen fluoride, performed by Buslaev et al., revealed the presence of $NbF_6^-$ and $NbF_7^{2-}$ complexes [57].

Anhydrous hydrogen fluoride is widely used for the synthesis of fluoride compounds [68]. In particular, $NaNbF_6$ and $Na_2NbF_7$ were prepared using a solution of anhydrous hydrogen fluoride, HF, containing dissolved $NbF_5$ and NaF [69].

Another anhydrous solvent that is frequently used for the synthesis of tantalum and niobium fluoride compounds is bromine trifluoride, $BrF_3$. At ambient temperature, bromine trifluoride is light yellow liquid characterized by a boiling point of 126°C, a melting point of ~9°C and a density of 2.84 g/cm$^3$ at melting temperature.

In its liquid form, bromine trifluoride dissociates according to Equation (6):

$$2\ BrF_3 = BrF_2^+ + BrF_4^- \quad (6)$$

In solvents of this kind, compounds that are formed with F-donors possess alkaline properties, whereas compounds affiliated with F-acceptors take on acidic properties. For instance, $MBrF_4$ (where M = alkali metal) is alkaline whereas $BrF_2NbF_6$ displays the property of an acid. A typical interaction that takes place during the synthesis can be represented as follows:

$$Br_2Nb(Ta)F_6 + MBrF_4 = MNb(Ta)F_6 + 2\ BrF_3 \quad (7)$$

Using $BrF_3$ solutions, Gutmann and Emeleus [70] prepared a large number of hexafluoroniobates and hexafluorotantalates of alkali and alkali earth metals.

## 2.3. Interactions with $TaF_5$ and $NbF_5$

The most universal method for the synthesis of tantalum and niobium fluoride compounds is based on direct interaction between their pentafluorides, $TaF_5$ or $NbF_5$, and fluorides of other metals. Some physical–chemical properties of these compounds are presented in Table 8 [71, 72].

$TaF_5$ and $NbF_5$ are prepared from their respective oxides by fluorination with fluorine, $F_2$, or with anhydrous hydrogen fluoride, HF [73-75]. Rakov et al. reported the interaction between niobium metal and anhydrous hydrogen fluoride as being the most effective way of preparing $NbF_5$ [76].

Bizot obtained compounds of $MNbF_6$, $M_2NbF_7$ and $M_3NbF_8$ type (M = Li, Na, K [77] and M = Rb and Cs [78]) by the direct interaction between $NbF_5$ and alkali metal fluorides.

Rakov et al. also describe the preparation of $Ca(NbF_6)_2$ [79] and $MgNbF_7$ [80].

Galy, Andersson and Portier reported on the thermal treatment (at 700°C), in a sealed ampule, of a mixture containing LiF, $Nb_2O_5$ and $NbF_5$, leading to the preparation of $Li_2NbOF_5$ [81].

*Table 8. Physical-chemical properties of $NbF_5$ and $TaF_5$ (after Galkin [71] and Rabinovich and Havin [72]).*

| Properties | $NbF_5$ | $TaF_5$ |
|---|---|---|
| Molecule weight | 187.90 | 275.94 |
| Density (standard conditions), g/cc | 3.3 | 4.98 |
| Melting point, °C | 79.5 | 96 |
| Boiling point, °C | 234.5 | 229.2 |
| Vapor pressure – P(t°C), torr | 0.1(45); 1(67); 10(104);100(163) | 1(80); 10(104); 100(161) |
| Standard molar heat, $C_p^0$, J/mol·K | 134.85 | 130.5 |
| Standard molar entropy, $S^0$, J/mol·K | 157.3 | 170 |
| Standard molar enthalpy, ΔH, J/mol·K | - 1813.8 | - 1903.6 |
| Standard Gibbs Energy, ΔG, J/mol·K | - 1698.7 | - 1790.8 |
| Dissolves in | HCl; $HNO_3$; Conc. $H_2SO_4$; Ethanol; Chloroform; $CCl_4$; $CH_3COOH$ | Conc. $HNO_3$; Conc. HCl; Hot $H_2SO_4$; Chloroform; $CCl_4$; $CS_2$ |

The process can be represented as follows:

$$10\ LiF + Nb_2O_5 + 3\ NbF_5 = 5\ Li_2NbOF_5 \quad (8)$$

The same compound, $Li_2NbOF_5$, can be obtained by another method as well [81], in which LiF interacts with gaseous $NbOF_3$. Niobium oxytrifluoride, $NbOF_3$, is generated from the thermal decomposition of $NbO_2F$ at 700-800°C. This decomposition process was first investigated by Andersson and Aström [82] and later by Yampolsky, Rakov et al. [83]. The decomposition of $NbO_2F$ yields solid and gaseous components, as follows:

$$4\ NbO_2F = Nb_3O_7F_{(solid)} + NbOF_{3\ (gas)} \quad (9)$$

## 2.4. Synthesis of oxyfluoride compounds using $NbO_2F$ and $TaO_2F$

Niobium dioxyfluoride, $NbO_2F$, and tantalum dioxyfluoride, $TaO_2F$, can be successfully used as precursors for the synthesis of many oxyfluoride compounds of niobium and tantalum. Systematic investigations performed on $MeO_2F$ – $M_2CO_3$ systems, in which Me = Nb or Ta and M = alkali metal, provided necessary information on optimal synthesis procedures and imparted some conformity on the mechanism of the chemical interaction between the components.

### 2.4.1. Interactions in $NbO_2F$ – $M_2CO_3$ systems

Reaction of $NbO_2F$ with an alkali metal carbonate, $M_2CO_3$, yields carbon dioxide, $CO_2$, in an amount equivalent to that of a chemical compound forming at the first stage of the reaction. The general form of the reaction between niobium dioxyfluoride and an alkali metal carbonate, $M_2CO_3$, is:

$$NbO_2F + m\,M_2CO_3 = (M_2O)_n \cdot NbO_2F + (m-n)\,M_2CO_3 + n\,CO_2 \quad (10)$$

When the reaction is performed at relatively low temperatures that prevent strong thermal decomposition of the alkali metal carbonate, the formation of $CO_2$ will be related only to the reaction and will indicate the stoichiometry of the process. Fig 8 presents mass loss isotherms of $NbO_2F$ – $M_2CO_3$ mixtures (in which M - Li, Na, K, Rb, Cs) that were subjected to thermal treatment in air at 850°C [84, 85]. It is important to mention that parallel experiments performed without the addition of $NbO_2F$, resulted in alkali metal carbonate mass losses that were in the same order of magnitude as the measurement errors at temperatures below 850°C.

Maximum losses correspond to a $NbO_2F$ molar fraction of 0.3–0.36. At higher concentrations of $NbO_2F$, alkali metal carbonate was not found in any of the systems. This indicates that the components $M_2CO_3$ and $NbO_2F$ interact at a molar ratio of 2:1, which corresponds to m=2 in Reaction (10). Precision thermal analysis [86] of the mixtures displays endothermic effects that correspond to the interaction of the compounds. The reaction temperatures and melting points of the carbonates are shown in Table 9. A relatively low temperature, in the case of the system containing $Li_2CO_3$, corresponds to particular properties of lithium and its position in the series of alkali metals. In general terms, reaction temperatures correlate with the melting points of alkali metal carbonates remaining to be lower.

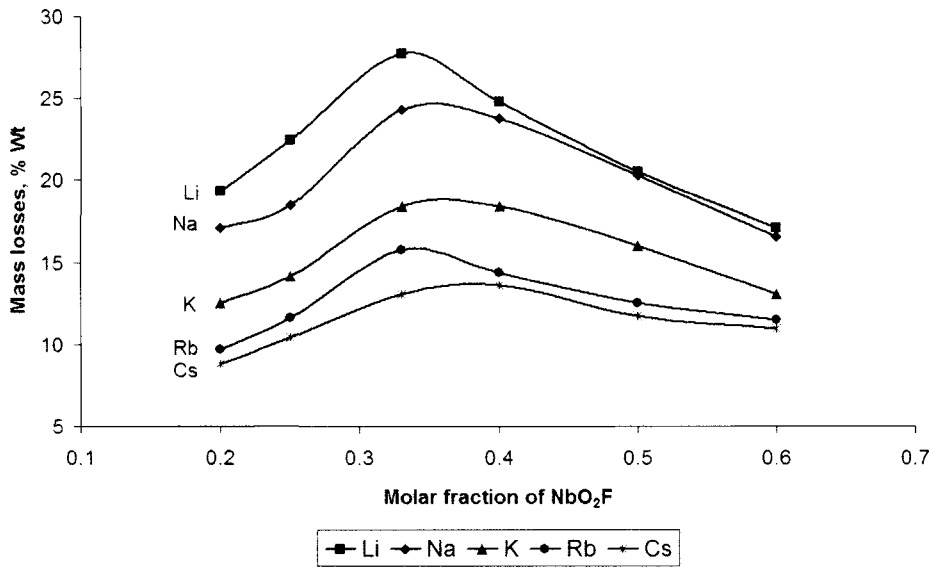


*Fig. 8. Mass loss isotherms (850°C) for $NbO_2F$ – $M_2CO_3$, mixtures in which M = Li, Na, K, Rb or Cs (after Agulyansky et al. [85]).*

$Li_2CO_3$ reacts with $NbO_2F$ yielding $Li_4NbO_4F$ according to Equation (11), as follows [87]:

$$2\ Li_2CO_3 + NbO_2F = Li_4NbO_4F + 2\ CO_2 \quad (11)$$

Additional evidence of the reaction described in Equation (11) is the section of the $Li_2CO_3$ – $NbO_2F$ system's melting diagram presented in Fig. 9 [87].

*Table 9. Melting points and reaction temperatures of $M_2CO_3$ with $NbO_2F$*

| | $Li_2CO_3$ | $Na_2CO_3$ | $K_2CO_3$ | $Rb_2CO_3$ | $Cs_2CO_3$ |
|---|---|---|---|---|---|
| Reaction point, °C | 607 | 710 | 680 | 628 | 530 |
| Melting point, °C | 732 | 852 | 891 | 835 | 600 |

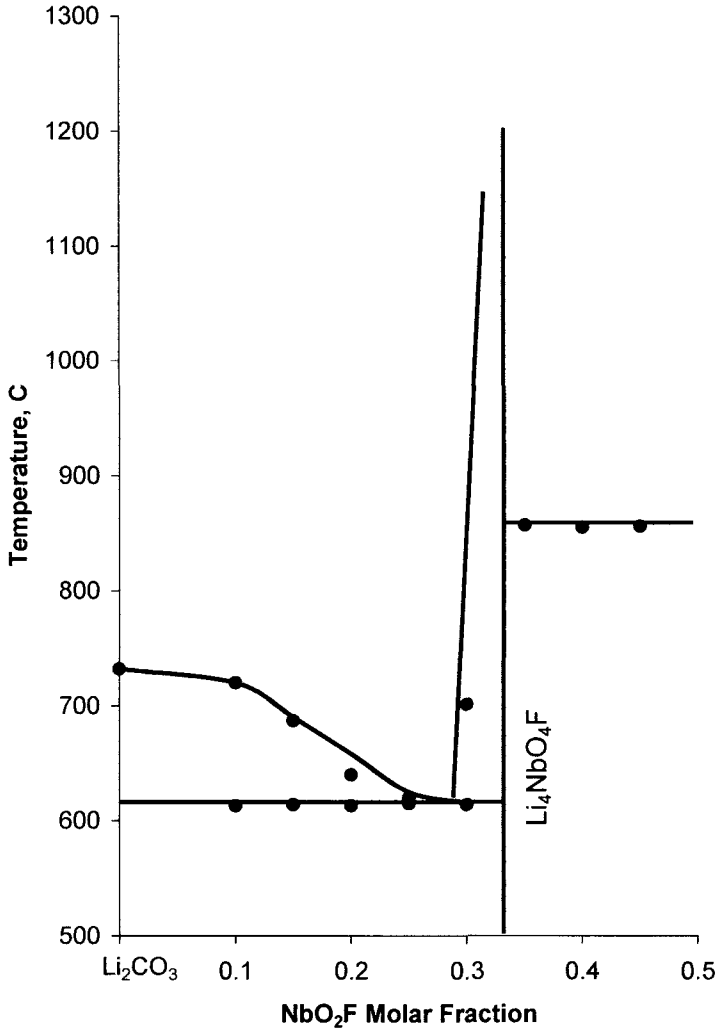


*Fig. 9. Melting diagram of $Li_2CO_3$ – $NbO_2F$ system. Reproduced from [87], A. I. Agulyansky, V. A. Bessonova, V. Y. Kuznetsov, V. T. Kalinnikov, Zh. Neorg. Khim. 29 (1984) 1066, Copyright 1984, with permission of "Nauka" (Russian Academy of Sciences) publishing.*

$LiNbO_3$ appeared in the treated mixtures that contained more than a 0.33 mol fraction of $NbO_2F$. This indicates that the system is not pseudo-binary in mixtures with higher $NbO_2F$ mol fraction compositions.

Niobium tetraoxyfluoride, $Li_4NbO_4F$, can also be prepared by the interaction between lithium fluoride, LiF, with lithium orthoniobate, $Li_3NbO_4$. The melting diagram for the compound shows that $Li_4NbO_4F$ undergoes incongruent melting at 1100°C as seen in Fig. 10 [87].

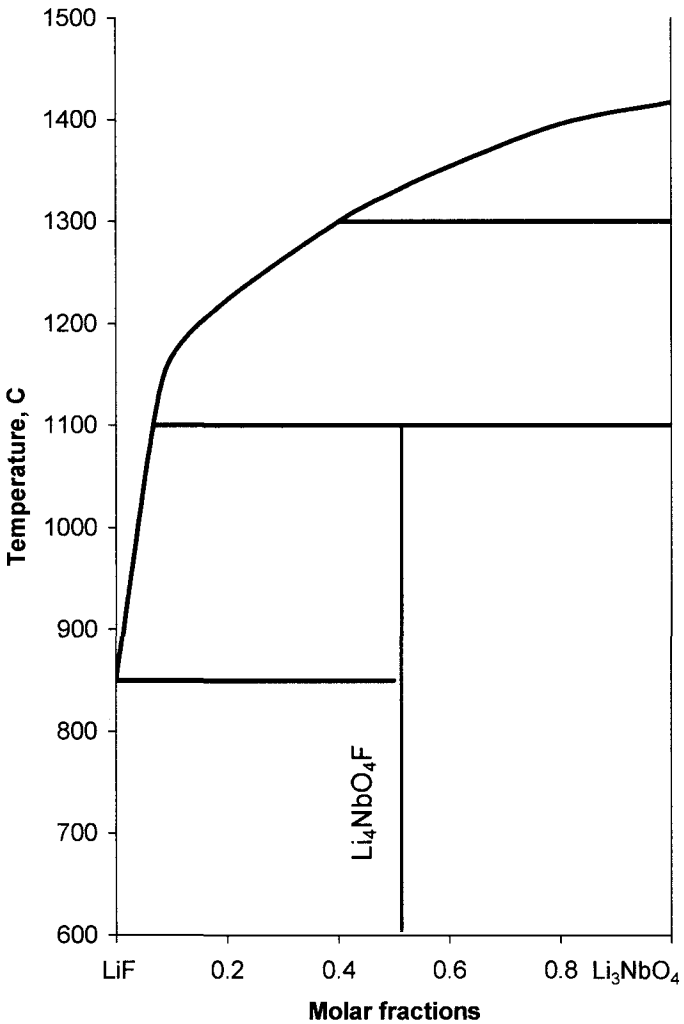


*Fig. 10. Melting diagram of LiF – $Li_3NbO_4$ system. Reproduced from [87], A. I. Agulyansky, V. A. Bessonova, V. Y. Kuznetsov, V. T. Kalinnikov, Zh. Neorg. Khim. 29 (1984) 1066, Copyright 1984, with permission of "Nauka" (Russian Academy of Sciences) publishing.*

The compound $Li_4NbO_4F$ crystallizes in cubic syngony, with a cell parameter of 4.192 Å and a Rock Salt (NaCl) structure. The compound's X-ray diffraction pattern and cell parameter are very similar to those of nickel oxide, NiO.

The above-mentioned data clearly indicate that the first step in the interaction between $NbO_2F$ and alkali metal carbonates takes place at a molar ratio of 1:2. In the case of lithium carbonate, $Li_4NbO_4F$ is obtained according to above Equation (11). A subsequent increase in the concentration of $NbO_2F$ in the lithium carbonate mixture leads to the formation of lithium metaniobate, $LiNbO_3$. The mechanism of $LiNbO_3$ formation can be represented by a two-step reaction. The first step consists of the formation of an intermediate compound according to the following equation:

$$Li_4NbO_4F + NbO_2F = 2\,Li_2NbO_3F \quad (12)$$

The product of the interaction (12), $Li_2NbO_3F$, is unstable and decomposes as follows:

$$Li_2NbO_3F = LiNbO_3 + LiF \quad (13)$$

The instability of $Li_2NbO_3F$ can be explained based on the 4:3 anion:cation ratio. Taking in to account the similar ionic radii of $O^{2-}$ and $F^-$ as well as the steric similarity of $Nb^{5+}$ and $Li^+$, it is possible to imagine the compound as having the general formula of $Me_3X_4$. In this case, one of the cations must have a coordination number of 4, which is highly improbable. Another possible way of stabilizing the compound is to crystallize it as a Galasso salt [88]. In this case, however, lithium's coordination number must increase, which is atypical for lithium cations.

Analysis of weight loss isotherms displayed in Fig. 8 shows that the first step in the interaction between $NbO_2F$ and carbonates of other alkali metals is similar to the interaction described by Equation (11). However, compounds of the $M_4NbO_4F$ form, where M = Na, K, Rb, Cs, were not found [85]. The instability of such compounds is related to the ionic radii of the alkali metals, which are greater than that of $Nb^{5+}$, thus the ions are too large to occupy the octahedral cavities formed by the oxygen and fluorine ions.

In mixtures containing excessive amounts of alkali metal carbonates (molar ratios of $M_2CO_3$:$NbO_2F$ equal to 4:1, 3:1 and 2:1), orthoniobate or a mixture of ortho- and metaniobate and alkali metal fluorides were found. A subsequent increase in the $NbO_2F$ concentration in the initial mixture leads to the

formation of metaniobates and oxyfluoroniobates of alkali metals. For instance, $Na_2Nb_3O_5F_2$ is formed at $Na_2CO_3$:$NbO_2F$ molar ratios of 1:1, 2:3 and 1:2.

X-ray diffraction analysis of compounds obtained from a $K_2CO_3$ – $NbO_2F$ system shows that the Galasso salt, $K_2NbO_3F$ [88], forms at temperatures of 690-790°C. A further increase in temperature, to 800-900°C, leads to predomination of the $KF{\cdot}4KNbO_3$ phase as described by Rogachov, Kuznetsov et al. [89]. This phase remains the main product of the interaction following thermal treatment of the mixture at 900°C. $Rb_2NbO_3F$, which is similar to Galasso salt, was found in the $Rb_2CO_3$ – $NbO_2F$ system, whereas cesium-containing systems yield the orthoniobate of cesium, $Cs_3NbO_4$ [85].

Analysis of the composition of compounds formed in systems containing $NbO_2F$ and alkali metal carbonates reveals several common peculiarities. The first stage of the interaction takes place according to Equation (11) and can be formulated in general as follows:

$$2\ M_2CO_3 + NbO_2F = M_4NbO_4F + 2\ CO_2 \qquad (14)$$

$M_4NbO_4F$ compounds have a NaCl-type structure, and are stable only in the case of lithium due to the steric similarity between the lithium ion and $Nb^{5+}$. In the case of other alkali metal cations with larger ionic diameters, the $M_4NbO_4F$ compounds decompose yielding orthoniobates and simple fluorides of alkali metals, as follows:

$$M_4NbO_4F = M_3NbO_4 + MF \qquad (15)$$

In $M_2CO_3$ – $NbO_2F$ mixtures with 1:1 molar ratios, Galasso-type compounds are formed:

$$M_4NbO_4F + NbO_2F = 2\ M_2NbO_3F \qquad (16)$$

The structure of the Galasso salt, $K_2NbO_3F$, which is made up of octahedral $NbO_4F_2$ ions and potassium ions [88] is rendered unstable when it contains the smaller alkali metal cations. Thus, compounds containingg sodium and lithium decompose according to the following scheme, yielding metaniobates, $MNbO_3$:

$$M_2NbO_3F = MNbO_3 + MF \qquad (17)$$

*Table 10. Main compounds formed in $M_2O$ ($M_2CO_3$) – $NbO_2F$ systems (after Agulyansky et al. [85]).*

| $M_2O$ | $M_2O$ : $NbO_2F$ molar ratio | | |
|---|---|---|---|
| | 2:1 | 1:1 | 1:2 |
| Li | $Li_4NbO_4F$ | $LiNbO_3$+LiF | $LiNbO_3$+$Nb_2O_5$+LiF |
| Na | $Na_3NbO_4$+NaF | $NaNbO_3$+NaF | $Na_2Nb_2O_5F_2$ |
| K | $K_3NbO_4$+KF | $K_2NbO_3F$ or KF·4$KNbO_3$+KF | |
| Rb | $Rb_3NbO_4$+RbF | $Rb_2NbO_3F$ | |
| Cs | $Cs_3NbO_4$+CsF | | |

In addition, it should be noted that $K_2NbO_3F$ is less stable that its rubidium and cesium analogs and that it too decomposes at relatively high temperatures, as follows:

$$4\ K_2NbO_3F = KF{\cdot}4KNbO_3 + 3\ KF \quad (18)$$

The apparently high relative stability of KF·4$KNbO_3$ can be related to the steric similarity between potassium and fluorine ions, which is hardly the case with other alkali metals. Table 10 presents a general list of compounds that can be obtained by the interaction of $NbO_2F$ with alkali metal carbonates.

## 2.4.2. Interactions in $TaO_2F$ – $M_2CO_3$ systems

Thermogravimetric analyses of $M_2CO_3$ – $TaO_2F$ systems, in which M = Li, Na, K, show that the temperatures that correspond to the interactions are not dependent on the composition of the initial mixtures and are very similar to the corresponding temperatures indicated for niobium-containing systems [90]. Interaction temperatures are 604°C, 682°C and 675°C for lithium-, sodium- and potassium carbonate, respectively. A mixture of $2Li_2CO_3$ and $TaO_2F$ yields the compound $Li_4TaO_4F$, which has similar structure with its niobium-containing analog. Further increasing the initial amount of $TaO_2F$ in the mixture leads to the formation of $LiTaO_3$, $Ta_2O_5$ and LiF. The amount of $Ta_2O_5$ obtained in this reaction increases with the initial concentration of $TaO_2F$. At

the same time, increasing the thermal treatment temperature in the range of 780-850°C leads to a significant increase in the $LiTaO_3$ concentration in the treated mixture. In the light of the above, the main interactions can be described as follows [90]:

$$2\ Li_2CO_3 + TaO_2F = Li_4TaO_4F + 2\ CO_2 \quad (19)$$

In the systems containing sodium or potassium carbonates found no $M_4TaO_4F$ type compounds were found (M = Na, K). A phase with a composition similar to that of sodium metatantalate was identified in a 2:1 (molar ratio) mixture of $Na_2CO_3$ and $TaO_2F$. The composition of this phase was found to be $Na_{0.95}TaO_{2.95}F_{0.05}$ and was described by Chaminad, Pouchard and Hagenmuller [91]. A further increasing in $TaO_2F$ concentration leads to the formation of compounds containing even higher levels of fluorine. A mixture of $Na_2CO_3$ and $TaO_2F$ (molar ratio 1:1) yields $Na_2Ta_2O_5F_2$ according to the following interaction:

$$Na_2TaO_3F + TaO_2F = Na_2Ta_2O_5F_2 \quad (20)$$

The compound $NaTaO_2F_2$ was found in treated mixtures that contained a higher concentration of $TaO_2F$. The formation of this compound can be explained by the following decomposition process:

$$Na_2Ta_2O_5F_2 = NaTaO_2F_2 + NaTaO_3 \quad (21)$$

A potassium-containing system yields $K_2TaO_3F$, but this phase is metastable and can only be identified during the brief pause of the 2:1 mixture of $K_2CO_3$ and $TaO_2F$ at 686°C. At higher temperatures or under longer thermal treatment, potassium metatantalate, $KTaO_3$, and potassium fluoride, KF are formed [90]. It is possible that the interaction begins with the formation of $K_4TaO_4F$, which sequentially decomposes by two mechanisms:

$$\text{First, } K_4TaO_4F = K_3TaO_4 + KF \quad (22)$$

$$\text{Second, } K_4TaO_4F = K_2TaO_3F + K_2O = KTaO_3 + K_2O + KF \quad (23)$$

Further increase in $TaO_2F$ concentration leads to the formation of a phase with a variable composition, $K_6Ta_{6+X}O_{15+X}F_{6+7X}$, described in [92].

The main phases formed in $M_2O$ ($M_2CO_3$) – $TaO_2F$ systems in which M = Li, Na, K, are listed in Table 11.

*Table 11. The main phases formed in $M_2O$ ($M_2CO_3$) – $TaO_2F$ systems*

| $M_2O$ | $M_2O$ : $TaO_2F$ molar ratio | | |
|---|---|---|---|
| | 2:1 | 1:1 | 1:2 |
| Li | $Li_4TaO_4F$ | $LiTaO_3$+LiF | $LiTaO_3$+$Ta_2O_5$+LiF |
| Na | $Na_{0.95}TaO_{2.95}F_{0.05}$ | $Na_2Ta_2O_5F_2$ + $NaTaO_2F_2$ | |
| K | $K_2TaO_3F$ + $K_3TaO_4$ + $KTaO_3$ + KF | | $K_6Ta_{6+X}O_{15+X}F_{6+7X}$ |

## 2.4.3. Interaction mechanism in systems containing carbonates

Determining the stoichiometry of a reaction's first step and the composition of the reaction's first product is a key point in the definition of heterogeneous processes. The most fundamental feature of the different interactions that take place in systems containing alkali metal carbonates is their similar mechanism. In all cases discussed here, components interact yielding the same intermediate compound, $M_4MeO_4F$, where M = alkali metal, Me – tantalum or niobium. Further products of the interactions depend on the properties of the alkali metal (primarily on its ionic radius) and on the initial composition of the mixture. The interaction temperature is close to the melting point of the respective alkali metal carbonate [85, 90]. Furthermore, the interaction temperature depends mainly on the nature of alkali metal carbonate and depends much less on the nature of the second compound. Interaction temperatures for systems that contain $Li_2CO_3$ and a second oxide compound are shown in Table 12 [93]. The interaction temperatures were defined by differential thermal analysis (DTA) and electroconductivity measurements. The DTA pattern generally remains unchanged for different types of the second compound and the only strong exothermal effect appears at temperatures that are close to lithium carbonate's melting point. This leads to the conclusion that the interaction temperature is not strongly dependent on the properties of the second compound but rather is defined by the melting of the alkali metal carbonate.

The compound formed in the first step of the reaction between the solid components and the molten alkali metal carbonate can passivate the surface and prevent subsequent development of the interaction. This special property of $M_4MeO_4F$, the compound formed in the first step, leads, in effect, to a single-stage interaction.

*Table 12. Interaction temperatures in systems containing lithium carbonate (after Agulyansky et al. [93]).*

| System | Molar ratio | Interaction temperature, °C |
|---|---|---|
| $Li_2CO_3$ | pure | 720 |
| $Li_2CO_3 - Nb_2O_5$ | 1:1 | 745 |
| $Li_2CO_3 - LiNb_3O_8$ | 1:1 | 740 |
| $Li_2CO_3 - LiNbO_3$ | 1:1 | 755 |
| $Li_2CO_3 - Li_3NbO_4$ | 1:1 | 740 |
| $Li_2CO_3 - Ta_2O_5$ | 1:1 | 745 |
| $Li_2CO_3 - TiO_2$ | 1:1 | 755 |

This is confirmed by thermal mass spectrometry analysis performed on a $Li_2CO_3$ – $NbO_2F$ (molar ratio 2:1) mixture [94]. The pressure of $CO_2$ that separated from the mixture upon heating was recorded using a mass spectrometer. The polytherm of the pressure gives a single symmetrical bell–type curve. A typical mass spectral pattern for the partial pressure of $CO_2$ is shown in Fig. 11. The maximum pressure corresponds to a temperature of about 600-610°C, which is in good correlation with DTA data. In the case of interactions that take place in $M_2CO_3 - MeO_2F$ systems (M = alkali metal, Me = Nb or Ta), the compound $M_4MeO_4F$ is not stable if M = Na, K, Rb or Cs. $Li_4MeO_4F$ is stable but it seems that the compound quickly dissolves in the melt. Thus, in both cases no passivation of the surface of the solid components takes place.

A different situation is observed in the case of the interaction between lithium carbonate and tantalum- or niobium oxide. According to various investigations [95-98], the interaction between $Li_2CO_3$ and $Me_2O_5$ (Me = Nb or Ta) proceeds in several stages. It is also reported that at least one of the components interacts in a liquid phase such as a melt [96, 99]. Indeed mass spectral patterns of $CO_2$ pressure for such systems exhibit several peaks (Fig. 12), which means that the process proceeds in several stages, with and without the release of $CO_2$ [94, 100-102]. Such isotherms are explained by the formation of $Li_3MeO_4$ type compounds during the first stage of the reaction. This compound cannot interact with $Li_2CO_3$ and thus passivates the solid $Me_2O_5$ preventing further interaction with lithium carbonate.

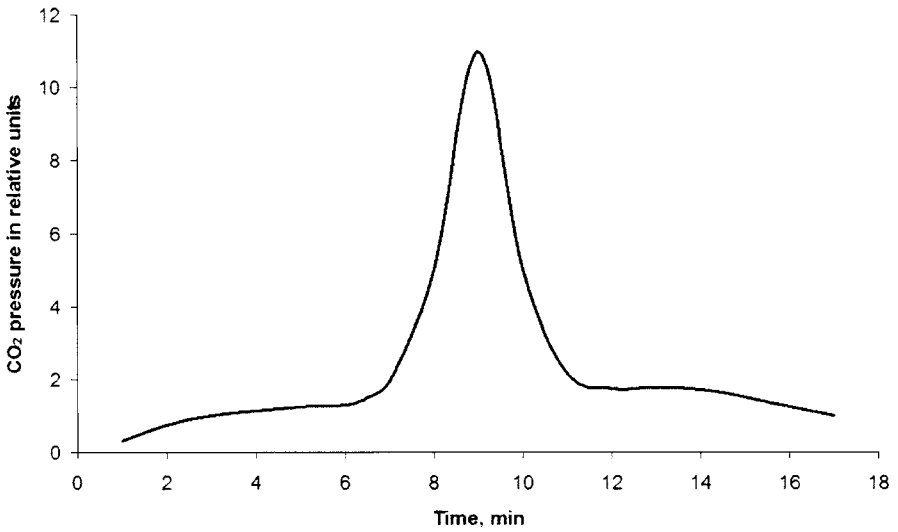


*Fig. 11. Mass spectral pattern of $CO_2$ pressure for $Li_2CO_3$ – $NbO_2F$ mixture (molar ratio 2:1, heating rate - 10°C per minute) (after Agulyansky et al. [94]).*

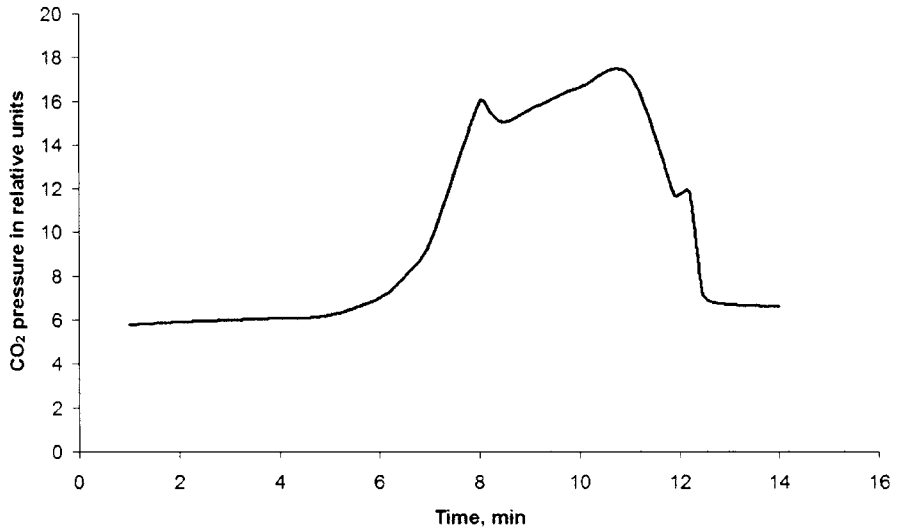


*Fig. 12. Mass spectral pattern of $CO_2$ pressure for $Li_2CO_3$ – $Nb_2O_5$ mixture (molar ratio 1:1, heating rate - 10°C per minute) (after Agulyansky et al. [100])*

However, $Li_3MeO_4$ does interact with $Me_2O_5$, yielding $LiMeO_3$. Metametalate of lithium, $LiMeO_3$, also interacts, both with $Li_2CO_3$ yielding $Li_3MeO_4$, and with $Me_2O_5$ yielding $LiMe_3O_8$. The mechanism described for these reactions consists of sequential interactions with $Li_2CO_3$ but not with lithium carbonate. The first kind of interaction leads to the decomposition of $Li_2CO_3$ and the release of $CO_2$ into the gas phase.

The second kind of interaction takes place between solids and as a pure solid phase interaction, does not release any $CO_2$.

This mechanism is also confirmed by X-ray diffraction measurements [94, 100]. It is also mentioned that the absence of reflexes belonging to $Li_3NbO_4$, in X-ray diffraction patterns obtained for mixtures treated at relatively low temperatures, could be explained by the formation of an amorphous material at the very beginning of the process [103].

The composition of the products that are formed as a result of the interaction with alkali metal carbonates can be determined using melting diagrams. It is obvious that in the first stage of the interaction, the compound can passivate the solid parts and prevent any further interaction. The passivation is achieved when the compound cannot interact chemically with the carbonate, i.e. the closest compound to the carbonate side of the melting diagram. For instance, the melting diagram of the $Li_2CO_3$ – $Nb_2O_5$ system [104] indicates that $Li_3NbO_4$ is the closest compound to $Li_2CO_3$. In the $Li_2CO_3$ – $NbO_2F$ system (Fig. 9), the passivating compound is $Li_4NbO_4F$. The probable formation of $M_4MeO_4F$ during the first stage of the interaction with alkali metal carbonates is typical for other types of fluoride compounds containing niobium and tantalum. $Li_4TaO_4F$ was also found during the investigation of the $Li_2CO_3$ – $LiTaF_6$ system. The melting diagram of the system is shown in Fig. 13. The interaction yielding $Li_4TaO_4F$ can be described by the following scheme:

$$LiTaF_6 + 4\,Li_2CO_3 = Li_4TaO_4F + 5\,LiF + 4\,CO_2 \qquad (24)$$

Summarizing the above results, the following peculiarities of the interactions of niobium and tantalum compounds with alkali metal carbonates can be mentioned:

- Alkali metal carbonates interact in molten form;
- The interaction takes place as a single-stage process;
- The results of the interaction is a compound incapable of any further interaction with the carbonate;
- In the case of oxyfluorides, $M_4MeO_4F$ compounds are formed;
- In the case of pure oxides, $M_3MeO_4$ compounds are formed.

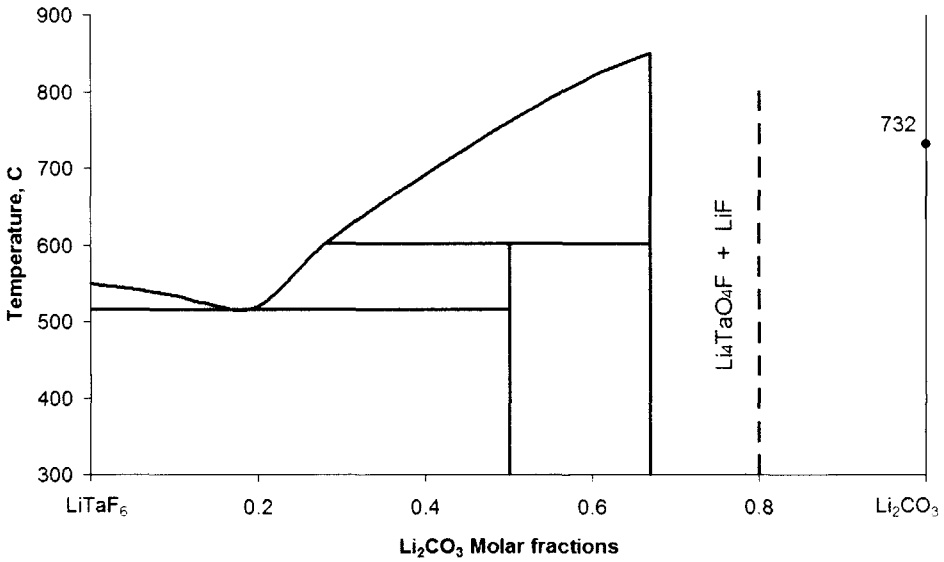


*Fig. 13. Part of melting diagram for $LiTaF_6 - Li_2CO_3$ system. Reproduced from [87], A. I. Agulyansky, V. A. Bessonova, V. Y. Kuznetsov, V. T. Kalinnikov, Zh. Neorg. Khim. 29 (1984) 1066, Copyright 1984, with permission of "Nauka" (Russian Academy of Sciences) publishing.*

## 2.5. Hydrofluoride synthesis of niobium and tantalum compounds

Hydrofluoride synthesis is based on the simultaneous fluorination by ammonium hydrofluoride of niobium or tantalum oxides with other metals compounds (oxides, halides, carbonates etc.) [105]. Table 13 presents some properties of ammonium hydrofluoride, $NH_4HF_2$ [51, 71]. Ammonium hydrofluoride is similar to anhydrous HF in its reactivity, but possesses some indisputable advantages. The cost of ammonium hydrofluoride is relatively low, it can be dried and handled easily, recycled from gaseous components, and its processing requires no special equipment.

*Table 13. Chemical properties of ammonium hydrofluoride (after Rakov [51] and Galkin [ 71]).*

| Property | Description |
|---|---|
| Formula | $NH_4HF_2$ |
| Molecular weight | 57.05 |
| Color | Colorless |
| Hygroscopic nature | Slightly hygroscopic at >50% humidity |
| Syngony | Rhombic |
| Space group | Pman |
| Cell parameters, nm | a = 0.84; b = 0.816; c = 0.367; Z = 4 |
| Density, g/cc | 1.505 |
| Melting point, °C | 126.45 |
| Melting enthalpy, kJ/mol | 19.096 |
| Boiling point, °C | 239.5 |

The interaction between metal oxides and ammonium hydrofluoride at 100-250°C yields complex fluorometalates of ammonium and water. The water formed evaporates from the mixture, but can also lead to hydrolysis of the fluorination product in the process. In the very common form the fluorination of metal oxides by ammonium hydrofluoride can be described as follows:

$$MeO_{n/2} + n\ NH_4HF_2 = (NH_4)_xMeF_{n+x} + n/2\ H_2O + (n-x)\ NH_3 + (n-x)\ HF \quad (25)$$

Ammonium complex fluorometalates are generally susceptible to hydrolysis by water formed in the course of the fluorination process (see 25). Such interactions, resulting in the formation of oxyfluoride metalates can be described as follows:

$$(NH_4)_xMeF_{n+x} + m\ H_2O = (NH_4)_xMeO_mF_{n+x-m/2} + 2\ m\ HF \quad (26)$$

Furthermore, both complex fluoromataletes and oxyfluorometalates of ammonium are prone to thermal decomposition. The decomposition is

accompanied by the release of gaseous ammonia and hydrogen fluoride. In the case of complex fluorometalates, the decomposition process is as follows:

$$(NH_4)_xMeF_{n+x} = (NH_4)_{x-y}MeF_{n+x-y} + y\,HF + y\,NH_3 \quad (27)$$

Complex oxyfluorometalates usually decompose by the same mechanism, maintaining the same Me/O ratio:

$$(NH_4)_xMeO_mF_{n+x-m/2} = (NH_4)_{x-y}MeO_mF_{n+x-m/2-y} + y\,HF + y\,NH_3 \quad (28)$$

Predominant formation of either complex fluoride or complex oxyfluoride depends on the interaction rates ratio of processes (25) and (26). The relatively high interaction rates of (27) and (28) lead to the synthesis of simple fluorides or oxyfluorides, respectively. With the availability of two or more cations in the system, the ammonium complex fluorometalates interact forming stable binary fluorides or oxyfluorides or mixtures thereof.

Ikrami and coworkers investigated interactions that take place in systems containing either lithium carbonate or alkali earth metals or some transition metals and ammonium hydrofluoride. Thus, the fluorination of lithium carbonate, $Li_2CO_3$, [106], Magnesium oxide, MgO, [107], oxides or carbonates of calcium and barium [108] results in the formation of simple fluorides characterized by a low oxygen impurity level. Fluorination of cobalt oxide, CoO, and nickel oxide, NiO, yield stable complex fluorometalates of ammonium – $(NH_4)_2MF_4$ and $(NH_4)_3MF_5$, where M = Co or Ni. The thermal decomposition of the above complex compounds results in the simple fluorides $CoF_2$ and $NiF_2$ [109].

Hexafluorometalates of ammonia are formed in the presence of trivalent metals [51, 52]. It was shown, for instance, that fluorination of chromium oxides using ammonium hydrofluoride yields $(NH_4)_3CrF_6$. It was also found that the oxidation degree of chromium does not depend on the initial valency of the original oxide used as a precursor [110].

The fluorination of tantalum oxide, $Ta_2O_5$, is described by Rakov [51]. The interaction begins at a temperature of 156-190°C, yielding heptafluorotantalate of ammonium:

$$Ta_2O_5 + 7\,NH_4HF_2 = 2\,(NH_4)_2TaF_7 + 3\,NH_3 + 5\,H_2O \quad (29)$$

Increasing the temperature to 260-300°C leads to the decomposition of the ammonium-tantalum complex fluoride:

$$(NH_4)_2TaF_7 = NH_4TaF_6 + NH_3 + HF \quad (30)$$

The sublimation and hydrolysis of $NH_4TaF_6$ take place at a higher temperature. Extended thermal treatment at 360-390°C yields tantalum dioxyfluoride as a final product:

$$NH_4TaF_6 + H_2O = TaO_2F + NH_3 + 5\,HF \quad (31)$$

Fluorination of niobium oxide, $Nb_2O_5$, by ammonium hydrofluoride was investigated by Rao et al. [111] and by Rakov et al. [51, 52]. The fluorination product at 100-130°C is $(NH_4)_3NbOF_6 \cdot 1.5H_2O$ according to Rao [111], or $(NH_4)_3NbOF_6$ according to Rakov [51, 52].

Buslaev et al. investigated the synthesis and mechanism of the thermal decomposition of $(NH_4)_3NbOF_6$ and $(NH_4)_3TaOF_6$ [112]. These compounds decompose in three steps, corresponding to three increasing temperatures, to yield $(NH_4)_2MeOF_5$, $NH_4MeOF_4$ and $MeO_2F$. For niobium containing compounds (Me = Nb) decomposition occurs at 255°C, 320°C and 420°C, respectively, while in the case of tantalum containing oxyfluoride (Me = Ta) decomposition temperatures are 175°C, 290°C and 320°C, respectively. The third step of the decomposition is related to the formation of $NbF_5$ or $TaF_5$ as components of the gaseous phase [112]:

$$2\,NH_4MeOF_4 = 2\,NH_3 + 2\,HF + TaF_5 + MeO_2F \quad (32)$$

## 2.5.1. Synthesis of fluorotantalates

The mechanism of the synthesis of alkali metal fluorotantalates using hydrofluoride can be illustrated by the $LiF - Ta_2O_5 - NH_4HF_2$ system [113, 114]. Differential thermal analysis (DTA) of $Ta_2O_5 - NH_4HF_2$ (molar ratio 1:7) (Fig. 14, curve 1) indicates several endothermic effects. The first effect refers to the melting of $NH_4HF_2$ and to the beginning of the reaction. This effect is also characterized by an intensive release of water vapor from the interacting mixture. Other strong effects, seen at higher temperatures in the range of 220-350°C, are related to the decomposition of ammonium fluorotantalates with different stoichiometries. These effects are accompanied by the release of

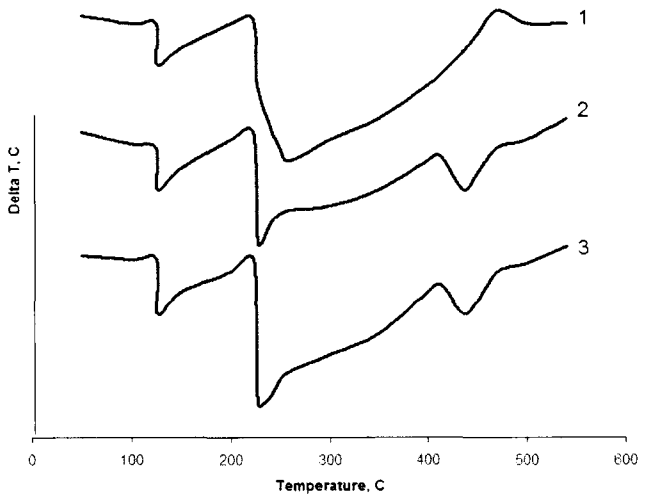


*Fig. 14. DTA patterns of mixtures:*
*$Ta_2O_5 - NH_4HF_2$ (1); $LiTaO_3 - NH_4HF_2$ (2) and $LiF - Ta_2O_5 - NH_4HF_2$ (3).*
*Reproduced from [113], V. T. Kalinnikov, Y. I. Balabanov, L. A. Agulyansky, A. I. Agulyansky, Y. A. Serebryakov, Zh. Obschei. Khim. 54 (1984) 1929, Copyright 1984, with permission of "Nauka" (Russian Academy of Sciences) publishing.*

ammonia, $NH_3$, and hydrogen fluoride, HF. The described interaction scheme was confirmed by mass spectral analysis of the system. The mass spectral patterns are shown in Fig. 15. Lithium containing mixtures display similar thermal behavior except for an additional effect at 435°C (Fig. 14, curves 2 and 3).

This additional effect corresponds to the exchange reaction between ammonium fluorotantalate and lithium fluoride that yields lithium heptafluorotantalate:

$$NH_4TaF_6 + LiF = LiTaF_6 + NH_3 + HF \quad (33)$$

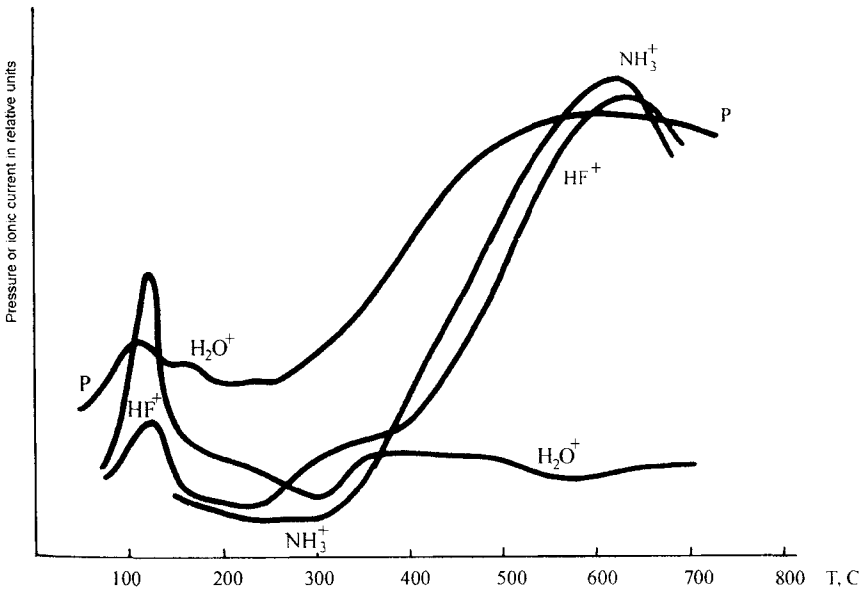


*Fig. 15. Mass spectral pattern: Polytherms of total pressure (P) and ionic currents of gaseous components in the form of ions separating from a $Ta_2O_5$ – $NH_4HF_2$ system versus heating temperature (after Agulyansky et al. [114]).*

Fig. 16 shows infrared (IR) spectra of the products obtained in the LiF – $Ta_2O_5$ – $NH_4HF_2$ system at different temperatures [113]. Analysis of the spectra indicates that the main product obtained at 230°C (Fig. 16, curve 1) is ammonium heptafluorotantalate, $(NH_4)_2TaF_7$ [115]. Slight absorption close to 1200 $cm^{-1}$ corresponds to remaining traces of $NH_4HF_2$ [116]. Increasing the temperature leads to a more complete reaction (Fig. 16, curve 2). At 350°C, a band is observed at about 600 $cm^{-1}$ (Fig. 16, curve 3) indicating that $(NH_4)_2TaF_7$ has decomposed down to ammonium hexafluorotantalate, $NH_4TaF_6$. Further increase in temperature leads to the disappearing of the ammonium vibration bands (Fig.16, curve 4). The correspondence of this curve to lithium fluorotantalate, $LiTaF_6$, was also confirmed by X-ray diffraction analysis [113].


*Fig. 16. IR absorption spectra of the products obtained from a $LiF - Ta_2O_5 - NH_4HF_2$ mixture (molar ratio 2:1:10) at 230°C (1), 290°C (2), 350°C (3) and 435°C (4). Reproduced from [113], V. T. Kalinnikov, Y. I. Balabanov, L. A. Agulyansky, A. I. Agulyansky, Y. A. Serebryakov, Zh. Obschei. Khim. 54 (1984) 1929, Copyright 1984, with permission of "Nauka" (Russian Academy of Sciences) publishing.*

Complex fluorotantalates of all other alkali metals can be prepared successfully using the same method, and appropriate adjustment of the initial mixture composition enables to obtain hexa-, hepta- and octafluorotantalates [117, 118].

Thus, the formation of alkali metal fluorotantalates as summarized above can be represented as follows:

$$Ta_2O_5 + 10NH_4HF_2 + nMF = 2M_{n/2}TaF_{4+n} + 5H_2O + 10NH_3 + 10HF \quad (34)$$

Where M = Li, Na, K, Rb, Cs; n = 2, 4 or 6, resulting in the preparation of $MTaF_6$, $M_2TaF_7$ or $M_3TaF_8$. Reaction temperatures are in the 200-450°C range, depending on the alkali metal and drops when going from Li to Cs.

Use of hydrofluoride is also appropriate for the synthesis of alkali earth metal fluorotantalates [119]. Investigation of the $Ta_2O_5 - 3BaF_2 - 10NH_4HF_2$ system shows that the mechanism of the interaction is similar to previously-described systems containing alkali metal fluorides. At 250°C, the main product is $NH_4TaF_6$, which interacts further with $BaF_2$ at about 400°C yielding $BaTaF_7$. Excess $BaF_2$ interacts with $BaTaF_7$ at 500°C yielding $Ba_3(TaF_8)_2$. In systems that contained $SrF_2$ or $CaF_2$, heptafluorotantalates of strontium or calcium, $SrTaF_7$ or $CaTaF_7$ were obtained at 460°C and 530°C, respectively.

All attempts to prepare magnesium fluorotantalate were unsuccessful. As a result of the interaction the mixture of $MgF_2$ and $TaO_2F$ were found out after performing of the process [119]. This inability to obtain magnesium fluorotantalates is related to the poor thermal stability of the compounds due to the similarity between the ionic radii of magnesium and tantalum. Analogous niobium-containing compounds, $MNbF_7$, are known and have been investigated, in which M = Mg, Ca, Mn, Fe, Co, Ni, Zn, Cd [120], but they are not exactly typical island-type complexes. $MNbF_7$ crystallizes in a manner similar to $MNbF_6$, with a seventh fluorine atom positioned between specific sites in the lattice of a $ReO_3$-type crystal. From this standpoint, $MNbF_7$ can be regarded as a non-stoichiometric phase of the $AB_{3+X}$ type. Attempts to obtain complex fluorotantalates of metals such as Cu, Fe and Cr, using the hydrofluoride method were unsuccessful.

Table 14 presents the conditions required for the preparation of several fluorotantalates using the hydrofluoride method. The procedure of hydrofluoride synthesis is very simple. Initial components are mixed and loaded into a platinum or carbon-glass crucible. The material is heated to the final temperature at the rate of about 20-40°C per minute. The mixture should be stirred continuously or intermittently by appropriate means especially during the melting phase and following solidification. Completion of the synthesis can be verified by weighing and by qualitative determination of ammonia residues using an appropriate method, e.g. using Nessler Reagent.

*Table 14. Conditions for fluorotantalate preparation*

| Compound | Initial mixture, mol | Final temperature of process, °C | Product weight at end of process, % initial weight |
|---|---|---|---|
| $LiTaF_6$ | $Ta_2O_5+2LiF+10NH_4HF_2$ | 450 | 56.77 |
| $NaTaF_6$ | $Ta_2O_5+2NaF+10NH_4HF_2$ | 420 | 58.03 |
| $KTaF_6$ | $Ta_2O_5+2KF+10NH_4HF_2$ | 400 | 59.22 |
| $RbTaF_6$ | $Ta_2O_5+2RbF+10NH_4HF_2$ | 350 | 62.33 |
| $CsTaF_6$ | $Ta_2O_5+2CsF+10NH_4HF_2$ | 250 | 65.05 |
| $Na_2TaF_7$ | $Ta_2O_5+4NaF+10NH_4HF_2$ | 500 | 61.02 |
| $K_2TaF_7$ | $Ta_2O_5+4KF+10NH_4HF_2$ | 450 | 63.02 |
| $Rb_2TaF_7$ | $Ta_2O_5+4RbF+10NH_4HF_2$ | 430 | 67.83 |
| $Cs_2TaF_7$ | $Ta_2O_5+4CsF+10NH_4HF_2$ | 420 | 71.60 |
| $CaTaF_7$ | $Ta_2O_5+2CaF_2+10NH_4HF_2$ | 530 | 64.95 |
| $SrTaF_7$ | $Ta_2O_5+2SrF_2+10NH_4HF_2$ | 460 | 63.58 |
| $Ba_3(TaF_8)_2$ | $Ta_2O_5+3BaF_2+10NH_4HF_2$ | 500 | 70.07 |

Oxides, hydroxides, chlorides or carbonates of the second metal can be used for synthesis instead of fluorides, but the necessary amount of ammonium hydrofluoride must be recalculated and added in order to assure complete fluorination of the second compound. Some excess of ammonium hydrofluoride is recommended to avoid insufficient fluorination. Remainders of $NH_4HF_2$ decompose and separate out from the system upon reaching the final temperature.

Since hydrofluoride synthesis is based on thermal treatment at relatively high temperatures, the possibility of obtaining certain fluorotantalates can be predicted according to thermal stability of the compounds. In the case of compounds whose crystal structure is made up of an octahedral complex of ions, the most important parameter is the anion–cation ratio. Therefore, it is very important to take in to account the ionic radius of the second cation in relation to the ionic radius of tantalum. "Large" cations, are not included in the

anion/cation ratio, which is calculated simply as F/Ta, and which must not be lower than 6. In the case of "small" second cations, with ionic radii similar to that of tantalum, the number of cations is included in the calculation of the ratio. Such cations will also be situated in the position that has an octahedral surrounding corresponding to a coordination number of 6. The ratio in this case, F/(M+Ta), must not exceed 3.

Table 15 summarizes anion–cation ratio for different types of fluorotantalates. Thermally stable compounds that can be prepared using the hydrofluoride method are noted in bold.

IR absorption spectra of several fluorotantalates of alkali and alkali earth metals prepared by hydrofluoride synthesis are presented in Fig. 17.

*Table 15. X/Me (F/Ta or F/(Ta+M)) ratios for some fluorotantalates of mono-, bi- and trivalent metals. ($r_M$ and $r_{Ta}$ – ionic radii, stable compounds are noted in bold and are underlined.)*

| Compound | $r_M > r_{Ta}$ | | | $r_M \approx r_{Ta}$ | | |
|---|---|---|---|---|---|---|
| | F | Ta | F/Ta | F | Ta + M | F/(Ta + M) |
| $M^{I}TaF_6$ | 6 | 1 | **6** | 6 | 2 | **3** |
| $M_2^{I}TaF_7$ | 7 | 1 | **7** | 7 | 3 | **2.3** |
| $M_3^{I}TaF_8$ | 8 | 1 | **8** | 8 | 4 | **2** |
| $M^{II}(TaF_6)_2$ | 12 | 2 | **6** | 12 | 3 | 4 |
| $M^{II}TaF_7$ | 7 | 1 | **7** | 7 | 2 | 3.5 |
| $M_3^{II}(TaF_8)_2$ | 16 | 2 | **8** | 16 | 5 | 3.2 |
| $M^{III}(TaF_6)_3$ | 18 | 3 | **6** | 18 | 4 | 4.5 |
| $M_2^{III}(TaF_7)_3$ | 21 | 3 | **7** | 21 | 5 | 4.2 |
| $M^{III}TaF_8$ | 8 | 1 | **8** | 8 | 2 | 4 |

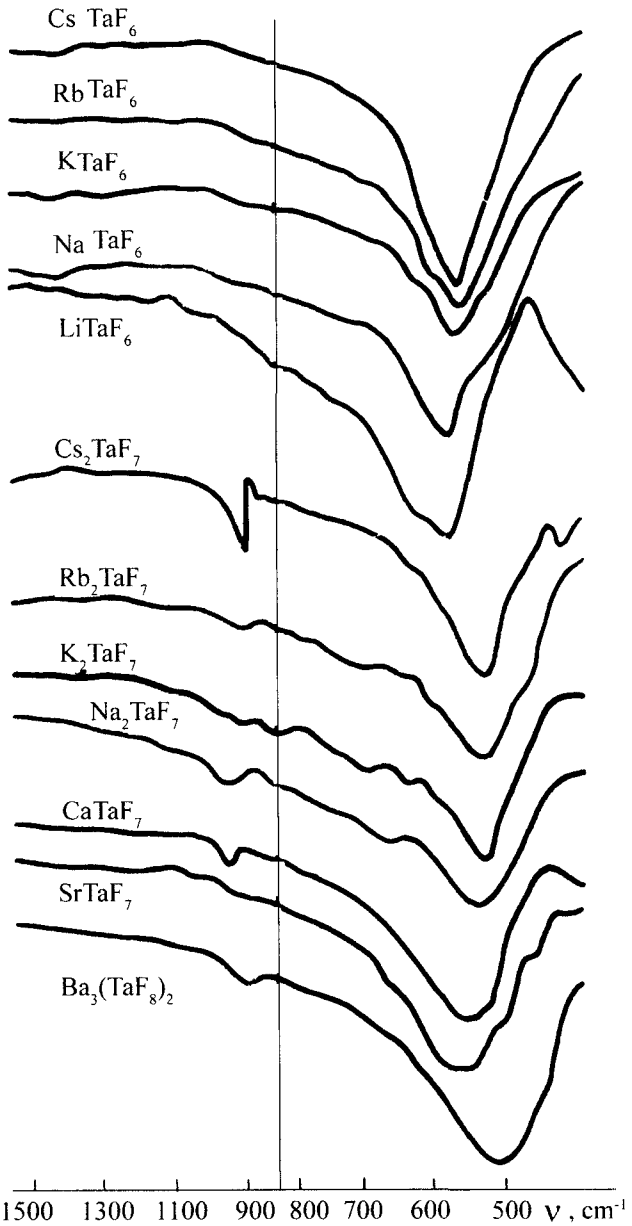


*Fig. 17. IR absorption spectra of alkali and alkali earth fluorotantalates synthesized using the hydrofluoride method.*

## 2.5.2. Synthesis of oxyfluoroniobates

The stoichiometry of the prepared compounds depends not only on the composition of the initial mixture, but also on the initial oxide's fluorination activity. Unlike tantalum oxide, fluorination of niobium oxide by an ammonium hydrofluoride melt results in the formation of oxyfluoroniobates, but not of fluoroniobates. During the first step of $Nb_2O_5$ fluorination, $(NH_4)_3NbOF_6$ is formed according to the following interaction [51, 52, 105, 111, 121, 122]:

$$Nb_2O_5 + 6\,NH_4HF_2 = 2\,(NH_4)_3NbOF_6 + 3\,H_2O \qquad (35)$$

The formation of $(NH_4)_3NbOF_6$ and its decomposition products define the composition of the niobium fluoride compounds that can be prepared by the hydrofluoride method [123-125].

Interaction between niobium oxide and fluorides, chlorides or carbonates of alkali metals in an ammonium hydrofluoride melt, yielded monooxyfluoroniobates with different compositions, $M_XNbOF_{3+X}$, where they were subsequently investigated [123-127]. According to DTA patterns of the $Nb_2O_5 - 6NH_4HF_2 - 2MF$ system, (Fig. 18) a rich variety of endothermic effects result from the formation of ammonium monooxyfluoroniobate, its thermal decomposition and its interaction with alkali metal fluorides. The number of effects decreases and separation of ammonium ceases at lower temperatures and when going from lithium to cesium in the sequence of alkali metal fluorides.

Fig 19 shows IR absorption spectra that verify change in phase composition as a function of the reaction temperature in an $Nb_2O_5 - NH_4HF_2 - LiF$ system. The first spectrum (curve 1) indicates the formation of $(NH_4)_3NbOF_6$ (bands, $cm^{-1}$: 470 – νNbF, 910 – νNbO, 1420 – $\delta NH_4^+$) and the remainders of untreated $NH_4HF_2$ (~1200 $cm^{-1}$ – $\delta_S HF_2^-$). Increasing the temperature leads to a more complete interaction, to the disappearing of the $NH_4HF_2$ remainders and to the subsequent thermal decomposition of $(NH_4)_3NbOF_6$ in particular to $(NH_4)_2NbOF_5$, which is confirmed by bands ($cm^{-1}$) at 550 – νNbF and 920 – νNbO that belong to the complex $NbOF_5^{2-}$ (see curve 3). According to the spectrum (curve 4), no ammonium-containing compounds were found at 400°C. The bands at ~620 and ~800 $cm^{-1}$ can be assigned to vibrations of NbF and NbO bonds of octahedral fragments connected through oxygen bridge atoms in the $(NbOF_4^-)_n$ chains. This type of spectrum is related to $LiNbOF_4$, whose composition was also confirmed by X-ray, crystal-optical and chemical analyses. Further increasing in temperature leads to an interaction between

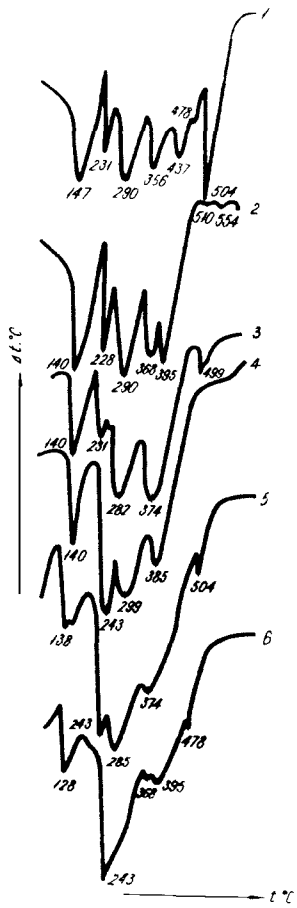


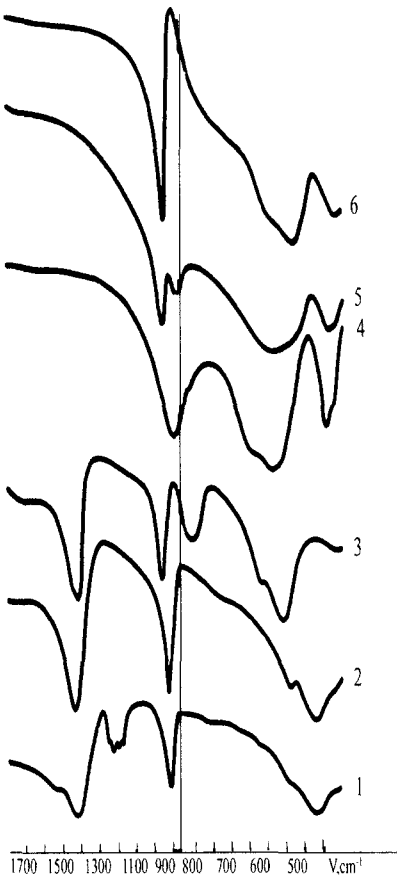


*Fig. 18* *Fig. 19*

*Fig. 18. DTA patterns of $Nb_2O_5$–$6NH_4HF_2$ (1) and $Nb_2O_5$–$6NH_4HF_2$–2MF, where M = Li (2), Na (3), K (4), Rb (5), Cs (6). Reproduced from [126], A. I. Agulyansky, E. L. Tikhomirova, V. Y. Kuznetsov, V. T. Kalinnikov, Zh. Neorg. Khim. 33 (1988) 85, Copyright 1988, with permission of "Nauka" (Russian Academy of Sciences) publishing.*

*Fig. 19. IR absorption spectra of $Nb_2O_5$-$NH_4HF_2$-LiF mixture (molar ratio 1:6:4) treated at 160°C (1), 200°C (2), 350°C (3), 400°C (4), 460°C (5) and 500°C (6). Reproduced from [126], A. I. Agulyansky, E. L. Tikhomirova, V. Y. Kuznetsov, V. T. Kalinnikov, Zh. Neorg. Khim. 33 (1988) 85, Copyright 1988, with permission of "Nauka" (Russian Academy of Sciences) publishing.*

$LiNbOF_4$ and remainders of LiF, yielding $Li_2NbOF_5$ (curve 6) [126].
Thus, the sequence of phases that are formed in hydrofluoride synthesis of lithium-niobium fluoride compounds is: $(NH_4)_3NbOF_6$ – $(NH_4)_2NbOF_5$ – $LiNbOF_4$ – $Li_2NbOF_5$.

The same method was successfully used for the synthesis of other alkali metal oxyfluoroniobates, $MNbOF_4$ and $M_2NbOF_5$, where M = Li, Na, K, Rb and Cs. In general, the reaction steps in a $Nb_2O_5$ – $NH_4HF_2$ – MF system can be represented as follows:

$$Nb_2O_5 + 6\,NH_4HF_2 = 2\,(NH_4)_3NbOF_6 + 3\,H_2O \quad (36)$$

$$(NH_4)_3NbOF_6 = (NH_4)_2NbOF_5 + NH_3 + HF \quad (37)$$

$$(NH_4)_2NbOF_5 = NH_4NbOF_4 + NH_3 + HF \quad (38)$$

$$(NH_4)_2NbOF_5 + MF = MNbOF_4 + 2\,NH_3 + 2\,HF \quad (39)$$

$$NH_4NbOF_4 + MF = MNbOF_4 + NH_3 + HF \quad (40)$$

Interactions (39) and (40) are consecutive and occur in parallel. When an excess of MF is present, $M_2NbOF_5$ and $M_3NbOF_6$ can be obtained, except for $Li_3NbOF_6$, which has never been prepared by any method [105, 126]. The interaction can be presented in the following schematic manner:

$$Nb_2O_5 + 6NH_4HF_2 + nMF = 2M_{n/2}NbOF_{3+n/2} + 3H_2O + 6NH_3 + 6HF \quad (41)$$

$M_3NbOF_6$ type compounds can be prepared also by direct interaction with alkali metal hydrofluorides, $MHF_2$ [127]:

$$Nb_2O_5 + 6\,MHF_2 = 2\,M_3NbOF_6 + 3\,H_2O \quad (42)$$

This process occurs at temperatures of about 200-300°C, but in order to complete evaporation of water and homogenization of the product, the temperature of the thermal treatment must be increased, in the final stages of the process, to 400-500°C. Nevertheless, extended thermal treatment or higher temperatures can lead to hydrolysis of the compound according to the following interaction:

$$M_3NbOF_6 + H_2O = M_3NbO_2F_4 + 2\,HF \quad (43)$$

There is no doubt that performing the synthesis of $M_3NbOF_6$ according to Equation (42) in dry air or an inert atmosphere allows to avoid hydrolysis as shown in Equation (43) [128].

Combined fluorination of niobium oxide and oxides of bivalent metals by ammonium hydrofluoride allows to obtain anhydrous compounds of the $M^{II}NbOF_5$ type. The interaction of such components can be illustrated by the $Nb_2O_5 - CoO - NH_4HF_2$ system [129]. Fig. 20 presents the DTA pattern of a $Nb_2O_5 - CoO - NH_4HF_2$ mixture (molar ratio 1:2:10) (curve 1). The first endothermic effect corresponds to the melting of $NH_4HF_2$, and all other effects are related to the oxide's fluorination, and the formation, decomposition and interaction of complex fluorometallates of ammonium. Nevertheless, fluorination of CoO and $Nb_2O_5$ begins at 160°C [109] and at 130°C [123], respectively. The temperature of interaction between niobium and cobalt fluoride compounds can be estimated from the DTA pattern of the $CoF_2 - (NH_4)_2NbOF_5$ system (Fig. 20, curve 2) as ~270°C.

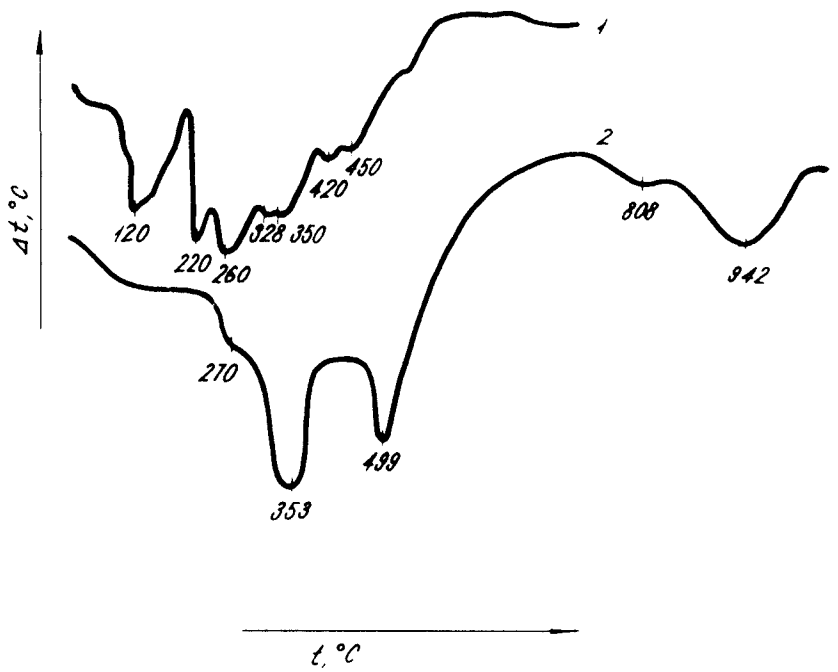


*Fig. 20. DTA patterns of 2 CoO – $Nb_2O_5$ – 10 $NH_4HF_2$ (1) and $CoF_2 – (NH_4)_2NbOF_5$ (2). Reproduced from [129], A. I. Agulyansky, E. L. Tikhomirova, V. T. Kalinnikov, Zh. Neorg. Khim. 32 (1987) 2079, Copyright 1987, with permission of "Nauka" (Russian Academy of Sciences) publishing.*

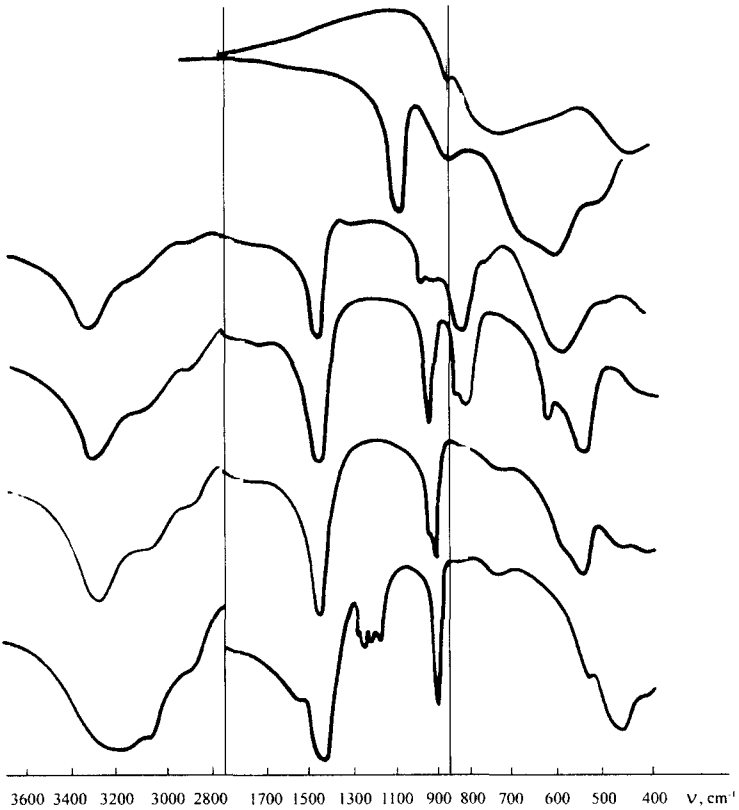


*Fig. 21. IR absorption spectra of mixture 2 CoO – Nb2O5 – 10 NH4HF2, treated at 170°C (1), 225°C (2), 250°C (3), 350°C (4) 400°C (5) and 900°C (6). Reproduced from [129], A. I. Agulyansky, E. L. Tikhomirova, V. T. Kalinnikov, Zh. Neorg. Khim. 32 (1987) 2079, Copyright 1987, with permission of "Nauka" (Russian Academy of Sciences) publishing.*

Phase composition changes as a function of temperature are similar to these that were observed for the lithium-containing system (see Fig. 21), except that individual stable ammonium-cobalt-oxyfluoroniobate occurs prior to the formation of $CoNbOF_5$ (Fig.21, curve 4). It is assumed that the composition of this intermediate phase, formed at 330-350°C, is $(NH_4)_2CoNbOF_7$ [129]. Complete removal of ammonium occurs at about 400°C (Fig. 21, curve 5) and leads to the formation of $CoNbOF_5$. The compound is defined as practically isotropic rose-colored crystals with a refractive index of N = 1.500. The

compound crystallizes in tetragonal syngony with the parameters: a = 7.81 Å, c = 9.02 Å, Z = 4, ρ = 3.19 g/cm$^3$. The structure of $CoNbOF_5$ can be presented as a tetragonally distorted $ReO_3$ lattice, built from linked octahedral complexes with Nb or Co in their centers [129]. The IR spectrum of the compound exhibits two groups of bands. The first, at 500-700 cm$^{-1}$, is ascribed to NbF, CoO and CoF bond vibrations, while the second band, at about 950 cm$^{-1}$, is ascribed to NbO bond vibrations.

According to Davidovich et al. [130], thermal decomposition of $CoNbOF_5$ leads to the release of NbF5 into the gas phase, yielding a mixture of $CoF_2$ and $NbO_2F$. But results described in [129] show that thermal treatment of $CoNbOF_5$, at up to 900°C in air, an inert atmosphere or vacuum, lead to a mass loss of 41.8%. X-ray analysis confirms the presence of neither $CoF_2$ nor $NbO_2F$ in the remainder. The product was identified as violet anisotropic crystals with refractive indexes of Np = 1.765 and Ng = 1.832. Chemical analysis of the crystals corresponds to the compound $Co_2NbO_3F_3$ (calculated mass loss – 41.94%). The compound crystallizes in tetragonal syngony with cell parameters (Å): a = 4.65, b = 3.03. The compound structure is close to a rutile type – $TiO_2$ structure. Such compounds have no narrow bands in their vibration spectra. The IR spectrum of $Co_2NbO_3F_3$ is shown in Fig. 20, curve 6. The decomposition process of $Co_2NbO_3F_3$ is still unclear, but can be shown schematically as follows:

$$3\ CoNbOF_5 = Co_2NbO_3F_3 + CoNb_2F_{12}\ (gas) \qquad (44)$$

It is possible, in general, that $CoNb_2F_{12}$ is present only in the gaseous phase at increased temperatures due to insufficient amounts of ligands that are necessary for the formation of a stable solid compound. Further thermal treatment of $Co_2NbO_3F_3$ at temperatures of ~1000-1100°C leads to the formation of $Co_4Nb_2O_9$ crystals with a pseudoilmenite structure.

Nickel and copper containing compounds have been prepared in a similar manner. The phases obtained by the simultaneous fluorination of niobium oxide and other bivalent metal oxides were $M^{II}NbOF_5$, $M_2^{II}NbO_3F_3$ and $M_4^{II}Nb_2O_9$, where $M^{II}$ = Co Ni, Cu [129, 131].

Simultaneous fluorination of niobium oxide and oxides of trivalent metals using an ammonium hydrofluoride melt leads only to oxide-type compounds, $M^{III}NbO_4$ due to low thermal stability of fluoride or oxyfluoride compounds that contain both niobium and trivalent metals.

IR absorption spectra of some oxyfluoroniobates prepared by the hydrofluoride method are displayed in Fig. 22.

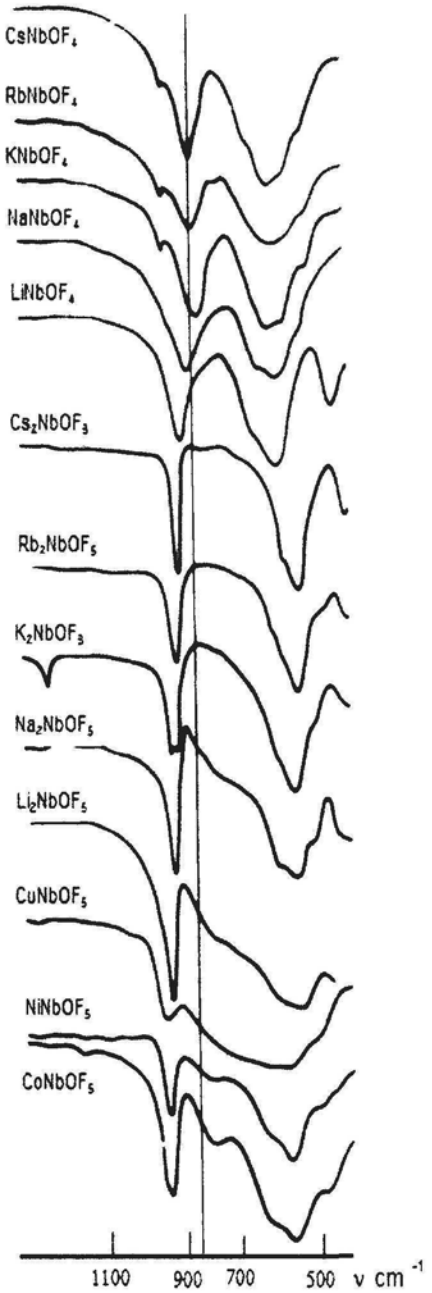


*Fig. 22. IR absorption spectra of some fluoroniobates prepared by the hydrofluoride method.*

### 2.5.3. Hydrofluoride synthesis: performance and capability

Table 16 presents the list of compounds that were successfully prepared using the hydrofluoride method together with the general conditions of synthesis. The preparation procedure is very simple. The initial compounds are mixed carefully and loaded into the container. Use of Teflon, carbon-glass or platinum containers is recommended, according to the process temperature. Teflon can be used at up to200–300°C depending on the type of the material. Carbon-glass can be used at up to 350-400°C in air. Nevertheless, it is strongly recommended to avoid using platinum containers at the initial stages of the processes in order to avoid catalytic oxidation of the ammonium ion in the presence of platinum [132]. Effective exhaust ventilation must be provided to collect gaseous components released during the reaction. Release of gaseous components occurs mainly between 200°C and -300°C, as was shown by mass-spectral investigation [133]. Gaseous $NH_3$ and HF can be condensed as $NH_4F$ on a surface with a temperature of 90-110°C. Due to its decomposition upon heating to ammonium hydrofluoride, ammonium fluoride, $NH_4F$, can be used in hydrofluoride synthesis, just as successfully as ammonium hydrofluoride, $NH_4HF_2$:

$$2\,NH_4F = NH_4HF_2 + NH_3 \qquad (45)$$

If applied, it is necessary to double the amount of ammonium fluoride compared to ammonium hydrofluoride, and to take into account the increased amount of gaseous $NH_3$ released.

If the quality of the product is not so critical or if further purification steps are planned, hydrofluoride synthesis can be performed using a regular black steel container.

The hydrofluoride method can be used successfully both for the preparation of complex fluoride compounds and of complex oxides. The main advantage is that the synthesis is performed at relatively lower temperatures. In addition, the complex oxide material is formed through its respective fluoride compound and the product obtained is therefore more consistent. For instance, $Co_4Nb_2O_9$ can be prepared using the hydrofluoride method at 900-1100°C, whereas the regular synthesis, based on the interaction of simple oxides, requires extended treatment at about 1400°C.

*Table 16. Conditions for the synthesis of niobium and tantalum fluoride compounds using the hydrofluoride method.*

| Compound | Initial composition and temperature, °C | Gaseous components |
|---|---|---|
| $M^{I}TaF_6$ | $Ta_2O_5 + 10NH_4HF_2 + 2M^{I}F$ | $H_2O$, $NH_3$, HF |
| ($M^{I}$=Li, Na, K, Rb, Cs) | 200 - 450 | |
| $M^{I}_2TaF_7$ | $Ta_2O_5 + 10NH_4HF_2 + 4M^{I}F$ | $H_2O$, $NH_3$, HF |
| ($M^{I}$=Na, K, Rb, Cs | 500 – 700 | |
| $M^{I}TaF_8$ | $Ta_2O_5 + 10NH_4HF_2 + 6M^{I}F$ | $H_2O$, $NH_3$, HF |
| ($M^{I}$=Na, K, Rb, Cs) | 600 – 800 | |
| $M^{II}TaF_7$ | $Ta_2O_5 + 10NH_4HF_2 + 2M^{II}F2$ | $H_2O$, $NH_3$, HF |
| ($M^{II}$=Ca, Sr, Ba) | 400 | |
| $M^{II}_3TaF_8$ | $Ta_2O_5 + 10NH_4HF_2 + 3M^{II}F2$ | $H_2O$, $NH_3$, HF |
| ($M^{II}$=Ba) | 500 | |
| $M^{I}NbOF_4$ | $Nb_2O_5 + 6NH_4HF_2 + 2M^{I}F$ | $H_2O$, $NH_3$, HF |
| ($M^{I}$=Li, Na, K, Rb, Cs) | 400 - 500 | |
| $M^{I}_2NbOF_5$ | $Nb_2O_5 + 6NH_4HF_2 + 4M^{I}F$ | $H_2O$, $NH_3$, HF |
| ($M^{I}$=Li, Na, K, Rb, Cs) | 400 - 500 | |
| $M^{I}_3NbOF_6$ | $Nb_2O_5 + 6NH_4HF_2 + 6M^{I}F$ | $H_2O$, $NH_3$, HF |
| ($M^{I}$=Na, K, Rb, Cs) | 400 - 500 | |
| | $Nb_2O_5 + 6M^{I}HF_2$ | $H_2O$ |
| | 300 - 400 | |
| $M^{I}_3NbO_2F_4$ | $Nb_2O_5 + 6M^{I}HF_2$ | $H_2O$, HF |
| ($M^{I}$=K, Rb, Cs) | 600 - 700 | |
| $M^{II}NbOF_5$ | $Nb_2O_5 + 10NH_4HF_2 + 2M^{II}O$ | $H_2O$, $NH_3$, HF |
| ($M^{II}$=Co, Ni, Cu) | 400 | |
| $M^{II}NbO_3F_3$ | $Nb_2O_5 + 10NH_4HF_2 + 2M^{II}O$ | $H_2O$, $NH_3$, HF, $NbOF_3$ |
| ($M^{II}$=Co, Ni, Cu) | 600 - 900 | |
| $M^{II}_4Nb_2O_9$ | $Nb_2O_5 + 10NH_4HF_2 + 2M^{II}O$ | $H_2O$, $NH_3$, HF, $NbOF_3$ |
| ($M^{II}$=Co, Ni, Cu) | 900 - 1100 | |
| $M^{III}NbO_4$ | $Nb_2O_5 + 10NH_4HF_2 + M^{III}_2O_3$ | $H_2O$, $NH_3$, HF |
| ($M^{III}$=Al, Fe, Cr, Ln) | 600 - 800 | |

This Page Intentionally Left Blank

# 3.

# CRYSTAL CHEMISTRY OF TANTALUM AND NIOBIUM FLUORIDE COMPOUNDS

One of the most important parameters that defines the structure and stability of inorganic crystals is their stoichiometry – the quantitative relationship between the anions and the cations [134]. Oxygen and fluorine ions, $O^{2-}$ and $F^{-}$, have very similar ionic radii of 1.36 and 1.33 Å, respectively. The steric similarity enables isomorphic substitution of oxygen and fluorine ions in the anionic sub-lattice as well as the combination of complex fluoride, oxyfluoride and some oxide compounds in the same system. On the other hand, tantalum or niobium, which are the central atoms in the fluoride and oxyfluoride complexes, have identical ionic radii equal to 0.66 Å. Several other cations of transition metals are also sterically similar or even identical to tantalum and niobium, which allows for certain isomorphic substitutions in the cation sub-lattice.

The ratio between the anionic and cationic radii leads to coordination numbers, the lowest of which is 6, which correspond to a octahedral polyhedron of anions around a central cation [135]. In this case, the compound structure type depends on the ratio of total number of anions and cations. The total number of anions (X) is calculated by summing up the number of oxygen (O) ions and of fluorine (F) ions: X=O+F, while the total number of cations (Me) is the number of tantalum ions, niobium ions and other similar cations.

The structure of such compounds is discussed from the viewpoint of the ratio X:Me (number of anions surrounding one cation or central atom) in a descending order from 8 to 1.

## 3.1. Island-type structure compounds

Island-type structures are inherent for compounds with X:Me ≥ 6. Typically X:Me equals to 6, 7 or 8. We have found no documentation of niobium- or tantalum-containing compounds characterizing by X:Me ≥ 9.

Lithium octafluoroniobate, $Li_3NbF_8$, was found by Bizot and Malek-Zadeh while they were investigating melting in the system LiF – $NbF_5$ [77]. The compound is not stable at room temperature, but exists in the temperature range of 548-585°C. X-ray diffraction was obtained for the powdered material after quenching with liquid nitrogen. Structural data on the compound is not available, and no tantalum-containing analog has been described in the literature.

Structural characteristics of compounds with X:Me = 8 are collected in Table 17. $Na_3NbF_8$ and $Na_3TaF_8$ compounds that form similar crystal structure [77]. The structure of $Na_3TaF_8$ was determined by Hoard et al. [136], by means of X–ray diffraction of a single crystal. $Na_3TaF_8$ is composed of sodium cations and isolated complex ions $TaF_8^{3-}$, in an Archimedean antiprism configuration, as shown in Fig. 23.

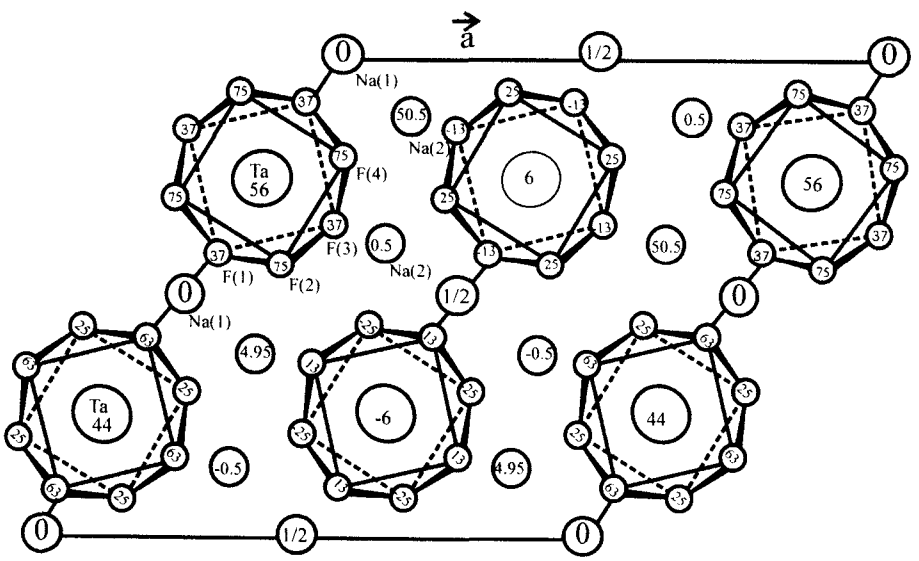


*Fig. 23. Projection on the XZ plane of $Na_3TaF_8$ structure. Numbers denote the Y coordinates of the atom (x100). Reproduced from [136], J. L. Hoard, W. J. Martin, M. E. Smith, J. Amer. Chem. Soc. 76 (1954) 3820, Copyright 1954, with permission of American Chemical Society.*

*Table 17. Structural parameters of octafluorotantalates and octafluoroniobates – X:Me=8*

| Compound | Syngony | Cell parameters, Å | | | | | Z | Space Group | Density | Reference |
|---|---|---|---|---|---|---|---|---|---|---|
| | | a | b | c | α | β | | | ρ, g/cm$^3$ | |
| $Na_3NbF_8$ | Monoclinic | 11.52 | 5.38 | 11.21 | | 120.9° | 4 | | 3.48 | [77] |
| $Na_3TaF_8$ | Monoclinic | 11.52 | 5.38 | 11.21 | | 120°55′ | 4 | $C_{2h}^6$ | 4.33 | [136] |
| $K_3NbF_8$ | Trigonal | 32.8 | | | 44° | | 81 | $C_{3i}^2$ | 3.15 | [139] |
| $K_3TaF_8$ | Trigonal | 32.8 | | | 44° | | 81 | $C_{3i}^2$ | 3.91 | [139] |
| $Rb_5NbF_8$ | Monoclinic | 10.65 | 9.40 | 8.58 | | 91°2′ | 3 | | 3.04 | [78] |
| $Cs_3NbF_8$ | Monoclinic | 11.20 | 9.85 | 8.93 | | 91°5′ | 3 | | 3.57 | [78] |
| $Ti_3NbF_8$ | Hexagonal | 8.59 | | 6.69 | | | | | 7.06 | [78] |

The $TaF_8^{3-}$ polyhedrons have a $D_{4d}$ symmetry. The length of Ta-F bonds in the $TaF_8^{3-}$ complex varies in the range of 1.93–2.01 Å, but the F-F distance is about 2.41 Å. Sodium atoms are located in two different positions. Na (1) atoms have an octahedral surrounding, and Na (1)-F distances vary in the range of 2.26–2.45 Å. The second type of sodium atoms, Na (2), occurs in the common positions and has a coordination number of 8 (Na (2)-F distances are in the range 2.26 – 2.45 Å).

According to different authors [28, 77, 78, 115], all compounds mentioned in Table 17 have isolated complexes $TaF_8^{3-}$ or $NbF_8^{3-}$ in their crystal structure. This is confirmed by similar IR absorption spectra indicating a strong band at ~500 $cm^{-1}$ for all such compounds [115, 119, 137, 138].

Values of absorption frequencies for $M_3NbF_8$ (M = Na, K, Tl) mentioned in [77] are not in agreement with data published in [115, 137, 138] and seem to be systematically higher. Other chloride-fluoride and oxyfluoride compounds with X:Me = 8, such as $K_3TaF_7Cl$, $K_3NbF_7Cl$ [37, 139] and $(N_2H_6)_2NbOF_7$ [140], can also be assigned to the same group since they, two, contain isolated heteroligand complexes $MeX_8^{n-}$.

Table 18 presents the main structural characteristics of heptafluorometalates. Many publications are devoted to investigations of the compounds $K_2TaF_7$ and $K_2NbF_7$ having similar type structure. These compounds are made up of potassium ions and isolated complexes $TaF_7^{2-}$ and $NbF_7^{2-}$, respectively [141-144]. According to data presented by Hoard [141], the polyhedral $MeF_7^{2-}$ is defined as a trigonal prism with six fluorine ions at its vertices. The seventh fluorine ion is situated above the center of the rectangular face of the prism, leading to a $C_{2V}$ symmetry. Precise X–ray investigations [143, 144] and investigations of vibration and $^{19}F$ NMR spectra at different temperatures [143] showed that the polyhedron $MeF_7^{2-}$, in the form of a face-centered prism with a $C_{2V}$ symmetry, can exist in stable form only at relatively low temperatures, and in particular, at temperatures lower than 150K. Increasing the temperature leads to the deformation of the polyhedron and to a lowering of the symmetry down to $C_1$ due to reorientation processes. Fig. 24 shows the structure of coordination polyhedrons of tantalum and potassium in $K_2TaF_7$.

Ta-F distances in the $TaF_7^{2-}$ polyhedron are unequal and vary in the range of 1.976–1.919 Å. Two types of fluorine polyhedrons form around the potassium atoms. The first polyhedron is characterized by K-F distances in the range of 2.905–2.646 Å, while K-F distances in the second polyhedron are in the range of 2.956–2.651 Å [144].

Both $K_2TaF_7$ and $K_2NbF_7$ exhibit a reversible phase transition at about 200°C, which is characterized by a significant change in density [148].

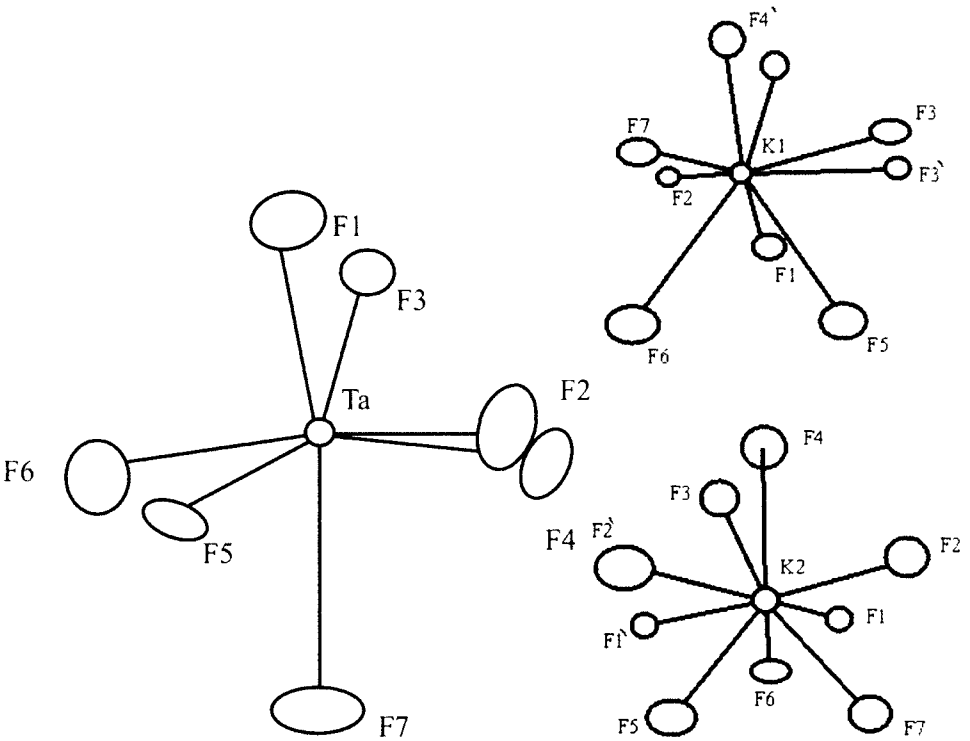


*Fig. 24. The structure of coordination polyhedrons of Ta and K in $K_2TaF_7$. Reproduced from [144], C. C. Torardi, L. H. Brixner, J. Solid State Chem. 67 (1987) 21, Copyright 1987, with permission of Elsevier.*

English et al. analyzed normal vibrations of the $TaF_7^{2-}$ ion for the distorted prism having a $C_{2V}$ symmetry and for the pentagonal bi-pyramid with a $D_{5h}$ configuration [143]. The Raman spectrum of the compound is characterized by a strong intensive Ta-F mode at 639 $cm^{-1}$, a weak doublet at 377/390 $cm^{-1}$, a weak singlet at 272 $cm^{-1}$ and some additional very weak peaks. The IR spectrum displays a very strong band at about 530 $cm^{-1}$ with a shoulder at a higher frequency, two strong bands at 309 and 279 $cm^{-1}$, a doublet at 150/160 $cm^{-1}$ and two more bands at 106 and 63 $cm^{-1}$ of medium intensity that correspond to lattice modes. The spectra do not confirm the $D_{5h}$ configuration according to the "alternative interdiction" rule (bands appearing in IR spectrum do not appear in Raman spectrum).

*Table 18. Structural parameters of heptafluorotantalates and heptafluoroniobates – X:Me=7*

| Compound | Syngony | Cell parameters, Å | | | | Z | Space Group | Density | Reference |
|---|---|---|---|---|---|---|---|---|---|
| | | a | b | c | β | | | ρ, g/cm$^3$ | |
| $Li_2NbF_7$ | Tetragonal | 9.76 | | 6.28 | | | | | [77] |
| $Na_2NbF_7$ | Monoclinic | 5.38 | 11.84 | 8.03 | 90° | 4 | | 3.51 | [77] |
| $Na_2TaF_7$ | Monoclinic | 5.40 | 11.83 | 7.97 | ~90° | 4 | | | [145] |
| $K_2NbF_7$ | Monoclinic | 5.846 | 12.693 | 8.515 | 90° | 4 | $C_{2h}^5$ | 3.19 | [142] |
| $K_2TaF_7$ | Monoclinic | 5.85 | 12.67 | 8.50 | 90° | 4 | $C_{2h}^5$ | 4.11 | [141] |
| | | 5.861(5) | 12.782(5) | 8.522(5) | 90.23(2)° | | | 4.08 | [143] |
| | | 5.8559(6) | 12.708(1) | 8.5125(9) | 90.17(1)° | | | 4.11 | [144] |
| $Rb_2NbF_7$ | Monoclinic | 10.60 | 10.10 | 9.65 | 99.5° | | | 3.10 | [78] |
| $Cs_2NbF_7$ | Monoclinic | 11.50 | 10.97 | 9.08 | 95° | | | 3.57 | [78] |

Complete cataloging of the spectra is not yet available, but some bands can be assigned as follows:
IR: 530 $cm^{-1}$ – asymmetric valence vibration – $\nu_{as}(TaF)$;
Raman: 639 $cm^{-1}$ – symmetric valence vibration – $\nu_s(TaF)$;
Doublet 377/390 $cm^{-1}$ and singlet 72 $cm^{-1}$ refer to deformational vibrations – $\delta(FTaF)$.

The same type of vibration spectra is obtained for other heptafluorotantalates and heptafluoroniobates of alkali metals as well, with the degree of similarity depending to a certain degree on the nature of the second cation. The bands usually shift to the red when going from Li to Cs. This shift is related to a slight increase in the share of Ta-F bond covalence.

Table 19 shows cell parameters of bivalent metal heptafluorotantalates and heptafluoroniobates. Investigation of the crystal structure of such compounds has not yet been performed. Nevertheless, similarities between the IR spectra of both crystal hydrates $M^{II}TaF_7 \cdot nH_2O$ and anhydrous compounds described in [62, 63, 115, 119] and the spectra of alkali metal fluorotantalates lead to the conclusion that bivalent fluorotantalates also contain isolated $TaF_7^{2-}$ ions. Heptafluoroniobates of bivalent metals are characterized by polymorphism and crystallize as $NaNbF_6$ type crystals (super-structure of $ReO_3$) or in rhombohedric syngony – $LiNbF_6$ type structure (super-structure of $VF_3$) [146, 147].

Such structures can exist if one fluorine atom is situated between atoms that are embedded in specific sites in the lattice of the crystal.

The only known compounds that contain trivalent metals are heptaluoroniobates (IV) of lantanides – $LnNbF_7$. Such compounds crystallize in monoclinic syngony, and have an $LnZrF_7$ type structure.

The space group of $LnNbF_7$ compounds is most probably $P2_1$, and the volume of the elementary cell increases linearly with the increase in the $Ln^{3+}$ ionic radius as reported by Bizot et al. [149].

Most of the $M_3MeOF_6$ type compounds belong to the highest symmetry class, except for $Na_3NbOF_6$. The main structural characteristics of the $M_3MeOF_6$ type compounds are collected in Table 20.

Some disagreement exists regarding the structure of $K_3TaOF_6$. According to investigations performed by Fouad et al. [150], the compounds $K_3NbOF_6$ and $K_3TaOF_6$ undergo a phase transition at a temperature of 283±10K and 310±10K, respectively. High temperature modifications result in cubic syngony crystallization, while low temperature phases lead to a tetragonal symmetry.

*Table 19. Cell parameters of heptafluorotantalates and heptafluoroniobates containing bivalent cations.*

| Compound | Syngony | Cell parameters, Å | | | Z | Density ρ, g/cm$^3$ | | Reference |
|---|---|---|---|---|---|---|---|---|
| | | a | c | α | | Calculated | Experimental | |
| $MnTaF_7 \cdot 6H_2O$ | Hexagonal | 9.86 | 10.24 | | 3 | 2.75 | 2.30 | [63] |
| $CoTaF_7 \cdot 6H_2O$ | Hexagonal | 9.59 | 10.02 | | 3 | 3.00 | 2.69 | [63] |
| $NiTaF_7 \cdot 6H_2O$ | Hexagonal | 9.56 | 9.94 | | 3 | 3.04 | 2.85 | [63] |
| $ZnTaF_7 \cdot 6H_2O$ | Hexagonal | 9.61 | 10.16 | | 3 | 2.99 | 2.93 | [63] |
| $CdTaF_7 \cdot 6H_2O$ | Hexagonal | 9.92 | 10.23 | | 3 | 3.05 | 2.73 | [63] |
| $MnNbF_7$ | Cubic | 8.040 | | | 4 | 3.587 | 3.66 | [146, 147] |
| $FeNbF_7$ | Cubic | 7.923 | | | 4 | 3.761 | 3.81 | [146, 147] |
| | Rhomb. | 7.90 | | 88.85° | | | | |
| $CoNbF_7$ | Cubic | 7.868 | | | 4 | 3.910 | 3.95 | [146, 147] |
| | Rhomb. | 7.90 | | 89.33° | | | | |
| $NiNbF_7$ | Cubic | 7.76 | | | 4 | 4.045 | 4.09 | [146, 147] |
| | Rhomb. | 7.775 | | 89.13° | | | | |
| $ZnNbF_7$ | Cubic | 7.840 | | | 4 | 4.012 | 3.90 | [146, 147] |
| | Rhomb. | 7.777 | | 87.98° | | | | |

Stomberg investigated the crystal structure of $Na_3NbOF_6$ [58]. Niobium atoms are surrounded by six fluorine atoms that form a pentagonal bi-pyramid, in which five fluorine atoms occupy an equatorial plane and the fifth fluorine atom and the oxygen atom are located in the apical positions. Fig. 25 shows the structure of the $NbOF_6^{3-}$ polyhedron and corresponding interatomic distances. The niobium atom is shifted from its position in the equatorial plane by 0.19 Å in the direction of the oxygen atom. Na-F and Na-O distances vary in the range of 2.414–2.510 and 2.376–2.587 Å, respectively.

According to Williams and Hoard [151], the structure of $K_3NbOF_6$ also consists of isolated $NbOF_6^{3-}$ complex ions and cations of potassium. The polyhedron $NbOF_6^{3-}$ is defined as an octahedron with the seventh atom located in the center of one of the planes. Interatomic distances are about 2.0 Å. Despite this, Pakhomov, Kaidalova and Davidovich [154] determined that $NbOF_6^{3-}$ in monooxyhexafluorniobate of guanidine has the form of a distorted pentagonal bi-pyramid. Slightly different Nb-F and Nb-O distances were mentioned for the $NbOF_6^{3-}$ complex.

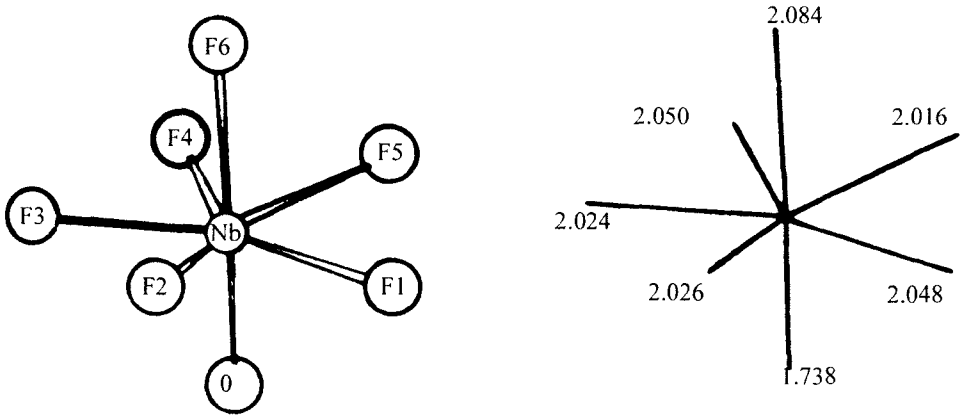


Fig. 25. *Structure of the $NbOF_6^{3-}$ polyhedron in $Na_3NbOF_6$ (after Stomberg [58]).*

*Table 20. Structural parameters of $M_3MeOF_6$ type compounds – X:Me=7.*

| Compound | Syngony | Cell parameters, Å | | | Z | Space group | Density ρ, g/cm$^3$ | | Reference |
|---|---|---|---|---|---|---|---|---|---|
| | | a | b | c | | | Calculated | Experimental | |
| $Na_3NbOF_6$ | Rhombic | 5.648 | 5.766 | 16.943 | 4 | $D_2^3$ | 3.52 | 3.53 | [58] |
| $K_3NbOF_6$ | Cubic | 8.87 | | | 4 | $O_h^5$ | 3.24 | 3.01 | [115, 151, 152] |
| $K_3TaOF_6$ | Cubic | 8.906 | | | 4 | $O_h^5$ | | 3.97 | [152, 153] |
| | Cubic | 8.88 | | | 4 | | 4.06 | | [115] |
| | Tetragonal | 6.280 | 8.955 | | 2 | | 4.03 | 3.99 | [150] |
| $Rb_3TaOF_6$ | Cubic | 9.21 | | | 4 | $O_h^5$ | 4.82 | | [115] |
| $(NH_4)_3NbOF_6$ | Cubic | 9.31 | | | 4 | $O_h^5$ | 2.28 | | [152] |
| $(NH_4)_3TaOF_6$ | Cubic | 9.35 | | | 4 | $O_h^5$ | | 3.00 | [115, 152] |

Alongside this, IR spectra of $M_3NbOF_6$ type compounds display a strong absorption band at 920 $cm^{-1}$ indicating the presence of a double niobium-oxygen bond, Nb=O [57, 115, 155, 156]. Kaidalova [156] explained this contradiction as a phenomenon that is related to the hampered rotation of the $NbOF_6^{3-}$ polyhedron in the equatorial plane.

Vibration spectra of $M_3MeOF_6$ type compounds (Me=Ta, Nb) are collected in Table 21.

The compound $K_4Ta_2F_{12}O$, with an X:Me = 6.5 (tetragonal syngony, cell parameters: a=12.50 Å and c=8.51 Å, decomposition at 310°C) should also be mentioned. IR absorption spectrum of the compound indicates the following bands (in $cm^{-1}$): 975, 910, 675, 660, 555, 500; Raman spectrum ($cm^{-1}$): 635, 600, 465, 270 [59]. The structure of $K_4Ta_2F_{12}O$ has not yet been determined.

*Table 21. Vibration spectra of* $M_3MeOF_6$ *type compounds – X:Me=7 (wave numbers are given in* $cm^{-1}$*, vibrations of* $NH_4^+$ *ion are not shown)*

| $(NH_4)_3NbOF_6$ | | | $K_3NbOF_6$ | $(NH_4)_3TaOF_6$ | $K_3TaOF_6$ | $Rb_3TaOF_6$ | Assignment |
|---|---|---|---|---|---|---|---|
| [157] | | [57] | [115] | [57] | [115] | [115] | |
| IR | Raman | IR | IR | IR | IR | IR | |
| 916 | 908 | 913 | 914 | 880 | 900 | 892 | νMeO |
| 533 | 541 | 535 | 538 | 550 | 552 | 548 | νMeF |
| 464 | | 465 | 480 | 465 | 472 | 474 | νMeF |
| 410 | | 417 | 430 | | 440 | 422 | νMeF |
| | | | 416 | | 417 | | νMeF |
| 325 | | | | | | | δMeOF |
| 318 | | 310 | | | | | δMeOF |
| | | 300 | | | | | δMeOF |
| 258 | | | | | | | δMeF |
| 227 | | | | | | | δMeF |
| | | 206 | | | | | δMeF |

Among the different families of tantalum and niobium complex fluorides and oxyfluorides, the family of compounds with an X:Me ratio equal to 6 is the largest. Table 22 presents the main structural characteristics of hexafluoroniobates and hexafluorotantalates. All known cases of niobium- and tantalum-containing formulary analogs have the same crystal structure type, at least at ambient temperature.

The compounds $LiNbF_6$ and $LiTaF_6$ [158, 159] crystallize similar to $LiSbF_6$ [160]. The structure of these compounds can be described as a rhombohedrically distorted NaCl lattice composed of lithium ions and $MeF_6^-$ complex ions. Each lithium ion is located in an octahedron made up of fluorine ions from six different $MeF_6^-$ complex ions. This structure is somewhat similar to the structure of $VF_3$. A similar structure is observed for hexafluoroniobates (IV) of some bivalent metals, $M^{II}NbF_6$. In the case of $M^{II}$ = Mg, Ca, Mn, Cd, the compounds form $ReO_3$ type crystal structures. In the case of $M^{II}$ = Fe, Co, Ni, Zn, $LiSbF_6$ type $M^{II}NbF_6$ compounds are obtained [161]. The difference in the structure type of the compounds is supposedly related to phase transitions, the temperature of which depends on the nature of the second cation. For instance, the compound $FeNbF_6$ crystallizes in cubic syngony (a = 7.954 Å, Z = 4, Space group – $O_h^5$) at 293K but transforms to a rhombohedral system (a = 5.420 Å, c = 14.072 Å, Z = 3, Space group - $C_{3i}^2$) at 150K [162].

The compounds $NaNbF_6$ and $NaTaF_6$ [158, 163] have similar crystal structure belonging to a $NaSbF_6$ type structure [164]. The compounds form a cubic lattice that is packed with $Na^+$ and $MeF_6^-$ ions, similar to the structure of NaCl.

The structure of $KNbF_6$ consists of potassium ions and isolated $NbF_6^-$ complex ions that were shown by Bode and Döhren to occur in the lattice in a configuration similar to that of α-CsCl [165]. The complex anion $Nb(Ta)F_6^-$ has a configuration of a distorted bi-pyramid (four fluorine atoms are shifted in pairs from their positions in the basic plane, towards the vertexes). The structure of $KNb(Ta)F_6$ compounds and of the $Nb(Ta)F_6^-$ polyhedron are shown in Fig. 26. Nb/Ta–F distances are equal to 2.13 and 2.15 Å, respectively, and F–F distances are 2.61, 3.03, 3.22 and 3.55 Å. Each potassium atom is surrounded by 12 fluorine atoms that are at unequal distances from each other: 8 of them are 2.50 Å apart and four others are 2.94 Å apart.

Hexafluoroniobates and hexafluorotantalates of rubidium, cesium and ammonium [78, 158, 163, 165] are similar and crystallize in a $BaSiF_6$ type structure. In general, the structure of the compounds can be described as a rhombically distorted CsCl type lattice.

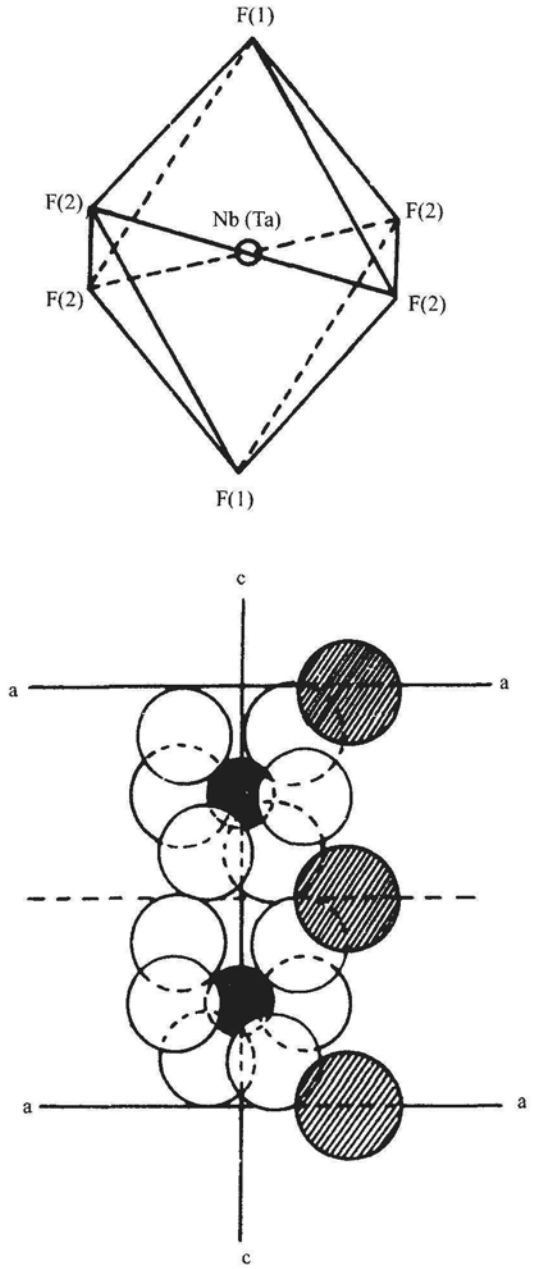


*Fig. 26. Structure of $Nb(Ta)F_6^-$ polyhedron and of $KNb(Ta)F_6$. Reproduced from [165], H. Bode, H. Döhren, Acta Cryst. 11 (1958) 80, Copyright 1958, with permission of Blackwell Publishing.*

*Table 22. Structural characteristics of hexafluoroniobates and hexafluorotantalates – X:Me=6*

| Compound | Syngony | Cell parameters, Å a | c | α | Z | Space Group | Density ρ, g/cm$^3$ | Reference |
|---|---|---|---|---|---|---|---|---|
| $LiNbF_6$ | Trigonal | 5.473 | | 58.09° | 1 | $C_{3i}^2$ | 3.20 | [158] |
| $LiTaF_6$ | Trigonal | 5.479 | | 58.05° | 1 | $C_{3i}^2$ | 4.52 | [158] |
| | | 5.480 | | 58°03′ | | | 4.51 | [159] |
| $NaNbF_6$ | Cubic | 8.26 | | | 4 | $O_h^5$ | 2.71 | [158, 163] |
| $NaTaF_6$ | Cubic | 8.28 | | | 4 | $O_h^5$ | 3.72 | [158, 163] |
| | | 8.273 | | | | | 3.73 | [159] |
| $KNbF_6$ | Tetragonal | 5.18 | 10.05 | | 2 | $D_{2d}^6$ | 3.02 | [165] |
| | Cubic | 10.29 | | | 8 | $O_h^5$ | 3.00 | [165] |
| $KTaF_6$ | Tetragonal | 5.20 | 10.05 | | 2 | $D_{2d}^6$ | 4.17 | [165] |
| | | 5.186 | 10.04 | | | | 4.12 | [159] |
| | Cubic | 10.29 | | | 8 | $O_h^5$ | 4.07 | [165] |
| $RbNbF_6$ | Trigonal | 5.14 | | 96.4° | 1 | $D_{3d}^5$ | 3.65 | [163] |
| $RbTaF_6$ | Trigonal | 5.14 | | 96.4° | 1 | $D_{3d}^5$ | 4.75 | [163] |
| | | 5.155 | | 96°04′ | | | 4.68 | [159] |
| $CsNbF_6$ | Trigonal | 5.32 | | 95.8° | 1 | $D_{3d}^5$ | 3.81 | [163] |
| $CsTaF_6$ | Trigonal | 5.32 | | 95.8° | 1 | $D_{3d}^5$ | 4.80 | [163] |
| | | 5.327 | | 96°17′ | | | 4.77 | [159] |

Muller [166] described the structure of $Ag(TaF_6)_2$ prepared in an autoclave under fluorine pressure of 3 Kbar.

The compound $Ag(TaF_6)_2$ crystallizes in triclinic syngony with cell parameters (Å, grad.) as follows: a = 9.061, b = 5.607, c = 5.207, α = 118.7, β = 91.61, γ = 102.3. $Ag(TaF_6)_2$ is composed of two separate layers made up of octahedral ions $AgF_6^{4-}$ and distorted octahedral complexes $NbF_6^-$ that are linked through the planes.

According to the approach described in [115, 167], vibration spectra of $NbF_6^-$ and $TaF_6^-$ can be interpreted according to the octahedral approximation. Claasen [168] and Linnet and Simpson [169] analyzed normal vibrations and general force fields of $XF_6$ type hexafluoride molecules. Such molecules have fifteen normal vibrations: $\Gamma = A_{1g}(R, p) + E_g(R, dp) + 2F_{1u}(I) + F_{2u}$, where R indicates activity in Raman spectrum, I – activity in IR spectrum, and p and dp denote polarized or depolarized vibrations. Increasing the ionic radius of the second cation leads to an insignificant shift to the red in the IR absorption frequencies [159], which enables the comparison of spectra obtained for different compounds containing different second cations. Table 23 presents wave numbers for $NbF_6^-$ and $TaF_6^-$ complexes.

To end the discussion of octa-, hepta- and hexafluorotantalates (-niobates) of alkali metals, it should be mentioned that indication of the uniformity of bond energy was found using X-ray electronic spectroscopy [172] based on the

*Table 23. Vibration spectra ($cm^{-1}$) of hexafluoroniobates and hexafluorortantalates in the compounds $MNbF_6$ and $MTaF_6$ containing different alkali metals (M).*

| Vibration | $MNbF_6$ | | | | $MTaF_6$ | | | |
|---|---|---|---|---|---|---|---|---|
| | [167] | | [170] | [171] | [169] | | [170] | [115] |
| | IR | Raman | IR | Raman | IR | Raman | IR | IR |
| $\nu_1$ ($A_{1g}$) | | 683 | | 683 | | 693 | | |
| $\nu_2$ ($E_g$) | | 568 | | 562 | | | | 610 |
| $\nu_3$ ($F_{1u}$) | 580 | | 580 | | 578 | | 580 | 587 |
| $\nu_4$ ($F_{1u}$) | | | | | 490 | 470 | | 410 |
| $\nu_5$ ($F_{2g}$) | | 280 | | 280 | | 271 | | |

example of sodium-containing compounds $NaTaF_6$, $Na_2TaF_7$ and $Na_3TaF_8$. This means that the increase in the complex anion's formal negative charge does not lead to a significant change in the charge of the ions that form this complex ion.

Table 24 presents structural parameters of oxypentafluoroniobates (-tantalates). These compounds can also be referred to as the X:Me=6 group (where X corresponds to sum of fluorine and oxygen atoms and Me is Ta or Nb). $Li_2NbOF_5$, which was investigated by Galy, Andersson and Portier [81], is structurally similar with $Li_2ZrF_6$ and contains in its structure nearly-regular shaped octahedral oxyfluoride ions containing lithium or niobium. The distances Nb-(O, F) and Li-(O, F) correspond to 1.95 and 2.05 Å, respectively.

According to crystal analysis performed by Stomberg [173], $Na_2NbOF_5$ is made up of sodium ions and isolated $NbOF_5^{2-}$ complex ions and is similar in structure to $FeWO_6$. $NbOF_5^{2-}$ polyhedrons comprise slightly distorted octahedrons that are located in one of two equivalent positions. The niobium atom is shifted 0.234 Å from the equatorial plane towards the oxygen atom.

The crystal structure of $K_2NbOF_5$ was investigated by Pinsker using the electron graphical method [174]. The compound is made up of isolated bi-pyramidal $NbOF_5^{2-}$ complexes and potassium ions (see Fig. 27). Polyhedrons of $NbOF_5^{2-}$ alternate, in statistical disorder, with potassium ions along the rotation tetrad axis, occupying one of two equivalent positions.

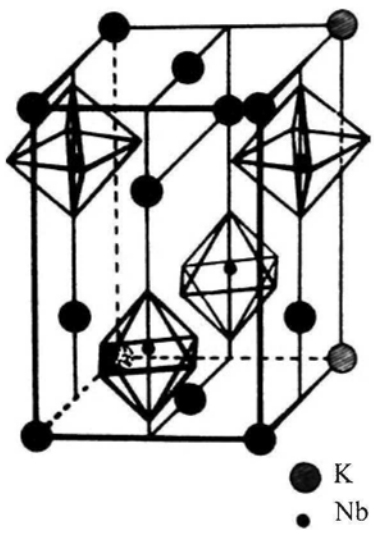


*Fig. 27. Structure of $K_2NbOF_5$. Reproduced from [174], G. Z. Pinsker Kristallografiya, 11 (1966) 741, Copyright 1966, with permission of "Nauka" (Russian Academy of Sciences) publishing.*

*Table 24. Structural parameters of oxypentafluoroniobate (-tantalates) – X:Me=6.*

| Compound | Syngony | Cell parameters, Å | | | Z | Space group | Density ρ, g/cm$^3$ | | Reference |
|---|---|---|---|---|---|---|---|---|---|
| | | a | b | c | | | Calculated | Experimental | |
| $Li_2NbOF_5$ | Hexagonal | 4.965 | | 4.572 | 1 | $D^1_{3d}$ | 3.71 | 3.8 | [81] |
| $Na_2NbOF_5$ | Orthorhombic | 5.089 | 5.512 | 18.207 | 4 | $D^{14}_{2h}$ | 3.250 | | [173] |
| $K_2NbOF_5$ | Tetragonal | 6.12 | | 8.98 | 2 | $D^7_{4h}$ | 2.78 | 2.66 | [174] |
| $Rb_2NbOF_5$ | Trigonal | 6.06 | | 4.85 | 1 | $D^3_{3d}$ | 4.04 | 4.03 | [115, 175] |
| $Cs_2NbOF_5$ | Trigonal | 6.32 | | 5.03 | 1 | $D^3_{3d}$ | 4.49 | 4.31 | [115, 175] |
| $Cs_2TaOF_5$ | Trigonal | 6.33 | | 5.03 | 1 | $D^3_{3d}$ | 5.33 | 5.20 | [176] |
| $(NH_4)_2NbOF_5$ | Orthorhombic | 14.34 | 7.20 | 5.96 | 4 | | 4.59 | 4.52 | [115, 175] |
| $N_2H_6NbOF_5 \cdot H_2O$ | Orthorhombic | 9.47 | 7.69 | 9.06 | 4 | $D^{16}_{2h}$ | 2.63 | | [115, 177] |
| $K_2NbOF_5 \cdot H_2O$ | Monoclinic (β=95°03′) | 6.241 | 6.197 | 17.935 | 4 | $C^5_{2h}$ | 2.80 | | [178] |
| $MnNbOF_5 \cdot 4H_2O$ | Orthorhombic | 7.62 | 9.28 | 10.69 | 4 | | 2.76 | 2.91 | [63] |
| $CdNbOF_5 \cdot 4H_2O$ | Orthorhombic | 7.33 | 9.16 | 10.79 | 4 | | 3.55 | 3.40 | [63] |
| $CoNbOF_5 \cdot 6H_2O$ | Hexagonal | 9.66 | | 10.12 | 3 | | 2.25 | 2.30 | [63] |
| $NiNbOF_5 \cdot 6H_2O$ | Hexagonal | 9.63 | | 10.09 | 3 | | 2.27 | 2.19 | [63] |
| $ZnNbOF_5 \cdot 6H_2O$ | Hexagonal | 9.64 | | 10.09 | 3 | | 2.31 | 2.30 | [63] |

Interatomic distances in $K_2NbOF_5$ are as follows (in Å): Nb-O – 1.68; Nb-F – 1.84 and 2.06 (Trans); K-O – 2.64; K-F – 2.61, 2.68 and 3.10; F-F – 2.59 and 2.65; F-O – 2.61. The relatively short Nb-O distance indicates that the bond is a multiple bond. The niobium atom is shifted from the basic plane of the bi-pyramid by 0.15 Å.

No investigations of the structures of crystal hydrates were found in the literature. Nevertheless, since the compounds $K_2NbOF_5 \cdot H_2O$ and $K_2MoO_2F_4$ have similar type structure [178], it can be assumed that the former also contains isolated $NbOF_5^{2-}$ complexes, the configuration of which is very close to being octahedral. Comparative analysis of the structures of $K_2MoO_2F_4 \cdot H_2O$ [179] and $K_2NbOF_5$ [174] shows that, notwithstanding some differences in cell parameters and atom coordinates, the compounds seem to be quite similar. It was found that the structure of the anhydrous salt contains some relative voids in places that, in the crystal hydrate, are occupied by water molecules. It is assumed that the above structure can explain the hygroscopic property of $K_2NbOF_5$. In this context it should be added that $K_2NbOF_5$ exhibits the highest hygroscopic activity among the compounds of the $M_2NbOF_5$ family, where M = alkali metal or ammonium. In addition, the investigation of water molecule polarization [180] and magnetic resonance of $^1H$ and $^{19}F$ [181] in the compound $K_2NbOF_5 \cdot H_2O$ indicate that water molecules do not enter into the coordination polyhedron of the niobium compound and that their removal has no influence on the compound's $^{19}F$ NMR spectra.

The $NbOF_5^{2-}$ complex ions in $N_2H_6NbOF_5 \cdot H_2O$ [177, 182] and in the binary salt $K_2NbOF_5 \cdot KHF_2$ [183] have a similar structure. According to data by Gorbunova [177], the distance Nb-O is 1.75 Å, which is too short for a single bond and indicates the presence of a double bond. Bond distances for Nb-F correspond to 2.21 and 1.93–1.96 Å for trans and cis positions of fluorine, respectively. The niobium atom is closer to the oxygen atom, which is shifted from the equatorial plane by 0.27 Å.

According to X-ray powder diffraction data, compounds $Rb_2NbOF_5$, $Cs_2NbOF_5$ [174] and $Cs_2TaOF_5$ [176] have similar type structure and are similar to $K_2GeF_6$, whereas $(NH_4)_2NbOF_5$ crystal structure is similar with $Rb_2MoO_2F_4$ [184]. The above-mentioned compounds contain isolated $NbOF_5^{2-}$ complex ions [185].

IR absorption spectra of oxypentafluoroniobates are discussed in several publications [115, 157, 167, 185, 186], but only Surandra et al. [187] performed a complete assignment of the spectra. Force constants were defined in the modified Urey-Bradley field using Wilson's FG matrix method. Based on data by Gorbunova et al. [188], the point group of the $NbOF_5^{2-}$ ion was defined as $C_{4V}$. Fifteen normal modes are identified for this group, as follows:

$4A_1(I, R) + 2B_1(R) + B_2(R) + 4E(I, R)$, where I indicates activity in IR absorption spectra and R indicates activity in Raman spectra. Kharitonov and Buslaev [186] determined the force constant of the Nb=O bond as being ~7.0 mD/Å for $K_2NbOF_5 \cdot H_2O$. This datum seems to be very close to the data mentioned in Table 25, in which assignment of calculated and observed vibration modes is presented for $Rb_2NbOF_5$ and $Cs_2TaOF_5$.

*Table 25. Calculated and observed wave numbers ($cm^{-1}$) for $NbOF_5^{2-}$ in $Rb_2NbOF_5$ and for $TaOF_5^{2-}$ in $Cs_2TaOF_5$ and their assignments. Reproduced from [187], L. Surandra, D. N. Sathyanarayana, G. V. Jeve, J. Fluor. Chem. 23 (1983) 115, Copyright 1983, with permission of Elsevier.*

| Vibration class and frequency designations | | Wave number of ions | | | | | | Assignment (Me=Nb,Ta) |
|---|---|---|---|---|---|---|---|---|
| | | $NbOF_5^{2-}$ | | | $TaOF_5^{2-}$ | | | |
| | | Raman | IR | Calculated | Raman | IR | Calculated | |
| $A_1$ | $\nu_1$ | 918 | 917 | 912 | 898 | 896 | 890 | ν Me=O |
| | $\nu_2$ | 583 | 581 | 584 | 595 | 590 | 600 | ν Me-F |
| | $\nu_3$ | - | 410 | 413 | - | 415 | 415 | ν Me-F′ |
| | | | 399 | | | | | |
| | $\nu_4$ | 266 | 266 | 237 | 258 | 261 | 225 | δ FMeO |
| | | 260 | | | | 256 | | |
| $B_1$ | $\nu_5$ | - | - | 492 | - | - | 512 | ν Me-F |
| | $\nu_6$ | - | - | 200 | - | - | 206 | δ FMeO |
| $B_2$ | $\nu_7$ | 289 | 290 | 289 | - | - | 318 | δ FMeF |
| | | | 278 | | | | | |
| E | $\nu_8$ | - | 536 | 534 | - | 520 | 523 | ν Me-F |
| | $\nu_9$ | 310 | 310 | 308 | 310 | 308 | 305 | δ FMeO |
| | | | 303 | | | | | |
| | $\nu_{10}$ | - | 253 | 242 | - | 245 | 247 | δ FMeF |
| | | | 247 | | | | | |
| | $\nu_{11}$ | - | 210 | 217 | 205 | 209 | 224 | δ FMeO |

Dioxytetrafluoroniobates (-tantalates) of alkali metals for the general $M_3MeO_2F_4$ type also belong to the family characterized by X:Me=6. Structural characteristics of the compounds are collected in Table 26.

$M_3TaO_2F_4$ and $M_3NbO_2F_4$, where M = K, Rb, Cs, form crystal structures similar to that of $Rb_3TiF_6$, which is described by Bode and Voss [189]. The structure of the compounds can be described as a tetragonally distorted cubic cell of the $(NH_4)_3FeF_6$ type, the structure of which is described by Steward and Rockby [190].

Fouad, Chaminad, Ravez and Hagenmuller [191] showed that all compounds of the $M_3MeO_2F_4$ type (M = K, Rb, Cs; Me = Ta, Nb) undergo a reversible phase transition into the cubic phase at the following temperatures (in °C): $K_3NbO_2F_4$ – 145; $Rb_3NbO_2F_4$ – 195; $Cs_3NbO_2F_4$ – 200; $K_3TaO_2F_4$ – 90; $Rb_3TaO_2F_4$ – 170. The transition, which consists of the modification of the cubic $(NH_4)_3FeF_6$ into a low temperature pseudotetragonal-type structure, is performed by the rotation of oxyfluoride octahedral ions $Ta(Nb)O_2F_4^{3-}$ by an angle of $\pi/4$ around the [001] axis, as demonstrated by Chaminade and Pouchard [192]. This transformation leads to the formation of a tetragonal cell of octahedrons and to a change in the coordination number of potassium.

Compounds of the $A_2A'NbO_2F_4$ type, in which A = K, Rb, Cs and A′ = Na, K, Rb, crystallize in a structure similar to that of alpasolite – $K_2NaAlF_6$. The structure of such lithium-containing compounds has not yet been determined. Based on X–ray data, it is not possible to distinguish the position of the oxygen ligand in the isolated $NbO_2F_4^{3-}$ complex. According to investigations performed by Pausewang et al. [157], this uncertainty might be related to the statistical orientation of the complexes in the crystal lattice. The position of the oxygen atom within the structure of the $NbO_2F_4^{3-}$ ion, as trans or cis, corresponds to its symmetry - $C_{2v}$ or $D_{4h}$, respectively. Factor group analysis of vibrations and the assignment of the IR absorption spectrum bands obtained for the compound $K_2NaNbO_2F_4$ indicate that the complex ion $NbO_2F_4^{3-}$ has a $D_{4h}$ point symmetry group that corresponds to a cis configuraion of the oxygen ligand [195]. Table 27 presents wave numbers and bands assignment of the $NbO_2F_4^{3-}$ ion in the IR absorption spectrum of $K_2NaNbO_2F_4$.

The radius of the second cation in known $M^{II}NbOF_5$, $M^{II}_2NbO_3F_3$ and $M^{III}_2NbO_5F$ compounds containing bi- and trivalent metals, is usually similar to that of niobium's ionic radius. Such compounds cannot be considered as having an island-type structure and will be discussed later on. Only bismuth-containing compounds ($Bi^{3+}$) display the presence of different cationic sub-lattices in their crystal structure.

*Table 26. Structural parameters of dioxytetrafluoroniobates (-tantalates) – X:Me=6.*

| Compound | Syngony | Cell parameters, Å | | Z | Space group | Density ρ, g/cm$^3$ | | Reference |
|---|---|---|---|---|---|---|---|---|
| | | a | c | | | Calculated | Experimental | |
| $K_3NbO_2F_4$ | Pseudotetragonal | 6.18 | 8.80 | 2 | | 3.138 | 3.138 | [193] |
| | | 6.188 | 8.872 | 2 | | 3.108 | 3.09 | [150] |
| $K_3TaO_2F_4$ | Tetragonal | 6.158 | 8.790 | 2 | $D_{4h}^{17}$ | 3.983 | 3.94 | [192] |
| | Pseudotetragonal | 6.197 | 8.862 | 2 | | 3.964 | 3.94 | [150] |
| $Rb_3NbO_2F_4$ | Pseudotetragonal | 6.399 | 9.149 | 2 | | 4.054 | 4.039 | [193] |
| $K_2NaNbO_2F_4$ | Cubic | 8.474 | | 4 | $O_h^5$ | 3.296 | 3.273 | [193] |
| $Rb_2NaNbO_2F_4$ | Cubic | 8.625 | | 4 | $O_h^5$ | 4.086 | 4.068 | [193] |
| $Rb_2KNbO_2F_4$ | Cubic | 8.999 | | 4 | $O_h^5$ | 3.745 | 3.732 | [193] |
| $Cs_2KNbO_2F_4$ | Cubic | 9.188 | | 4 | $O_h^5$ | 4.334 | 4.321 | [193] |
| $Cs_2RbNbO_2F_4$ | Cubic | 9.431 | | 4 | $O_h^5$ | 4.499 | 4.405 | [193] |
| $K_2LiNbO_2F_4$ | Hexagonal | 13.06 | 3.892 | 5 | $C_{6h}^1$ | 4.131 | | [194] |
| $Rb_2LiNbO_2F_4$ | Hexagonal | 13.50 | 3.958 | 5 | $C_{6h}^1$ | 5.06 | 4.98 | [194] |

*Table 27. IR absorption spectrum and band assignment of $NbO_2F_4^{3-}$ ($D_{4h}$) in the compound $K_2NaNbO_2F_4$ (F' – occurs in tran -position relative to the oxygen ion). Reproduced from [195], K. Dehnike, G. Pausewang, W. Rüdorff, Z. Anorg. Allg. Chem. 366 (1969) 64, Copyright 1969, with permission of Wiley-VCH.*

| ν, $cm^{-1}$ | Vibration class | Assignment |
|---|---|---|
| 894 | $A_1$ | $\nu_s$ $NbO_2$ |
| 825 | $B_1$ | $\nu_{as}$ $NbO_2$ |
| 513 | $B_1$, $B_2$ | $\nu_{as}$ $NbF_2$, $\nu_{as}$ $NbF'_2$ |
| 421 | $A_1$ | $\nu_s$ $NbF_2$ |
| 394 | $A_1$ | $\nu_s$ $NbF'_2$ |
| 285 | $A_1$ | δ $NbO_2$ |
| 233 | $B_1$, $B_2$ | δ NbOF, γ $NbO_2$ |
| 222 | | |
| 136 | | |
| 131 | $A_1$, $A_1$, $B_2$ | δ $NbF_2$, δ $NbF'_2$, γ $NbF_2$ |
| 125 | | |
| 102 | $B_2$ | ρ $NbF'_2$ |

Anrivillius [196] investigated the isostructural compounds $Bi_2NbO_5F$ and $Bi_2TaO_5F$. $Bi_2NbO_5F$ crystallizes in tetragonal syngony with cell parameters: a = 3.835 Å, c = 16.63 Å, Z = 2, calculated density, ρ = 8.26 $g/cm^3$. Cell parameters of $Bi_2TaO_5F$ are: a = 3.829 Å, c = 16.64 Å, Z = 2, calculated density, ρ = 9.50 $g/cm^3$.

Fig. 28 shows the crystal structure of $Bi_2NbO_5F$ with a space group of I4/mmm - $D_{4h}^{17}$. Bismuth ions, along with anions, form $Bi_2O_2$ type $Bi_2(O,F)_2$ layers with a tetragonal configuration. These layers alternate with planes that have the general composition of $Nb(O,F)_4$ in an octahedral configuration. From this point of view, the structural formula of the compound can be presented as

$Bi_2(O,F)_2Nb(O,F)_4$. Positions of oxygen and fluorine in the structure have not yet been determined. The main interatomic distances are (in Å): Nb-(O,F) – 2.0 and 1.92; Bi-(O,F) – 2.29 and 2.90.

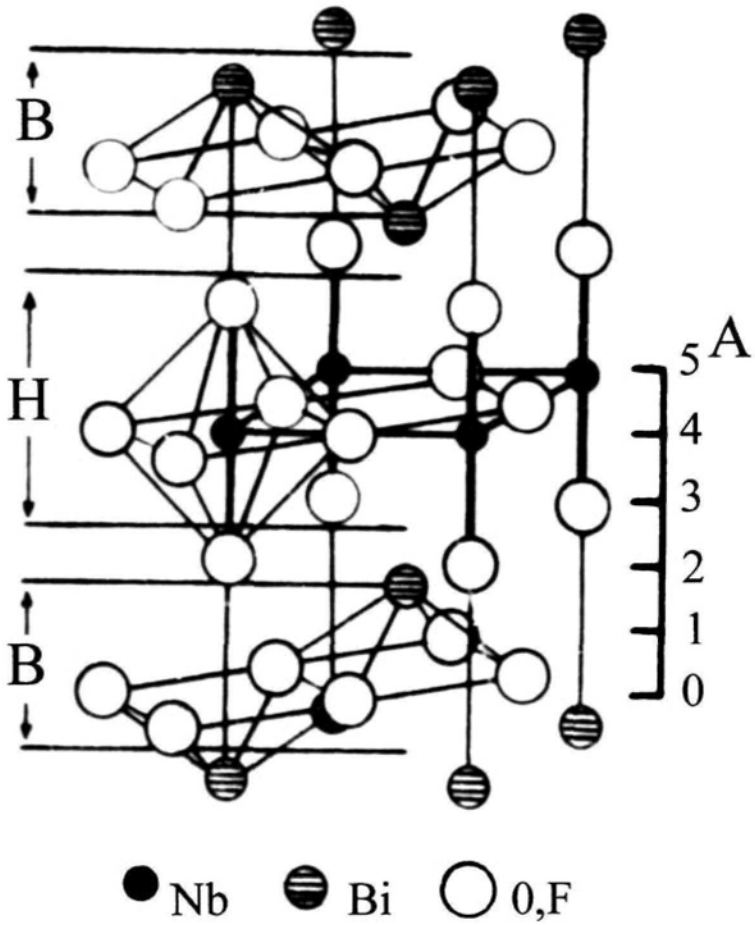


*Fig. 28. Partial structure of $Bi_2NbO_5F$ (after Anrivillius [196]).*

## 3.2. Compounds with chain-type structures

Since the coordination number of tantalum or niobium in fluoride and oxyfluoride compounds cannot be lower than 6 due to steric limitations, further decrease of the X:Me ratio (lower than 6) leads to linkage between complex ions in order to achieve coordination saturation by sharing of ligands between different central atoms of the complexes. The resulting compounds have X:Me ratios between 6 and 4, and form crystals with a chain-type structure.

Table 28 presents structural characteristics of compounds with X:Me ratios between 6 and 5 (5.67, 5.5, 5.33, 5.25). According to data provided by Kaidalova et al. [197], $M_5Nb_3O_3F_{14}$ type compounds contain one molecule of water to form $M_5Nb_3O_3F_{14}\cdot H_2O$, where M = K, Rb, Cs, $NH_4$. Cell parameters for both anhydrous compounds [115] and crystal-hydrates [197] were, nevertheless, found to be identical. Table 28 includes only anhydrous compound compositions because IR absorption spectra of the above compounds display no bands that refer to vibrations of the water molecule [115].

*Table 28. Structural characteristics of compounds with X:Me ratios between 6 and 5.*

| Compound | Syngony | a, Å | c, Å | α, ° | Z | Density, ρ, g/cm$^3$ | Reference |
|---|---|---|---|---|---|---|---|
| $K_5Nb_3O_3F_{14}$ | Hexagonal | 20.12 | 7.87 | | | | [115] |
| $Rb_5Nb_3O_3F_{14}$ | Hexagonal | 20.48 | 8.14 | | | | [115] |
| $Cs_5Nb_3O_3F_{14}$ | Hexagonal | 21.33 | 8.51 | | | | [115] |
| $(NH_4)_5Nb_3O_3F_{14}$ | Hexagonal | 20.51 | 8.06 | | | | [115] |
| $CsNb_2F_{11}$ | Trigonal | 12.47 | | 91.3 | 8 | 3.56 | [78] |
| $RbNb_2F_{11}$ | Trigonal | 12.76 | | 91.2 | 8 | 3.32 | [78] |
| $TlNb_2F_{11}$ | Trigonal | 10.70 | | 94.5 | 6 | 5.10 | [78] |
| $RbNb_3F_{16}$ | Trigonal | 11.3 | | 95.0 | 4 | 3.38 | [78] |
| $CsNb_4F_{21}$ | Trigonal | 9.52 | | 88.8 | 2 | 3.56 | [78] |

Kaidalova et al. established [197] that the crystal structure of $K_5Nb_3O_3F_{14}\cdot H_2O$ has the space group $P6_3mc$ - $C_{6v}^4$ [197]. It was found that the final R-factor equals 0.16 at $B_{common}$ =3.35 Å$^2$.

Due to the relatively low accuracy (~0.1 Å) in measurements of interatomic distances Nb-(O,F), the determination of the positions of oxygen and fluorine atoms in the crystal structure has been unsuccessful. The structure of $K_5Nb_3O_3F_{14}\cdot H_2O$ contains $K^+$ ions and three crystallographically independent island groups. Two groups have a prism configuration and the third group has a pyramidal configuration. There is, however, no indication that $NbO_2F_4^{3-}$, $NbF_6^-$ or $NbOF_5^{2-}$ has ternary prism configurations. The distance $Nb_1$-$Nb_2$ was found to be 4.27 Å, which is typical for niobium atoms that are linked through another light, "bridge" atom, such as fluorine.

Information regarding the structure of other compounds listed in Table 28 is unavailable.

Table 29 presents IR absorption spectra of the above compounds. All spectra display bimodal absorption in the high frequency range, which is attributed to Nb-O vibrations. In addition, the Nb-F part of the spectra seems to be different from the typical spectra observed for isolated complex ions. Such differences in the structure of the spectra can be related to vibrations of both the bridge and the terminal ligands.

*Table 29. IR absorption bands of Nb-O and Nb-F bond vibrations in the compounds $M_5Nb_3O_3F_{14}$ [115], $Cs_3Nb_2O_2F_9$ and $Rb_7Nb_4O_4F_{19}$ [198] (underlined numbers refer to highest intensity bands)*

| Compound | ν NbO, cm$^{-1}$ | | ν NbF, cm$^{-1}$ | | | |
|---|---|---|---|---|---|---|
| $K_5Nb_3O_3F_{14}$ | <u>954</u> | 890 | 610 | <u>560</u> | | |
| $Rb_5Nb_3O_3F_{14}$ | <u>952</u> | 890 | 603 | <u>558</u> | | |
| $Cs_5Nb_3O_3F_{14}$ | <u>947</u> | 890 | 595 | <u>555</u> | 505 | 450 |
| $(NH_4)_5Nb_3O_3F_{14}$ | <u>953</u> | 896 | 600 | <u>570</u> | 557 | 406 |
| $Cs_3Nb_2O_2F_9$ | <u>956</u> | 888 | | <u>560</u> | | 432 |
| $Rb_7Nb_4O_4F_{19}$ | <u>946</u> | 886 | | <u>555</u> | | 420 |

Available data on compounds with X:Me ratios between 6 and 5 provide no clear indication as to the association of complex ions, but rather display a more intricate picture than in the case of isolated complexes. Compounds with X:Me ratios of 5 and lower display more clearly the tendency of the complex ions to be linked in chains of different configurations.

Typical examples of compounds that form chain-type structures are simple pentafluorides of tantalum and niobium, $TaF_5$ and $NbF_5$, which were investigated by Edwards [199]. The crystal structure of $NbF_5$ consists of rings made up of four $NbF_6$ octahedrons that are linked by fluorine ligands that are each shared by two neighboring octahedrons, as shown in Fig. 29. The main interatomic distances (in Å) are as follows: Nb-Nb – 5.80, 5.90 and 4.13; Nb-$F_{end}$ – 1.75 and 1.78; Nb-$F_{bridge}$ – 2.06 and 2.07; angle Nb-$F_{bridge}$-Nb – 182.5°.

The linked $MeF_6$ octahedron structure remains unchanged when moving from solid to gaseous phase [200]. Various researchers indicate that the gaseous phase above niobium pentafluoride, $NbF_5$, predominantly consists of trimers, $(NbF_5)_3$ with a $D_{3h}$ symmetry [201-203].

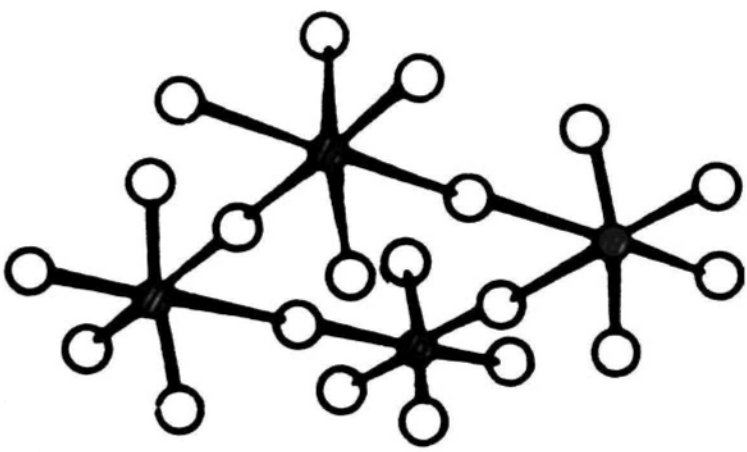

*Fig. 29. Fragment of $NbF_5$ crystal structure. Reproduced from [199], A. J. Adwards, J. Chem. Soc. 10 (1964) 3714, Copyright 1964, with permission of The Royal Society of Chemistry.*

*Table 30. Structural parameters of monoxytetrafluoroniobates – X:Me=5 and related compounds.*

| Compound | Syngony | Cell parameters, Å | | | | Space | Density ρ, g/cm$^3$ | | Reference |
|---|---|---|---|---|---|---|---|---|---|
| | | a | b | c | Z | group | Calculated | Experimental | |
| $NbF_5$ | Monoclinic | 9.62 | 14.43 | 5.12 | 8 | $C_{2h}^3$ | 3.53 | 3.29 | [199] |
| $TaF_5$ | Monoclinic | 9.64 | 14.45 | 5.12 | 8 | $C_{2h}^3$ | 5.17 | 4.98 | [199] |
| $NH_4NbOF_4$ | Tetragonal | 8.04 | | 3.95 | 2 | $D_{4h}^7$ | 2.64 | 2.61 | [204, 205] |
| $LiNbOF_4$ | Tetragonal | 6.26 | | 3.98 | 2 | | | 3.40 | [126] |
| $KNbOF_4$ | Tetragonal | 15.451 | | 7.755 | 16 | $C_4^5$ | 3.21 | 3.56 | [139] |
| $(NH_4)_5Nb_3OF_{18}$ | Tetragonal | 15.710 | | 7.744 | 4 | $C_{4v}^{10}$ | 2.57 | | [206] |
| $K_5Nb_3OF_{18}$ | Tetragonal | 14.877 | | 7.697 | 4 | $C_{4v}^{10}$ | 3.00 | | [206] |
| $Rb_5Nb_3OF_{18}$ | Tetragonal | 15.525 | | 7.794 | 4 | $C_{4v}^{10}$ | 3.76 | | [206] |

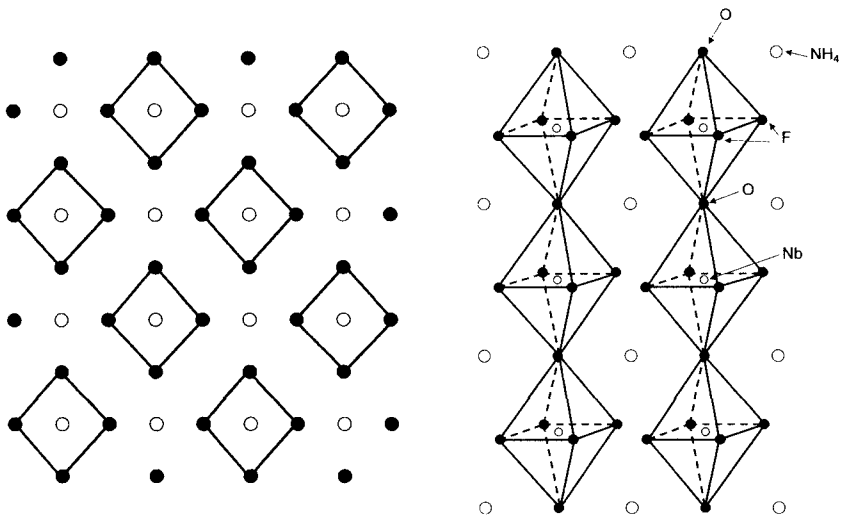


*Fig. 30. Projection of $NH_4NbOF_4$ structure on the planes (001) and (010). Reproduced from [204], V. I. Pakhomov, T.A. Kaidalova, Kristallografiya 19 (1974) 733, Copyright 1974, with permission of "Nauka" (Russian Academy of Sciences) publishing.*

Typical chain-type crystal structure is observed for compounds with the general formula $MNbOF_4$. Table 30 presents cell parameters of tantalum and niobium pentafluorides and of other compounds with X:Me = 5.

According to investigations performed by Pakhomov and Kaidalova [204], the crystal structure of $NH_4NbOF_4$ consists of infinite chains made up of distorted octahedral ions ($NbOF_4^-$) linked by oxygen atoms. Ammonium cations, $NH_4^+$, occupy the spaces between the chains, as shown in Fig. 30. The packing of the structural units in the $NH_4NbOF_4$ crystal can be described as a CsCl type structure in which $Cl^-$ ions are replaced by $NbO_2F_4$ complexes and $Cs^+$ ions are replaced by ammonium ions.

The niobium atom has a slightly distorted octahedral coordination. Interatomic distances between the niobium atom and the two oxygen atoms in trans positions, O-Nb-O are 1.81 and 2.14 Å. The niobium atom is shifted from the base plane of the octahedron by 0.23 Å, and this shift, in adjacent chains, is in opposite directions. Pakhomov and Kaidalova [204] concluded that the shorter Nb-O bond (1.81 Å) is an intermediate between a single and double bond.

Kuznetzov et al. [139] showed that the structure of $KNbOF_4$ consists of potassium ions and two types of infinite chains running along the c axis. The first type of chain is similar to the $NH_4NbOF_4$ chains and is made up of octahedrons that are linked together in a simple manner. The second type of chain has branches due to linkage of additional octahedrons. Each unit of such chain consists of three octahedrons with a common axis, which is perpendicular to the rotation-inversion tetrad axis. Potassium atoms are situated in two sets of eight-fold positions characterized by a coordination number of either nine or ten. This structure corresponds to K-O,F distances of 2.06–3.62 and 2.71–3.53 Å, respectively. Nb-O,F distances vary in the range of 1.64–2.24 Å. $KNbOF_4$ crystal structure is similar to $BaFeF_5$, which is described in [207].

According to the classification of chain-type compounds developed by Von Der Mühll and Ravez [208], the formation of branched octahedron chains in compounds of the $ABF_5$ type is typical in cases in which the ratio between the ionic radii of the cations is $r(B^{3+})/r(A^{2+}) \leq 0.57$, where $r(A^{2+}) \geq 1$ Å. This approach is in good correlation with the structural peculiarities of $KNbOF_4$. On the other hand, one would expect the same branching of chains to be found in the case of $NH_4NbOF_4$, since the ionic radius of $NH_4^+$ is 1.43 Å. One possible explanation of this discrepancy is the influence of the hydrogen bond N-H...F on the crystal structure of $NH_4NbOF_4$ [204].

A chain-type structure can also be attributed to $M_5Nb_3OF_{18}$, where M = $NH_4$, K, Rb, even when the X:Me ratio is greater than 6. As a matter of fact, the compounds contain both isolated complex ions and chains composed of octahedral ions. The composition of the compounds can be presented as $2M_2NbF_7 \cdot MNbOF_4$. The crystal structure of $Rb_5Nb_3OF_{18}$ is described in [209] and presented in Fig. 31. The structure consists of infinite anion chains ($NbOF_4^-$), isolated ions $NbF_7^{2-}$ and cations of rubidium, $Rb^+$. Infinite chains extend along the c axis and are made up of octahedrons that are linked by a shared oxygen atom. The niobium atom is shifted from the base plane (Nb-O distances along the chain are 1.741 and 2.156 Å).

There are two main differences between the structure of the $NH_4NbOF_4$ chains and that of the $Rb_5Nb_3OF_{18}$ chains. The first difference is, that in the case of $Rb_5Nb_3OF_{18}$ neighboring octahedrons along the chain are rotated by $\pi/4$ relative to one another (the rotation axis coincides with z-axis), as shown in Fig. 31. The second difference is that in the $NbOF_4^-$ complexes, the niobium atoms are all shifted in the same direction, forming a polar structure.

The polyhedron $NbF_7^{2-}$ is more similar to a pentagonal bi-pyramid but is distorted due to a strong shift of $F_6$ towards $F_3$ ($F_6F_3$ and $F_1F_6$ distances are 2.39 and 3.08 Å, respectively). This distortion renders the polyhedron structure closer to an Archimedes antiprism with a truncated corner, as shown in Fig. 31.

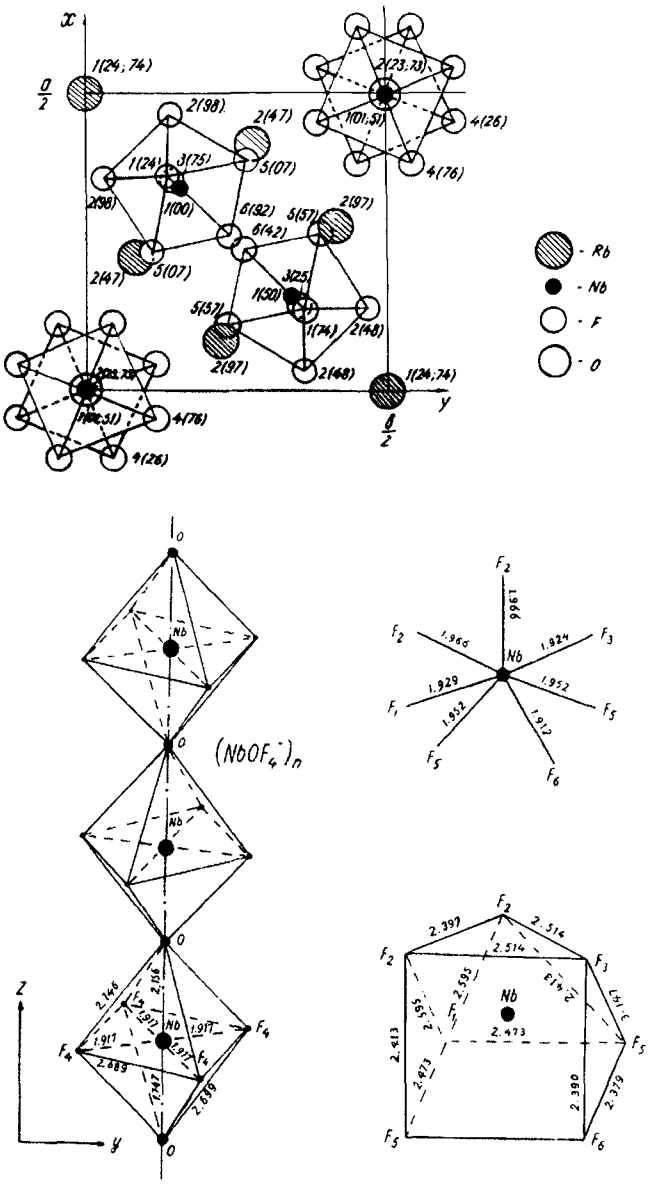


*Fig. 31 Crystal structure of $Rb_5Nb_3OF_{18}$. Projection on the plane (001). Numbers in brackets are the atom coordinates on the z-axis in percents of c parameter. Structure of $NbOF_4^-$ chains and $NbF_7^{2-}$ polyhedron. Reproduced from [209], A. I. Agulyansky, V. E. Zavodnik, V.Y. Kuznetzov et al. Neorgan. Mater. 27 (1991) 380, Copyright 1991, with permission of "Nauka" (Russian Academy of Sciences) publishing.*

Sharing of an oxygen atom by two central atoms in compounds with chain-type structures weakens the binary Nb=O bond compared to the corresponding bond in pure isolated ions such as $NbOF_5^{2-}$. This phenomenon affects the vibration spectra and increases wave numbers of NbO vibrations in the case of isolated oxyfluoride complex ions. Table 31 displays IR absorption spectra of some chain- type compounds. Raman spectra are discussed in [212].

Bands at a higher frequency of 955–975 $cm^{-1}$ are attributed to vibrations of isolated MeO bonds that occur at the ends of the chain branches.

Regarding dioxytrifluoroniobates (-tantalates) of alkali metals, information on the synthesis of $K_2NbO_2F_3$ and $K_2TaO_2F_3$ is available in [213] and [214], respectively.

Table 32 presents the structural characteristics of compounds with X:Me ratios in the range of 5 - 4.

Rogachev and Kuznetzov et al. [215] and Chaminad et al. [153] investigated the crystal structure and actual composition of $K_2Ta_2O_3F_6$, Marignac's salt, which is the hydrolysis product of $K_2TaF_7$ (using boiling water). It should be recalled that for a long time the general formula of Marignac's salt was believed to be $K_4Ta_4O_3F_6$.

According to investigations [215], the structure of Marignac's salt corresponds to the formula $K_2Ta_2O_3F_6$. The compound crystallizes in orthorhombic syngony, with a space group of Pnma - $D_{2h}^{16}$, Z = 4.

*Table 31. Wave numbers ($cm^{-1}$) of IR absorption spectra of chain-type compounds (Me = Nb or Ta).*

| Compound | ν (MeO) | ν (Me-O-Me) | ν (MeF) | Reference |
|---|---|---|---|---|
| $NH_4NbOF_4$ | | 828 | 620, 587, 405 | [115, 205] |
| $LiNbOF_4$ | | 875 | 580 | [126] |
| $NaNbOF_4$ | | 850 | 590 | [126] |
| $KNbOF_4$ | 970 | 800 | 590 | [126] |
| $RbNbOF_4$ | 975 | 820 | 595 | [126] |
| $CsTaOF_4$ | 955 | 710-620 | 580, 475 | [210] |
| $(NH_4)_5Nb_3OF_{18}$ | | 800 | 620, 550 | [209, 211] |
| $K_5Nb_3OF_{18}$ | | 800 | 620, 550 | [209, 211] |
| $Rb_5Nb_3OF_{18}$ | | 800 | 620, 550 | [209, 211] |

*Table 32. Structural characteristics of $M_2Ta_2O_3F_6$ compounds (M = $NH_4$, K, Rb) and $Cs_7Ta_8O_{13}F_{21}$, with 4 < X:Me<5 (all compounds have orthorhombic syngony).*

| Compound | a, Å | b, Å | c, Å | Z | Density, ρ, g/cm$^3$ | | Reference |
|---|---|---|---|---|---|---|---|
| | | | | | Calculated | Measured | |
| $K_2Ta_2O_3F_6$ | 10.22 | 5.57 | 14.52 | 4 | 4.84 | 4.72 | [215] |
| | 10.215 | 5.581 | 14.493 | 4 | 4.837 | 4.79 | [153] |
| $Rb_2Ta_2O_3F_6$ | 10.45 | 5.65 | 14.86 | 4 | 5.26 | | [215] |
| $(NH_4)_2Ta_2O_3F_6$ | 10.43 | 5.64 | 14.84 | 4 | 4.26 | | [215] |
| $Cs_7Ta_8O_{13}F_{21}$ | 10.86 | 5.73 | 15.47 | | | | [215] |

Fig. 32 presents the crystal structure of $K_2Ta_2O_3F_6$. Eight tantalum atoms are located in two sets of four- fold positions on reflection planes. Each tantalum atom is coordinated to six anions, oxygen or fluorine (O, F), forming slightly distorted octahedrons. The octahedrons are linked via double zig-zag chains. The chains are arranged in parallel to the b axis, with potassium ions located between the chains. Analysis of Ta-(O, F) interatomic distances indicates that the bridging atoms between the connected octahedrons can only be oxygen atoms.

The tantalum atoms are shifted from the equatorial planes of the octahedrons by 0.15 Å. Potassium ions are situated between the chains and each ion is surrounded by nine fluorine atoms. The distances $K_1$-F and $K_2$-F vary in the ranges of 2.63-2.95 and 2.85-3.07 Å, respectively [215].

Lastochkina et al. [216] reported on the preparation of $KTaO_{1.5}F_3 \cdot H_2O$, but the X-ray powder diffraction pattern obtained for the anhydrous product, $KTaO_{1.5}F_3$, does not correspond with the pattern given for $K_2Ta_2O_3F_6$ in [215].

IR absorption spectra of $Rb_2Ta_2O_3F_6$ and $Cs_7Ta_8O_{13}F_{21}$ are practically identical and are characterized by intensive bands as follows (in cm$^{-1}$) [115]:

$Rb_2Ta_2O_3F_6$ – 988, 926, 668, 553, 508, 495
$Cs_7Ta_8O_{13}F_{21}$ – 988, 916, 664, 547, 503, 485

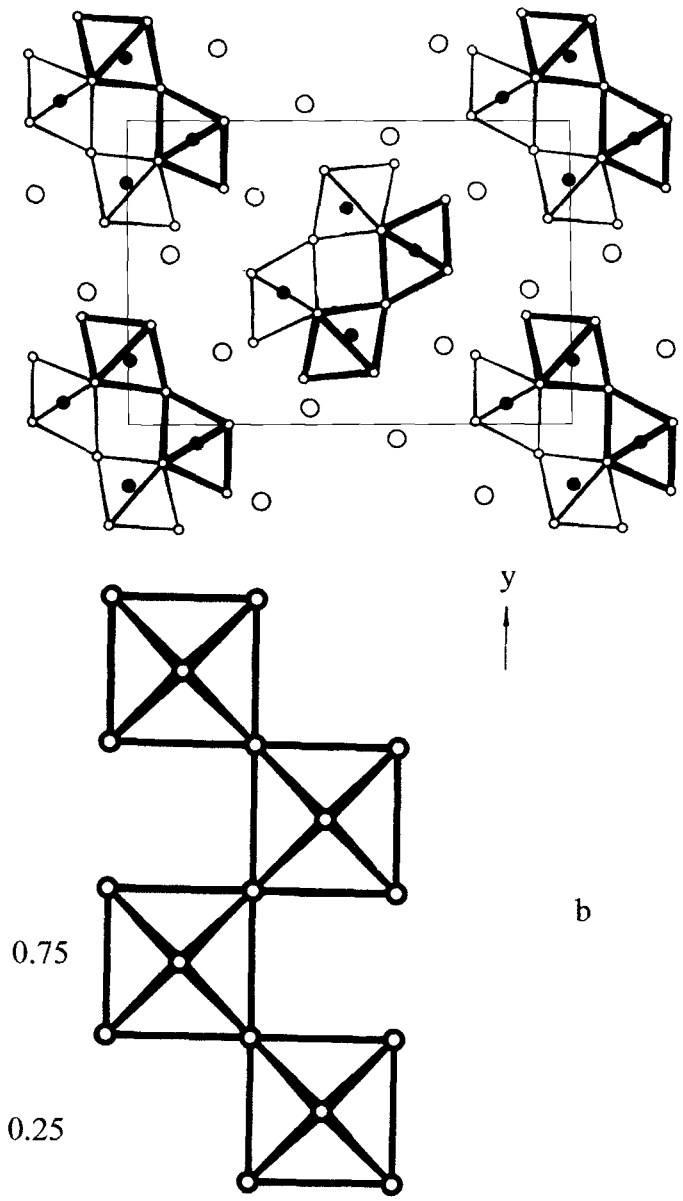


*Fig. 32. Crystal structure of Marignac's salt, $K_2Ta_2O_3F_6$, and the arrangement of oxyfluoride octahedrons (b). Reproduced from [215], D. L. Rogachev, V. Y. Kuznetzov, A. N. Bogdanova et al., Zh. Strukt. Khim. 17 (1976) 129, Copyright 1976, with permission of "Nauka" (Russian Academy of Sciences) publishing.*

## 3.3. Compounds with layered-type structures

A further decrease in the X:Me ratio, to 4, leads to linkage of the octahedral units by sharing more than one ligand so as to achieve coordination saturation. Sharing of two vertexes (two corners of the each octahedron) leads to the formation of compounds with layered-type structures.

Table 33 presents structural parameters of compounds with X:Me ratios equal to 4.

$NbOF_3$ and $TaOF_3$ are characterized by very low stability, are sensitive to moisture and decompose in air even at ambient temperature. Nevertheless, Köhler et al. [217] succeeded in investigating these compounds. Both compounds crystallize in a $SnF_4$ type structure forming planes that share oxyfluoride octahedrons with each other, at four corners. These planes are stacked in a three-dimensional lattice via van der Waals interactions [217].

The structure of $LiTaO_2F_2$, as reported by Vlasse et al. [218], is similar to a $ReO_3$ type structure and consists of triple layers of octahedrons linked together through their vertexes. The layers are perpendicular to the c axis, and each layer is shifted, relative to the layer below, by half a cell in the direction (110). Lithium atoms are situated in the centers of the tetragonal pyramids (coordination number = 5). The other lithium atoms are statistically distributed along with tantalum atoms (coordination number = 6) at a ratio of 1:3. The sequence of the metal atoms in alternating layers is (Ta-Li) – Ta – (Ta-Li). Positions of oxygen and fluorine atoms were not determined. The main interatomic distances are (in Å): Ta-(O, F) – 1.845-2.114; Li-(O, F) – 2.087-2.048; (O, F)-(O,F) – 2.717-2.844.

$NaNbO_2F_2$ and $NaTaO_2F_2$ are isostructural compounds. Their crystal structure was reported by Andersson and Galy [219] and Chaminade, Pouchard and Hagenmuller [91] to consist of layers made up of $Nb(Ta)O_4F_2$ octahedrons that are linked via their angles (vertexes). Fig. 33 presents the structure of $NaNbO_2F_2$ layers. These compounds can be considered to have a $\alpha PbO_2$ type structure. The main interatomic distances are (in Å): Nb-O – 1.94; Nb-F – 2.015; Na-F – 2.22-2.36.

The crystal structure of $KTaO_2F_2$ is made up of $Ta(O, F)_6$ octahedrons that are linked via six hexagonal rings. The rings are connected via their vertexes forming infinite empty channels along the c axis [139].

Galasso and Darby [220] prepared and investigated the oxyfluoride $K_2NbO_3F$, which has crystal structure similar to $K_2TaO_3F$ and crystallizes in a $K_2NiF_4$ type structure. The structure of the compound consists of infinite layers of octahedrons, $NbO_4F_2$, that are oriented perpendicular to the c axis, as shown in Fig. 34.

*Table 33. Structural characteristics of compounds having X:Me=4.*

| Compound | Syngony | Cell parameters, Å | | | Z | Space group | Density ρ, g/cm$^3$ | | Reference |
|---|---|---|---|---|---|---|---|---|---|
| | | a | b | c | | | Calculated | Measured | |
| $NbOF_3$ | Tetragonal | 3.9675(1) | | 8.4033(1) | 10 | $D_{4h}^{17}$ | 4.16 | | [217] |
| $TaOF_3$ | Tetragonal | 3.9448(1) | | 8.4860(1) | 10 | $D_{4h}^{17}$ | 6.43 | | [217] |
| $LiTaO_2F_2$ | Tetragonal | 3.903 | | 25.38 | 5 | $D_{4h}^{17}$ | 5.54 | 5.53 | [218] |
| $NaNbO_2F_2$ | Monoclinic | 8.091 | 5.434 | 7.498 | 4 | $C_{2h}^{5}$ | 3.83 | | [219] |
| | | (β = 101.15°) | | | | | | | |
| $NaTaO_2F_2$ | Monoclinic | 8.013 | 5.405 | 7.626 | 4 | $C_{2h}^{5}$ | 5.64 | 5.62 | [91] |
| | | (β = 101.70°) | | | | | | | |
| $KTaO_2F_2$ | Hexagonal | 13.12 | | 3.89 | | $C_{6h}^{1}$ | | | [139] |
| $K_2NbO_3F$ | Tetragonal | 3.956 | | 13.67 | 2 | $D_{4h}^{17}$ | 3.68 | 3.64 | [220] |
| $K_2TaO_3F$ | Tetragonal | 3.95 | | 13.67 | 2 | | 5.06 | 5.07 | [221] |
| $CuNbO_3F$ | Triclinic | 7.305 | 6.594 | 3.766 | 2 | $C_1^1$ | 4.97 | 4.98 | [222] |
| | | (α=87.39°; β=85.19°; γ=123.81°) | | | | | | | |

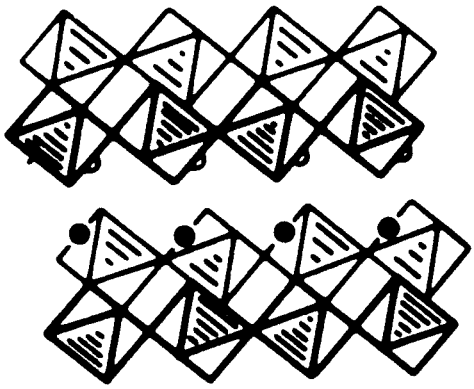

*Fig. 33. Structure of $NaNbO_2F_2$. Reproduced from [219], S. Andersssson, J. Galy Acta Cryst. 25 (1969) 847, Copyright 1969, with permission of Blackwell Publishing.*

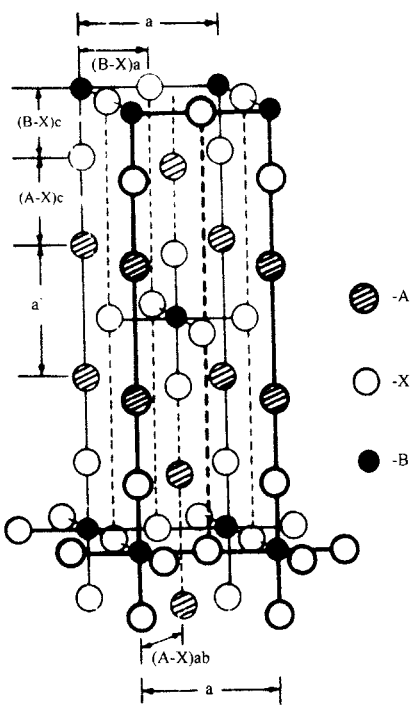


*Fig. 34. Structure of $K_2NbO_3F$. Reproduced from [220], F. Galasso, W. Darby, J. Phys. Chem. 66 (1962) 1318, Copyright 1962, with permission of American Chemical Society.*

Potassium ions are located between the layers. Interatomic distances are as follows (in Å): Nb-Nb – 3.96; K-K – 4.10; Nb-O – 1.98; Nb-F – 2.06; K-F – 2.72 and 2.80 [220].

Lundberg and Sävborg [222] reported that the crystal structure of $CuNbO_3F$ is composed of $Nb(O, F)_6$ octahedrons linked via two shared corners. The linked octahedrons form zig-zag chains along the c axis. The chains are connected to one another via copper atoms, each of which is surrounded by four anions that form a four-sided structure and two additional anions positioned at a greater distance from the copper atom. Fig. 35 shows the structural elements of $CuNbO_3F$.

Table 34 presents structural parameters of compounds with $3 < X:Me < 4$.

Chaminade, Pouchard and Hagenmuller [91] discussed the crystal structure of compounds $Na_4Ta_5O_{10}F_9$ and $Na_2Ta_3O_6F_5$ but such structure was never investigated. Nevertheless, the similarity of these two compounds to compounds formed in the $Ca_2Nb_2O_7 - NaNbO_3$ [223] and $La_2Ti_2O_7 - CaTiO_3$ [224] systems allows the proposal of a possible structure for $Na_4Ta_5O_{10}F_9$ and $Na_2Ta_3O_6F_5$. The phases of the two compounds can be represented as layers of octahedrons that are arranged parallel to the plane xz, and are attached to one another via terminal ligands. From the standpoint of the $A_nB_nX_{3n+2}$ type [224] group, the layers can be either binary (n = 2) or ternary (n = 3). Atoms A are positioned within and between perovskite layers.

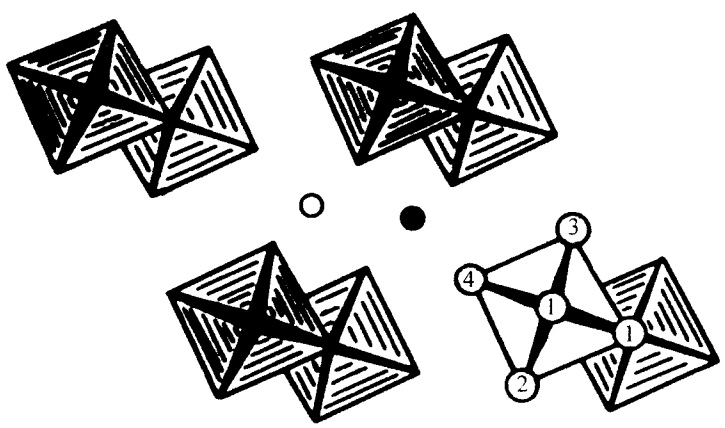


*Fig. 35. The surroundings of $Cu^{2+}$ and $Nb(O,F)_6$ octahedrons in the crystal structure of $CuNbO_3F$. Ends of the bold and thin lines correspond to metals positioned at Z~0.75 and Z~0.25. Reproduced from [222], M. Lundberg, Ö. Sävborg, Chem. Scripta 13 (1978-79) 197, Copyright 1979, with permission of The Royal Swedish Academy of Sciences.*

*Table 34. Structural characteristics of compounds having 3 < X:Me <4.*

| Compound | Syngony | Cell parameters, Å a | b | c | Z | Space group | Density ρ, g/cm³ Calculated | Measured | Reference |
|---|---|---|---|---|---|---|---|---|---|
| $Na_4Ta_5O_{10}F_9$ | Orthorhombic | 7.620 | 36.905 | 5.438 | 4 | | 5.766 | 5.68 | [91] |
| $Na_2Ta_3O_6F_5$ | Orthorhombic | 3.845 | 21.110 | 5.426 | 2 | | 5.878 | 5.81 | [91] |
| $K_3Ta_4O_8F_7$ | Orthorhombic | 3.918 | 18.072 | 19.057 | 4 | $C_{2v}^7$ | 5.35 | 5.42 | [225] |
| $K_6Ta_{6.5}O_{14.5}F_{9.5}$ | Hexagonal | 13.109 | | 3.880 | 1 | $C_{3h}^1$ | 5.27 | 5.23 | [226] |
| $K_6Nb_{6.5}O_{14.5}F_{9.5}$ | Hexagonal | 13.126 | | 3.883 | 1 | $C_{3h}^1$ | 3.60 | 3.65 | [227] |
| $K_{12}Nb_{15.5}O_{35.5}F_{18.5}$ | Hexagonal | 19.26 | | 3.873 | 1 | $C_{3h}^1$ | 3.77 | 3.73 | [226, 227] |
| $K_{12}Ta_{15.5}O_{35.5}F_{18.5}$ | Hexagonal | 19.32 | | 3.878 | 1 | $C_{3h}^1$ | 5.55 | 5.57 | [227, 228] |
| $Na_2Nb_2O_5F_2$ | Monoclinic | 12.91 (β = 90°) | 7.45 | 18.24 | 12 | | 4.00 | 4.18 | [229] |
| $Na_2Ta_2O_5F_2$ (I) | Monoclinic | 12.89 (β = 105°) | 7.42 | 25.12 | 16 | | 6.02 | 5.79 | [230] |
| $Na_2Ta_2O_5F_2$ (II) | Monoclinic | 12.771 (β = 108.79°) | 7.428 | 12.86 | 8 | | 6.048 | 6.02 | [230] |
| $Ag_2Nb_2O_5F_2$ | Orthorhombic | 7.455 | 10.500 | 7.72 | 4 | | 5.71 | 5.67 | [230] |
| $Ag_2Ta_2O_5F_2$ | Monoclinic | 12.87 | 7.469 | 25.02 | 16 | | 7.77 | 7.50 | [230] |
| $NaTa_4O_8F_5$ | Orthorhombic | 6.481 | 10.496 | 3.905 | 1 | | 6.06 | 6.50 | [91] |
| $K_2Ta_4F_4O_9$ | Hexagonal | 15.936 | | 3.892 | 3 | $C_6^1$ | 5.90 | 5.89 | [231] |

This method of approach, when applied to the above mentioned compounds leads to a $Na_2Ta_3O_6F_5$ structure in which n = 3 (n denotes the number of layers) if the perovskite positions remain vacant, as shown in Fig. 36 (a). The $Na_4Ta_5O_{10}F_9$ phase corresponds to n = 2.5, which leads to the proposed structure consisting of two types of alternating layers, characterized by n = 2 and n = 3, as shown in Fig. 36 (b). The central positions of the perovskite layers remain vacant in this structure as well.

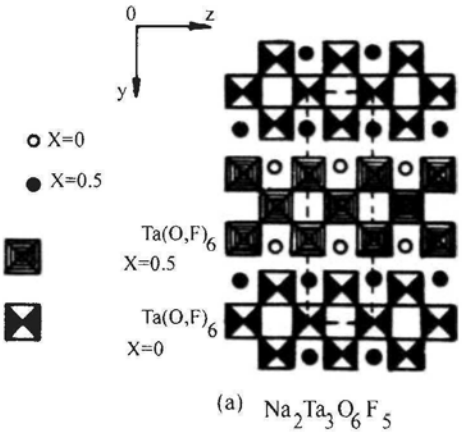


(a) $Na_2Ta_3O_6F_5$

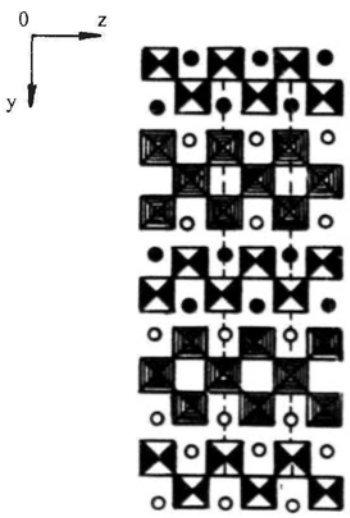


(b) $Na_4Ta_5O_{10}F_8$

*Fig. 36. Possible packing of layers for $Na_2Ta_3O_6F_5$ (a) and $Na_4Ta_5O_{10}F_9$ (b) (after Chaminad, Pouhard, Hagenmuller [91]).*

$K_3Ta_4O_8F_7$ [225] too has a layered structure and contains clusters of the $Ta_3X_{15}$ type. Each cluster is composed of three $TaX_6$ type octahedrons that are linked to one another via their vertexes.

Boukhari, Chaminade, Pouchard and Vlasse [226-228] investigated the compounds $K_6Me_{6.5}O_{14.5}F_{9.5}$ and $K_{12}Me_{15.5}F_{18.5}O_{35.5}$, where Me = Nb or Ta, and found the compounds to have similar structures. The structure of $K_6Me_{6.5}O_{14.5}F_{9.5}$ consists of two sub-lattices made up of $[Me_{0.5}X_3]_n$ and $[Me_6X_{21}]_n$ type units, whereas $K_{12}Me_{15.5}F_{18.5}O_{35.5}$ is made up of $[Me_{0.5}X_3]_n$ and $[Me_5X_{17}]_n$ type units. X corresponds to oxygen or fluorine anions. The sub-lattice, which is identical for all $[Me_{0.5}X_3]_n$ type compounds of this group, consists of infinite chains of trigonal prisms with a metal atom in the center of each. The second type of sub-lattice is formed from $MeX_6$ octahedrons that are linked via their vertexes (see Fig. 37).

The compounds characterized by X:Me = 3.5 have a common formula of $M_2Me_2O_5F_2$ and crystallize either in a pyrochlore [192] or a veberite [229] type structure. According to X-ray powder diffraction patterns, the structure of $Na_2Nb_2O_5F_2$ can be regarded as a super-structure of pyrochlore, which is made up of octahedrons connected in layers and arranged in the (111) direction . The layers are linked via octahedrons so that each octahedron in one layer shares three vertexes with an octahedron in the adjacent layer.

The structure of the low-temperature modification of the compound, $Na_2Ta_2O_5F_2$ (I), has not yet been determined. The high-temperature modification, $Na_2Ta_2O_5F_2$ (II), can be conceived as two sub-lattices: $Ta_{16}X_{52}$, which is composed of $TaX_6$ octahedrons and $Na_{14}X_4$, which contains $Na_4X_2$ tetrahedrons [192]. Fig. 38 shows the structure of $Na_2Ta_2O_5F_2$ (II). Two additional sodium atoms occupy the centers of two bi-pyramids with distorted hexagonal bases.

The compounds $K_2Ta_4O_9F_4$ and $K_7Ta_{12}O_{28}F_{11}$ [231] belong to the same homological series and have similar structure with $K_2W_4O_{13}$. Oxyfluoride octahedrons, $TaX_6$, are connected via their vertexes to form hexagonal rings. Six additional octahedrons are linked to the outer side of each ring. These double hexagonal rings are connected to one another via the octahedrons of the outer layer. Potassium atoms are located in the centers of the rings and between the rings.

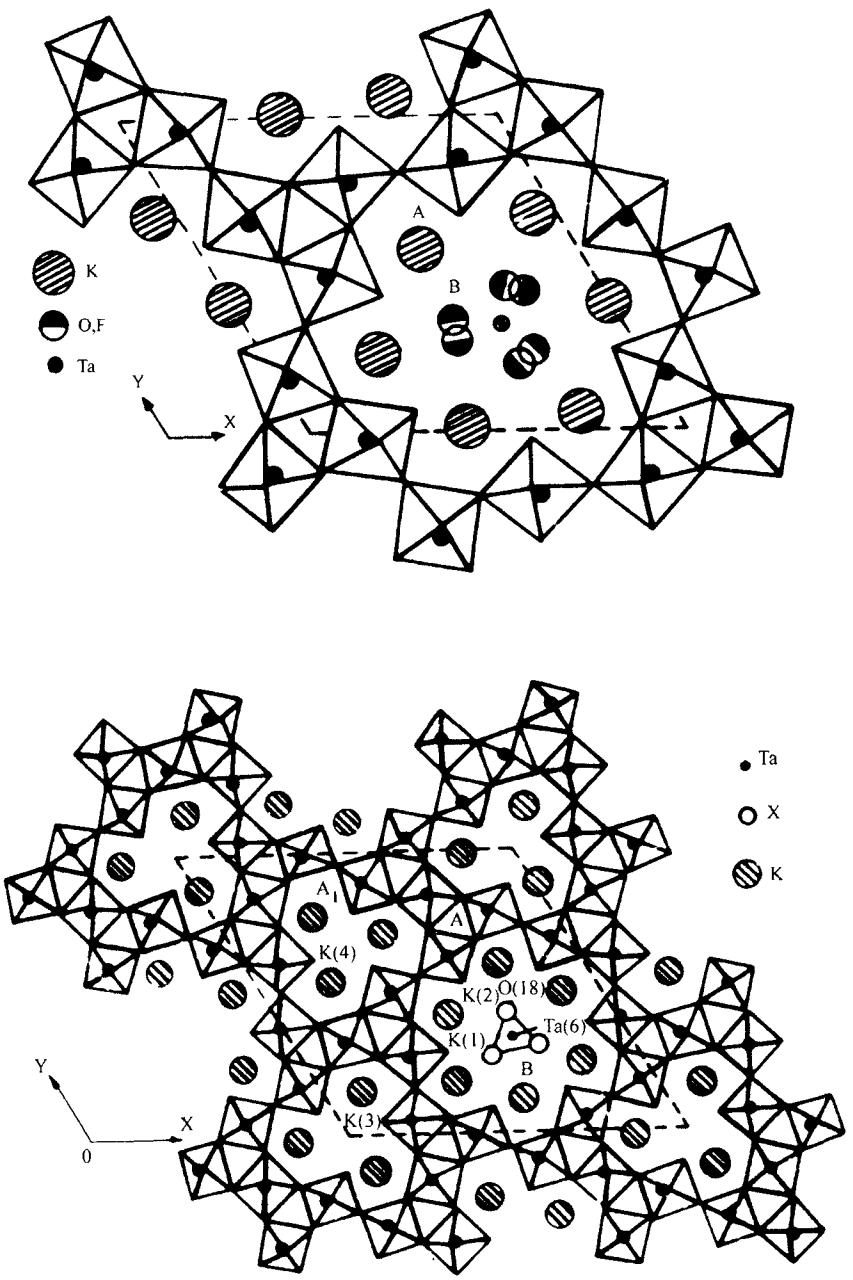


*Fig. 37 Structure of $K_6Me_{6.5}O_{14.5}F_{9.5}$ (top) and $K_{12}Me_{15.5}F_{18.5}O_{35.5}$ (bottom). Projection on (001) (after Boukhari, Chaminade, Vlasse, Pouchard, [227]).*

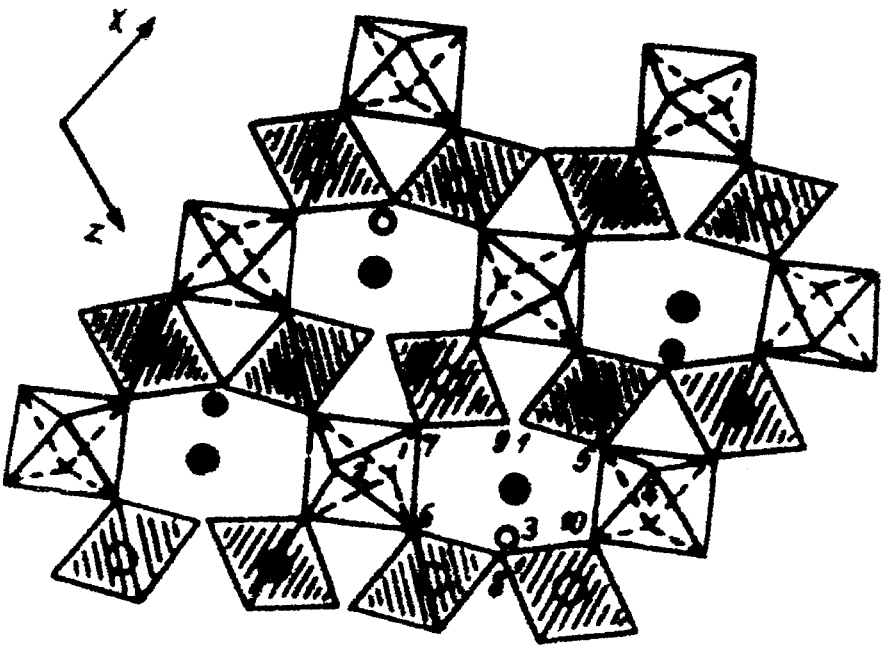


*Fig. 38. Projection of $Na_2Ta_2O_5F_2$ (II) structure (after Chaminade and Pouhard [192]).*

Kuznetzov, Rogachev et al. [232] investigated the binary salt $KF{\cdot}4KNbO_3$ with X:Me = 3.25. The $KF{\cdot}4KNbO_3$ crystal contains binary columns of $NbO_6$ octahedrons that are connected by two shared angles. Potassium and fluorine atoms separate the binary columns. The structure of the compound can be represented satisfactorily by the formula $(FK_5)_{1\infty}[Nb_4O_{12}]_{1\infty}$. Potassium and fluorine form chains of F-K octahedrons that are connected via potassium atoms. Anion columns $[Nb_4O_{12}]^{4-}$ and cation chains $[FK_5]^{4+}$ are arranged in the plane (100) in a chess-board order. One of the possible reasons for this type of structure is the steric similarity of fluorine and potassium ions.

## 3.4. Compounds with framework-type structures

Known oxyfluoroniobates (-tantalates) with compositions that correspond to X:Me = 3 crystallize in typical structures of $ReO_3$, pyrochlore, and hexagonal and tetragonal tungsten bronze. Table 35 presents structural parameters of such compounds.

The crystal structure of tantalum and niobium dioxyfluorides, $TaO_2F$ and $NbO_2F$, consists of oxyfluoride octahedrons linked via their vertexes to form a three-dimensional lattice with a $ReO_3$ type structure, as demonstrated by Andersson and Astrom [233] and by Frevel and Rinn [234]. Fig. 39 shows the structure of $NbO_2F$.

The compounds of the $MMe_2O_5F$ type, where Me = Nb or Ta; M = Rb, Cs, Tl, crystallize in cubic symmetry and correspond to a pyrochlore-type structure [235-237]. This structure can be obtained from a fluorite structure by replacing half of the calcium-containing cubic polyhedrons with oxyfluoride octahedrons.

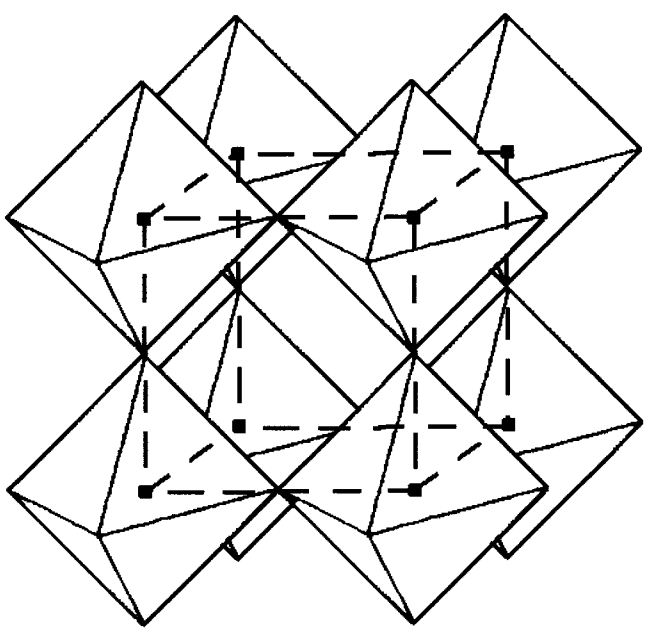

*Fig. 39. Structure of $NbO_2F$ ($ReO_3$ type structure).*

*Table 35. Structural characteristics of compounds having X:Me = 3.*

| Compound | Syngony | Cell parameters, Å a | b | c | Z | Space group | Density ρ, g/cm$^3$ Calculated | Measured | Reference |
|---|---|---|---|---|---|---|---|---|---|
| $NbO_2F$ | Cubic | 3.902 | | | 1 | $O_h^1$ | 4.02 | | [233] |
| $TaO_2F$ | Cubic | 3.896 | | | 1 | $O_h^1$ | 6.51 | 5.99 | [234] |
| $RbTa_2O_5F$ | Cubic | 10.47 | | | | $O_h^7$ | | | [235] |
| $CsNb_2O_5F$ | Cubic | 10.57 | | | | $O_h^7$ | | | [236] |
| $CsTa_2O_5F$ | Cubic | 10.50 | | | | $O_h^7$ | | | [236] |
| $TlNb_2O_5F$ | Cubic | 10.506 | | | 8 | $O_h^7$ | 5.60 | | [237] |
| $AgNb_2O_5F$ | Orthorhombic | 12.461 | 12.264 | 7.676 | 10 | $D_{2h}^9$ | 5.56 | 5.38 | [238] |
| $K_{0.3}NbF_3$ | Orthorhombic | 7.54 | 13.06 | 7.75 | 12 | $D_2^5$ | 4.20 | | [239] |
| $NaNb_2O_5F$ | Tetragonal | 12.355 | | 3.943 | 5 | $D_{4h}^5$ | 4.24 | | [240] |
| $KNb_2O_5F$ | Tetragonal | 12.632 | | 3.950 | 5 | $D_{4h}^5$ | 4.29 | 4.26 | [241, 242] |
| $KTa_2O_5F$ | Tetragonal | 12.569 | | 3.961 | 5 | $D_{4h}^5$ | 6.56 | 6.6 | [241] |
| $K_{0.4}NbO_{2.4}F_{0.6}$ | Tetragonal | 12.586 | | 3.917 | 10 | $D_{4h}^5$ | 4.24 | 4.22 | [242] |
| $K_{0.6}NbO_{2.6}F_{0.4}$ | Tetragonal | 12.642 | | 3.952 | 10 | $D_{4h}^5$ | 4.35 | 4.34 | [242] |
| $K_3Nb_5O_{13}F_2$ | Tetragonal | 12.60 | | 3.95 | 2 | $D_{4h}^5$ | 4.37 | 4.25 | [139, 242] |
| $Na_3Ta_5O_{13}F_2$ | Tetragonal | 12.343 | | 3.918 | 2 | $D_{4h}^5$ | 7.84 | 7.26 | [243] |
| $K_{0.4}TaO_{2.4}F_{0.6}$ | Tetragonal | 12.50 | | 3.94 | 10 | $D_{4h}^5$ | 7.04 | 6.98 | [244] |

Fourgnet, Plet and Pape [238] obtained $AgNb_2O_5F$ while investigating phases formed in an $NbO_2F$ – $AgNbO_3$ system. This compound can also be represented by the general formula $Ag_xNbO_{2+x}F_{1-x}$. When $0 < x < 0.25$, solid solutions based on $NbO_2F$ are formed. The solid solutions are characterized by perovskite-type structures, and the cell parameter increases linearly from 3.901 to 3.916 Å, with the increase in x.

When $0.4 < x < 0.53$, an orthorhombic phase is observed in the $Ag_xNbO_{2+x}F_{1-x}$ system. This phase undergoes a phase transition at 900°C that leads to the formation of a tetragonal phase, which crystallizes in a tetragonal tungsten bronze-type structure with cell parameters: a = 12.343 and c = 3.905 Å. When $0.82 < x < 1$, solid solutions based on $AgNbO_3$ were found, which crystallize in a perovskite-type structure.

The compound $K_{0.3}NbF_3$ has an average niobium valency of 2.7 and forms a crystal structure that is referred to as hexagonal tungsten bronze [239].

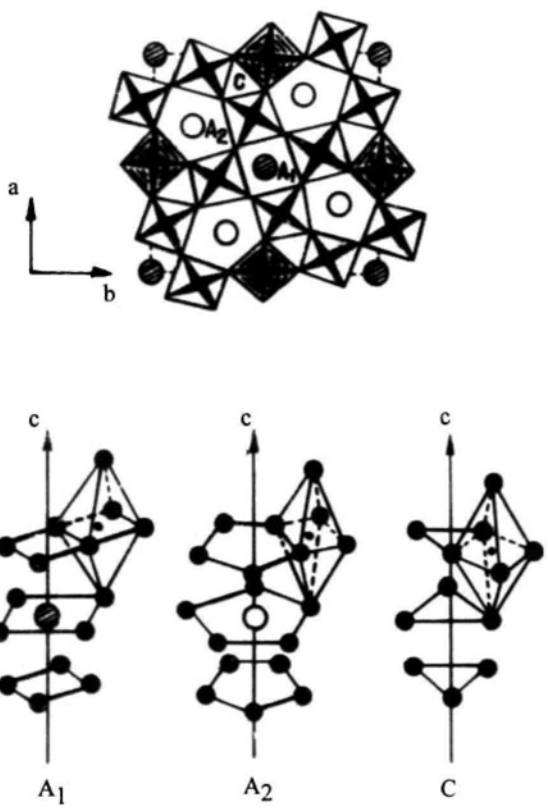


*Fig. 40. Structure of $M_xMeO_{2+x}F_{1-x}$ type compounds – tetragonal tungsten bronze- type structure.*

Another group of compounds with the general formula $M_xMeO_{2+x}F_{1-x}$ crystallizes in a manner similar to a tetragonal tungsten bronze structure [240-244]. In this case, $Me(O,F)_6$ octahedrons are linked by shared vertexes, forming tri-, quadra- and pentagonal chains. Alkali metal occurs in the two last chains. Fig. 40 shows the structure of $M_xMeO_{2+x}F_{1-x}$.

Magneli [245] reported on alkali metal oxyfluoroniobates that crystallize in a hexagonal tungsten bronze-type structure. Typical to this group is the compound $K_{0.25}NbO_{2.25}F_{0.75}$. The compound crystallizes in hexagonal syngony – space group $P6_3/mcm$ ($D^3_{6h}$), Z = 6, and its cell parameters are: a = 7.543 and c = 7.760 Å. The crystal structure is made up of $Nb(O,F)_6$ octahedrons that are linked via their vertexes to form hexagonal rings. The rings are connected to form hexagonal channels that contain potassium atoms.

Solid solutions, $Li_{1-x}MeO_{3-x}F_x$, where Me = Nb or Ta, are formed in the $LiMeO_3$ – $MeO_2F$ system and crystallize in a pseudo-ilmenite, $LiNbO_3$ type structure, as reported by Guelin, Ravez and Hagenmuller [246].

Lithium dioxyfluoroniobate (IV), $LiNbO_2F$, also has a $LiNbO_3$-type crystal structure, while dioxyfluoroniobates of sodium and potassium, $NaNbO_2F$ and $KNbO_2F$, crystallize in a perovskite-type structure [247].

There are two ways to further reduce the X:Me ratio to a value lower than 3. The first is to arrange simple similar to coordination type structure that requests steric similarity of all cations so as to be able to occupy octahedral voids. This method will be discussed separately. The second way is to arrange the linking of the octahedrons so as to render additional structural elements, namely pentagonal "blocks".

Table 36 presents structural characteristics of oxyfluoride compounds with X:Me < 3.

Two structural modifications are known for $Me_3O_7F$ compounds (Me = Nb or Ta), namely low-density and high-density phases, $Nb_3O_7F$ and $\alpha Ta_3O_7F$ or $\beta Ta_3O_7F$, respectively [192, 248-250].

The structure of $Nb_3O_7F$ (low density) consists of $ReO_3$ type blocks connected via their sides to form infinite layers. The layers are arranged along the b and c axes and have a certain thickness along each axis. Compounds $Nb_3O_7F$ (high density) and $\alpha Ta_3O_7F$ have similar crystal structure and are composed of tetragonal bi-pyramids linked via their sides to form chains. The connection between chains is achieved via common vertexes of the bi-pyramids. $MeX_6$ octahedrons are located in the voids between the chains. The same types of layers are observed in the structure of $\beta U_3O_8$.

*Table 36. Structural characteristics of compounds having X:Me < 3.*

| Compound | Syngony | Cell parameters, Å a | b | c | β° | Z | Space group | Density ρ, g/cm³ Calculated | Measured | Reference |
|---|---|---|---|---|---|---|---|---|---|---|
| $Nb_3O_7F$ | Orthorhombic | 20.67 | 3.833 | 3.927 | | 2 | $D_{2h}^{19}$ | 4.37 | 4.27 | [248] |
| $Nb_3O_7F$ (hi density) | Orthorhombic | 6.475 | 10.514 | 3.927 | | 2 | | 5.09 | | [249] |
| $\alpha Ta_3O_7F$ | Orthorhombic | 6.478 | 10.496 | 3.907 | | 2 | | 8.42 | | [250] |
| $\beta Ta_3O_7F$ | Orthorhombic | 16.690 | 3.935 | 8.915 | | 2 | | 7.64 | 7.64 | [192] |
| $Nb_{59}O_{147}F$ | Monoclinic | 73.29 | 3.828 | 21.17 | 104,29 | | | | | [251] |
| $Nb_{31}O_{77}F$ | Monoclinic | 37.54 | 3.832 | 21.18 | 91.92 | | | | | [251] |
| $Nb_{65}O_{161}F_3$ | Monoclinic | 81.16 | 3.829 | 21.15 | 103.97 | | | | | [251] |
| $Nb_{34}O_{84}F_2$ | Monoclinic | 21.09 | 3.827 | 23.02 | 116.22 | | | | | [251] |
| $LiNb_6O_{15}F$ | Orthorhombic | 16.635 | 3.964 | 8.888 | | 2 | | 4.66 | | [252] |
| $LiTa_6O_{15}F$ | Orthorhombic | 16.680 | 3.915 | 8.930 | | 2 | | 7.65 | 7.59 | [253] |
| $NaNb_6O_{15}F$ | Orthorhombic | 3.949 | 10.192 | 14.721 | | 2 | | 4.70 | | [254] |
| $NaTa_6O_{15}F$ | Orthorhombic | 3.912 | 10.204 | 14.776 | | 2 | | 7.70 | 7.50 | [91] |
| $Cu_{0.6}Nb_6O_{14.6}F_{1.4}$ | Orthorhombic | 16.772 | 3.876 | 8.973 | | 2 | $D_{2h}^{5}$ | 4.84 | | [255] |
| $KNb_4O_{10}F$ | Tetragonal | 12.4605 | | 3.9606 | | 2 | | 4.55 | 4.49 | [242] |
| $KNb_6O_{15}F$ | Tetragonal | 17.786 | | 3.9629 | | 4 | | 4.58 | 4.61 | [242] |
| | Orthorhombic | 17.532 | 17.707 | 3.9663 | | 4 | | 4.61 | | [256] |
| $Na_3Nb_{12}O_{31}F$ | Tetragonal | 17.494 | | 3.9442 | | | $C_4^1$ | | | [257] |
| $K_3Nb_{12}O_{31}F$ | Tetragonal | 12.4927 | | 3.9656 | | | | | | [256] |
| $KNb_{12}O_{29}F_3$ | Tetragonal | 17.5939 | | 3.9473 | | | | | | [256] |

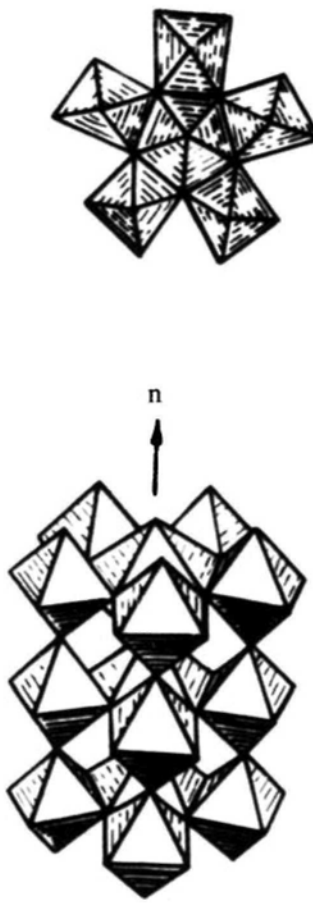


*Fig. 41. Structure of basic $Me_6(O,F)_{27}$ block (top) and of $[Me_6(O,F)_{21}]_n$ cluster (bottom).*

Formation of $Me_6(O,F)_{27}$-type blocks is typical of compounds $\beta Ta_3O_7F$, $Nb_{59}O_{147}F$, $Nb_{31}O_{77}F$, $Nb_{65}O_{161}F_3$, $Nb_{34}O_{84}F_2$, $MMe_6O_{15}F$ (M = Li, Na; Me = Nb, Ta) and $Cu_{0.6}Nb_6O_{14.6}F_{1.4}$ –[91, 192, 242, 251-255]. The blocks are arranged in $[M_6(O,F)_{21}]_n$ clusters. The arrangement of octahedrons into blocks and subsequently into clusters is shown in Fig. 41.

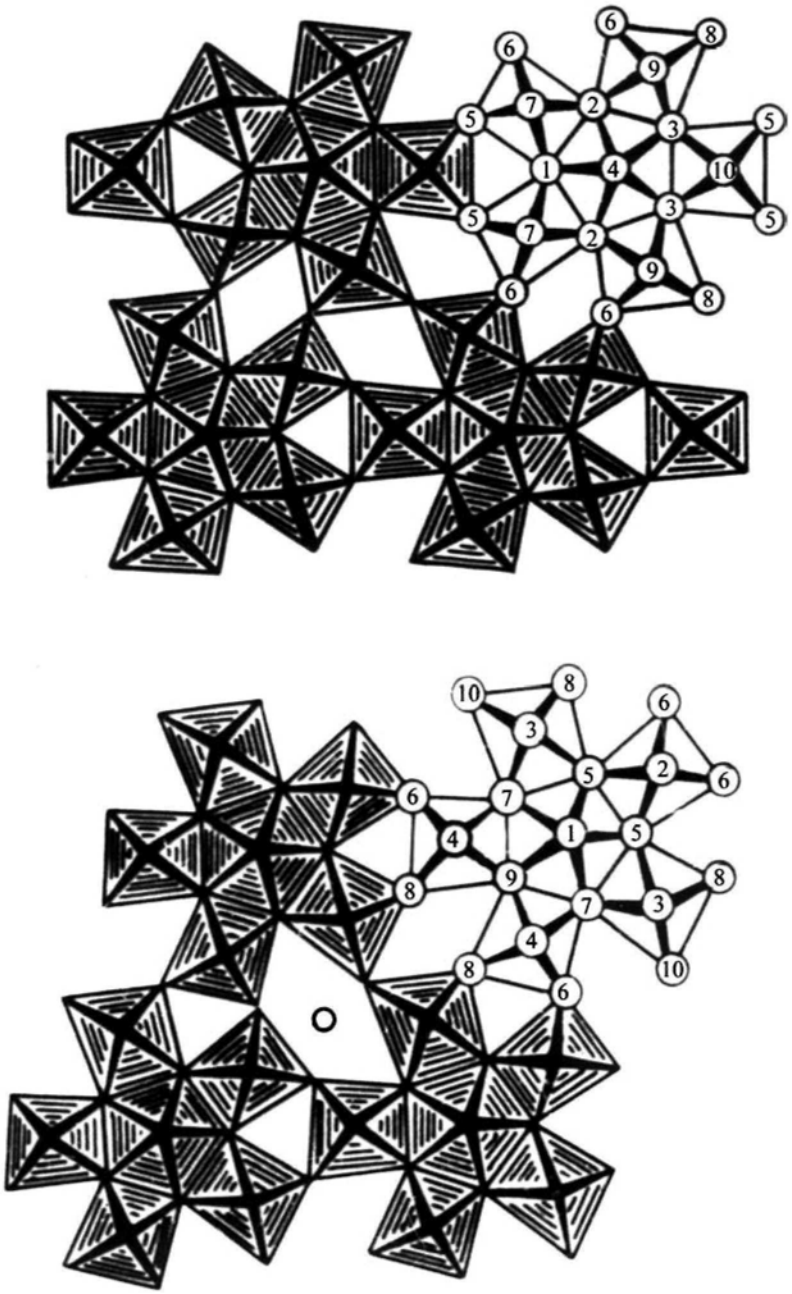

*Fig. 42. Structure of $LiTa_6O_{15}F$ (top) and of $NaTa_6O_{15}F$ (bottom) (after Chaminade, Pouhard, Hagenmuller [91]).*

The main differences between the structures of the above compounds are related to the alkali metals that they contain. For instance, $\beta Ta_3O_7F$ and $LiTa_6O_{15}F$ have a similar crystal structure, but in the former, the voids between the basic blocks are empty, whereas in the latter, lithium atoms occupy the voids. Moving to sodium-containing compounds $NaTa_6O_{15}F$ and $NaNb_6O_{15}F$ requires the rearrangement of the connected $[Me_6(O,F)_{21}]_n$ clusters to allow for the presence of the larger sodium ions in the structural voids. Fig. 42 shows the arrangement of the clusters for $LiTa_6O_{15}F$ and $NaTa_6O_{15}F$.

The variation that exists in the O:F ratio of $MMe_6O_{15}F$-type compounds enables isomorphic replacement of alkali metal cations by other cations with appropriate radii. For instance, a copper-containing compound, $Cu_{0.6}Nb_6O_{14.6}F_{1.4}$, which crystallizes in a $LiNb_6O_{15}F$ type structure, was obtained [255].

The presence of cations that have ionic radii greater than that of sodium ion, $Na^+$, leads to the formation of clusters that are connected via additional individual octahedrons in such a way that the number of large pentagonal voids is increased. This tendency leads to the formation of tetragonal tungsten bronze crystal structures [242, 256]. The same type of structure is also formed when the increase in the number of alkali metal cations includes an increase in the number of niobium cations in the compound. Hence, when progressing from $NaNb_6O_{15}F$ to $Na_3Nb_{12}O_{31}F$ [257] (in which X:Me = 2.67, in both cases), the structure of $NaNb_6O_{15}F$ undergoes transformation into a tetragonal tungsten bronze structure.

One difficulty that exists in the crystal chemistry of oxyfluorides is the distinguishing of oxygen and fluorine in their structures. In most of the cases discussed above, X–ray measurements do not provide information on oxygen and fluorine positions. Some additional information on the possible character of the cation/anion surroundings can be obtained using Pauling's valence bond method of calculation. Calculations of the valence bonds were performed for some fluoride and oxyfluoride compounds [258]. The results of calculations made for niobium- and tantalum-containing compounds show the tendency of fluorine ions to be located at the polyhedrons' vertexes, with the lowest rate of sharing with the different central atoms. For instance, in $CuNbO_3F$ and $Na_2Ta_2O_5F_2$ (II), the fluorine ions occupy the position of the terminal ligand, and in the case of $LiNb_6O_{15}F$ and $NaNb_6O_{15}F$, fluorine ions appear mostly at the vertexes of the basic blocks.

## 3.5. Compounds with coordination-type structures

The steric similarity of oxygen and fluorine ions enables the formation of coordination-type structures in some tantalum and niobium oxyfluoride compounds.

The lowest coordination number of tantalum or niobium permitted by crystal chemistry formalism is 6, which corresponds to an octahedral configuration. X:Me ratios that equal 3, 2 or 1 can, therefore, be obtained by corresponding substitutions in the cationic sub-lattice. A condition for such substitution is no doubt steric similarity between the second cation and the tantalum or niobium ion so as to enable its replacement in the octahedral polyhedron. In such cases, the structure of the compound consists of oxyfluoride octahedrons that are linked by their vertexes, sides or faces, according to the compound type, $MeX_3$, $MeX_2$ or MeX respectively. Table 37 lists compounds that have a coordination-type structure [259-261].

Typical examples of compounds with a coordination-type structure are $NbO_2F$ and $TaO_2F$, which crystallize in a $ReO_3$ type structure [233, 243]. Oxygen and fluorine ions are statistically distributed in the anionic sub-lattice. The compounds are characterized by X:Me = 3 and can be described as $MeX_3$ type compounds.

*Table 37. Fluoride and oxyfluoride compounds with coordination-type structures*

| X:Me | Compound | Structure type |
|---|---|---|
| 3 | $NbO_2F$; $TaO_2F$ | $ReO_3$ |
| | $LiTaF_6$; $LiNbF_6$ | $AlF_3$ |
| | $MNbOF_5$ (M = Co, Ni, Cu) | $ReO_3$ (distorted) |
| 2 | $M_{1.5}Nb_{1.5}O_{5.5}F_{0.5}$ (M = Mn, Co, Fe) | $\alpha PbO_2$ |
| | $M_2NbO_3F_3$ (M = Co, Ni, Cu) | Rutile |
| | $M_2NbO_5F$ (M = Ti, V, Cr) | Rutile (Tri-rutile) |
| 1 | $Li_4TaO_4F$; $Li_4NbO_4F$ | NaCl |

Other examples of compounds that are considered $MeX_3$-type compounds are lithium hexafluorotantalate (-niobate), $LiTaF_6$ and $LiTaF_6$, which have crystal structures similar to $AlF_3$. Both lithium and tantalum (niobium) cations have similar ionic radii and are located in the centers of octahedrons that are composed of fluorine anions.

$CoNbOF_5$ [129] can also be considered an $MeX_3$ type compound due to the steric similarity of cobalt and niobium ions. This compound crystallizes in tetragonal syngony with cell parameters: a = 7.81 and c = 9.02 Å (Z = 4; ρ = 3.19 g/cm$^3$), and can be considered to have a distorted cubic $ReO_3$ structure. Both cobalt and niobium occur in the center of oxyfluoride octahedrons that are linked via their vertexes.

Table 38 presents structural parameters of $MeX_2$-type compounds.

Compounds of the general form $M_{1.5}Nb_{1.5}O_{5.5}F_{0.5}$, where M = Mn, Co, Fe, were obtained by Senegas and Galy while investigating solid solutions in $FeNbO_{4-x}F_x$, $MnNb_{2-x}O_{6-x}F_x$ and $CoNb_{2-x}O_{6-x}F_x$ systems [262]. It was determined that the compounds crystallize in a structure similar to an $\alpha PbO_2$-type structure. Cations are situated within octahedrons that are linked via their sides i.e. by sharing of two adjacent angles.

$Co_2NbO_3F_3$ was obtained as a result of the thermal treatment of $CoNbOF_5$, predominantly prepared by the hydrofluoride method [129]. This compound crystallizes in a rutile-type structure that can be achieved due to the statistical distribution of cations within the oxyfluoride octahedrons.

Senegas and Galy obtained the same type of structure for $Ni_2NbO_3F_3$, while investigating solid solutions in a $NiF_2 - NiNb_2O_6$ system [263]. Niobium and nickel cations are randomly located in the oxyfluoride octahedrons, which are linked via their sides.

Oxyfluoroniobates, $M_2NbO_5F$, containing trivalent metals (where M = Ti, V, Cr) have the same type of structure [264], except for $Cr_2NbO_5F$, which has a tri-rutile type structure. This exception is related to the ordered, rather than statistical, distribution of chromium and niobium cations in the oxyfluoride octahedrons, which leads to a corresponding increase in cell parameter c.

In order to construct an MeX-type compound (X:Me = 1) using only octahedral elements, the octahedrons must be linked via their faces i.e. by sharing of three angles. This arrangement of the octahedral polyhedrons yields a rock-salt type structure (NaCl type structure).

*Table 38. Structural characteristics of $MeX_2$ type compounds.*

| Compound | Syngony | Cell parameters in Å: | | | Reference |
|---|---|---|---|---|---|
| | | a | b | c | |
| $Mn_{1.5}Nb_{1.5}O_{5.5}F_{0.5}$ | Orthorhombic | 14.402 | 5.676 | 5.074 | [262] |
| $Co_{1.5}Nb_{1.5}O_{5.5}F_{0.5}$ | Orthorhombic | 14.130 | 5.709 | 4.970 | [262] |
| $Fe_{1.5}Nb_{1.5}O_{5.5}F_{0.5}$ | Orthorhombic | 14.678 | 5.661 | 5.052 | [262] |
| $Co_2NbO_3F_3$ | Tetragonal | 4.65 | | 3.03 | [129] |
| $Ni_2NbO_3F_3$ | Tetragonal | 4.71 | | 3.07 | [263] |
| $Ti_2NbO_5F$ | Tetragonal | 4.703 | | 3.008 | [264] |
| $V_2NbO_5F$ | Tetragonal | 4.655 | | 3.032 | [264] |
| $Cr_2NbO_5F$ | Tetragonal | 4.700 | | 9.180 | [264] |

Crystal modifications of binary oxides of lithium and some tri- and tetravalent metals, with the general formulas $LiM^{III}O_2$ and $Li_2M^{IV}O_3$, having a rock-salt type structure with disordered cation arrangement, are known to exist and are described in [265, 266]. Appropriate thermal treatment of the compounds leads to the ordered entry of different cations to occupy certain positions. This disorder–order transition is accompanied by a structural transformation from the original cubic symmetry to a tetragonal symmetry, in most cases. Phases with rock-salt-type structures were also found for other lithium-containing compounds, such as $Li_3NbO_4$ [267, 268], $Li_3TaO_4$ [269-271], $Li_4MoO_5$ and $Li_4WO_5$ [272]. Some order in the cations alternation related to the compound's stoichiometry affects the cubic crystal lattice, lowering its symmetry down to a pseudo-tetragonal, monoclinic or triclinic structure. Nevertheless, after further and more precise investigation of the products obtained in the interaction between $LiTaO_3$ and $Li_2CO_3$, Roth identified the meta-stable cubic phase of $Li_3TaO_4$ [273]. This phase crystallizes in a rock-salt-type structure with disordered alternation of lithium and tantalum cations in the oxide octahedrons. Conformation of the statistical cation distribution is found not only in the crystallization of the $Li_3TaO_4$ phase in cubic syngony with a cell parameter of 4.2 Å, but also in the presence of relatively broad reflections in the X–ray powder diffraction pattern. Thermal treatment at a temperature higher than 800°C leads to the disappearance of this meta-stable

phase and to the formation of a stable, well-known modification with a crystal structure and polymorphism that are described in detail in publications [269-271].

In the case of lithium orthoniobate, $Li_3NbO_4$, no meta-stable phase was found that had a rock-salt crystal structure with disordered cation distribution [268]. Nevertheless, solid solutions $Li_{2+x}Ti_{1-4x}Nb_{3x}O_3$, where $0 < x \leq 0.22$, have a monoclinic structure at low temperatures and undergo transformation to a disordered NaCl type structure at high temperatures [274].

In the case of pure oxide compounds, a state of disordered cation distribution destabilizes by uniform anionic sub-lattice consists only oxygen anions. From this point of view, the isomorphic substitution of oxygen by fluorine ions, which have similar ionic radii, stabilizes the disordered meta-stable anionic/cationic arrangement of the compound crystal structure. Typical examples of oxyfluoride compounds that form relatively stable disordered crystal structures are $Li_4NbO_4F$ and $Li_4TaO_4F$, which are described in [260, 261, 275]. Table 39 lists the preparation conditions and parameters of oxyfluoride compounds with rock-salt-type structures. The table is based mostly on data published in [275]. Compounds $Li_4NbO_4F$ and $Li_4TaO_4F$ were prepared similarly to all other compounds mentioned, using no $NbO_2F$ or $TaO_2F$.

In all cases except $Li_3NbO_4$, phases similar to $Li_4NbO_4F$ and $Li_4TaO_4F$ were found. Pure binary oxides transform easily to modified structures characterized by ordered cation distribution, while oxyfluorides are more stable and require treatment at a high temperature, for an extended period of time, in order to be transformed into a state of ordered cation distribution.

Fig. 43 shows fragments of X–ray powder diffraction patterns of compounds with rock-salt-type structures.

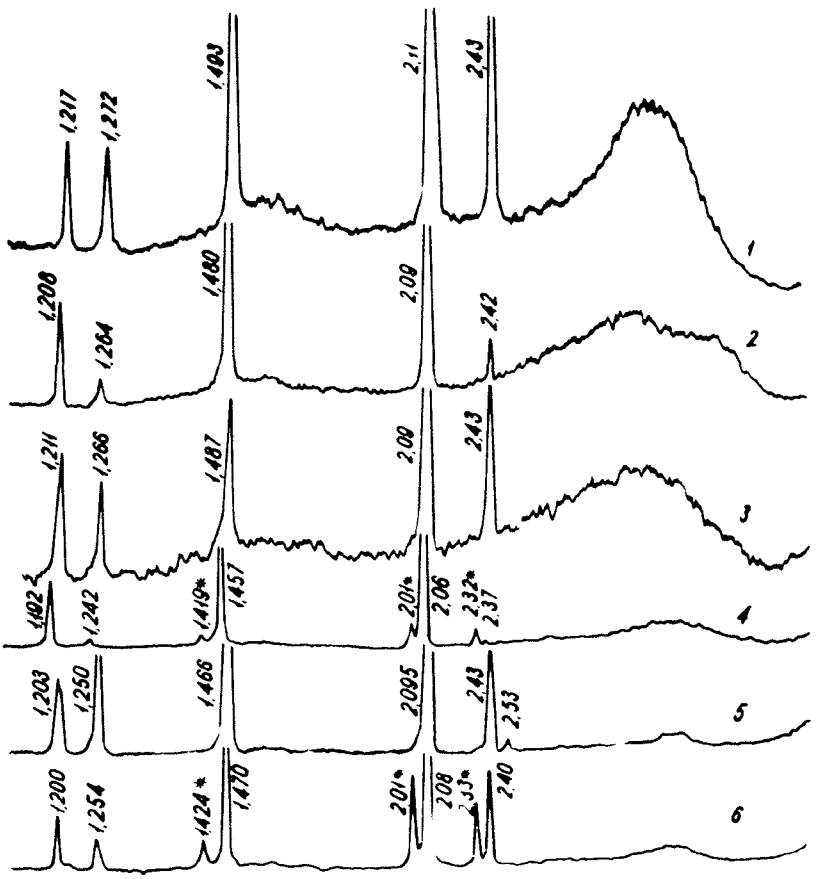


*Fig. 43. Fragments of X–ray powder diffraction patterns of compounds with rock-salt structures that underwent modification to a state of disordered ionic arrangement. 1 – $Li_3TaO_4$; 2 – $Li_4NbO_4F$; 3 – $Li_4TaO_4F$; 4 – $Li_3TiO_3F$; 5 – $Li_2FeO_2F$; 6 – LiNiOF (Reflections attributed to LiF are marked by an asterisk).*

*Reproduced from [275], A. I. Agulyansky, V. A. Bessonova, V. Y. Kuznetsov, V.T. Kalinnikov, Zh. Neorg. Khim. 31 (1986) 2683, Copyright 1986, with permission of "Nauka" (Russian Academy of Sciences) publishing.*

*Table 39. Synthesis conditions and modifications of compounds crystallizing in NaCl type structure (X:Me = 1).*

| Compound | Precursors | Synthesis Conditions | Type structure | Cell parameters (Å): a | c | Refractive Index |
|---|---|---|---|---|---|---|
| $Li_3TaO_4$ | $3Li_2CO_3 + Ta_2O_5$ | 700°C, 10 hours | NaCl | 4.22 | | |
| | | 900°C, 10 hours | $Li_3TaO_4$ | 6.01 | 16.67 | 1.933; 1.940 |
| $Li_3NbO_4$ | $3Li_2CO_3 + Nb_2O_5$ | 700°C, 10 hours | $Li_3NbO_4$ | 8.43 | | 1.951 |
| $Li_4NbO_4F$ | $3Li_2CO_3 + Nb_2O_5 + 2LiF$ | 800°C, 8 hours | NaCl | 4.19 | | 1.845 |
| | | 1100°C, 20 hours | $Li_3NbO_4$ | 8.42 | | 1.945 |
| $Li_4TaO_4F$ | $3Li_2CO_3 + Ta_2O_5 + 2LiF$ | 800°C, 8 hours | NaCl | 4.20 | | 1.785 |
| | | 1100°C, 10 hours | $Li_3TaO_4$ | 5.03 | 16.68 | 1.85; > 1.93 |
| $Li_3TiO_3F$ | $Li_2CO_3 + 2TiO_2 + LiF$ | 900-1100°C, 10 hours | NaCl | 4.12 | | > 2.06 |
| $Li_2FeO_2F$ | $Li_2CO_3 + Fe_2O_3 + 2LiF$ | 900-1100°C, 40 hours | NaCl | 4.18 | | > 2.06 |
| LiNiOF | LiF + NiO | 1000°C, 40 hours | NaCl | 4.16 | | |

In all cases, broad diffuse reflections are observed in the high interface distance range of X-ray powder diffraction patterns. The presence of such diffuse reflection is related to a high-order distortion in the crystal structure. The intensity of the diffuse reflections drops, the closer the valencies of the cations contained in the compound are. Such compounds characterizing by similar type of crystal structure also have approximately the same type of IR absorption spectra [261]. Compounds with rock-salt-type structures with disordered ion distributions display a practically continuous absorption in the range of 900–400 $cm^{-1}$ (see Fig. 44, curves 1 – 4). However, the transition into a tetragonal phase or cubic modification, characterized by the entry of the ions into certain positions in the compound, generates discrete bands in the IR absorption spectra (see Fig. 44, curves 5 – 8).

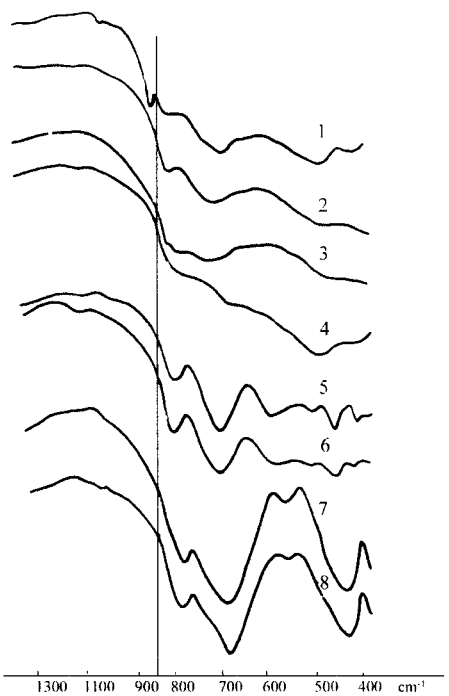


*Fig. 44. IR absorption spectra of $Li_3TaO_4$ (1), $Li_4TaO_4F$ (2), $Li_4NbO_4F$ (3), $Li_3TiO_3F$ (4) – rock-salt-type structures with disordered ionic arrangement and high-temperature modifications of $Li_3TaO_4$ (5), $Li_4TaO_4F$ (6), $Li_3NbO_4$ (7), $Li_4NbO_4F$ (8).*

*Reproduced from [261], V. T. Kalinnikov, A. I. Agulyamsky, Jap. J. Appl. Phys. 24 (1985) 628, Copyright 1985, with permission of Institute of Pure and Applied Physics, Tokyo, Japan.*

## 3.6. Crystal chemical classification

As mentioned earlier, the main distinction of compounds formed in the M – Ta (Nb) – O – F system stems from the steric similarity between tantalum and niobium ions on the one hand, and oxygen and fluorine ions on the other hand. The ratio between the ionic radii of niobium (tantalum) and oxygen (fluorine) leads to a metal coordination number of 6, which is typical for a significant number of acido ligands [276]. In a homological sequence of compounds of the $MNb(Ta)F_{6+2x}O_x$ type, the structure depends on the ratio between the number of anions (oxygen and fluorine) and the number of cations (tantalum/niobium), assuming that the valence of the metal remains unchanged. Subsequent substitution of fluorine by oxygen lowers this ratio. Lowering the X:Me ratio to a value less than 6 requires sharing of ligands in order to achieve coordination saturation while maintaining an octahedral configuration. This leads to the formation of chains, layers and in turn to a framework-type structure. Table 40 illustrates the crystal structure of compounds versus X:Me (Me = Nb or Ta) ratio.

The basis of the crystal chemical classification of tantalum and niobium fluoride compounds was first formulated by Kuznetzov and Rogachov [232]. The main tenets of the classification are as follows:

1) Reduction of X:Me from 8 to 6 leads to a reduction of the metal coordination number from 8 to 6, respectively, and to the formation of octahedrons (distorted octahedrons) as a basic unit.
2) Further reduction of X:Me brings about no change in the coordination number but leads to a sharing of ligands. This results in the linkage of octahedrons into chains and rings (X:Me = 5), double chains (X:Me = 4.5), layers (X:Me = 4 – 3.25) and a framework structure (X:Me = 3.25 – 3).
3) When X:Me < 3, some anions are shared by three metal atoms, which in turn leads to the formation of blocks.

The formulated principals correlating crystal structure features with the X:Nb(Ta) ratio do not take into account the impact of the second cation. Nevertheless, substitution of a second cation in compounds of similar types can change the character of the bonds within complex ions. Specifically, the decrease in the ionic radius of the second (outer-sphere) cation leads not only to a decrease in its coordination number but also to a decrease in the ionic bond component of the complex [277].

*Table 40. Structural changes versus X:Me ratio.*

| X:Me | Typical Compound | Features of crystal structure | Notes |
|---|---|---|---|
| 8 | $Na_3TaF_8$ | Isolated complexes $TaF_8^{3-}$ | Similar compounds with K, Rb, Cs, Tl and Nb are known. |
| 7 | $K_2TaF_7$<br>$K_2NbF_7$ | Isolated complexes $TaF_7^{2-}$ | $M_2Nb(Ta)F_7$ are all isostructural except for $Li_2NbF_7$. |
| | $K_3NbOF_6$<br>$K_3TaOF_6$ | Isolated complexes $NbOF_6^{3-}$ or $TaOF_6^{3-}$ | Known compounds are isostructural. |
| 6 | $KTaF_6$<br>$KNbF_6$ | Isolated complexes $TaF_6^-$ or $NbF_6^-$ | $LiNb(Ta)F_6$ crystallizes in a $LiSbF_6$ type structure. All cations are located in octahedral voids. |
| | $K_2NbOF_5$ | Isolated complexes $NbOF_5^{2-}$ | $Li_2NbOF_5$ is composed of (O,F) linked octahedrons. |
| | $K_3TaO_2F_4$ | Isolated complexes $TaO_2F_4^{3-}$ | Niobium analogues with K, Rb or Cs have similar structure. |
| 5 | $NbF_5$ | Four-folded rings of $NbF_6^-$ octahedrons | No outer-sphere cation, rings are linked via Van der Waals forces only, low melting point, low stability. |
| | $NH_4NbOF_4$ | Infinite chains of octahedrons – $NbO_2F_4^{3-}$ | $MNbOF_4$ (M=K, Rb, Cs) refers also to a chain-type structure. |
| 4.5 | $K_2Ta_2O_3F_6$ | Binary chains | Zig-zag shape |
| 4 | $NaNb(Ta)O_2F_2$<br>$K_2Nb(Ta)O_3F$ | Layers of octahedrons | $Nb(Ta)O_4F_2$ octahedrons are linked via vertexes. |
| 3.5 | $Na_2Nb_2O_5F_2$ | Linear layers | Linkage via octahedrons |
| 3 | $Nb(Ta)O_2F$ | Framework | $ReO_3$ type structure |
| 2.67 | $Nb_3(Ta_3)O_7F$ | Basic blocks | Metal ions located in pentagonal bi-pyramid void |
| 2 | $Co_2NbO_3F_3$ | Framework | Rutile-type structure |
| 1 | $Li_4Nb(Ta)O_4F$ | Framework | Rock-salt type structure |

According to the above classification, the structures of $LiNb(Ta)F_6$ and $Li_2Nb(Ta)OF_5$ should be composed of lithium cations and isolated octahedral complex ions, $Nb(Ta)F_6^-$ or $Nb(Ta)OF_5^{2-}$, respectively. It is known, however, that the structure of these compounds consists only of octahedrons linked via their vertexes in the first case, and via their sides in the second case. The same behavior is observed in compounds containing bi- and trivalent metals.

Compounds of the same stoichiometry type usually have the same type crystal structure within the row of alkali metals K – Rb – Cs; rarely the same type structure with sodium-containing analogues; and never crystallize similarly with lithium-containing compounds. The crystal structure analysis of different fluoride and oxyfluoride compounds clearly indicates that the steric similarity between all cations and tantalum or niobium must be taken into account when calculating the X:Me ratio.

More developed principals of classification were formulated in [278]. The central point of the classification can be formulated as follows:
*The structure of the crystal has a tendency to utilize steric similarity of its component ions and is defined by the number of anions (oxygen and fluorine) per cation in each oxyfluoride octahedron.*

The affinity of different cations to the octahedral coordination can be estimated based on the Octahedral Site Preference Energy [279-281]. The above-defined ratio characterizes the way in which the octahedrons are linked [282]. Table 41 illustrates the correlation between the value of the X:Me ratio and the way in which the octahedrons are linked.

The family of coordination-type compounds contains only compounds with ions that can occupy octahedral positions. It is obvious that the X:Me ratio for this type of compound cannot be greater than 3.

In its finalized version, the classification of tantalum and niobium fluoride compounds can be presented as shown in Table 42 and formulated as follows:

1) The type of crystal structure depends on the ratio X:Me, where X is the total number of anions (oxygen and fluorine) and Me is the total number of all cations that can fit into/occupy octahedral voids (tantalum, niobium, lithium and other metals with similar ionic radii).
2) When $8 \leq X:Me \leq 6$ the structure remains an island-type structure with a respective increase in the coordination number.
3) When $6 < X:Me \leq 3$ the structure consists of chains (5), double chains (4.5), layers (4) or a framework structure (3).

4) When X:Me ≤ 3 two possibilities exist: coordination-type structure (3, 2, 1) or blocks (2.67), when the stoichiometry of the compounds does not correspond to the formation of any coordination- type compound.

*Table 41. Structural features and octahedron linkage for different X:Me ratios.*

| X:Me | Compound type | Form of polyhedron linkage |
|---|---|---|
| | | **Isolated complexes:** |
| 8 | $M_3MeF_8$ | $MeF_8^{3-}$ |
| 7 | $M_2MeF_7$ | $MeF_7^{2-}$ |
| | $M_3MeOF_6$ | $MeOF_6^{3-}$ |
| 6 | $MMeF_6$ | $MeF_6^{-}$ |
| | $M_2MeOF_5$ | $MeOF_5^{2-}$ |
| | $M_3MeO_2F_4$ | $MeO_2F_4^{3-}$ |
| | | **Linkage of octahedrons into:** |
| 5 | $MMeOF_4$ | Chains with fragments – $(MeOF_4^{-})_n$ |
| | $M_2MeO_2F_3$ | Chains with fragments – $(MeO_2F_3^{2-})_n$ |
| 4.5 | $M_2Me_2O_3F_6$ | Double chains |
| 4 | $MMeO_2F_2$ | Layers |
| | $M_2MeO_3F$ | Layers |
| 3 | $M_xMeO_{2+x}F_{1-x}$ | Framework structure |
| | | **Coordination-type structures:** |
| 3 | $MeO_2F$ | Shared vertexes – $MeX_3$ |
| | $LiMeF_6$ | |
| | $M^{II}MeOF_5$ | |
| 2 | $LiMeO_2F_2$ | Shared sides – $MeX_2$ |
| | $M^{II}MeO_3F_3$ | |
| | $M^{III}MeO_5F$ | |
| 1 | $Li_4MeO_4F$ | Shared faces – MeX |

*Table 42. General classification of tantalum and niobium fluoride compounds*

| X:Me | Second cation present, with coordination number greater than 6 (second cation's ionic radius > tantalum/niobium ionic radius) | Only cations that can fit into/occupy octahedral voids are present (second cation's ionic radius ≈ tantalum/niobium ionic radius) |
|---|---|---|
| ≥ 6 | Island-type structure | The compounds either do not exist or exist under very limited conditions (have low stability, low melting and boiling points, etc.) |
| from 5 to 4 | Chain-type structure | |
| from 4 to 3 | Layer-type structure | |
| ≤ 3 | Framework-type structure (Perovskite, pyrochlore, tungsten bronze etc.) | Coordination-type structure ($ReO_3$, $TiO_2$, $\alpha PbO_2$, NaCl etc.) |

The main condition for the formation of stable compounds with island-, chain- and layer-type structures (X:Me > 3) is the presence of a second cation (or cations) that is unable to occupy the oxyfluoride octahedral polyhedron. The ionic radius of the cation must be significantly greater than that of tantalum or niobium in order to ensure a coordination number higher than 6. In compounds with X:Me > 6, complete linkage of all octahedrons cannot be achieved. When no second cations with coordination numbers higher 6 are present, the linkage between the structural elements is performed by Van der Waals interactions only. Such compounds usually have low thermal stability, low melting and boiling points and can be prepared and stored only under very special and limited conditions. Several compounds are known to exist, which have X:Me > 3 and contain no large, second cation: Nb(Ta) $OF_3$, Nb(Ta)$F_5$, $Ag(NbF_6)_2$ and others.

The formation of compounds of the MeX, $MeX_2$ and $MeX_3$ types is also limited by the ionic radii of the second cations and by the formal stoichiometry of the compound. For instance, it is obvious that compounds of the MeX type cannot be obtained using polyvalent second cations, while $MeX_3$ cannot be obtained using tetravalent cations (see Table 43).

Thus, the formulated classification allows for the definition of the compound's crystal structure type based on its composition. In this process, the most important stage is the correct definition of the X:Me ratio.

Vibration spectra of fluoride and oxyfuoride compounds correspond to X:Me ratios, especially in the case of island-type structure compounds. Analysis of IR absorption spectra provides additional indication of the coordination number of the central atom. Fig. 45 shows the dependence on the X:Me ratio of the most intensive IR bands, which correspond to asymmetric Me-F modes in fluoride complexes, as well as ν(Me=O) and ν(Me-F) in oxyfluoride complexes. Wave numbers of $TaF_5$, $NbF_5$ and $NbOF_3$ IR spectra were taken from [283-286].

*Table 43. Binary systems that can be used for the synthesis of MeX, $MeX_2$ and $MeX_3$ type compounds (Me = A + B; X = O + F).*

| Compound | $A^+$ | $A^{2+}$ | $A^{3+}$ | $A^{4+}$ |
|---|---|---|---|---|
| MeX | $LiF - Li_3BO_4$ | n/a | n/a | n/a |
| $MeX_2$ | $Li_3BF_8 - LiB_3O_8$ | $AF_2 - AB_2O_6$ | $AOF - ABO_4$ | n/a |
| $MeX_3$ | $LiBF_6 - BO_2F$ | $A_2BF_9 - BO_2F$ | $AF_3 - BO_2F$ | $AOF_2 - BO_2F$ |
| | | $A^{2+}$ = Mg, Ni, Fe, Co, Cu, Ge | $A^{3+}$ = Ti, V, Mn, Fe, Cr, Al | $A^{4+}$ = Ti, V, Zr, Mn, Cr, |

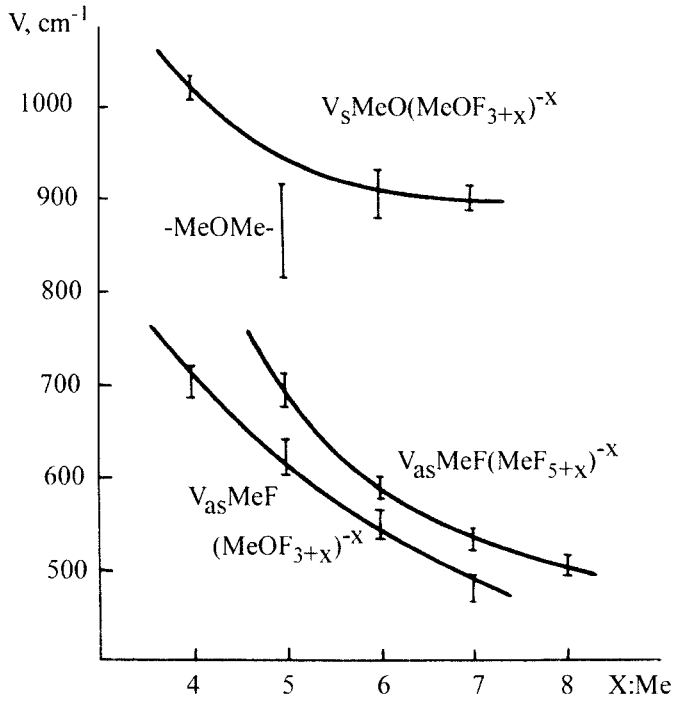


*Fig. 45. Wave numbers of MeO and MeF vibrations in $MeF_{5+x}^{x-}$ and $MeOF_{3+x}^{x-}$ complexes (Me = Nb, Ta) versus X:Me (X = O, F).*

An increase in the coordination number of the central atom leads to a systematic decrease in the wave numbers that correspond to the expected behavior of valence vibrations. [287]. In general terms, increasing the coordination number extends the bond length in the complex, which in turn reduces the force constant of the bond. In the case of $MMeOF_4$ type compounds, the ν(MeO) wave number seems to be incompatibly lower than expected. This drop is related to the linking of octahedrons to form $(MeOF_4)_n^-$ chains via shared oxygen atoms. The bridging action of the oxygen leads to additional attenuation of NbO bond strength.

Changes in the charge of the central atom also strongly affect the metal–ligand bond length and the ionic–covalent share in fluoride complexes, which in turn impact the vibration spectra. Fig. 46 shows the dependence of asymmetric valence vibrations on the charge of the central atom. The spectral data for Mo, W, Zr, Hf fluoride compounds were taken from [71, 115, 137].

Very slight changes in wave numbers observed when moving within the same group, from Mo to W, from Nb to Ta and from Zr to Hf (see Fig. 46), indicate that the contribution of the change in the central atom's mass is compensated for by respective changes in the metal–ligand force constant.

The high stability of fluoride complexes maintains the configuration and vibration parameters of different compounds in various media. This special feature enables clear distinguishing of different complex ion types using vibration spectroscopy in solid, liquid and molten media.

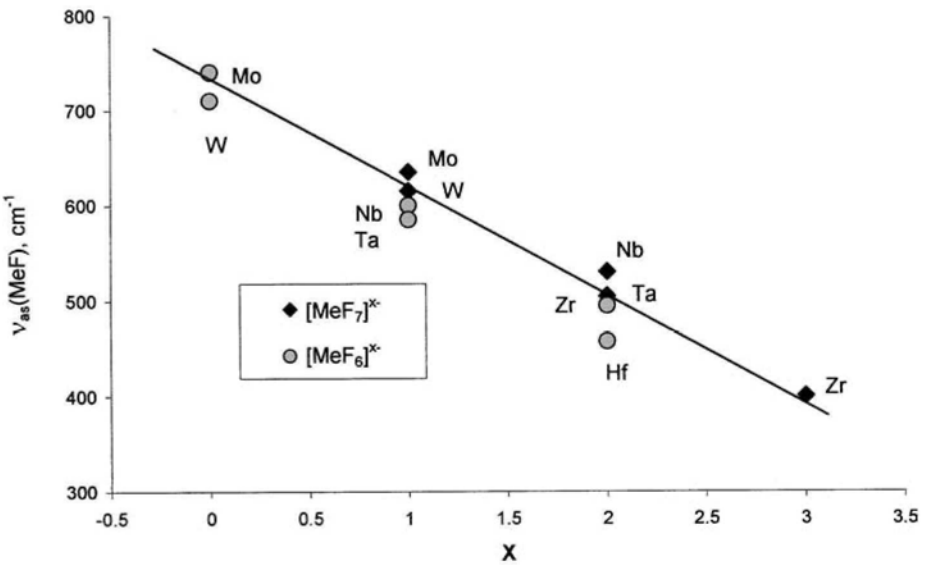


*Fig. 46. Dependence of asymmetric vibration modes (νMeF) in hexa- and heptafluorometalate complexes on the charge of the central ion.*

This Page Intentionally Left Blank

# 4.

# TANTALUM AND NIOBIUM COMPLEXES IN FLUORIDE SOLUTIONS

The fact that tantalum and niobium complexes form in fluoride solutions not only supplements fundamental data on the coordination chemistry of fluoride compounds, but also has a broad practical importance. This type of solution is widely used in the technology of tantalum and niobium compounds in raw material digestion, liquid-liquid extraction, precipitation and re-pulping of hydroxides, and in the crystallization and re-crystallization of K–salts and other complex fluoride compounds.

NMR, Raman and IR spectroscopy are most frequently used to investigate the complex structures of fluoride solutions containing tantalum and niobium. Most investigations of such solutions were performed on the liquid-liquid extraction of tantalum and niobium, with the objective of describing the mechanism of the process. These publications will be discussed separately.

This chapter focuses on tantalum and niobium fluoride complex ions that occur in solutions containing hydrofluoric acid.

## 4.1. Niobium-containing solutions

Based on a comprehensive investigation of solubility isotherms and of conductometric and potentiometric titration in the $NbF_5 - HF - H_2O$ system, Nicolaev and Buslaev [288] concluded that $H_2NbOF_5$ is the predominant niobium-containing form present in such solutions.

Raman spectra of fluoride solutions containing niobium were investigated by Keller [171]. Solutions were prepared by dissolving niobium fluoride compounds in solutions of hydrofluoride acid, HF, of different concentrations.

Two types of solutions were investigated. The first type of solution was prepared by dissolving $K_2NbOF_5 \cdot H_2O$ in water and the second type was obtained by dissolving $K_2NbF_7$ in 1-50% hydrofluoride acid solutions. Comparative analysis of Raman spectra of the solutions and of spectra obtained for solid $K_2NbOF_5 \cdot H_2O$ and $CsNbF_6$ compounds showed that niobium is present in the above solutions in the form of $NbOF_5^{2-}$ and $NbF_6^-$ complex ions. In addition, the researchers mentioned that no $NbF_7^{2-}$ complex was found in the solutions investigated.

The type of complex present in each solution depends on the acidity of the solution. In particular, HF solutions with concentrations lower than 25% contain niobium only in the form of $NbOF_5^{2-}$ complexes, whereas significant amounts of $NbF_6^-$ ions are found in solutions containing 35% HF and higher. Table 44 shows the composition of complex ions in solutions of different concentrations, as found by Keller [171].

Howell and Moss [289] confirmed, by $^{19}F$ NMR spectroscopy, that $NbOF_5^{2-}$ complex is present in hydrofluoric acid solutions of up to 30%. Increase in HF concentration leads to the formation of $NbF_6^-$ complex ions.

The $NbOF_5^{2-}$ ion has a tetragonal bi-pyramidal structure and can be considered to be an octahedron distorted as a result of the replacement of fluorine by an oxygen ligand. The oxygen ligand is connected by a multiple bond to the niobium atom, which is the central atom of the complex. The fluorine ligand, which is situated in the trans position relative to the oxygen atom, can be replaced by a water molecule. Thus, Buslaev et al. [57] reported that, using $^{19}F$ NMR spectroscopy, the F/Nb molar ratio of the complex $NbOF_4 \cdot H_2O^-$ in the solutions examined was found to be less than 5.

*Table 44. Composition of niobium-containing complexes in fluoride solutions of different concentrations (after Keller [171]).*

| HF concentration, mol/l | Nb concentration, mol/l | $K^+/Nb^{5+}$ | Complex found | Percentage |
|---|---|---|---|---|
| 23 | 0.39 | 2 | $NbF_6^-$ | 100% |
| 11 | 0.22 | 2 | $NbOF_5^{2-}$ | 100% |
| 5.2 | 0.34 | 2 | $NbOF_5^{2-}$ | 100% |
| ~0 | 0.34 | 2 | $NbOF_5^{2-}$ | 100% |

Tsikaeva et al. [290, 291] investigated the Raman and IR absorption spectra of hydrofluoric acid solutions containing a wide range of concentrations of niobium, but no other additional cations.

An initial solution was prepared by dissolving metallic niobium powder in 40% hydrofluoric acid. The dissolution was performed at elevated temperature with the addition of a small amount of nitric acid, $HNO_3$, to accelerate the process. The completeness of niobium oxidation was verified by UV absorption spectroscopy [21]. The prepared solution was evaporated to obtain a small amount of precipitate, which was separated from the solution by filtration. A saturated solution, containing Nb – 7.01 mol/l, HF – 42.63 mol/l, and corresponding to a molar ratio F:Nb = 6.08, was prepared by the above method. The density of the solution at ambient temperature was $\rho = 2.0$ g/cc. Concentrations needed for the measurements were obtained by diluting the saturated solution with water or hydrofluoric acid.

The complex structure of the various solutions was investigated by Raman and IR absorption spectroscopy. Containers made of sapphire and KRS-5 were used for Raman and IR spectra measurements, respectively. Vibration spectra analysis was performed based on the band assignment [171, 187] presented in Table 45.

The main peaks observed in the Raman spectra of niobium-containing solutions were at 686 and 933 $cm^{-1}$, and correspond to $\nu_1$ vibrations of $NbF_6^-$ and $NbOF_5^{2-}$, respectively. An increase in HF and niobium contents leads to the disappearance of the line indicating the presence of $NbOF_5^{2-}$ ions and arising of the line referring to $NbF_6^-$ ions. Analysis of bands intensities versus concentration enabled researchers to define the predominant presence fields of the two ions as shown in Fig. 47 [291].

*Table 45. Vibration spectra band assignment of hydrofluoric solutions containing niobium (after Keller [171] and Surandra et al. [187]).*

| Spectra | Wave number, $cm^{-1}$ | Assignment |
|---|---|---|
| Raman | 280 | $\nu_5$ $NbF_6^-$ or $\nu_7$ $NbOF_5^{2-}$ |
| | 686 | $\nu_1$ $NbF_6^-$ |
| | 933 | $\nu_1$ $NbOF_5^{2-}$ |
| IR absorption | 600 | $\nu_3$ $NbF_6^-$ |
| | 940 | $\nu_1$ $NbOF_5^{2-}$ |

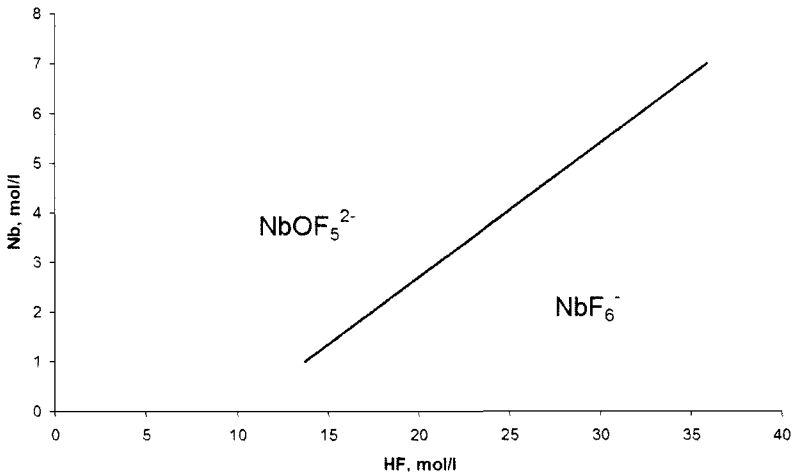


*Fig. 47. Predominant presence fields of $NbOF_5^{2-}$ and $NbF_6^-$ complexes in a $Nb_2O_5$ – HF – $H_2O$ system. Reproduced from [291], D. V. Tsikaeva, S. D. Nikitina, A. I. Agulyansky, V. T. Kalinnikov, Zh. Obschei. Khim. 57 (1987) 974, Copyright 1987, with permission of "Nauka" (Russian Academy of Sciences) publishing.*

The coordinates of the line between the presence fields is described satisfactorily by Equation (46):

$$[F] = 3.7\,[Nb] + 10 \qquad (46)$$

where [F] and [Nb] denote fluorine and niobium concentrations in the solution in mol/l.

The spectra of the initial saturated solution, with a F:Nb of approximately 6, are of particular interest because of the presence of a weak band at about 900–930 $cm^{-1}$. This band can be attributed to NbO bonds in oxyfluoride complexes. Even small additions of HF lead to the disappearance of the above effect. This can be explained based on a complex solvatation model. In solutions with a F:Nb ratio of about 6, hexafluoroniobate complex, $NbF_6^-$, initiates the formation of HF that interacts with complex ions as a solvate. This process is called "autosolvatation" and is represented by two interactions. The first is a hydrolysis process that leads to the formation of HF:

$$NbF_6^- + 2\,H_2O = NbOF_5^{2-} + HF + H_3O^+ \qquad (47)$$

The second is a solvatation process:

$$NbF_6^- + n\,HF = NbF_6^- \cdot nHF \qquad (48)$$

It is obvious that the addition of HF will lead to a F:Nb ratio that is greater than 6 and will shift Equation (47) to the left, leading in turn to the disappearance of $NbOF_5^{2-}$ ions from the solution.

Only two types of complex ions are present in fluoride solutions: $NbOF_5^{2-}$ and $NbF_6^-$, the equilibrium of which is described by Equation (47). Higher concentrations of HF lead to the formation of $NbF_6^-$ ions.

The addition of alkali metal or ammonium fluorides reduce the acidity of the system and shift the equilibrium between the two ions toward the formation of $NbOF_5^{2-}$ ions [60,61]. The shift depends on the alkalinity of the cation. The more alkaline the cation is (higher atomic weight), the stronger the shift toward $NbOF_5^{2-}$ ion formation. Fig. 48 shows typical Raman spectra of niobium-containing solutions before and after such additions were made.

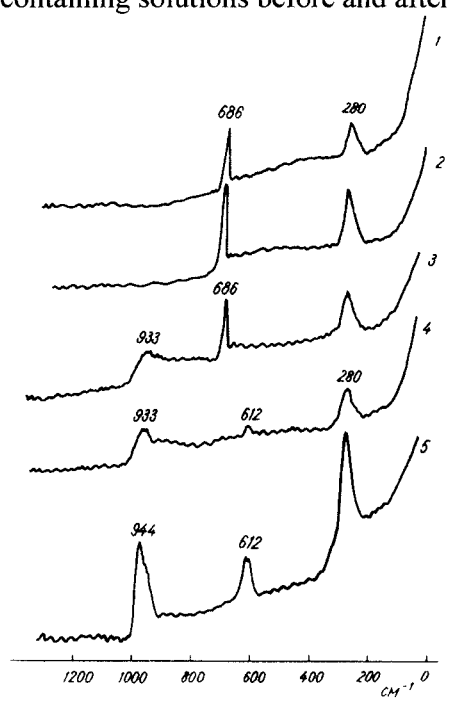


*Fig. 48. Raman spectra of initial solution (1) and following additions of (expressed as molar ratios) $NH_4F$:Nb=1:1 (2); $NH_4F$:Nb=4:1 (3); KF:Nb=1:1 (4); RbF:Nb=0.5:1. Reproduced from [291], D. V. Tsikaeva, S. D. Nikitina, A. I. Agulyansky, V. T. Kalinnikov, Zh. Obschei. Khim. 57 (1987) 974, Copyright 1987, with permission of "Nauka" (Russian Academy of Sciences) publishing.*

## 4.2. Tantalum-containing solutions

The first comprehensive investigation of the $TaF_5$ – HF – $H_2O$ system was performed by Buslaev and Nikolaev [292]. Based on the analysis of solubility isotherms, and on conductometric and potentiometric titrations, the authors concluded that in this solution, tantalum forms oxyfluorotantalic acid, $H_2TaOF_5$, similar to the formation of $H_2NbOF_5$ in solutions containing $NbF_5$.

Keller and Chetham-Strode [155] subsequently investigated Raman spectra of solutions containing tantalum, ammonium and hydrofluoride acid. Two types of complex ions were identified based on a comparative analysis of the spectra, namely $TaF_7^{2-}$ and $TaF_6^-$. In solutions that contain either no HF or relatively low HF concentrations, $TaF_7^{2-}$ ions are predominant. At an HF concentration of 24 mol/l, $TaF_6^-$ ions are predominantly observed in the solution, while $TaF_7^{2-}$ is barely detectable. Both complex ions are observed at intermediate HF concentrations. It should also be mentioned that $TaF_8^{3-}$ ion has not yet been found under any investigated conditions. Table 46 presents the ionic composition of solutions investigated by Keller and Chetham-Strode [155].

Tsikaeva et al. investigated the Raman and IR absorption spectra of solutions containing tantalum in hydrofluoric acid with no additional cations [290, 291].

Preparation of the solutions was similar to that of niobium-containing solutions, i.e. by dissolving tantalum metal powder in hydrofluoric acid, HF, at a concentration of about 40% weight.

*Table 46. Composition of tantalum-containing complexes in fluoride solutions of different concentrations (after Keller and Chetham-Strode [155]).*

| HF concentration, mol/l | Ta concentration, mol/l | $NH_4^+/Ta^{5+}$ | Complexes found | % $TaF_7^{2-}$ of total complexes |
|---|---|---|---|---|
| 22 | 0.977 | 1.92 | $TaF_6^-$, $TaF_7^{2-}$ | 33% |
| 10 | 0.939 | 2.91 | $TaF_6^-$, $TaF_7^{2-}$ | 92% |
| 2.6 | 0.976 | 1.99 | $TaF_6^-$, $TaF_7^{2-}$ | 91% |
| ~0 | 0.945 | 2.02 | $TaF_7^{2-}$ | ~100% |

The tantalum dissolution process takes longer compared to the preparation of the corresponding niobium solution, therefore the solution is heated and a small amount of nitric acid is added. A grey precipitate indicates saturation of the solution. The prepared solution is separated from the precipitate by filtration and used as the initial solution.

The initial saturated solution contains 6.90 mol/l Ta and 40.42 mol/l HF. Its F:Ta ratio is 5.86, and its density is $\rho = 2.5$ g/cm$^3$.

Solutions of various concentrations were prepared by diluting the initial saturated solution (40% HF weight) with water.

Table 47 shows wave numbers of vibration spectra bands and their assignment.

In practically all cases, Raman spectra display bands at 699 and 280 cm$^{-1}$. These bands correspond to $\nu_1$ and $\nu_5$ of the $TaF_6^-$ complex ion, respectively. Decrease in the concentration of both HF and tantalum leads to a decrease in the intensity of the band at 699 cm$^-$ and to an increase in the intensity of the band at 645 cm$^{-1}$. A further decrease in HF or/and tantalum concentrations initiates the appearance of a band at 674 cm$^{-1}$. These changes in the Raman spectra attest to the fact that with the decrease in HF or/and tantalum concentrations, $TaF_6^-$ is replaced by $TaF_7^{2-}$ complex ion. Fig. 49 shows typical changes in Raman spectra versus HF concentration.

*Table 47. Vibration spectra bands assignment of hydrofluoric solutions containing tantalum.*

| Spectra | Wave numbers, cm$^{-1}$ | Assignment |
|---|---|---|
| Raman | 280 | $\nu_5$ $TaF_6^-$ or $\nu$ $TaF_7^{2-}$ |
| | 645 | $\nu$ $TaF_7^{2-}$ |
| | 674 | $\nu$ Ta-F ? |
| | 699 | $\nu_1$ $TaF_6^-$ |
| IR absorption | 600 | $\nu_3$ $TaF_6^-$ |
| | 550 | $\nu$ $TaF_7^{2-}$ |
| | 880 | $\nu$ TaO |

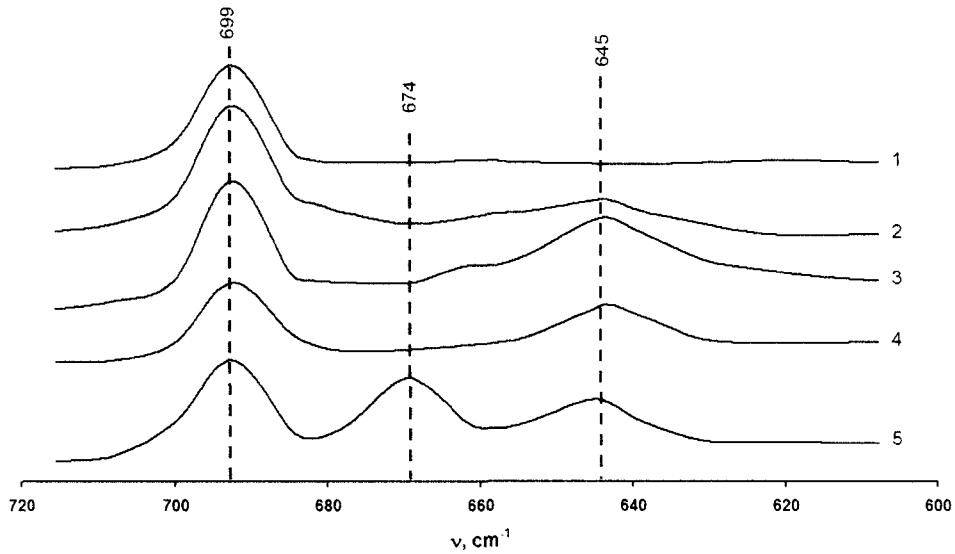


*Fig. 49. Raman spectra of solutions containing Ta - 1.5 mol/l and HF – 25.7 (curve 1); 21.7 (curve 2); 17.2 (curve 3); 12.9 (curve 4) and 9.25 (curve 5) Reproduced from [291], D. V. Tsikaeva, S. D. Nikitina, A. I. Agulyansky, V. T. Kalinnikov, Zh. Obschei. Khim. 57 (1987) 974, Copyright 1987, with permission of "Nauka" (Russian Academy of Sciences) publishing.*

Unfortunately, no clear assignment of the band at 674 $cm^{-1}$ has been made.

Analysis of the correlation between concentrations and the intensity of the bands at 699 $cm^{-1}$ and 645 $cm^{-1}$, which refer to $TaF_6^-$ and $TaF_7^{2-}$ complex ions respectively, enable definition of the predominant presence fields of the two ions. These fields are shown in Fig. 50.

Coordinates of the line between the two presence fields are approximated satisfactory by the following equation [291]:

$$[F] = 1.7\,[Ta] + 20;$$

where [F] and [Ta] denote fluorine and tantalum concentrations in mol/l.

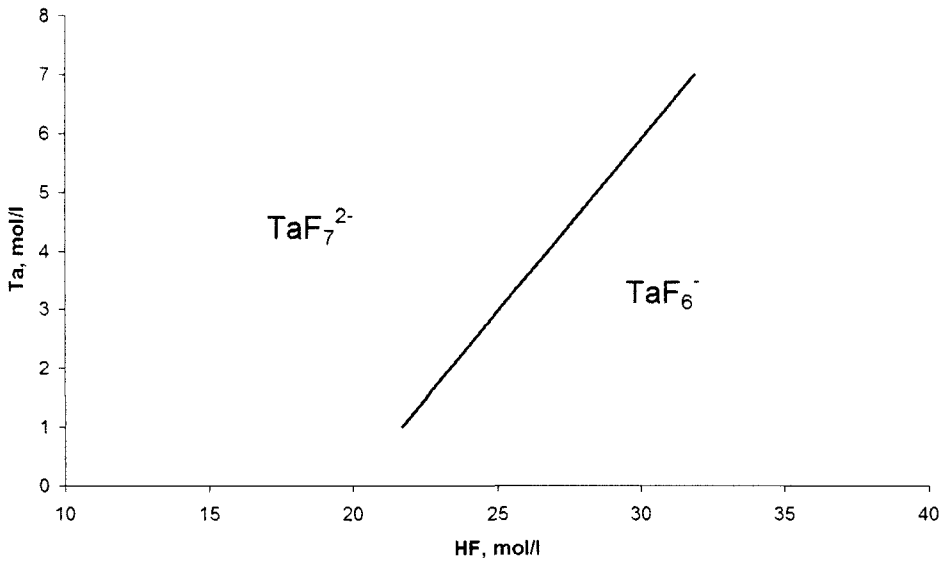


*Fig. 50. Predominant presence fields of $TaF_7^{2-}$ and $TaF_6^-$ complexes in a $Ta_2O_5$ – HF – $H_2O$ system.*
*Reproduced from [291], D. V. Tsikaeva, S. D. Nikitina, A. I. Agulyansky, V. T. Kalinnikov, Zh. Obschei. Khim. 57 (1987) 974, Copyright 1987, with permission of "Nauka" (Russian Academy of Sciences) publishing.*

IR absorption spectrum of the initial tantalum-saturated solution displays a weak band at about 880 $cm^{-1}$, which corresponds to TaO bonds. The formation of the oxyfluorotantalate complex seems to be similar to the formation of oxyfluoroniobate in a niobium-saturated solution, but in the case of tantalum, the above effect is more emphasized.

This difference can also be explained based on the difference in solvation interactions. In addition, a stronger effect is related to tantalum's higher effective charge compared to that of niobium.

The "autosolvation process" can be represented by the two following equations:

$$TaF_6^- + 2\,H_2O = TaOF_5^{2-} + HF + H_3O^+ \quad (49)$$

$$TaF_6^- + n\,HF = TaF_6^-\cdot nHF \quad (50)$$

The high tendency of the $TaF_6^-$ complex to undergo solvation initiates partial hydrolysis of the $TaF_6^-$ complex yielding HF. Any addition of HF to the solution leads to an increase in the F:Ta ratio, which in turn shifts Equilibrium (49) to the left and results in the disappearance of the band at 880 $cm^{-1}$.

In summary, it can be said that tantalum-containing fluoride solutions generally consist of two types of ions: $TaF_7^{2-}$ and $TaF_6^-$. Low acidity of the solution (i.e. low HF concentration) leads to the predominant formation of $TaF_7^{2-}$ complex ions, while higher concentrations of HF lead to the presence of $TaF_6^-$ complex ions .

One explanation of this phenomenon is based on the formation of hydrofluride ions at high concentrations of HF. This model is described by the following ionic equation:

$$TaF_6^- + HF_2^- = TaF_7^{2-} + HF \qquad (51)$$

On the other hand, $TaF_7^{2-}$ and $TaF_6^-$ can be said to be Lewis bases, the acidity of which increases when moving from $TaF_7^{2-}$ to $TaF_6^-$ (i.e. when decreasing the coordination number). Thus, the more acidic complex preferably exists in the more acidic media. In addition, the more acidic complex also has a greater tendency to undergo solvation. From this point of view, the ionic equilibrium can be represented as follows:

$$TaF_6^- \cdot nHF + H_2O = TaF_7^{2-} + (n-1)\,HF + H_3O^+ \qquad (52).$$

Chemical interaction with other metal ions shifts Equilibrium (52) to the right (alkaline side) and yields certain types of compounds according to the acidity of the added metal.

# 5.

# TANTALUM AND NIOBIUM COMPLEXES IN FLUORIDE MELTS

## 5.1. Preliminary notes

For a long period of time, molten salts containing niobium and tantalum were widely used for the production by electrolysis of metals and alloys. This situation initiated intensive investigations into the electrochemical processes that take place in molten fluorides containing dissolved tantalum and niobium in the form of complex fluoride compounds. Well-developed sodium reduction processes currently used are also based on molten salt media. In addition, molten salts are a suitable reagent media for the synthesis of various compounds, in the form of both single crystals and powdered material. The mechanisms of the chemical interactions and the compositions of the compounds depend on the structure of the melt.

Molten salts are characterized by the formation of discrete complex ions that are subjected to coordination phenomenon. Such complex ions have specific compositions that are related to the rearrangement of their electronic configuration and to the formation of partially covalent bonds. The life time of the coordinated ions is longer than the contact period of the individual ions [293].

Molten salt investigation methods can be divided into two classes: thermodynamic and kinetic. In some cases, the analysis of melting diagrams and isotherms of physical-chemical properties such as density, surface tension, viscosity and electroconductivity enables the determination of the ionic composition of the melt. Direct investigation of the complex structure is performed using spectral methods [294].

Investigation of fluoride melts containing tantalum or niobium is a very difficult procedure that involves high temperatures, corrosion activity and the

*Table 48. Changes in Gibbs potential (ΔG) for some interactions in molten systems (after Amosov [295, 296]).*

| Interaction | ΔG, in cal/mol (T – temperature, K) |
|---|---|
| $KF + TaF_5 = KTaF_6$ | -55250 + 42.77T |
| $KF + KTaF_6 = K_2TaF_7$ | -27750 + 4.27T |
| $KF + K_2TaF_7 = K_3TaF_8$ | -20750 + 3.57T |
| $2\,KF + TaOF_3 = K_2TaOF_5$ | -38900 + 35.0T |
| $3\,KF + TaOF_3 = K_3TaOF_6$ | -44900 + 39.2T |
| $K_2TaF_7 + KCl = K_3TaF_7Cl$ | -20900 + 3.74T |

extremely high sensitivity of such molten systems to interaction with air and moisture.

Three conceptual steps can be discerned in the definition of the ionic structure of fluoride melts containing tantalum or niobium. Based on the very first thermodynamic calculations and melting diagram analysis, it was initially believed that the coordination numbers of tantalum and niobium, in a molten system containing alkali metal fluorides, increase up to 8.

Amosov [295, 296] made the first attempt to define the composition of compounds occurring in the molten system K – Ta – O – F – Cl by applying thermodynamic analysis based on main estimated parameters. Table 48 presents changes in Gibbs potential for the main possible interactions. According to the above calculations, it was assumed that tantalum forms complex ions with the following compositions: $Ta_nCl_m^{3-}$ ($TaF_8^{3-}$, $TaF_7Cl^{3-}$) or $TaO_yF_x^{x-}$ ($TaOF_6^{3-}$, $TaO_2F_3^{2-}$).

An investigation of the physical-chemical properties and IR spectra of melts with relatively low metal concentrations indicated that heptafluorometalate ions, $TaF_7^{2-}$, are also present in the melt. These measurements initiated the second conceptual step and it was assumed that there are two types of complex ions, namely octafluorometalate, $MeF_8^{3-}$, and heptafluorometalate, $MeF_7^{2-}$, that determine the melt's various properties.

The third step consisted of the direct investigation of IR emission spectra for a wide range of concentrations. The investigation showed the tendency of the metals to reduce their coordination number when moving from solid to molten state. This property of the melt depends on the equilibrium between two types of complex ions, $MeF_7^{2-}$ and $MeF_6^{-}$.

## 5.2. Melting diagrams

### 5.2.1. Niobium-containing systems

Bizot and Malek-Zadeh [77, 78] performed detailed investigations of melting in MF – $NbF_5$ binary systems, in which M = Li, Na, K, Rb, Cs. Such systems are characterized by the formation of significant amounts of compounds such as $MNb_4F_{21}$, $MNb_3F_{16}$, $MNb_2F_{11}$, $MNbF_6$, $M_2NbF_7$ and $M_3NbF_8$. Some of the compounds undergo congruent melting, while others undergo incongruent melting. Figs. 51 and 52 present melting diagrams of the above-mentioned compounds.

It is important to note that the number of different compounds found in such systems increases significantly when moving along the sequence of alkali metals, from lithium to cesium, as does their thermal stability. This phenomenon is related to the systematic increase of both ionic radii and polarity of alkali metals ions when moving from lithium to cesium.

Presence of the compound $K_3NbF_8$ was detected in the KF – $K_2NbF_7$ system. This compound undergoes congruent melting, as demonstrated by Mukhtar and Winand [297] and McCawley and Barelay [298]. Coordinates of invariant points on the temperature vs. composition diagram are not significantly different than data provided by Bizot [77]. Kamenskaya and Konstantinov investigated the ternary systems KCl – NaF – $K_2NbF_7$ and KF – NaF – $K_2NbF_7$ [299, 300]. Fig. 53 shows projections of the crystallization surfaces of the KCl – NaF – $K_2NbF_7$ and KF – NaF – $K_2NbF_7$ systems. In the first system, five crystallization fields were found that correspond to the following five compounds: KCl, KF, $K_2NbF_7$, $K_3NbF_8$ and $K_3NbF_7Cl$. In addition, three invariant points were defined, two of which refer to ternary eutectics ($E_1$ and $E_2$), and the third to the peritectic transformation:

$$L + K_3NbF_8 = K_3NbF_7Cl + KF \qquad (53)$$

where L denotes liquid (melt).

Fig. 54 displays projections of the crystallization surfaces of the interconnecting ternary systems $K^+$, $Na^+//Cl^-$, $NbF_7^{2-}$ and $K^+$, $Na^+//Cl^-$, $NbF_8^{3-}$ [37, 221, 301-303]. The first system was investigated along the diagonal line $K_2NbF_7$ – NaCl. $K_3NbF_7Cl$ displays the largest crystallization field, which also crosses the diagonal KCl – $Na_2NbF_7$, and is an unstable compound.

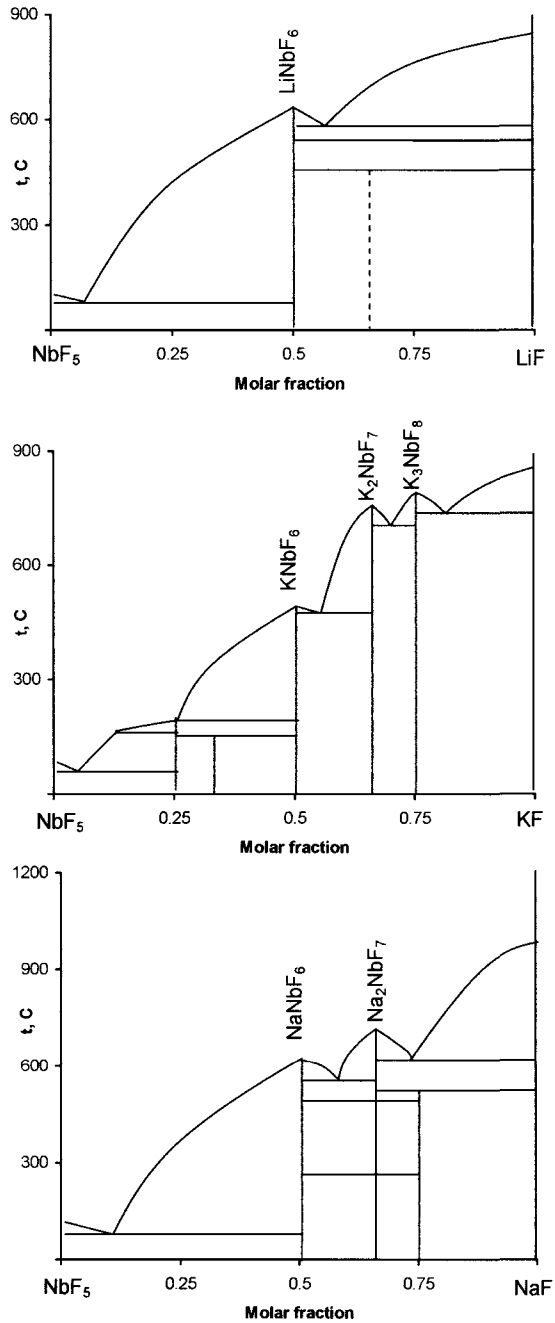


*Fig. 51. Melting diagrams of $NbF_5$ – MF systems, where M = Li, Na, K (after Bizot and Makek-Zadeh [77]).*

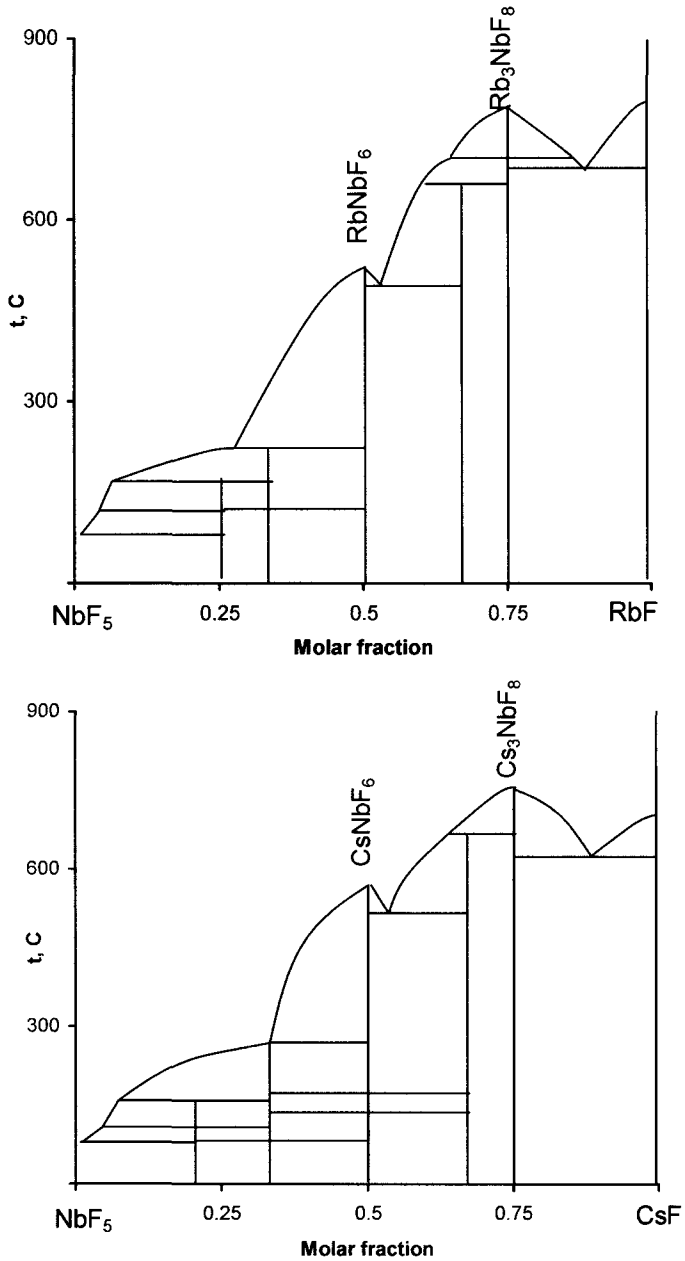


*Fig. 52. Melting diagrams of $NbF_5$ – MF systems, where M = Rb, Cs. Reproduced from [78], D. Bizot, J. Fluor. Chem. 11 (1978) 497, Copyright 1978, with permission of Elsevier.*

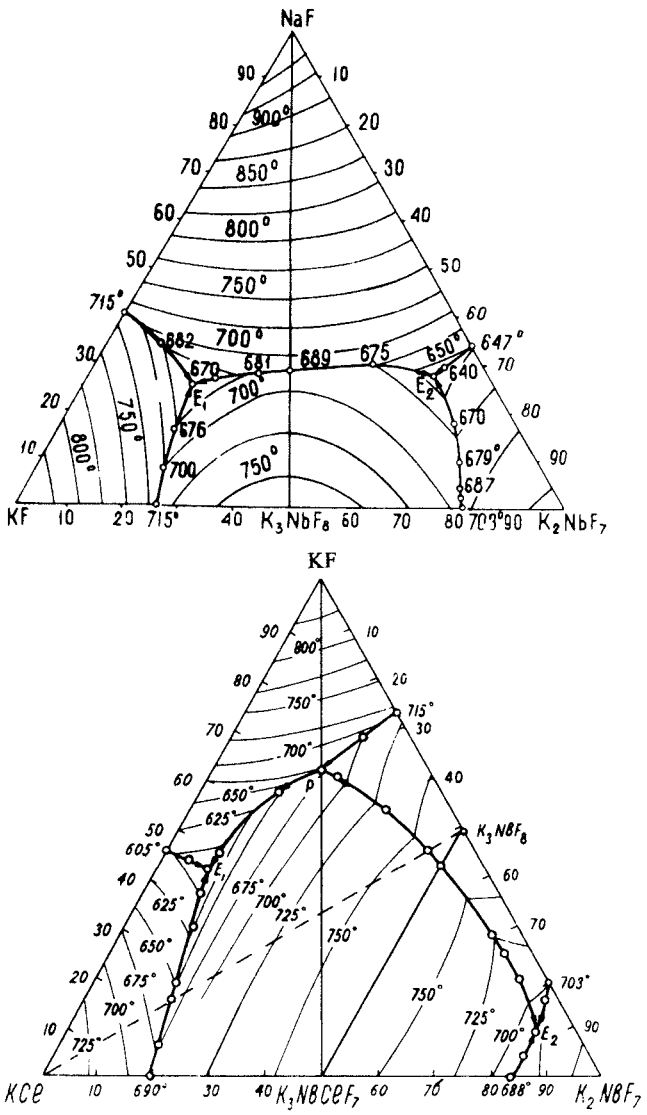


*Fig. 53. Ternary melting diagrams of the KF – NaF – $K_2NbF_7$ system (top). Reproduced from [299], L. A. Kamenskaya, V. I. Konstantinov, Zh. Neorg. Khim. 16 (1971) 2003, Copyright 1971, with permission of "Nauka" (Russian Academy of Sciences) publishing.*
*Ternary melting diagrams of the KCl – NaF – $K_2NbF_7$ system (bottom). Reproduced from [300], L. A. Kamenskaya, V. I. Konstantinov, A. M. Matveev, Zh. Neorg. Khim. 17 (1972) 2567, Copyright 1972, with permission of "Nauka" (Russian Academy of Sciences) publishing.*

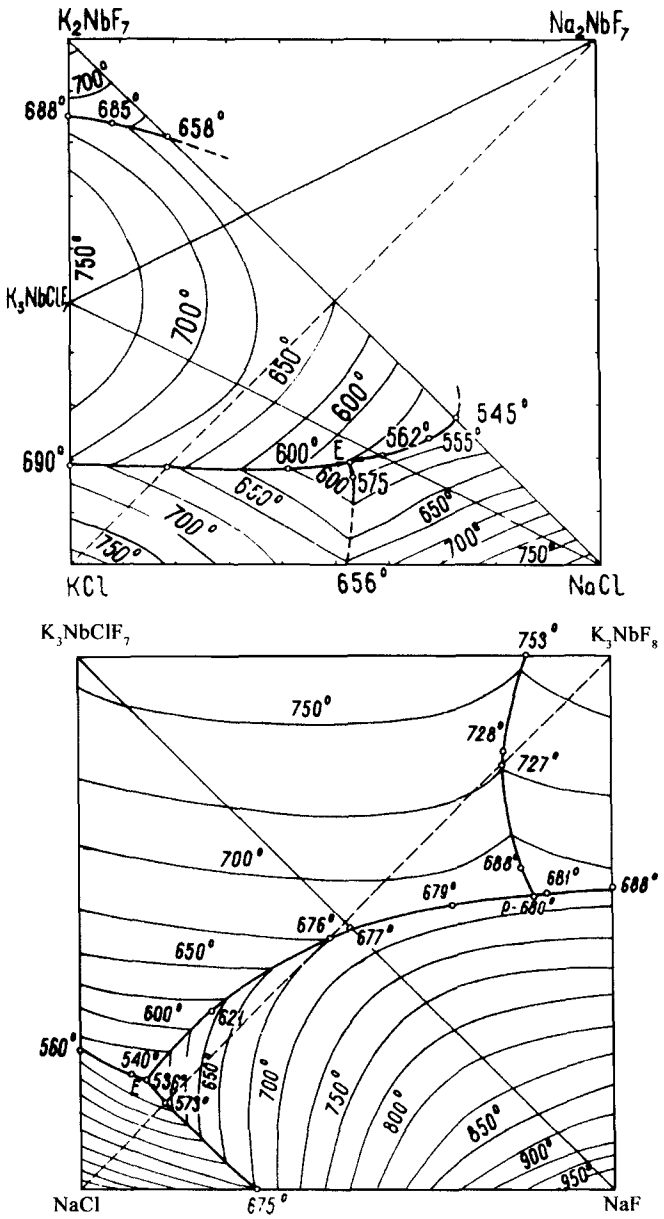


*Fig. 54. Projections of crystallization surfaces of ternary interconnecting systems $K^+$, $Na^+//Cl^-$, $NbF_7^{2-}$ (top) and $K^+$, $Na^+//Cl^-$, $NbF_8^{3-}$ (bottom). Reproduced from [37], V. I. Konstantinov, Electrochemical obtaining of tantalum niobium and their alloys, Metallurgiya, Moscow, 1977, Copyright 1977, with permission of "Metallurgiya - Mir".*

Kovalev, Ioffe and Karzev [304] investigated the ternary system $K_2NbF_7$ – NaF – NaCl and mentioned the formation of $2K_2NbF_7 \cdot NaCl$. According to Konstantinov [37] and Kamenskaya [221], however, the dystectic maximum of the compound corresponding to $2K_2NbF_7 \cdot NaCl$ is significantly blurred and seems to be quite far from having a singular shape. The researchers proposed attributing the maximum observed on the liquidus curve to the interaction that leads to cationic exchange, as shown below:

$$3\ K_2NbF_7 + 2\ NaCl = 2\ K_3NbF_7Cl + Na_2NbF_7 \qquad (54)$$

This interpretation correlates with data obtained for the ternary interconnecting system $K^+$, $Na^+//Cl^-$, $NbF_7^{2-}$.

Kamenskaya [221] and Konstantinov [37] investigated the concentration field adjacent to the KF – $NbF_5$ side of the ternary interconnected system $K^+$, $Nb^{5+}//O^{2-}$, $F^-$. Fig. 55 shows the projection of the crystallization fields.

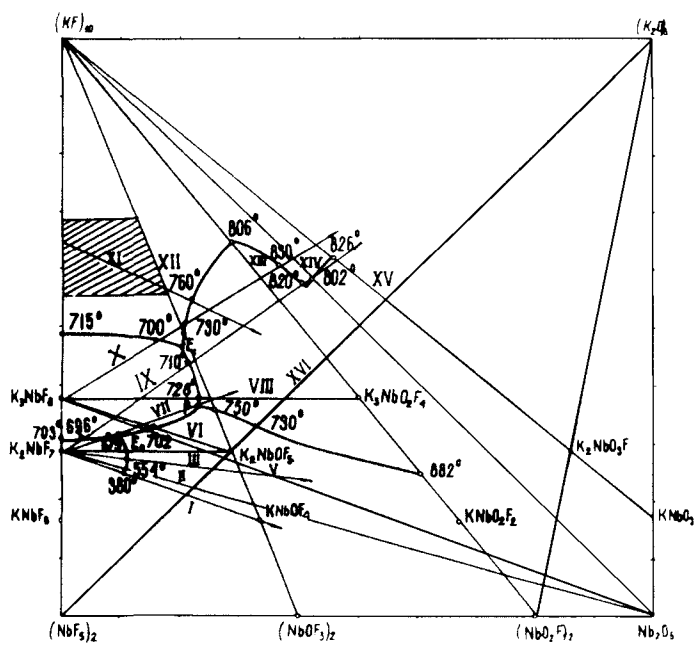


*Fig. 55. Crystallization fields of compounds formed in the ternary interconnected system $K^+$, $Nb^{5+}//O^{2-}$, $F^-$. Reproduced from [37], V. I. Konstantinov, Electrochemical obtaining of tantalum niobium and their alloys, Metallurgiya, Moscow, 1977, Copyright 1977, with permission of "Metallurgiya - Mir".*

The largest crystallization field belongs to $K_3NbO_2F_4$, which undergoes congruent melting at 986°C.

Analysis of the melting diagrams led to the conclusion that fluoride, fluoride–chloride and oxyfluoride-chloride melts containing niobium contain the complex ions $NbF_8^{3-}$, $NbF_7Cl^{3-}$, $NbO_2F_4^{3-}$.

Among the systems that contain bivalent metals, only the $NbF_5$ – $MnF_2$ system was investigated by Bizot et al. [148]. Fig. 56 presents the melting diagram for this system. Two compounds, $MnNb_2F_{12}$ and $MnNbF_7$, were found that undergo incongruent melting at 885 and 630°C, respectively.

Table 49 lists the melting points of some niobium-containing fluoride compounds.

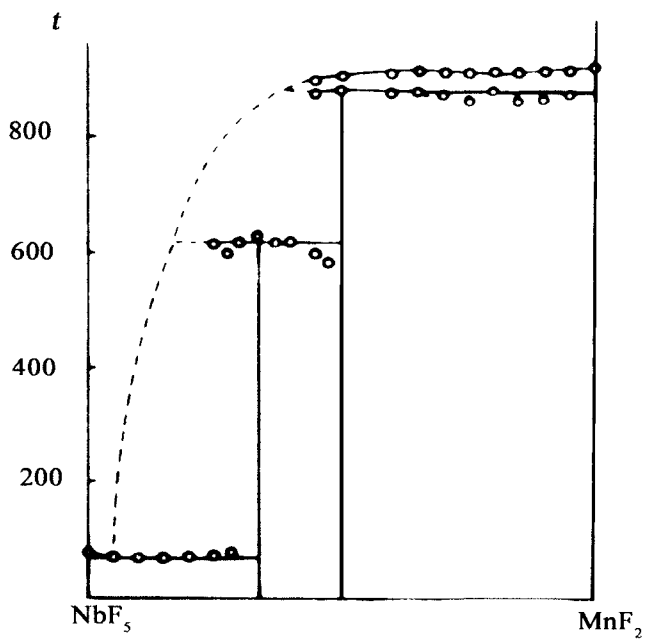


*Fig. 56. Melting diagram of $NbF_5$ – $MnF_2$ system.*
*Reproduced from [78], D. Bizot, J. Chassaing, A. Erb, J. Less-Common Metals 79 (1981) 39, Copyright 1981, with permission of Elsevier.*

*Table 49. Melting points of some niobium-containing fluoride compounds*

| Compound | Melting point, °C | Melting mechanism |
|---|---|---|
| $NbF_5$ | 80 | Congruent |
| $KNbF_6$ | 478 | Congruent |
| $K_2NbF_7$ | 732 | Incongruent |
| $K_3NbF_8$ | 768 - 770 | Congruent |
| $K_3NbF_7Cl$ | 745 - 753 | Congruent |
| $K_3NbO_2F_4$ | 986 | Congruent |
| $K_3NbOF_6$ | 700 (decomposition in solid phase) | $K_3NbF_8 + K_3NbO_2F_4$ |

## 5.2.2. Tantalum-containing systems

Various researchers [305 – 310] investigated and reported on melting in the binary system $K_2TaF_7$ – KF. The compound $K_3TaF_8$ ($K_2TaF_7 \cdot KF$) was found, that undergoes congruent melting at 776°C, along with two eutectics. One is in the KF – $K_3TaF_8$ side and melts at 717-718°C, the other in the $K_3TaF_8$ – $K_2TaF_7$ side and melts at 695-697°C [305 – 307], or at 727°C [310].

A typical interaction was observed in the KCl – $K_2TaF_7$ system that yields $K_3TaF_7Cl$ ($K_2TaF_7 \cdot KCl$), which undergoes congruent melting at 758°C as reported in [305, 306], or at 776°C as reported in [310]. An eutectic compound in the KCl – $K_3TaF_7Cl$ side melts at 695-700°C, while the eutectic compound in the $K_3TaF_7Cl$ – $K_2TaF_7$ side melts at 697°C [305, 306], or at 710 -712°C [310].

Iuchi and Matsuchima [305] and Zui Bin-Sin, Lushnaya and Konstantinov [306] investigated the melting diagram of the ternary system $K_2TaF_7$ – KF – KCl and observed the compound $K_3TaF_7Cl$ along with its initial components.

Kovalev, Kartsev, Ioffe and Leonov [310] investigated melting in the ternary system $K_2TaF_7$ – KF – NaF, which is also characterized by the formation of $K_3TaF_8$.

Fig. 57 shows projections of the crystallization surfaces of the $K_2TaF_7$ – KF – KCl and $K_2TaF_7$ – KF – NaF systems.

An analysis of the melting diagram led to the conclusion that, in fluoride and fluoride–chloride melts, tantalum forms the complex ions $TaF_8^{3-}$ or $TaF_7Cl^{3-}$, respectively [37, 306].

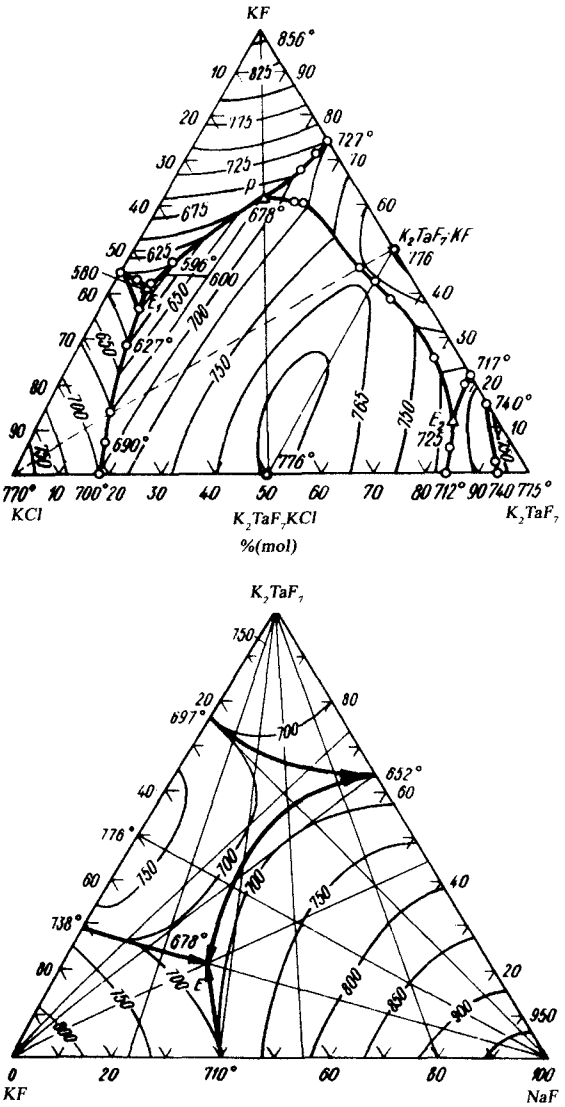


*Fig. 57. Projections of the crystallization surfaces of the ternary systems $K_2TaF_7$ – KF – KCl (top). Reproduced from [306], Z. Bin-Sin, N. P. Lushnaya, V. I. Konstantinov, Zh. Neorg. Khim. 8 (1963) 389, Copyright 1963, with permission of "Nauka" (Russian Academy of Sciences) publishing.*
*Projections of the crystallization surfaces of the ternary systems $K_2TaF_7$ – KF – NaF (bottom). Reproduced from [310], F. V. Kovalev, V. E. Kartsev, V. M. Ioffe, M. E. Leonov, Zh. Neorg. Khim. 18 (1973) 1352, Copyright 1973, with permission of "Nauka" (Russian Academy of Sciences) publishing.*

It was assumed that tantalum, when added to the melt in the form of potassium heptafluorotantalate, $K_2TaF_7$, interacts with KF or KCl to form a compound with an increased tantalum coordination number of up to eight. The compound is present in the melt in its dissociated form, yielding potassium ions and octa-coordinated complexes of tantalum, namely $TaF_8^{3-}$ or $TaF_7Cl^{3-}$.

Konstantinov, Kamenskaya, Zui Bin-Sin and Lushnaya [37, 221, 311] investigated the ternary interconnected system $K^+$, $Ta^{5+}//O^{2-}$, $F^-$ and the quaternary system $K^+$, $Ta^{5+}//F^-$, $Cl^-$, $O^{2-}$. Fig. 58 presents a projection of the crystallization surfaces of the ternary interconnected system $K^+$, $Ta^{5+}//O^{2-}$, $F^-$.

It was shown that in tantalum-containing oxyfluoride systems, three types of oxyfluoride compounds are formed: $K_3TaO_2F_4$, $K_3TaOF_6$ and $KTaOF_4$, the thermal stability of which decreases from $K_3TaO_2F_4$ to $K_3TaOF_6$ to $KTaOF_4$. Analysis of the melting diagrams led to the conclusion that oxyfluoride melts contain $TaOF_6^{3-}$ or $TaO_2F_4^{3-}$ complex ions depending on the concentration of tantalum oxide, $Ta_2O_5$, in the melt.

Table 50 lists melting points of some tantalum-containing fluoride compounds.

Investigation of the formation of complexes using melting diagrams is a widely used method, which in some cases provides positive results. In particular, in most chloride systems that have relatively low melting points, presence of a dystectic melting point allows the prediction of the composition of a complex ion based on the composition of the parent compound. Fluoride-containing systems are usually more refractory, therefore the analysis of the melting diagrams must take into account not only the correlation of the crystallization fields, but also the shape of the liquidus curve near the dystectic melting point.

Available data on binary and pseudo-binary systems containing tantalum and niobium fluorides indicate that in most cases there is no singularity near compounds that undergo congruent melting. It should be mentioned that the only systems that can be considered to have singular maximum points are the LiF – $NbF_5$ and NaF – $NbF_5$ systems. In all other known systems, relatively significant curvature radii are observed near the dystectic melting points. This indicates that most compounds formed in the solid phase have a tendency to dissociate in the molten state, yielding complex ions with lower coordination numbers [312].

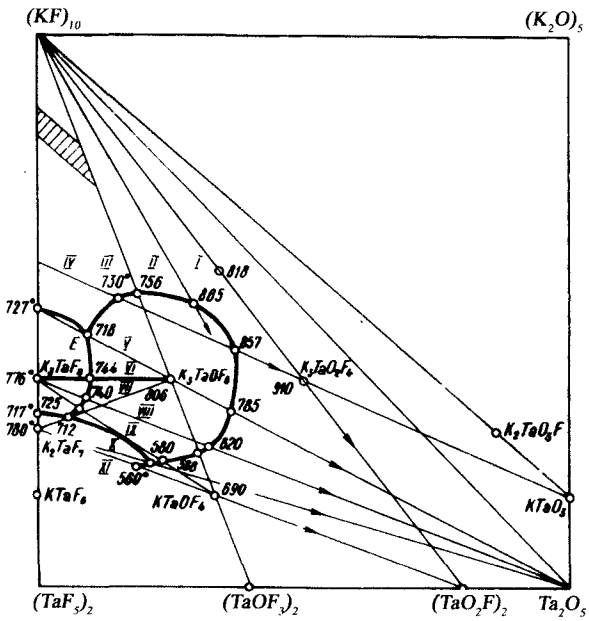


*Fig. 58. Crystallization fields of compounds formed in the ternary interconnected system $K^+$, $Ta^{5+}//O^{2-}$, $F^-$. Reproduced from [37], V. I. Konstantinov, Electrochemical obtaining of tantalum niobium and their alloys, Metallurgiya, Moscow, 1977, Copyright 1977, with permission of "Metallurgiya - Mir".*

*Table 50. Melting points of some niobium-containing fluoride compounds*

| Compound | Melting point, °C | Melting mechanism |
|---|---|---|
| $TaF_5$ | 96 | Congruent |
| $KTaF_6$ | 513 | Congruent |
| $K_2TaF_7$ | 746 | Incongruent |
| $K_3TaF_8$ | 778 | Congruent |
| $K_3TaF_7Cl$ | 776 | Congruent |
| $K_3TaO_2F_4$ | 860 - 880 | Congruent |
| $K_3TaOF_6$ | 806 | Congruent |

## 5.3. Physicochemical properties

### 5.3.1. General observations

Physicochemical properties of molten systems have an applied significance due to their wide use in both technological process planning and in production equipment design. Analysis of various melt properties versus different parameters of the melt enables to infer the interaction mechanism between the initial components, and in some cases, even to estimate the possible composition of the main complex ions formed in the melt [312]. From this point of view, the analysis of isotherms of physicochemical properties versus melt composition and of the magnitude of their deviation from ideal conditions is of most interest.

In order to draw the "property – composition" diagram, coordinates are usually chosen so that the ideal system values correspond with the additive law regarding concentration [313]. It is known, for instance, that in an ideal system, molar volume changes additively with the concentration, and is expressed in molar fractions or molar percentages, whereas specific volume changes linearly with the concentration, and is expressed in mass fractions or mass percentages.

In this case, the deviations from the ideal system property can be used to estimate the type of interaction between the initial components. In general, deviations in the values of a property from the ideal condition can be positive, negative or S–shaped.

Fig. 59 shows, schematically, possible property variations for a hypothetical binary system composed of components A and B. Variation of the values of the property in accordance with the additive law indicates that the system's behavior is close to that of an ideal system.

In most cases, the formation of complexes in molten salts leads to an increase in the molar volume relative to the additive volume. This phenomenon is usually explained by an increase in bond covalency. Nevertheless, the nature of the initial components should be taken into account when analyzing deviations in property values, as was shown by Markov, Prisyagny and Volkov [314]. In particular, this rule applies absolutely when the system consists of pure ionic components. The presence of initial components with a significant share of covalent bonds leads to an S–shaped isotherm [314].

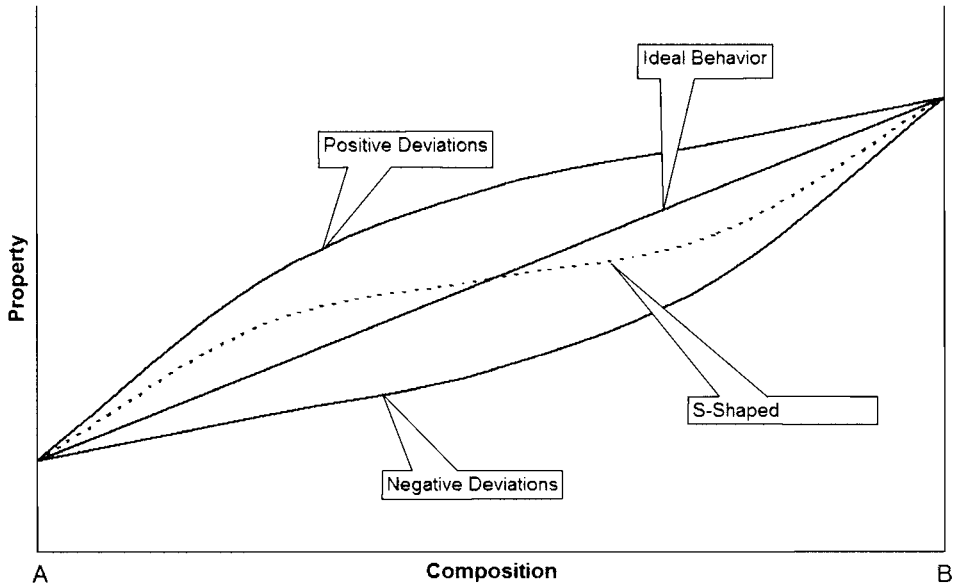


*Fig. 59. Possible deviations from the ideal behavior of a binary system A-B*

In the limiting case, if one of the components possesses a very strong covalency the molar volume of the system will decrease. Melts of NaF – $AlF_3$ are an example of such systems.

Electro-conductivity of molten salts is a kinetic property that depends on the nature of the mobile ions and ionic interactions. The interaction that leads to the formation of complex ions has a varying influence on the electro-conductivity of the melts, depending on the nature of the initial components. When the initial components are purely ionic, forming of complexes leads to a decrease in conductivity, whereas associated initial compounds result in an increase in conductivity compared to the behavior of an ideal system. Since electro-conductivity is never an additive property, the calculation of the conductivity for an ideal system is performed using the well-known equation proposed by Markov and Shumina (Markov's Equation) [315].

## 5.3.2. Physicochemical properties of fluoride melts containing niobium

Konstantinov, Kuznetsov and Stangrit [316] investigated the density of the molten systems KF – $K_2NbF_7$, KCl – $K_2NbF_7$, KCl – KF – $K_2NbF_7$ and KCl – KF – $K_2NbF_7$ – $Ta_2O_5$ in the temperature range of 730-950°C using the hydrostatic weighing method. The density of the two latter systems, KCl – KF – $K_2NbF_7$ and KCl – KF – $K_2NbF_7$ – $Ta_2O_5$, was not investigated over the complete range of concentrations, but rather, measurements were performed over a limited concentration range, close to the electrolyte concentration used for electrolytic reduction of niobium. The first two systems, KF – $K_2NbF_7$ and KCl – $K_2NbF_7$, were investigated over the entire range since binary systems enable the analysis of density isotherms from the standpoint of complex ion formation.

The value of the specific volume of the melts KF – $K_2NbF_7$ and KCl – $K_2NbF_7$ changes almost linearly with the melt composition, as expressed in mass percents. This indicates that the systems' behavior is close to that of an ideal system. At melt masses close to 50%, which correspond to the formation of the compounds $K_3NbF_8$ and $K_3NbF_7Cl$, a slight deviation from the additive law was observed. In the case of the KF – $K_2NbF_7$ system, the specific volume exhibits a negative deviation from the ideal system, while the KCl – $K_2NbF_7$ system is characterized by a positive volume deviation from the ideal system. Nevertheless, it was concluded [316] that the above deviations are related to the formation of $NbF_8^{3-}$ and $NbF_7Cl^{3-}$ complex ions, respectively, whereas other compositions that contain even higher concentrations of KF or KCl, correspond to the formation of $NbF_7^{2-}$ complexes.

The addition of $Nb_2O_5$ to molten KCl – KF – $K_2NbF_7$ leads to a consistent increase in density with the increase in $Nb_2O_5$ concentration. The density temperature coefficient is at a minimum at an $Nb_2O_5$ concentration that corresponds to a $K_2NbF_7$:$Nb_2O_5$ ratio of 3.43. This unique point on the density temperature coefficient graph is explained by an interaction that yields $K_3NbOF_6$:

$$3\ K_2NbF_7 + Nb_2O_5 + 9\ KF = 5\ K_3NbOF_6 \qquad (55)$$

Based on Equation (55), it was concluded/assumed that niobium-containing oxyfluoride melts are characterized by the formation of complex ions $NbOF_6^{3-}$.

Systematic investigations of the electro-conductivity of niobium-containing fluoride and oxyfluoride melts were not performed. Some measurements were performed on the molten mixtures KCl – $K_2NbF_7$, KCl – KF – $K_2NbF_7$ by

Kuznetsov, Polyakov and Stangrit [317, 318] and on KCl – NaCl – NaF – $K_2NbF_7$ by Kovalev, Ioffe and Datlina [319], all in the concentration range of up to 20-25% mass of $K_2NbF_7$. In all cases, maximum electro-conductivity was observed at concentrations of about 5–10% mass of $K_2NbF_7$. The peaking of the electro-conductivity is explained by the occurrence of two processes with opposite characters. The increase in electro-conductivity is related to the increase in the concentration of potassium ions [319] and fluorine ions [317, 318], whereas the drop in conductivity results from a decrease in free volume due to an increase in $NbF_7^{2-}$ ion concentration.

### 5.3.3. Physicochemical properties of fluoride melts containing tantalum

Konstantinov et al. [320, 321] investigated the surface tension and density of molten systems $K_2TaF_7$ – KCl and $K_2TaF_7$ – KF as well as some molten mixtures containing $K_2TaF_7$, KCl, KF and $Ta_2O_5$, using the method of maximum pressure in gas bubble.

The results were presented in the form of isotherms, in which the properties are plotted versus the concentration. Nevertheless analysis of the isotherms was made based on available melting diagrams approach that the melts consist of $TaF_8^{3-}$ and $TaF_7Cl^{3-}$ complex ions. However, according to this general conception [312 – 314], the isotherm of the surface tension must, in such a case, have either a minimum or at least display prominence of the dependence in the direction of the concentration axis.

Systematic investigation of the density of molten systems $K_2TaF_7$ – KF, $K_2TaF_7$ – KCl and some compositions of KF – KCl – $K_2TaF_7$ and KF – KCl – $K_2TaF_7$ – $Ta_2O_5$ mixtures was reported in [322]. The measurements were performed by means of hydrostatic weighing. In order to avoid contaminating the melts with oxygen-containing compounds, all measurements were performed in a purified inert atmosphere and initial components were also purified. KCl was treated by the directed crystallization method, while KF was prepared by thermal decomposition of $K_2SiF_6$ as described in [323].

All compositions investigated showed a linear dependence of the density ($\rho$) on the absolute temperature (T in K), as follows:

$$\rho = a - b \cdot T \qquad (56)$$

The values of a and b were calculated for the molten systems $K_2TaF_7$ – KF and $K_2TaF_7$ – KCl, and are collected in Table 51 [322].

*Table 51. Density (ρ) of molten systems $K_2TaF_7$ – KF and $K_2TaF_7$ – KCl. Reproduced from [322], A. I. Agulyansky, P. T. Stangrit, V. I. Konstantinov, Zh. Prikl. Khim. 51 (1978) 789, Copyright 1978, with permission of "Nauka" (Russian Academy of Sciences) publishing.*

| System | $K_2TaF_7$ content (mol %) | ρ (g/cc) a | $b \cdot 10^3$ | Temperature range, °C |
|---|---|---|---|---|
| $K_2TaF_7$ – KF | 100 | 4.780 | 1.530 | 775 – 920 |
| | 90 | 4.347 | 1.157 | 765 – 900 |
| | 80 | 4.260 | 1.118 | 740 – 900 |
| | 70 | 3.971 | 0.902 | 760 – 910 |
| | 60 | 3.929 | 0.896 | 780 – 900 |
| | 50 | 3.800 | 0.841 | 780 – 900 |
| | 40 | 3.703 | 0.831 | 770 – 910 |
| | 30 | 3.535 | 0.787 | 760 – 900 |
| | 20 | 3.336 | 0.721 | 775 – 910 |
| | 10 | 3.039 | 0.687 | 790 – 900 |
| | 0 | 2.683 | 0.677 | 860 – 920 |
| $K_2TaF_7$ – KCl | 100 | 4.780 | 1.530 | 775 – 920 |
| | 90 | 3.946 | 0.870 | 740 – 910 |
| | 80 | 3.841 | 0.856 | 750 – 920 |
| | 70 | 3.737 | 0.874 | 770 – 920 |
| | 60 | 3.517 | 0.737 | 780 – 900 |
| | 50 | 3.557 | 0.879 | 790 – 910 |
| | 40 | 3.028 | 0.550 | 780 – 920 |
| | 30 | 3.025 | 0.709 | 760 – 920 |
| | 20 | 2.621 | 0.556 | 740 – 920 |
| | 10 | 2.281 | 0.480 | 740 – 920 |
| | 0 | 2.227 | 0.576 | 780 - 930 |

Electro-conductivity measurements were performed on the above systems using the double-electrode method described by Sheiko [325], and are reported in [324].

Specific conductivity ($\chi$) of all investigated mixtures showed quadratic dependence on the absolute temperature (T), which can be presented as follows:

$$\chi = a + b \cdot T + c \cdot T^2 \qquad (57)$$

Table 52 presents values of the conductivity coefficients a, b, and c as calculated for the systems $K_2TaF_7$ – KF and $K_2TaF_7$ – KCl.

Due to the fact that $K_2TaF_7$ – KF is considered to be part of the $TaF_5$ – KF binary system, while the $K_2TaF_7$ – KCl system is a component of the interconnected ternary system $K^+$, $Ta^{5+}$//$F^-$, $Cl^-$, the single-molecule conductivity and activation energy of the systems was calculated based on density and specific conductivity data [322, 324]. Molar conductivity ($\mu$) depends on the absolute temperature (T), according to the following exponential equation:

$$\log(\mu) = A - B/T \qquad (58)$$

Table 53 presents coefficients of the molar conductivity of molten systems $K_2TaF_7$ – KF and $K_2TaF_7$ – KCl.

Fig. 60 presents isotherms of the molar volume and molar conductivity at 800°C for the systems $K_2TaF_7$ – KF and $K_2TaF_7$ – KCl. For KF and for a mixture containing 0.1 molar fraction of $K_2TaF_7$, values were extrapolated to 800°C. Isotherms of the properties of $K_2TaF_7$ – KF melts were very similar to those of an ideal simple system in which no specific chemical interactions occur. For the second system, $K_2TaF_7$ – KCl, some mellowing of the melt was observed that results in the increased conductivity. This approach is typical and non-informative from the standpoint of the melt complex structure analysis. It must be taken into account that the system $K_2TaF_7$ – KF is, in general terms, part of a true binary system KF – $TaF_5$, whereas the mixture $K_2TaF_7$ – KCl is part of the interconnected ternary system $K^+$, $Ta^{5+}$//$F^-$, $Cl^-$. From this point of view, it is more informative to consider isotherms that plot properties versus melt concentration, as expressed in terms of $TaF_5$. Fig. 61 shows an isotherm (at 800°C) of the specific volume of the melts $K_2TaF_7$ – KF and $K_2TaF_7$ – KCl versus the concentration of $TaF_5$, as expressed in mass percent. In this case, the specific volume of an ideal system varies according to the additive law [313].

*Table 52. Specific conductivity ($\chi$) of molten systems $KF - K_2TaF_7$ and $KCl - K_2TaF_7$. Reproduced from [324], A. I. Agulyansky, P. T. Stangrit, V. I. Konstantinov, Zh. Prikl. Khim. 51 (1978) 2720, Copyright 1978, with permission of "Nauka" (Russian Academy of Sciences) publishing.*

| System | $K_2TaF_7$, mol fractions | $\chi = a + bT + cT^2$ $(ohm \cdot cm)^{-1}$ - a | $+b \cdot 10^3$ | $- c \cdot 10^6$ | Temperature range, °C |
|---|---|---|---|---|---|
| $KF - K_2TaF_7$ | 0 | 3.340 | 11.897 | 4.778 | 860 – 920 |
| | 0.1 | 3.433 | 11.336 | 7.590 | 770 – 910 |
| | 0.2 | 6.551 | 15.667 | 6.595 | 730 – 900 |
| | 0.3 | 10.455 | 22.171 | 9.498 | 760 – 920 |
| | 0.4 | 5.448 | 12.368 | 4.971 | 775 – 920 |
| | 0.5 | 4.644 | 10.309 | 3.948 | 785 – 920 |
| | 0.6 | 9.254 | 18.700 | 7.866 | 780 – 920 |
| | 0.7 | 9.479 | 18.900 | 7.938 | 760 – 910 |
| | 0.8 | 9.731 | 19.335 | 8.142 | 775 – 920 |
| | 0.9 | 6.767 | 13.640 | 5.602 | 800 – 920 |
| | 1.0 | 9.130 | 15.735 | 5.837 | 780 – 910 |
| $KCl - K_2TaF_7$ | 0 | 3.990 | 9.021 | 3.000 | 780 – 920 |
| | 0.1 | 9.707 | -15.152 | -7.690 | 740 – 910 |
| | 0.2 | 1.426 | -0.391 | -1.057 | 740 – 920 |
| | 0.3 | 3.277 | 7.345 | 2.113 | 755 – 920 |
| | 0.4 | 6.401 | -9.178 | -4.844 | 780 – 920 |
| | 0.5 | 6.565 | 14.469 | 5.999 | 780 – 920 |
| | 0.6 | 2.784 | 7.061 | 2.513 | 780 – 920 |
| | 0.7 | 6.482 | 13.817 | 5.628 | 765 – 910 |
| | 0.8 | 4.090 | 8.669 | 3.246 | 745 – 910 |
| | 0.9 | 6.252 | -11.656 | -6.411 | 740 - 900 |
| | 1.0 | 9.130 | 15.735 | 5.837 | 780 – 910 |

*Table 53. Molar conductivity ($\mu$, $cm^2ohm^{-1}mol^{-1}$) and conductivity activation energy ($U_\mu$) of molten systems $KF - K_2TaF_7$ and $KCl - K_2TaF_7$. Reproduced from [324], A. I. Agulyansky, P. T. Stangrit, V. I. Konstantinov, Zh. Prikl. Khim. 51 (1978) 2720, Copyright 1978, with permission of "Nauka" (Russian Academy of Sciences) publishing.*

| System | Molar fraction | | $\log(\mu) = A - B/T$ | | $U_\mu$, |
|---|---|---|---|---|---|
| | $K_2TaF_7$ | $TaF_5$ | A | $B \cdot 10^{-3}$ | Kcal/mol |
| $KF - K_2TaF_7$ | 0 | 0 | 2.746 | 0.555 | 2.540 |
| | 0.1 | 0.083 | 2.374 | 0.273 | 1.249 |
| | 0.2 | 0.143 | 2.286 | 0.329 | 1.505 |
| | 0.3 | 0.188 | 2.272 | 0.350 | 1.602 |
| | 0.4 | 0.222 | 2.337 | 0.468 | 2.141 |
| | 0.5 | 0.25 | 2.389 | 0.566 | 2.590 |
| | 0.6 | 0.273 | 2.288 | 0.478 | 2.187 |
| | 0.7 | 0.292 | 2.304 | 0.511 | 2.338 |
| | 0.8 | 0.308 | 2.332 | 0.542 | 2.480 |
| | 0.9 | 0.321 | 2.185 | 0.448 | 2.050 |
| | 1.0 | 0.333 | 3.080 | 1.552 | 7.102 |
| $KCl - K_2TaF_7$ | 0 | 0 | 2.741 | 0.749 | 3.427 |
| | 0.1 | 0.083 | 2.653 | 0.634 | 2.901 |
| | 0.2 | 0.143 | 2.613 | 0.621 | 2.842 |
| | 0.3 | 0.188 | 2.747 | 0.793 | 3.629 |
| | 0.4 | 0.222 | 2.501 | 0.548 | 2.507 |
| | 0.5 | 0.25 | 2.379 | 0.447 | 2.045 |
| | 0.6 | 0.273 | 2.431 | 0.544 | 2.489 |
| | 0.7 | 0.292 | 2.607 | 0.763 | 3.491 |
| | 0.8 | 0.308 | 2.409 | 0.648 | 2.965 |
| | 0.9 | 0.321 | 2.945 | 1.356 | 6.205 |
| | 1.0 | 0.333 | 3.080 | 1.552 | 7.102 |

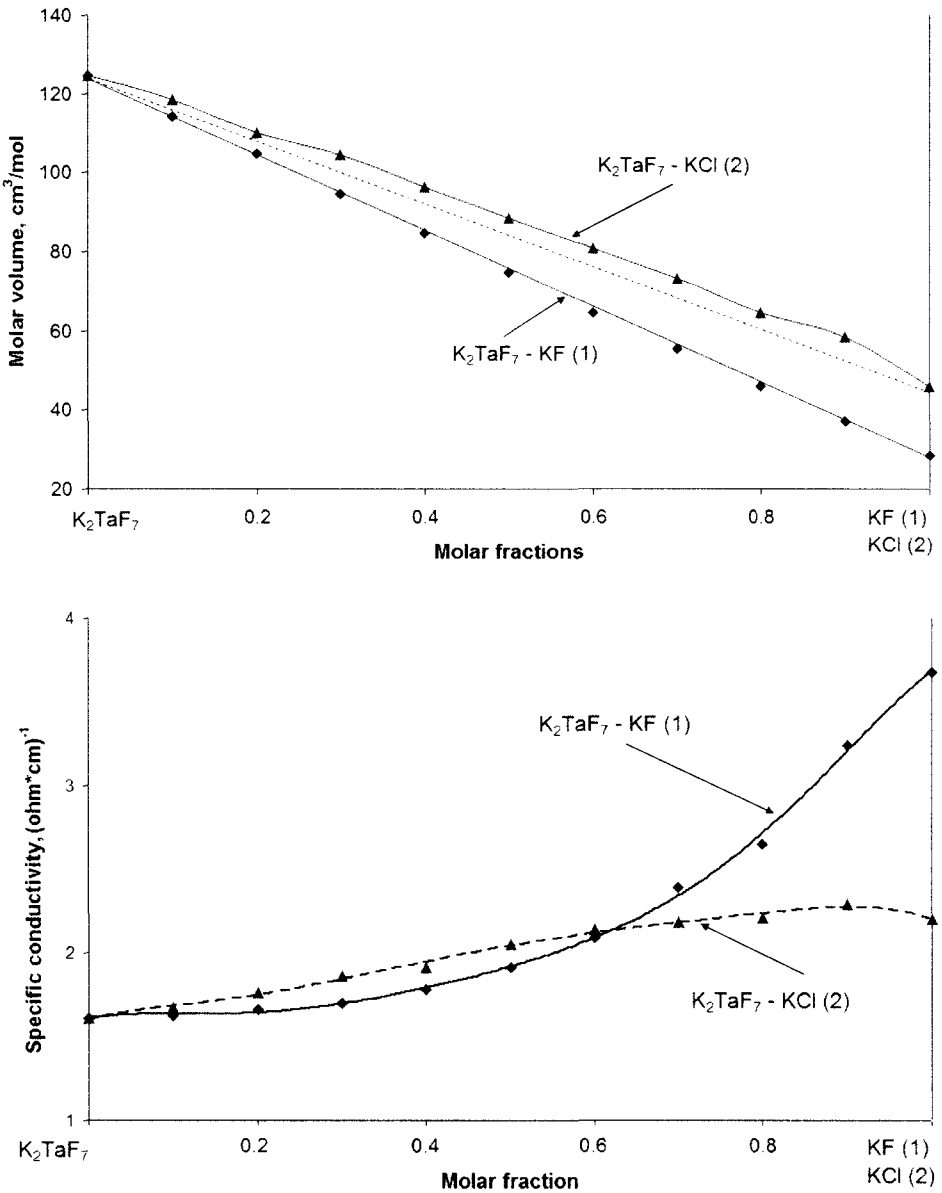


*Fig. 60. Isotherms (800°C) of molar volume (top) (after Agulyansky et al. [322]) and specific conductivity (bottom)(after Agulyansky et al. [324]) of the melts KF – $K_2TaF_7$ (1) and KCl – $K_2TaF_7$ (2).*

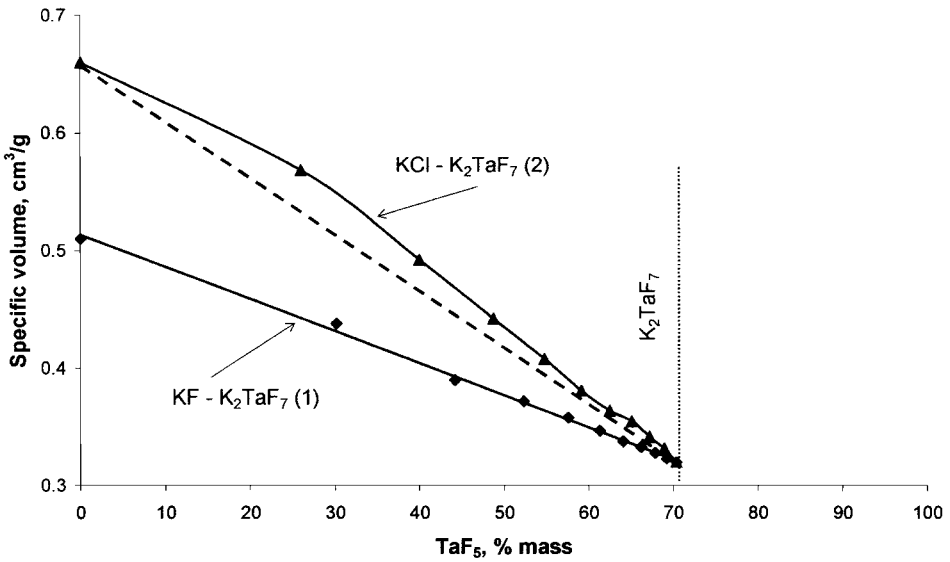


*Fig. 61. Isotherms (800°C) of specific volume versus $TaF_5$ concentration in mass percent for the molten systems KF – $K_2TaF_7$ (1) and KCl – $K_2TaF_7$ (after Agulyansky et al. [324]).*

Possible variants of the interactions for the system KF – $K_2TaF_7$ are as follows:

$$TaF_7^{2-} + F^- = TaF_8^{3-} \quad (59)$$

$$TaF_7^{2-} = 2\,F^- + TaF_5 \quad (60)$$

$$TaF_7^{2-} = F^- + TaF_6^- \quad (61)$$

Judging by the shape of the isotherms, the occurrence of the additive interaction (59) seems unlikely. No special points on the isotherms in the concentration range corresponding to the formation of $K_3TaF_8$ were observed. Based on the analysis of the isotherm of the complete system KF – $TaF_5$, the dissociation scheme described in Equation (60) is possible. Fig. 62 shows a fragment of this type of diagram. The value of the specific volume of $TaF_5$ (0.966 $cm^3/g$) was calculated by extrapolating the value reported by Fairbrother, Grundy and Thompson [326].

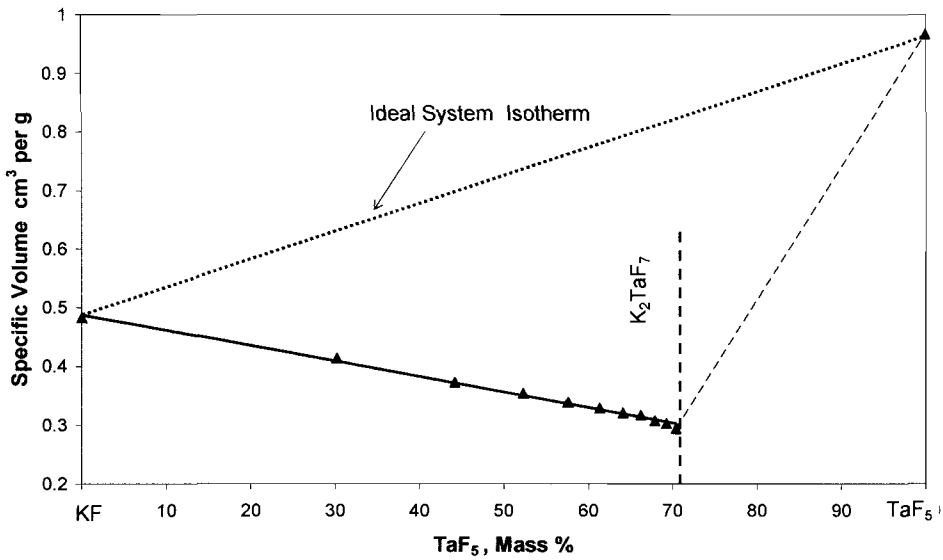


*Fig. 62. Isotherm (800°C) of the specific volume of the molten system KF – $TaF_5$.*

This approach enables to assign the KF – $TaF_5$ system to the group of systems that consist of initial components that are significantly different from one another in the nature of their chemical bonds. Formation of complexes in such systems leads to a strong compression of the melt. From this point of view, the system under discussion indeed seems to be similar to the molten system NaF – $AlF_3$ [327].

Attempts to determine the equilibrium constant for Equation (60), applying the method proposed by Fialkov [313] for an $AB_2 = A+2B$ type interaction, provided values that defy physical logic. This means that the equilibrium in Equation (60) shifts almost completely to the left, and that it is also disturbed by A + B = AB type interactions [313], which, in this case, correspond to the interaction $F^- + TaF_5 = TaF_6^-$ . Due to the improbability of the presence of $TaF_5$ in the melts, it makes more sense to attribute the $TaF_6^-$ ions to the equilibrium described in Equation (61), which provides an analogical effect on the additive values of the property.

Such a model of the melt structure does not contradict conductivity data [324], if plotted against the composition of the KF – $TaF_5$ system. Fig. 63 presents isotherms of molar conductivity, in which molar conductivity of the ideal system was calculated using Markov's Equation [315], and extrapolation

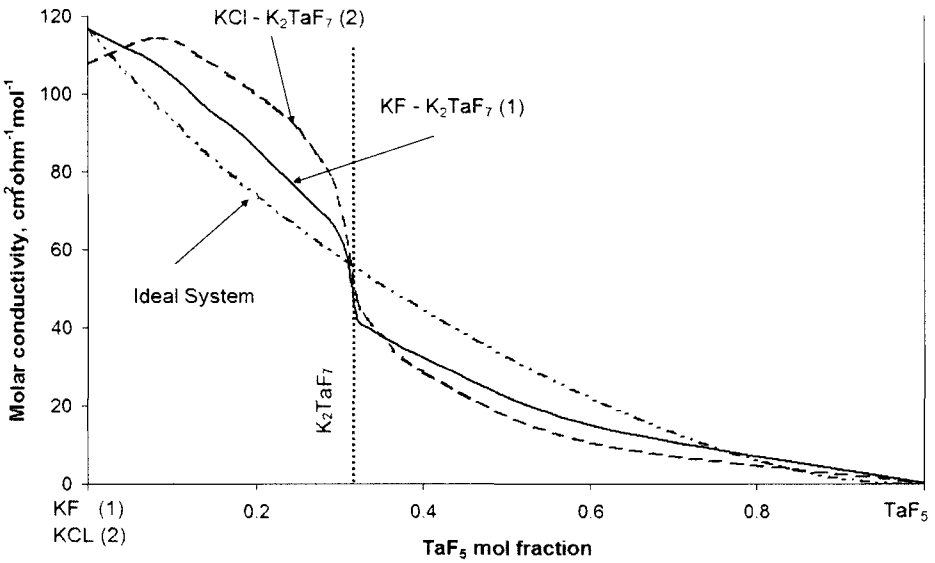


*Fig. 63. Isotherms (800°C) of the molar conductivity of molten systems KF – $K_2TaF_7$ (1), KCl – $K_2TaF_7$ (2) and an ideal system versus the concentration of $TaF_5$.*

to 800°C of the molar conductivity of $TaF_5$ was performed from data reported by Fairbrother, Grundy and Thompson [326] - $\mu_{TaF5} = 0.14$ $cm^2ohm^{-1}mol^{-1}$.

Positive deviations of molar conductivity from the values calculated for the ideal system correspond to the interaction of ionic and associated components of the system. Dissolution of KF in $TaF_5$ and the solution generated as a result, cause the dissociation of the $(TaF_5)_n$ polyanionic structure in to separate groups, leading to the ionization of the system, which undoubtedly leads in turn to an increase in its conductivity.

On the other hand, the formation of the complex ions as $TaF_{5+n}^{n-}$ leads to the opposite tendency - a decrease in conductivity. In the investigated range of the concentrations corresponding to KF – $K_2TaF_7$ side of the diagram, the first effect (i.e. the dissociation of $TaF_5$ polyanions and ionization of the melt) predominates, while in melts containing higher concentrations of $TaF_5$, the second mechanism, leading to a decrease in conductivity, is more significant [328].

As a whole, the KF – $TaF_5$ system forms melts that are characterized by a decrease in molar volume and increase in molar conductivity, as demonstrated in Fig. 64. This behavior enables classification of the system as a IIb-type

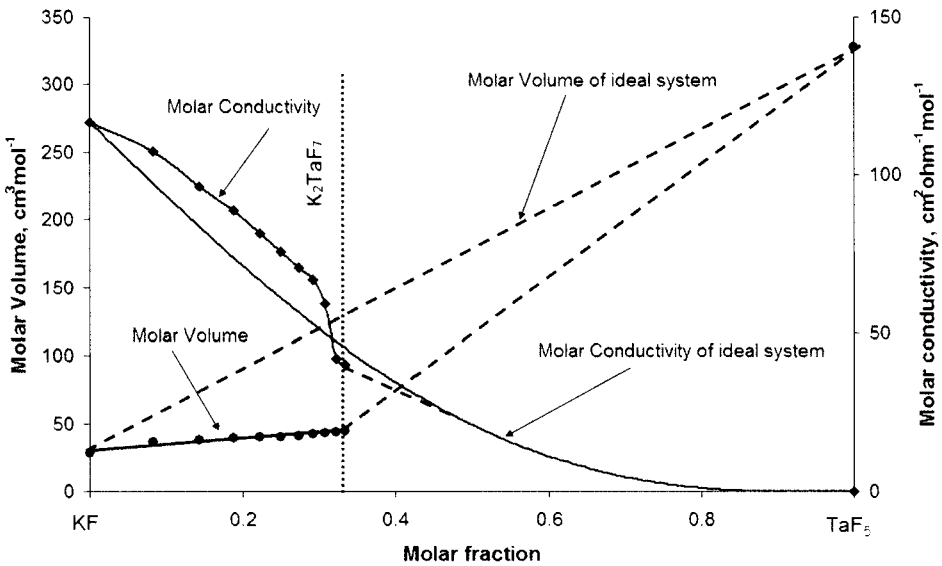


*Fig. 64.Isotherms of molecular properties of the molten system KF – $TaF_5$.*

system according to the classification method developed by Markov, Prisyagny and Volkov [314]. Such systems consist of an ionic component and associated initial components, which, during the melting process, form complex ions.

The same analysis of the properties of niobium-containing melts [316, 317] shows that the KF – $NbF_5$ system exhibits behavior similar to that of the tantalum-containing melts.

The specific concave shape of the isotherms of the properties of KCl – $K_2TaF_7$ melts can be explained by the following ligand-replacement interaction:

$$TaF_7^{2-} + Cl^- = TaF_6Cl^{2-} + F^- \qquad (62)$$

The interaction (62) yields a more mobile $F^-$ ion and a volumetric complex ion – $TaF_6Cl^{2-}$.

In order to estimate the value of the dissociation constant of the $TaF_7^{2-}$ complex according to the aforementioned scheme (61), $TaF_7^{2-} = F^- + TaF_6^-$, analysis of the available volume values was performed using a modified method developed by Frank and Foster [329]. This method is based on two main initial assumptions. The first is that the dissociation constant remains

constant with the change in the melt composition, and the second is that the total volume consists of the added contributions of the partial volumes of the initial and forming components. Despite the above assumptions, the method provides an adequate fit with experimental results obtained for molten systems NaF – $AlF_3$ [329] and LiF – $AlF_3$ [330]. A detail description of the model developed and adapted to tantalum-containing melts, as well as the deduction of the main equation, are presented in [331].

Calculations were performed for the dissociation reaction, as represented in molecular form, as follows:

$$K_2TaF_7 = KF + KTaF_6 \tag{63}$$

The equilibrium constant, $K_F$, for the above equation can be written as:

$$K_F = \frac{[KF]\cdot[KTaF_6]}{[K_2TaF_7]} = \frac{\beta_i}{1-\beta_i}\cdot\frac{1-N_i(3-\beta_i)}{1-N(2-\beta_i)} \tag{64}$$

Where [KF], [$KTaF_6$] and [$K_2TaF_7$] are molar concentrations of KF, $KTaF_6$ and $K_2TaF_7$, respectively; $N_i$ = variable molar fraction of $TaF_5$; $\beta_i$ = variable degree of dissociation of $K_2TaF_7$.

It is easy to show that the partial densities (ρ) of the components can be presented as follows:

$$\rho_{KF} = 1-\rho_i(1+2k-\beta_i k) \tag{65}$$

$$\rho_{KTaF_6} = \rho_i\beta_i(1+k) \tag{66}$$

$$\rho_{K_2TaF_7} = \rho_i(1-\beta_i)(1+2k) \tag{67}$$

where $\rho_i$ = variable density of the melt; $k$ = molecular weight ratio, $M_{KF}/M_{TaF_5}$.

Based on the assumption that the total specific volume can be calculated as the sum of the partial specific volumes of the initial and forming components, and expressed $\rho_i$ by $TaF_5$ molar fraction – $N_i$ using equation (64), an equation representing the total variable density of the melt ($\rho_i$) can be written as follows:

$$\frac{1}{\rho_i} = \frac{1}{\rho_{KF}} + \frac{A\cdot N_i\cdot(B-\beta_i)}{k+N_i(1-k)} \tag{68}$$

where $\beta_i = \frac{1-3N_i}{2N_i} + \sqrt{\left(\frac{1-3N_i}{2N_i}\right)^2 + \frac{k(1-2N_i)}{N_i(k+1)}}$

Constants $A$ and $B$ depend on the dissociation constant, $K_F$. For the molten system KF – $TaF_5$ at 900°C, the calculation, based on a nonlinear regression using the least squares method, gives the values: $A = 0.23 \pm 0.01$; $B = 1.87 \pm 0.01$ and $K_F = 0.82 \pm 0.02$. Taking into account that the dissociation constant $K_F$ is related to $\alpha$, the degree of dissociation of pure $K_2TaF_7$ according to $K_F = \alpha^2/(1 - \alpha^2)$, can be estimated to be $\alpha = 0.67$.

This means that in its molten state, $K_2TaF_7$ is significantly dissociated, yielding KF and $KTaF_6$.

Using the defined dependence on $TaF_5$ concentration of the degree of dissociation $\beta_i$, the molecular composition of the melt was calculated and is presented in Fig. 65.

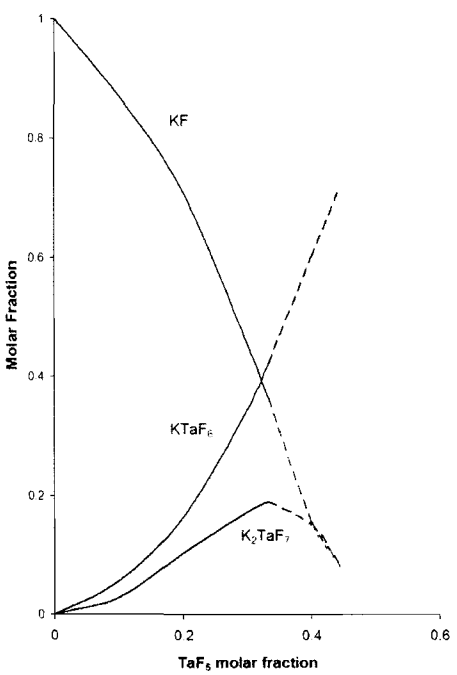


*Fig. 65. Molar composition of molten system KF – $TaF_5$ at 900°C (after Agulyansky and Khomchenko [331]).*

The calculation of the ionic composition (see Fig. 66) is based on the assumption that the salts dissociate completely, yielding potassium ions, $K^+$, fluorine ions, $F^-$, and complex fluorotantalete ions, $TaF_6^-$ or $TaF_7^{2-}$, as described below:

$$KF = K^+ + F^- \tag{69}$$

$$KTaF_6 = K^+ + TaF_6^- \tag{70}$$

$$K_2TaF_7 = 2\,K^+ + TaF_7^{2-} \tag{71}$$

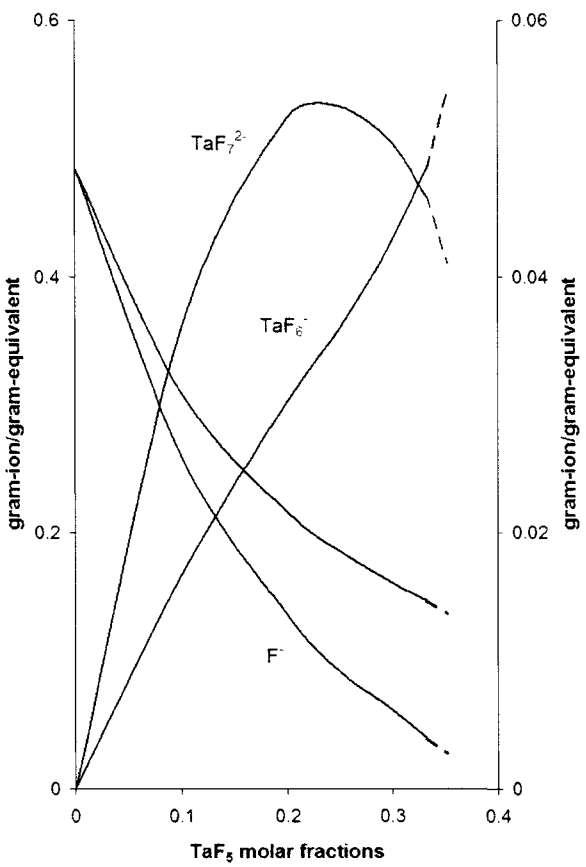


*Fig. 66. Ionic composition of molten system KF – $TaF_5$ at 900°C (after Agulyansky and Khomchenko [331]).*

The molten system KCl – $K_2TaF_7$ was analyzed using the same method and the ionic equilibrium calculated is as follows:

$$2\ TaF_7^{2-} + Cl^- = 2\ F^- + TaF_6^- + TaF_6Cl^{2-} \quad (72)$$

This equilibrium covers the presence of all inferred types of complex ions. The equilibrium constant of Equation (72) can be written as $K = K_F^{\ 2} / K_{Cl}$, where $K_F$ and $K_{Cl}$ are the dissociation constants of complex ions $TaF_7^{2-}$ and $TaF_6Cl^{2-}$, respectively. The calculation indicated that $K_{Cl} \approx 0.2$. The most important conclusion from the above calculations is that both dissociation constants, $K_F$ and $K_{Cl}$, are of the same order of magnitude. This indicates that the formation of $TaF_7^{2-}$ and $TaF_6Cl^{2-}$ complexes occurs essentially with equal probability, a fact that confirms the validity of the ionic exchange interaction (62).

The concept of the formation of heteroligand complexes in the melts explains the appearance of peaks in the range of 5 – 10 % (mass) of $K_2TaF_7$ [324] on the isotherms of the specific conductivity of molten mixtures KCl – KF – $K_2TaF_7$ (Fig. 67).

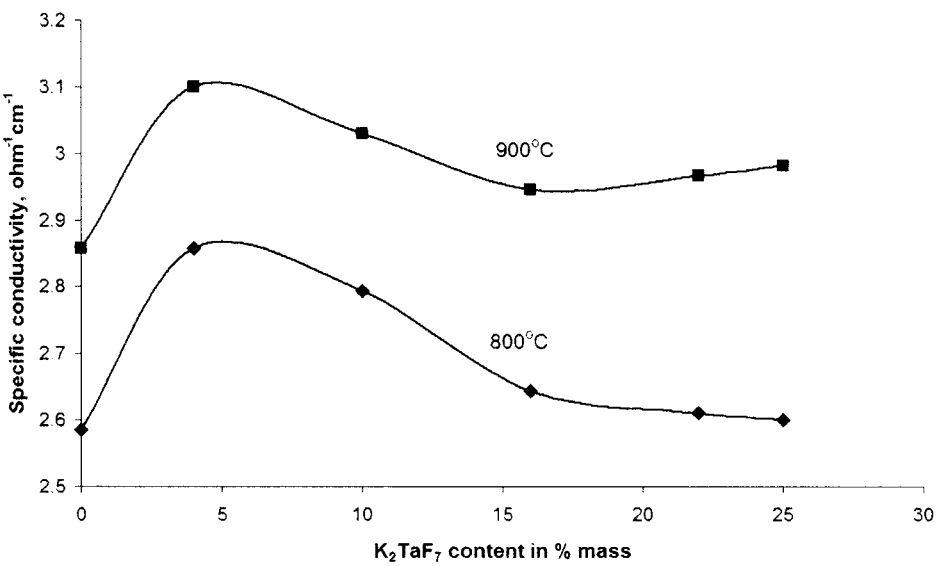


*Fig. 67. Isotherms of the specific conductivity of KF – KCl – $K_2TaF_7$ melts (KF:KCl = 1:2 mass). Reproduced from [324], A. I. Agulyansky, P. T. Stangrit, V. I. Konstantinov, Zh. Prikl. Khim. 51 (1978) 2720, Copyright 1978, with permission of "Nauka" (Russian Academy of Sciences) publishing.*

At low $K_2TaF_7$ concentrations (< 5% mass), the increase in conductivity is related to the dissociation of $TaF_7^{2-}$ ions, according to Equation (61), whereas the decrease in conductivity at higher concentrations of $K_2TaF_7$ can be explained by the formation of $TaF_6Cl^{2-}$ complexes according to the following interaction:

$$TaF_6^- + Cl^- = TaF_6Cl^{2-} \quad (73)$$

Using the same mechanism based on interactions (61) and (73), the peaks of the conductivity isotherms for niobium-containing molten systems KCl – $K_2NbF_7$, KCl – KF – $K_2NbF_7$ [317, 318], KCl – NaF – $K_2NbF_7$ [319] can be explained.

Analysis of isotherms of physicochemical properties can also clarify the interactions within molten systems that contain oxides. For example, the interaction between potassium fluorotantalate and tantalum oxide, $Ta_2O_5$, can be studied using density isotherms of molten mixtures. Fig. 68 demonstrates the dependence of the density on $K_2TaF_7$ concentration for mixtures $K_2TaF_7$ – KF – KCl and $K_2TaF_7$ – KF – KCl – $Ta_2O_5$.

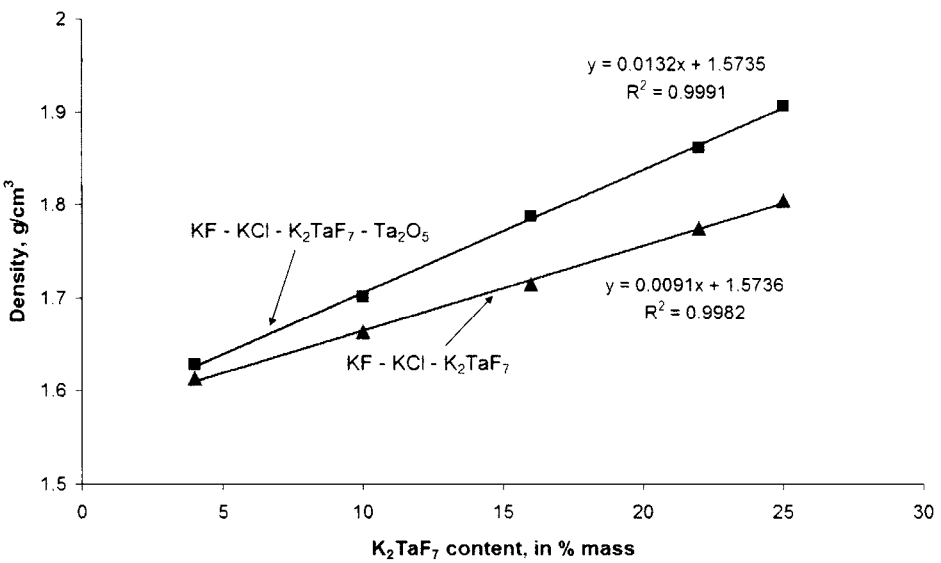


*Fig. 68. Density of molten mixtures $K_2TaF_7$ – KF – KCl and $K_2TaF_7$ – KF – KCl – $Ta_2O_5$ versus concentration of $K_2TaF_7$ at 800°C. KF:KCl = 1:2 (mass ratio) and $K_2TaF_7$:$Ta_2O_5$ = 3 (molar ratio).*

It should be mentioned that systematic investigations of the solubility of $Ta_2O_5$ in KF – KCl melts containing $K_2TaF_7$ performed by Konstantinov and coworkers [332] indicated that the solubility of tantalum oxide depends on the concentration of $K_2TaF_7$ achieving a maximum $K_2TaF_7$:$Ta_2O_5$ molar ratio of 3 for relatively dilute melts.

Thus, the composition of the melts used for the density measurements (see Fig. 68) was such that a KF:KCl ratio of 1:2 (mass) was maintained in both cases and a $K_2TaF_7$:$Ta_2O_5$ ratio of 3:1 (mol) was maintained in the second set of the experiments. Such compositions led to the inferring of the following interaction:

$$3\ TaF_7^{2-} + Ta_2O_5 + m\ F^- = 5\ TaOF_{(21+m)/5}^{(6+m)/5-} \qquad (74)$$

When it is considered that the partial densities of pure fluoride and oxyfluoride complexes are approximately equal, the changes in density caused by the addition of tantalum oxide can be attributed to the concentration changes only. These concentration changes can occur according to Equation (74), as a result of the formation of five oxyfluoride ions from only three heptafluorotantalate ions and the consequent drop in fluoride ion concentration. This assumption is indeed logical and reasonable, especially in case of relatively dilute systems with relatively low concentrations of tantalum-containing ions. On the other hand, the above model enablesto estimate the magnitude of m mentioned in Equation (74). It was found that m varies from 9 to 4.5 with an increase in $K_2TaF_7$ concentration from 5 to 25% (mass). The results indicate that melts that contain low concentrations of tantalum are characterized by the formation of the complex ion $TaOF_6^{3-}$ according to the following interaction:

$$3\ TaF_7^{2-} + Ta_2O_5 + 9\ KF = 5\ TaOF_6^{3-} \qquad (75)$$

Increasing the concentration of tantalum in the melt can lead to the formation of complex oxyfluorides with lower coordination numbers, such as $TaOF_5^{2-}$ or $TaOF_4^-$. Nevertheless, as can be seen in the melting diagram of the ternary interconnected system K, Ta//O, F, which displays no dystectic point that corresponds with the compound $K_2TaOF_5$, the formation of $TaOF_5^{2-}$ ions seems hardly probable. Hence, it seems more likely that polyanions are formed, which are made up of oxyfluorotantale ions linked by oxygen "bridge" atoms as was found among the $(-TaOF_4^-)_n$. chains in solid state.

The proposed model of the structure of oxyfluoride melts corresponds with the conductivity results shown in Fig. 69. The specific conductivity of the melt drops abruptly and asymptotically approaches a constant value with the increase in tantalum oxide concentration. This can be regarded as an additional indication of the formation of oxyfluorotantale-associated polyanions, which leads to a decrease in the volume in which light ions, such as potassium and fluorine, can move. The formation of the polyanions can be presented as follows:

$$3\ n\ TaF_7^{2-} + n\ Ta_2O_5 = 5\ (TaOF_4^-)_n + n\ F^- \quad (76)$$

Analysis of the physicochemical properties of fluoride and oxyfluoride melts reveals that the complex ions are characterized by coordination numbers that do not exceed seven. Fluoride melts consist of the complex ions $MeF_7^{2-}$ and $MeF_6^-$. Molten chloride-fluoride systems initiate the formation of heteroligand complexes of the form $MeF_6Cl^{2-}$. Oxyfluoride and oxyfluoride-chloride melts can contain oxyfluoride complexes $MeOF_6^{3-}$ at relatively low concentrations. The behavior of the more concentrated melts can be attributed to the formation of oxyfluorometalate polyanions.

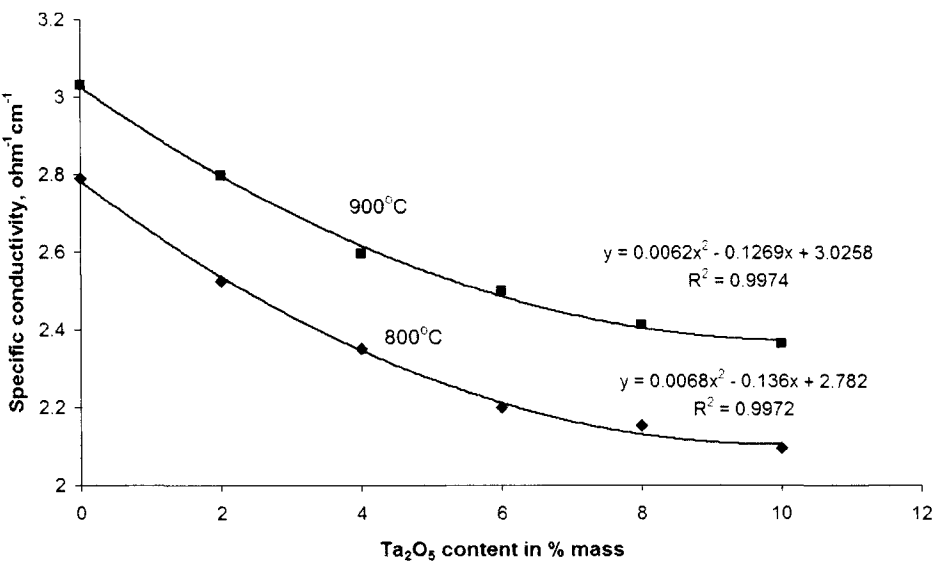


*Fig. 69. Specific conductivity of molten mixtures KCl – KF – $K_2TaF_7$ – $Ta_2O_5$ versus $Ta_2O_5$ content at 800 and 900°C*

## 5.4. Vibration spectroscopy of fluoride melts

### 5.4.1. Experimental techniques

High refractory properties, extremely strong sensitivity to moisture and exceptionally high chemical activity of fluoride melts, especially of those containing ions of polyvalent metals, make spectral measurements of such melts extremely complicated. In order to obtain reliable results, the measurement cell must comply with three main requirements:

- high melting point and high thermal stability;
- transparency in the appropriate spectral range;
- chemical inertness relative to the investigated molten material.

Due to the above requirements, typical optically-transparent materials, such as oxides (glass, quartz, alumina, zirconium oxide etc.) and halides (sodium chloride, lithium fluoride, calcium fluoride, potassium bromide, cesium bromide etc.) are usually unsuitable for use with fluoride melts. Therefore, no standard procedure exists at present for the spectral investigation of fluoride melts, and an original apparatus must be created especially for each particular case.

Experimental methods of IR spectroscopy measurements can be divided into three main groups:

- Traditional scheme using diamond or graphite windowless cells;
- Transmission spectra of thin layers held by nets or plates;
- Reflection spectra;
- Emission spectra from thin or thick layers.

Information exists about the use of measuring cells made entirely of diamond or graphite with or without embedded diamond windows. Diamond cells were used, for instance, by Toth and Gilpatrick [333] in the investigation of the Nb(IV) spectrum in a LiF – $BeF_2$ molten system at 550°C. Windowless graphite cells for the IR spectroscopy of melts were developed by Veneraky, Khlebnikov and Deshko [334]. Diamond, and in some cases windowless sapphire or graphite micro-cells, were also applied for Raman spectroscopy measurements of molten fluorides.

Figs. 70, 71 and 72 show schematic descriptions of the three latter above-listed methods. The main advantages and disadvantages of the methods were discussed in general by Volkov and Yazimirsky [294], for all types of molten salts. Regarding the application of the above-mentioned techniques in the investigation of molten fluorides, the following points should be mentioned.

Volkov and Sushko [335] described a technique that is based on the use of nets. This method provides direct absorption spectra, but is very complex to perform: The net must be placed in a chamber that ensures a pure inert atmosphere so as to avoid hydrolysis of the melt, and the temperature and geometry of the net must be kept very stable. Other major limitations of the method are the requirements that the surface tension of the melt be such that its position on the net is ensured, and that the vapor pressure of the material in molten state be as low as possible

The method based on a net melt-holder is used successfully for materials with relatively low melting points and is less promising for the investigation of fluoride melts containing tantalum and niobium.

The second method, based on measurements of IR reflection spectra, is simpler and enables working with larger volumes of molten salt. No special problems involving temperature and atmosphere control exist. The method was used successfully by Fordyce and Baum [336-338] in the investigation of fluoride melts containing tantalum and niobium.

The main disadvantage of this method is that the IR reflection spectra must be recalculated and converted to absorption spectra, and possible distortion of the spectra by the thermal emission of the melt must be taken into account.

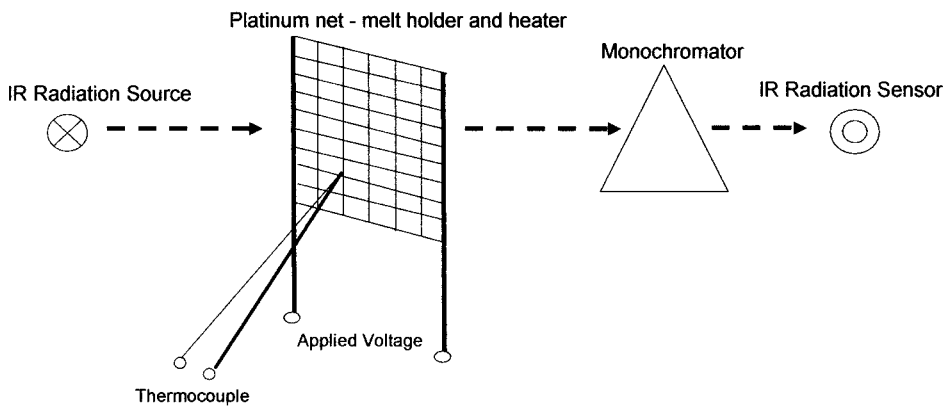


*Fig. 70. IR transmission spectroscopy. A thin layer of melt is held and heated by the net.*

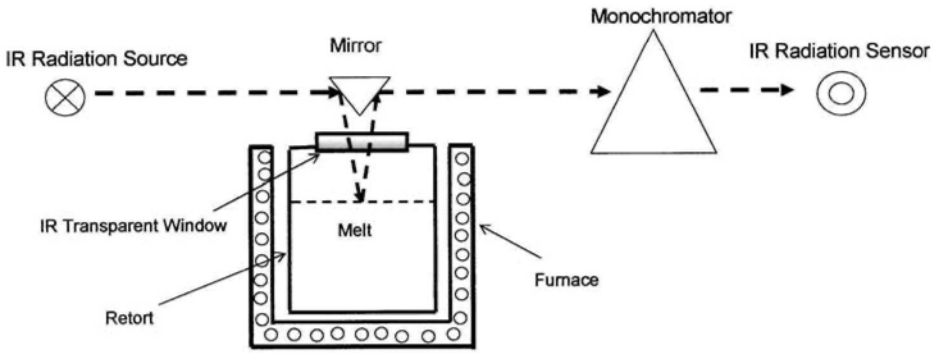


*Fig. 71. IR reflection spectroscopy.*

The simplest technique is the IR emission spectroscopy method, as presented schematically in Fig. 72. The method allows the successful investigation of aggressive molten materials and is generally applicable over a very wide range of temperatures and concentrations.

Two modifications of the technique are used: emission from "thin" layers [339 – 341] and emission from "thick" layers of the melt [342].

The emission capability $\varepsilon(\lambda,T)$ of the melt depends on the wavelength ($\lambda$) and temperature (T), and can be represented by following the equation, as demonstrated by Kozlowski (77) [339]:

$$\varepsilon(\lambda,T) = (1 - r_1)[1 + (r_1 - r_2)\exp(-kd) + (r_2 - r_1)r_1\exp(-2kd) - r_1r_2\exp(-2kd)] \quad (77)$$

where d = melt layer thickness, k = absorption coefficient of the melt, and $r_1$ and $r_2$ = reflection coefficients of the melt surface and bottom surface of the container, respectively.

A quick analysis of Equation (77) shows that if the melt layer is thin ($kd << 1$), the emission spectrum corresponds to an absorption spectrum. This means that the emission peaks occur at the same wave numbers as the absorption bands. In case of thick melt layers ($kd >> 1$) Equation (77) becomes the following expression:

$$\varepsilon(\lambda, T) = 1 - r_1 \quad (78)$$

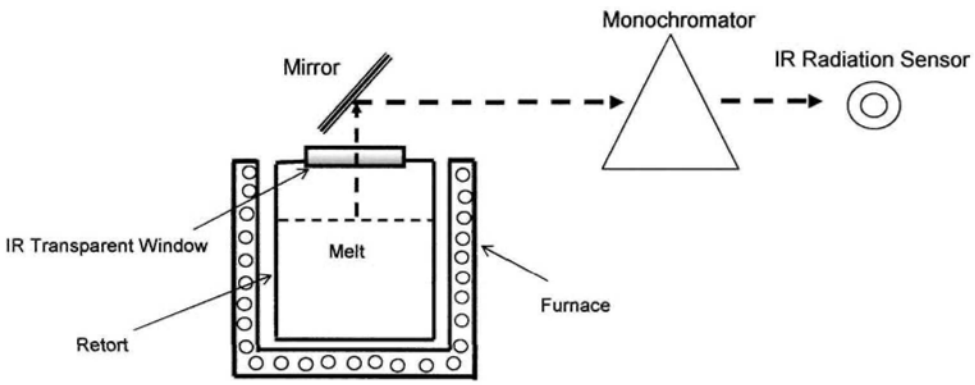


*Fig. 72. IR emission spectroscopy.*

Consequently, in the emission spectrum of thick layers (kd >> 1) the minimums occur at wave numbers that correspond to the maximums of the reflection spectrum. Fig. 73 shows a typical example of this spectrum transformation.

The spectra obtained using the apparatus described in [342] is appropriate for IR emission measurements of both thin and thick layers of melts.

Measurements were performed on a potassium nitrite melt ($KNO_3$) at 450°C. Fig. 73, curve 1 presents the spectrum obtained for a melt layer 0.05–0.1 mm thick, which was placed on a reflective surface (polished platinum). Fig. 73, curve 2 presents the inverted spectrum (relative to curve 1) of a relatively thin layer placed on an absorptive bottom surface (carbon-glass).

In the first case, a typical emission spectrum of a thin layer melt is observed, because the emission from the bottom surface is negligible compared to that from the melt itself. In the second case, the relationship between the emission from the bottom surface and the emission from the melt is reversed, so that the spectrum reverts to being similar to a regular absorption spectrum.

Increasing the layer thickness (Fig. 73, curve 3) changes the shape of the bands as a result of the increased influence of the reflection capability of the melt. Nevertheless, the shift in bands is not significant.

Further increasing of the melt layer thickness leads to a decrease in the intensity of the bands until complete disappearance thereof.

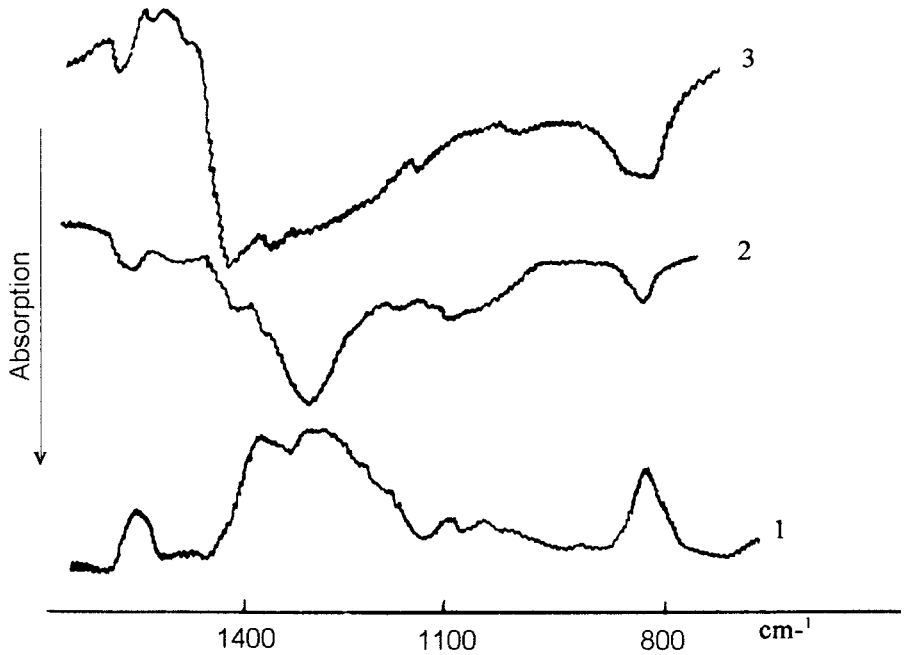


*Fig. 73. IR emission spectra of $KNO_3$ melt at 450°C.*
*Curve 1 – Layer thickness - ~0.05 mm, reflective surface*
*Curve 2 – Layer thickness - ~0.1 mm, absorptive surface*
*Curve 3 – Layer thickness - ~0.2 mm, absorptive surface*
*(after Agulyansky and Sakharov [342]).*

Opposite behavior was displayed by molten fluoride systems. For instance, no bands were observed in the thin layer emission spectrum of a KF – $K_2SiF_6$ melt, whereas increasing the melt layer to 10–20 mm led to the appearance of two intensive bands at 730 and 476 $cm^{-1}$. These bands correspond to $\nu_3$ and $\nu_4$ vibrations of the complex ion $SiF_6^{2-}$. Solid $K_2SiF_6$ is characterized by IR absorption bands at 741 and 483 $cm^{-1}$ [343].

Such differences of the thermal IR emission spectra of compounds that consist of oxygen-containing ions and halide ions are related to the relationships between the compounds' optical parameters.

There is no doubt that IR emission spectroscopy of thick layers is preferable for investigations of fluoride melts containing tantalum and niobium.

Analysis of the dependence of absorption and reflection coefficients on the frequency shows that the emission spectra of thick layers of melts are similar to their molecular scattering and are actually quite close to their absorption spectra. This analysis enables the assessment of the emission spectra of similar compounds with no need for any additional calculations [294, 344].

The investigation of IR emission spectra from samples of varying thickness is widely used for solids as well [345, 346].

## 5.4.2. Brief review of molten fluoride systems

Fluoride systems containing aluminum trifluoride, $AlF_3$, were investigated in greater detail. Based on Raman spectra, researchers repeatedly demonstrated the presence of two types of complex ions, $AlF_4^-$ and $AlF_6^{3-}$ [347 – 350]. The spectral parameters of these complexes are as follows (wave numbers in $cm^{-1}$):

$AlF_4^-$ ($T_d$) – 625 ($\nu_1$, $A_1$); 210 ($\nu_2$, E); 760 ($\nu_3$, $T_2$); 322 ($\nu_4$, $T_2$)

$AlF_6^{2-}$ ($O_h$) – 555 ($\nu_1$, $A_{1g}$); 247 ($\nu_5$, $T_{2g}$).

Quist, Bates and Boyd investigated Raman spectra of the molten systems NaF – LiF – $BeF_2$ [351] and $NaBF_4$ – NaF [352] and characterized the complexes $BeF_4^{2-}$ and $BF_4^-$ as having a tetragonal configuration. Wave numbers are as follows ($cm^{-1}$):

$BeF_4^{2-}$ ($T_d$) – 547 ($\nu_1$); 255 ($\nu_2$); 800 ($\nu_3$); 385 ($\nu_4$);

For the $BF_4^-$ complex, a band corresponding to $\nu_1$ at 773 $cm^{-1}$ was observed. Additional bands were found in the range of 660–715 $cm^{-1}$ and were assigned to bond vibrations of the complexes $SiF_5^-$ and $SiF_6^{2-}$ [352].

Wilmshurst [353] observed the following bands were in the IR reflection spectra of some mixtures belonging to the LiF – NaF – KF – $ZrF_4$ system ($cm^{-1}$): 720, 520, 480, 240. The band at 480 $cm^{-1}$ was assigned to bond vibrations of either $ZrF_5^-$ or $ZrF_6^{2-}$, while bands at 520 and 240 $cm^{-1}$ were

attributed to vibrations of a quasi-lattice formed by fluorozirconate ions and of alkali metal fluoride ions, respectively.

Toth, Quist and Boyd [354] investigated the Raman spectra of LiF – NaF – $ZrF_4$ melts and showed that increasing the $ZrF_4$ concentration from 14% to 40% (mol), leads to a shift in the intensive polarized band from 555 to 593 $cm^{-1}$. A similar effect was observed also for LiF – NaF – $ThF_4$ melts [355], whereby a frequency shift of the symmetric vibration occurred when concentration of polyvalent metal was increased. This phenomenon was explained by the reduction of the polyvalent metal's coordination number.

Fordyce and Baum investigated the IR reflection spectra of niobium- and tantalum-containing fluoride melts. In LiF – NaF – KF melts that contained up to 0.1 molar fraction of either $TaF_5$ or $NbF_5$, a pair of bands were observed at 535 and 300 $cm^{-1}$ [336] or at 555 and 315 $cm^{-1}$ [337], respectively. Based on a comparison of this spectra with the spectra obtained for solid phases with a known structure, it was concluded that $TaF_7^{2-}$ and $NbF_7^{2-}$ are present in the corresponding melts. Measurements performed on melts that contained no KF led to the conclusion that $TaF_6^-$ or $NbF_6^-$ can occur in the melts as well.

The hydrolysis of melts containing KF – LiF and $NbF_5$ [337] or $TaF_5$ [338] was investigated. Hydrolysis was performed by bubbling of moisturized inert gas through the melt. IR reflection spectra of the resultant system displayed bands in the range of 900–920 $cm^{-1}$, in addition to those mentioned above. Comparative analysis of the spectra [337, 338] led to the conclusion that, following hydrolysis, melts with low concentrations of $NbF_5$ or $TaF_5$ yield oxyfluoride complexes $NbOF_6^{3-}$ or $TaOF_6^{3-}$.

The same results were obtained in the investigation of IR emission spectra of thick layers of the melts [342]. In the case of molten potassium fluoride containing up to 0.1 mol fraction $K_2TaF_7$ at 850°C, a band was observed at 545 $cm^{-1}$, which confirms the presence of the complex ion $TaF_7^{2-}$. The addition of 0.01 mol fraction of potassium hydroxide, KOH, to the above melt leads to the appearance of an additional band at 910 $cm^{-1}$, which indicates the formation of $TaOF_6^{3-}$ complex ions. IR emission spectrum of molten $K_2TaF_7$ at 850°C displays two bands, at 546 and 610 $cm^{-1}$, which are assigned to $TaF_7^{2-}$ and $TaF_6^-$ complex ions, respectively [356].

The formation of complexes in fluoride and oxyfluoride melts containing tantalum and niobium will be discussed later on in detail.

Table 54 contains general information on molten fluoride systems reviewed here.

*Table 54. Vibration spectra of complex ions in fluoride melts.*

| System | Complex ions | Wave numbers, $cm^{-1}$ | Spectrum | Ref. |
|---|---|---|---|---|
| $NaF–LiF–BeF_2$ | $BeF_4^{2-}$ | 547, 255, 800, 385 | Raman | [351] |
| $NaF–NaBF_4$ | $BF_4^{2-}$ | 773 | Raman | [352] |
| $MF–AlF_3$ | $AlF_4^-$ | 625, 210, 760, 320 | Raman | [347– |
| | $AlF_6^{3-}$ | 555, 247 | Raman | - 350] |
| $LiF–NaF–ThF_4$ | $ThF_7^{3-}$, $ThF_8^{4-}$ | 474-478, 250 | Raman | [355] |
| $LiF–NaF–KF–ZrF_4$ | $ZrF_5^-$, $ZrF_6^{2-}$ | 720, 520, 480, 240 | IR | [353] |
| $LiF–NaF–ZrF_4$ | $ZrF_8^{4-}$ - $ZrF_4$ | 555–593, 320, 250 | Raman | [354] |
| $LiF–KF–TaF_5$ | $TaF_7^{2-}$ | 535, 300 | IR | [336] |
| $KF – K_2TaF_7$ | $TaF_7^{2-}$ | 545 | IR | [342] |
| $K_2TaF_7$ | $TaF_7^{2-}$ | 546 | IR | [356] |
| | $TaF_6^-$ | 610 | IR | [356] |
| $LiF–KF–TaF_5$ (Hydrolysis) | $TaOF_6^{3-}$ | 910 | IR | [338] |
| $KF-K_2TaF_7$ - KOH | $TaOF_6^{3-}$ | 910 | IR | [356] |
| $LiF–KF–NbF_5$ | $NbF_7^{2-}$ | 555, 315 | IR | [337] |
| $LiF–KF–NbF_5$ (Hydrolysis) | $NbOF_6^{3-}$ | 920 | IR | [337] |

## 5.4.3. Tantalum-containing fluoride melts

The melting process of potassium fluorotantalate, $K_2TaF_7$, was investigated by IR emission spectroscopy using thick layers of the melt [356]. It should be mentioned that in some cases, if the temperature of the sample is high enough, the above method enables to obtain spectra of the material in solid state as well.

Fig. 74 shows the IR emission spectrum of the transition of $K_2TaF_7$ from solid to molten state.

The IR spectrum obtained at ambient temperature (Fig. 74, curve 1) shows the presence of a strong wide band at 535 $cm^{-1}$ and a weak shoulder at about 643 $cm^{-1}$. At the melting temperature (curve 2), the only discernable band observed is shifted slightly toward the higher wave numbers and occurs at 535–540 $cm^{-1}$. This high frequency shift, which accompanies the melting, is related to changes in the distances between the central atom and the first and second coordination spheres, as illustrated in Fig. 75.

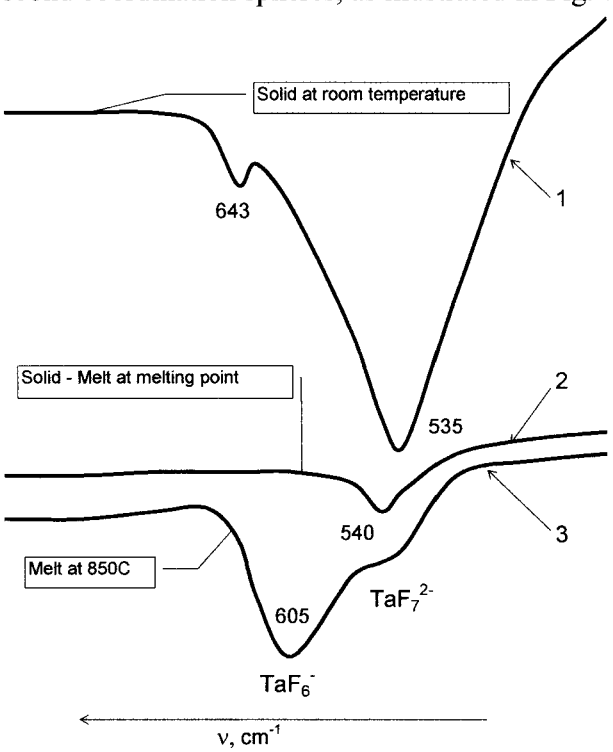


*Fig. 74. IR spectra of $K_2TaF_7$ at ambient temperature (curve 1), at melting point (curve 2) and at 850°C (curve 3) (after Agulyansky, Kirillov, Prisyagny [356]).*

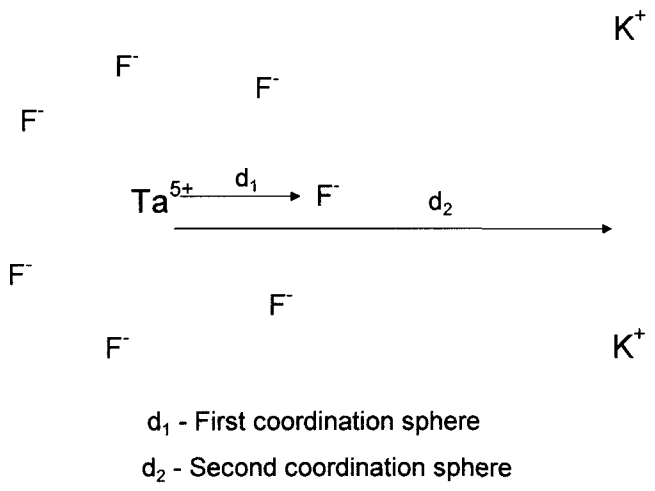


*Fig. 75. Schematic structure of the first and second coordination spheres*

Fluorine ions form the first coordination sphere around the tantalum ion, which is the central atom of the complex. Potassium ions form the second coordination sphere, which significantly affects the geometry and force field of the first coordination sphere. The melting of $K_2TaF_7$ leads to the dissociation of the compound into ions, as follows:

$$K_2TaF_7 = TaF_7^{2-} + 2\,K^+ \qquad (79)$$

This dissociation is in effect an extension of the diameter $d_2$ of the second coordination sphere and the subsequent decrease in the intrinsic interaction potential of the outer sphere. Therewith, the inter-spherical interaction potential between the central atom and the first coordination sphere increases, leading to shortening of the distance $d_1$, which in turn leads to an increase in the frequency of the Ta-F bond vibration.

Further increase of the temperature leads to the appearance of a strong band at ~605 $cm^{-1}$ (see Fig. 74, curve 3) along with the band at ~540 $cm^{-1}$, which remains unchanged. Comparative analysis of the spectra shows that the above bands refer to the vibrations of the complex ions $TaF_6^-$ and $TaF_7^{2-}$, respectively.

The spectral bands corresponding to $TaF_6^-$ and $TaF_7^2$ in molten state are shifted towards higher frequencies, compared to their position in corresponding spectra obtained for the crystals. This phenomenon is common and is observed for other systems as well.

Particularly, Gadgiev and Kirillov [357] showed that the frequency shift that occurs in crystals due to an increase in temperature coincides with the shift that is due to the melting of the crystal.

The formation of $TaF_6^-$ ions is related to the dissociation of $TaF_7^{2-}$ complexes by a known mechanism:

$$TaF_7^{2-} = TaF_6^- + F^- \quad (80)$$

The equilibrium between the complexes formed according to Equation (80) depends both on the concentration of fluorine ions and on the potential of interionic interactions, namely the nature of the outer-sphere cations [358]. The influence of the concentration of fluorine ions and of the nature of the outer-sphere cations on the equilibrium in Equation (80) can be demonstrated by the spectral transformations observed at 850°C for $M_2TaF_7$ – MF systems, where M = alkali metal [358].

The IR emission spectrum of molten $Na_2TaF_7$ consists of a single band at 605–610 $cm^{-1}$ and a very weak shoulder at about 540 $cm^{-1}$ (Fig. 76, a). This spectrum indicates, that for molten $Na_2TaF_7$, the equilibrium in Equation (80) is shifted strongly to the right, forming $TaF_6^-$ complex ions. The addition of NaF to molten $Na_2TaF_7$ does not change the spectrum; the band at 605–610 $cm^{-1}$ remains the strongest up to an NaF concentration of 0.9 mol fraction. This indicates that in all investigated concentrations, the melt contains mostly $TaF_6^-$ ions and the addition of NaF does not significantly shift the equilibrium in Equation (80) to the left.

IR spectra of the molten system $K_2TaF_7$ – KF are more sensitive to the concentration of KF (Fig. 76, b). Molten $K_2TaF_7$ is characterized by a strong band at 605 $cm^{-1}$ and a shoulder at ~540 $cm^{-1}$, as shown before (see Fig. 74, curve 3). The addition of KF to molten $K_2TaF_7$ leads to a decrease in the intensity of the above band and to the appearance of a band at 540 $cm^{-1}$. When the KF concentration equals or exceeds 0.9 mol fraction, a band is observed at 540 $cm^{-1}$ only. This spectral transformation indicates that the equilibrium in Equation (80) shifts to the left with the increase in KF concentration, and that at KF concentrations above 0.9 mol fraction, only $TaF_7^{2-}$ complexes are present, while $TaF_6^-$ ions are not observed by IR emission spectral methods.

The rubidium-containing system $Rb_2TaF_7$ – RbF displays similar behavior, but the band attributed to the $TaF_6^-$ ion vibration disappears at a RbF concentration of 0.6 mol fraction and higher (Fig. 76, c). This means that in the case of rubidium-containing melts, the equilibrium in Equation (89) is more significantly shifted to the left.

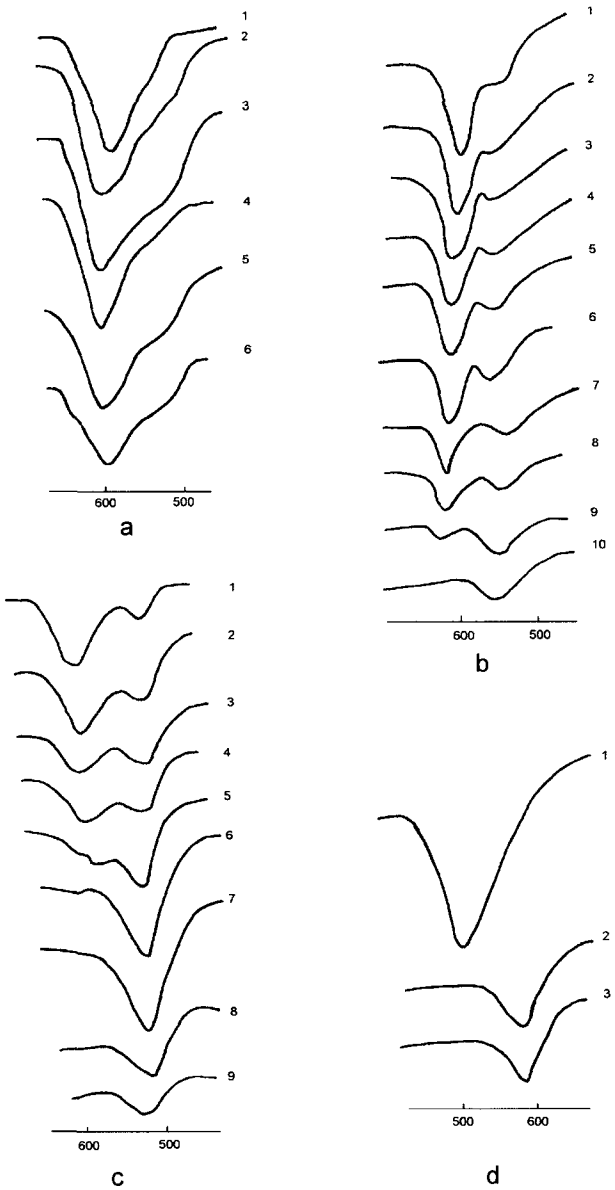


*Fig. 76. IR spectra of the systems $Na_2TaF_7$ – NaF (a), $K_2TaF_7$ – KF (b), $Rb_2TaF_7$ – RbF (c). Curves 1, 2, 3 etc. correspond to 0, 0.1, 0.3 etc. molar fraction of alkali fluoride. The $CsTaF_6$ – CsF system (d) is represented by spectra of $CsTaF_6$ (curve 1), $Cs_2TaF_7$ (curve 2) and $Cs_3TaF_8$ (curve 3). Reproduced from [358], A. I. Agulyansky, Zh. Neorg. Khim. 25 (1980) 2998, Copyright 1980, with permission of "Nauka" (Russian Academy of Sciences) publishing.*

In the case of the cesium-containing molten system $Cs_2TaF_7$ – CsF, the band attributed to the $TaF_6^-$ ion vibrations does not appear at any concentration of $Cs_2TaF_7$. The spectra consist only of a band at 516 $cm^{-1}$, indicating the presence of $TaF_7^{2-}$ ions. The $TaF_6^-$ band at 593 $cm^{-1}$ was observed only for molten $CsTaF_6$.

Fig. 76d shows fragments of IR emission spectra of molten $CsTaF_6$, $Cs_2TaF_7$ and $Cs_3TaF_8$ at 850°C. The band at ~600 $cm^{-1}$, which is attributed to the $TaF_6^-$ complex, appears only in molten $CsTaF_6$, whereas the band at 516 $cm^{-1}$, which characterizes the complex $TaF_7^{2-}$, appears in $Cs_2TaF_7$ – CsF melts, at all concentrations.

Table 55 presents the results discussed above. Fluoride melts containing tantalum contain two types of complex ions, namely $TaF_6^-$ and $TaF_7^{2-}$. The equilibrium between the complexes depends on the concentration of fluoride ions in the system, but mostly upon the nature of the outer-sphere cations. The complex ionic structure of the melts can be adjusted by adding cations with a certain polarization potential. For instance, the presence of low polarization potential cations, such as cesium, leads primarily to the formation of $TaF_7^{2-}$ complexes, while the addition of cations with relatively high polarization potentials, such as lithium or sodium, shifts the equilibrium towards the formation of $TaF_6^-$ ions.

*Table 55. IR spectra and complex structure of $M_2TaF_7$ – MF melts at 800°C.*

| System | $\nu(TaF_6^-)$, $cm^{-1}$ | $\nu(TaF_7^{2-})$, $cm^{-1}$ | Complex ions found |
|---|---|---|---|
| $Na_2TaF_7$ - NaF | 607 | 542 | Only $TaF_6^-$ is found, at all concentrations |
| $K_2TaF_7$ - KF | 605 | 540 | $TaF_6^-$ is observed up to 0.9 mol fraction of KF, at KF ≥ 0.9 mol fraction, only $TaF_7^{2-}$ is observed |
| $Rb_2TaF_7$ - RbF | 600 | 520 | $TaF_6^-$ is observed up to 0.6 mol fraction of RbF, at RbF ≥ 0.6 mol fraction, only $TaF_7^{2-}$ is observed |
| $Cs_2TaF_7$ - CsF | 593 | 516 | Only $TaF_7^{2-}$ is found, at all concentrations |

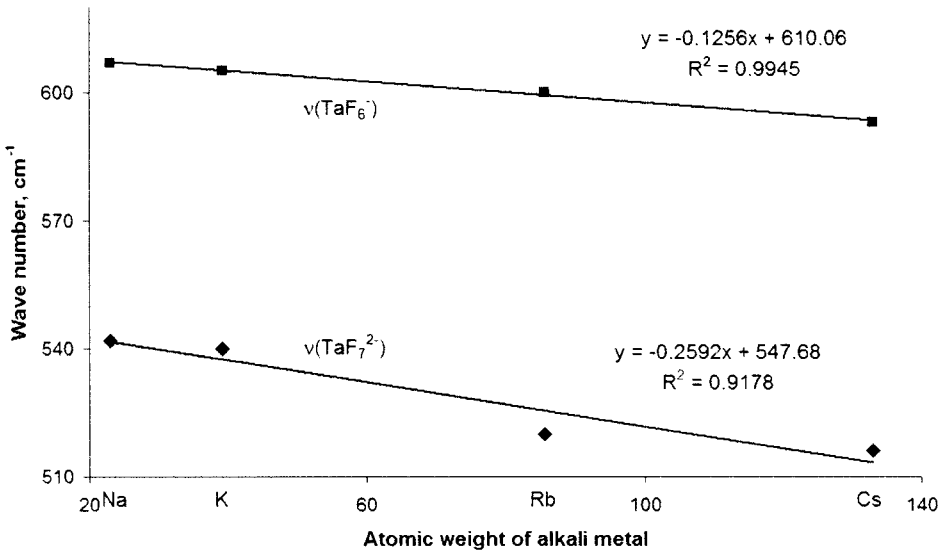


*Fig. 77. Dependence of $\nu(TaF_6^-)$ and $\nu(TaF_7^{2-})$ on the atomic weight of alkali metal.*

The nature of outer-sphere alkali metal cations can actually define the ionic equilibrium and also has an affect on complex anions. Fig. 77 illustrates the influence of the cationic surrounding on the wave numbers.

A slight but systematic decrease in the wave number of the complexes' bond vibrations, observed when moving from sodium to cesium, corresponds to the increase in the covalency of the inner-sphere bonds. Taking into account that the ionic radii of rubidium and cesium are greater than that of fluorine, it can be assumed that the covalent bond share results not only from the polarization of the complex ion but from that of the outer-sphere cation as well. This mechanism could explain the main differences between fluoride ions and oxides. For instance, melts of alkali metal nitrates display a similar influence of the alkali metal on the vibration frequency, but covalent interactions are affected mostly by the polarization of nitrate ions in the field of the outer-sphere alkali metal cations [359].

The conception of the formation of hetero-ligand complexes and the nature of anion-anion interactions can be clarified using IR spectra of $K_2TaF_7$ – KX mixtures, where X = Cl, Br or I [356, 360]. Fig. 78 shows the spectral transformation due to the dilution of molten $K_2TaF_7$ with potassium halide.

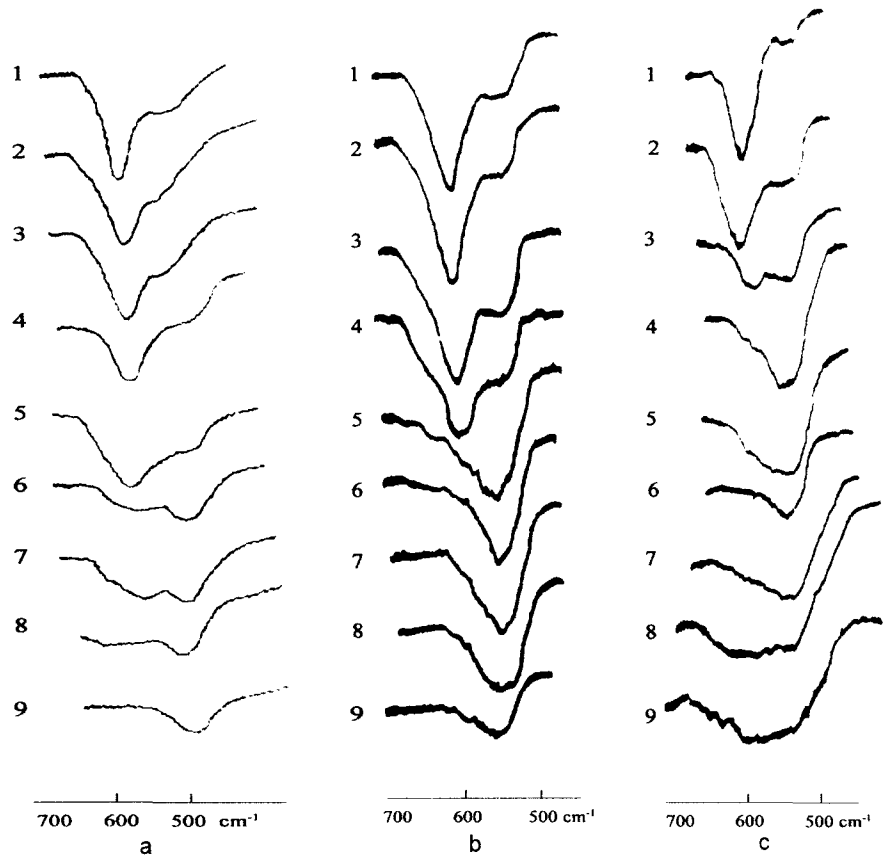


*Fig. 78. IR spectra of molten mixtures $K_2TaF_7$ – KX, where X – Cl (a), Br (b) and I (c). Curves 1, 2, etc. correspond to 0.1, 0.2, etc. mol fractions of KX (after Agulyansky, Kirillov, Prisyagny [356]).*

Increasing the concentration of potassium chloride, KCl, in the molten system $K_2TaF_7$ – KCl leads to the spectral transformation (Fig. 78, a), which is similar to that observed in the case of $K_2TaF_7$ – KF. The intensity of the band at ~600 $cm^{-1}$ decreases while the intensity of the band at ~540 $cm^{-1}$ increases. When KCl concentration is equal to, or greater than 0.8 mol fractions, the band at ~600 $cm^{-1}$ disappears and the only band observed is at ~ 540 $cm^{-1}$. The above behavior of the system can be explained by the following interaction between hexafluorotantalate ions, $TaF_6^-$ and chloride ions, $Cl^-$:

$$TaF_6^- + Cl^- = TaF_6Cl^{2-} \qquad (81)$$

In addition, a chlorine ion most probably replaces the fluoride ion located on the rotation diad axis of the heptacoordinated complex with $C_{2v}$ symmetry; otherwise splitting of the band would be observed. Replacement of the ligand in any other position would reduce the symmetry from $C_{2v}$ to $C_1$.

The disappearance of the first band at ~600 $cm^{-1}$ in IR spectra of melts $K_2TaF_7$ - KBr takes place at a lower KBr concentration compared to both KF and KCl containing systems (see Fig. 78, b). If KBr concentration equals or exceeds 0.5 mol fraction, a single band, which is attributed to hexacoordinated complex ions is observed. In the case of the $K_2TaF_7$ – KI molten system (Fig. 78, c) this phenomenon is observed at KI concentration as low as 0.4 mol fraction.

An examination of the IR spectral transformations versus concentration of the components in $K_2TaF_7$ – KX systems indicates that an increase in the KX concentration leads to a shift to the right in the following equilibrium:

$$TaF_6^- + X^- = TaF_6X^{2-} \qquad (82)$$

Furthermore, under identical conditions, the higher the polarity of anion X, the greater is the shift to the right of Equation (82). The observed distortion and expansion of the band that occurs in the $K_2TaF_7$ – KI system at high KI concentrations, can be related to the distortion of $TaF_6I^{2-}$ complex due to a charge transfer process from $I^-$ to $Ta^{5+}$, leading in turn to a partial reduction of the tantalum ion:

$$Ta^{5+} + 2\,I^- = Ta^{3+} + I_2 \qquad (83)$$

Additional confirmation of the above process can be found in the fact that some iodine separation is observed from melts containing more than 0.1 mol fraction KI [359, 360]. Chernov [361] noted a similar phenomenon of iodine separation when investigating the molten system $K_2ZrF_6$ – KI.

Adding potassium hydroxide, KOH, to a melt containing KF and a 0.1 mol fraction of $K_2TaF_7$ leads to the appearance of an additional band at ~900 $cm^{-1}$, as shown in Fig. 79 [342]. This band corresponds to TaO bond vibrations in $TaOF_6^{3-}$ complex ions. Interpretation of IR spectra obtained from more concentrated melts is less clear (Fig. 80). The observed absorption in the range of 900–700 $cm^{-1}$ indicates the formation of oxyfluoride polyanions with oxygen bridges ...OTaO.... The appearance of a fine band structure could be related to very low concentrations of some isolated components. These isolated conditions prevent resonance interaction between components and thus also prevent expansion of the bands by a mechanism of resonance [362].

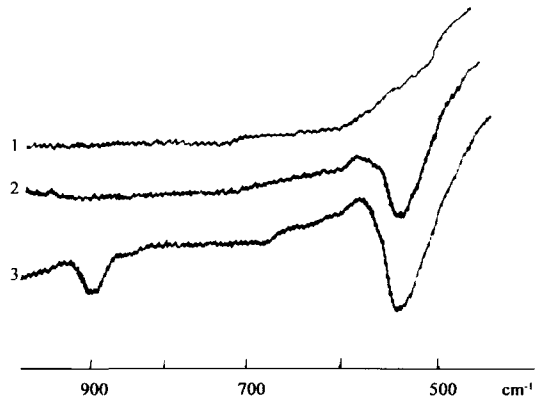


*Fig. 79. IR spectra of molten KF (1), KF + $K_2TaF_7$ (0.1 mol fraction) (2) and KF + $K_2TaF_7$ (0.1 mol fraction) + KOH (0.01 mol fraction) (3) at 850°C (after Agulyansky and Sakharov [342]).*

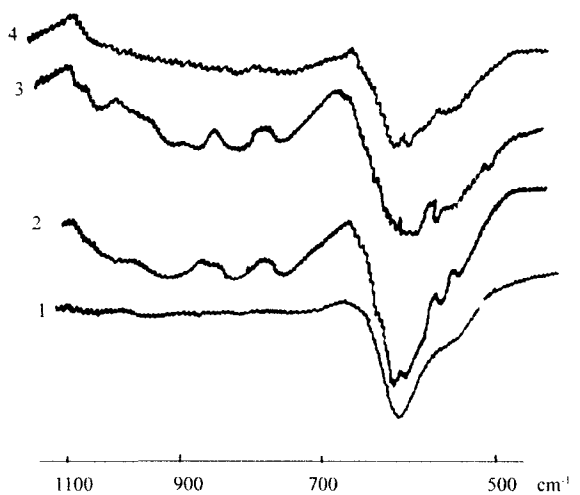


*Fig. 80. IR spectra of $K_2TaF_7$ (1) with additions of $Ta_2O_5$ in $K_2TaF_7$:$Ta_2O_5$ molar ratios of 4:1 (2), 3:1 (3) and 2:1 (4) (after Agulyansky and Sakharov [342]).*

## 5.4.4. Niobium-containing fluoride melts

Fluoride melts containing niobium have a significantly high tendency to undergo hydrolysis. The presence of niobium fluoride hydrolysis products can significantly distort the results of spectroscopy measurements. Another problem with the system is related to the intensive separation of niobium-containing compounds in the gaseous phase. The results of IR emission spectroscopy performed on molten $K_2NbF_7$ in air, vacuum and inert atmospheres were reported in [363]. Fig. 81 presents IR emission spectra of molten $K_2NbF_7$ in air.

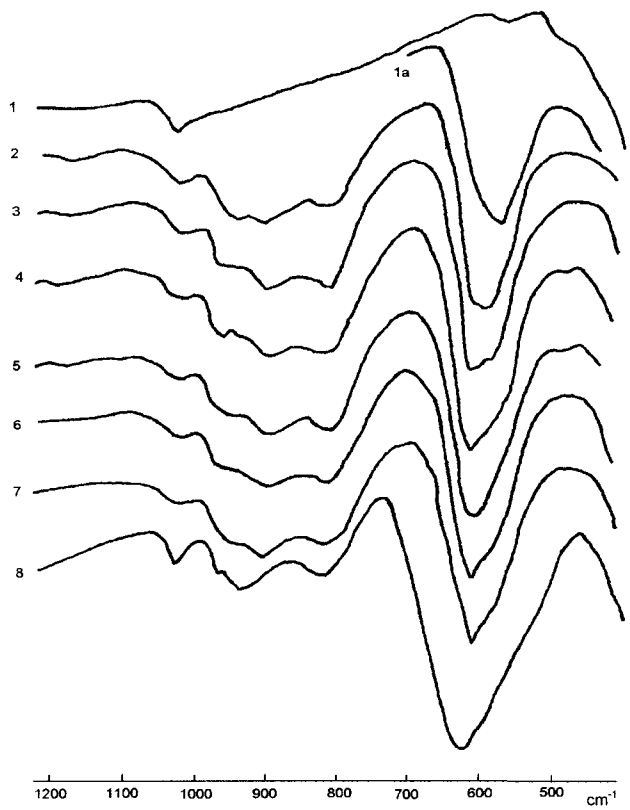


*Fig. 81. IR emission spectra of molten $K_2NbF_7$ in air.*
*1 – 1a – melting point; 2 – 7 - 780°C (15-minutes intervals); 8 - 900°C. Reproduced from [363], A. I. Agulyansky, V. A. Bessonova, Zh. Neorg. Khim. 29 (1984) 79, Copyright 1984, with permission of "Nauka" (Russian Academy of Sciences) publishing.*

The spectra presented in curves 1 and 1a of Fig. 81 were obtained at the melting point of $K_2NbF_7$. At the onset of melting, the heterogeneous material (curve 1) indicates two weak bands at 1030 and 575 $cm^{-1}$. The end of the melting process is characterized by homogenization of the melt (curve 1 a), which leads to a strong increase in the intensity of the second band. This increase in intensity occurs as a result of the increase in the effective surface of direct thermal radiation. All other spectra (curves 2 – 7) were also obtained in air, at 780°C at 15-minute intervals. A relatively weak complex absorption in the range of 1000–800 $cm^{-1}$ can be observed, and at the same time the strong band at 575 $cm^{-1}$ shifts towards the higher frequencies, up to 630 $cm^{-1}$. Complete assignment of the spectra is difficult and cannot be performed at this time. Nevertheless, some preliminary descriptions have been made [363].

The wide complex band at ~630 $cm^{-1}$ refers to NbF bond vibrations in the complex ions $NbF_6^-$. It is important to mention that wave numbers of NbF bond vibrations in oxyfluoroniobate complexes that have a total coordination number of 6 fall into the same range as well. Particularly, the shoulder at about ~560 $cm^{-1}$ indicates the formation of $NbOF_5^{2-}$ complexes rather than $NbOF_6^{3-}$, because NbF vibrations of the latter are expected to appear at a lower range of wave numbers. This is confirmed also by the presence of corresponding bands in the range of 1000–800 $cm^{-1}$. The band at ~820 $cm^{-1}$ can be assigned to the vibrations of bridging NbONb bonds in the structure of the infinite chains with fragment $NbOF_4^-$, while the band at 960–940 $cm^{-1}$ can be allocated to the terminal TaO bonds in the isolated complex $NbOF_5^{2-}$. At first glance, the weak band at 1030 $cm^{-1}$ could be assigned to NbO modes of $NbOF_3$, which could form during thermal decomposition of oxyfluoroniobate. In this case, however, significant absorption at 700 and 770 $cm^{-1}$ would be expected, as mentioned in [286]. In addition, the spectrum does not correspond to the data presented in [217]. The band at 1030 $cm^{-1}$ will be discussed separately.

Analysis of the ingot formed following the melting of $K_2NbF_7$ in air showed that along with $K_2NbF_7$, potassium oxyfluoroniobates are also present, but that the major component is $K_2NbOF_5$. $KNbOF_4$ was also identified in the condensate that was deposited on the cold parts of the retort. None of the IR spectra of the analyzed solids indicated any absorption at 1030 $cm^{-1}$. Since the spectra remain practically unchanged over relatively long periods of time (see Fig. 81, curves 2 – 7), the coexistence of two opposing processes can be assumed, i.e. the formation of oxyfluoroniobates along with the decomposition of the compounds and separation of some oxygen-containing compounds into the gaseous phase. This was confirmed by another experiment.

Fig. 82 presents IR emission spectra of molten $K_2NbF_7$ in an inert atmosphere (sealed retort) and in air. Curves 1 and 2 were obtained in an inert

atmosphere at temperature 770°C and 850°C, respectively. Curves 3, 4 and 5 were obtained at 850°C, at 20-minute intervals, with the retort open to the air. Two bands are observed close to the melting point of $K_2NbF_7$ (curve 1). It can be seen that increasing the temperature leads to a significant increase in the intensity of both bands, at ~602 and at 1030 $cm^{-1}$, and to the appearance of a shoulder at about 640 $cm^{-1}$. As a result of opening the retort to the air, new bands appear in the range of 1000–800 $cm^{-1}$ (curves 3 – 5), along with a decrease in the intensity of the band at 1030 $cm^{-1}$.

While the band at 602 $cm^{-1}$ can be unambiguously attributed to the $\nu_3$ mode of $NbF_6^-$ ions, the interpretation of the bands at 1030 and 640 $cm^{-1}$ requires additional explanations.

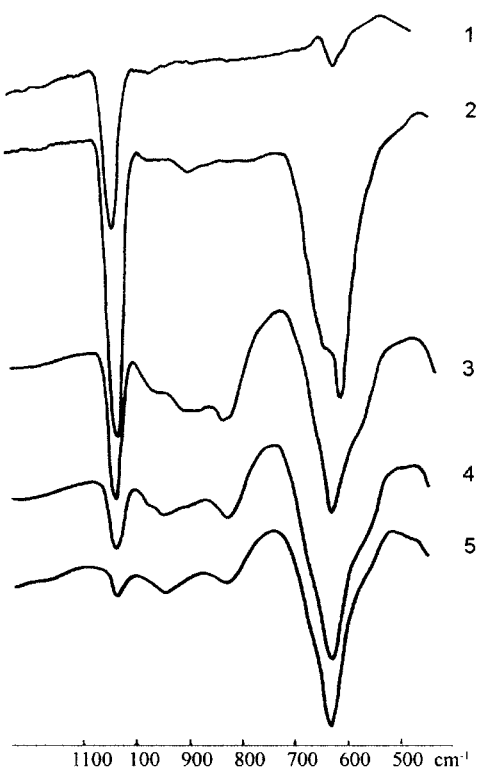


*Fig. 82. IR spectra of $K_2NbF_7$ undergoing melting in an inert atmosphere (1 - 770°C; 2 - 850°C) and after opening the retort to the air (curves 3 – 5). Reproduced from [363], A. I. Agulyansky, V. A. Bessonova, Zh. Neorg. Khim. 29 (1984) 79, Copyright 1984, with permission of "Nauka" (Russian Academy of Sciences) publishing.*

While the band at 1030 $cm^{-1}$ appears to be most intensive when melting takes place in a sealed inert atmosphere, its intensity decreases significantly when the system is opened to the air. This behavior can be elucidated by examining spectra obtained under weak vacuum created by pumping out the gaseous phase above the melt. Fig. 83 shows the spectral changes that occur under the above conditions. Curve 1 corresponds to molten $K_2NbF_7$ in an inert atmosphere at 820°C. Increasing the temperature up to 880°C (curve 2) leads to an increase in the intensity of the observed bands, and to the appearance of a shoulder at 640 $cm^{-1}$. The spectrum in curve 3 was obtained immediately after connecting the retort to a mechanical vacuum pump. As can be seen, removal of the inert gas leads to a significant decrease in the intensity of the band at 640 $cm^{-1}$. After 20 minutes of pumping out the gaseous phase above the surface of the melt (curve 4), the band at 1030 $cm^{-1}$ practically disappears, and an increase of temperature up to 900°C causes no essential changes in the spectrum.

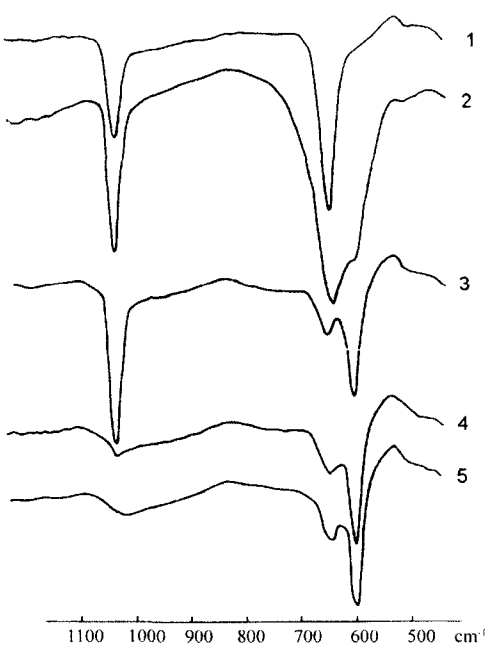


*Fig. 83. IR spectra of $K_2NbF_7$ undergoing melting in an inert atmosphere (1 - 820°C; 2 - 880°C) and in weak vacuum (curves 3 and 4, 20-minute interval, 5 - 800°C). (Reproduced from [363], A. I. Agulyansky, V. A. Bessonova, Zh. Neorg. Khim. 29 (1984) 79, Copyright 1984, with permission of "Nauka" (Russian Academy of Sciences) publishing.*

It is important to mention that the band at 1030 $cm^{-1}$ increases along with the band at 640 $cm^{-1}$, while no bands are observed in the range of 1000–800 $cm^{-1}$.

Comparison of the above data with information obtained for tantalum-containing melts [358] leads to the conclusion that the presence of the two bands at 640 and ~600 $cm^{-1}$ is not related to the splitting of $\nu_3$ $NbF_6^-$ mode degeneration but rather stems from the existence of two differently polarized $NbF_6^-$ complex ions. The main outer-sphere cation is definitely potassium, $K^+$, and the second cation with a higher polarization potential is possibly hydrogen, $H^+$. The presence of hydrogen cations is related to the hydrolysis of $K_2NbF_7$, which yields HF, and which in turn dissolves and dissociates in the melt. Taking into account that the mode wave number of complex ions increases with the increase in the polarization potential of outer-sphere cation, it is reasonable to assume that the bands at 640 and ~600 $cm^{-1}$ refer to $NbF_6^-$ complex ions that are polarized by hydrogen and potassium, respectively.

Higher melt temperatures lead to an increase in band intensity and merging thereof, as shown in Fig. 84. The merging of bands that occurs at increased temperatures can be explained by the augmentation of ion diffusion that causes an averaging of the potential of inter-ionic interactions between the $NbF_6^-$ ions and the outer-sphere cations.

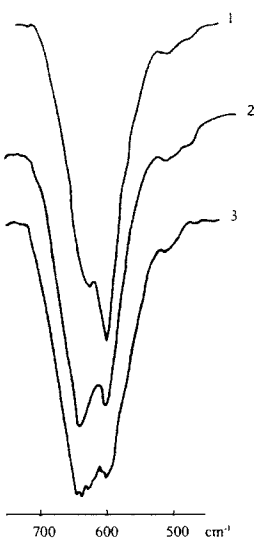


*Fig. 84. Fragments of IR spectra of molten $K_2NbF_7$ at 810°C (curve 1), 840°C (curve 2) and 900°C (curve 3). Reproduced from [363], A. I. Agulyansky, V. A. Bessonova, Zh. Neorg. Khim. 29 (1984) 79, Copyright 1984, with permission of "Nauka" (Russian Academy of Sciences) publishing.*

Thus, hydrogen fluoride is formed as a result of the hydrolysis of molten $K_2NbF_7$ by the following known mechanism [48]:

$$K_2NbF_7 + H_2O = K_2NbOF_5 + 2\,HF \qquad (84)$$

Hydrogen fluoride does not separate completely from the system, but rather dissolves significantly in the melt, interacting with fluoroniobate complexes.

Repeated attempts to obtain the band at 1030 $cm^{-1}$ in spectra of the respective solids of various compositions did not furnish the desired result. Nevertheless, the band was observed in IR transmission spectra of gaseous components that separated from molten $K_2NbF_7$ and were collected in a standard gas phase cell with CsI windows appropriate for IR measurements. Fig. 85 presents the structure of the band and exact wave numbers of its components. Storage of the gas in the cell for several days resulted in a yellow deposit on the windows due to oxidation and subsequent separation of iodine. Analysis of available reported data [364 – 367] enables to assign the band observed at ~1030 $cm^{-1}$ to vibrations of OF radicals. It should be emphasized that a single mode was observed for OF in the argon matrix; while in the case of nitrogen, two modes were indicated [367].

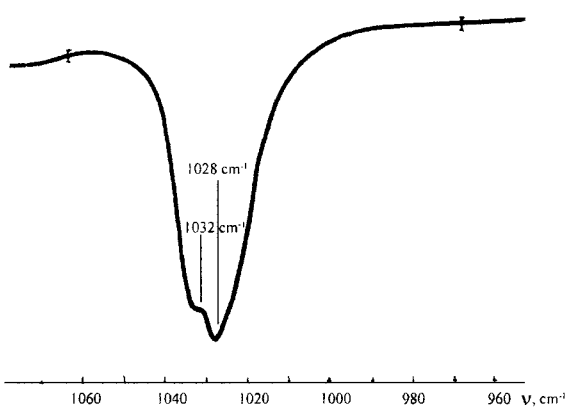


*Fig. 85. IR absorption spectra of gaseous OF collected from the retort atmosphere.*
*Reproduced from [363], A. I. Agulyansky, V. A. Bessonova, Zh. Neorg. Khim. 29 (1984) 79, Copyright 1984, with permission of "Nauka" (Russian Academy of Sciences) publishing.*

Fluoride melts containing niobium form $NbF_6^-$ complex ions. Investigation of IR spectra of $K_2NbF_7$ – KF melts show behavior similar to that described for corresponding tantalum-containing systems. Dissolution of molten $K_2NbF_7$ in potassium fluoride leads to the formation of $NbF_7^{2-}$ complexes. In the case of oxyfluoride melts, the presence of $NbOF_5^{2-}$ complex ions and polyoxyanions, formed by linkage of octahedrons via oxygen bridges, is most probable.

## 5.5. Main conclusions

The most common property of molten systems containing tantalum or niobium is the ionic equilibrium between hexa- and heptacoordinated complexes, with the general compositions $MeF_6^-$ and $MeF_6X^{(n+1)-}$:

$$\mathbf{MeF_6^- + X^{n-} = MeF_6X^{(n+1)-}} \quad \textbf{(85)}$$

Where Me = Ta, Nb;

and $X^{n-} = F^-, Cl^-, Br^-, I^-, O^{2-}$. (86)

The equilibrium in Equation (85) depends on three conditions: the concentration of the components, the nature of the X ions, and the nature of the outer-sphere cations.

An increase in the concentration of fluorometalate shifts the equilibrium in Equation (85) to the left.

The nature of the anion $X^{n-}$ also has a strong affect on the equilibrium. In general terms, the shift in Equation (85) depends on the polarity of the added anion: the higher the polarity of the anion, the greater is the shift to the right of Equation (85).

The only exception to this rule is the oxygen anion. Oxygen has a polarity of $2.74 \cdot 10^{-24}$ $cm^3$, which should place the anion, in sequence (86), between the chlorine and bromine ligands. It should be taken into account that, for the most part, oxygen anions form multiple bonds with tantalum or niobium while metal-halide bonds are always single bonds. The strength of the resultant bond between the metal and oxygen is, therefore, incomparably higher.

It seems reasonable to assume that both polarity and polarization potential of the anions must be taken into account in the definition of anion activity. It is quite indicative to arrange the anions by increasing order of the product of the polarity and polarization potential, $\alpha \cdot Z/r$,

where $\alpha$ = polarity, Z = effective charge, and r = ionic radius. In this case, the order of anions is as presented in Table 56.
Thus, each anion ($X^{n-}$) in sequence (86) or in the above Table 56 replaces all preceding anions ($Y^{k-}$) in the complex $MeF_6X^{(n+k)-}$. In other words, the following equilibrium will shift to the right:

$$MeF_6Y^{(k+1)-} + X^{n-} = MeF_6X^{(n+1)-} + Y^{k-} \quad (87)$$

Volkov, Grischenko and Delimarsky [293] mentioned a similar tendency of the complexes to increase in strength with the increase in the polarity of ligands along the sequence $F^-$ to $I^-$. This concept confirms the significance of the covalent share in the energetics of the formation of complex ions in molten media.

The only significant difference between halide melts and oxyhalide melts is that oxyfluoride complexes have a tendency to dissociate at relatively high concentrations yielding polyanion groups. This phenomenon is related with the need to achieve coordination saturation.

The third factor that strongly affects the equilibrium between hexa- and heptacoordinated complexes (85) is the nature of the second, outer-sphere cations. Increasing the ionic radii of the cations causes the equilibrium in Equation (85) to shift to the left, forming mostly hexacoordinated complexes $MeF_6^-$. The mechanism of interionic equilibrium in fluoride melts can be presented schematically as follows:

$$\mathbf{...M^+ - MeF_6^- - X^{n-} - M^+...} \quad \mathbf{(88)}$$

The anions $MeF_6^-$ and $X^{n-}$ approach each other closely to form the heptacoordinated complex $MeF_6X^{(n+1)-}$, or separate from one another, according to the polarization potential of the outer-sphere cation (alkali metal cation – $M^+$). This process is unique in that the mode frequencies of the complexes remain practically unchanged despite varying conditions. This particular stability of the complexes is due to the high charge density of $Ta^{5+}$ and $Nb^{5+}$.

*Table 56. Ligands versus product of polarity ($\alpha$) and polarization potential ($Z/r$) - $\alpha Z/r$.*

| Ligand | $F^-$ | $Cl^-$ | $Br^-$ | $I^-$ | $O^{2-}$ |
|---|---|---|---|---|---|
| $\alpha \cdot Z/r$ | 0.72 | 1.97 | 2.55 | 3.44 | 4.03 |

The appearance of the seventh ligand ($X^{n-}$) predominantly in the first coordination sphere of the complex or outside of the complex depends on the polarization potential of the alkali metal cation, $M^+$, and on the polarity of the seventh anion, $X^{n-}$. Increased polarity of the anion favors its entering into the first coordination sphere of the complex ion.

All of the above enables the interpretation of peaks in the conductivity isotherms of fluoride-chloride melts containing both $K_2TaF_7$ and $K_2NbF_7$ [37, 317–319, 324]. An increase in $K_2MeF_7$ concentration shifts the equilibrium (Equation 85) to the left ($X^{n-} = F^-$), which in turn increases conductivity. On the other hand, increasing the concentration of $MeF_6^-$ ions in the melt initiates interaction between this complex and the chloride ion, $Cl^-$, shifting the equilibrium (85) to the right ($X^{n-} = Cl^-$) and forming the complex ion $MeF_6Cl^{2-}$. This last process is accompanied by a decrease in conductivity. From this point of view, the presence of local maximums in the isotherms describing physicochemical properties can indicate the formation of heteroligand complexes.

The scheme of the interaction mechanism (Equation 88) testifies to an electro-affinity of $MeF_6^-$ ions. In addition, $MeF_6^-$ ions have a lower negative charge, smaller size and higher mobility compared to $MeF_6X^{(n+1)-}$ ions. The above arguments lead to the assumption that the reduction to metal form of niobium or tantalum from melts, both by electrolysis [368] and by alkali metals, most probably occurs due to interaction with $MeF_6^-$ ions. The kinetics of the reduction processes are defined by flowing equilibriums between hexa- and heptacoordinated complexes.

In conclusion, it should be mentioned that fluoride melts containing tantalum and niobium are, from the standpoint of their complex structure, in an "intermediate position" between crystals and solutions. Along the sequence crystal – melt – solution, the maximum coordination number decreases in the order 8 – 7 – 6, respectively. It should also be noted that the concentration of $TaF_7^{2-}$ ions in such solutions is low relative to the concentration of $TaF_6^-$ ions; no heptafuoroniobate ions were found in niobium-containing solutions. A similar decrease in the coordination number of complexes undergoing transition from crystal form to melts is observed in systems that contain complex fluorides of transition metals, while the maximum coordination number of fluorides of s- and p-elements usually remains unchanged, as shown below:

| Maximum coordination number of fluorides | Be | B | Al | Si | Zr | Nb | Ta |
|---|---|---|---|---|---|---|---|
| in crystals | 4 | 4 | 6 | 6 | 7 | 8 | 8 |
| in melts | 4 | 4 | 6 | 6 | 6 | 7 | 7 |

This Page Intentionally Left Blank

# 6.

# THERMAL PROPERTIES AND DECOMPOSITION OF TANTALUM- AND NIOBIUM-CONTAINING FLUORIDE COMPOUNDS

## 6.1. Impact of temperature on solid fluoride complexes

The main problems encountered in the investigation of tantalum- and niobium-containing fluoride and oxyfluoride complexes are related to the tendency of the compounds to undergo hydrolysis, particularly at elevated/high temperatures. In addition, the interpretations of the observed effects are often nontrivial and unclear due to the relatively complicated inter-particular interactions and changes that occur under thermal treatment. From this point of view, vibration spectroscopy methods are of high importance due to the dependence of solid phase spectra on the temperature, which, above all, stems from the nature of such inter-ionic interactions [369].

In general, increasing the temperature within the stability range of a single crystal structure modification leads to a smooth change in all three parameters of vibration spectra: frequency, half-width and intensity. The dependency of the frequency (wave number) on the temperature is usually related to variations in bond lengths and force constants [370]; the half-width of the band represents parameters of the particles' Brownian motion [371]; and the intensity of the bands is related to characteristics of the chemical bonds [372].

Fig. 86 presents IR absorption spectra of $K_2NbF_7$ and $K_2TaF_7$ at different temperatures. It was noted that for both $K_2NbF_7$ and $K_2TaF_7$, as well as for some other complex hexafluorometalates of potassium such as $K_2SiF_6$, $K_2GeF_6$ and $K_2TiF_6$, a smooth decrease in intensity was observed only upon increasing of the temperature [373].

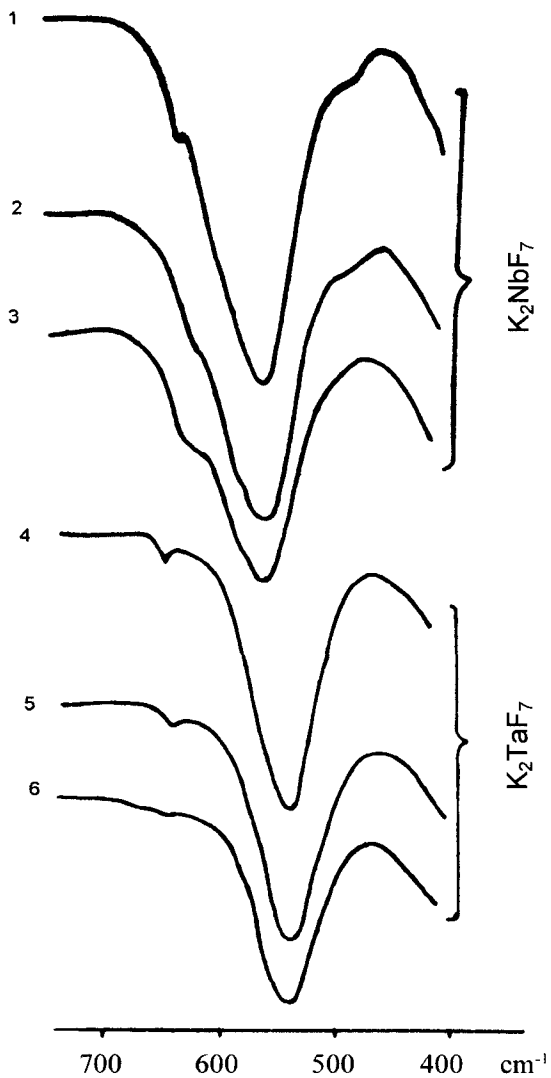


*Fig. 86. IR absorption spectra of $K_2NbF_7$ (curves 1 – 3) and $K_2TaF_7$ (curves 4 – 6); Curve numbers correspond to temperatures in °C: 1 – 36; 2 – 148; 3 – 246; 4 – 48; 5 – 148; 6 – 233.*
*Reproduced from [373], A. I. Agulyansky, O. A. Zalkind, V. A. Masloboev, Zh. Prikl. Spectr. 39 (1986) 341, Copyright 1986, with permission of "Nauka" (Russian Academy of Sciences) publishing.*

The dependence of the intensity on the temperature, for the above compounds, is approximated satisfactorily by the following equation:

$$I = I_0(1 - \beta t) \tag{89}$$

where $I_0$ = intensity at 0°C; $\beta$ = temperature coefficient; $t$ = temperature in °C.

One of the possible mechanisms of the intensity decrease is related to the change in occupancy of the base and excited levels [374]. The magnitude of the contribution of the occupancy change in to the intensity variation was estimated in [373]. Table 57 presents experimental and calculated values of coefficient β.

It is obvious that calculated values are systematically lower than the experimental data. Comparison of the experimental and calculated values of coefficient β shows that along with the changes in occupancy levels that appear at elevated temperatures, inter-particular interactions also make a significant contribution. Band intensity is generally defined as the derivative of the dipole moment with respect to the normal coordinate. It is, therefore, logical to assume that thermal extension and outer-sphere cation replacement have a similar influence on the potential of inter-ionic interactions, which, in turn, lead to the intensity changes.

Sergienko et al. [375, 376] showed that the band intensity of fluoride complexes increases systematically when outer-sphere cations undergo sequential transition from lithium to cesium.

*Table 57. Frequency (ν) ,Me – F bond length (r) and temperature coefficient (β) for several fluoride complex compounds (after Agulyansky et al. [373]).*

| Compounds | ν, $cm^{-1}$ | $r_{Me-F}$, Å | $\beta \cdot 10^3$, $grad^{-1}$ | |
|---|---|---|---|---|
| | | | Experimental | Calculated |
| $K_2SiF_6$ | 745 | 1.71 | 0.80 | 0.37 |
| $K_2GeF_6$ | 605 | 1.77 | 1.00 | 0.50 |
| $K_2TiF_6$ | 587 | 1.91 | 1.03 | 0.52 |
| $K_2NbF_7$ | 557 | 1.97 | 1.40 | 0.55 |
| $K_2TaF_7$ | 536 | 1.97 | 1.43 | 0.57 |

This phenomenon was explained by the reduction of the overlapping integral of the ligand–outer-sphere cation. This point was subsequently clarified by Zasukha and Volkov [377], based on a computation method by which the intensity is increased by increasing the outer-sphere cation ionic radius, which, in turn, leads to an increase in the ionic contribution to the energy of interaction between complex ions and outer-sphere cations. Based on this concept, the decrease in intensity observed while increasing the temperature can be explained by the increase in the covalent share of the bonds between complex ions and outer-sphere cations. The tendency of the intensity to change with the variation in temperature depends on the chemical bonds strength properties of the complex ions. Table 57 illustrates the correlation between β coefficients, vibration frequencies and the lengths of inner-sphere bonds.

Contrary to the cases discussed above, phase transitions are observed, that occur along with the reconstruction of the first coordination sphere, causing cardinal changes in IR spectra. Fig. 87 [373] shows IR absorption spectra of $K_2ZrF_6$ and $K_2HfF_6$ obtained at different temperatures. The shift of bands to a higher frequency range at temperatures above 240°C is related to a decrease in the metal's coordination number. Low temperature modifications consist of chains of dodecahedrons that are linked through their sides, leading to a coordination number of 8, for both zirconium and hafnium. The phase transition occurs concurrently with the destruction of the chains and the formation of isolated octahedrons, $ZrF_6^{2-}$ or $HfF_6^{2-}$, with a coordination number of 6.

Thus, increasing the temperature exerts an influence on the fluoride complexes that is similar to the influence of outer-sphere cations and is expressed by an increase of the covalent contribution to the bonds between fluoride complexes and outer-sphere cations.

An irreversible phase transition at about 240°C was observed for both $K_2NbF_7$ and $K_2TaF_7$ [130]. It was later shown that, in both cases, the transition occurs at about ~200°C by a reversible mechanism and is characterized by a relatively significant temperature hysteresis and a strong change in density [148]. Taking in to account that the transition does not cause any significant changes in the IR absorption spectra (see Fig. 86), it can be assumed that the solid polymorphism of $K_2NbF_7$ and $K_2TaF_7$ is most probably related to the rearrangement of the cationic sub-lattice, whereas the structure of the complex ions $NbF_7^{2-}$ or $TaF_7^{2-}$ remains practically unchanged. The aforementioned increase in band intensity indicates an increase in the overlapping integral of orbits 4s – potassium and 2p – fluorine; nevertheless the seventh fluorine-ligand is not removed from the metal's first coordination sphere.

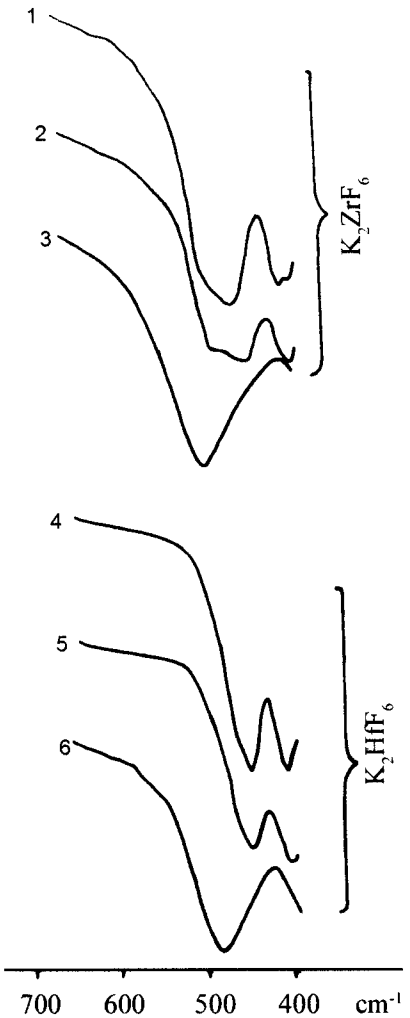


*Fig. 87. IR absorption spectra of $K_2ZrF_6$ (curves 1 – 3) and $K_2HfF_2$ (curves 4 – 6). Curve numbers correspond to temperatures in °C: 1 – 20; 2 – 185; 3 – 249; 4 – 23; 5 – 185; 6 – 243.*
*Reproduced from [373], A. I. Agulyansky, O. A. Zalkind, V. A. Masloboev, Zh. Prikl. Spectr. 39 (1986) 341, Copyright 1986, with permission of "Nauka" (Russian Academy of Sciences) publishing.*

## 6.2. Melting processes

The complicated character of inter-ionic interactions leads to some uncertainty when attempting to define the melting mechanism of the fluoride complex compounds. In particular, according to data provided by different researchers, the melting point of $K_2TaF_7$ varies within the very wide interval of 630-820°C and therefore the discussion of the thermal analysis of $K_2TaF_7$ merits a more detailed consideration [378]. The differential curve of the heating of $K_2TaF_7$ in the range of 700-800°C exhibits three endothermic effects at 730, 746 and 778°C, as seen in Fig. 88, curve 1, whereas cooling of the melt displays only two exothermic effects, at 746 and 778°C. This alludes to the irreversible nature of the process that occurs at 730°C (Fig. 88, curve 2). In addition, a sharp increase in conductivity is observed at 730°C (Fig. 88, curve 3), which indicates the formation of a melt that is a liquid conductive phase.

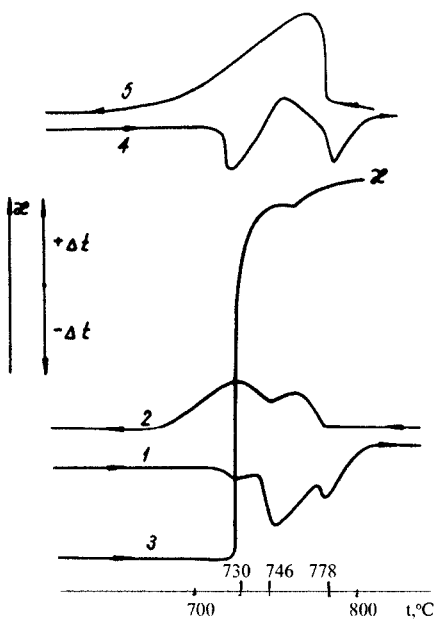


*Fig. 88. Thermal pattern and electroconductivity dependence of $K_2TaF_7$ (curves 1 – 3), heating thermal pattern of an equimolar mixture $K_2TaF_7$ – KF (curve 4) and crystallization of $K_3TaF_8$ (curve 5); t = temperature in °C, χ = conductivity in relative units.*
*Reproduced from [378], A. I. Agulyansky, V. A. Bessonova, Zh. Prikl. Khim. 33 (1983) 489, Copyright 1983, with permission of "Nauka" (Russian Academy of Sciences) publishing.*

To identify the above effects, a differential temperature curve of a $K_2TaF_7$ – KF mixture (molar ratio 1:1) was plotted. The heating curve displays two effects, at 730 and 780°C (see Fig. 88, curve 4), whereas cooling provides only one effect, at 778°C (Fig. 88, curve 5).

The above measurements and additional data lead to the proposal of the following melting mechanism of $K_2TaF_7$. The effect observed at 730°C corresponds to the partial decomposition of potassium heptafluorotantalate, yielding molten $KTaF_6$ and solid $K_3TaF_8$. The effects observed at 746°C and at 778°C can probably be attributed to the melting of $K_2TaF_7$ and $K_3TaF_8$, respectively. During the cooling of the homogenized melt, $K_3TaF_8$ crystallizes first which further interacts with the melt by a peritectic reaction, forming solid $K_2TaF_7$. The proposed melting scheme was confirmed by visual observations. Lowering the temperature of the melt down to 778°C leads to the formation of crystals that rise to the surface of the melt due to the lower density of $K_3TaF_8$ compared with that of $K_2TaF_7$ - 3.68 and 4.11 g/cm$^3$, respectively. The formation of $KTaF_6$ was confirmed by X-ray diffraction analysis of the condensate above the melt.

This complicated melting mechanism of $K_2TaF_7$ is related to differences in the nature of the chemical bonds of the products formed as a result of the decomposition of the compound. Taking in to account the formation of $KTaF_6$ melting diagram of system KF – $K_2TaF_7$ usually provided in the literature from a thermodynamic point of view, cannot be considered as a completely equilibrious system. The melting point of $K_2TaF_7$ (770-776°C) commonly mentioned in the literature, corresponds more or less to the melting of $K_3TaF_8$. Fig. 89 presents melting points versus the coordination number of niobium- and tantalum-containing fluoride compounds.

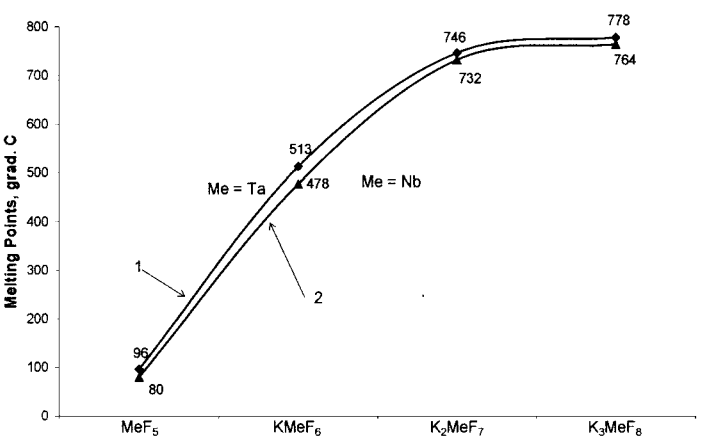


*Fig. 89. Melting points of fluorotantalates (1) and fluoroniobates (2).*

## 6.3. Thermal decomposition of oxyfluoroniobates

The thermal decomposition of alkali metal oxyfluoroniobates is also not a trivial process. $MNbOF_4$ compounds (where M = alkali metal) with a chain-type structure are relatively stable up to temperatures in the range of 500-600°C. Fig. 90 presents mass loss dependences on temperature of several $MNbOF_4$ compounds. As can be seen, among the compounds presented, only $CsNbOF_4$ exhibits significantly different behavior, beginning its thermal decomposition at a lower temperature of about 400°C.

The phase composition of products obtained from the thermal treatment of $LiNbOF_4$ and $NaNbOF_4$ was investigated using X–ray diffraction and vibration spectroscopy, as reported in [379]. Compounds with the following structures were found: $M_2NbOF_5$ , $MNbO_2F_2$ and $MNbO_3$, where M = Li or Na.

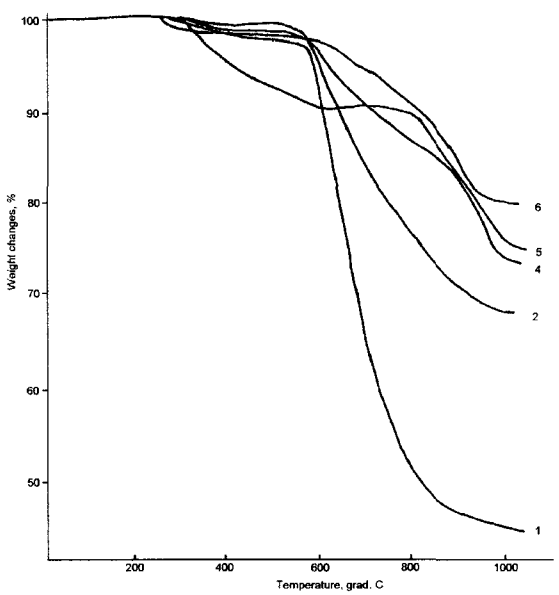


*Fig. 90. Mass loss temperature dependences for compounds with chain-type structure – $MNbOF_4$, where M = Li (curve 1); Na (curve 2); K (curve 3); Rb (curve 4); Cs (curve 5) (after Agulyansky et al. [379]).*

The formation of $M_2NbOF_5$ can be expressed by the following decomposition mechanism:

$$2\ MNbOF_4 = M_2NbOF_5 + NbOF_3 \quad (90)$$

During the thermal treatment of the compound, $NbOF_3$ is eliminated from the material and passes into the gaseous phase. Alternatively, $MNbOF_4$ can decompose also to form solid $MNbO_2F_2$ and $MNbO_3$ according to the following equation:

$$2\ MNbOF_4 = MNbO_2F_2 + MNbF_6 \quad (91)$$

The formation of $MNbO_2F_2$ serves as a source for the following decomposition process, which yields metaniobate of the alkali metal, $MNbO_3$:

$$2\ MNbO_2F_2 = MNbOF_4 + MNbO_3 \quad (92)$$

The $MNbOF_4$ formed in the interaction described by Equation (92) then participates again in the decomposition processes described by Equations (90) and (91).

Decomposition processes of oxyfluorides, in which two compounds are formed, one with a higher oxygen content than the precursor and the other with a lower oxygen content, seem to be common among oxyfluoroniobates. In general, this reaction can be represented as follows:

$$2\ M_nNbO_mF_{(5+n)-2m} = M_nNbO_{m-1}F_{(5+n)-2(m-1)} + M_nNbO_{m+1}F_{(5+n)-2(m+1)} \quad (93)$$

An analogical rearrangement of oxygen and the corresponding rearrangement of fluorine take place also during the decomposition of island-type compounds, $M_3NbOF_6$ [37, 221, 128]. This decomposition mechanism can be represented as follows:

$$2\ M_3NbOF_6 = M_3NbF_8 + M_3NbO_2F_4 \quad (94)$$

$M_2NbOF_5$-type compounds decompose to yield metaniobates by two possible pathways [128]. The first includes two decomposition steps:

$$3\ M_2NbOF_5 = 2\ M_2NbF_7 + M_2NbO_3F \quad (95)$$

$$M_2NbO_3F = MNbO_3 + MF \quad (96)$$

The second pathway consists of three steps, but provides the same type of final decomposition products:

$$2\ M_2NbOF_5 = M_3NbOF_6 + MNbOF_4 \quad (97)$$

$$2\ MNbOF_4 = MNbF_6 + MNbO_2F_2 \quad (98)$$

$$2\ MNbO_2F_2 = MNbOF_4 + MNbO_3 \quad (99)$$

The above decomposition mechanism is very important for the understanding of the hydrolysis, at elevated temperatures, of potassium heptafluoroniobate, $K_2NbF_7$, and of the thermal behavior of $K_2NbOF_5$.

Koltsov [380] reported that a mixture of potassium fluoride, KF, and potassium metaniobate, $KNbO_3$, was obtained as a final product after the hydrolysis of $K_2NbF_7$ at an increased temperature. Other researchers noted [37, 128, 380] that, in some cases, especially after thermal treatment of the material in an inert atmosphere, $KNbO_3$ and $Nb_2O_5$ are identified as final decomposition products. This can be explained by the spontaneous reduction of niobium, which occurs at high temperatures. Krilov et al. [381] investigated the thermal decomposition of sodium and potassium metaniobates, $NaNbO_3$ and $KNbO_3$, in vacuum. It was shown that both compounds decompose in the temperature range of 400-800°C yielding oxygen, while the alkali metal is formed at temperatures as high as 800-1200°C. The residue after complete decomposition was mostly niobium dioxide, $NbO_2$. It is evident that the $NbO_2$ formed serves as a source of $Nb_2O_5$, due to disproportion decomposition (100) or oxidation by atmospheric oxygen when performed in weak vacuum or in air:

$$3\ NbO_2 = Nb_2O_5 + NbO \quad (100)$$

In general, the decomposition of potassium metaniobate, forming niobium oxide, can be represented as follows:

$$KNbO_3 = K_{1-x}NbO_{3-y} + x\,K + y\,O = NbO_2 + K + O \quad (101)$$

Niobium pentaoxide, $Nb_2O_5$, also has a tendency to release oxygen into the gaseous phase upon heating [28], forming a colored substance that results from defects in the oxygen sub-lattice.

A dark color is also observed in material containing $K_2NbOF_5$ or $K_2NbF_7$ and its hydrolysis product, $K_2NbOF_5$, upon heating or melting and following cooling. The color stems from the decomposition of $K_2NbOF_5$ and the formation of partially reduced potassium niobate, $KNbO_{3-x}$, niobium oxide, $Nb_2O_{5-x}$ or niobium dioxide, $NbO_2$. Ultimately, the decomposition process can be represented by the following equilibrium [378]:

$$4\,K_2NbOF_5 = 2\,K_2NbF_7 + K_3NbOF_6 + NbO_2 + K + O \qquad (102)$$

This decomposition mechanism, which includes the separation off of oxygen, enables to explain the thermal peculiarities of systems containing $K_2NbF_7$. It is well known that melts that contain $K_2NbF_7$ display a significantly high corrosion activity compared to similar tantalum-containing systems. In addition, niobium metal obtained, for instance, by the electrolysis of NaCl – KCl melts containing $K_2NbF_7$ is about ten times more contaminated by oxygen compared to tantalum obtained from tantalum-containing melts with the same conditions [382]. Hence, the main difference is in the mechanism and products of hydrolysis. In the case of tantalum-containing melts, hydrolytic processes carried out in the presence of potassium fluoride yield $K_3TaOF_6$ that decomposes by the mechanism described by Equation (94). This mechanism yields no oxyfluoride compounds with a tendency to release oxygen. In contrast to tantalum, the hydrolysis of melts containing $K_2NbF_7$ yields $K_2NbOF_5$ as a product. The decomposition of $K_2NbOF_5$ takes place by the mechanism described by Equations (97 – 102), resulting in the release of active oxygen, which causes significant corrosion activity in the system, and oxidized niobium metal obtained from the melt [128].

## 6.4. Gaseous components

Knowledge of the composition of the gaseous components that separate off during the thermal decomposition of oxyfluoride compounds has significant importance for the understanding of the process. In general terms, a homological sequence of alkali metal monooxyfluoroniobates, $M_nNbOF_{3+n}$, can be obtained by adding $NbOF_3$ to an equivalent amount of alkali metal fluoride, MF, where M = alkali metal. The resultant addition reaction can be represented as follows:

$$n\,MF(solid) + NbOF_3(gas) = M_nNbOF_{3+n}(solid) \qquad (103)$$

The interaction (103) is shifted completely to the right and is correct from the standpoint of the synthesis of the complex oxyfluoride compounds that can actually be prepared using solid alkali metal fluoride and gaseous $NbOF_3$. Nevertheless, the composition of gaseous components that are released during thermal treatment of oxyfluoroniobates as $M_nNbOF_{3+n}$ in vacuum does not correspond to that as per Equation (103). The process described by Equation (103) is mostly irreversible. The gaseous components composition rather depends on the crystal structure and on the nature of the inter-ionic interactions in oxyfluoroniobate than its precursors.

Mass spectral investigation of gaseous components released from alkali metal oxyfluoroniobates with various types of structures was reported in [383]. Fig. 91 presents polytherms showing both total pressure and ionic currents of gaseous components released during thermal treatment of chain-type compounds, $MNbOF_4$ (M = alkali metal). Mass numbers (m/e) noted on the curves correspond to the following excited ions: 18 – $H_2O^+$; 19 – $F^+$; 20 – $HF^+$; 46.5 – $Nb^{2+}$; 56 – $NbF^{2+}$; 64 – $NbOF^{2+}$ (band intensities of niobium-containing ions were increased threefold compared to the unexcited ions). The four mass numbers 46.5, 56, 64 and 19 were also observed in mass spectral patterns of the thermal decomposition of $NbO_2F$ [286, 384], confirming the release of $NbOF_3$ into the gaseous phase.

Water separation polytherms show that the hygroscopic tendency of the compounds increases when moving along the sequence from $LiNbOF_4$ to $KNbOF_4$, reaching a maximum, then slightly dropping for $RbNbOF_4$ and $CsNbOF_4$. This unique behavior, exhibited by potassium-containing compounds can be attributed to the fact that the potassium ion is sterically similar to the fluorine ion. Hence, the ionic radii of lithium and sodium ions are smaller than that of fluorine, whereas those of rubidium and cesium ions are larger.

The separation of hydrogen fluoride, HF (see Fig. 91, curve 20) occurs inversely to the separation of water, $H_2O$, (see Fig. 91, curve 18): the peak in HF separation corresponds to the minimum water concentration. Residual water that is usually adsorbed by the material and the surface of the inner parts of the vacuum cell clearly indicate the hydrolysis of the compounds.

In the case of thermal decomposition of compounds with island-type structures, the composition of the gaseous components is different. Fig. 92 shows mass spectral parameters (total pressure and ionic current) of gaseous components that appear during the thermal decomposition of $Li_2NbOF_5$, $Na_2NbOF_5$ and $K_2NbOF_5$ versus temperature. $K_2NbOF_5$ has strong hygroscopic properties that cause a significant amount of water separation in the very beginning of thermal treatment of the compound.

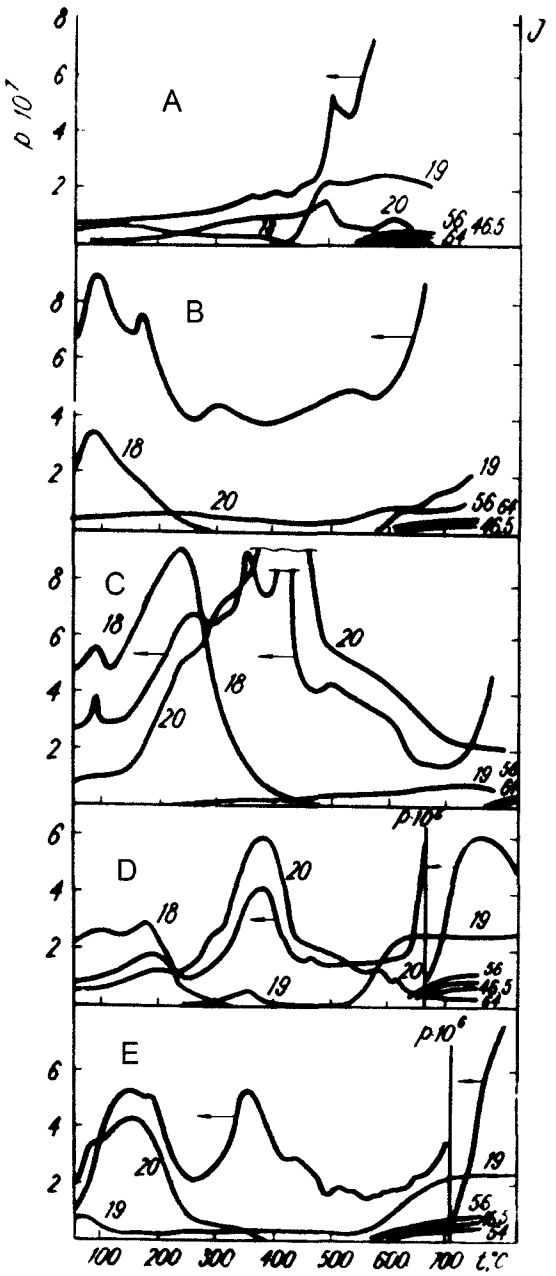


*Fig. 91. Polytherms of pressure (p in torr) and ionic currents (J in relative units) of $MNbOF_4$, where M = Li (A); Na (B); K (C); Rb (D); Cs (E).*
*Mass numbers (m/e) correspond to ions: 18 – $H_2O^+$; 19 – $F^+$; 20 – $HF^+$; 46.5 – $Nb^{2+}$; 56 – $NbF^{2+}$; 64 – $NbOF^{2+}$ (after Agulyansky et al., [383]).*

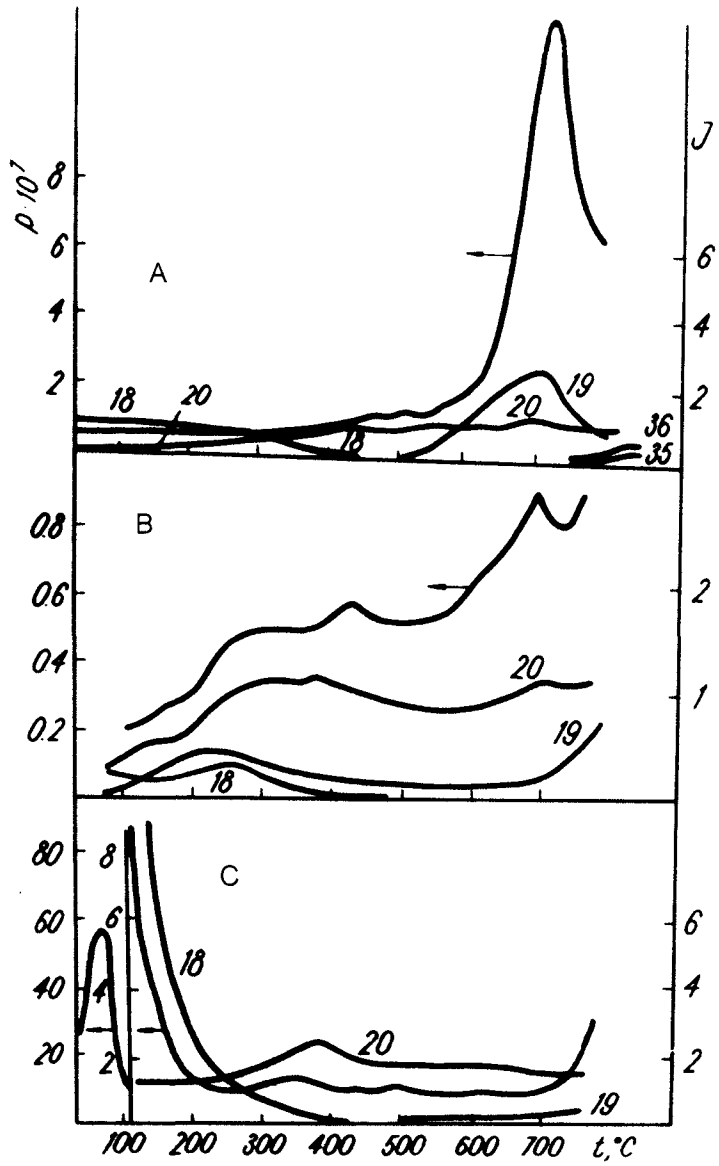


*Fig. 92. Mass spectral parameters: pressure (p in torr) and ionic currents (J in relative units) of $Li_2NbOF_5$ (A), $Na_2NbOF_5$ (B) and $K_2NbOF_5$ (C) versus temperature in °C (after Agulyansky et al., [383]). Numbers on the curves correspond to ions as shown in Fig. 91.*

compared to compounds containing lithium or sodium. Nevertheless, in all cases investigated, the hydrolysis of the compounds was not very significant. The amount of HF separated just slightly exceeded the background current level. The main difference in the behavior of the island-type compounds is the separation of fluorine. Special experiments performed and reported in [383] showed that the observed fluorine is not formed as a fragment of gaseous $NbOF_3$, but rather appears to originate in the solid material. Yagodin et al. [385] observed similar separation of fluorine while investigating the thermal decomposition of binary oxyfluorides of rhenium. As can be seen from the polytherms in Fig. 92, the concentration of gaseous fluorine increases with the temperature, and in the case of $Li_2NbOF_5$ even displays an extreme rise. The peak in fluorine separation corresponds approximately to 700°C. At higher temperatures, the concentration of the separating fluorine decreases along with the appearance of two new ions, mass numbers of 35 and 36, that can be attributed to the single-charge ions OF and HOF, respectively.

Thus, it is possible to make a very important assumption that chain-type compounds decompose forming gaseous niobium-containing components, while island-type compounds release upon thermal decomposition only light atoms and molecules into the gaseous phase [383].

Fig. 93 presents mass spectra of the decomposition of $NbO_2F$, $LiNbOF_4$ and $CoNbOF_5$ in the mass range of up to 400 a. m. u. The interpretation of the masses observed is as follows: 93 – $Nb^+$; 112 – $NbF^+$; 128 – $NbOF^+$; 131 – $NbF_2^+$; 147 – $NbOF_2^+$; 150 – $NbF_3^+$; 166 – $NbOF_3^+$; 169 – $NbF_4^+$. Based on the mass spectral data presented in Fig. 93, it is obvious that the separation of niobium-containing molecules, such as $NbOF_3$, is typical for framework-type compounds as well as for compounds that crystallize in a chain-type structure. It seems reasonable to assume that the thermal decomposition that leads to the separation of niobium-containing molecules is related to the presence of common ligands of oxyfluoride octahedrons in the crystal structure.

It should be emphasized that spectra indicating the separation of $NbF_5$ have yet to be investigated [383]. Nevertheless, Yampolsky et al. [285] reported that niobium pentafluoride, $NbF_5$, was observed as a product of the thermal decomposition of $NbOF_3$. Alikhanian et al. [384] also concluded that $NbF_5$ is present in the gaseous phase, based on the presence of a peak at 169 atomic mass units that corresponds to the $NbF_4^+$ ion.

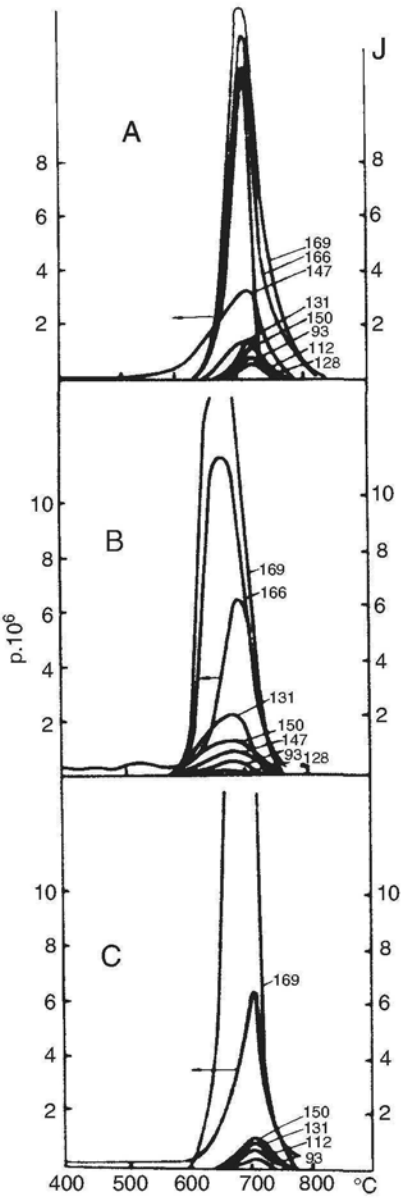


*Fig. 93. Mass spectra of $NbO_2F$ (A); $LiNbOF_4$ (B) and $CoNbOF_5$ (C). Peak assignment: 93 – $Nb^+$; 112 – $NbF^+$; 128 – $NbOF^+$; 131 – $NbF_2^+$; 147 – $NbOF_2^+$; 150 – $NbF_3^+$; 166 – $NbOF_3^+$; 169 – $NbF_4^+$ (after Agulyansky et al. [383]).*

Nonetheless, the absence, from even the high range of the accelerating potential, of even very weak peaks corresponding to $NbF_5$ ions was especially mentioned in [383].

It is possible that $NbF_5$ separates due to $NbOF_3$ decomposition according to the following known process, as evident from $NbF_5$ deposits found on the cold parts of the vacuum chamber of the measuring equipment:

$$2\ NbOF_3 = NbF_5 + NbO_2F \quad (104)$$

The ionic current intensity corresponding to the peak at 169 amu was analyzed under isothermal and polythermal conditions [383]. It was found that in a gaseous atmosphere, the intensity changes are in correlation with the CO content and in negative correlation with the $CO_2$ content. The presence of CO in vacuum systems equipped with heating elements is usually related to thermo-cycling and desorption of CO by nickel atoms [386]. Based on the above, the presence of $NbF_4^+$ ions in mass spectra is most probably related to the niobium reduction process, which can be represented as follows:

$$5\ NbO_2F_{(solid)} + CO_{(gas)} = Nb_3O_7F_{(solid)} + NbO_{2\,(solid)} + NbF_{4\,(gas)} + CO_{2\,(gas)} \quad (105)$$

Alikhanian et al. [384] observed niobium oxides, $NbO_2$ and $Nb_2O_5$, as additional phases along with $Nb_3O_7F$ in the solid product of the thermal decomposition of $NbO_2F$ and in experiments discussed in [383]. The formation of $Nb_2O_5$ therewith could result from the oxidation of niobium suboxide, $NbO_2$ by atmospheric oxygen. The tendency of $Nb^{5+}$ to undergo reduction following thermal treatment of oxide compounds in vacuum or in inert atmospheres is commonly known [387]. It seems that, the partial reduction of penta-valent niobium can take place along with the separation of both oxygen and fluorine.

The most probable spontaneous reduction process can be described as follows:

$$2\ NbO_2F_{(solid)} = NbOF_{2\,(solid)} + NbO_{2\,(solid)} + O_{(gas)} \quad (106)$$

$$2\ NbOF_{2\,(solid)} = NbF_{4\,(gas)} + NbO_{2\,(solid)} \quad (107)$$

$$2\ NbOF_{2\,(solid)} + O_{2\,(gas)} = NbOF_{3\,(gas)} + Nb_3O_7F_{\,(solid)} \quad (108)$$

In the case of $LiNbOF_4$, the gaseous phase is slightly more enriched with $NbF_4$, which is to be expected if the decomposition of the compound proceeds according to the following interactions:

$$3\ LiNbOF_{4\,(solid)} = Li_2NbOF_{5\,(solid)} + LiNbO_2F_{2\,(solid)} + NbF_{4\,(gas)} + F_{(gas)} \quad (109)$$

$$2\ LiNbO_2F_{2\,(solid)} = LiF_{(solid)} + LiNbO_{3\,(solid)} + NbOF_{3\,(gas)} \quad (110)$$

The thermal decomposition of $LiNbOF_4$ can be also represented based on the formation of a complex fluoride compound with partially reduced niobium. But the resulting products remain unchanged:

$$3\ LiNbOF_{4\,(solid)} = Li_2NbF_{6\,(solid)} + LiNbO_2F_{2\,(solid)} + NbF_{4\,(gas)} + O_{(gas)} \quad (111)$$

$$Li_2NbF_{6\,(solid)} + O_{2\,(gas)} = Li_2NbOF_{5\,(solid)} + OF_{(gas)} \quad (112)$$

Lack of any peaks corresponding to oxygen-containing components in the mass spectra of $CoNbOF_5$ (see Fig. 93, C) leads to the conclusion that the compound decomposes without releasing $NbOF_3$ molecules. Hence, the decomposition scheme can be represented by the following interactions:

$$2\ CoNbOF_{5\,(solid)} = Co_2NbO_2F_{4\,(solid)} + NbF_{4\,(gas)} + 2\ F_{(gas)} \quad (113)$$

$$Co_2NbO_2F_{4\,(solid)} + O_{2\,(gas)} = Co_2NbO_3F_{3\,(solid)} + OF_{(gas)} \quad (114)$$

The intermediate solid niobium-containing compounds that are formed during the thermal decomposition of both $LiNbOF_4$ and $CoNbOF_5$ are stable in oxidizer-free atmospheres. Such compounds are characterized by an anion cation (X:Me) ratio of 2 that enables the formation of a stable $MeX_2$ type crystal structure. Nevertheless, atmospheric oxygen leads to the oxidation of $Nb^{4+}$ resulting in the formation of $Li_2NbOF_5$ or $Co_2NbO_3F_3$, respectively. Specifically, $CoNbOF_5$ that is removed from the vacuum chamber after undergoing thermal decomposition changes its color, and its X–ray diffraction analysis indicates the formation of $Co_2NbO_3F_3$. This color change can be explained by the rapid oxidation of the intermediate product by atmospheric oxygen.

Based on the above, the oxidation of $NbF_4$ can be represented as follows:

$$NbF_4 + O_2 = NbOF_3 + OF \quad (115)$$

The addition of lithium fluoride, LiF, to the chain-type compound $LiNbOF_4$ leads to an abnormally strong release of fluorine into the gaseous phase at about 300°C [379], which, it seems,, is also related to the occurrence of oxidation–reduction processes. The addition of lithium fluoride, LiF, to $LiNbOF_4$ does not lead to the splitting off of isolated $NbOF_5^{2-}$ complexes, but rather to the breaking down of oxyfluorride chains into shorter chain fragments. The process of chain breakdown can be presented as follows:

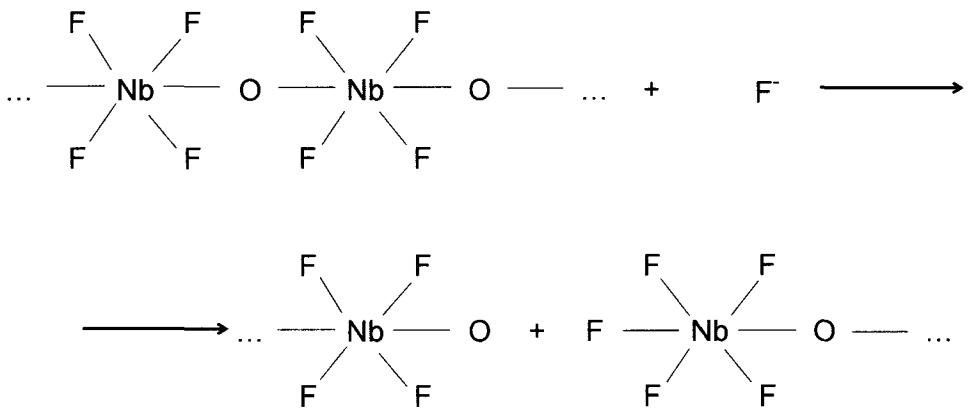


Nevertheless, the system, composed of chain fragments of oxyfluoroniobate complexes, is thermodynamically less stable. Dipole properties of fragments of a certain length are re-orientated so as to be linked into typical infinite chains. There is no doubt that the fragment re-orientation and linking process initiates the partial reduction of niobium to $Nb^{4+}$ and the oxidation of fluoride to elementary fluorine. The process scheme can be presented as follows:

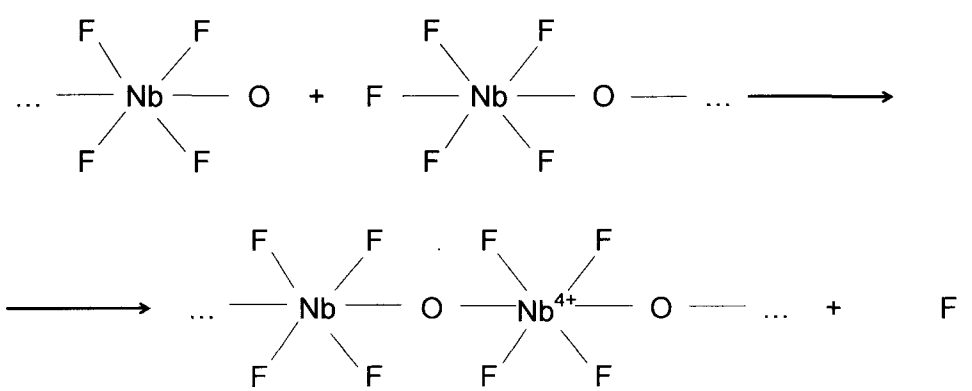

The partially reduced form of niobium accounts for the color change of samples that underwent thermal treatment in vacuum or inert atmospheres. Whereas the thermal treatment of the mixture in air leads to the simultaneous oxidation of $Nb^{4+}$ by oxygen, this is actually equivalent to the replacement of fluorine ions by oxygen ions in the complex structure of oxyfluoroniobate. Extended thermal treatment of systems containing $LiNbOF_4$ and LiF yields a mixture of LiF and $LiNbO_3$ as the final thermal decomposition product.

The occurrence of oxyfluoride chains in MF – $MNbOF_4$ molten mixtures was confirmed by IR emission spectra [379]. Fig. 94 presents a typical example, the spectrum of molten LiF – $LiNbOF_4$. The strong band at about 780–800 $cm^{-1}$ is characteristic of Nb-O-Nb vibrations of the octahedrons that are linked into chains via oxygen "bridge" atoms.

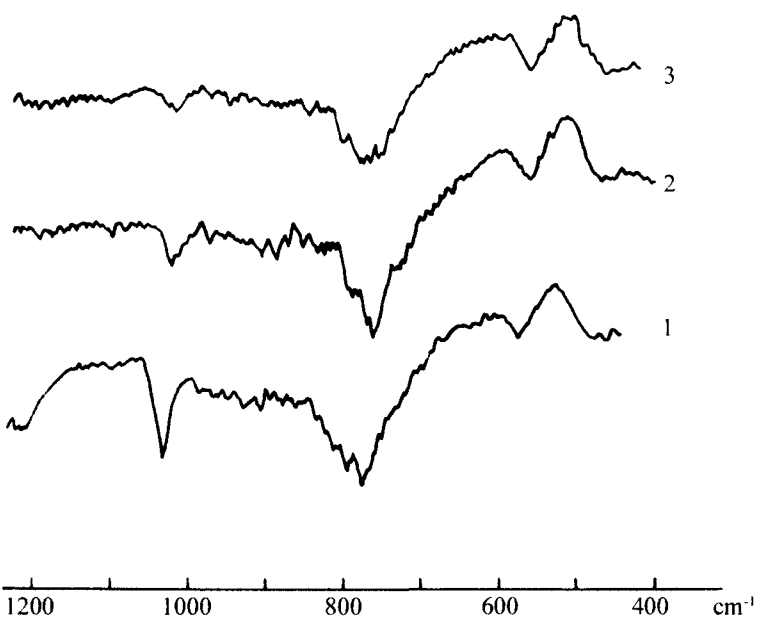


*Fig. 94. IR emission spectra of molten system $LiNbOF_4$ – LiF at 660°C. Curves 1, 2 and 3 correspond to $LiNbOF_4$ concentrations of 1.0, 0.8 and 0.6 molar fraction, respectively. Reproduced from [379], A. I. Agulyansky, E. L. Tikhomirova, V. T. Kalinnikov, Zh. Neorg. Khim., 33 (1988) 1155, Copyright 1988, with permission of "Nauka" (Russian Academy of Sciences) publishing.*

## 6.5. Main conclusions

The data presented and discussed indicates that the mechanism of thermal decomposition of niobium oxyfluoride complex compounds is not trivial, but that some regularity can nonetheless be formulated regarding the processes, as follows:

- Increasing the temperature generally promotes an increase in the covalent contribution to the bond between complex anions and outer-sphere cations;
- Thermal decomposition of oxyfluoroniobates yields two main compounds containing higher and lower oxygen concentrations relative to the initial compound;
- Oxyfluoride compounds that crystallize in island-type structures decompose and release light atoms into the gaseous phase;
- Oxyfluoride compounds whose crystal structure is made up of linked octahedrons decompose and release niobium-containing molecules into the gaseous phase;
- The separation of oxygen and fluorine into the gaseous phase is related to the tendency of niobium (V) to undergo partial reduction during thermal treatment;
- The formation of oxide compounds as a result of the thermal treatment of oxyfluorides is due to high temperature hydrolysis and reduction–oxidation processes.

This Page Intentionally Left Blank

# 7.

# FERROELECTRIC PROPERTIES OF NIOBIUM AND TANTALUM FLUORIDE COMPOUNDS

## 7.1. General notes

Crystals with one of the ten polar point-group symmetries ($C_1$, $C_2$, $C_s$, $C_{2v}$, $C_4$, $C_{4v}$, $C_3$, $C_{3v}$, $C_6$, $C_{6v}$) are called polar crystals. They display spontaneous polarization and form a family of ferroelectric materials. The main properties of ferroelectric materials include relatively high dielectric permittivity, ferroelectric–paraelectric phase transition that occurs at a certain temperature called the Curie temperature, piezoelectric effect, pyroelectric effect, non-linear optic property – the ability to multiply frequencies, ferroelectric hysteresis loop, and electrostrictive, electro-optic and other properties [16, 388].

The main source of spontaneous polarization in crystals is the relative "freedom" of cations that fit loosely into the crystal's octahedral cavities. The number of degrees of freedom of the octahedrons affects the spontaneous polarization value and hence influences the crystal's ferroelectric properties. Abrahams and Keve [389] classified ferroelectric materials into three structural categories according to their atomic displacement mechanisms: one-dimensional, two-dimensional and three-dimensional.

When all of the atomic displacement vectors are parallel to a polar axis of the crystal structure, the compound belongs to the one-dimensional category. In this case, linkage manner of octahedrons, $MeX_6$, is of fundamental significance of spontaneous polarization appearance. Typical examples of compounds that belong to the one-dimensional category include perovskites,

$LiNbO_3$ type crystals and compounds that crystallize in a tungsten bronze-type structure.

Compounds that belong to the two-dimensional category undergo polarization reversal due to atomic displacement in a plane that contains a polar axis. The displacement can be imagined as the rotation of atomic groups around an axis that is perpendicular to a reflection plane. Typical examples of two-dimensional compounds include $BaMF_4$ type compounds, where M = Mg, Mn, Fe, Co, Ni, Zn.

In crystals that belong to the three-dimensional category, reorientation of the polarization occurs due to displacements that appear to be relatively equal in all three directions. Such displacements are observed in the case of island-type crystals.

The variation in the repolarization character causes systematic changes in the properties of the materials. Particularly, the transition from one-dimensional structure compounds to three-dimensional structure compounds is accompanied by a decrease in the spontaneous polarization value and in the compound's Curie temperature, and a change in the character of the compound's chemical bonds [390].

From a steric point of view, the high charge and relatively small ionic radii of Nb(V) and Ta(V), which are surrounded by an octahedral arrangement of oxygen or fluorine ions, enable cation displacement within the crystal cavities. On the other hand, according to the pseudo Jahn-Teller effect, the absence of electrons in the external d orbital leads to the vibronic intolerance of the system in relation to metal ion displacements [391]. This vibronic instability is the driving force behind the cation displacements. This effect is further enhanced with the increase in the contribution of the covalence metal–ligand bonds [392]. From this point of view, the replacement of oxygen ions by fluorine ions in the coordination sphere of niobium or tantalum generally leads to an increase in the ionic contribution of the inner-sphere bonds and to a decrease in the overall structural distortion. Isomorphic substitution of oxygen by fluorine thus decreases the spontaneous polarization value and lowers the Curie temperature [45, 47, 246].

In other cases, if the fluorination process leads to cardinal changes in the crystal structure of the initial oxide compounds, new compounds with polar structures can be obtained. A demonstrative example of such materials are compounds that belongs to the system $Na_5(W_{3-x}Nb_x)O_{9-x}F_{5+x}$ and that have chiolite-type structures, when neither pure fluoride nor oxide display any ferroelectric properties [393 – 395].

A rich variety of complex oxyfluoride compounds containing tungsten, molybdenum, and titanium and displaying spontaneous polarization was discovered and described in [396 – 399].

According to a classification method presented by Ravez [400], inorganic fluoride ferroelectric compounds belong to one of the following six families: $(NH_4)_2BeF_4$, $BaMnF_4$, $SrAlF_5$, $Na_2MgAlF_7$, $K_3Fe_5F_{15}$ and $Pb_5Cr_3F_{19}$.

Oxyfluorides can be subdivided into two general groups. The first group is the group of "true" ferroelectrics that exhibit polar crystal structures. Not all related fluorides and oxides are necessarily ferroelectrics. "True" oxyfluoride compounds usually have a relatively high F/O ratio and crystallize in the following types of structures: $K_3MoO_3F_3$, $Bi_2TiO_4F_2$, $Na_5W_3O_9F_5$, $Pb_5W_3O_9F_{10}$ and $Mg_3B_7O_{13}F$.

The second group is the group of oxyfluorides that are derived from ferroelectric oxides by means of fluorine–oxygen substitution. The basic oxides are usually perovskite, tetragonal tungsten bronze, pyrochlore, lithium tantalate etc. [400].

In particular cases, oxyfluoride compounds with island-type crystal structures, such as $K_3NbOF_6$, $K_3TaOF_6$, $K_3NbO_2F_4$ and $K_3TaO_2F_4$, display ferroelectric–ferroelastic properties, with Curie temperatures of 283, 310, 420, 465°K, respectively [150, 191].

Among the alkali metal hexafluorometalates, potassium hexafluoronibate ($KNbF_6$) was investigated in detail. An anomaly in the dependence of temperature on dielectric permittivity was observed at 240–265°K [401].

Compounds with $MNbOF_4$ chain-type structures are also of great interest from the standpoint of the investigation of electro-physical properties, because ferroelectric properties were also found in their structural analogs, the compounds of the $SrAlF_5$ family [402, 403]. It was found that $MNbOF_4$ compounds (M = alkali metal) exhibit the same properties exhibited by ionic conductors, with the conductivity increasing upon moving from cesium to lithium [379].

Tantalum and niobium fluoride compounds that crystallize in coordination-type structures also seem to be perspective candidates for the investigation of ferroelectric properties. Ravez and Mogus-Milancovic [404] showed that some fluoride and oxyfluoride compounds with crystal structures similar to the $ReO_3$ type exhibit ferroelastic properties. For instance, ferroelastic properties were found in some solid solutions based on $NbO_2F$ and $TaO_2F$ [405, 406].

## 7.2. Compounds derived from lithium metatantalate

Fluorinated materials derived from lithium metatantalate, $LiTaO_3$, or lithium metaniobate, $LiNbO_3$, in the form of high-density ceramics or single crystals were comprehensively investigated by Ye, Von Der Mühll, Raves and Hagenmuller [407 – 412].

Dielectric, piezoelectric and pyroelectric properties of $LiTaO_3$ derived ceramics containing additives of LiF and $MgF_2$ were investigated and reported on in [407]. The materials were prepared at 900°C by means of two methods:

- Reaction sintering, yielding powdered polycrystalline material:

$$(1 - x)\ LiTaO_3 + x\ (LiF + MgF_2)$$

- Simultaneous preparation and sintering:

$$(1 - x)/2\ (Li_2CO_3 + Ta_2O_5) + x\ (LiF + MgF_2)$$

It was assumed that fluoride-containing precursors undergo partial hydrolysis by atmospheric moisture. For instance, for an initial composition corresponding to x = 0.05, the final composition was found, using mass loss and chemical analyses, to be $Li_{0.89}(Mg_{0.050}Ta_{0.95})O_{2.795}F_{0.090}(OH)_{0.060}$.

Partial substitution of oxygen by fluorine and the corresponding substitution of tantalum by magnesium to compensate for the differences in charge, enabled to obtain high-density ceramics with elevated Curie temperatures. The piezoelectric and pyroelectric coefficients of the ceramic material were approximately 30 and 20% of the corresponding values reported for the $LiTaO_3$ single crystal.

Fig. 95 shows the change in cell parameters, density and Curie temperature for ceramics with initial compositions of $Li(Ta_{1-x}Mg_x)O_{3-3x}F_{3x}$ (where $0 \leq x \leq 0.2$) versus x value. It should also be mentioned that the pyroelectric coefficient for x = 0.05 was found to be 4.0 nC $cm^{-2}$ $K^{-1}$.

Sintering processes in the system

$$(1 - x)\ LiTaO_3 + x\ [(1 - y)\ \text{“}LiMgF_3\text{”} + y\ \text{“}LiMg(OH)_3\text{”}]$$

were investigated and reported on in [409]. It was shown that high-density ceramics can be obtained by thermal treatment at 900°C in air. Dielectric permittivity at temperatures close to the ferroelectric–paraelectric phase transition systematically increased with an increase in $OH^-$ concentration.

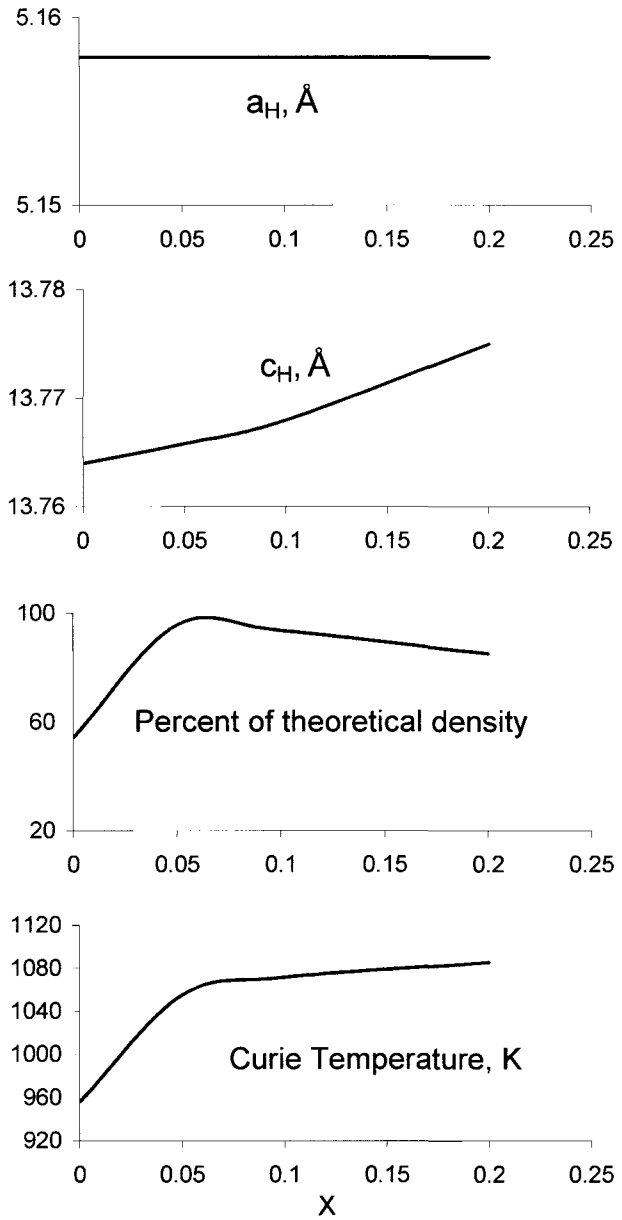


*Fig. 95. Change in cell parameters ($a_H$ and $c_H$), density of ceramics normalized by theoretical value and Curie temperature versus x value for $Li(Ta_{1-x}Mg_x)O_{3-3x}F_{3x}$ system. Reproduced from [407], Z-G. Ye, R. Von Der Mühll, J. Ravez, P. Hagenmuller, J. Mater. Res., 3 (1988) 112, Copyright 1988, with permission of MRS Journal of Material Research.*

Maximum density was achieved for the ceramic material that corresponds to the composition $Li(Ta_{0.925}Mg_{0.075})O_{2.775}F_{0.169}(OH)_{0.056}$, with a Curie temperature of 1060 ± 10 K.

Fluoride-containing additives, such as $MgF_2$ + LiF, enable to obtain high-density ceramics of solid solutions at low sintering temperatures compared to the sintering of oxide materials. It is assumed that the formation of a hydrofluoride liquid phase during the sintering is responsible for the high densification that occurs at temperatures as low as about 900°C [411].

An oxyfluoride compound that is related to $LiTaO_3$ and has a composition similar to $Li(Mg_{0.05}Ta_{0.95})O_{2.85}F_{0.15}$ was prepared in the form of a single crystal using the flux growth method [408]. The material was investigated in comparison with single-crystal $LiTaO_3$. It was shown that the material that underwent limited substitution of tantalum by magnesium and corresponding substitution of oxygen by fluorine offers several advantages over pure lithium tantalate. First, the derived material displays lower dielectric losses at high temperatures, which leads to easier polarization of the crystal. Second, the crystals exhibit lower birefringence at room temperature. Another very important advantage is directly related to the presence of fluorine in the compound composition, which provides higher optical transparency, especially in the visible and UV spectrum ranges.

Oxyfluoride compounds and highly densified ceramics that are related to lithium niobate, $LiNbO_3$, were obtained in the system:

$$(1 - x)\ LiNbO_3 + x\ (LiF + MgF_2) = Li(Nb_{1-x}Mg_x)O_{3-3x}F_{3x} \qquad (116)$$

where $0 \leq x \leq 0.065$. Ceramics of maximum density were prepared at $0.025 \leq x \leq 0.05$ [412].

The compensative substitution

$$Me^{5+} + 3\ O^{2-} = Mg^{2+} + 3\ F^-$$

is of great interest in the preparation of high-density ceramics of $LiMeO_3$ related compounds with perspective ferroelectric properties (where Me = Ta or Nb).

## 7.3. Spontaneous polarization and non-linear optical effect in niobium and tantalum fluoride compounds

### 7.3.1. General notes

The material's ability to multiply the frequency of laser radiation is related to the non-centrosymmetric crystal structure, required in order to classify the material as a ferroelectric substance. The second harmonic generation (SHG) method enables the effective investigation of both single crystals and powdered fine crystalline substances [413]. A qualitative approach, using second harmonic intensity analysis, is usually based on the assumption that centrosymmetric phases provide an SHG signal that is weaker than the alpha-quartz signal by 0.01 [414]. In addition to the qualitative analysis, the magnitude of the SHG signal is a measure of crystal asymmetry and in some cases can be used for quantitative estimations of spontaneous polarization values [415, 416].

A very simple equation exists that relates spontaneous polarization to the intensity of the second harmonic signal. Spontaneous polarization is conceived as the sum of the products of each of the charges in a dielectric material by each of their displacements from the centrosymmetric positions. Hence, the relationship between spontaneous polarization and the second harmonic signal value can be presented as follows:

$$P_S = Const \cdot \frac{\sqrt{I_{2\omega}}}{(n+1)^3} \tag{117}$$

where $P_S$ = spontaneous polarization; $I_{2\omega}$ = intensity of second harmonic signal; $n$ = refractive index of the material; $Const$ = constant that depends on the measurement conditions.

In order to avoid defining the constant, relative measurements are usually applied for at least two materials, A and B, one of which is used as an etalon. In this case, if material A is an etalon, the spontaneous polarization of material B can be calculated using the following equation:

$$P_{S(B)} = P_{S(A)} \cdot \frac{(n_A+1)^3}{(n_B+1)^3} \cdot \sqrt{I_{2\omega}(B) / I_{2\omega}(A)} \tag{118}$$

Barium titanate, $BaTiO_3$, is frequently used as an etalon and is characterized by the following parameters: $P_S = 25$ μC/cm$^2$; $n = 2.4$; $I_{2\omega} = 300 \cdot I_{2\omega}(SiO_2)$.

Stefanovich, Leonov and Venevtsev [417] describe a typical procedure of SHG measurement. The scheme of the SHG equipment enables to perform measurements at different temperatures, as shown in Fig. 96. SHG measurements of some tantalum and niobium complex fluoride and oxyfluoride compounds in the powdered form were reported in [206, 211] and some results are presented in Table 58.

## 7.3.2. Order–disorder mechanism

A relatively significant SHG signal was observed for the coordination-type compounds $L_4NbO_4F$ and $Li_4TaO_4F$. It is also mentioned in the literature [418] that the signal intensity is not very stable and varies as a function of the method of synthesis and temperature of thermal treatment. In order to understand the main reasons for the signal instability and the nature of spontaneous polarization in compounds with a rock-salt crystal structure, the interaction between $Li_2CO_3$ and $NbO_2F$ was investigated in situ [418, 419]. Fig. 97 shows the dependence of the SHG signal $I_{2\omega}$ on the temperature. The polytherm of the SHG signal of the mixture $Li_2CO_3$ – $NbO_2F$ (molar ratio 2:1) starts at a temperature of 550-570°C, which is the temperature at which the compounds interact, yielding compound $Li_4NbO_4F$ characterizing as non-symmetric phase (Fig. 97, curve a).

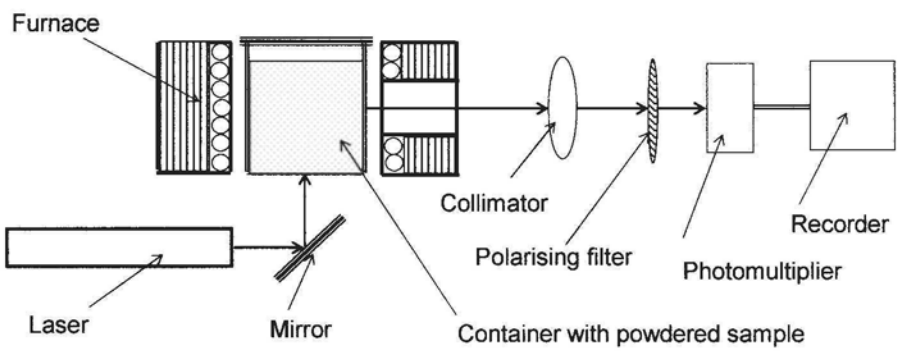


*Fig.96. Investigation of powdered materials using SHG measurements.*

*Table 58. SHG intensity values ($I_{2\omega}/I_{2\omega}$ ($SiO_2$)) of some tantalum and niobium fluorides and oxyfluorides after normalization by alpha-quartz signal $I_{2\omega}$ ($SiO_2$). Measurements were taken before and after thermal treatment, up to extinction of signal.*

| Compound | SHG signal $I_{2\omega}/I_{2\omega}$ ($SiO_2$) | | Curie Temp., °C | Description |
|---|---|---|---|---|
| | Initial | After heating | | |
| | *Solid phase synthesis at 700 - 800°* | | | |
| $Li_4NbO_4F$ | 45 | < 0.1 | | Irreversible signal extinction at > 850°C |
| $Li_4TaO_4F$ | 10<br>10 | | 660 | Reversible type II phase transition |
| | *Hydrofluoride synthesis at 200 - 400°C* | | | |
| $LiNbOF_4$ | < 0.01 | | | Centrosymmetric phase |
| $NaNbOF_4$ | 4 | < 0.1 | | Irreversible signal extinction at 150–200°C |
| $KNbOF_4$ | < 0.1 | | | Centrosymmetric phase |
| $RbNbOF_4$ | 1.2 | < 0.1 | | Irreversible signal extinction at 150-200°C |
| $CsNbOF_4$ | < 0.1 | | | Centrosymmetric phase |
| $CoNbOF_5$ | < 0.1 | | | Centrosymmetric phase |
| $Co_2NbO_3F_3$ | < 0.1 | | | Centrosymmetric phase |
| | *Precipitation from solutions at about room/ambient temperature* | | | |
| $Rb_2NbOF_5$ | 0.8 | < 0.1 | | Irreversible signal extinction at 150°C |
| $RbNbF_6$ | 0.8 | < 0.1 | | Irreversible signal extinction at 130°C |
| $(NH_4)_5Nb_3OF_{18}$ | 15 | 12 | 240 | Reversible type I phase transition |
| $K_5Nb_3OF_{18}$ | 90 | 80 | 320 | Reversible type I phase transition |
| $Rb_5Nb_3OF_{18}$ | 60 | 50 | 320 | Reversible type I phase transition |

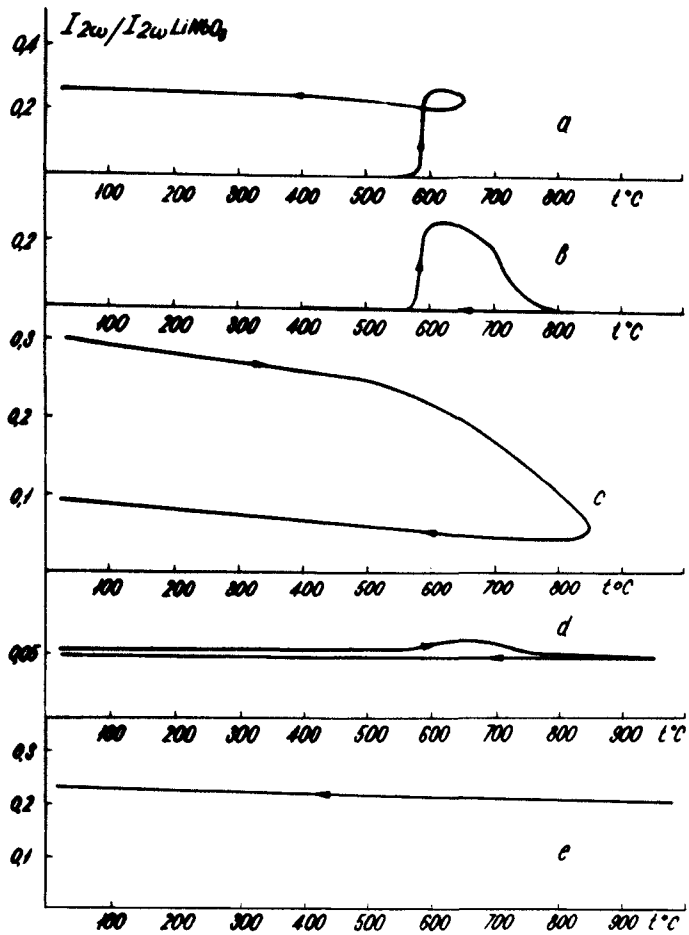


*Fig. 97. Temperature dependence of SHG signals normalized by signal of powdered $LiNbO_3$ ($I_{2\omega}/I_{2\omega\ LiNbO_3}$). Curves a and b – synthesis of $Li_4NbO_4F$ by in situ interaction between $Li_2CO_3$ and $NbO_2F$; curve c and d – $Li_4NbO_4F$ after holding at 800 and 1100°C, respectively; curve e – $Li_3NbO_4$ synthesized at ~ 600°C. Reproduced from [419], S. Y. Stefanovich, B. A. Strukov, A. P. Leonov, A. I. Agulyansky, V. T. Kalinnikov, Jap. J. Appl. Phys., 24 (1985) 630, Copyright 1985, with permission of Institute of Pure and Applied Physics, Tokyo, Japan.*

Further increase in temperature, up to 800°C, leads to a slight decrease in the signal, which remains unchanged following the cooling of the sample and repeated heating up to at least 600-650°C.

Increasing the temperature up to ~800°C leads to a practically complete irreversible extinction of the previously observed SHG signal (see Fig. 97, curve b). This indicates that a metastable non-centrosymmetric phase of $Li_4NbO_4F$ is formed during the initial stages of the synthesis. Relatively extended thermal treatment at 800°C of the phase formed, or even a short heating period at a higher temperature of about 1000-1100°C, leads to an irreversible transition of the rock-salt type compound into a $Li_3NbO_4$ type structure. This structural transformation is reflected in a stable SHG signal typical to $Li_3NbO_4$ type compounds (see Fig. 97, curves c and d).

The high temperature modification of $Li_4NbO_4F$ displays a weaker $I_{2\omega}$ signal compared to its structural analog, $Li_3NbO_4$, which is characterized by an ordered cation arrangement (compare curves d and e of Fig. 97). In the case of oxyfluoride compounds, the lower signal is related to lower spontaneous polarization values compared to pure oxide material and it is in good correlation with the general trend occurring due to the oxygen-fluorine substitution. The above compounds belong to the $Li_{3+x}NbO_4F_x$ family, in which x ranges between 0 and 1. Increasing the value of x leads to a higher ionic contribution of the chemical bonds, which in turn results in reduced displacement of cations and a decrease in the structural distortion. Nevertheless, the appearance of a relatively strong SHG signal for the metastable $Li_4NbO_4F$ phase obtained at low temperatures is of great interest and will be discussed separately based on investigations reported in [206, 419 – 421].

Fragments of X–ray diffraction patterns of a powdered mixture of $Li_2CO_3$ and $NbO_2F$ interacting to form $Li_4NbO_4F$ were obtained at different temperatures and are presented in Fig. 98. When the compound was formed at 650°C, several weak reflexes were observed in the high interplanar distance range, along with the main reflexes. As the temperature increased, the number and inventory of weak reflexes systematically decreased. At about 800-900°C, only a regular diffusive reflex remained. Such an X–ray diffraction pattern indicates that the cubic (or slightly distorted cubic) rock–salt type structure contains steric irregularities in its cationic composition, which differs from the average composition of the crystal. Hence, the appearance of an SHG signal in the low-temperature phase of $Li_4NbO_4F$ can be related to the formation and ordering of $Li^+$ - $Nb^{5+}$ dipoles as part of these said irregularities.

A relatively strong SHG signal observed at low temperatures, can be explained only based on the interaction between fields that contain ordered

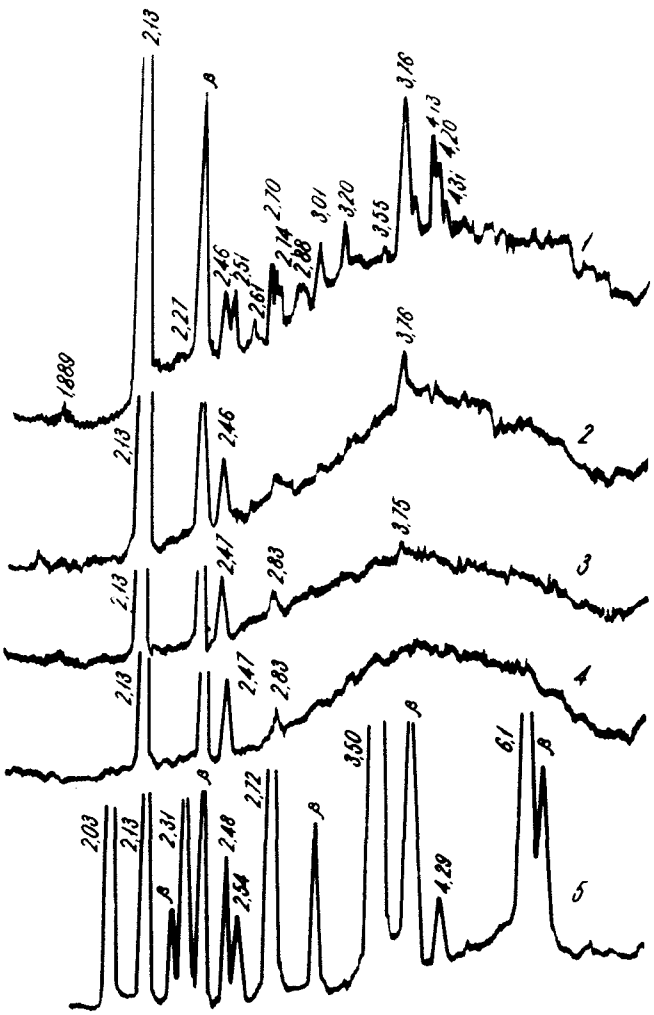


*Fig. 98. Fragments of X–ray diffraction patterns of an $Li_2CO_3$ and $NbO_2F$ mixture performed in situ during synthesis of $Li_4NbO_4F$ at several temperatures. Curve numbers correspond to: 580 (1); 730 (2); 830 (3); 900 (4) and 1150°C (5). Reproduced from [419], S. Y. Stefanovich, B. A. Strukov, A. P. Leonov, A. I. Agulyansky, V. T. Kalinnikov, Jap. J. Appl. Phys., 24 (1985) 630, Copyright 1985, with permission of Institute of Pure and Applied Physics, Tokyo, Japan.*

dipoles and which yield a macroscopic dipole moment that initiates a symmetry reduction with corresponding physical properties changes.

The weak reflexes that appear together with the diffused reflex in the non-centrosymmetric phase, and their disappearance in the centrosymmetric phase can be conceived as circumstantial evidence of the dipole ordering. From this point of view, the decrease in the diffused reflex intensity upon increasing of the temperature indicates that the degree of cation disorder decreases with the increase in temperature. It seems that the concentration of $Li^{+}$ - $Nb^{5+}$ dipoles is not high enough in order to form macro dipoles at higher temperatures. Thermal treatment also leads to a statistic distribution of cations in the rock-salt lattice, which leads to the irreversible extinction of the SHG signal even after cooling of the material.

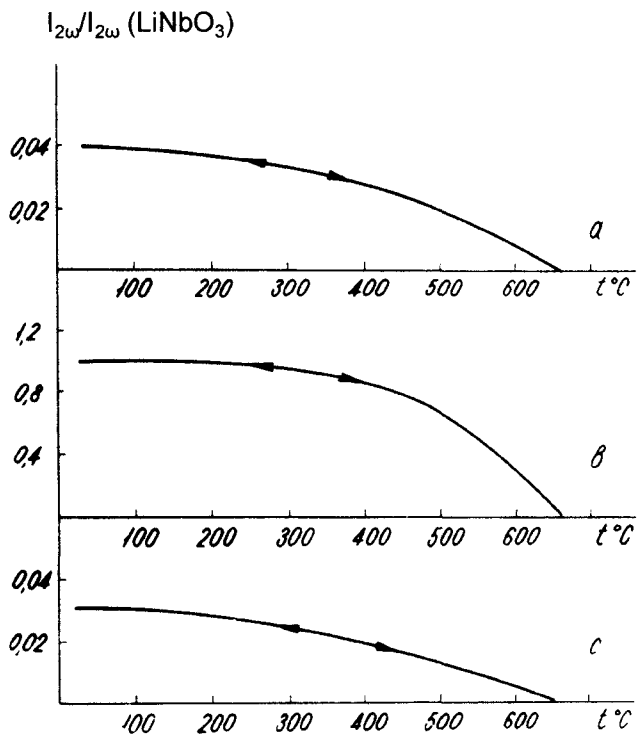


*Fig. 99. Polytherms of the SHG signal of $Li_3TaO_4$ synthesized at 650°C (a) and at 1100°C (b); and of $Li_4TaO_4F$ synthesized at 850°C (c). Reproduced from [419], S. Y. Stefanovich, B. A. Strukov, A. P. Leonov, A. I. Agulyansky, V. T. Kalinnikov, Jap. J. Appl. Phys., 24 (1985) 630, Copyright 1985, with permission of Institute of Pure and Applied Physics, Tokyo, Japan.*

The compound $Li_4TaO_4F$ displays a behavior similar to that of lithium orthotantalate, $Li_3TaO_4$, and undergoes modifications of a disordered and ordered NaCl-type structure. Fig. 99 shows the dependence of the SGH signal of $Li_3TaO_4$ and $Li_4TaO_4F$ on the temperature. $Li_3TaO_4$ prepared at a low temperature (660°C) and $Li_4TaO_4F$ prepared at 850°C appear to have the approximate same value of SHG signals, while lithium orthotantalate displays a significantly higher value when undergoing additional thermal treatment at 1100°C. In all three cases, reversible SHG signal extinction is observed at about 660°C.

The appearance of spontaneous polarization in the case of $Li_4TaO_4F$ is related to volumetric irregularities and ordering of the $Li^+$ - $Ta^{5+}$ dipoles, as is in the case of the similar niobium-containing compound $Li_4NbO_4F$. It can be assumed that the main difference between the two compounds is that the irregularities and the $Li^+$ - $Ta^{5+}$ dipoles are thermally more stable compared to the niobium-containing system. This increased stability of the dipoles leads to the reversible phase transition at 660°C.

The function of $I_{2\omega}$ (T) in the vicinity of the phase transition to centrosymmetric conditions usually has a linear character. Such behavior corresponds to ferroelectrics that undergo type II phase transitions and for which the SHG signal, $I_{2\omega}$, in the vicinity of the Curie temperature is described by the Curie - Weiss Equation:

$$I_{2\omega} \sim P_S^2 \sim (T_C - T) \qquad (119)$$

Thus, in cubic oxyfluorides of niobium and tantalum with rock-salt (NaCl) crystal structures, the formation and extinction of spontaneous polarization occurs due to polar ordering or disordering of $Li^+$ - $Nb^{5+}$($Ta^{5+}$) dipoles.

It seems that structural irregularities that cause spontaneous polarization are a relatively common property of niobium and tantalum oxyfluoride crystals. Fig. 100 shows the temperature dependence of SHG signals for several compounds that form island-type and chain-type structures.

An irreversible extinction of the SHG signal at 150-200°C is observed for a number of other fluoride and oxyfluoride compounds of tantalum and niobium that crystallize in centrosymmetric space groups. This phenomenon is especially typical for the compounds prepared by precipitation from solutions [206]. The appearance of the weak SHG signal for such compounds is related to imperfections in their crystal structure and the creation of dipoles. Nevertheless, appropriate thermal treatment improves the structure and leads to the disappearance of dipoles and to the irreversible disappearance of the corresponding SHG signal.

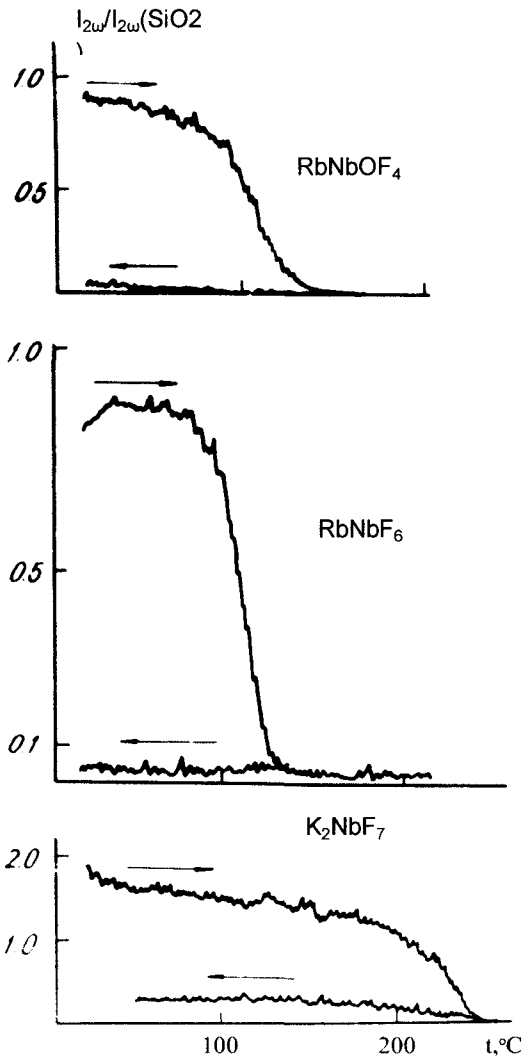


*Fig. 100. Irreversible extinction of SHG signal during heating of compounds that crystallize in centrosymmetric space groups. SHG signal is normalized by signal of alpha-quartz ($\alpha$-$SiO_2$).*
*Reproduced from [206], V. T. Kalinnikov, A. I. Agulyansky, S. Y. Stefanovich, Ferroelectrics, 92 (1989) 77, Copyright 1989, with permission of Taylor & Francis, Inc., http://www.routledge-ny.com.*

## 7.3.3. Displacement mechanism

Statistical analysis indicates that crystallization in centrosymmetric space groups is mostly observed in compounds that have centrosymmetric groups of atoms and ions in their structure [422]. Thus, spontaneously polarized conditions are predominantly created for niobium and tantalum fluoride and oxyfluoride compounds because non-centrosymmetric groups of ions form the basis of a large number of such compounds. Nevertheless, due to electrostatic interactions, dipoles that are created orientate themselves in such a way that in many cases the crystal lattice becomes centrosymmetric. Typical examples are compounds of the $M_2NbOF_5$ type, in which isolated non-centrosymmetric complex ions $NbOF_5^{2-}$ orientate themselves in one of two equivalent positions along a four-fold axis. Furthermore, infinite oxyfluoride chains in $MNbOF_4$ compounds consist of octahedrons that contain niobium that is shifted from the center of the octahedron toward one of the oxygen "bridge" ions, so that in adjacent chains, niobium is shifted in opposite directions. The decrease in the electrostatic interaction between non-centrosymmetric complex ions might promote the onset of spontaneous polarization. This decrease in interionic interaction can be achieved by increasing the interionic distance, for instance, by introducing additional complexes that separate the non-centrosymmetric groups.

The validity of this approach can be demonstrated by the example of several complex fluoride compounds that exhibit ferroelectric properties, such as compounds that belong to the $SrAlF_5$ family [402, 403]. The crystal structure of the compounds is made up of chains of fluoroaluminate octahedrons that are separated by another type of chains - ramified chains. Other examples are the compounds $Sr_3Fe_2F_{12}$ and $Pb_5W_3O_9F_{10}$. In this case, the chains of iron- or tungsten-containing octahedrons are separated from one another by isolated complexes with an octahedral configuration [423, 424].

The crystal structure of $M_5Nb_3OF_{18}$ compounds, where M = $NH_4$, K, Rb, is made up of infinite chains of oxyfluoroniobate octahedrons that are similar to $MNbOF_4$ chain-type compounds. Infinite chains are separated by isolated complexes $NbF_7^{2-}$, whose structure is similar to that found in the island-type compound $K_2NbF_7$. The structure of the $M_5Nb_3OF_{18}$ compounds was described and discussed in Chapter 3.2. Due to the separation of the chains, the displacement of the niobium ion is in the same direction in all chains. The above displacement leads to a spontaneous polarization value that is as high as $4 - 5\ \mu C/cm^2$.

Fig. 101 shows the temperature dependence of the SHG signal for $(NH_4)_5Nb_3OF_{18}$, $K_5Nb_3OF_{18}$ and $Rb_5Nb_3OF_{18}$. The function takes on the form

of $\sqrt{I_{2\omega}}$, which is proportional to the spontaneous polarization ($P_S$) of the compounds. In all cases, a reversible extinction of the signal was observed [211]. The steep slope of the signal and the relatively significant hysteresis that occurs near the Curie temperature indicate that the phase transition is of the first-order type [425, 426]. Values of the spontaneous polarization estimated from the SHG measurements correspond to 4.4; 11.4 and 8.8 μC/cm$^2$ for $(NH_4)_5Nb_3OF_{18}$, $K_5Nb_3OF_{18}$ and $Rb_5Nb_3OF_{18}$, respectively [211]. The estimated values are typical for fluoride compounds and are in good correlation with the spontaneous polarization value of, for instance, $BaCoF_4$, with $P_S$ = 8 μC/cm$^2$ [427].

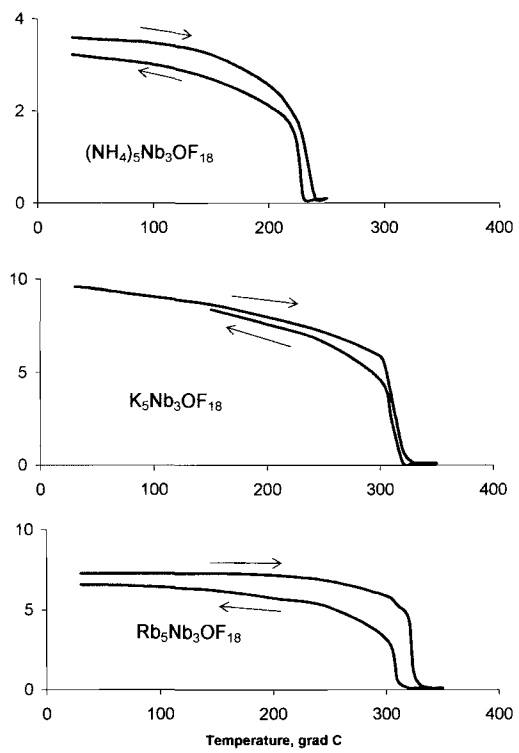


*Fig. 101. Temperature dependence (in relative units, vertical axis) of the SHG signal for $M_5Nb_3OF_{18}$ compounds, where M = $NH_4$; K or Rb. The curve has the form of $\sqrt{I_{2\omega}} \sim P_S$. Arrows indicate heating and cooling of the powdered sample. Reproduced from [211], A. I. Agulyansky, S. Y. Stefanovich, D. V. Tsikaeva, V. T. Kalinnikov, Zh. Neorg. Khim., 27 (1991) 380, Copyright 1991, with permission of "Nauka" (Russian Academy of Sciences) publishing.*

## 7.4. Piezoelectric, pyroelectric and related properties in $M_5Nb_3OF_{18}$ compounds.

### 7.4.1. General notes

$M_5Nb_3OF_{18}$ compounds, in which M = K or Rb, were investigated in greater detail and compared to other related fluoride compounds that contain tantalum or niobium, and are most promising for future practical application in the electronics and optics industries.

These compounds can be referred to as the ferroelectric family $A_5B_3X_{19}$. $Pb_5W_3O_9F_{10}$, a basic compound of the family, was discovered and investigated by Ravez, Abrahams, Marsh, Arquis and Chaminade [428]. A significant number of compounds that belong to the ferroelectric family $A_5B_3X_{19}$, where A = Sr, Ba, Pb and B = Al, Ti, V, Cr, Fe, Ga, Mo, W [428 – 437] have been prepared and investigated in the form of powder, ceramics or small single crystals.

$M_5Nb_3OF_{18}$ compounds, in which M = K or Rb, were investigated in the form of powders or single crystals. Table 59 presents the main physical properties of such materials. The publications devoted to the properties will be discussed below.

*Table 59. Main properties of $M_5Nb_3OF_{18}$, where M = K or Rb.*

| | $K_5Nb_3OF_{18}$ | $Rb_5Nb_3OF_{18}$ |
|---|---|---|
| ***Crystallographic data*** | | |
| Molecular weight | 823.23 | 1064.06 |
| Symmetry | Tetragonal | Tetragonal |
| Space group | $C_{4v}^{10} - I4cm$ | $C_{4v}^{10} - I4cm$ |
| Lattice parameters: | | |
| $a = b$, Å | 14.941(3) | 15.491(3) |
| $c$, Å | 7.718(1) | 7.759(1) |
| Molar volume: | | |
| $V$, Å$^3$ | 1723(7) | 1862(7) |
| $Z$ | 4 | 4 |
| Density: | | |
| $\rho_{measured}$, g·cm$^{-3}$ | 3.21(1) | 3.74(2) |
| $\rho_{calculated}$, g·cm$^{-3}$ | 3.208 | 3.795 |

*Table 59. Main properties of $M_5Nb_3OF_{18}$, where M = K or Rb (Continuation).*

| | | $K_5Nb_3OF_{18}$ | $Rb_5Nb_3OF_{18}$ |
|---|---|---|---|
| ***Optical data*** | | | |
| Refractive indexes (λ = 543 nm): | | | |
| $n_e$ | | 1.500(5) | 1.498(5) |
| $n_o$ | | 1.441(5) | 1.452(5) |
| Limit of UV transmission, μm | | 0.22(2) | 0.22(2) |
| ***Electro-physical data*** | | | |
| Dielectric constant, $\varepsilon_{33}/\varepsilon_0$: | | | |
| frequency – $10^3$ Hz | | 25(5) | 27(5) |
| frequency – $10^6$ Hz | | 15(5) | 15(5) |
| Dielectric losses, ***tan δ*** (along OZ): | | | |
| frequency – $10^3$ Hz | | 0.6(2) | 0.5(2) |
| frequency – $10^6$ Hz | | 0.03(2) | 0.05(2) |
| Pyroelectric coefficient: | | | |
| $p$ | $10^{-9} C \cdot cm^{-2} \cdot K^{-1}$ | 1.8(3) | 1.7(3) |
| Frequency constant | | | |
| $N = f_r \cdot l$ | $Hz \cdot m$ | 1670(50) | 1500(100) |
| Velocity of sound: | | | |
| $V$ | $m \cdot s^{-1}$ | 3300(100) | 2800(100) |
| Coupling factor: | | | |
| $k$ | % | 33(2) | 23(2) |
| Piezoelectric coefficients: | | | |
| $d_{33}$ | $10^{-12} \cdot C \cdot N^{-1}$ | 25(5) | 20(5) |
| $g_{33}$ | $10^{-3} \cdot V \cdot m \cdot N^{-1}$ | 100(20) | 100(20) |
| Elastic compliance constant: | | | |
| $s_{33}$ | $10^{-12} \cdot m^2 \cdot N^{-1}$ | 30(2) | 33(2) |
| Young's modulus: | | | |
| $Y$ | $10^{10} \cdot N \cdot m^{-2}$ | 3.5(2) | 3.0(2) |
| Mechanic quality: | | | |
| $Q_m$ | | 7(2) | 9(2) |

## 7.4.2. Preparation and thermal stability

$M_5Nb_3OF_{18}$ compounds can be prepared in the form of powder using the hydrofluoride method, according to the following interaction:

$$10\ MF + 3Nb_2O_5 + 14\ NH_4HF_2 = 2\ M_5Nb_3OF_{18} + 14\ H_2O + 14\ NH_3 \qquad (120)$$

where M = K or Rb. In order to avoid handling the highly hygroscopic potassium and rubidium fluorides, an interaction based on alkali metal carbonates can be used. The amount of fluorination agent must be re-calculated taking into account the fluorination of both niobium oxide and alkali metal carbonates. The process can be presented as follows and is performed at a temperature of 300°C:

$$5\ M_2CO_3 + 3\ Nb_2O_5 + 18\ NH_4HF_2 = 2\ M_5Nb_3OF_{18} + 5\ CO_2 + 18\ H_2O + 18\ NH_3 \qquad (121)$$

Using powder as a starting material, single crystals were grown from a solution of hydrofluoric acid containing appropriate concentrations of each type of compound (M = K or Rb), using the slow cooling method [206, 209, 211, 438].

At elevated temperatures, $M_5Nb_3OF_{18}$ compounds are sensitive to moisture. Upon heating in non-dry air, hydrolysis occurs at a temperature of above 550K, yielding hydrogen fluoride and two oxyfluoride compounds of different compositions, probably according to the following interaction [438]:

$$M_5Nb_3OF_{18} + H_2O = M_2NbOF_5 + M_3Nb_2OF_{11} + HF \qquad (122)$$

When thermal treatment is applied under conditions that prevent the hydrolysis of the compounds, partial decomposition takes place at a temperature above 600K. Extended thermal treatment at temperatures above 600K leads to complete decomposition according to the following process [438]:

$$M_5Nb_3OF_{18} = 2\ M_2NbF_7 + MNbOF_4 \qquad (123)$$

The processes described in Equations (120 – 123) apply to both potassium- and rubidium-containing compounds (M = K or Rb).

### 7.4.3. Crystal structure and powder X–ray diffraction

According to data obtained from powder X–ray diffraction, the compounds $K_5Nb_3OF_{18}$ and $Rb_5Nb_3OF_{18}$ have similar crystal structure.

The crystal structure of $Rb_5Nb_3OF_{18}$ was investigated and described in [209]. The crystalline network of $Rb_5Nb_3OF_{18}$ is made up of distorted oxyfluoride octahedrons, $NbO_2F_4$, which are linked via oxygen corners forming infinite chains along the Oz direction. Rubidium atoms and isolated $NbF_7^{2-}$ complexes separate the chains from each other. The structure of $Rb_5Nb_3OF_{18}$ is discussed in Chapter 3.2 and shown in Fig. 31.

Fig. 102 shows the temperature dependence of $K_5Nb_3OF_{18}$ and $Rb_5Nb_3OF_{18}$ unit cell parameters [438]. Parameter ***a*** increases with the increase in temperature, while parameter ***c*** displays a maximum at a temperature of about 490–500K. The changes in parameter values with respect to the temperature are reversible.

Such changes indicate the occurrence of a reversible phase transition. No other appreciable anomalies were observed at temperatures of up to 650K that do not correspond to the phase transition at about 595K described in [439].

### 7.4.4. Microcalorimetry

Microcalorimetric measurements also confirm the occurrence of the phase transition [440]. A small peak ($\Delta H \approx 1500$ J·mole$^{-1}$) was observed at about 480K for $Rb_5Nb_3OF_{18}$. A second peak ($\Delta H \approx 4850$ J·mole$^{-1}$) occurs at ~590K. The second peak also appears upon cooling, but with a significantly smaller thermal effect ($\Delta H \approx 1800$ J·mole$^{-1}$). This implies that even if the transition takes place at ~590K, it probably occurs along with at least partial decomposition.

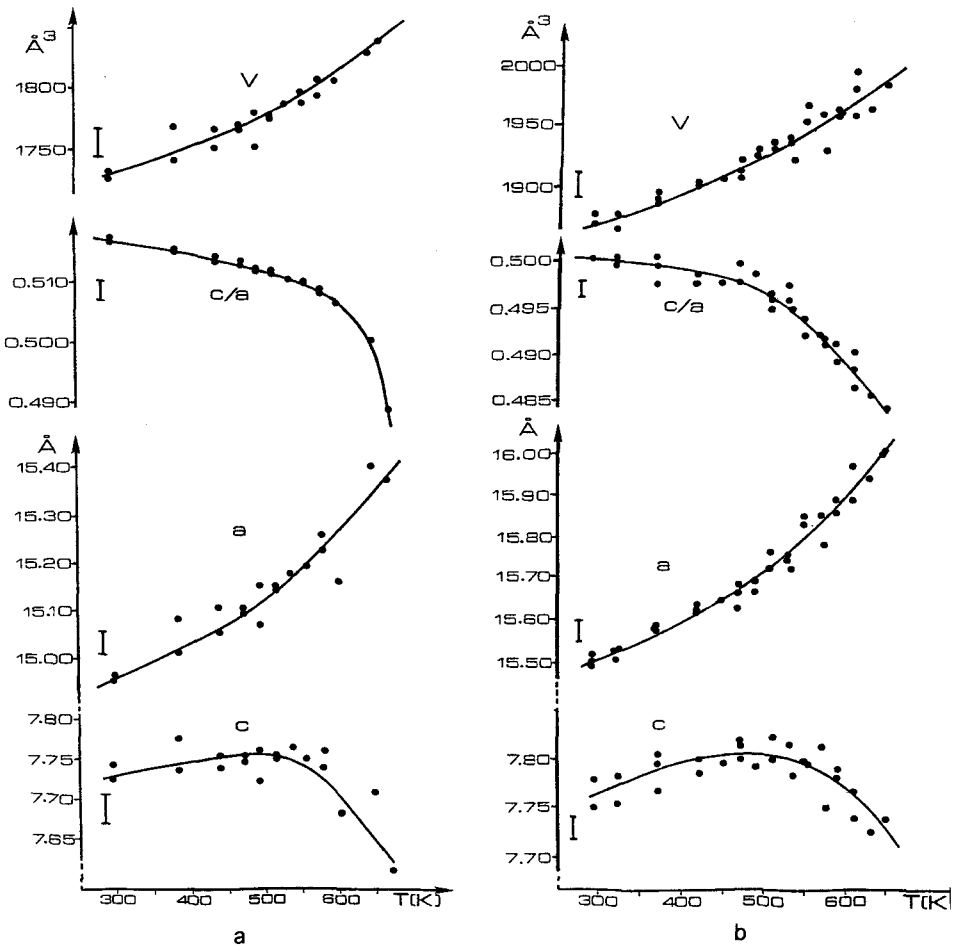


*Fig. 102. Temperature dependence of unit cell parameters* ***a*** *and* ***c****; ratio of parameters – c/a volume – V. Figure (a) - $K_5Nb_3OF_{18}$, figure (b) – $Rb_5Nb_3OF_{18}$ (after Agulyansky and Ravez [438]).*

## 7.4.5. Thermal dependence of birefringence

$K_5Nb_3OF_{18}$ and $Rb_5Nb_3OF_{18}$ crystals are positive uniaxial at room temperature. The resulting thermal dependence of the birefringence $\Delta n$ shows a change in slope at about 490K for $Rb_5Nb_3OF_{18}$ [440]. In the case of $K_5Nb_3OF_{18}$ crystals, the birefringence decreases less drastically, as seen in Fig. 103. The observed changes are reversible up until 550K. This is not the case at temperatures that exceed 600K, at which the crystals become progressively opaque.

The dependence of birefringence on the temperature seems to be correlated to the temperature dependence of the lattice parameters ratio ***c/a*** shown in Fig. 102.

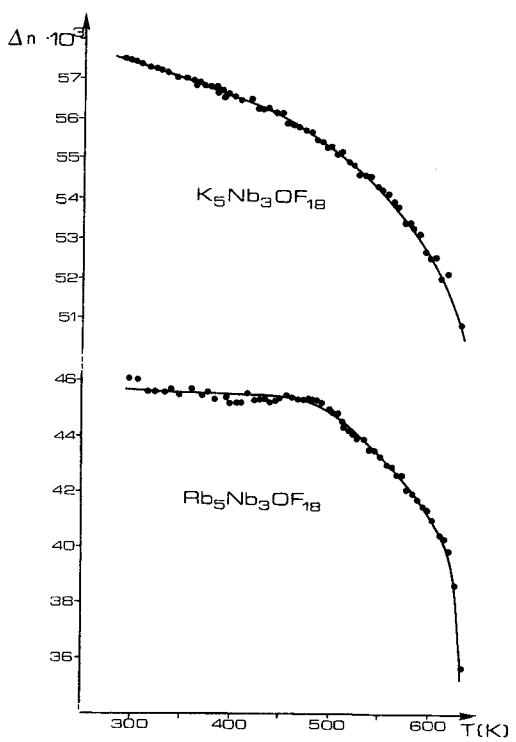


*Fig. 103. Temperature dependence of birefringence.*
*Reproduced from [440], A. I. Agulyansky, J. Ravez, Eur. J. Solid State Inorg. Chem. 30 (1993) 673, Copyright 1993, with permission of Elsevier.*

## 7.4.6. Raman spectra

A Raman study was carried out on single crystals of $Rb_5Nb_3OF_{18}$ using various scattering geometries at room temperature as well as during heating under dry nitrogen to avoid hydrolysis [441, 442].

According to a factor group analysis of R (space group I4cm with Z = 4), vibration modes can be presented in the center of the Brillouin zone (wave vector $\vec{k} = 0$) as follows:

$$\Gamma_{vib.} = 22A_1 + 18A_2 + 16B_1 + 21B_2 + 41E$$

The $A_1$, $B_1$, $B_2$ and E modes are active in the Raman spectrum, $A_1$ is polarized along $\vec{c}$ and E mode is polarized perpendicular to $\vec{c}$. $A_1$ and E modes are active in the IR spectrum as well.

Raman spectra obtained at different orientations of the crystal are presented in Fig. 104. Axes denoted as $a'$, $b'$ and $c'$ correspond to directions $[110]$, $[1\bar{1}0]$ and $[001]$, respectively.

The strongest mode observed near 800 $cm^{-1}$ is polarized along $\vec{c}$ and is a totally symmetrical vibration mode ($A_1$) corresponding to the niobium–oxygen vibrations $\nu_S$ (NbO) of infinite chains $(NbOF_4^-)_n$ running along the $c$-axis. The mode observed at 615 $cm^{-1}$ is polarized perpendicular to $\vec{c}$ and corresponds to the NbF vibrations of the octahedrons of the same chains. The mode at 626 $cm^{-1}$ is attributed to NbF vibrations of isolated complex ions – $NbF_7^{2-}$. The lines at 377, 390 and 272 $cm^{-1}$ correspond to deformation modes δ(FNbF) of the two polyhedrons.

The most striking peculiarity concerns the TO–LO splitting (788–847 $cm^{-1}$) that was observed for the NbO stretching mode ($A_1$ symmetry) polarized along the $c$ axis. Fig. 105 shows the transformation of the spectrum as dependent on scattering geometry. When the wave vector $(\vec{k})$ is perpendicular or parallel to $\vec{c}$, pure TO or LO modes are observed. In the case of intermediate orientation, for instance, a 45° quasi–mode (phonon oblique) is observed [441, 442].

The TO–LO splitting phenomenon was witnessed over the entire investigated temperature range, showing that this crystal belongs to the polar space group up to a temperature of 635K.

The wave numbers of both niobium–oxygen and niobium–fluorine modes change slightly, but systematically, upon heating. The value of $\nu_S$(NbO) increases, indicating an inflection point at about 490K, whereas $\nu_S$(NbF) decreases slowly, ultimately reaching a constant wave number value. Fig. 106

shows the temperature dependences of n. The aforementioned results correlate with data on the temperature dependence of the lattice parameters and indicate the occurrence of a phase transition at 490K. Furthermore, Raman spectra investigations [441, 442] show that even at high temperatures the phase remains polar.

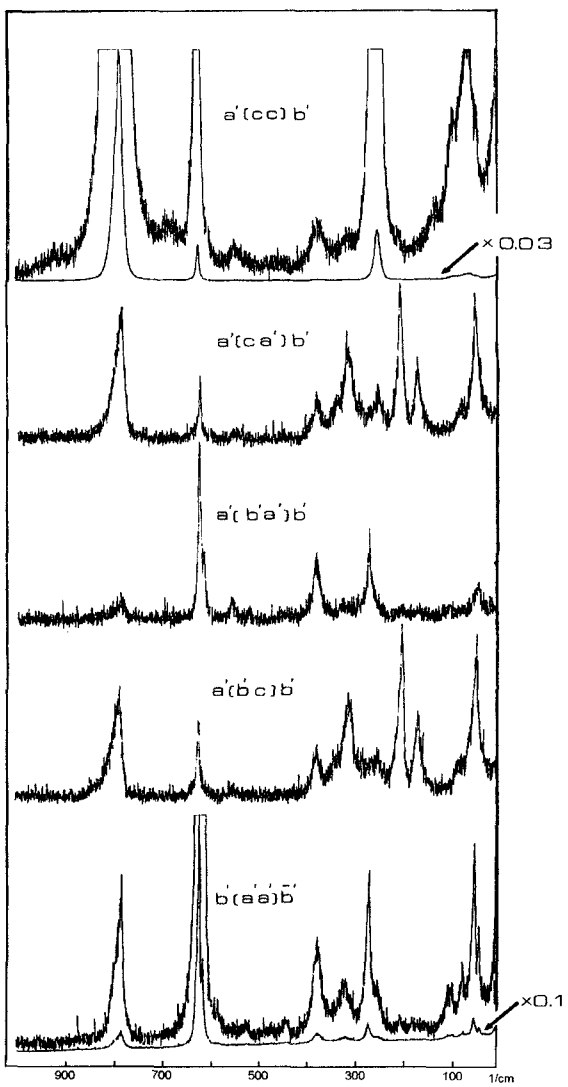


*Fig. 104. Raman spectra of a single crystal of $Rb_5Nb_3OF_{18}$. Reproduced from [441], A. I. Agulyansky, R. Cavagnat, M. Couzi, J. Ravez, Phys. Stat. Sol. (a) 138 (1993) 327, Copyright 1993, with permission of Wiley-VCH.*

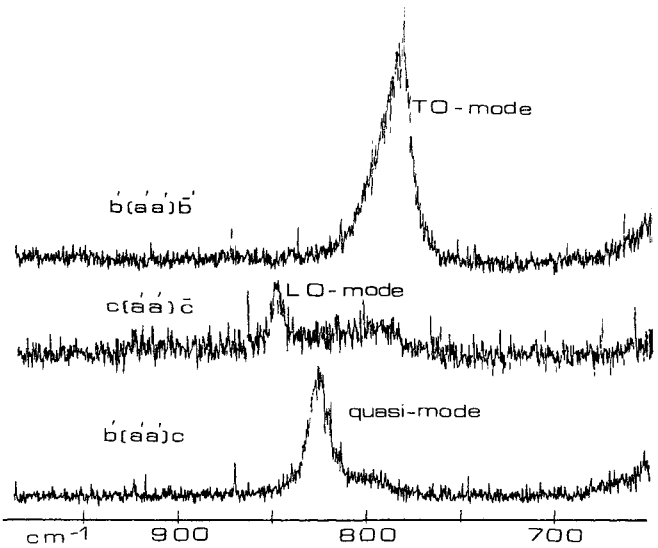


*Fig. 105. TO–LO splitting of totally symmetrical mode $A_1$ (NbO vibration of $Rb_5Nb_3OF_{18}$). Reproduced from [441], A. I. Agulyansky, R. Cavagnat, M. Couzi, J. Ravez, Phys. Stat. Sol. (a) 138 (1993) 327, Copyright 1993, with permission of Wiley-VCH.*

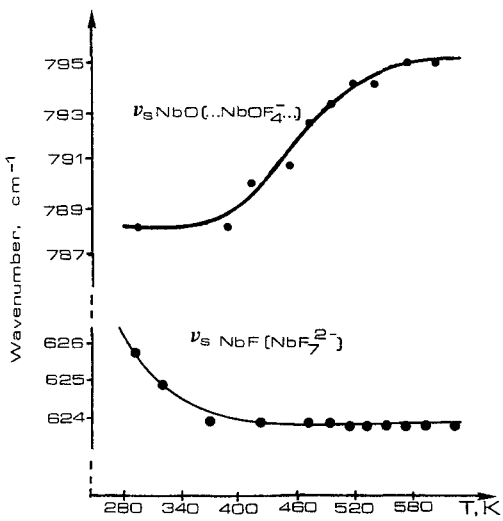


*Fig. 106. Temperature dependence of $\nu_S$(NbO) and $\nu_S$(NbF) wave numbers for a single crystal of $Rb_5Nb_3OF_{18}$. Reproduced from [442], A. I. Agulyansky, J. Ravez, R. Cavagnat, M. Couzi, Ferroelectrics 152 (1993) 373, Copyright 1993, with permission of Taylor & Francis, Inc., http://www.routledge-ny.com.*

## 7.4.7. Dielectric measurements

The temperature dependence of the dielectric permittivity, $\varepsilon_r'$, and of the loss tangent, $\tan\delta = \varepsilon_r''/\varepsilon_r'$, was investigated in an inert gas atmosphere in the frequency range of $10^2$-$10^5$ Hz [440, 443].

A ceramic sample of $Rb_5Nb_3OF_{18}$ shows a maximum $\varepsilon_r'$ at a temperature of about 475K, as seen in Fig. 107. The increased frequency leads to a decrease in $\varepsilon_r'$ and to a stronger dispersion. In addition, it is noted that a very strong increase in permittivity occurs at temperatures >530K. This strong increase, which occurs especially at low frequencies, is probably related to the ionic conductivity of the material. Experiments performed on single crystals along the Oz direction revealed no maximum, but only a slope change in $\varepsilon_r'$ versus the temperature at about 485K. A strong, but irreversible maximum occurs at about 600K for both types of samples.

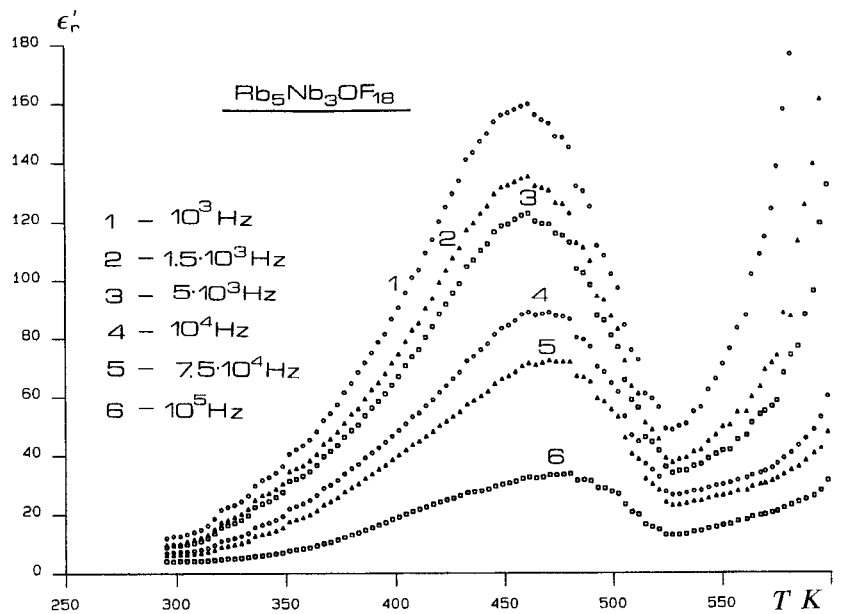


*Fig. 107. Temperature dependence of the dielectric permittivity $\varepsilon_r'$ determined at various frequencies for a ceramic sample of $Rb_5Nb_3OF_{18}$.*
*Reproduced from [443], A. I. Agulyansky, J. Ravez, R. Von Der Mühll, A. Simon, Ferroelectrics 158 (1994) 139, Copyright 1994, with permission of Taylor & Francis, Inc., http://www.routledge-ny.com.*

In the case of single crystals of $K_5Nb_3OF_{18}$, a maximum in the dielectric permittivity $\varepsilon_{33}'$ was observed at about 400K. Fig. 108 shows the temperature dependence of b at different frequencies.

The temperature dependence of $\varepsilon_r''$ shows two or more maxima, especially at low frequencies. The estimated conductivity values indicate that the temperature dependence of this parameter has an inflection point around 450K.

Maxima observed on the plot of the temperature dependences of the dielectric permittivity confirm a phase transition at a temperature of about 480–500K.

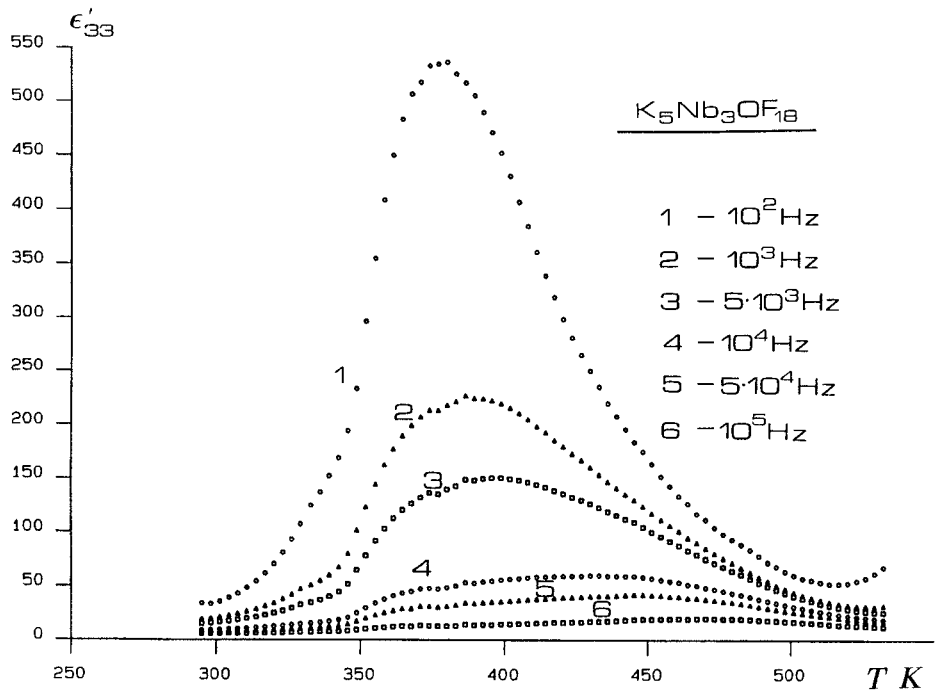


*Fig. 108. Temperature dependence of dielectric permittivity $\varepsilon_r'$ determined at various frequencies for a single crystal of $K_5Nb_3OF_{18}$ along the c axis. Reproduced from [443], A. I. Agulyansky, J. Ravez, R. Von Der Mühll, A. Simon, Ferroelectrics 158 (1994) 139, Copyright 1994, with permission of Taylor & Francis, Inc., http://www.routledge-ny.com.*

## 7.4.8. Piezoelectric resonance and electromechanical properties

Piezoelectric measurements were performed on single crystals oriented along the *c* axis using the resonance method, in the frequency range $10^2$-$3\times10^6$ Hz. The samples were investigated in the temperature range of 280–550K and were heated in an inert atmosphere [443]. Fig. 109 shows typical plots of conductivity versus frequency for $Rb_5Nb_3OF_{18}$ and $K_5Nb_3OF_{18}$, including main resonance and overtones. Temperature dependence of some electromechanical parameters calculated from the measurements are shown in Figs. 110 and 111 for $Rb_5Nb_3OF_{18}$ and $K_5Nb_3OF_{18}$, respectively.

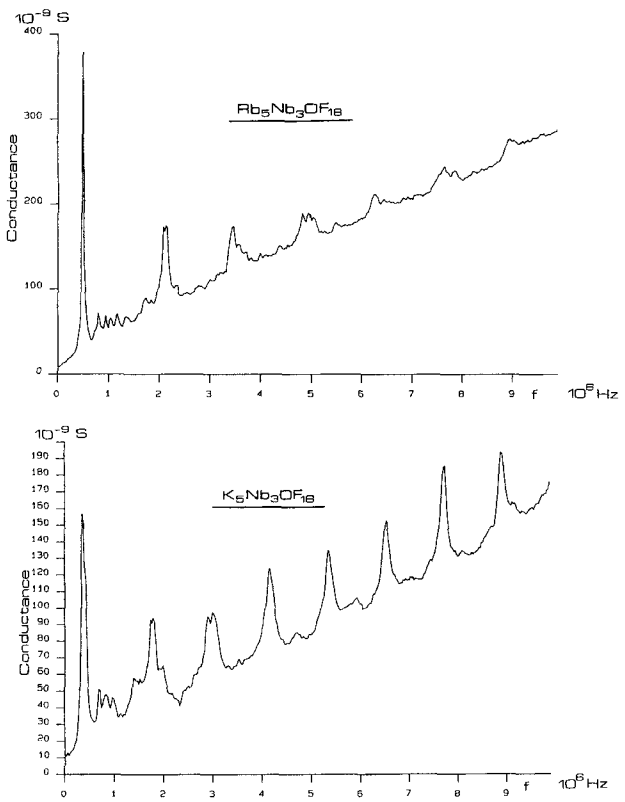


*Fig. 109. Frequency dependence of conductivity (G) for single crystals of $M_5Nb_3OF_{18}$ and $K_5Nb_3OF_{18}$ (electrodes were deposited onto the (001) faces). Reproduced from [443], A. I. Agulyansky, J. Ravez, R. Von Der Mühll, A. Simon, Ferroelectrics 158 (1994) 139, Copyright 1994, with permission of Taylor & Francis, Inc., http://www.routledge-ny.com.*

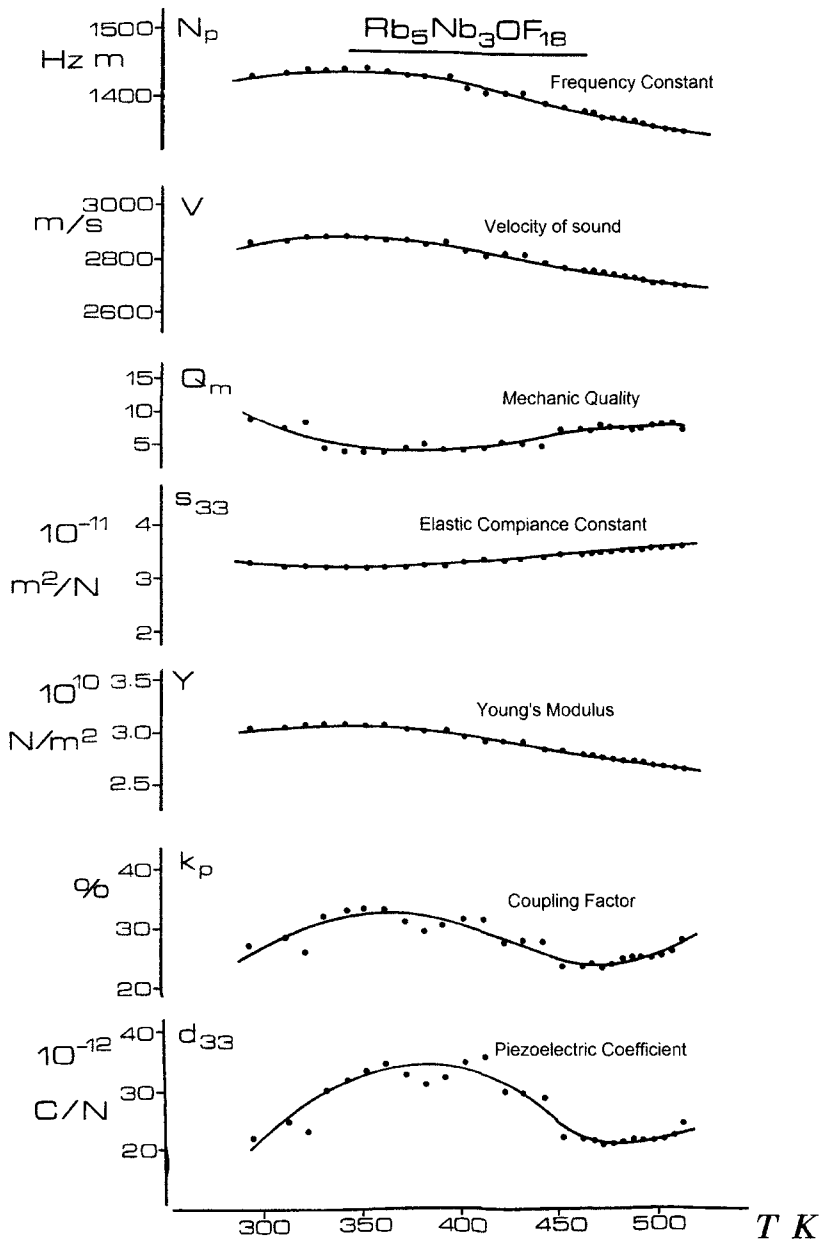


*Fig. 110. Temperature dependence of some electromechanical properties of $Rb_5Nb_3OF_{18}$ crystals. Reproduced from [443], A. I. Agulyansky, J. Ravez, R. Von Der Mühll, A. Simon, Ferroelectrics 158 (1994) 139, Copyright 1994, with permission of Taylor & Francis, Inc., http://www.routledge-ny.com.*

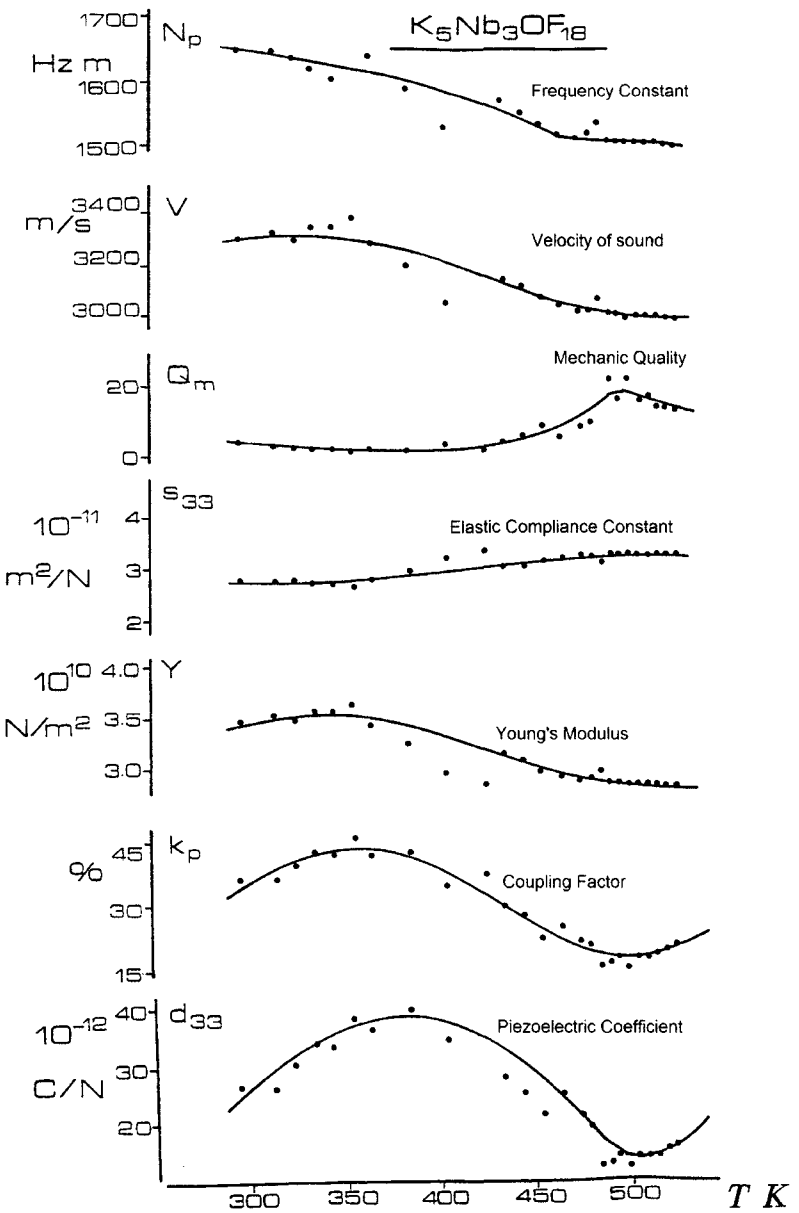


*Fig. 111. Temperature dependence of some electromechanical properties of $K_5Nb_3OF_{18}$ crystals. Reproduced from [443], A. I. Agulyansky, J. Ravez, R. Von Der Mühll, A. Simon, Ferroelectrics 158 (1994) 139, Copyright 1994, with permission of Taylor & Francis, Inc., http://www.routledge-ny.com.*

## 7.4.9. Pyroelectric measurements

Pyroelectric effects occur only in crystals that are characterized by spontaneous polarization. The pyroelectric coefficient describes the change in the electric charge per unit of surface area following a temperature change of one degree. The pyroelectric coefficient of a free sample or of a sample subject to a constant stress and a constant electric field depends on the change in the spontaneous polarization with the change in temperature, but not on the value of the spontaneous polarization itself. The pyroelectric coefficient is equal to the negative derivative of spontaneous polarization with respect to the temperature, and can be expressed as follows:

$$p = -{}^{dP_S}\!/_{dT} \tag{124}$$

where $p$ = pyroelectric coefficient, $P_S$ = spontaneous polarization. When $dT$ is positive, the minus sign turns $p$ into a positive value [16].

Thermocurrent measurements were performed on crystals of $Rb_5Nb_3OF_{18}$ and $K_5Nb_3OF_{18}$ along the $c$ direction [440, 443]. Fig. 112 shows the temperature dependences of the pyroelectric coefficients close to room temperature .

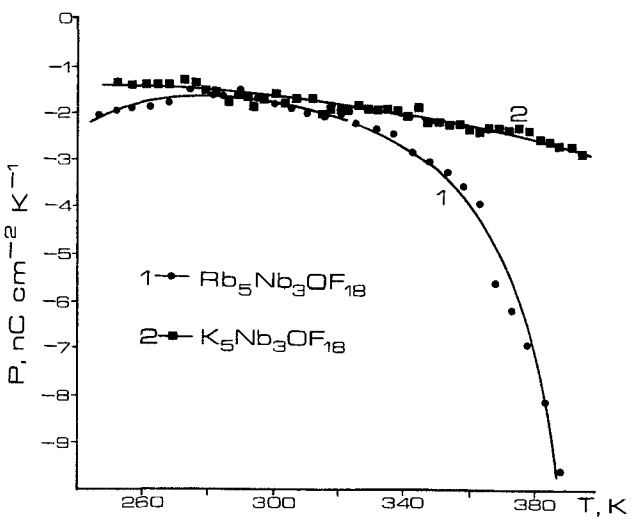


*Fig. 112. Pyroelectric coefficients of $Rb_5Nb_3OF_{18}$ and $K_5Nb_3OF_{18}$ crystals in the temperature range around room/ambient temperature. Reproduced from [443], A. I. Agulyansky, J. Ravez, R. Von Der Mühll, A. Simon, Ferroelectrics 158 (1994) 139, Copyright 1994, with permission of Taylor & Francis, Inc., http://www.routledge-ny.com.*

At high temperatures, the module of the pyroelectric constants of both compounds increases more significantly and reaches an extremum at about 480K. Fig. 113 shows the temperature dependence of the pyroelectric coefficients. This phenomenon could be related to the change in dilatation mechanism that was observed while investigating the temperature dependence of the lattice parameters (see Fig. 102).

In general terms, the pyroelectric coefficient of a free sample consists of three components. The first, called the real coefficient, depends on the derivative of spontaneous polarization with respect to the temperature. The second is derived from the temperature dilatation and can be calculated based on mechanical parameters. The third coefficient is related to the piezoelectric effect and results from the temperature gradient that exists along the polar axis of the crystal.

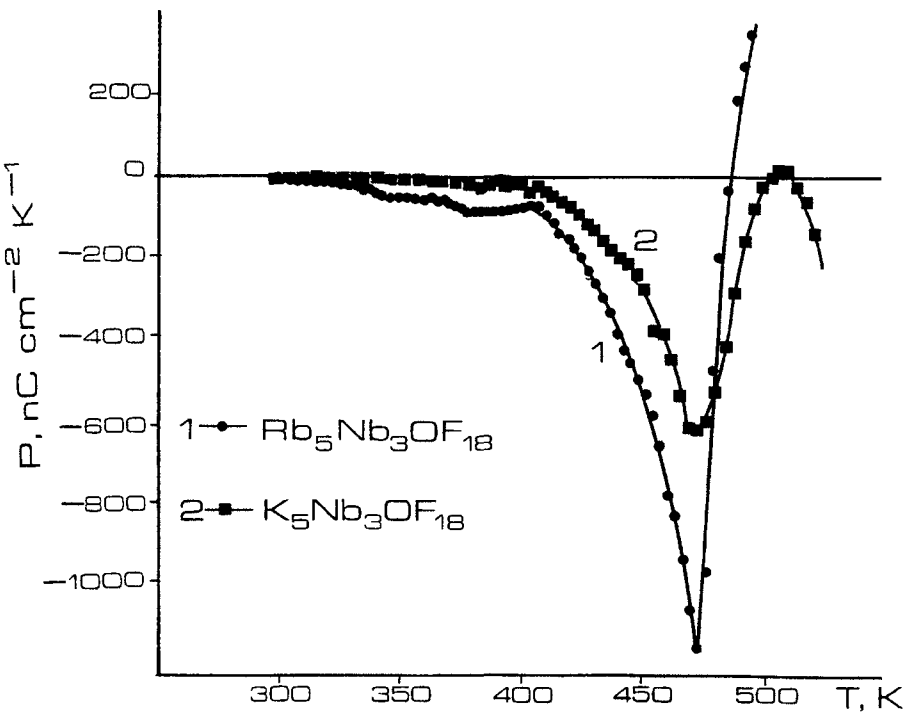


*Fig. 113. Pyroelectric coefficients of $Rb_5Nb_3OF_{18}$ and $K_5Nb_3OF_{18}$ crystals measured in the high temperature range. Reproduced from [443], A. I. Agulyansky, J. Ravez, R. Von Der Mühll, A. Simon, Ferroelectrics 158 (1994) 139, Copyright 1994, with permission of Taylor & Francis, Inc., http://www.routledge-ny.com.*

In the case of relatively small samples, the third coefficient is usually significantly low compared to the first and second coefficients; nevertheless, the second coefficient in such cases is too significant not to be taken into consideration.

The measured pyroelectric coefficient can be represented as the sum of the first coefficient (real pyroelectric coefficient - $p_i^{T,E}$) and the second coefficient, which depends on the piezoelectric constant ($d_{ij}$), the thermal expansion coefficient ($\alpha_{ij}^{E}$) and the elastic compliance coefficient ($s_{ij}^{E}$) as follows [16]:

$$p_i^{T,E} = p_i^{S,E} + d_{ij}\alpha_{ij}^{E} / s_{ij}^{E} \tag{125}$$

Using data obtained from thermocurrent, piezoelectric and dilatometric measurements, the first and second pyroelectric coefficients were calculated for the $Rb_5Nb_3OF_{18}$ crystal. Fig. 114 presents the results.

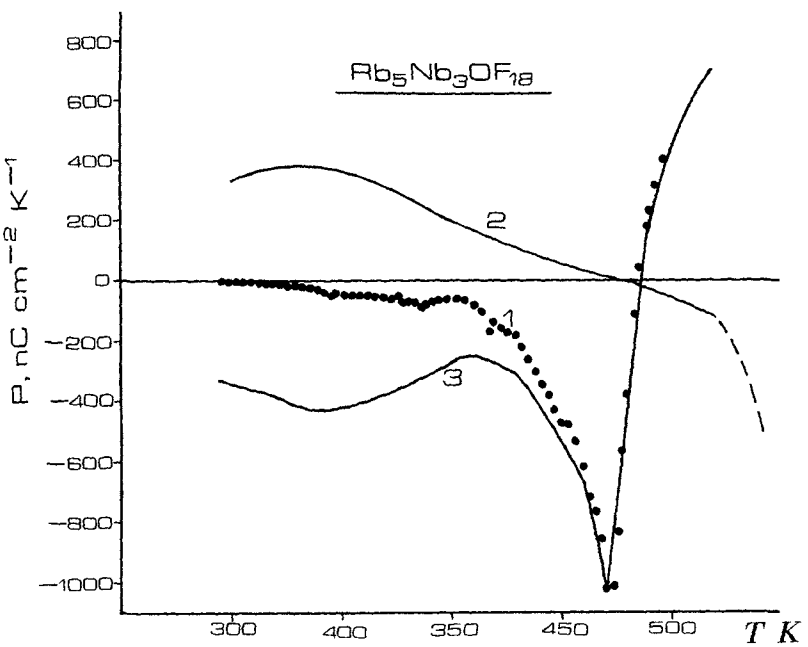


*Fig. 114. Pyroelectric coefficients of $Rb_5Nb_3OF_{18}$ crystal (free sample). 1 – Measured coefficient; 2 – Second coefficient; 3 – First coefficient.*

Based on the results of the calculations, it should be mentioned that the first pyroelectric coefficient seems to be significantly higher than the measured value even at room temperature. This high value of the coefficient can be achieved by clamping (compressing) the sample.

## 7.4.10. Conclusions

The various studies performed on $K_5Nb_3OF_{18}$ and $Rb_5Nb_3OF_{18}$ crystals and ceramics are in agreement regarding the reversible transition that takes place at about 470–490°K. The transition seems to be related mainly to a modification of the NbO bonds in the infinite chains ($NbOF_4^-$) of the structure. The lack of ferroelastic domains implies that the transition occurs without any change in the crystalline system. Raman scattering study results indicate that both the low- and high-temperature phases crystallize in a polar space group, which excludes a ferroelectric–paraelectric transition, which appears always with the transition from a polar to a non-polar group.

The small effects and the progressive evolutions observed seem to be in agreement with a second order phase transition. The lack of coexistence of the low- and high-temperature phases in the temperature range close to the transition temperature and the apparent lack of thermal hysteresis confirm this conclusion.

The hiding of the pyroelectric coefficients seems to be correlated to the maximum $c$ parameter, which in turn corresponds to the transition temperature. The shift along the Oz direction, $\Delta z$, of the niobium atoms, which are located within the octahedrons, is responsible for the compound's polar properties. When $c$ is at its maximum, this shift is enhanced and leads apparently to maximum spontaneous polarization $P_S$. The value of $P_S$ increases in the temperature range of 300 to 490K and then decreases at temperatures above 490°K.

These materials are piezoelectric and pyroelectric; ferroelectricity has not been clearly proven [443].

The compounds $K_5Nb_3OF_{18}$ and $Rb_5Nb_3OF_{18}$ display promising properties for their application in electronics and optics. The compounds can be used as piezoelectric and pyroelectric elements due to sufficient piezo- and pyroelectric coefficients coupled with very low dielectric permittivity. In addition, the materials can successfully be applied in optic and optoelectronic systems due to their wide transparency range. High transparency in the ultraviolet region enables use of the materials as multipliers of laser radiation frequencies up to the second, and even fourth optical harmonic generation.

This page is intentionally left blank

# 8.

# FLUORINE CHEMISTRY IN THE PROCESSING OF TANTALUM AND NIOBIUM

## 8.1. General notes

Modern processing of tantalum and niobium metals and their compounds is related to the treatment of fluoride compounds. Hence, successful technological improvements, the development of novel methods and the manufacturing of high-grade products depend on the application of technological achievements in the area of fluorine chemistry.

The processing of tantalum and niobium begins with the fluorination of the raw material, which always consists of complex oxide compounds containing tantalum and niobium. The main types of tantalum- and niobium-containing minerals are discussed in Chapter 1, and typical compositions of such minerals are presented in Table 2.

Concentrates of columbate-tantalate are most suitable for processing and are most frequently used in the production of tantalum, niobium and their compounds.

The fluorination process aims to decompose the material and convert tantalum and niobium oxides into complex fluoride compounds to be dissolved in aqueous solutions. The correct and successful performance of the decomposition process requires a clear understanding of the oxygen–fluorine substitution mechanism of the interaction itself.

The next technological step is the purification and separation of tantalum and niobium in the form of complex fluoride compounds of tantalum and niobium. This process is performed using liquid–liquid extraction, using appropriate organic solvents. This technological step requires knowledge on

the complex structure of tantalum and niobium fluorides in solutions. It is very important to understand what type of complexes are present in the solution, which parameters of the solution can affect the equilibrium between the complexes and what type of complexes are extracted into the organic solvent from water or stripped from the organic phase into the aqueous solution.

The process of separating the intermediate products from the purified solutions, in the form of solid complex fluoride salts or hydroxides, is also related to the behavior of tantalum and niobium complexes in solutions of different compositions. The precipitation of complex fluoride compounds must be performed under conditions that prevent hydrolysis, whereas the precipitation of hydroxides is intended to be performed along with hydrolysis in order to reduce contamination of the oxide material by fluorine.

Tantalum powder is produced by reduction of potassium heptafluorotantalate, $K_2TaF_7$, dissolved in a molten mixture of alkali halides. The reduction is performed at high temperatures using molten sodium. The process and product performance are very sensitive to the melt composition. There is no doubt that effective process control and development of powders with improved properties require an understanding of the complex fluoride chemistry of the melts. For instance, it is very important to take into account that changes both in the concentration of potassium heptafluorotantalate and in the composition of the background melt (molten alkali halides) can initiate cardinal changes in the complex structure of the melt itself.

This chapter is devoted to a discussion of the main steps in the currently-applied technology of tantalum and niobium compounds from the standpoint of the chemistry of complex tantalum and niobium fluoride compounds.

Fig. 115 presents the general process flow chart. The raw material is decomposed in order to digest the material for conversion into soluble fluoride compounds. The obtained solution is treated by the liquid–liquid extraction method to obtain two solutions. The first is a high-purity tantalum-containing solution that is ready for further application. The tantalum-containing solution is used for two processes. The first process is the precipitation of potassium heptafluorotantalate, $K_2TaF_7$. Potassium heptafluorotantalate is also called K–salt and is used as an initial material in the production of tantalum metal powder. Reduction of tantalum is performed in the melt by adding molten sodium. This process is also called a sodium reduction process. Tantalum-containing solution is also used in the preparation of tantalum oxide, $Ta_2O_5$. The process is based on the precipitation of tantalum hydroxide, filtration and subsequent thermal treatment of tantalum hydroxide to form tantalum oxide powder.

The second solution that results from the liquid–liquid extraction process is a high-purity niobium-containing solution. This solution is used in the preparation of niobium oxide, $Nb_2O_5$. The process is similar to the above-described process of tantalum oxide preparation and consists of the precipitation of niobium hydroxide and subsequent thermal treatment to obtain niobium oxide powder.

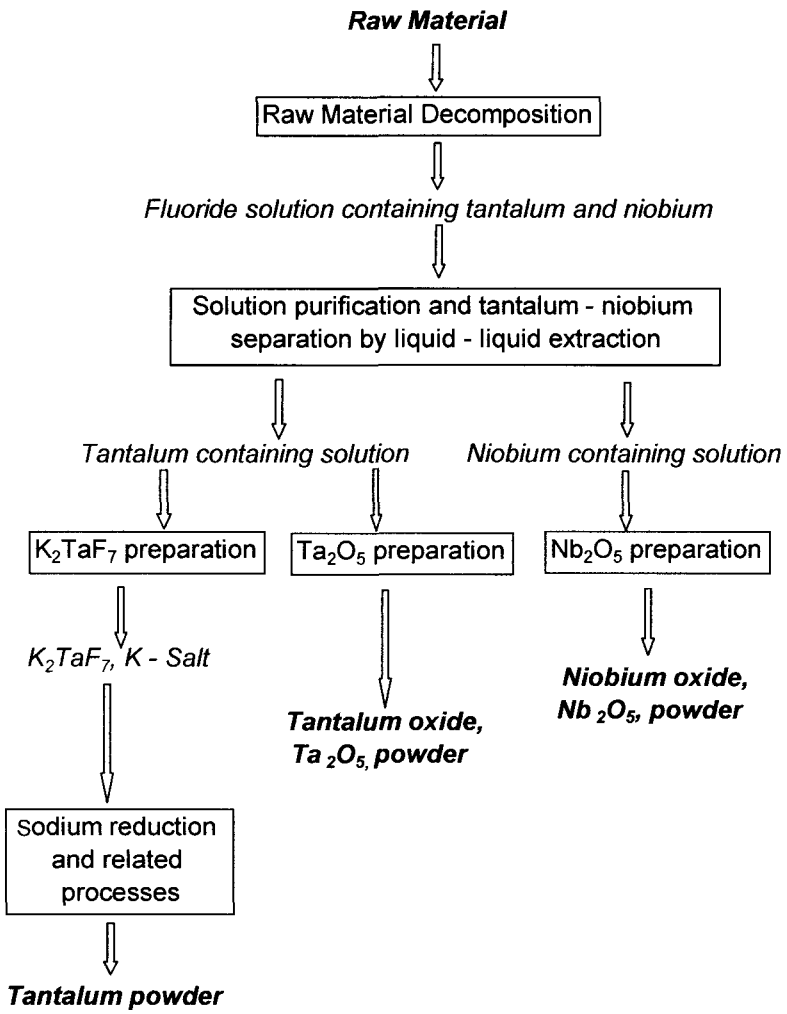


*Fig. 115. General scheme of the processing of tantalum and niobium including treatment of fluoride compounds.*

## 8.2. Raw material decomposition

### 8.2.1. Digestion using hydrofluoric and sulfuric acids

The purpose of the decomposition of raw materials is to convert tantalum and niobium compounds into a soluble form and prepare the solution for use in subsequent procedures. Fig. 116 presents the process flow chart. The most typical and frequently used raw materials are columbite–tantalite concentrates with the general formula (Fe, Mn)(Nb, $Ta)_2O_6$.

Two types of digestion solutions are usually used for the chemical decomposition of the raw material hydrofluoric acid, HF, or a mixture of hydrofluoric and sulfuric acids, HF and $H_2SO_4$ [32]. The process is performed using solutions with relatively high acid concentrations, at elevated temperatures and under intensive stirring for several hours to ensure effective digestion. The raw material is nearly completely dissolved.

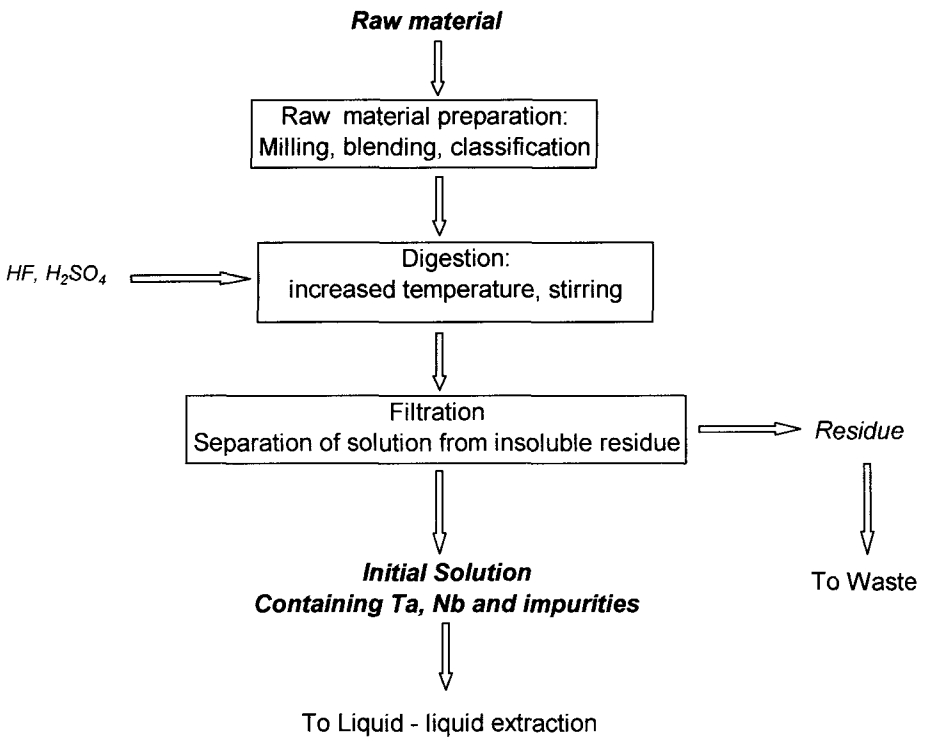


*Fig. 116. Flow chart of the raw material decomposition process.*

A residual phase, usually consisting of insoluble fluorides and oxyfluorides of alkali earth and rare earth metals, is separated from the solution by filtration. The mechanism of the chemical decomposition of raw materials of the tantalum- and niobium-containing oxide type seems to be complicated, and unfortunately, the process has yet to be adequately investigated.

The mechanism and kinetics of the dissolution of tantalum and niobium oxides both in hydrofluoric acid and in a mixture of hydrofluoric and sulfuric acids were investigated by Baram [444 – 447]. It was shown that the dissolution rate of $Nb_2O_5$ and $Ta_2O_5$ in hydrofluoric acid solutions depends on the initial concentration of HF and corresponds to a second-order interaction. Tantalum oxide, $Ta_2O_5$, dissolves in HF solutions significantly slower than does niobium oxide, $Nb_2O_5$. This phenomenon is explained by the difference in the dissolution mechanisms of the two compounds. Thus, it was found that the dissolution rate of $Nb_2O_5$ is described by a kinetic equation, whereas the dissolution rate of $Ta_2O_5$ in hydrofluoric acid is limited by diffusion, a process that proceeds at a slower pace than does a chemical interaction.

It was proposed [445 – 447] that the dissolution of tantalum and niobium oxides in mixtures of hydrofluoric and sulfuric acids takes place through the formation of fluoride-sulfate complexes, at least during the initial steps of the interaction and at relatively low acid concentrations. Nevertheless, it was also assumed that both tantalum and niobium fluoride-sulfate complexes are prone to hydrolysis yielding pure fluoride complexes and sulfuric acid. No data was provided, however, to confirm the formation of fluoride sulfate complexes of tantalum and niobium in the solutions.

Nevertheless, $Ta^{5+}$ and $Nb^{5+}$ interact with aqueous media containing fluorine ions, such as solutions of hydrofluoric acid. On the other hand, as was clearly shown by Majima et al. [448 – 450], the increased hydrogen ion activity can also significantly enhance the dissolution rate of oxides. The activity of hydrogen ions can be increased by the addition of mineral salts or mineral acids to the solution.

Majima, Awakura, Mashima and Hirato [451] investigated in detail the kinetics of the dissolution process of columbite and tantalite in aqueous solutions of HF, HF – HCl, $NH_4F$ – HCl and $NH_4F$ – $H_2SO_4$, in the 60-80°C temperature range.

Results of the measurements were analyzed in the form of the initial dissolution rate ($R_i$), which is the first derivative of the dissolution fraction of a said element, in this case, niobium or tantalum. The dissolution fraction is defined as the molar ratio between the amount of metal dissolved and its total concentration in the said sample, in this case, columbite or tantalite. Table 60 presents some relevant values of the initial dissolution rate taken from [451].

*Table 60. Initial dissolution rates ($R_i$) of niobium and tantalum dissolved from columbite or tantalite in different solutions, at 80°C. (Compositions of solutions are given in mol/l)(after Majima et al. [415]).*

| HF | $H_2SO_4$ | $NH_4F$ | $R_{Nb}/10^{-3}$ min$^{-1}$ | $R_{Ta}/10^{-3}$ min$^{-1}$ |
|---|---|---|---|---|
| Columbite (in Wt %): $Nb_2O_5$ – 62.19; $Ta_2O_5$ – 5.86 | | | | |
| 1 | - | - | 0.339 | 0.393 |
| 2 | - | - | 1.61 | 2.11 |
| 5 | - | - | 6.22 | 8.25 |
| 10 | - | - | 27.3 | 23.4 |
| 1 | 0.1 | - | 0.826 | |
| 1 | 1 | - | 1.53 | |
| 1 | 2 | - | 3.34 | |
| - | 1 | 1 | 0.662 | |
| - | 1 | 2 | 0.195 | |
| - | 2 | 1 | 1.55 | |
| Tantalite (in Wt %): $Nb_2O_5$ – 41.94; $Ta_2O_5$ – 26.83 | | | | |
| 0.1 | - | - | 0.009 | 0.010 |
| 1 | - | - | 0.135 | 0.201 |
| 10 | - | - | 7.82 | 11.5 |

Based on an analysis of the initial dissolution rate in different solutions at different temperatures, several very useful conclusions and recommendations were made. It was found that the apparent activation energies for the dissolution of niobium and tantalum in 10 mol/l HF solution are 56.5 and 65.5 kJ/mol, respectively for columbite, and 42.7 and 61.1, respectively, in the case of tantalite. It was also concluded that the mechanism of dissolution is the same for both columbite and tantalite. In addition, the initial dissolution rate of niobium ($R_{Nb}$) from columbite is controlled primarily by the activities of the

hydrogen and fluorine ions, whereas the presence of other ions is of minor importance.

The dependence of $R_{Nb}$ on these two parameters is expressed by the experimental equation as follows:

$$R_{Nb} = k_0 a(H^-)^{1.2} C(F^-)^{1.1} exp(-E_a/RT) \quad (126)$$

where $k_0$ and $E_a$ are the initial rate constant and apparent activation energy, respectively.

The addition of strong acids or neutral salts, such as $NH_4F$, to the hydrofluoric acid solution was recommended in order to increase the concentrations and activities of fluorine and hydrogen ions [451].

Akimov and Chernyak [452] investigated and reported on the mechanism of the interaction between columbite and tantalite and sulfuric acid. The said interaction is presented as comprising two steps. The first step is related to the formation of iron and manganese sulfates and of tantalum and niobium hydroxides:

$$(Fe, Mn)(Ta, Nb)_2O_6 + H_2SO_4 = (Fe, Mn)SO_4 + (Ta, Nb)_2O_5 \cdot H_2O \quad (127)$$

It is assumed that at the second step, tantalum and niobium hydroxides are converted into oxysulfate compounds, as represented by Equation (128):

$$2\,(Ta, Nb)_2O_5 \cdot H_2O + H_2SO_4 = 2\,(Ta, Nb)_2O_3(SO_4)_2 + H_2O \quad (128)$$

The results of a thermodynamic analysis of the interactions in Equations (127) and (128), as presented in [452], show that a coherent shell of tantalum and niobium hydroxides is formed on the surface of the columbite or tantalite during the interaction with sulfuric acid. The formation of the shell drives the process towards a forced thermodynamic equilibrium between the initial components and the products of the interaction, making any further interaction thermodynamically disadvantageous. It was also shown that, from a thermodynamic standpoint, the formation of a pseudomorphic structure on the surface of columbite or tantalite components is preferable to the formation of tantalum and niobium oxysulfates. Hence, the formation of the pseudomorphic phases catalyzes the interaction described by Equation (127) while halting that described by Equation (128).

This approach explains the experimental fact that the complete decomposition of columbite or tantalite by sulfuric acid yields hydroxides of tantalum and niobium according to the first step of Equation (127).

The decomposition process can be significantly intensified by the mechanical activation of the material prior to chemical decomposition. Based on a thermodynamic analysis of the system, Akimov and Chernyak [452] showed that the mechanical activation initiates dislocations mostly on the surface of the grains, and that heterogeneities in the surface cause the predominant migration of iron and manganese to the grain boundaries. It is noted that this phenomenon is more pronounced for manganese than it is for iron.

Analysis of the volumetric effects indicates that as a result of such mechanical activation, iron and manganese are concentrated in the extended part of the crystal, while tantalum and niobium are predominantly collected in the compressed part of the distorted crystal structure. It is interesting to note that this effect is more pronounced in the case of tantalite than it is for columbite, due to the higher "rigidity" of the former. Akimov and Chernyak [452] concluded that the effect of redistribution of the ions might cause the selective predominant dissolution of iron and manganese during the interaction with sulfuric acid and other acids.

Welham [453] investigated in detail the effect of extended grinding on the dissolution process of tantalum- and niobium-containing concentrates. The measurements were performed using concentrates prepared from a West Australian pegmatite deposit. The material was milled in a ball mill under wet or dry conditions and in air or argon atmosphere for different periods of time. X-ray powder diffraction patterns of the milled product indicated no significant changes, but extended milling (100 hours) provided no X–ray powder diffraction peaks at all. This indicates that the material becomes amorphous or can be called X–ray amorphous, since its particle size is too small to provide a regular X–ray pattern. The general relationship between the particle size and the milling duration is given by Equation (129), as follows [453, 454]:

$$r_0(t) = r_0(0)(1 + at)^{-1/n} \tag{129}$$

where $a$ is a constant indicating the milling efficiency, $r_0(0)$ is the crystalline radius at $t = 0$.

All of the experiments described by Welham in [453] are compatible with Equation (129), and give the values $r_0(0) = 35.5 \pm 0.9$ nm and $n = 3.0 \pm 0.2$

for all types of milling, whereas the value of $a$ varies, depending on the presence of water, from 1.15 to 0.17 for dry and wet milling, respectively.

Analysis of specific changes in surface area during milling shows the difference between wet and dry conditions. In addition, dry milling under argon and in air also provides different results. Thus, the specific surface areas at the end of the size-reduction milling process were estimated at 4.6 and 3.9 $m^2\ g^{-1}$ for milling in air and under argon, respectively. This phenomenon is explained by the interaction with oxygen of the freshly formed broken surface, which prevents rewelding of the particles. In the case of an argon atmosphere, no oxidized layer is formed and the surface remains highly susceptible to rewelding.

The difference between the specific surface areas of materials treated by the wet or dry method can also be explained by the rewelding mechanism. The surface area of wet milled powders continuously increases during milling, while extended dry milling causes a decrease in surface area.

Nevertheless, it was clearly shown [453] that dry extended milling efficiently increases the dissolution rate of the material. Thus, a powder milled for 50 hours exhibits a dissolution rate 4500 times higher than a powder after only two hours of milling.

It was found that the dissolution rate of the material depends both on its surface area and on its crystalline size, but the importance of the crystalline size seems to be greater. The empiric equation describing the above dependence of the leaching rate on these two parameters is as follows (130):

$$\%(leached) = C_1 / r + C_2 A \tag{130}$$

where $C_1$ and $C_2$ are constants and $r$ and $A$ are crystalline size in nm and specific surface area in $m^2\ g^{-1}$, respectively. For the investigated material, $C_1$ and $C_2$ were found to be 677.79 and 1.2208, respectively. It was found that the dissolution process takes place in two stages. The first stage is controlled by diffusion and its extent can be increased by extended milling. The second stage is assumed to be limited by chemical interaction.

Based on a comprehensive investigation, Welham [453] recommends the use of a strong acid or high fluoride concentration in order to achieve optimal leaching. Specifically, the use of hydrofluoric acid with a concentration > 18% or fluoride concentration > 0.5 mol/l was indicated. It is also noted that leaching at elevated temperatures leads to the separation of titanium by hydrolytic precipitation from the solution.

Summarizing the said investigations on the dissolution of tantalum- and niobium-containing raw materials in liquid media, the following points can be noted.

Hydrofluoric acid, at relatively high concentrations and at elevated temperatures, dissolves columbite–tantalite concentrates at a reasonable rate. The dissolution process is based on the fluorination of tantalum, niobium and other metal oxides and their conversion into soluble complex fluoride acids yielding complex fluoride ions.

Formulation of the complete formal chemical interaction between hydrofluoric acid, HF, and a columbite–tantalite concentrate with the general formula (Fe, Mn)(Ta, $Nb)_2O_6$ is not trivial. Nevertheless, some assumptions regarding the final products of the dissolution can be made based on available knowledge on the chemistry of tantalum and niobium in fluoride solutions. First, it must be taken into account that hydrofluoric acid of relatively low concentrations does not interact with oxide-type raw materials containing tantalum and niobium at a reasonable dissolution rate. Specifically, industrial processes use up to 70% HF acid at a temperature of about 70-90°C in order to achieve a reasonable production capacity of raw material decomposition. Hydrofluoric acid of such high concentration contains a significant amount of hydrofluoride ions, $HF_2^-$, which are the most chemically active component in the media. In addition, due to the high concentration of hydrofluoric acid and the high acidity of the resulting solution, hexafluorotantalate, $TaF_6^-$, and hexafluoroniobate, $NbF_6^-$, complex ions are most probably formed in the solution. Iron and manganese are converted into complex fluoride ions as well, but their final valence and coordination numbers are unclear.

In the case of a mixture of hydrofluoric and sulfuric acids, the process is more complex. It can be noted that sulfuric acid most probably interacts mainly with iron and manganese, whereas hydrofluoric acid serves mostly in the dissolution of tantalum and niobium and their conversion into soluble fluoride complexes. Nevertheless, due to the high acidity of the solution, here too the formation of hexafluorotantalate and hexafluoroniobate complex ions, $TaF_6^-$ and $NbF_6^-$, is expected. Hence, it is noted that the acid dissolution of tantalum- and niobium-containing raw material leads to the formation of hexafluoro-acids – $HTaF_6$ and $HNbF_6$.

The digestion of columbite, tantalite and other raw materials containing tantalum and niobium using both hydrofluoric acid and a mixture of hydrofluoric and sulfuric acids is widely applied in the industry. The main advantage of the method is its simplicity. The method has, nevertheless, several disadvantages that should be noted, as follows.

First, handling of highly concentrated acids, including hydrofluoric acid, especially at elevated temperatures, is very dangerous and requires use of special equipment and appropriate training of personnel. Second, the required amount of fluorine (or HF) is well above the amount needed based on the interaction stoichiometry. This results in large amounts of liquid waste, the treatment of which is very expensive.

The method is based on the complete dissolution of the raw material. Only alkali earth metals and rare earth metals that form insoluble salts do not usually provide any significant preliminary concentration of the material during decomposition. In addition, concentration of tantalum and niobium in the final solution yielding by dissolution depends on the composition of the raw material.

Another point is related to the high acidity level of the final solution, which leads to certain limitations in the subsequent technological steps. Specifically, the high acidity of the initial solution eliminates any possibility for selective extraction, i.e. sequential separation of tantalum and then of niobium. Due to the high concentration of acids, only collective extraction (of tantalum and niobium together) can be performed, at least at the first step. In addition, extraction from a highly acidic solution might cause additional contamination of the final products with antimony and other related impurities. In order to reduce the level of contaminants in the initial solution, some special additives are applied prior to the liquid–liquid extraction. For instance, some mineral acids and base metals are added to the solution at certain temperatures to cause the precipitation of antimony [455 – 457].

### 8.2.2. Decomposition by molten ammonium hydrofluoride

Another method of raw material decomposition is based on the fluorination of the raw material by the hydrofluoride method. No published data exists on hydrofluoride decomposition of columbite or tantalite concentrates. The interaction can, nevertheless, be discussed based on available information on the decomposition of lithium tantalate, $LiTaO_3$, and lithium niobate, $LiNbO_3$, using the hydrofluoride method [113, 118, 122].

The chemical interaction of lithium tantalate with molten ammonium hydrofluoride can be represented as follows:

$$LiTaO_3 + 6\,NH_4HF_2 = (NH_4)_2TaF_7 + LiF + 3\,H_2O + 4\,NH_3 + 4\,HF \qquad (131)$$

The process, as described by Equation (131), is performed at a temperature of about 200-350°C [113]. Vapors of the water formed, ammonia and hydrogen fluoride, are separated from the interaction zone and collected for reuse by condensation at appropriate temperatures in the form of ammonium fluoride, $NH_4F$, or ammonium hydrofluoride, $NH_4HF_2$.

The optimal temperature range for the fluorination process was found to be about 230-290°C. The resulting cake was leached with water. The prepared solution was separated from the precipitate by regular filtration and the separated insoluble precipitate was identified as lithium fluoride, LiF. The solution contained up to 90 g/l $Ta_2O_5$. Solution acidity was relatively low, with a typical pH = 3–4, and was suitable for the precipitation of potassium heptafluorotantalate, $K_2TaF_7$, tantalum hydroxide or further purification by liquid–liquid extraction after appropriate adjustment of the solution acidity [113].

Decomposition of lithium niobate, $LiNbO_3$, by molten ammonium hydrofluoride can be performed even at temperatures as low as 130-260°C [122]. The process also enables the separation of niobium and lithium, yielding ammonium oxyfluoroniobate and lithium fluoride. The interaction can be represented by Equation (132):

$$LiNbO_3 + 4\ NH_4HF_2 = (NH_4)_3NbOF_6 + LiF + 2\ H_2O + NH_3 + HF \qquad (132)$$

The optimal temperature range for the interaction was found to be 150-230°C. The cake resulting from the fluorination process was also successfully leached with water, dissolving ammonium oxyfluoroniobate, $(NH_4)_3NbOF_6$. The solution was separated from the precipitate of lithium fluoride. The main parameters of the solution were a niobium concentration of about 75 g/l $Nb_2O_5$, pH = 3–4.

The filtrated solution can be successfully used for the precipitation of potassium heptafluoroniobate, $K_2NbF_7$ or niobium hydroxide. In addition, the solution is suitable for further purification by liquid–liquid extraction after adjustment of its acidity [118, 122].

In both cases, the fluorination of the complex oxides of tantalum and niobium leads to the formation of the water-soluble compounds $(NH_4)_2TaF_7$ and $(NH_4)_3NbOF_6$, the insoluble lithium fluoride and the gaseous components $H_2O$, $NH_3$ and HF.

Since the fluorination enables to separate components of complex oxide compounds containing tantalum and niobium, it seems that it is applicable for

the decomposition of columbite – tantalite raw material as well. The possible interaction, based on equal concentrations of tantalum and niobium in the concentrate, can be represented by Equation (133):

$$(M)(Ta, Nb)_2O_6 + 12\,NH_4HF_2 = NH_4MF_3 + (NH_4)_2TaF_7 + \\ + (NH_4)_3NbOF_6 + 5\,H_2O + 6\,NH_3 + 8\,HF \quad (133)$$

where M = Fe or Mn.

In order to increase the efficiency of the fluorination process, the tantalum-niobium-containing raw material must be milled and well mixed with ammonium hydrofluoride. It is assumed that the process temperature can be set between 200-350°C.

In general, the process flow chart of raw material decomposition by the hydrofluoride method can be represented as shown in Fig. 117.

The separated ammonia and hydrogen fluoride can be condensed and collected in the form of $NH_4F$ or $NH_4HF_2$ according to temperature condenser.

The cake is leached with water in order to dissolve tantalum and niobium (and other related compounds) in the form of fluoride salts of ammonium. Ammonium fluoroferrate and fluoromanganate are unstable in aqueous solutions of low acidity. It is assumed that iron and manganese will form precipitates of insoluble fluorides or oxyfluorides that can be separated from the solution by filtration.

The main advantages of the method can be formulated as follows. First, hydrofluoric acid is not needed for the decomposition stage; the amount of fluorine required for the raw material decomposition can be calculated and adjusted as closely as possible to the stoichiometry of the interaction. Since the leaching of the fluorinated material is performed with water, a significant fraction of the impurities are precipitated in the form of insoluble compounds that can be separated from the solution, hence the filtrated solution is essentially purified. There is no doubt that solutions prepared in this way can be of consistent concentrations of tantalum and niobium, independent of the initial raw material composition.

The most important property of the solution is its low acidity. Such solutions can be treated by liquid–liquid extraction using both the collective and selective methods after an appropriate acidity adjustment.

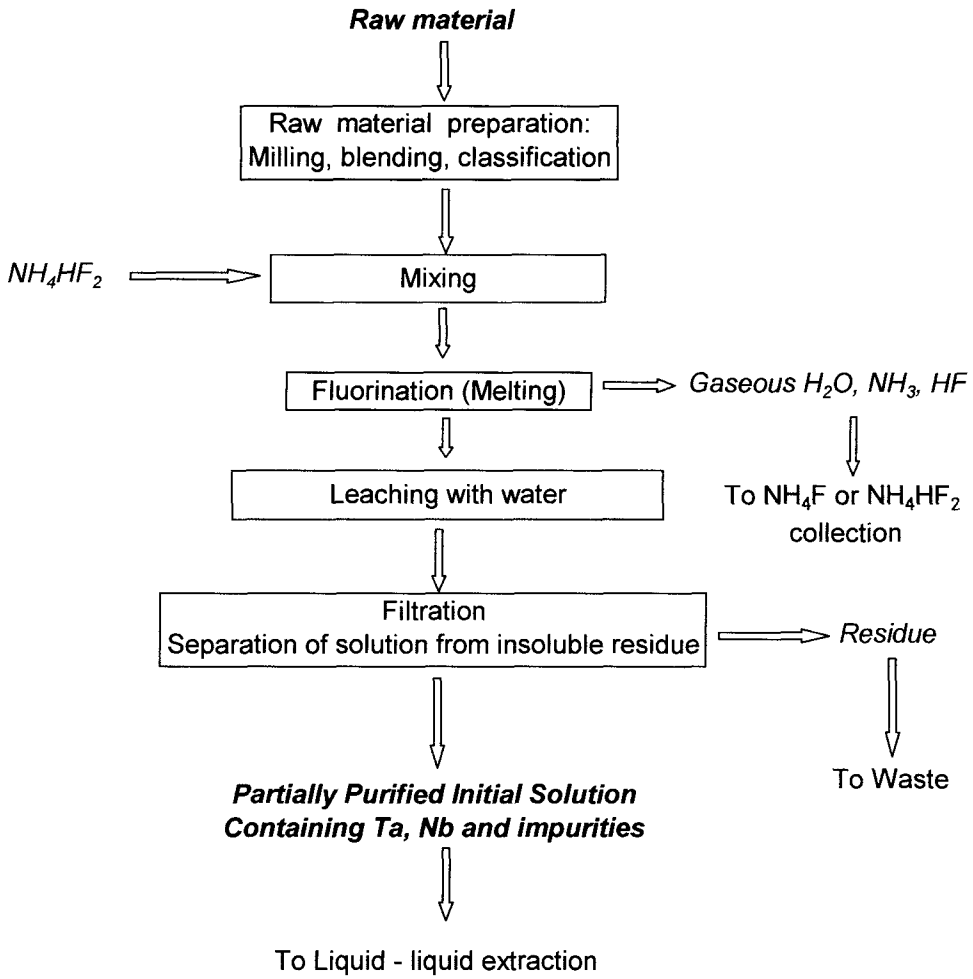


*Fig. 117. Possible flow chart of decomposition of tantalum- or niobium-containing raw material by the hydrofluoride method.*

## 8.3. Liquid–liquid extraction

### 8.3.1. General notes

The liquid–liquid extraction (solvent extraction) process was developed about 50 years ago and has found wide application in the hydrometallurgy of rare refractory and rare earth metals. Liquid–liquid extraction is used successfully for the separation of "problematic" pairs of metals such as niobium and tantalum, zirconium and hafnium, cobalt and nickel etc. Moreover, liquid–liquid extraction is the only method available for the separation of rare earth group elements to obtain individual metals.

The method is very effective for the separation of dissolved components and enables the production of high-purity products, in addition to its advantages of being a low-cost and simple method. Liquid–liquid extraction is performed continuously using simple equipment, which can be completely automated and does not require constant labor and service.

The liquid–liquid extraction process is based on the specific distribution of dissolved components between two immiscible fluids, for instance, between aqueous and organic liquids. The process refers to a mass exchange processes in which the mass transport of component (j) from phase (1) to phase (2) by means of convection or molecular diffusion acts to achieve the chemical potential (μ) equilibrium (134):

$$\mu_{(1j)} = \mu_{(2j)} \tag{134}$$

The distribution coefficient is defined as the ratio of the concentrations of the components in the two immiscible fluids at equilibrium.

The rate of extraction depends on the mass transport coefficient $(K)$, the phase contact area $(F)$ and the difference between the equilibrium concentration and the initial concentration of the dissolved component, which is usually expressed as the driving force of the process $(\Delta)$. The rate of extraction $(V)$ can be calculated as shown in Equation (135):

$$V = K \times F \times \Delta \tag{135}$$

As can be seen from Equation (135), the only effective way to increase the extraction rate is by increasing the phase contact area. This can be achieved by

intensive mixing of small drops of one phase into the other phase. The rate of extraction is a very important parameter that influences the production capacity of the process.

The subsequent step in the liquid–liquid extraction process is the separation of the two phases. This step is also of high importance because its performance impacts the quality of the separation and, ultimately, the purity of the final product.

Fig. 118 shows the principal scheme and main parameters of the extraction process for a system containing two dissolved components. The initial solution (I) is an aqueous phase (X) containing two dissolved components, A and B, with initial concentrations $X_{A,I}$ and $X_{B,I}$, respectively. The extractant (solvent) (S) is an organic phase (Y) containing no dissolved components in the initial state, prior to the interaction between the phases; thus, $Y_{A,S} = 0$ and $Y_{B,S} = 0$. The extraction process consists of mixing the aqueous and organic phases for a specified period of time, i.e. emulsification, followed by their separation. The two resultant phases following separation are also aqueous and organic.

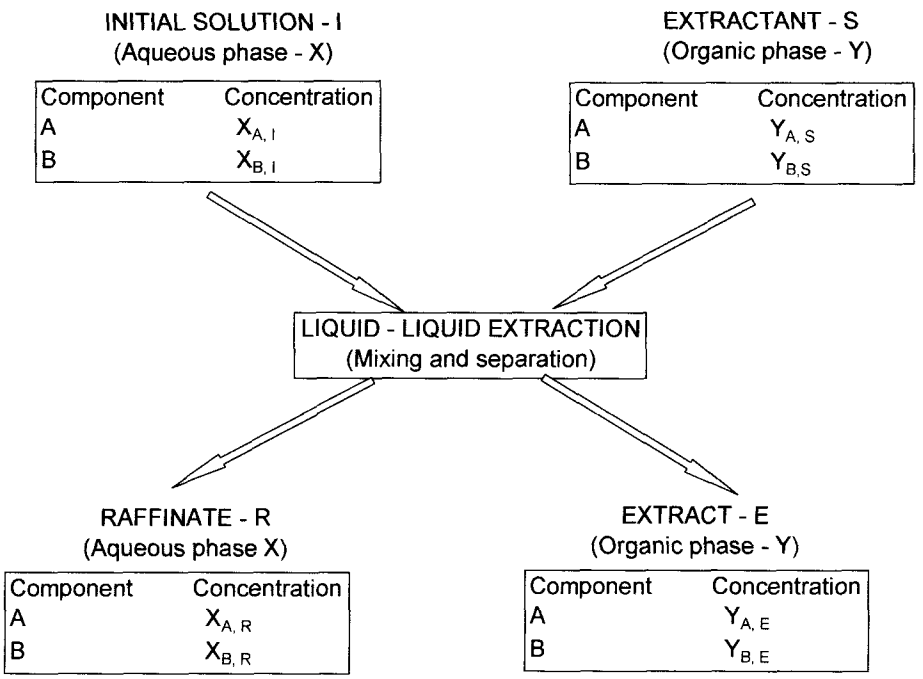


*Fig. 118. General scheme of liquid–liquid extraction of a system containing two dissolved components.*

The first phase is the raffinate (R), an aqueous phase (X) containing components A and B at concentrations $X_{A,\ R}$ and $X_{B,\ R}$, respectively. The second phase is the extract (E), an organic phase (Y) in which the concentrations of components A and B are denoted $Y_{A,E}$ and $Y_{B,E}$.

Based on the above, the main parameters of the extraction process can be represented as follows:

The extractant selectivity with respect to the components:

Component A: $Y_{A,E} >> X_{A,R}$ and $Y_{B,E} << X_{B,R} \cong X_{B,I}$

Component B: $Y_{B,E} >> X_{B,R}$ and $Y_{A,E} << X_{A,R} \cong X_{A,I}$

Distribution coefficients $\alpha_A$ and $\alpha_B$ of components A and B can be calculated as follows:

$$\alpha_A = {Y_{A,E}}/{X_{A,R}} \quad \text{and} \quad \alpha_B = {Y_{B,E}}/{X_{B,R}} \tag{136}$$

The separation coefficient, $\beta$, is calculated as the ratio between the two distribution coefficients, $\alpha_A$ and $\alpha_B$:

$$\beta = {\alpha_A}/{\alpha_B} \tag{137}$$

The process of liquid–liquid extraction, which includes the mixing of two immiscible fluids (emulsification) and separation of two immiscible fluids from the emulsion (settling), is applied in industry in one of the following three forms:

- One stage;
- Multistage cross-current;
- Multistage counter-current.

The three types of process performance can be understood using $Y_j = f(X_j)$ diagrams. One-stage extraction implies a single contact between the initial aqueous solution and the extractant. A one-stage extraction process can be

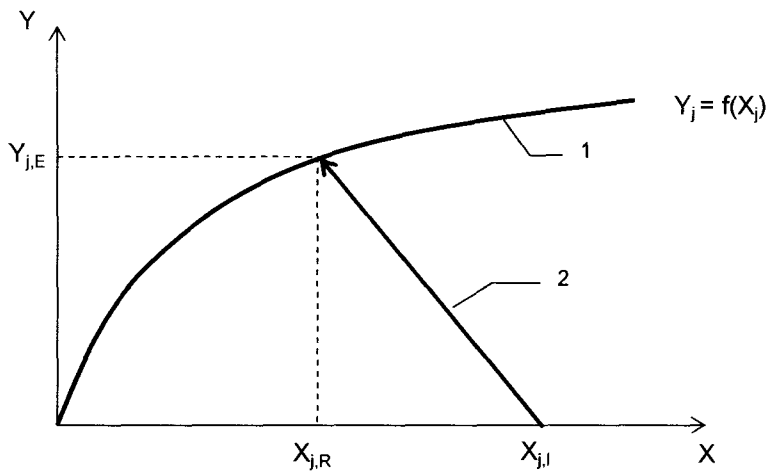


*Fig. 119. Diagram of one- stage liquid–liquid extraction*
*(1 – equilibrium curve, 2 – one-stage process)*
*X – concentration of component (j = A or B) in aqueous phase;*
*$X_{j,R}$ – concentration of j-component in raffinate (R);.*
*$X_{j,I}$ – concentration of j-component in initial solution (I);*
*Y – concentration of j-component in organic phase;*
*$Y_{j,E}$ – concentration of j-component in extract (E).*

either a batch or a continuous process. Fig. 119 shows a diagram of the one-stage extraction process.

One-stage extractions display lower efficiency compared to the other two procedures.

A multistage cross-current process consists of several heavily-connected stages, as shown in Fig. 120. The raffinate from a previous stage (stage *n*), with a concentration of $X_{j,R(n)}$, proceeds to the following stage as an initial solution, which is to be mixed with a "fresh" portion of the extractant. The extracts from each stage are collected into one common batch to be treated integrally during the next technological step. The multistage cross-current process uses a relatively large volume of extractant, thus the resulting concentration of an element in the extract collected from different stages is lower than its concentration under saturation conditions and can be defined as follows (138):

$$Y_{j,E} = \sum Y_{j,E(n)} / n \tag{138}$$

where $n$ is the number of stages performed.

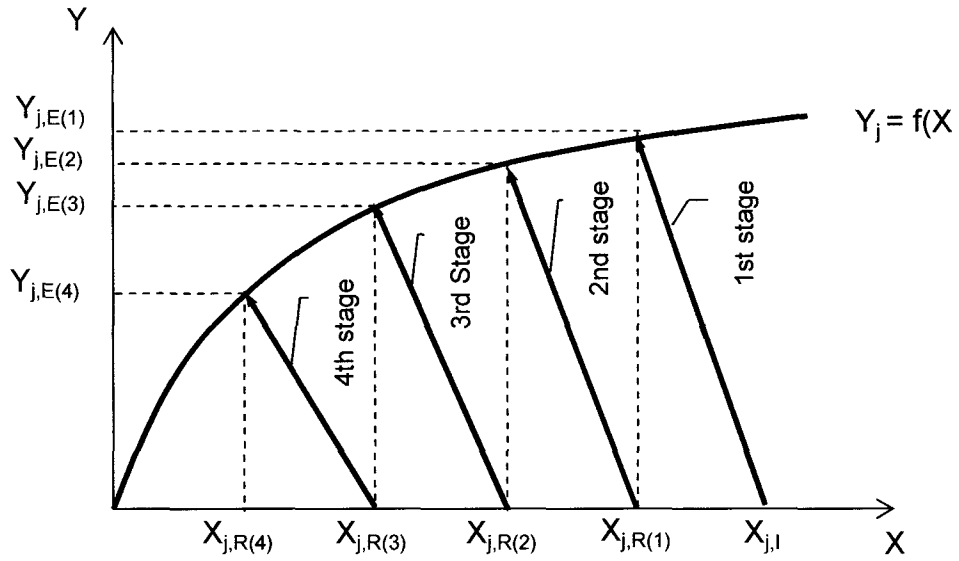


*Fig. 120. Multistage cross-current liquid–liquid extraction diagram.*

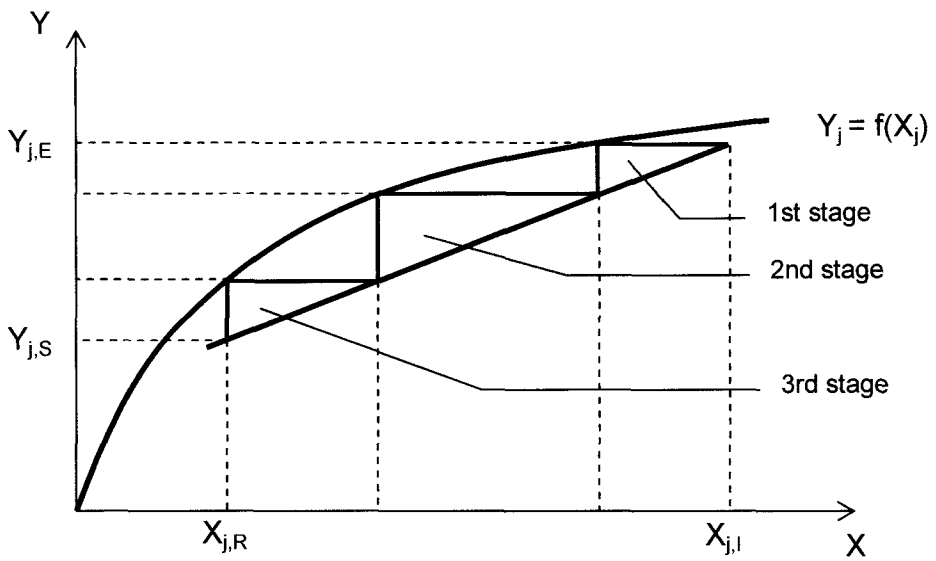


*Fig. 121. Diagram of multistage counter-current liquid–liquid extraction.*

Multistage counter-current liquid–liquid extraction is a typical continuous process. Fig. 121 shows a schematic diagram of the process. The slope of the line depends on the volumetric ratio of the aqueous and organic phases. The aqueous and organic phases move through the system as two counter currents. The raffinate from a specific extraction stage moves on to the next stage, to be mixed with a relatively "fresh" portion of the extract, i.e. extractant that was previously mixed with a low-concentration aqueous solution.

Multistage counter-current liquid–liquid extraction is characterized by a high production capacity and economic efficiency.

Mixer–settler extraction cells are frequently used in the hydrometallurgical processing of tantalum and niobium compounds. The overall process usually consists of three steps. The first step aims to extract the components into the extract and leave the impurities in the raffinate. This step can be referred to as the extraction step. In the second step, the extract is washed using an appropriate aqueous solution to obtain a pure extract containing only the targeted component. This step can be referred to as the washing step. The objective of the third step is to obtain a pure aqueous solution containing the targeted component by striping the component from the extract into an appropriate aqueous phase. This step can be referred to as the re-extraction or stripping step. The organic phase that results from the stripping stage usually contains a very low concentration of the targeted component and is reused as an extractant in the first extraction step. Fig. 122 shows the general scheme of the overall process.

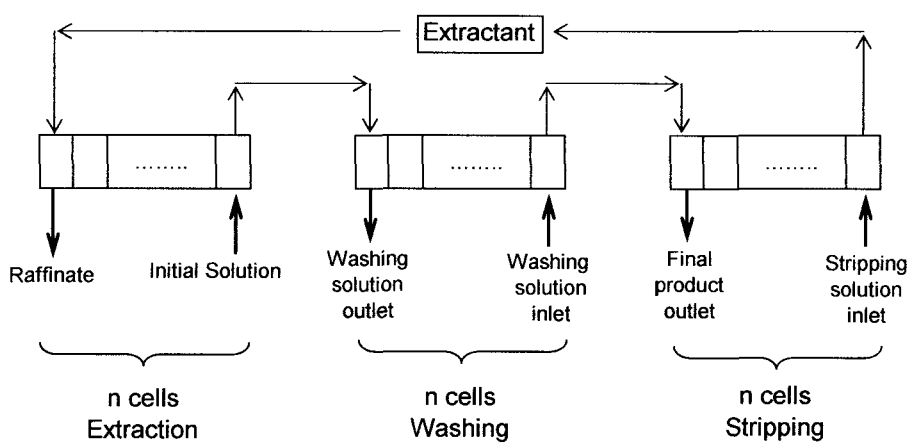


*Fig.122. General scheme of liquid–liquid extraction process using the multistage counter-current method. The three main steps are: extraction, washing and stripping.*

Each cell in the extraction system presented in Fig. 122 is called a mixer–settler extractor and is made up of two parts. The role of the first part, the mixer, is to emulsify the incoming aqueous and organic phases and to transfer the emulsion to the second part of the extractor–settler cell. The purpose of the settler is to stratify the phases and enable the separation of the two liquids.

Fig. 123 shows the typical construction of a mixer–settler extractor. The main parameters usually required for the design of an extractor are maximum output, total holding capacity, organic reagent capacity, mixer capacity, phase contact time, settler surface area and specific settler output.

The number of cells required for each step of the overall extraction process - extraction, washing and stripping - is determined empirically.

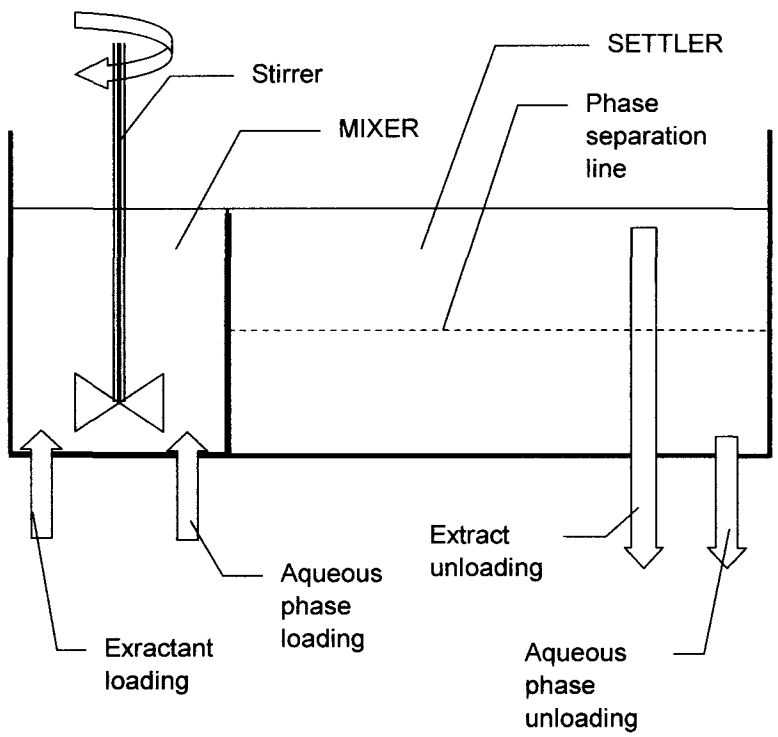


*Fig. 123. Schematic structure of a mixer–settler extraction cell.*

## 8.3.2. Mechanism of tantalum and niobium extraction

As was discussed in Chapter 4, tantalum and niobium dissolve in fluorine-containing solutions in the form of complex fluoride ions of two types, namely $TaF_7^{2-}/TaF_6^-$ and $NbOF_5^{2-}/NbF_6^-$ [61, 155, 171, 291]. The equilibrium between the complexes depends on the acidity of the solution and can be represented schematically as shown in Equations (139) and (140) for tantalum and niobium, respectively:

$$TaF_7^{2-} + HF = TaF_6^- + HF_2^- \quad (139)$$

$$NbOF_5^{2-} + 3\,HF = NbF_6^- + HF_2^- + H_2O \quad (140)$$

The complexes can be considered to be Lewis acids, the acidity of which increases with the reduction in the metal's coordination number or when moving along the complex sequence from $TaF_7^{2-}$ or $NbOF_5^{2-}$ to $TaF_6^-$ or $NbF_6^-$. The reduction in coordination number also leads to a reduction in the charge on the complex.

The enhanced acidity of the solution causes the equilibriums in Equations (139) and (140) to shift to the right, yielding mostly complexes with lower charges, namely $TaF_6^-$ and $NbF_6^-$ [291], which are, for the most part, extracted into the organic phase. At a lower acidity of the solution, Equations (139) and (140) shift to the left, leading to the formation of mostly low-acidity complexes, namely $TaF_7^{2-}$ and $NbOF_5^{2-}$. Such complexes are more stable in aqueous solutions and strip into the aqueous phase from the organic phase.

The difference in behavior between tantalum and niobium complexes is related to the difference in their molecular weights. Niobium complexes have lower molecular weights and are stronger Lewis acids compared to the corresponding tantalum-containing complexes. The high Lewis acidity of the niobium complexes requires that the solution acidity be respectively higher in order to be converted into $NbF_6^-$ complexes.

This particular difference in the Lewis acidity of tantalum and niobium complexes provides the possibility of an effective separation between the elements using liquid–liquid extraction. It is obvious that tantalum will extract into the organic phase at a lower acidity of the aqueous solution, whereas niobium will require a higher level of acidity in order to be extracted. The stripping of the elements from the organic phase into the aqueous phase will take place in reverse order.

A possible mechanism of the extraction of tantalum and niobium using different solvents, and their stripping into the aqueous phase, was reviewed comprehensively by Babkin, Maiorov and Nikolaev [458, 459].

Nikolaev et al. [460] investigated the mechanism of tantalum and niobium extraction from solutions containing hydrofluoric and sulfuric acids using oxygen-containing extractants.. Based on measurements performed using $^{19}F$ and $^{93}Nb$ NMR and IR spectroscopy methods [460], a hydrate–solvate mechanism was proposed. According to this mechanism, the extraction occurs in the form of $TaF_6^-$ and $NbF_6^-$ complexes. No oxyfluoride compounds of either niobium or tantalum were detected during the investigation of the extraction process [460].

Kuterev, Stoyanov, Bagreev and Zolotov [461] reported on the investigation, using IR spectroscopy, of the composition of niobium and tantalum complexes extracted by amines from fluoride solutions. It was shown that in solutions that contain hydrofluoric acid in concentrations ranging from 1M to 12M, both niobium and tantalum were extracted in the form of $NbF_6^-$ and $TaF_6^-$.

Using $^{19}F$ NMR and IR spectroscopy, Golubkov, Travkin, Il'in, Karamushko and Kovalev [462] investigated the extraction forms of tantalum and niobium when aliphatic alcohols were used. Three groups of signals were observed in $^{19}F$ NMR spectra of extracts containing tantalum, two of which correspond to the presence of $TaF_6^-$ ions and $TaF_5L$, where L = alkoxil group. A relatively weak signal at a strong field range was attributed to the co-extraction of hydrofluoric acid. Nevertheless, it is noted that the coincidental observation of $TaF_6^-$ and HF indicates that no exchange interaction takes place between fluorine ions of the complex ion and hydrogen fluoride.

The spectrum of the niobium-containing extract was concluded to be related to the presence of $NbF_6^-$ and $NbF_5OR^-$ ions [462]. Investigation of the IR absorption spectra confirms the presence of $TaF_6^-$ and $NbF_6^-$ complex ions in the tantalum and niobium extracts, respectively.

Based on recent [462] and previous measurements [463, 464], it was concluded in [462] that the extraction of tantalum and niobium from solutions containing hydrofluoric and sulfuric acids, using aliphatic alcohols, occurs in the form of the complex acids $HTaF_6$ or $HNbF_6$.

The stripping of tantalum and niobium from the organic phase into aqueous media occurs in solutions with low acidity levels, leading to the formation of $TaF_7^{2-}$ and $NbOF_5^{2-}$, which have a lower charge and weaker Lewis acidity.

Extraction and stripping (re-extraction) of tantalum and niobium complex acids are shown schematically in Fig. 124.

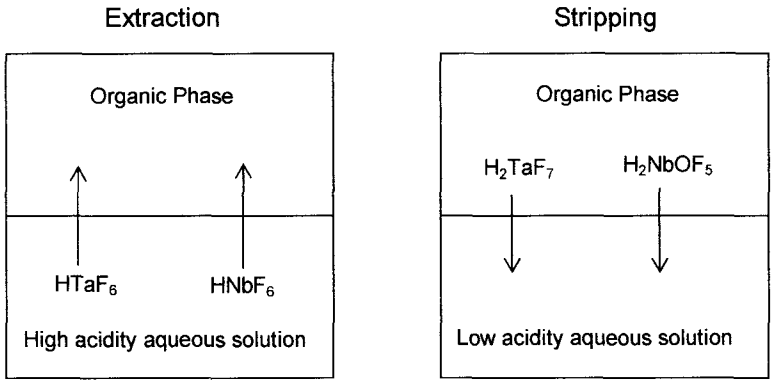


*Fig. 124. Distribution of complex acids between organic and aqueous phases during extraction and stripping of tantalum and niobium.*

## 8.3.3. Extraction schemes

Two main schemes exist for the separation and purification of tantalum and niobium using liquid–liquid extraction. The first is based on the collective extraction of tantalum and niobium from an initial solution into an organic phase so as to separate them from impurities that remain in the aqueous media, the raffinate. The separation of tantalum and niobium is subsequently performed by fractional stripping into two different aqueous solutions. In this case, stripping of niobium is performed using relatively weak acids prior to the stripping of tantalum. Fig. 125 presents a flow chart of the process.

The second method is based on selective extraction that consists of extraction into two different organic solutions. In the first step, tantalum is extracted into an organic phase. In the second step of the procedure, niobium is extracted into a separate portion of the extractant. Fig. 126 presents a flow chart of the process based on the selective extraction scheme.

In both cases, the extraction process includes washing (scrubbing) of the extract, a stage that is not shown separately. The organic phase that results from the stripping process is returned to the beginning of the extraction process for reuse as an extractant.

The second process of selective extraction is more effective and leads to better separation of tantalum and niobium and to more effective purification. Its performance, however, requires the initial solution to be of relatively low acidity.

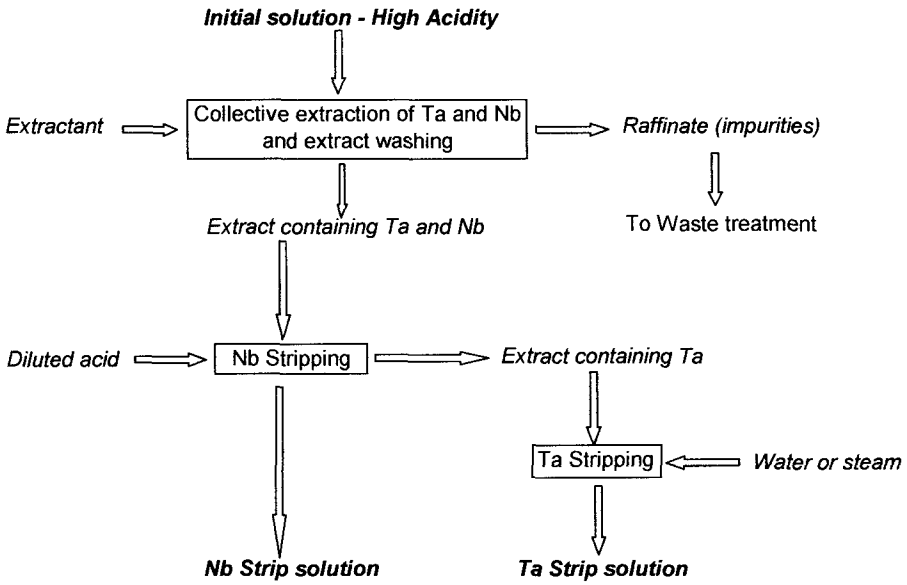


*Fig. 125 Collective extraction.*

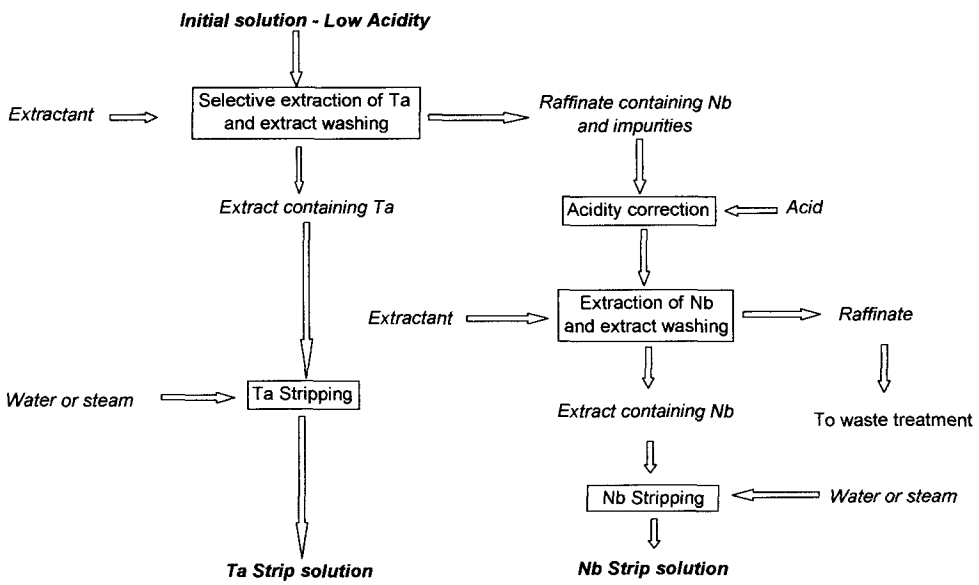


*Fig. 126. Selective extraction*

Nevertheless, current processes of raw material decomposition that are based on digestion of the material by highly concentrated hydrofluoric and sulfuric acids yield highly acidic solutions.

The initial solution is characterized by a high level of acidity that excludes the possibility of selective extraction. Such solutions can be treated only using the collective extraction procedure.

Eckert [32] reported on the modification of the traditional scheme so as to enable selective extraction of tantalum. Fig. 127 shows the flow chart of the process. The process begins with the traditional collective extraction of tantalum and niobium into an organic phase, from an initial solution of high acidity. To ensure effective separation and purification of the products, collective stripping of tantalum and niobium is performed using steam. This stage enables the separation of tantalum and niobium from the impurities. In addition, the resulting strip solution, which contains tantalum and niobium, has a relatively low level of acidity, which ensures the effective selective extraction of tantalum in the following step.

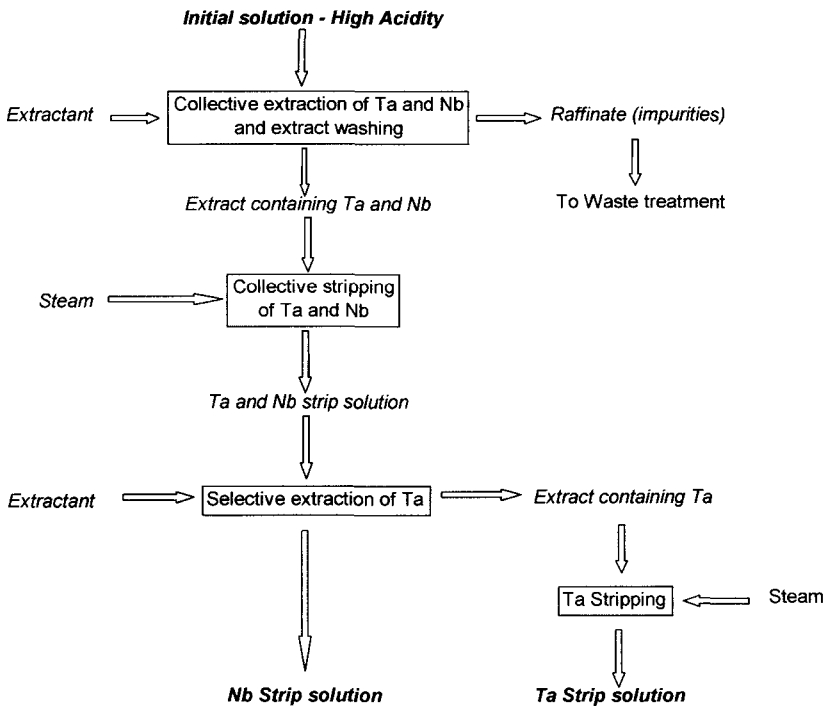


*Fig. 127. Modified scheme of collective extraction, including selective extraction of tantalum.*

The raffinate from the selective extraction process contains mostly niobium. The tantalum extract is treated by steam stripping to obtain a tantalum strip solution. The method results in the effective separation and relatively high concentration of tantalum and niobium in the respective strip solutions.

Another way of applying the selective extraction method directly on the initial solution is to produce a solution of low acidity. This can be achieved by using the hydrofluoride method for fluorination and decomposition of raw material. As was discussed in Paragraph 8.2.2, the raw material is fluorinated by molten ammonium hydrofluoride yielding soluble complex fluorides of ammonium and tantalum or niobium. The cake obtained following fluorination is dissolved in water, leading to a solution of low initial acidity that is related for the most part to the partial hydrolysis of complex fluoride compounds. The acidity of the solution is first adjusted to ensure selective tantalum extraction. In the second step, the acidity of the raffinate is increased to provide the necessary conditions for niobium extraction.

## 8.3.4. Frequently used extractants

The extraction of tantalum and niobium from solutions containing hydrofluoric and sulfuric acids can be performed using a wide variety of extractants, including organic acids and organic salts, basic dyes, amines and quaternary ammonium salts, neutral oxygen-containing solvents including ethers, ketones, derivatives of pyrazole, phosphoric acid, alcohols and so on [458]. Some of the extractants listed above have no application in the hydrometallurgy of tantalum and niobium but are used for analytical purposes.

Three extractants are currently used commercially in the production of tantalum and niobium production: methyl iso-butyl ketone – $C_6H_{12}O$ (MIBK), tributyl phosphate – $C_{12}H_{27}O_4P$ (TBP) and cyclohexanone - $C_6H_{10}O$ [32, 458, 459, 462]. MIBK is most frequently used as an extractant due to its low density, low viscosity and several other properties that enable to obtain high-purity products. The main disadvantages of all three materials are their relatively high solubility in aqueous phases as well as the high solubility of aqueous solutions in the organic compounds themselves. In particular, MIBK can exist in an aqueous raffinate in concentrations of up to 1.7% wt. This leads to the need for complicated and expensive systems for the recovery of the extractant [465]. In addition, MIBK is a highly volatile compound with a low flash point. These properties render the use of this extractant dangerous and special handling conditions must be observed. Cyclohexanone has a higher

solubility in aqueous solutions compared to MIBK and is also characterized by high volatility and other flammable properties.

TBP is less soluble and less dangerous but is more problematic due to its relatively high density. This can lead to poor stratification, especially during the stripping process. Hence, insufficient separation of the strip solution from the extractant can lead to additional contamination, by phosphorous, of the final products [458, 462].

Alcohols with a $C_8 - C_{12}$ chain length, characterized by low solubility in aqueous media, may have a particular commercial potential as perspective extractants for tantalum and niobium hydrometallurgical processing. Particular emphasis has been placed recently on the investigation of tantalum and niobium extraction using octanol ($C_8H_{18}O$) in the forms of 1-octanol and 2-octanol [462, 466 – 473].

Table 61 presents some important and useful properties of MIBK, TBP and 2–Octanol [72, 458, 474 – 476] .

*Table 61. Some properties of MIBK, TBP and 2–octanol.*

| Properties | Methyl iso-butyl ketone (MIBK) | Tributyl phosphate (TBP) | 2-octanol |
|---|---|---|---|
| Alternative names | Isopropylaceton; 4-Methyl-1-2-pentanone; 2-pentanone,4-methyl; "Hexone"; MIBK; MIK. | Phosphoric acid tributyl ester; Celluphos – 4 ®. | Capryl alcohol; sec-Caprylic alcohol; Hexyl methylcarbinol; Methylhexyl carbinol; Secondary n-octyl alcohol. |
| CAS # | 108-10-1 | 126-73-8 | 123-96-6 |
| Formula | $C_6H_{12}O$ or $CH_3CO{\cdot}CH_2CH(CH_3)_2$ | $C_{12}H_{27}O_4P$ or $[CH_3(CH_2)_3O]_3PO$ | $C_8H_{18}O$ or $CH_3CH(OH)(CH_2)_5CH_3$ |
| Molecular weight | 100.16 | 266.32 | 130.23 |
| Density at 25°C | 0.7965 g/cm$^3$ | 0.9727 g/cm$^3$ | 0.8188 g/cm$^3$ |

*Table 61. Some properties of MIBK, TBP and 2–octanol (cont.)*

| Properties | Methyl *iso*-butyl ketone (MIBK) | Tributyl phosphate (TBP) | 2-octanol |
|---|---|---|---|
| Melting point, °C | -84 | -80 | -31.6 |
| Surface tension, mN/m | 23.64 at 20°C | 27.2 at 25°C | 27.10 at 25°C<br>25.12 at 50°C |
| Boiling point, °C | 116.5 | 289 (decomposition) | 180 |
| Refractive index | 1.3962 | 1.4224 | 1.4203 |
| Vapor pressure | 1 kPa at 9°C<br>10 kPa at 51.5°C<br>100 kPa at 116.1°C | 9 Pa at 25°C<br>133 Pa at 100°C<br>973 Pa at 150°C | 1 kPa at 69.9°C<br>10 kPa at 112.5°C<br>100 kPa at 179.4°C |
| Viscosity | 0.585 m Pa s at 20°C | 3.3 - 3.7 m Pa s at 25°C | 7.3 m Pa s at 25°C |
| Flash point | 18°C | 146°C | 60 – 88°C |
| Solubility in water | 2.26 % wt at 10°C<br>1.63 % wt at 30°C<br>1.39% wt at 50°C | 0.4 % wt at 20°C | 0.096 % wt at 25°C |
| Solubility of water in extractant | ~2 % wt at 25°C<br>2.2 % wt at 30°C | ~6% wt at 25°C | very low |

## 8.3.5. Process performance

Details of the tantalum and niobium extraction process depend on the type of raw material used, decomposition method, initial solution composition, extractant type, equipment specifications, type of final products and desired purity. Therefore, process parameters are usually defined individually for each specific case. This may be the reason for the existence of the wide variety of publications devoted to the liquid–liquid extraction of tantalum and niobium. Nevertheless, some common features of the process should be emphasized.

First, it is important to note that complete fluorination of the elements ensures an effective separation process. Particularly, Maiorov and Nikolaev [477] developed and reported on the conversion of tantalum, niobium and titanium sulfates and chlorides into their respective fluorides. It was shown that such conversion leads to significant improvement in/enhancement of the separation of the elements.

Concentration of free HF in the initial solution is of high importance and can affect the separation efficiency. Prasad, Ranganathan and Sastri [478] recommended the performance of selective extraction using TBP from an initial solution that contained no free HF in order to achieve the effective separation and purification of tantalum and niobium. Kim Yong Hyon, Li Gwi Song and Choe Chag Bong [479] investigated the effect of the concentrations of tantalum, niobium, hydrofluoric and sulfuric acids on the rate of extraction using MIBK. It was shown that the separation coefficient depends solely on the HF concentration. In addition, the separation coefficient increases with the decrease in HF concentration. Maiorov and Nikolaev [480] reported recently that the most efficient separation and purification of tantalum and niobium was observed for solutions that contained only a minimal concentration of HF.

It is recommended that the concentration of sulfuric acid in the initial solution be kept at 2–4 mol per liter for the extraction of tantalum, whereas for the extraction of niobium, the concentration of sulfuric acid must be increased to a minimum of 6 mol per liter [458, 481]. In some cases, the presence, in the initial solution, of titanium in the form of fluorotitanic acid ensures the successful and selective extraction and purification of tantalum and niobium with no addition of any other mineral acid [482].

The composition of solutions that are used for washing and stripping of extracts is also different and is adjusted for each specific case; however, some common conditions can be noted. It is recommended that the extract obtained following collective extraction, which contains both tantalum and niobium, be washed (scrubbed) using sulfuric acid solutions that contain at least 6 mol per liter of $H_2SO_4$. Collective stripping of the elements, on the other hand, can be

successfully performed using water or steam. The extracts obtained from the selective extraction process are washed and stripped using an altogether different type of solution. Thus, tantalum extract is usually washed using a solution of relatively low acidity that typically contains sulfuric acid at about 2 mol per liter, whereas niobium-containing extract requires the application of solutions with sulfuric acid concentrations equal to or greater than 6 mol per liter. Stripping is typically performed using water, steam or solutions containing low concentrations of acids or salts [32, 458, 467].

The extraction technology is applied for scrap recycling of tantalum and niobium and for the treatment of related materials. Recovery of tantalum and niobium from secondary material, such as Sn slag, Ti slag, W slag, catalyst wastes, used cemented carbide and used tantalum capacitors was reviewed by Dai, Zhong, Li and Li [483].

Uchino and Azuma [484] proposed a method for the recovery of tantalum or niobium from carbide–based raw materials. The process includes crushing of the raw material, roasting it in air while providing good contact between the crushed material and the air, dissolution in HF or in a mixture of HF and some other mineral acid, and subsequent recovery of tantalum and niobium by known methods. Another process, proposed by Azuma and Kinoshita [485] for recycling of the material, is based on treatment using strong basics. Raw material containing niobium, tantalum and fluorine with impurities is treated with a strong alkali solution to obtain a slurry. The slurry is washed with water, followed by filtration. The residue obtained is washed with a mineral acid other than HF, and the acid is then filtered off. The processed raw material can be further treated to produce tantalum or niobium oxides. The oxides obtained by the above method are suitable for the production of tantalum and niobium carbides.

The method for the recovery of tantalum and niobium was developed for use on secondary raw materials in the form of oil-contaminated sludge. Uchino and Azuma [486] suggested using solid–liquid separation of oil from the slurry prior to the recovery of tantalum and niobium from the raw material.

A method for the purification or recycling of tantalum-containing salts was also proposed. According to reports by Eberts [487], potassium fluorotantalate, $K_2TaF_7$, is dissolved in sulfuric acid, followed by extraction with MIBK and neutralization of the extract using an ammonium solution. Zakharov, Korovin, Kluchnikov and Apraksin [488] noted that tantalum is not extracted from the solution of $K_2TaF_7$ using TBP. Nevertheless, they found that the addition of magnesium and lithium in the form of soluble salts – chlorides, nitrates and sulfates - significantly enhances tantalum extraction efficiency.

## 8.3.6. Extraction of tantalum and niobium with 2-octanol – definition of the process parameters

Different isomers of octanol seem to be very promising as extractants for the separation and purification of tantalum and niobium using initial solutions containing HF and $H_2SO_4$ [466, 467]. Maiorov and Nikolaev [467] reported on the investigation of the extraction of tantalum and niobium using 1-octanol. The process displays good results and a definite application potential of the extractant for the production of pure tantalum and niobium from tantalite, columbite and loparite. The extraction equilibrium can be achieved in less than 5 minutes. The process consists of the collective extraction of tantalum and niobium (5-7 extraction stages), scrubbing (6-8 extraction stages), niobium stripping (5-7 extraction stages), and tantalum stripping (4-6 extraction stages). Near complete separation of tantalum and niobium is obtained, as well as the extensive purification, i.e. removal of impurities.

Comprehensive comparative investigation of the main extraction parameters shows that 2-octanol is more selective than 1-octanol, with $\beta_{Ta/Nb}$ equal to 133.6 for 2-octanal as compared with 70.9 for 1-octanol [462]. It was also determined that 2-octanol has a separation coefficient of 238 compared to 97 for 1-octanol. 2-octanol is also more selective than other aliphatic alcohols.

Definition and verification of the process parameters when making the transition from laboratory measurements to a laboratory extraction system and ultimately to a pilot extraction plant, are reported in [471 – 473] and will be discussed below as an example of the process development.

An initial solution was prepared by the hydrofluoride method, i.e. melting of a mixture of ammonium hydrofluoride and tantalite, followed by the digestion of soluble components with water and separation of the solution by filtration. The prepared initial solution contained no free HF or any other acid, and had a pH $\approx$ 3. In order to obtain an optimal acidity level, sulfuric acid was added to the solution. Concentrations of $Ta_2O_5$ (50-60 g/l) and $Nb_2O_5$ (~30 g/l) were kept approximately constant during the preparation of the solutions. Extraction was performed using a polypropylene beaker and a magnetic stirrer.

Fig. 128 shows the extraction of tantalum and niobium versus $H_2SO_4$ concentration. It is evident that the optimal $H_2SO_4$ concentration for tantalum extraction is about 2.5–3.5M. It can also be seen that niobium begins to move into the organic phase at an $H_2SO_4$ concentration exceeding 5M. 2-octanol provides both good separation and good purification of the elements. Fig. 129 shows the extraction of some impurities compared with niobium extraction.

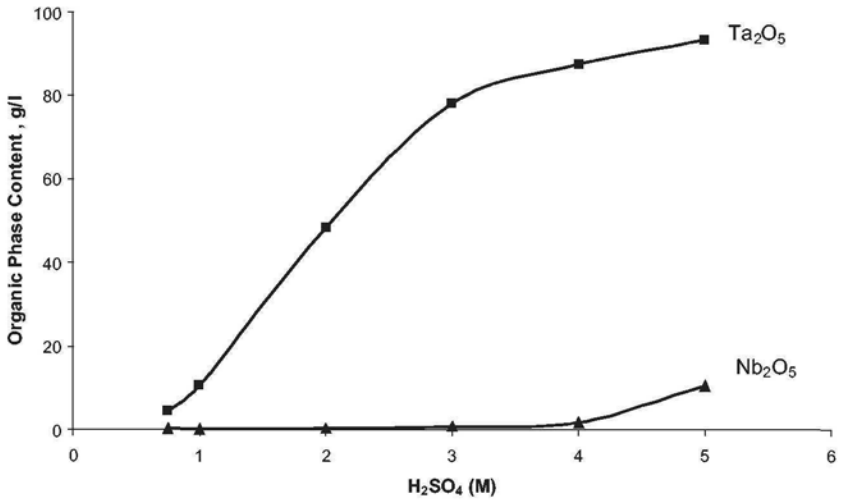


*Fig. 128. Extraction of tantalum and niobium versus $H_2SO_4$ concentration. Reproduced from [473], A. Agulyansky, L. Agulyansky, V. F. Travkin, Chemical Engineering and Processing 43 (2004) 1231, Copyright 2004, with permission of Elsevier.*

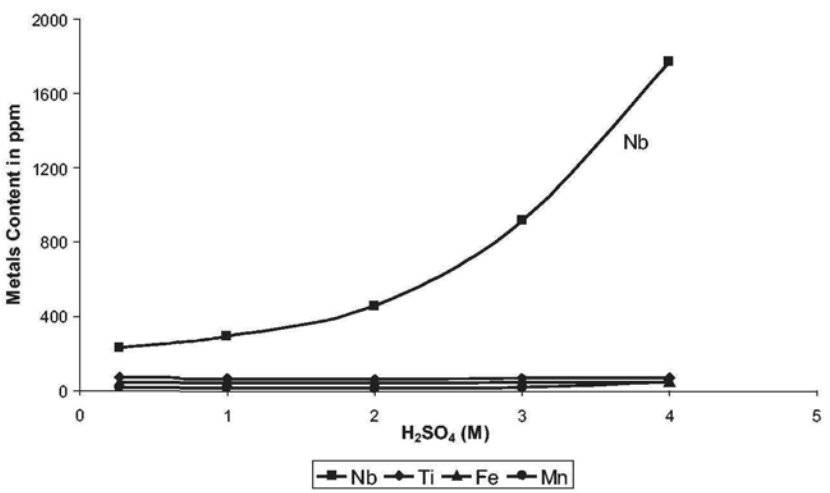


*Fig. 129. Extraction of niobium and impurities versus $H_2SO_4$ concentration. Reproduced from [473], A. Agulyansky, L. Agulyansky, V. F. Travkin, Chemical Engineering and Processing 43 (2004) 1231, Copyright 2004, with permission of Elsevier.*

The second step in the process is the definition of the optimal mixing time and solution temperature. It was found that for both niobium and tantalum, the mixing time for extraction and stripping must not exceed one minute. No concentration changes were observed in the temperature range of 25-50°C.

The next step is related to the analysis of extraction and stripping isotherms intended to define the capacity of the process and verify the required number of extraction steps. Fig. 130 presents the extraction and stripping isotherms for tantalum at 25°C, using 2-octanol as an extractant and water as a strip solution. Curve 1 clearly shows that the organic phase capacity, in terms of $Ta_2O_5$ content, is about 130 g/l. The linearity and the slope of the stripping isotherm indicate two important issues. First, even an infinite number of steps will not achieve complete stripping of tantalum into water; and second, a counter-current mixer-settler extraction system must include more stripping steps than extraction steps.

A small extraction system, consisting of a total of 18 cells, was used for laboratory evaluation of the process. The volumes of the mixer and settler were 10 ml and 30 ml, respectively. Production capacity of the system was 200-300 ml per hour. The cells were divided among the functions as follows: extraction – 8 cells, washing – 3 cells, stripping – 8 cells. Several experiments were performed using the laboratory system.

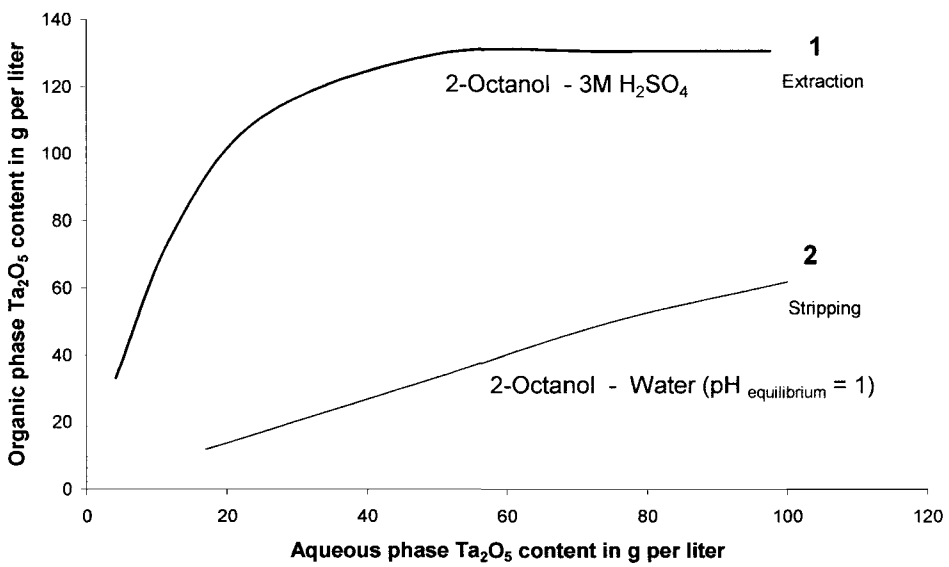


*Fig. 130 Isotherms of tantalum extraction (curve 1) and stripping (curve 2) at 25°C (after Agulyansky et al., [473]).*

Conditions for one of the experiments were:
Initial solution: $Ta_2O_5$ – 101 g/l; $H_2SO_4$ – 3 M;
Volume ratios – $V_{org.}$:$V_{aqu.}$ extraction – 1.2:1; washing – 20:1; stripping – 2.5:1.
Fig. 131 shows the distribution of tantalum content among the different cells for the organic and aqueous phases.

Based on the laboratory extractor experiments it was concluded that five to six cells are sufficient for successful extraction at $V_{org}$:$V_{aqu}$ = 1.2:1 and that washing and stripping can be performed at $V_{org.}$: $V_{aqu}$ = (20-5):1 and 3:1, respectively.

The chosen conditions were applied in the pilot production experiments. The pilot extraction system included a total of 18 cells divided as follows: extraction – 6 cells, washing – 5 cells and stripping – 7 cells. The various cell parameters were: Mixer volume 2 liters with 50-mm diameter stirrer, 800–1000 rpm; Settler volume 18 liters. Total production capacity was 110–170 liters per hour (50–80 liters per hour for aqueous phase). The initial solution, containing about 105–145 g of $Ta_2O_5$ per liter, was prepared by digestion of tantalum scrap using a solution of ammonium hydrofluoride and sulfuric acid at concentrations that ensured minimum free fluorine content and $H_2SO_4$ 3M in excess for the extraction of tantalum. Volume ratios, $V_{org}$:$V_{aqu}$ were chosen to be 1.2:1, 7:1 and 3:1 for extraction, washing and stripping, respectively.

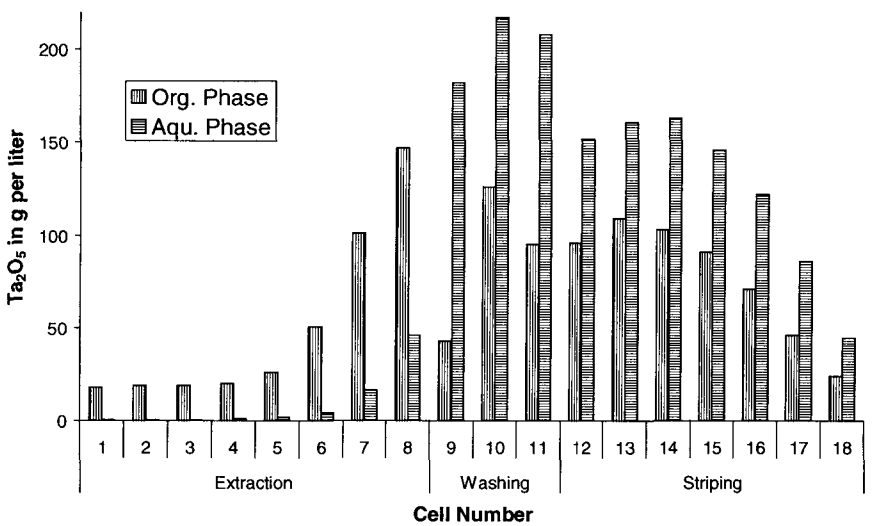


*Fig. 131. Distribution of tantalum between cells of laboratory extractor, for organic and aqueous phases. Reproduced from [473], A. Agulyansky, L. Agulyansky, V. F. Travkin, Chemical Engineering and Processing 43 (2004) 1231, Copyright 2004, with permission of Elsevier.*

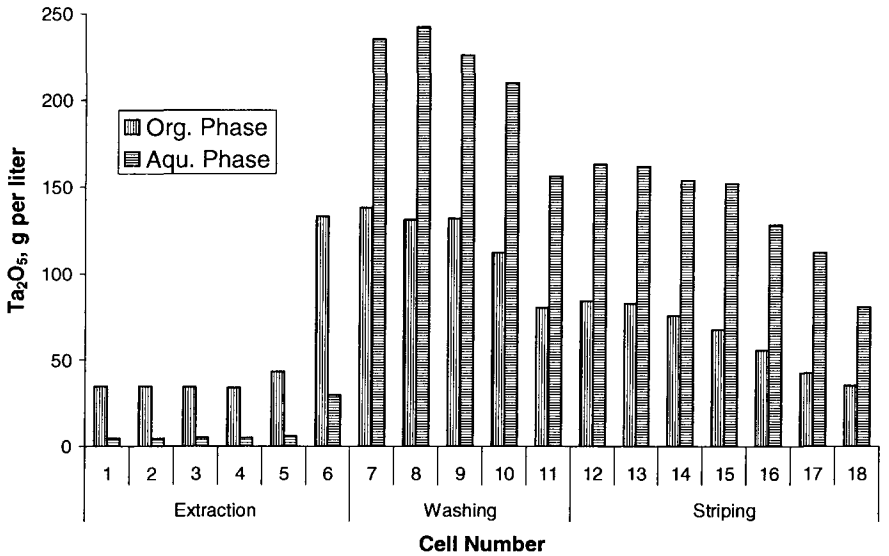


*Fig. 132. Distribution of tantalum oxide between cells of pilot extraction system, for organic and aqueous phases. Reproduced from [473], A. Agulyansky, L. Agulyansky, V. F. Travkin, Chemical Engineering and Processing 43 (2004) 1231, Copyright 2004, with permission of Elsevier.*

Fig. 132 shows the content distribution of tantalum oxide among the cells, for the organic and aqueous phases.

The tantalum strip solution was used for the preparation, by precipitation and thermal treatment, of tantalum oxide. The product was determined to be of high purity grade. Table 62 presents typical analysis results.

The optimal parameters of tantalum extraction with 2–octanol are as follows:

- Extraction: Initial solution contains about 300 g/l sulfuric acid; number of cells – 6, $V_{org}$:$V_{aqu}$ = (1-1.2):1;
- Washing: Washing solution – water; number of cells – 5-6; $V_{org}$:$V_{aqu}$ = (5-10):1;
- Stripping: Stripping solution – water; number of cells 6-7; $V_{org}$:$V_{aqu}$ = 3:1.

The raffinate obtained following selective extraction of tantalum is used as the initial solution for niobium extraction. The acidity of the initial solution is increased by adding sulfuric acid up to a concentration of at least 6M. It was

found that the mixing time and temperature influence the extraction of both niobium and tantalum. Fig. 133 presents an isotherm of niobium extraction for an $H_2SO_4$ 6M solution. The capacity of the extractant, in terms of $Nb_2O_5$, is about 130–134 g/l. Analysis of the stripping process indicated that stripping by water leads to near complete results, and a large number of steps is not required.

Optimal parameters for the extraction, washing and stripping of niobium were determined to be: number of stages for all three processes - 4, volumetric ratios $V_{org}$:$V_{aqu}$ are 1:1, 20:1 and 8:1, respectively. Additional fine purification of the extractant was recommended by stripping of tantalum and niobium remainders using a ~0.5% wt. ammonia solution. This additional stripping leads to final concentrations of both tantalum and niobium in the extractant that are < 0.001 g/l. Table 62 shows the purity of niobium oxide prepared by the described method.

Table 63 presents the complete process parameters, including tantalum and niobium extraction. Fig. 134 gives the flow chart of the complete process.

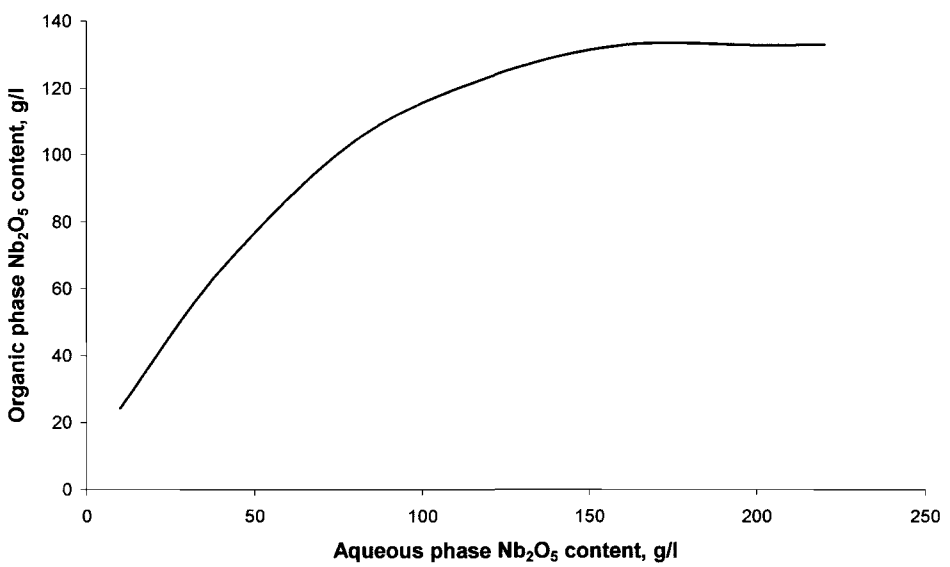


*Fig. 133. Isotherm of distribution of niobium between organic and aqueous phases during extraction by 2-octanol from initial solution containing 6 M $H_2SO_4$ (after Agulyansky et al., [473]).*

*Table 62. Typical purity of tantalum and niobium oxides prepared from strip solutions after extraction with 2–octanol. Impurity level is given in ppm.*

| Elements | Tantalum oxide | Niobium oxide |
|---|---|---|
| Total Purity, % | 99.995 | 99.986 |
| Nb (Ta) | <10 | <10 |
| Fe | <1 | <1 |
| Ca | <10 | <15 |
| Si | <10 | <10 |
| Al | <1 | <10 |
| Na | <15 | <15 |
| Mg | <7 | <10 |
| P | <10 | <10 |
| W | <10 | <10 |
| Ti | <2 | <10 |
| Co | <3 | <3 |

*Table 63. Optimal parameters of tantalum and niobium extraction with 2-octanol.*

| Process | Aqueous solution - description | Number of stages | $V_{org.}$: $V_{aqu}$ |
|---|---|---|---|
| Ta extraction | Initial solution, 3 M $H_2SO_4$ | 6 | (1.2-1):1 |
| Ta extract washing | Water | 5 - 6 | (10-5):1 |
| Ta stripping | Water | 6 - 7 | 3:1 |
| Nb extraction | Raffinate after Ta extraction, 6 M $H_2SO_4$ | 4 | 1:1 |
| Nb extract washing | Water | 4 | 20:1 |
| Nb stripping | Water | 4 | 15:1 |
| Final stripping | 0.5% wt $NH_4OH$ | 2 | 8:1 |

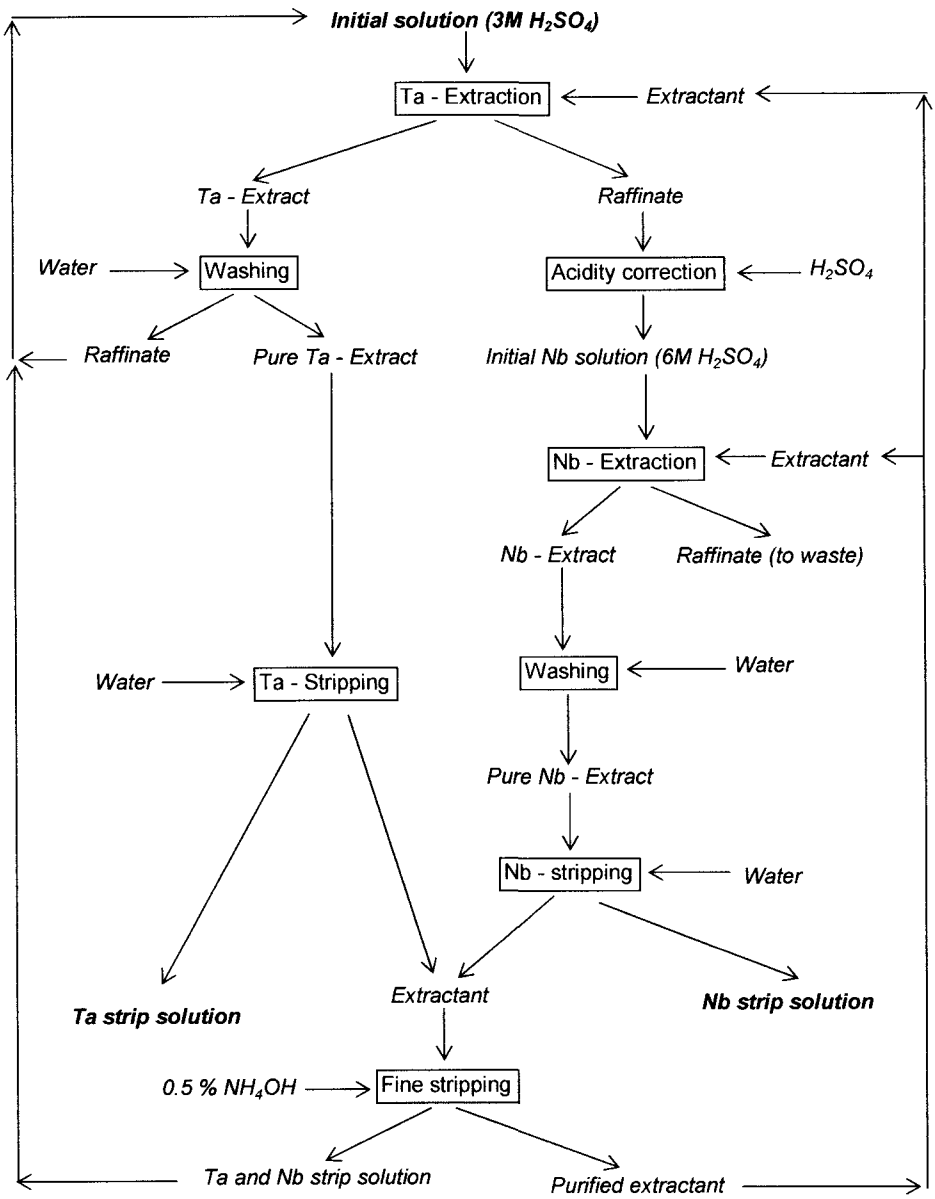


*Fig. 134. Flow chart of complete process of tantalum and niobium extraction with 2-octanol.*

## 8.4. Preparation of tantalum and niobium oxides

### 8.4.1. General notes

Tantalum and niobium oxides, $Ta_2O_5$ and $Nb_2O_5$, are among the final products obtained from tantalum and niobium strip solutions following liquid–liquid extraction processes. The strip solutions of tantalum and niobium consist of solutions of fluorotantalic and oxyfluoroniobic acids, $H_2TaF_7$ and $H_2NbOF_5$, respectively.

Several possibilities exist for the conversion of the liquid acids into solid tantalum and niobium oxides. The most common steps performed in all such methods are:

- Substitution of fluoride ions by other suitable ions in the complex acid so as to separate the fluorine ions from tantalum and niobium (liquid–liquid interaction);
- Precipitation of niobium and tantalum compounds in forms that are suitable for separation from the aqueous media (liquid–solid interaction);
- Decomposition following thermal treatment of the separated material yielding solid oxides and gaseous components (solid–gas interaction).

The main difference between the methods is usually related to the first step, namely fluorine substitution and precipitation of tantalum or niobium compounds.

The defluorination of the complex acids is a key step in the production of tantalum and niobium oxides as it defines the quality of the products and durability of the production equipment.

In some cases, the degree of fluorine contamination of tantalum and niobium oxides containing increased fluorine levels is not very critical to the later application of the oxides. Applications related to the manufacturing of optic and electronic devices, however, require significant limitations of the fluorine content of tantalum and niobium oxides.

Fluorine is usually present in the oxides in the form of oxyfluorides of tantalum or niobium: $MeO_2F$, $Me_3O_7F$ (Me = Ta or Nb). The impurities can interact with components of the subsequent processes, yielding stable complex oxyfluoride phases. For instance, the presence of fluorine can significantly modify some electrophysical parameters of ceramic materials [489]. During the synthesis of lithium niobate, $LiNbO_3$, and lithium tantalate, $LiTaO_3$, oxides that are contaminated with fluorine yield a foreign phase of $Li_4TaO_4F$ or $Li_4NbO_4F$

[87, 132]. The contaminated powdered material usually causes problems during crystal growth and degraded the electric and optic properties of the final products.

## 8.4.2. Precipitation of hydroxides by ammonia solution

Preparation of tantalum and niobium oxides based on the precipitation by ammonium solution of tantalum or niobium hydroxides from strip solutions is the most frequently used method in the industry and consists of several steps. Fig. 135 presents a flow chart of the process.

The interaction between fluorotantalic or oxyfluoroniobic acids and ammonia solution initiates the hydrolysis of complex fluoride compounds. The complete process can be represented as follows:

In the case of tantalum strip solution:

$$2\ H_2TaF_7 + 14\ NH_4OH = Ta_2O_5{\cdot}nH_2O_{(solid)} + 14\ NH_4F + (9\text{-}n)\ H_2O \qquad (141)$$

In the case of niobium strip solution:

$$2\ H_2NbOF_5 + 10\ NH_4OH = Nb_2O_5{\cdot}nH_2O_{(solid)} + 10\ NH_4F + (7\text{-}n)\ H_2O \qquad (142)$$

Equations (141) and (142) describe the equilibrium between the hydrolysis of complex fluoride acids (shift to the right) and the fluorination of hydroxides (shift to the left). Near complete precipitation of hydroxides can be achieved by applying an excessive amount of ammonia. Typically, precipitation is performed by adding ammonia solution up to pH = 8–9. However, the precipitate that separates from the mother solution can be contaminated with as much as 20% wt. fluorine [490]. Analysis of niobium hydroxides obtained under different precipitation conditions showed that the most important parameter affecting the fluorine content of the resultant hydroxide is the amount of ammonia added [490]. Sheka et al. [491] found that increasing the pH to 9.6 toward the end of the precipitation process leads to a significant reduction in fluorine content of the niobium hydroxide.

Agulyansky et al. [492, 493] investigated the complex structure and composition of solid phases precipitated by ammonia solution from experimental and industrial niobium and tantalum strip solutions. Fig. 136 shows isotherms (20°C) of $Nb_2O_5$ content versus pH for solutions prepared by the dissolution of $(NH_4)_3NbOF_6$ and $(NH_4)_2NbOF_5$ in water and of Nb metal in

HF acid. The acidity (pH) of the solutions was modified by adding HF or $NH_4OH$ solutions. The minimums observed on the isotherms are related to the precipitation of complex oxyfluoroniobates of various compositions, namely $(NH_4)_3NbOF_6$, $(NH_4)_2NbOF_5$ and $(NH_4)_5Nb_3OF_{18}$.

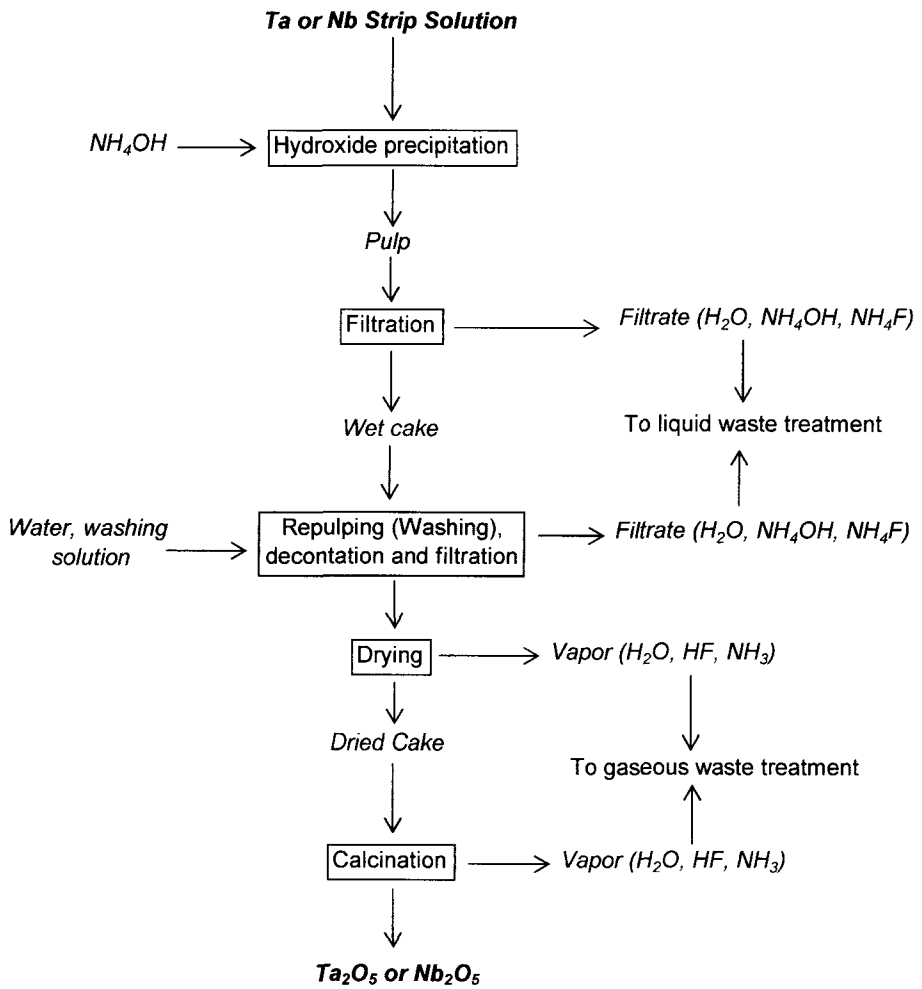


*Fig. 135. Flow chart of tantalum/niobium oxide preparation - precipitation of hydroxides by ammonia solution.*

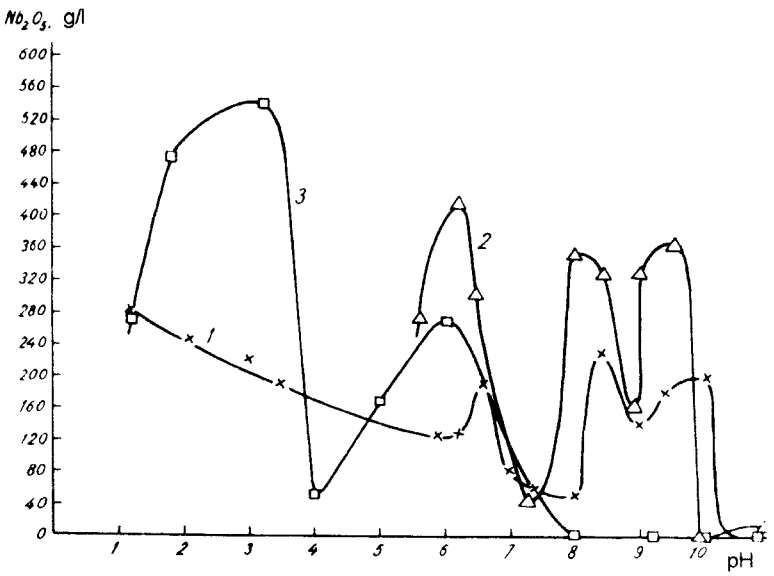


*Fig. 136. $Nb_2O_5$ concentration versus pH of solutions prepared by dissolution of $(NH_4)_3NbOF_6$ (1) and $(NH_4)_2NbOF_5$ (2) in water or Nb in HF solution (3) (after Agulyanskaya et al., [492, 493]).*

Increasing the pH to 10–11 (in the case of Nb – HF solution - pH = ~8) reduced the $Nb_2O_5$ concentration in the solutions to 0.5–0.3 g/l and the solid precipitate was identified as a pure amorphous substance, which after thermal treatment was identified as niobium oxide.

In the case of tantalum-containing solutions, a sharp drop in $Ta_2O_5$ concentration was observed also at pH > 10. The precipitated material was identified as a pure amorphous powder, which after appropriate thermal treatment was converted into tantalum oxide. Fig. 137 presents isotherms (20°C) of $Ta_2O_5$ concentration versus pH for solutions with compositions close to those of industrial strip solutions.

Two types of compounds, crystalline and amorphous, can be precipitated from tantalum or niobium solutions by an initial ammonia solution containing ammonium ions, with an interface at about pH = 10. Such solutions are used for the stripping of tantalum or niobium from TBP extracts. In the case of pure fluorotantalic or fluoroniobic acids that result from the stripping process with water, the interface occurs at a lower pH level.

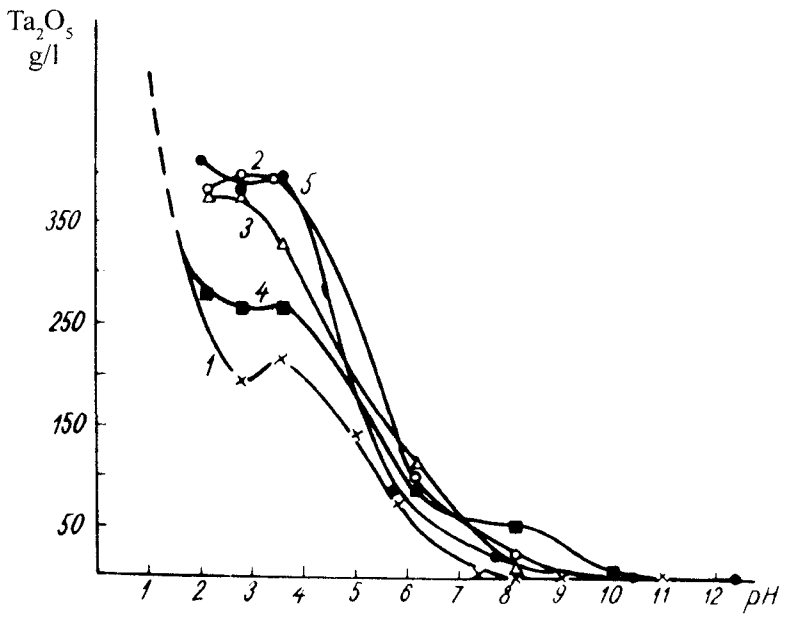


*Fig. 137. Tantalum oxide content versus pH. Curve 1 – solution containing no ammonium fluoride. Curves 2–5 – solutions with increased initial ammonium fluoride content (after Agulyanskaya et al., [492, 493]).*

Based on the above approach, the phases that are obtained from the strip solutions by precipitation with ammonium solution can be represented by the general formula: $xNH_4F \cdot yMe_2O_5 \cdot zH_2O$ or by the following interaction:

$$x\,NH_4F \overset{1}{\leftrightarrow} y\,Me_2O_5 \overset{2}{\leftrightarrow} z\,H_2O \qquad (143)$$

The resulting product depends on the precipitation conditions, and in particular, on the over-saturation level of the solution. Formation of ammonium oxyfluorometalate crystalline compounds occurs at a relatively low pH of the solution. From the standpoint of the interactions described in Equation (143), this means that the interaction between $NH_4F$ and $Me_2O_5$ (denoted as interaction 1) is stronger than the interaction denoted as interaction 2. In this case, subsequent processes of the hydroxide treatment lead to some defluorination of the product, but the performance of such processes is usually very problematic. Precipitation at high pH values leads to a strong over-saturation of niobium- or tantalum-containing compounds, which in turn

ensures the formation of amorphous phases. It should be noted that interaction 2 is predominate in relation to interaction 1 (see Equation 143).

It is possible to create the over-saturated conditions required for the formation of hydroxides not only by adding ammonia to the strip solutions. It was reported in [492] that fast cooling to 0°C (quenching) of a hot solution saturated with $(NH_4)_2NbOF_5$ leads to a precipitate containing significant amounts of an amorphous phase. Thermal treatment of the obtained material yielded white powder that consisted mainly of $Nb_2O_5$. However, similar thermal treatment of the precipitate performed by slow cooling of the same solution led to the formation of crystalline $NbO_2F$ or $Nb_3O_7F$, depending on the calcination temperature.

Thus, in order to achieve precipitation of tantalum and niobium hydroxides with minimal levels of fluorine contamination, it is recommended to perform the process at a pH no lower than 10.

Brown et al. [494] developed a method for the production of hydrated niobium or tantalum pentoxide from fluoride-containing solutions. The essence of the method is that the fluorotantalic or oxyfluoroniobic acid solution is mixed in stages with aqueous ammonia at controlled pH, temperature, and precipitation time. The above conditions enable to produce tantalum or niobium hydroxides with a narrow particle size distribution. The precipitated hydroxides are calcinated at temperatures above 790°C, yielding tantalum oxide powder that is characterized by a pack density of approximately 3 g/cm$^3$. Niobium oxide is obtained by thermal treatment of niobium hydroxide at temperatures above 650°C. The product obtained has a pack density of approximately 1.8 g/cm$^3$. The specific surface area of tantalum oxide and niobium oxide is nominally about 3 or 2 m$^2$/g, respectively.

The way in which ammonia solution is added to tantalum or niobium strip solutions is also important for the quality of the precipitated hydroxides and final oxides. The traditional method by which ammonia is poured into a container of strip solution and the mixture agitated is not optimal. According to this method, the first portion of ammonia is added to a solution of high acidity, the pH of which continues to drop gradually with each addition of ammonia, until the final addition of ammonia is made into a low-acidity solution. This procedure leads to a relatively slow increase in pH that can cause contamination of the hydroxide with crystalline oxyfluoride compounds.

The opposite process, i.e. pouring the strip solution into the ammonia solution, significantly reduces the fluorine concentration in the hydroxides formed. Bludssus et al. [495] developed a process comprising the introduction of tantalum- or niobium-containing acid solution to an ammonia solution until achieving pH = 9. It is reported that this method enables the production of tantalum or niobium hydroxides with fluoride contents as low as 0.5% wt. with

a relatively low consumption of ammonia solution. According to our laboratory experience, the precipitate usually consists of very fine particles that cause some problems during filtration. More acceptable results were obtained using a double-stream system with concurrent stirring of the relatively small components of the mixture [492, 493]. Fig. 138 presents the general scheme of the reactor.

The equipment consists of a mixing tank and stirrer that is equipped with a relatively small premixing plate. Predetermined volumes of strip and ammonia solutions are loaded onto the rotating premixing plate. The premixed pulp is unloaded into the mixing tank for continuation of interaction and homogenization of the mixture.

Application of an excessive amount of ammonia solution in the precipitation of tantalum and niobium hydroxides from strip solutions usually ensures good quality of the products. Nevertheless, the method has two general problems. First, hydroxides containing low levels of fluorine contamination

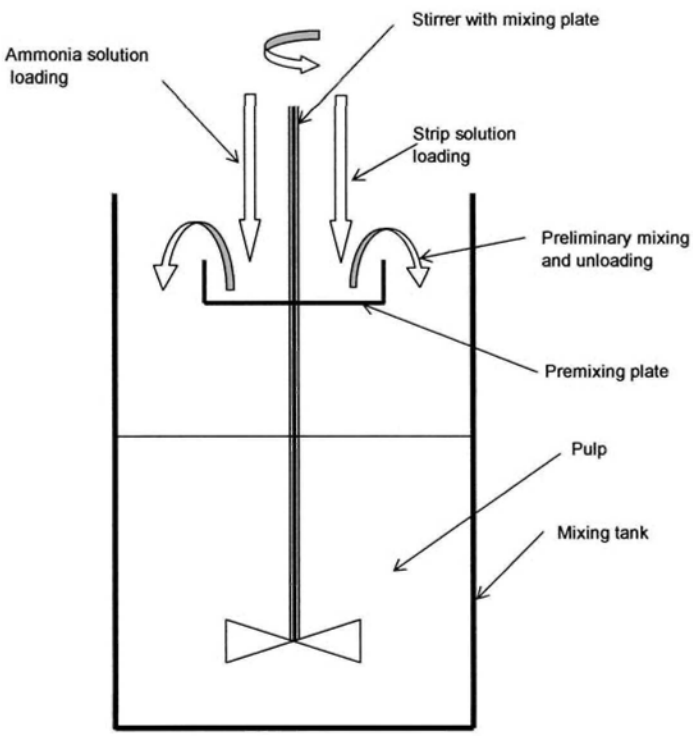


*Fig. 138. Scheme of reactor for precipitation of hydroxides including double-stream solution loading and premixing plate.*

precipitate in the form of very fine particles that lead to slow and problematic filtration, especially in the case of niobium hydroxide. Second, the method generates a huge amount of liquid waste in the form of ammonia solution filtrates.

Some improvement in the filtration rate can be achieved by increasing the temperature and concentration of the solid component of the pulp [496, 497].

Uchino and Azuma [498] proposed a way in which to recycle the filtrate solutions. The process consists of adding calcium hydroxide, $Ca(OH)_2$, to the filtrate, yielding a calcium fluoride, $CaF_2$ precipitate and gaseous ammonia, $NH_3$. The fluorine and ammonia are recovered in forms that are suitable for reutilization.

### 8.4.3. Washing of hydroxides

The subsequent steps in the production of tantalum and niobium are washing and thermal treatment of the precipitated hydroxides. For effective washing of precipitated hydroxides, Vaicenberg et al. [490] recommended the use of a 2% wt. ammonia solution that is added at a solid–liquid volumetric ratio of 1:15. It is reported that the above conditions ensure the preparation of dry hydroxides with fluorine contents of less than 2%. Sheka et al. [491] proposed precipitation with ammonia at pH = 8.7–9 (20-40°C) and the subsequent use of 0.5-10% $NH_4OH$ with a solid-liquid volumetric ratio of 1:5 for washing (re-pulping). This method enables to reduce the fluorine content in the dry hydroxides to 0.2% wt.

Balabanov et al. [499] investigated the efficiency of different solutions for the washing of niobium hydroxide. The effectiveness of water and solutions of ammonia, $NH_4OH$, ammonium acetate, $CH_3COONH_4$, and ammonium carbonate, $(NH_4)_2CO_3$, were tested. It was shown that ammonium acetate interacts with solid ammonium oxyfluoroniobates yielding niobium oxide even at temperatures as low as 125°C. The interaction that takes place between the solid components can be presented as follows (144):

$$2\,(NH_4)_3NbOF_6 + 6\,NH_4CH_3COO + 12\,O_2 =$$

$$= Nb_2O_5 + 12\,NH_3 + 12\,HF + 12\,CO_2 + 9\,H_2O \quad (144)$$

Hence, water, ammonia, hydrogen fluoride and carbon dioxide separate from the mixture into the gaseous phase. However, despite the possibility of a solid-state interaction, the application of ammonium acetate solutions for washing of

niobium hydroxide was not sufficiently successful for the effective reduction of fluorine contamination. One of the possible reasons might be related to insufficient amounts of oxygen in the liquid system.

Ammonia solutions are significantly more efficient than ammonium acetate as washing reagents. The process of fluorine content reduction is related to subsequent hydrolysis of fluoride and oxyfluoride contaminants by ammonia.

The most effective of the proposed solutions seem to be solutions of ammonium carbonate, $(NH_4)_2CO_3$. Such solutions were also recommended by Mulyarchuk and Panchenko [500] for the decomposition of potassium fluorosilicate, $K_2SiF_6$.

Ammonium carbonate interacts with ammonium oxyfluoroniobates yielding niobium oxide, as shown below [497]:

$$2\ (NH_4)_3NbOF_6 + 3\ (NH_4)_2CO_3 = Nb_2O_5 + 12\ NH_3 + 12\ HF + 3\ CO_2 \qquad (145)$$

Ammonia, hydrogen fluoride and carbon dioxide separate from the system in the form of gaseous components.

The most efficient washing of the hydroxide was achieved applying a three-step process using an ammonium carbonate solution as the first step, followed by an ammonia solution, and water as the final step. This washing process brings about a ten-fold reduction in the concentration of fluorine compared with laboratory and industrial experience, in which a 2–4 fold reduction in the fluorine content of tantalum or niobium hydroxides following a one-step washing process was obtained.

### 8.4.4. Thermal treatment of hydroxides

Precipitated, washed and filtrated hydroxides consisting of wet powder contain two kinds of water. The first is moisture, i.e. water remainders that include adsorbed water. This kind of water can be successfully removed by drying at 100-200°C. The second type is molecules of water that are incorporated with tantalum or niobium to form hydroxides. Because hydroxyl groups form relatively strong bonds with tantalum or niobium, the separation of the second kind of water requires thermal treatment at higher temperatures [501].

Lapizki et al. [502] reported that niobium hydroxide can be completely dried by thermal treatment at 50-500°C. Titova et al. [503] argued that the number of water molecules incorporated with niobium in niobium hydroxide

can be altered by thermal treatment at different temperatures: 25°C – $Nb_2O_5 \cdot 4H_2O$, 200°C – $Nb_2O_5 \cdot 0.5H_2O$, 400°C – $Nb_2O_5$.

Balabanov et al. [499] found an endothermic effect in the thermographic pattern of the decomposition of niobium hydroxide at 435°C that corresponds to complete removal of water. At the above temperature, amorphous niobium hydroxide also converts into amorphous niobium oxide. Crystallization of the amorphous oxide occurs at a higher temperature with the release of energy [28]. Researchers [499] reported on another exothermal effect at 549°C that was attributed to the crystallization temperature of amorphous niobium oxide. Decomposition of tantalum hydroxide and its conversion into crystalline tantalum oxide occurs at about 710°C [502] or at 670–700°C according to another source [132].

Thus, tantalum and niobium hydroxides are converted into oxides following a two-step thermal treatment. The first step is usually performed at relatively low temperatures in the range of 100-200°C in order to dry the wet precursors. The second thermal treatment brings about the decomposition of hydroxides, removes the rest of the water and converts the material into crystalline oxides. The second thermal treatment is usually performed at temperatures as high as 900-1000°C.

Uchino and Azuma [504] developed and proposed a two-step calcination process of tantalum and niobium hydroxides to obtain oxides. The first treatment is recommended to be performed at 500-700°C, and the second– at 750-1000°C. It is reported that the above method ensures the production of oxides that contain only negligible concentrations of fluorine and silicon impurities.

The fluorine concentration in hydrofluorides of tantalum and niobium is an extremely important issue. Fluorine that separates into the gaseous phase interacts with the construction elements of the furnaces, leading to additional contamination of the final product by silicon, aluminum, etc. Thus, it is recommended to perform drying in crucibles made of Teflon or polypropylene with appropriate temperature limitations. Use of crucibles made of carbon-glass ensures high quality and a broad working temperature range, at least up to 300-350°C.

Calcination is performed in crucibles made of platinum or related metals. Tantalum or niobium oxide can be successfully used in the manufacturing of such crucibles. Frolov et al. [505, 506] developed a method for coating various ceramic materials with tantalum or niobium oxide using an optical furnace.

Fluorine appears in hydroxides in the form of ammonium oxyfluoro-metalates, yielding ammonium fluoride upon decomposition during thermal treatment. Ammonium fluoride is not a thermally stable compound and

decomposes without melting, yielding gaseous ammonia and hydrogen fluoride according to the following scheme:

$$NH_4F = HF + NH_3 \quad (146)$$

The decomposition described in Equation (146) takes place at relatively low temperatures; hence, thermal treatment at a relatively slow temperature rate can be sufficient in order to significantly reduce fluorine levels in the final oxides. Nevertheless, treatment at a high temperature rate can lead to another mechanism of ammonium fluoride decomposition yielding gaseous ammonia and molten ammonium hydrofluoride according to the following scheme:

$$2\,NH_4F = NH_4HF_2 + NH_3 \quad (147)$$

Ammonium hydrofluoride is relatively stable, even in the molten state. In addition to being in contact with tantalum or niobium oxide, the compound will initiate the fluorination process yielding complex tantalum or niobium fluoride compounds. There is no doubt that thermal treatment of the hydroxides at high temperatures and/or at a high temperature rate leads to the enhancement of the defluorination processes, which in turn results in an increase in fluorine content of the final oxides.

Different procedures for the precipitation, washing and thermal treatment of hydroxides result in different fluorine contamination levels in the final products – tantalum and niobium oxides. Laboratory and industrial experience confirms some correlation between the initial concentration of fluorine in the dried hydroxides and the fluorine content in the final oxides obtained after appropriate thermal treatment. For instance, it is reported in [499] that if the initial concentration of fluorine in niobium hydroxide equals A%, then the fluorine content in the final niobium oxide can be estimated according to the thermal treatment temperature as follows:

Temperature: 400°C – possible final fluorine content: 3.98A/(39.6–0.70A);

Temperature: 1000-1200°C – final fluorine content: 1.11A/(39.6–0.76A).

Agulyanskaya et al. [507] investigated the impact of fluorine content on the particle size of niobium and tantalum oxides and powdered lithium niobate and tantalate prepared from the oxides. It was shown that fluorine concentrations lower than $\sim 10^{-2}$% wt. do not influence particle size and result in a set minimum particle size. This concentration range was referred to as being non-

sensitive to fluorine contamination. In the case of fluorine concentrations higher than ~$10^{-2}$% wt., the particle size increases proportionally to the logarithm of the fluorine concentration. A correlation was also found between the particle sizes of oxides and powdered lithium tantalate or niobate, prepared by interaction of the oxides with lithium carbonate. Thus, controlling the fluorine content in tantalum and niobium oxides enables the effective management of the particle size of the powder.

Kobayashi et al. [508] developed an effective method to control particle size and fluoride content in granular tantalum oxide and niobium oxide. The resultant powders are suitable for application in the manufacturing of ceramics, single crystals, optical glass, etc.

## 8.4.5. Other methods for precipitation of tantalum and niobium oxide precursors

Other methods exist for the precipitation of tantalum and niobium hydroxides for subsequent use as oxide precursors. Application of ammonium carbonate, $(NH_4)_2CO_3$, instead of ammonia solution, also seems to have potential for the precipitation of tantalum and niobium hydroxides. Ammonium carbonate is relatively stable in aqueous media at room temperature and does not initiate the precipitation of hydroxides. Increasing the temperature of the solution causes hydrolysis and decomposition of ammonium carbonate yielding hydroxyl ions and an increase in pH, as follows:

$$(NH_4)_2CO_3 + H_2O = 2\,NH_4OH + CO_2 \qquad (148)$$

The interaction described in Equation (148), in which $CO_2$ separates from the solution and ammonia hydroxide is formed, reduces the acidity of the solution causing precipitation of tantalum or niobium hydroxide. The hydroxide powder precipitated using ammonium carbonate is usually coarser and has better filtering properties. Changing the ammonium carbonate concentration and temperature of the solution allows some control over the particle size and filtering properties of the precipitated hydroxides.

In addition to the possibility of controlling the particle size of the hydroxides, application of ammonium carbonate affords several other advantages compared to traditional precipitation of hydroxides using ammonia solution. First, ammonium carbonate does not increase the total volume of the solution as much as does the addition of ammonia. Second, the method enables to perform the interaction so as to precipitate stoichiometric mixtures, which

are then converted into niobates or tantalates after appropriate thermal treatment. The addition of carbonate-containing compounds to tantalum- or niobium-containing fluoride solutions up to pH = 7 is recommended for the precipitation of hydroxides which are then used successfully in the manufacturing of tantalates and niobates [509].

Another promising method for the preparation of tantalum and niobium oxide precursors involves the precipitation of peroxoniobate and peroxotantalate compounds.

Niobium and tantalum peroxoacids and salts were investigated and described as early as about 100 years ago by Balke and Smith [510]. $M_3NbO_8$, and $MgMNbO_8 \cdot aq.$ type compounds (where M = Na, K, Rb, Cs), as well as $CaMNbO_8 \cdot aq.$ type compounds (where M = Na, K), can be prepared by hydrogen peroxide treatment of strongly alkaline solutions containing soluble niobates or tantalates. Lithium- and ammonium-containing compounds of the $M_3NbO_8$ series have been obtained as well. In addition, it was shown that peroxide ions can replace fluorine ions in complex niobium and tantalum fluoride and oxyfluoride ions, yielding peroxofluoroniobate or peroxofluorotantalate compounds [28].

Latish, Chernyak and Serebrennikova [511] investigated the formation of complexes in $Nb^V - H_2O_2 - HF - H_2SO_4$ and $Ta^V - H_2O_2 - HF - H_2SO_4$ systems using spectrophotometric methods. It was found that in the niobium-containing system, four complexes occur that have a component ratio $Nb^V:H_2O_2:HF$ of 1:1:1; 1:1:2; 1:1:3 and 1:1:4, respectively. The instability constants of the complexes in the $Nb^VHF - H_2O_2$ series are $2.85\times10^{-4}$ for $Nb^VHF:H_2O_2$ = 1:1, and $2.17\times10^{-3}$ for $Nb^VHF:H_2O_2$ = 1:2. In the $Nb^VH_2O_2$ – HF series, $Nb^VH_2O_2$:HF complexes with ratios of 1:1; 1:2; 1:3 and 1:4 are characterized by instability constants equal to $2.42\times10^{-3}$; $1.93\times10^{-2}$; $2.66\times10^{-3}$ and $3.07\times10^{-2}$, respectively. The same types of complexes were found for the tantalum-containing system $Ta^V - H_2O_2 - HF - H_2SO_4$. The following instability constants were determined for the $Ta^VHF - H_2O_2$ and $Ta^VH_2O_2 - HF$ series, respectively: $4.60\times10^{-4}$ (for $Ta^VHF:H_2O_2$ = 1:1) and $1.48\times10^{-3}$ (for $Ta^VHF:H_2O_2$ = 1:2); $4.11\times10^{-3}$ (for $Ta^VH_2O_2$:HF = 1:1); $4.5\times10^{-3}$ (for $Ta^VH_2O_2$:HF = 1:2); $1.18\times10^{-2}$ (for $Ta^VH_2O_2$:HF = 1:3) and $1.49\times10^{-2}$ (for $Ta^VH_2O_2$:HF = 1:4).

The formation and stability of peroxoniobates and peroxotantalates can be used successfully in the technology of tantalum and niobium oxide production. Belov, Avdonina and Mikhlin [512] investigated processes of precipitation and thermal decomposition of high-purity ammonium tetraperoxoniobate and tetraperoxotantalate as precursors for the production of tantalum and niobium

oxides. It was shown that the method can be applied to fluoride-containing solutions for the production of high-purity oxides that are suitable for the manufacture of electronic and optic materials.

The essence of the process is the precipitation of ammonium peroxotantalate or peroxoniobate by the addition of solutions of ammonia and hydrogen peroxide, $H_2O_2$, to appropriate strip solutions. The process was described in general terms as follows:

$$H_xMOF_{(x+3)} + NH_4OH + H_2O_2 \rightarrow (NH_4)_3MO_8 + NH_4F \quad (149)$$

For the precipitation of ammonium peroxometalates (M = Ta or Nb), the above interaction takes place at pH > 8.

Nevertheless, the precipitation process can be specified based on data available on the complex structure of the strip solutions. In the case of tantalum strip solutions, the interaction can be written as follows:

$$H_2TaF_7 + 10\,NH_4OH + 4\,H_2O_2 = (NH_4)_3TaO_8 + 7\,NH_4F + 10\,H_2O \quad (150)$$

In the case of niobium-containing strip solutions, the interaction takes place at a lower concentration of added ammonia solution:

$$H_2NbOF_5 + 8\,NH_4OH + 4\,H_2O_2 = (NH_4)_3TaO_8 + 5\,NH_4F + 9\,H_2O \quad (151)$$

Subsequent steps of the process involve the decomposition of ammonium peroxometalates, $(NH_4)_3TaO_8$ and $(NH_4)_3TaO_8$, which takes place according to a hydrolytic mechanism. Belov et al. [512] presents the following interactions as occurring by different mechanisms in different media. Hydrolysis in acidic media at pH ≤ 3 appears to occur with the separation of oxygen, as shown in Equation (152):

$$(NH_4)_3MO_8 + H^+ \xrightarrow{t} HMO_4{\cdot}xH_2O + 3\,NH_4^+ + O_2 \quad (152)$$

Hydrolysis in neutral or slightly basic media (pH ≥ 7) yields gaseous ammonium:

$$(NH_4)_3MO_8 + H_2O \xrightarrow{t} (NH_4)M(OH)O(O_2){\cdot}xH_2O + 2\,NH_3 \quad (153)$$

It can be seen that x molecules of water must be added to the left side of Equations (152) and (153) in order to achieve mass equilibrium.

Thermal treatment of the compounds obtained from the hydrolysis leads to their decomposition, yielding tantalum or niobium oxides and gaseous oxygen. The processes of thermal decomposition are given as follows [512]:

$$2\ HMO_4 \cdot xH_2O \xrightarrow{t} M_2O_5 + H_2O + O_2 \quad (154)$$

$$2\ (NH_4)M(OH)O(O_2) \cdot xH_2O \xrightarrow{t} M_2O_5 + 2\ NH_3 + O_2 \quad (155)$$

Leaving aside the incompleteness of the equilibriums, Equations (154) and (155) indicate a clear possibility of producing tantalum and niobium oxides based on the precipitation of peroxometalate precursors.

Dry peroxometalates, $(NH_4)_3MO_8$ (M = Ta or Nb), decompose within the temperature range of 5-40°C, accompanied by the separation of oxygen and the formation of amorphous $(NH_4)_3MO_5$ according to following interaction:

$$(NH_4)_3MO_8 \xrightarrow{t} (NH_4)_3MO_5 + 3/2\ O_2 \quad (156)$$

$(NH_4)_3MO_5$ compounds are relatively stable at room temperature. No significant weight loss was observed at 25°C, even after 2 days.

At temperatures above 45°C, however, $(NH_4)_3MO_8$ compounds decompose yielding gaseous ammonia, $NH_3$, and oxygen as well as tantalum or niobium oxides:

$$2\ (NH_4)_3MO_8 \xrightarrow{t} M_2O_5 + 6\ NH_3 + 4\ O_2 + 3\ H_2O \quad (157)$$

At even higher temperatures - 80°C for $(NH_4)_3NbO_8$ and 90°C for $(NH_4)_3TaO_8$ - the decomposition process becomes explosive [512].

Table 64 presents the thermodynamic parameters of $(NH_4)_3MO_8$ compounds as determined by Belov et al. [512].

To avoid explosion, the compounds can be decomposed via hydrolysis in liquid solution. Ultra-fine particles are obtained in water and water-ammonia media. Hydrolysis in HCl and $HNO_3$ solutions leads to the precipitation of an agglomerated powder of both tantalum and niobium oxides. Agglomerates obtained are up to 12 μm in diameter, while the estimated diameter of the smallest crystalline particles varies in the range of 0.01–0.5 μm [512].

*Table 64. Thermodynamic parameters of ammonium peroxotantalate and peroxoniobate (after Belov et al. [512]).*

| Compound | $H_f$, kJ·mol$^{-1}$ | Explosion heat, kJ·mol$^{-1}$ | Detonation velocity, m·s$^{-1}$ |
|---|---|---|---|
| $(NH_4)_3NbO_8$ | 1425 | 3200 | 2060 |
| $(NH_4)_3TaO_8$ | 1280 | 2400 | 2370 |

To reduce fluorine content in $(NH_4)_3MO_8$, the precipitate is washed. Use of water as a washing solution ensures a significant reduction of the fluorine content; however, the process seems to be of low efficiency due to the relatively high solubility of ammonium peroxometalates. According to Belov et al. [512], solubility of the ammonium peroxometalates depends on the concentration of the ammonium salts. The solubility of ammonium peroxometalates ($C_{M_2O_5}$) in solutions of various ammonium salts can be calculated using the following expression:

$$C_{M_2O_5} = C_0 / \left(1 + KC_{NH_4A}\right) \tag{158}$$

where $C_0$ = solubility of ammonium peroxometalate in water, equal to 17 g/l for $Nb_2O_5$ and 21 g/l for $Ta_2O_5$; $K_{NH_4A}$ = coefficient for the various salts added, specifically $K_{NH_4F}$ = 0.096; $K_{(NH_4)_2SO_4}$ = 0.044; $K_{NH_4Cl}$=0.070; $K_{NH_4NO_3}$ = 0.063.

Thus, by adding ammonium salts, the properties of the washing solution can be adjusted and optimal process parameters achieved.

The method based on the precipitation of peroxometalate precursors enables to achieve additional purification during the process. Thus, the addition of complexonates, such as OEDP or EDTA, which form stable complexes with some polyvalent metals, prevents co-precipitation of the main impurities such as Fe, Co, Ni, Mn, Mg, etc., which in turn significantly increases the purity of the final product. Enhanced purification can also be achieved by re-crystallization of the precursor. Particularly, the precipitation of ammonium peroxofluorometalates, such as ammonium peroxofluoroniobate ($(NH_4)_3NbO_4F_4$), as a primary precursor, leads to significant reduction of the titanium contamination. Ammonium peroxofluoroniobate, $(NH_4)_3NbO_4F_4$, is

precipitated from fluoride solutions at pH = 5–7, separated from the solution by filtration and dissolved in mineral acids, to be subsequently converted to $(NH_4)_3NbO_8$ [512].

Ammonium peroxometalates, $(NH_4)_3NbO_8$ and $(NH_4)_3TaO_8$, can also be re-crystallized, but Belov et al. [512] noted that the process must be performed using citric acid solutions, which are stable at pH = 4–5 up to 100°C.

The precipitation of ammonium peroxometalate precursors seems to be very promising for development and implementation in the production of high-purity oxides of tantalum and niobium. The main advantages of the method are as follows:

- Ammonium peroxometalates or peroxofluorometalates are relatively coarse crystalline powders that precipitate rapidly and can be completely and quickly separated from the solution by filtration;
- The precipitated precursor can be dissolved and re-crystallized from fluorine-free solutions. This provides excellent conditions for deep purification of the material and reduction of problematic impurities such as titanium, fluorine, etc.;
- Peroxometalates decompose at relatively low temperatures forming tantalum or niobium oxides containing small amount of absorbed water. The absorbed water separation is achieved by further thermal treatment – drying and calcination – of the product;
- The method emphasizes perspective directions in the development and improvement of the technology of tantalum and niobium oxides.

The most difficult aspect of the method is the fact that it is based on the handling of compounds that unequivocally belong to the family of powerful explosives. There is no doubt that working with peroxide compounds is dangerous and requires the development and implementation of special procedures and safety equipment.

## 8.4.6. Plasma chemical decomposition of fluoride solutions

Tantalum and niobium strip solutions that originate in the liquid–liquid extraction process consist of fluorotantalic and oxyfluoroniobic acid solutions that contain $TaF_7^{2-}$ and $NbOF_5^{2-}$ complex ions. Standard thermal treatment of the solutions, including heating, evaporation and subsequent calcination of the precipitated solids, yields oxyfluorides of tantalum or niobium. The general composition of the solids can be represented as $MeO_2F$ or $Me_3O_7F$ (Me = Ta or Nb), depending on the treatment temperature. In some cases, very small amounts of pentoxides, $Me_2O_5$, are observed in the resultant material. Oxide formation is related to the partial hydrolysis of fluoride and oxyfluoride compounds containing tantalum or niobium. Hence, the regular thermal treatment process can be divided into different stages such as separation of water, thermal decomposition of fluoride complexes and possible hydrolysis of solid products. It is obvious that the process, which is based on rapid heating of the solution in order to ensure hydrolysis of the complex fluoride compounds, leads to the formation of tantalum and niobium oxides. The most suitable heat source for the above purposes, and which enables rapid heating, is low-temperature plasma.

Plasma chemical processes have been in wide use in chemical technology for a relatively long period [513]. The main application fields of low-temperature plasma involve metallurgy, high-temperature treatment of materials, reduction of metals from oxides, halides, sulfates and some other compounds, and synthesis of refractory oxides, carbides and nitrides [514, 515]. Numerous processes are known for plasma chemical treatment of solutions, containing salts of nitric, hydrochloric and sulfuric acids, in the production of metal oxides [516 – 518]. A method for the preparation of refractory metal oxides from volatile chlorides using oxygen-containing plasma is also known [519]. Niobium pentafluoride, $NbF_5$, and niobium pentachloride, $NbCl_5$, can be treated and converted into ultra-fine powders of niobium nitride, oxide or metal using low-temperature plasma that contains nitrogen or hydrogen, respectively [520 – 523].

The first experiments on the plasma chemical decomposition of fluoride solutions containing tantalum or niobium to obtain tantalum and niobium oxides were reported about fifteen years ago [524]. Subsequent publications were devoted to further development and expansion of the method for other refractory rare metals such as titanium and zirconium [525 – 532].

The plasma chemical method for the thermal decomposition of solutions has been preferred over gas-flame heating for the following reasons [532]:

- No fuel is required;
- Significantly higher initial temperature of heating source – up to 3000 –10000K;
- Significantly higher temperature can be achieved during the process – up to 2500K;
- No additional gaseous components that coming from gaseous heating source in the case of gas-flame process;
- Possibility to vary the type of gas used (in other words, possibility to vary interaction atmosphere).

The plasma chemical decomposition method is based on rapid heating, decomposition and hydrolysis of fluoride compounds to obtain powdered oxides following interaction with water. Rakov and Teslenko [533] showed that the following hydrolysis equilibrium

$$MeF_n + n/2\ H_2O = MeO_{n/2} + n\ HF \qquad (159)$$

shifts to the right when the temperature exceeds 1000K. The reverse interaction, fluorination, takes place at lower temperatures: below 500K for niobium, tantalum and titanium and below 700K in the case of zirconium.

The decomposition of solutions using plasma can be conceived as occurring in two steps. In the first step, evaporation of all system components takes place. Under such conditions, tantalum and niobium appear to be in the form of gaseous $TaF_5$ ($TaOF_3$) and $NbF_5$ ($NbOF_3$). The second step consists of the hydrolysis of the niobium- or tantalum-containing molecules by water vapors. This process leads to the formation of solid oxides and gaseous hydrogen fluoride, HF. The overall process can be described by Equations (160) and (161) for tantalum-containing fluorometalic acid solutions (strip solutions obtained after stripping by water):

$$2\ H_2TaF_7(liquid) + 5\ H_2O(liquid) \xrightarrow{t} Ta_2O_5(solid) + 14\ HF(gas) \qquad (160)$$

as well as for niobium-containing solutions:

$$2\ H_2NbOF_5(liquid) + 3\ H_2O(liquid) \xrightarrow{t} Nb_2O_5(solid) + 10\ HF\ (gas) \qquad (161)$$

The presence of ammonia ions in the solution causes no significant differences in the process (strip solution obtained after stripping by ammonium

fluoride or other salt-containing solutions). Due to the high temperatures, most of the ammonia decomposes and oxidizes forming decomposition products that include nitrogen, $N_2$, and hydrogen, $H_2$, or products of ammonia oxidation: $H_2O$, $N_2$ and nitrogen oxides.

The main requirements of the plasma chemical system can be formulated as follows:

- High-frequency plasma source having no consumable electrodes;
- Possibility of attaining temperatures of at least 1000K in the interaction zone;
- Separation of solid and gaseous decomposition products takes place at 500K;
- Solutions loading and unloading system, heat exchanger and all other wet parts are manufactured from materials that are suitable for use with aggressive fluoride liquids.

Fig. 139 shows the schematic arrangement of the plasma chemical installation.

Operation of the installation is as follows. The power supply (1) is connected to the plasma generator (4.5 kW) (2), which initiates a plasma jet by delivering plasma-forming gas (air, oxygen, nitrogen etc.). The solution is loaded onto the plasma by means of pneumatic nozzles (3) and dispersed using the same type of gas.

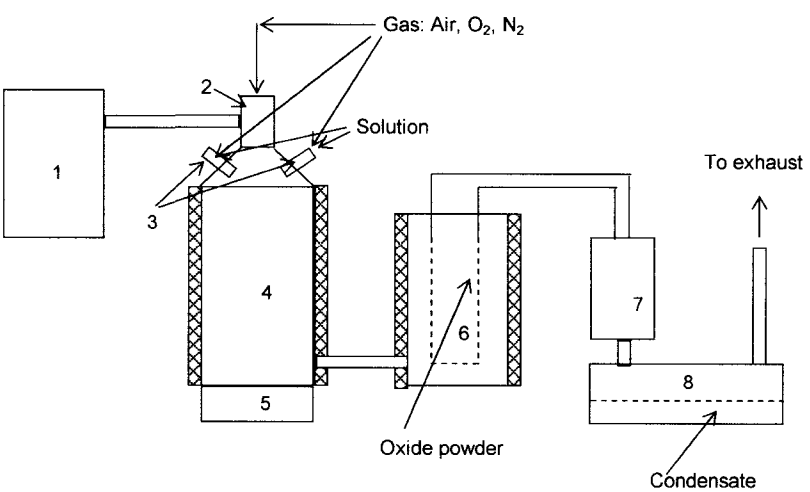


*Fig. 139. Plasma chemical installation. 1 – Plasma generator; 2 – plasma torch; 3 – pneumatic nozzles; 4 – reactor; 5 – solid parts collector; 6 – fine filter; 7 – heat exchanger; 8 – condensate collector.*

The interaction occurs in the reactor (4), which is equipped with exterior heaters and insulation. The coarsest parts of the solids are collected in the collector (5). The gaseous mixture is moved through the connecting tube to the filter (6), which is also equipped with a heater and heat shielding. The solid oxide powder is collected on the filter while the rest of the gaseous components are removed to the heat exchanger
(7), which is equipped with a cooling system that maintains a set condensation temperature. The condensate is collected by the collector (8), whereas the rest of the gases are separated from the system through exhaust ventilation.

Table 65 presents typical initial parameters of the process and compositions of final products - oxide powder and condensate.

Niobium oxide obtained by plasma chemical decomposition is an ultra-fine powder with a specific surface area, as determined by the BET method, of about 20–30 $m^2/g$. The estimated average particle size does not exceed 0.1 μm.

X–ray powder diffraction analysis of the obtained solid product indicated the presence of $Nb_2O_5$ only, in two main modifications, namely β-$Nb_2O_5$ and γ-$Nb_2O_5$. It is interesting to note that the particle diameters of the different crystallographic modifications of the powder are different. Particle diameters of β-$Nb_2O_5$ and γ-$Nb_2O_5$ were estimated, based on X–ray diffraction peak widths, to be 25 nm and 100 nm, respectively. No other peaks belonging to oxyfluoroniobates, $NbO_2F$ or $Nb_3O_7F$, were observed [528, 532]. Nevertheless, in some preliminary experiments [524], an impurity in the form of $NbO_2F$ was observed in products obtained at lower process temperatures, usually below 900°K.

In order to verify the nature of the increased level of fluorine in the obtained niobium oxide, the material was investigated by mass spectral methods [526]. Measurements were performed in situ while heating the samples. At temperatures of up to 1200K, no gaseous components containing niobium were observed and only HF was detected in the gaseous phase. These results clearly indicate that the fluorine contamination appears in the product in the form of HF, which is adsorbed by the fine powdered niobium oxide. Indeed, a trivial calculation shows that a monomolecular layer of HF that is adsorbed by niobium oxide powder and which has a particle diameter in the range of 0.1–0.5 μm, leads to an average fluorine content of about 1–3 % wt.

*Table 65. Typical results of plasma-chemical decomposition of niobium containing fluoride solutions*

| Initial solution composition in g/l | | | Process parameters | | | | Final products | | | | |
|---|---|---|---|---|---|---|---|---|---|---|---|
| | | | Gas Type | Gas flow, g/sec | | solution flow | Powder | | Condensate composition, g/l | | |
| $Nb_2O_5$ | F | $(NH_4)_2O$ | | Plasma | Nozzles | g/sec | Yield, % | F content, % wt | $Nb_2O_5$ | F | $(NH_4)_2O$ |
| 73.0 | 45.0 | 25.3 | Air | 1.3 | 0.2 | 0.2 | 93.2 | 1.1 | 0.010 | 75.0 | 0.4 |
| 36.5 | 23.5 | 14.0 | $O_2$ | 1.3 | 0.2 | 0.26 | 94.0 | 0.78 | 0.010 | 39.0 | 0.4 |
| 36.5 | 23.5 | 14.0 | Air | 1.3 | 0.2 | 0.33 | 86.9 | 1.3 | 0.132 | 35.0 | 0.4 |
| 116.0 | 122 | 119.4 | $O_2$ | 1.1 | 0.2 | 0.13 | - | 0.15 | 0.032 | 135 | 9.6 |
| 223.6 | 176.6 | 0 | Air | 1.6 | 0.11 | 0.245 | 99.4 | 0.55 | 0.002 | 183 | 0 |
| 223.6 | 176.6 | 0 | $N_2$ | 1.2 | 0.09 | 0.19 | 95.3 | 0.54 | 0.019 | 198 | 0 |
| 223.6 | 176.6 | 0 | $N_2$ | 1.05 | 0.09 | 0.18 | 98.8 | 0.50 | 0.037 | 290 | 0 |

Additional confirmation of the approach can be found in the fact that mere thermal treatment of powder obtained from fluoride solutions by plasma chemical decomposition at 1000–1200K for 2–3 hours in air brings about a 100-300 fold reduction in fluorine content. Hence, the plasma chemical process and subsequent thermal treatment of the powder enables to obtain final products with fluorine contents as low as $10^{-2}$–$10^{-3}$ % wt.

Analysis of some experimental results [527, 528, 532] suggests that niobium oxides are first formed as gaseous components resulting from the pure gas-phase hydrolysis:

$$NbOF_3(gas) + 3\,H_2O\,(gas) = Nb_2O_5\,(gas) + 6\,HF\,(gas) \qquad (162)$$

From this point of view, the filter serves not only as separator between the solid and gaseous components of the interaction, but also as a niobium oxide "condenser".

Chemical analysis of niobium oxide indicated that the purity of the final product depends strongly on the purity of the initial solution. Account should be taken of about 0.02–0.03% wt. cationic impurities, introduced due to interactions with metal parts of the equipment. The main added impurities are Fe, Ni, Cr, which originate mostly from the stainless steel filter. The purity of the final product can be significantly increased by using a filter made of niobium or other appropriate material. Nevertheless, the material obtained using a stainless steel filter is sufficient for use in ceramic applications or as an initial material for carbide manufacture.

The unique advantage of the plasma chemical method is the ability to collect the condensate, which can be used for raw material decomposition or even liquid–liquid extraction processes. The condensate consists of a hydrofluoric acid solution, the concentration of which can be adjusted by controlling the heat exchanger temperature according to a binary diagram of the HF – $H_2O$ system [534]. For instance, at a temperature of 80–100°C, the condensate composition corresponds to a 30–33% wt. HF solution.

Investigations of the plasma chemical decomposition of tantalum-containing fluoride solutions indicated no significant differences in the process and product parameters compared to the corresponding decomposition of niobium-containing fluoride solution [529, 532]. The particle diameter, shape and specific surface area of both niobium oxide and tantalum oxide powders attest to a gas-phase mechanism of the interaction, with sequential condensation and agglomeration of the oxides.

Table 66 presents a comparative analysis of different methods for the production of tantalum and niobium oxides.

*Table 66. Comparative analysis of different possible methods of the production of tantalum and niobium oxide powders from strip solutions.*

| Method | Added components | Products | Waste products | Notes |
|---|---|---|---|---|
| Precipitation by ammonia solution | $NH_4OH$ solution | High-purity $Me_2O_5$ | $NH_4OH$ solutions contaminated by fluorine, gaseous ammonia and HF during drying and calcinating | Huge amount of liquid wastes, filtration and washing stages are very long and problematic |
| Precipitation by ammonia carbonate | Solid $(NH_4)_2CO_3$ | High-purity $Me_2O_5$ | $NH_4OH$ solutions contaminated by fluorine, gaseous ammonia and HF during drying and calcinating | Significantly less amount of liquid wastes, less problematic filtration and washing |
| Precipitation of ammonia peroxometalates | $NH_4OH$, $H_2O_2$, citric acid | Highest-purity $Me_2O_5$ | $NH_4OH$ solutions contaminated by fluorine and $H_2O_2$, gaseous ammonia and $O_2$ during decomposition | Less amount of liquid wastes, no problems with filtration and washing, but handling of peroxide compounds is dangerous |
| Plasma chemical decomposition | No chemicals are added | Ceramic-grade $Me_2O_5$; reusable HF solutions | Vapors of water and HF | Special equipment is required |

## 8.5. K–salt production

Potassium heptafluorotantalate, $K_2TaF_7$, or as it is called by its commercial name K–salt, is a starting material for tantalum metal production. K–salt is produced by adding potassium fluoride, KF, or potassium chloride, KCl, to a tantalum strip solution that results from a liquid–liquid extraction process. In order to prevent hydrolysis and co-precipitation of potassium oxyfluorotantalate, a small excess of HF is added to the solution [24]. Another way to avoid the possible formation and co-precipitation of oxyfluoride phases is to use potassium hydrofluoride, $KHF_2$, as a potassium-containing agent. The yield of the precipitation depends mostly on the concentration of the potassium-containing salt and is independent of the HF concentration [535].

The main properties of potassium heptafluorotantalate in solid, molten and dissolved states were discussed in previous chapters of the monograph and are also collected and discussed in review [536].

The particle size of precipitated potassium heptafluorotantalate is one of the more important parameters. In order to achieve a certain particle size, potassium salts are added to the hot tantalum strip solution as a hot solution. The mixture is cooled down at a specific rate in order to enable the precipitation and crystallization of K–salt in the form of small, individual crystals.

Potassium heptafluorotantalate, $K_2TaF_7$, precipitates in the form of transparent needles. The precipitated particles must not be too fine, since fine powder usually promotes co-precipitation and adsorption of some impurities from the solution. Even niobium can be adsorbed by the surface of $K_2TaF_7$ developed during precipitation, as shown by Herak et al. [535]. On the other hand, the precipitation of large K-salt crystals should not be strived for either. Laboratory and industrial experience indicates that excessively large crystals usually contain small drops of solution trapped within the crystals. This "occluded" solution can remain inside of the crystal until drying and will certainly lead the hydrolysis of the material.

Precipitated K–salt crystals are carefully filtrated and washed so as to separate them from the mother solution. Drying of filtrated K–salt is also a very delicate and important process that must be performed under conditions that avoid hydrolysis of the material. Potassium heptafluorotantalate is sensitive to water, basic compounds and alcohols, especially at elevated temperatures. The main product of K–salt hydrolysis is Marignac's salt. For a long time it was believed that the composition of Marignac's salt is $K_4Ta_4O_3F_6$. However, X–ray crystal structure analysis and precise chemical analysis of the

compound have indicated that the actual composition of Marignac's salt is $K_2Ta_2O_3F_6$ [153, 215].

Based on the above composition, the hydrolysis of potassium heptafluorotantalate can be described as follows:

$$2\,K_2TaF_7 + 3\,H_2O = K_2Ta_2O_3F_6 + 2\,KF + 6\,HF \qquad (163)$$

If Equation (163) occurs in the solution during the precipitation of K–salt, KF and HF dissolve in the aqueous phase, and $K_2TaF_7$, contaminated with $K_2Ta_2O_3F_6$, will precipitate in the form of turbid crystals. In the case of hydrolysis during drying or storing, the potassium fluoride forms as a different phase. Separated KF imparts a hygroscopic property onto the product, since K–salt itself is not a hygroscopic compound. Moisture that is absorbed by KF causes the continuation of the $K_2TaF_7$ hydrolysis. Thus, the K–salt, which is contaminated with oxyfluorotantalate of potassium, displays an elevated oxygen level and seems to be "moisturized".

To minimize the possibility of contaminating the material during hydrolysis, it is recommended to dry the K–salt by slowly increasing the temperature, but not exceeding 160°C.

It is obvious that vacuum drying will not prevent the hydrolysis. On the contrary, evacuation of the air might stimulate and accelerate the hydrolytic process because HF saturation pressure is higher than that of water.

Additional purification of the product and improvement of particle size and shape can be achieved by re-crystallization. The process consists of sequential dissolutions of potassium heptafluorotantalate in appropriate solutions at increased temperatures, filtration of the solution to separate possible insoluble parts of the product and cooling of the filtrated solution at a certain rate. The precipitated crystals are filtrated, washed and dried to obtain the final product. Re-crystallization can be performed both after filtration of the preliminary precipitated salt or after drying if the quality of the product is not sufficient. HF solutions of low concentrations are usually used for re-crystallization. In general, even water can be used as a solvent if the process is performed fast enough. Nevertheless, practical experience suggested the use of a 30–40% HF solution within the temperature interval of 80-25°C, and a cooling rate of about 8–10°C per hour. The above conditions enable to achieve an acceptable process yield and good performance of the product.

Re-crystallization also leads to a significant reduction in the level of carbon and oxygen impurities; however, the reduction of cationic impurities is usually not efficient. To prevent co-precipitation of complex fluorotantalates of polyvalent metals, some suitable complexonates are added to the solution.

K–salt undergoes a phase transition at 202°C, which is characterized by a significant density change, and which leads in turn to the shattering of the initial crystals to form fine powder. This effect is so strong that pure potassium heptafluorotantalate can never be obtained in the form of a monolithic block. After melting and subsequent cooling, the phase transition occurs at 202°C, leading to a strong density change that shatters the block into fine separated parts.

Potassium heptafluoroniobate, $K_2NbF_7$, generally exhibits very similar behavior. The most important difference is that $K_2NbF_7$ is significantly more sensitive to moisture. The hydrolysis of potassium heptafluoroniobate yields $K_2NbOF_5$:

$$K_2NbF_7 + H_2O = K_2NbOF_5 + 2\,HF \qquad (164)$$

Another problem is that $K_2NbOF_5$ is extremely hygroscopic. The absorbed water converts the compound into crystal hydrate:

$$K_2NbOF_5 + H_2O = K_2NbOF_5 \cdot H_2O \qquad (165)$$

The presence of hydrated material causes the hydrolysis to continue at an increased temperature and the separating of HF affects the equipment leading to an additional contamination of materials or products manufactured using $K_2NbF_7$.

Table 67 presents some properties of potassium heptafluorotantalate, $K_2TaF_7$, as compared with potassium heptafluoniobate, $K_2NbF_7$.

*Table 67. Some properties of $K_2TaF_7$ and $K_2NbF_7$.*

| Properties | $K_2TaF_7$ | $K_2NbF_7$ |
|---|---|---|
| CAS # | 16924-00-8 | 16924-03-1 |
| Formula Weight | 392.14 | 304.10 |
| Density, g/cm$^3$ | 4.11 | 3.19 |
| Syngony | Monoclinic | Monoclinic |
| a, b, c, (Å), β° | 5.856; 12.708; 8.513; 90.17 | 5.846; 12.693; 8,515; 90 |
| Space group | $P2_1/c$ | $P2_1/c$ |
| Refractive indexes | 1.414 and 1.418 | 1.435 and 1.445 |
| Phase transition, °C | 202 (reversible transition occurring with strong density change and crystals cracking) | 202 (reversible transition occurring with strong density change and crystals cracking ) |
| Melting point, °C | 746 (incongruent melting) | 732 (incongruent melting) |
| Solubility in water | Slightly soluble in water | Soluble in water |
| Hydrolysis products | $K_2Ta_2O_3F_6$ + HF + KF | $K_2NbOF_5 \cdot H_2O$ + HF |
| Ions in HF solutions | $TaF_7^{2-}$ and $TaF_6^-$ | $NbOF_5^{2-}$ and $NbF_6^-$ |
| Ions in melt | $TaF_6^-$ and $TaF_7^{2-}$ | Mostly $NbF_6^-$ |

## 8.6. The production of tantalum and niobium metals by reduction of fluoride melts

### 8.6.1. General notes

Several methods are described for the production of tantalum and niobium metal. Metals can be obtained by reduction of pentachlorides with magnesium, sodium, hydrogen or by thermal decomposition in vacuum [24, 28]. Oxides can be reduced using carbon, aluminum, calcium, magnesium [28, 537, 538] or alkali and rare earth metals [539].

In line with the main subject of this monograph, we will discuss the reduction of complex fluoride compounds.

Only two processes of tantalum metal production are of worldwide commercial significance. These are the electrolysis of fluoride–chloride melts containing potassium heptafluorotantalate, $K_2TaF_7$, and tantalum oxide, $Ta_2O_5$, and the reduction with sodium of K–salt or K–salt that is dissolved in potassium fluoride–chloride melts.

### 8.6.2. Electrolysis of melts

Electrochemical reduction of tantalum in molten halide systems containing potassium heptafluorotantalate, $K_2TaF_7$, and tantalum oxide, $Ta_2O_5$, was originated by Balke [540] and realized as an industrial process in the United States by Fansteel Metallurgical Corporation. The most typical electrolyte consists of a eutectic mixture of KF – KCl with up to 25% wt. $K_2TaF_7$. Tantalum oxide is added to prevent an anodic effect. Three types of electrolytic baths are used: crucible–cathode, crucible-anode and cold crucible. The baths are shown schematically in Fig. 140 and the corresponding processes are described as follows. The first process is performed using an iron crucible as the melt container and cathode, and a graphite rot as the anode. The suspended anode is raised during the collection of the reduced tantalum in the crucible [37]. The second type is the opposite of the previous process, and consists of a graphite crucible-anode and a suspended cathode made of stainless steel, nickel, nickel-based alloys or some other suitable material. The third process consists of a metal crucible (container) that is equipped with external cooling and with suspended anodes and a cathode. The energy required to melt the material is provided by an electric current that is passed through the melt.

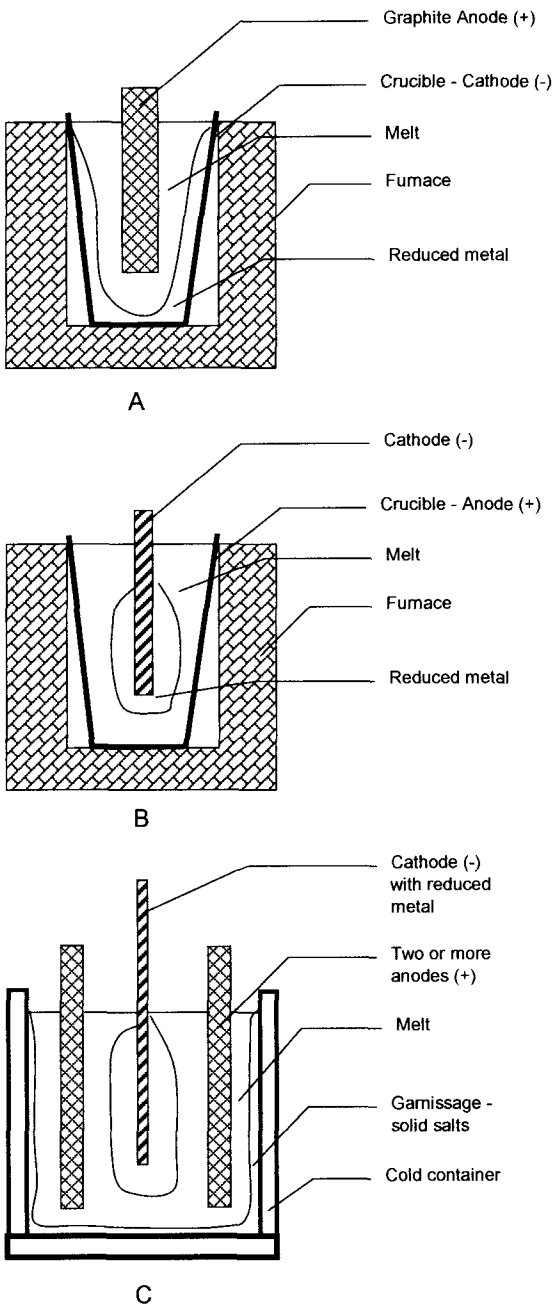


*Fig. 140. Three main types of electrolytic baths:*
*A – Crucible–cathode; B – Crucible-anode; C – Cold crucible.*

External cooling ensures the formation of a solid salt on the surface of the container, which protects the material the container is made of from interacting with the molten material [37, 541].

After the end of the interaction, the melt is cooled down to room/ambient temperature, and the metal and salts are crushed and leached using mineral acids and water to separate the metal. The metal precipitates mostly in the form of dendrites, which are pressed and sintered into bars to be converted into wire, sheet and powder.

A similar electrolyte, containing potassium heptafluoroniobate, $K_2NbF_7$, can be used for the electrolytic reduction of niobium [37, 542 - 544]. No industrial application, however, was found for the electrolysis of niobium in fluoride–chloride melts.

An ongoing debate continues among researchers regarding the mechanism of the electrochemical reduction of tantalum in fluoride melts. No unified model exists for the process. Espinola et al. [545] concluded, based on an investigation of the electrochemical reduction of tantalum from a molten LiF–NaF–KF eutectic solution, that the process takes place in two stages. The first, reversible step involves the transfer of two electrons:

$$Ta^{5+} + 2\,\bar{e} = Ta^{3+} \qquad (166)$$

In the second step, three other electrons are transfered to the tantalum ion, yielding a completely reduced tantalum metal atom:

$$Ta^{3+} + 3\,\bar{e} = Ta^{0} \qquad (167)$$

The majority of researchers, however, are inclined to believe that the tantalum reduction process takes place in a single step. Experimental results and discussions confirm that tantalum is reduced from fluoride, fluoride–chloride and oxyfluoride melts containing $K_2TaF_7$, via a single stage in which five electrons are transfered [546 – 548]:

$$Ta^{5+} + 5\,\bar{e} = Ta^{0} \qquad (168)$$

Single-stage reduction of tantalum seems to be typical mostly for fluoride complexes due to the ionic nature of the bonds.

Substitution of the fluoride ligands by ions that lead to higher covalence of the bonds can alter the mechanism of tantalum reduction. For instance, the investigation of pure chloride systems containing tantalum pentachloride,

$TaCl_5$, and a eutectic mixture of CsCl and NaCl, shows that tantalum reduction occurs in two steps [550]:

First step: $Ta^{5+} + \bar{e} = Ta^{4+}$ (169)

Second step: $Ta^{4+} + 4\,\bar{e} = Ta^{0}$ (170)

Niobium undergoes a two-stage electrochemical reduction from potassium heptafluoroniobate, $K_2NbF_7$, that is dissolved in fluoride–chloride melts [550 – 553]:

First step: $Nb^{5+} + \bar{e} = Nb^{4+}$ (171)

Second step: $Nb^{4+} + \bar{e} = Nb^{0}$ (172)

The niobium reduction mechanism is also confirmed by the observation of the slow spontaneous reduction of $Nb^{5+}$ to $Nb^{4+}$ in a LiF – NaF – KF eutectic melt, even with no added Nb metal. In the presence of a stoichiometric amount of Nb metal, the spontaneous reduction occurs more rapidly [554].

The electrochemical behavior of niobium in different types of molten electrolytes and the influence of ligand substitution in niobium-containing complex ions on the reduction mechanism is comprehensively reviewed by Polyakov [555].

Anode processes yield gaseous chlorine, fluorine, carbon chloride or fluoride. In the case of melts containing dissolved tantalum oxide, carbon oxides (mostly carbon dioxide) are formed on the graphite anode [28, 37].

The addition of oxygen ions, in the form of tantalum oxide or niobium oxide, to the respective melts alters their complex structure and impacts the products of the electrochemical reduction [556]. Nevertheless, tantalum and niobium display significantly different electrochemical behavior in similar oxyfluoride – chloride melts. Kazain et al. [557] found that KCl – NaCl melts containing $K_2TaF_7$ or $K_2NbF_7$, which are contaminated by oxygen in equal amounts, result in different oxygen concentrations in electrochemically reduced tantalum and niobium. Tantalum metal obtained by electrolysis contained oxygen at a concentration about 10 times lower than that of niobium that was obtained in a similar process. Grinevitch et al. [558] also reported on the investigation of the effect of oxygen on the electrolysis of tantalum and niobium in oxyfluoride – chloride melts, and found that for tantalum, a wider

range of melt compositions exists that enable the production of metal with negligible oxygen contamination. Nevertheless, the melt compositions and electrolysis conditions can be adjusted, either for the preparation of pure tantalum or niobium metals or for their oxygen-containing compounds. This aspect affords the possibility of performing the synthesis of different novel compounds by electrochemical reduction of oxyfluoride melts [558].

The anionic composition of the cathodic product is not the only parameter that can be controlled through electrolysis conditions. Grinevitch et al. [559] reported on the investigation of the co-deposition of tantalum and niobium during the electrolysis of fluoride – chloride melts. Appropriate electrodeposition conditions were found that enable to obtain either pure niobium or alloys.

It was also announced that tantalum diboride can be successfully synthesized from chloride – fluoride melts using the electrochemical method [560].

Electrolytic refining of tantalum and niobium is of great interest to researchers dealing with electrolysis. The refinery process is based on the use of a consumable anode made of some tantalum or niobium precursor material. Elyutin et al. [561] investigated the consumable anodic processes and kinetic characteristics of the dissolution of Ta, Nb, Fe, Ni and Mo. Elyutin, Kartsev and Kovalev [562] showed that niobium, which was obtained by carbothermic or alumothermic reduction, can be refined by electrolysis using molten salts. The product of the single-step process is sufficiently pure to be used as a precursor in the fabrication of ingots for application in ultra-high frequency techniques. The main parameters for refining tantalum using the electrochemical method were investigated and reported by Elyutin et al. [563]. It was indicated that the crystal size and current efficiency of the obtained tantalum deposit increase if 10–12% NaF is added to the electrolyte, as well as at enhanced $K_2TaF_7$ concentration and process temperature. The impurity behavior and electrolytic process parameters required to ensure the obtaining of pure tantalum from precursors that contain several percents of Nb, O, Fe, Ni and Mo were investigated and described in [564].

Another application of the electrolysis of tantalum and niobium in fluoride melts is in the preparation of intermetalic compounds as a result of the interaction between the electrochemically precipitating metal and the cathode material. Based on an investigation of the electrochemical reduction of $K_2TaF_7$ or $K_2NbF_7$ in a LiF – NaF melt on nickel cathodes, Taxil and Qiao [565] determined the appropriate conditions for the formation of $TaNi_3$ or $NbNi_3$ in the form of stable phases in the bulk of the obtained layer.

Kolosov, Matychenko and Novichkov reported [566] on the investigation of the electrolysis of pure niobium from $K_2NbF_7$ dissolved in a LiF – NaF – KF eutectic melt (called a FLINAK melt). Conditions for obtaining highly uniform niobium coatings thicker than 5 μm were determined.

Decroly, Muchtar and Winand [567] investigated the electrocrystallization of tantalum and niobium from molten fluoride mixtures containing $K_2NbF_7$ or $K_2TaF_7$. A comparative analysis of the results shows that the current efficiency is generally much lower in the case of niobium than for tantalum, under the same experimental conditions. It was also found that an increase in the $K_2NbF_7$ or $K_2TaF_7$ content in the bath leads to a significant decrease in the current efficiency, and the effect is much stronger in the case of niobium-containing melts. Increasing the $K_2NbF_7$ or $K_2TaF_7$ concentration also leads to a decrease in grain size of the electrochemically precipitated metals. In addition, the grain size decreases with the increase in temperature, while the current efficiency achieves a maximum at about 900°C.

Similar results were reported by Freidin et al. [568]. Moreover, a correlation was reported [360] between the particle size of tantalum powder obtained by electrolysis of fluoride – chloride melts and its electric conductivity.

Summarizing the reported results, it is reasonable to conclude that the current efficiency and grain size depend on the complex structure of the melts containing complex tantalum or niobium fluoride ions. As was discussed in Chapter 5, the melts consist of two types of complexes with coordination numbers equal to 6 or 7: $MeF_6^-$ and $MeF_6X^{2-}$, where Me = Ta or Nb and X = F or Cl. The main difference between the two types of ions in terms of their electrochemical behavior is related to their different polarity. The interaction of anions with the cathode can be conceived as an interionic interaction between a complex anion and cation. From this point of view, heptacoordinated ions $MeF_6X^{2-}$ seem to be the most effective for the electrochemical reduction process. Hence, increasing the concentration of $K_2NbF_7$ or $K_2TaF_7$ in the melts initiates the predominant formation of hexacoordinated complex ions, $TaF_6^-$ or $NbF_6^-$, which leads to a relatively low current efficiency and small grain size of the reduced material. Decreasing the $K_2NbF_7$ or $K_2TaF_7$ content in the melts shifts the ionic equilibrium toward the formation of heptacoordinated complex ions. $MeF_6X^{2-}$ complex ions, with their significantly higher polarity, ensure a higher current efficiency and enhanced crystal size of the reduced material. The difference in the electrochemical behavior between niobium- and tantalum-containing melts is related to the fact that the equilibrium between $NbF_6^-$ and $NbF_6X^{2-}$ complexes undergoes a much stronger shift toward the formation of $NbF_6^-$ ions. The formation of heptacoordinated complex ions can

be achieved at relatively low concentrations of $K_2NbF_7$. In the case of tantalum-containing melts, the complex structure is different. Even pure molten $K_2TaF_7$ already consists of both types of complex ions (see Chapter 5).

It should be noted that in addition to changes in $K_2NbF_7$ or $K_2TaF_7$ concentrations that afford control over the complex structure and electrolysis parameters, the cation type also affects the equilibrium between the complex ions. The heptacoordinated complexes become increasingly dominant when progressing along the cation series from Li to Cs.

Catodic reduction and anodic oxidation of tantalum and niobium can also be performed in other molten media. Descriptions of processes that take place in chloride molten systems can be found in the literature [569 – 571].

Use of low-temperature molten systems for electrolytic processes related with tantalum and niobium and other rare refractory metals seems to hold a promise for future industrial use, and is currently of great concern to researchers. The electrochemical behavior of tantalum, niobium and titanium in low-temperature carbamide-hilide melts has been investigated by Tumanova et al. [572]. Electrodeposition of tantalum and niobium from room/ambient temperature chloroaluminate molten systems has been studied by Cheek et al. [573].

### 8.6.3. Reduction of tantalum and niobium with sodium

Berzelius reported on the results of the first reduction of tantalum from $K_2TaF_7$ using metallic potassium in 1825 [574]. About thirty years later, Rose obtained sufficiently pure tantalum in an interaction between $Na_2TaF_7$ and metallic sodium [575]. The methods elaborated by Berzelius and Rose provided a basis for the development of the industrial-scale production of tantalum by the reduction of $K_2TaF_7$ using metallic sodium.

The sodium reduction process was first implemented in Germany by Siemens and Halske A.G. and it remained a principally European method, while the American tantalum industry was founded exclusively on the electrolysis of molten fluorides [28, 576]. The production of tantalum by sodium reduction has gained worldwide acceptance and currently, nearly 90% of the world's tantalum is produced by the sodium reduction method [538].

The main reason for the tantalum industry's drive toward the sodium reduction process is an increasing demand for tantalum powder by tantalum capacitor manufacturers. The modern tendency of the electronics industry to miniaturize their components calls for the improvement of tantalum powder

production, which focuses mainly on the development of high purity materials with high specific charges. The properties required of tantalum powder cannot be achieved by means of electrolysis, whereas the sodium reduction method affords very broad possibilities for the production of high-purity and high-specific charge tantalum powders. At present, nearly all capacitor-grade tantalum powder is produced exclusively by sodium reduction of molten $K_2TaF_7$ [576].

The process is based on the interaction between potassium heptafluorotantalate and metallic sodium:

$$K_2TaF_7 + 5\,Na = Ta + 2\,KF + 5\,NaF \qquad (173)$$

The interaction in Equation (173) is exothermic and occurs with the generation of 713 Kcal of heat per 1 kg of mixture, as reported by Bose and Gupta [538]. Kolchin and Vol'dman [577] investigated the thermal effects of tantalum and niobium reduction by sodium from molten $K_2TaF_7$ and $K_2NbF_7$, respectively. The interaction with $K_2NbF_7$ is similar to that shown is Eqaution (173). It was found that the thermal effects in the case of tantalum and niobium correspond to 385 cal/g and 510 cal/g at 1000°C, respectively.

The process of sodium reduction is generally performed by one of two methods: direct reduction of $K_2TaF_7$ or reduction of $K_2TaF_7$ dissolved in molten alkali halides. The first method consists of a direct interaction between $K_2TaF_7$ and Na that are arranged in alternating layers in a stainless steel crucible. The crucible is heated to initiate the reduction process. After cooling of the reactor, the excessive sodium is neutralized and the metal-salt mixture cake is removed from the crucible. The cake is crushed and the salts are leached out with water or appropriate solvents and finally dried. The direct reduction method usually results in a very coarse and non-uniform powder due to the inability to control process parameters. The powder produced by the direct method is usually used for further melting by electron-beam furnaces to obtain tantalum ingots. Tantalum that is treated by electron-beam melting can also be crushed by the hydration-dehydration method to obtain coarse tantalum powder that is used for tantalum capacitors of relatively low capacitance but high voltage applications. Fig. 141 shows the flow chart for the direct reduction process.

Despite the above disadvantages, some investigations show possible directions for further improvement and development of the process for the production of tantalum powder suitable for the manufacture of capacitors with no additional electron-beam melting and special crushing.

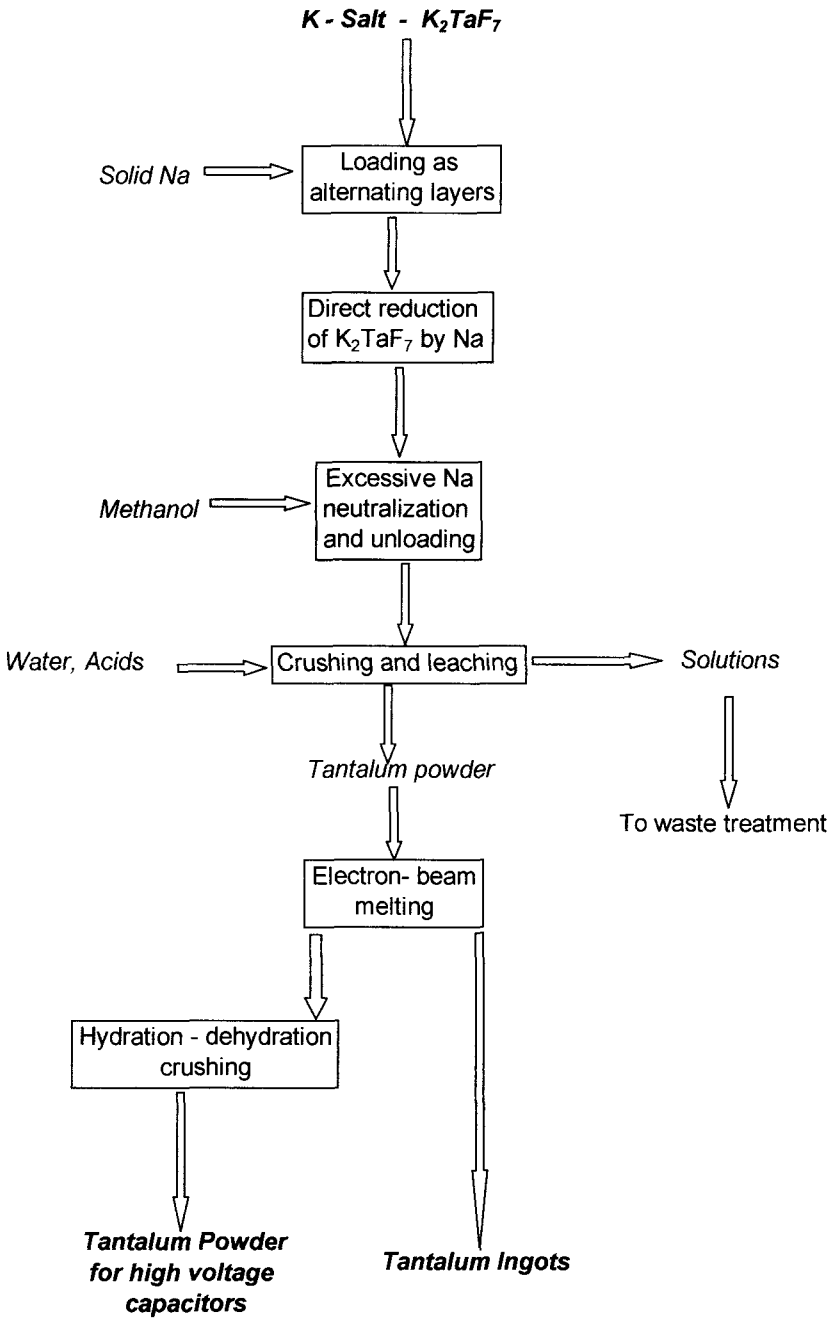


*Fig. 141. Flow chart of the direct reduction of $K_2TaF_7$ by sodium.*

Jain, Bose and Gupta [578] reported on pilot plant testing intended for the production of capacitor-grade tantalum powder. Two types of reactors were investigated and compared. The first type was a static bomb-type reactor with alternating layers of $K_2TaF_7$ and sodium. The second reactor was specially designed to maintain the interaction with continuous stirring, and the initial components – molten $K_2TaF_7$ and sodium – were fed into the reactor so as to maintain a semi-continuous process. It was found that the product obtained with the modified reactor equipped with stirrer, had a higher degree of purity and better particle size distribution. In addition, the modified reactor provided higher product yields compared with the regular process using the static bomb-type reactor.

In order to improve mixing of the interacting components, a method was patented according to which loading of molten sodium or potassium is effected by means of a distributor that has, in addition to the stirring action, twenty four 0.5 mm diameter holes [579]. The method refers to the reduction of both tantalum and niobium from $K_2TaF_7$ and $K_2NbF_7$ using molten sodium or potassium.

Further improvement of the process was achieved by the preliminary mixing of the components. A process was patented [580] that includes the mixing of thermally activated $K_2TaF_7$ with Na and KCl at a molar ratio of 1:5:1.5. The obtained paste is placed in tantalum vessels, cooled down to <50°C and ignited under air atmosphere at 700-780°C. The method gives a relatively high yield and the product, after appropriate thermal treatment, is classified as capacitor-grade powder with improved mechanical properties and increased breakdown voltage.

Tantalum powder with a smaller particle size compared with that obtained by the regular process was obtained by thermal treatment at 700-950°C of a mixture containing $KTaF_6$, $NH_4F$ and sodium [581]. Eighty three percent of the tantalum powder obtained appears to be smaller than 200 mesh.

In order to produce coarse-grained tantalum or niobium powder it is recommended to perform the reduction of molten $K_2TaF_7$ or $K_2NbF_7$ with sodium or potassium in the presence of tantalum or niobium metal particles, which are added to aid nucleation [582]. It is reported that tantalum powder with an average particle size of 2.7–4.2 μm was obtained at a yield of 90.1–94%.

The impact of the excess sodium on the properties of tantalum powder obtained by direct reduction of $K_2TaF_7$ with sodium in the stainless steel bomb reactor was investigated by Yoon et al. [583]. It was shown that the yield and amount of fines strongly depend on the amount of excess sodium present. With the increase in sodium excess, the proportion of the fine powder fraction (approximately 325 mesh) decreases appreciably and the yield of the process

improves to 94%. At a 5% sodium excess, the tantalum particle size increases up to 4 μm.

The reduction of $K_2TaF_7$ can also be performed using sodium vapors [584]. This process is conducted at an Na pressure as low as 0.1 torr, which enables the removal of interferring gases such as N, O and $H_2O$. The interaction begins at 350°C. The temperature further increases up to 800°C to prevent the condensation of sodium and the formation of colloidal tantalum powder. The product of the interaction is removed from the reactor after cooling and treated with boiled HCl and HF solutions. The method enables the production of coarse grain tantalum powder with 99.5% purity.

Attempts to adopt the process of direct reduction of $K_2TaF_7$ by sodium for the production of capacitor-grade powders are continuing in the direction of improving both the reduction process and the chemical leaching efficiency. Purushotham et al. [585] analyzed the main characteristics of the powder produced by direct reduction of the diluted melt. It was reported that the powder contained higher levels of impurities, but the authors nevertheless believe that the impurity levels can be reduced to acceptable limits.

The leaching process aims to remove the salts from the metal – salt mixture but also enables to achieve additional purification of the tantalum powder. Keller and Martin [586] found that the application of a leaching solution containing 0.1–10% HF and 0.5–10% $H_2O_2$ leads to a decrease in the oxygen content of the final tantalum powder obtained from the reduction of $K_2TaF_7$ with sodium.

An effective leaching process that enables to reduce residual oxygen content in tantalum powder obtained from the reduction of $K_2TaF_7$ with sodium, has been developed and proposed by Martin [587]. According to this process, the cake obtained after reduction is crushed to 4–100 mesh and leached with a solution containing sulfuric acid and aluminum sulfate, $Al_2(SO_4)_3$. The amount of added aluminum salt is calculated to correspond to a Al:F ratio of (0.17–1.0):1. The mixture is agitated for 60 minutes, allowed to settle and decanted. The residual solids are treated again with the same solution. The residual solids from the second treatment are leached with solutions containing HF and $H_2O_2$, followed by a solution containing $H_2SO_4$ and finally by an MeOH solution. The resulting solids are rinsed with water and dried in vacuum. The final product usually contains 0.02% oxygen.

The separation of the excess unreacted sodium is also subject to investigation and development. Miyazaki and Kuroki [588] proposed a reactor system for the reduction of $K_2TaF_7$ or $K_2NbF_7$ with Na or K, respectively. According to this method, the reduced melt is tapped into a special chamber for solidification, while unreacted Na or K is trapped with a condenser in the gas phase for recycling.

Gruner, Ibold and Naumann [589] proposed the performance of thermal treatment of the cake obtained after sodium reduction of $K_2TaF_7$ in vacuum. The application of a temperature of 800-1050°C and a residual pressure of 0.013–1.33 Pa was recommended. The process is performed with intermittent vibration in order to promote the separation of the impurities. It is reported that the resulting tantalum contains 31 and 40 ppm of Na and K, respectively.

Significant improvement of tantalum powder properties was achieved by the application of molten alkali halides as solvents for potassium heptafluorotantalate, $K_2TaF_7$. Variation of the initial concentration of $K_2TaF_7$ in the melt, stirring and rate of sodium loading enable a well-controllable production of tantalum powder with a wide variety of specific charges. Heller and Martin [590] proposed the use of a reactor equipped with a stirrer in 1960. Fig. 142 shows a typical scheme of the reactor [24, 576]. All metal parts of the reactor are made of nickel or nickel alloy.

The complete production process of capacitor-grade powder includes the reduction of $K_2TaF_7$ that is usually diluted in molten KCl and KF or some other molten alkali halide, followed by leaching, agglomeration and deoxidation of the product. Fig. 143 presents the flow chart of the process.

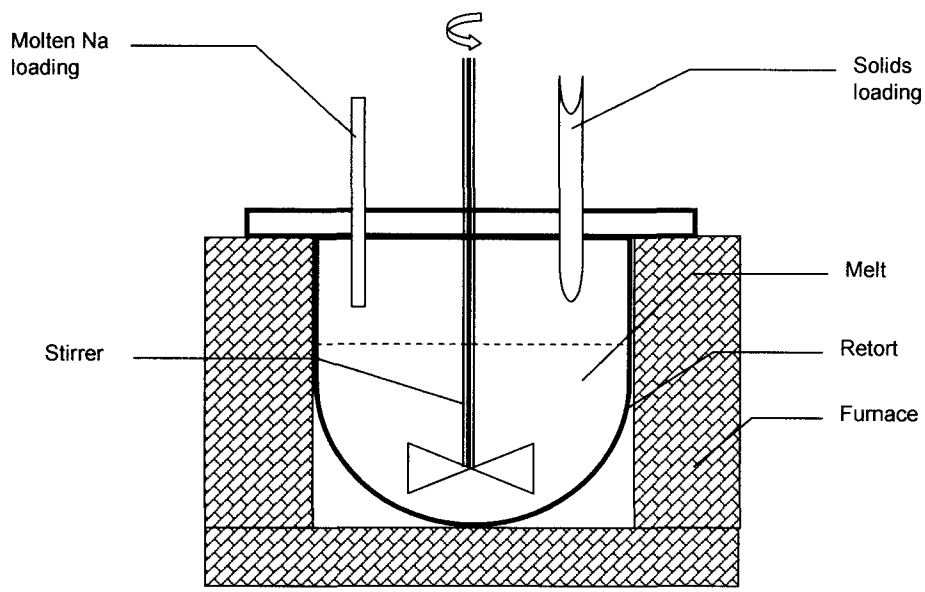


*Fig. 142. Schematic structure of reactor for the reduction by molten sodium of $K_2TaF_7$ diluted in molten salts.*

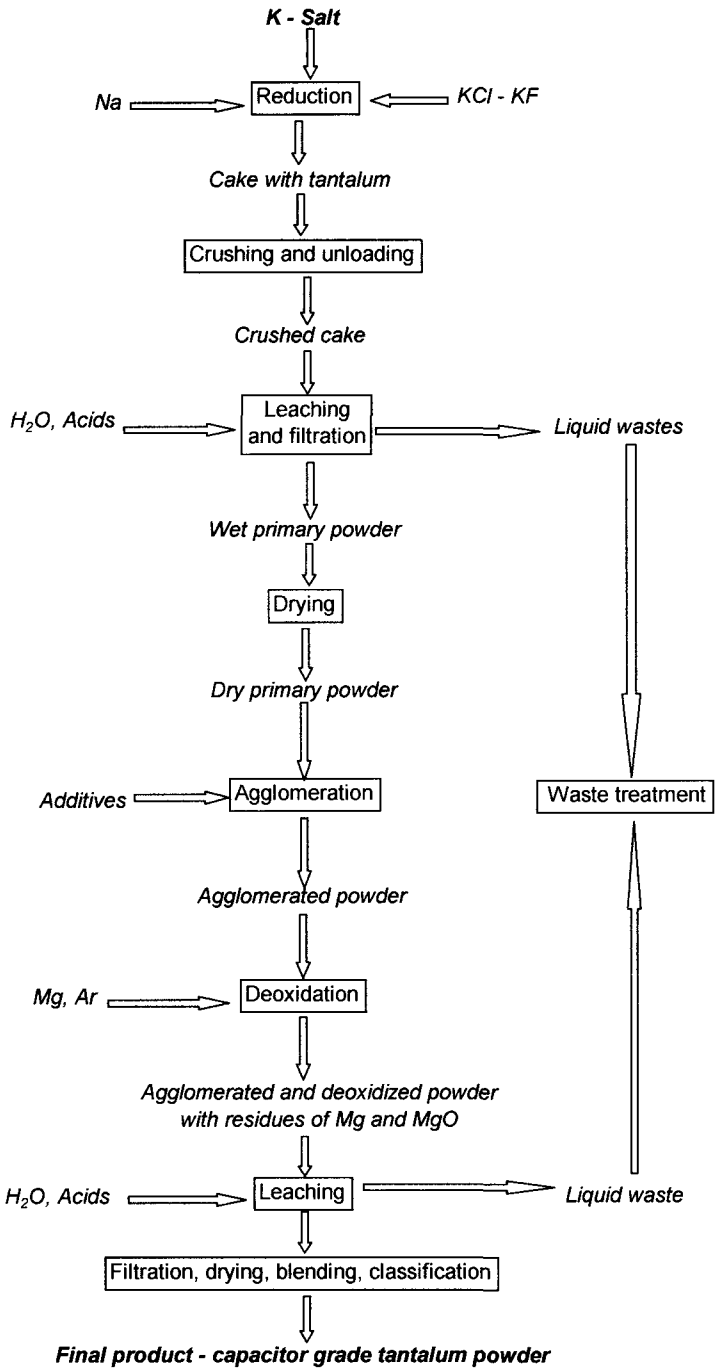


*Fig. 143. Flow chart for production of capacitor-grade tantalum powder.*

The reduction process is performed as follows. Diluents – potassium chloride (KCl) and potassium fluoride (KF), or some other alkali halite and potassium heptafluorotantalates ($K_2TaF_7$) – in predetermined concentrations are loaded into the reactor and melted under an inert atmosphere. After achieving the designed process temperature, molten purified sodium is loaded into the stirred melt at a certain rate, in an amount corresponding to the added amount of $K_2TaF_7$, but with some excess to ensure the completion of the tantalum reduction and some growing and agglomeration of tantalum particles. After finishing the sodium loading and subsequent stirring of the mixture, the reactor is cooled down enough to enable further safe handling. The cake is removed from the retort, crushed and leached with water to separate salts and possibly reduce impurities. The residual metal tantalum powder is separated from the solubale salt-containing solutions, leached by acids of relatively low concentrations, washed and, following final filtration, dried in a vacuum furnace at 150-200°C. The tantalum powder resulting from the reduction process is called a primary powder. The purity, particle size and shape of the primary powder define the main properties of the final capacitor-grade tantalum powder.

The main metallic impurities that contaminate the primary powder, due to chemical corrosion of the retort and other metal parts of the reactor, are Fe, Ni and Cr. From this point of view, reactors that are equipped with larger retorts usually provide better purity due to a relatively low ratio between the internal surface of the wet metal parts of the reactor and the total volume of the melt. Recent investigations on the decreasing of Fe, Ni and Cr impurities during the sodium reduction process were performed by Li [591]. It was shown that one of the most effective ways to reduce contamination of the product is to reduce the duration of time $K_2TaF_7$ is present in the reactor.

To achieve additional purification of tantalum obtained from sodium reduction of $K_2TaF_7$ in the presence of diluent salts, Chang [592] developed a process consisting of two steps of initial material loading. The first step includes pretreating the reactor and is performed by loading a small amount of sodium and sodium chloride into the reactor prior to the loading of $K_2TaF_7$. The preloaded reactor is purged with argon and heated to 850°C for proper drying and subsequent melting. The second step consists of the reduction and is performed by simultaneous loading into the pretreated reactor of a predetermined ratio of molten sodium and $K_2TaF_7$. The mixture is mixed for two hours, cooled, removed, washed and dried. It is claimed that the procedure results in purified tantalum powder with a high surface area. The Fe, Ni, Cr and Mo impurity levels do not exceed 5 ppm each, whereas the product of the process, in which no preliminary addition of sodium is made, is significantly more contaminated by Fe and Ni.

One of the main reasons for the reduced tantalum contamination is moisture remainders and the hydrolysis of potassium heptafluorotantalate. The mechanism is very simple. The remainder of moisture that enters the reactor along with $K_2TaF_7$ and the diluent salts interacts upon heating with $K_2TaF_7$, yielding potassium oxyfluorotantale and hydrogen fluoride, HF. The hydrogen fluoride, being in the form of a gas, dissolved gas or hydrofluorides, interacts aggressively with the metal part of the reactor causing contamination of the final product. There is no doubt that the moisture and resultant products of the hydrolysis significantly contaminate the metal powder with oxygen. In the case of the reduction of $K_2NbF_7$, the contamination effect is more dramatic due to a higher tendency and higher rate of hydrolysis characteristic of complex niobium fluoride compounds.

It is, therefore, required that all initial compounds be dried properly prior to performing the reduction. This procedure is not at all trivial and refers, first of all, to the diluent salts, and especially to potassium fluoride, KF, which is characterized by a strong hygroscopic property and a tendency to form stable crystal hydrates. The problem of contamination due to hydrolytic processes can usually be resolved in two manners. The first is to apply another tantalum-containing complex fluoride compound that does not undergo hydrolysis. The second involves the adjustment of the reduction process parameters and use of some additives that will "collect" the oxygen present, in the form of water, hydroxyl groups or other compounds.

According to the method developed by Izumi [593], magnesium chloride is added to the reactor as a diluent, along with $K_2TaF_7$ and NaCl, prior to the reduction process. The powder obtained by the above method is washed and treated thermally at 1200°C in vacuum. The final product has a specific capacitance of 12,000 μC/g, contains 1800 ppm of oxygen, and its Mg content is as low as 20 ppm.

The oxygen level in primary tantalum powder can be also increased by adjustment of the reduction process parameters [594] or by controlled step-wise additions of sodium to the reactor [595].

The reduction process parameters and composition and physical-chemical properties of the melts define the particle size and shape of the reduced tantalum powder. Kolosov et al. [596] investigated the influence of the melt surface tension on the morphology of the tantalum powder. They found that decreasing the surface area of the initial melt leads to the formation of powders with a higher specific surface area. Increasing the melt surface tension causes enlargement of fragments of dendritic particles and a corresponding decrease in their specific surface area.

The application of a high rate of reduction using an alkali metal in a molten salt bath was was proposed in order to produce tantalum or niobium powder with a desired particle size [597]. This process is performed using a molten $K_2TaF_7$ – NaCl system of 890 kg in total loading, containing about 51% wt. of $K_2TaF_7$. The reduction begins at an initial temperature of 640°C and stirring rate of 120 rpm. Liquid sodium is injected into the bath at a rate of 5.17 kg/min until a temperature of 820°C is achieved. The liquid sodium loading rate is then decreased to 1.563 kg/min. During that period, the temperature is maintained constant at 820°C by forced cooling for 66 minutes, the stirring rate is reduced down to 70 rpm, and the remaining 135.6 kg of sodium is added to the bath over 2.5 hours. Over 99% of the powder obtained by the above method is 80 mesh.

The concentration of $K_2TaF_7$ in the initial melt is the main parameter controlling the particle size and surface area of the reduced primary powder [598]. Typically, the increased concentration of $K_2TaF_7$ leads to the formation of coarse tantalum powder. According to Yoon et al. [599], the diluent prevents a strong increase in the temperature of the melt that is caused due to the exothermic effect of the reduction process. Based on the investigation of the reduction process in a $K_2TaF_7$ – KCl – KF system, it was shown that increased amounts of diluent lead to a decrease in particle size of the obtained tantalum powder.

Yoon et al. [600] investigated the influence of the process temperature on the yield of tantalum powder and amount of fine fraction obtained. The reduction was performed using $K_2TaF_7$ dissolved in a KCl – KF melt. The melt temperature varied in the range of 800-980°C. The analysis of the obtained results shows that the yield of the process increases at higher temperatures. In addition, higher temperatures lead to a decrease in the amount of fine fraction of tantalum powder produced. Nevertheless, it was noted that solely changing the process temperature does not ensure an improved yield.

Kim et al. [601] investigated the influence of both temperature and the excess amount of sodium compared with the stoichiometry of the interaction. The molten system $K_2TaF_7$ – KCl – KF was used for the experiments and the temperature varied in the range of 800-980°C. The excessive amount of sodium ranged from -10% to +10%. It was found that increasing either the temperature or the excess amount of added sodium led to an enhanced yield and increased the particle size of the tantalum powder. Optimal conditions were found to be 920°C and 5% excess reductant.

Chai and Zhong [602] investigated the melting properties of molten systems containing $K_2TaF_7$ and different alkali metal cations with respect to the optimization of the sodium reduction process. It was shown that the specific

capacitance of the tantalum powder obtained from the above molten systems decreases with the increase in the Na/K ratio.

Based on available results, it can be summarized that the particle size of tantalum powder increases (specific charge decreases) with the increase in temperature, $K_2TaF_7$ concentration and excess sodium. In addition, an increase in the specific surface area of the melt and Na/K ratio also leads to the formation of coarser tantalum powder. The most important conclusion is that for the production of finer tantalum powders with higher specific charges, the concentration of $K_2TaF_7$ in the melt must be relatively low. This effect is the opposite of that observed in the electrochemical reduction of melts.

Based on the results discussed in Chapter 5, it should be noted that lowering $K_2TaF_7$ concentrations leads not only to the dilution of tantalum-containing ions but also to a transformation of the melt structure. Melts that contain high concentrations of $K_2TaF_7$ consist mostly of $TaF_6^-$ complex ions, whereas lowering the $K_2TaF_7$ concentration leads to the formation of predominantly heptacoordinated complexes such as $TaF_7^{2-}$ and $TaF_6Cl^{2-}$. The equilibrium between the complexes can be formulated as follows:

$$TaF_6^- + X^- = TaF_6X^{2-} \qquad (174)$$

Higher temperatures, increased $K_2TaF_7$ concentrations and other factors mentioned above shift the equilibrium in Equation (174) to the left and lead to the formation of coarser tantalum particles. Form this point of view, it can be concluded that smaller hexacoordinated complexes, $TaF_6^-$, lead to the formation of coarser tantalum powder, whereas the predominant presence of larger heptacoordinated complexes ions initiates the formation of finer particles.

The discussion presented in Chapter 5 indicates that changing the $K_2TaF_7$ concentration is not the only way to transform the complex structure of the melt. Application of different halide ions or alkali metal ions can change the melt complex structure with no significant reduction in the tantalum concentration of the melt. Thus, the presence of alkali metal ions with lower polarizing potentials (Rb, Cs) shifts the equilibrium in Equation (174) to the right, towards the formation of predominantly heptacoordinated ions. This enables to obtain finer tantalum powder with a higher concentration of tantalum in the initial melt. It is assumed that the reduction of cesium heptafluorotantalate, $Cs_2TaF_7$, will ensure the production of fine powder at high concentrations of tantalum in the initial melt. The same effect can approximately be achieved using diluent salts containing high-polarity anions (Br, I).

The uniformity of tantalum powder is also a very important parameter of capacitor-grade tantalum powder. The loss of powder uniformity can initiate during the regular reduction process due to varying conditions at the beginning and end of the reduction process. At the end of the process, the concentration of tantalum in the melt is very low, while the sodium content increases. Based on the complex structure model of melts, it should be noted that the desired particle size of the powder is formed at the very beginning of the process, while the very fine fraction forms at the end of the process, independent of the initial content of the melt. The use of special equipment enables to perform a continuous reduction process with simultaneous loading of $K_2TaF_7$ and sodium, which can influence the improved uniformity of the primary powder [592, 603, 604].

After completion of the tantalum reduction process, the material is cooled down to a temperature that enables further operations. The cake is removed, crushed and leached with water, followed by mineral acid solutions, as discussed above. The separation of the metal powder from the solutions containing dissolved salts is performed by filtration. The wet leached product is dried and analyzed. The tantalum powder obtained cannot be applied immediately in the manufacture of tantalum capacitors due to insufficient reological properties. The primary powder has a relatively high specific charge and is usually characterized by a low bulk density and a very poor flow ability that prevents application of the powder in the industrial process of automatic pressing into pellets. In addition, the oxygen level of the primary powder is typically too high to achieve suitable electrical parameters of the anodes [605]. Therefore, in order to convert the primary powder into a true capacitor-grade powder, some post-reduction treatment steps are required.

To impart upon the powder necessary reological properties, the material is thermally treated in high vacuum. This process is called agglomeration. Some additives intended to prevent strong sintering of the parts during the agglomeration are added to the primary powder prior to the thermal treatment.

In order to reduce the oxygen content of the agglomerated powder, the material is treated using a special deoxidation process. The essence of the process is the reduction of the oxygen content in the tantalum powder by interaction with magnesium. The interaction is performed in an inert atmosphere at a temperature of about 900–1100°C [606]. The remainders of magnesium and magnesium oxide formed during the interaction are removed from the deoxidized powder by leaching.

Orlov et al. [607] investigated the process of tantalum powder deoxidation using both calcium and magnesium chips as oxygen getters. It is recommended to perform the process with calcium chips at temperature of 900-1300°C for

one hour, while the magnesium getter must be applied at a temperature range of 700-1100°C for 0.5–3 hours. It was found that the process enables the reduction of both oxygen and fluorine contents. Using the process on powders that have specific surface areas of 0.1–1 $m^2/g$, the oxygen content can be reduced from initial values of 0.3–1% wt. to a value of 0.05% wt.

Rare earth metals, as well as alkali earth metals, can be used as oxygen getters in the purification of tantalum powder. Osaku and Komukai [608] developed a method for the production of tantalum and niobium metal powder by a two-step reduction of their oxides. The second step was aimed at reducing the oxygen content and was performed by thermal treatment with the addition of rare metals. The powder obtained by the described method is uniform, had a low oxygen level and was suitable for application in the manufacturing of tantalum capacitors.

Subsequent processes related to the finishing of the capacitor-grade tantalum powder are beyond the scope of this monograph subject.

Modern requirements of the capacitor industry initiate further development of tantalum powder production processes. The tendency is to produce powder of higher purity with a higher specific charge and at lower cost. Further development of the processes can be successfully achieved based on current achievements in the chemistry of tantalum and niobium fluoride compounds.

# 9.

# MAIN PRINCIPALS OF THE CHEMISTRY OF TANTALUM AND NIOBIUM FLUORIDE COMPOUNDS

- ✓ Tantalum and niobium are present in the crystal structure in the form of complex ions. The lowest coordination number, 6, corresponds to the formation of slightly distorted octahedrons. The linking and packaging of the octahedrons depends on the X:Me ratio, where X is the total number of oxygen and fluorine atoms, and Me is the total number of tantalum or niobium ions as well as other metals that can replace tantalum or niobium in the octahedral polyhedron. The crystal structure type can be defined based on the X:Me ratio, as follows:

  $X:Me \geq 6$ – island-type structure;
  $5 \leq X:Me < 6$ – chain-type structure;
  $4 \leq X:Me < 5$ – layered-type structure;
  $3 \leq X:Me < 4$ – framework-type structure;
  $X:Me \leq 3$ – coordination-type structure.

- ✓ Thermal properties and decomposition mechanisms depend on the crystal structure type. Compounds with a crystal structure that includes shared octahedrons decompose forming tantalum- or niobium-containing gaseous components, while island-type compounds release light atoms and molecules into the gaseous phase.

- ✓ The properties of fluoride solutions containing tantalum or niobium are defined by the equilibriums between $TaF_6^-$ ↔ $TaF_7^{2-}$ and $NbF_6^-$ ↔ $NbOF_5^{2-}$ complex ions. Increasing the acidity of the solutions shifts the equilibriums toward the predominant formation of hexacoordinated complexes. Decreasing the acidity, by dilution or by adding alkali metal fluorides, initiates an opposite shift in the equilibriums. Precipitation of complex fluoride compounds from solutions that contain mostly $TaF_6^-$ or $NbF_6^-$ ions yields hexa- and heptafluorometates, while the presence of $TaF_7^{2-}$ or $NbOF_5^{2-}$ complexes leads to the formation of hepta- and octafluoro-tantalates and oxyfluoroniobates. In addition, decreasing the acidity of the added substance leads to the formation of complex fluoride compounds with lower coordination numbers.

- ✓ The properties of fluoride melts containing tantalum or niobium depend on the equilibriums that exist between two types of complex ions, $TaF_6^-$ ↔ $TaF_7^{2-}$ or $NbF_6^-$ ↔ $NbF_7^{2-}$. Such equilibriums depend on the concentration of tantalum or niobium and on the nature of the alkali metal. Increasing the Nb or Ta concentration shifts the equilibriums toward the formation of $TaF_6^-$ and $NbF_6^-$ ions. The equilibriums shift to the opposite direction when moving along the series of alkali metals, from Na to Cs. In the presence of chloride or other halites, heteroligand complex ions are formed. Hydrolysis of fluoride melts containing $K_2TaF_7$ or $K_2NbF_7$ leads to the formation of $TaOF_6^{3-}$ and $NbOF_5^{2-}$ complex ions.

- ✓ Fluorination of tantalum and niobium oxides by hydrofluorides of ammonium or alkali metals yields fluorotantalate or monooxy-fluoroniobate compounds. Fluorination of tantalum or niobium oxides in the presence of oxides of other metals yields complex fluoride compounds containing both tantalum or niobium and added metals.

# APPENDIX

## X – Ray powder diffraction data of some important tantalum and niobium fluoride compounds ($CuK_\alpha$ radiation)

### Niobium-containing compounds

$K_5Nb_3O_3F_{14}$
Hexgonal syngony; a = 20.12Å, c = 7.87Å (after Davidovich et al. [115])

| d, Å | $I/I_0$ | hkl | d, Å | $I/I_0$ | hkl | d, Å | $I/I_0$ | hkl |
|---|---|---|---|---|---|---|---|---|
| 9.87 | 36 | 110 | 2.54 | 4 | 332, 113 | 1.694 | 6 | 920 |
| 5.71 | 32 | 300, 201 | 2.32 | 19 | 602, 223 | 1.599 | 3 | 832 |
| 4.94 | 22 | 220, 211 | 2.26 | 2 | 522 | 1.594 | 3 | 841, 930 |
| 4.61 | 100 | 301 | 2.19 | 6 | 711, 323 | 1.527 | 3 | 760, 823 |
| 4.11 | 3 | 401 | 2.15 | 14 | 800 | 1.519 | 3 | 306 |
| 3.93 | 31 | 002 | 2.09 | 2 | 503, 702, 532 | 1.515 | 2 | 850 |
| 3.84 | 2 | 102 | 1.9888 | 8 | 550 | 1.491 | 2 | 714 |
| 3.75 | 7 | 410 | 1.971 | 10 | 004, 712 | 1.475 | 2 | 932 |
| 3.39 | 81 | 411 | 1.933 | 2 | 114, 730 | 1.453 | 1 | 415, 804 |
| 3.31 | 59 | 330 | 1.900 | 12 | 523, 632 | 1.438 | 1 | 724 |
| 3.24 | 41 | 302 | 1.880 | 4 | 820, 731 | 1.423 | 2 | 762, 425 |
| 3.08 | 21 | 222, 510 | 1.859 | 4 | 901, 613 | 1.415 | 1 | 860 |
| 2.69 | 10 | 601 | 1.828 | 15 | 821 | | | |
| 2.61 | 23 | 521, 103 | 1.774 | 12 | 552 | | | |

$K_2NbF_7$
Monoclinic syngony a = 5.85Å, b = 12.72Å, c = 8.51Å, β = 90°
(after Davidovich et al. [115])

| d, Å | $I/I_0$ | hkl | d, Å | $I/I_0$ | hkl | d, Å | $I/I_0$ | hkl |
|---|---|---|---|---|---|---|---|---|
| 5.32 | 60 | 110 | 2.12 | 25 | 060 | 1.465 | 4 | 400 |
| 5.07 | 100 | 021 | 2.10 | 45 | 014 | 1.435 | 3 | 360 |
| 4.51 | 44 | 111 | 2.06 | 48 | 061 | 1.415 | 5 | 006, 361 |
| 4.26 | 58 | 030, 002 | 1.991 | 11 | 150, 143 | 1.381 | 6 | 074 |
| 3.85 | 15 | 121 | 1.939 | 29 | 161, 223 | 1.373 | 6 | 190 |
| 3.79 | 13 | 031 | 1.924 | 18 | 242 | 1.356 | 9 | 191, 273 |
| 3.43 | 91 | 130, 102 | 1.882 | 4 | 311 | 1.327 | 4 | 282 |
| 3.32 | 68 | 112 | 1.803 | 11 | 153, 162 | 1.313 | 5 | 371, 441 |
| 3.19 | 64 | 040, 131 | 1.771 | 19 | 330, 302 | 1.294 | 4 | 046, 165 |
| 3.00 | 6 | 032 | 1.733 | 9 | 331 | 1.273 | 4 | 290, 084 |
| 2.93 | 27 | 200 | 1.699 | 28 | 005, 063, 171 | 1.243 | 4 | 433 |
| 2.67 | 5 | 132 | 1.682 | 22 | 261 | 1.225 | 2 | 335 |
| 2.53 | 9 | 221 | 1.626 | 7 | 163 | 1.203 | 3 | 460, 373 |
| 2.50 | 10 | 113 | 1.586 | 12 | 253 | 1.192 | 3 | 027, 461 |
| 2.42 | 8 | 230, 202 | 1.550 | 4 | 342 | 1.154 | 2 | 166, 194 |
| 2.32 | 18 | 231 | 1.529 | 5 | 073 | 1.144 | 3 | 390 |
| 2.26 | 24 | 222 | 1.513 | 6 | 244 | 1.123 | 3 | 512 |
| 2.19 | 6 | 052, 133 | 1.485 | 6 | 173 | | | |

$K_2NbF_7$
High temperature modification, measured at 230°C
(after Agulyansky et al. [148]).

| d, Å | $I/I_0$ | hkl | d, Å | $I/I_0$ | hkl | d, Å | $I/I_0$ | hkl |
|---|---|---|---|---|---|---|---|---|
| 5.33 | 24 | | 3.271 | 26 | | 2.330 | 9 | |
| 5.167 | 87 | | 3.184 | 20 | | 2.275 | 30 | |
| 5.073 | 100 | | 3.100 | 50 | | 2.144 | 7 | |
| 4.885 | 26 | | 2.978 | 8 | | 2.074 | 10 | |
| 4.585 | 38 | | 2.883 | 42 | | 2.053 | 19 | |
| 3.801 | 19 | | 2.856 | 19 | | 2.034 | 46 | |
| 3.729 | 9 | | 2.756 | 14 | | 1.949 | 8 | |
| 3.562 | 60 | | 2.719 | 8 | | | | |
| 3.432 | 1 | | 2.504 | 14 | | | | |

$KNbF_6$
Tetragonal syngony, a = 5.18 Å, c = 10.05 Å
(after Bizot and Malek-Zadeh [77]).

| d, Å | $I/I_0$ | hkl | d, Å | $I/I_0$ | hkl | d, Å | $I/I_0$ | hkl |
|---|---|---|---|---|---|---|---|---|
| 5.18 | 52 | 100 | 2.964 | 10 | 112 | 2.098 | 37 | 212 |
| 5.05 | 33 | 002 | 2.584 | 5 | 200 | 2.068 | 16 | 203 |
| 3.66 | 80 | 110 | 2.471 | 10 | 113 | 1.826 | 9 | 220 |
| 3.60 | 100 | 102 | 2.307 | 3 | 202 | | | |
| 3.403 | 5 | 111 | 2.258 | 4 | 211 | | | |

$(NH_4)_5Nb_3OF_{18}$
Tetragonal syngony, a = 15.710 Å, c = 7.744 Å (after Tsikaeva et al. [61]).

| d, Å | $I/I_0$ | hkl | d, Å | $I/I_0$ | hkl | d, Å | $I/I_0$ | hkl |
|---|---|---|---|---|---|---|---|---|
| 11.11 | 5 | 110 | 3.797 | 6 | 321 | 2.775 | 2 | 440 |
| 7.83 | 1 | 200 | 3.699 | 12 | 330 | 2.756 | 7 | 402 |
| 5.56 | 27 | 220 | 3.655 | 23 | 112 | 2.731 | 14 | 521 |
| 5.22 | 100 | 211 | 3.513 | 29 | 420 | 2.695 | 8 | 530 |
| 4.98 | 98 | 310 | 3.422 | 37 | 411 | 2.679 | 6 | 332 |
| 3.926 | 1 | 400 | 3.178 | 4 | 222 | 2.621 | 18 | 600 |
| 3.870 | 4 | 002 | 3.084 | 1 | 431 | 2.484 | 1 | 620 |

$K_5Nb_3OF_{18}$
Tetragonal syngony, a = 14.877 Å, c = 7.697 Å (after Tsikaeva et al. [61]).

| d, Å | $I/I_0$ | hkl | d, Å | $I/I_0$ | hkl | d, Å | $I/I_0$ | hkl |
|---|---|---|---|---|---|---|---|---|
| 10.45 | 1 | 110 | 3.51 | 17 | 330 | 2.676 | 11 | 402 |
| 7.42 | 1 | 200 | 3.42 | 87 | 202 | 2.607 | 46 | 521 |
| 5.26 | 28 | 220 | 3.33 | 84 | 420 | 2.556 | 12 | 530 |
| 5.04 | 100 | 211 | 3.27 | 76 | 411 | 2.484 | 11 | 600 |
| 4.71 | 85 | 310 | 3.118 | 28 | 222 | 2.356 | 22 | 620 |
| 3.85 | 21 | 002 | 2.978 | 6 | 312 | | | |
| 3.61 | 49 | 321 | 2.921 | 7 | 431 | | | |

$Rb_5Nb_3OF_{18}$
Tetragonal syngony, a = 15.511 Å, c = 7.785 Å (after Tsikaeva et al. [61]).

| d, Å | $I/I_0$ | hkl | d, Å | $I/I_0$ | hkl | d, Å | $I/I_0$ | hkl |
|---|---|---|---|---|---|---|---|---|
| 7.78 | 3 | 200 | 3.482 | 100 | 202 | 2.585 | 3 | 600 |
| 5.46 | 42 | 220 | 3.391 | 70 | 411 | 2.394 | 14 | 213 |
| 5.17 | 27 | 211 | 3.175 | 27 | 222 | 2.452 | 47 | 620 |
| 4.90 | 30 | 310 | 2.881 | 6 | 431 | | | |
| 3.890 | 30 | 400 | 2.742 | 30 | 440 | | | |
| 3.767 | 59 | 321 | 2.703 | 28 | 521 | | | |
| 3.654 | 69 | 330 | 2.659 | 12 | 530 | | | |

$LiNbOF_4$
Tetragonal syngony, a = 6.86 Å, c = 3.98 Å (after Agulyansky et al. [126]).

| d, Å | $I/I_0$ | hkl | d, Å | $I/I_0$ | hkl | d, Å | $I/I_0$ | hkl |
|---|---|---|---|---|---|---|---|---|
| 4.866 | 13 | 110 | 1.844 | 19 | 112 | 1.431 | 1 | 421 |
| 3.981 | 19 | 001 | 1.722 | 20 | 321, 202 | 1.377 | 5 | 322 |
| 3.446 | 100 | 101, 200 | 1.716 | 28 | 400 | 1.345 | 2 | 510 |
| 3.074 | 25 | 111 | 1.673 | 17 | 212 | 1.331 | 3 | 003 |
| 2.599 | 4 | 201 | 1.616 | 4 | 330 | 1.298 | 8 | 402, 501 |
| 2.429 | 22 | 220 | 1.575 | 1 | 401 | 1.283 | 7 | 113 |
| 2.167 | 45 | 310 | 1.534 | 31 | 420 | 1.280 | 5 | 511 |
| 1.993 | 90 | 002 | 1.503 | 3 | 302 | | | |
| 1.914 | 19 | 102 | 1.469 | 13 | 312 | | | |

$NaNbOF_4$ (after Tsikaeva et al. [61]).

| d, Å | $I/I_0$ | hkl | d, Å | $I/I_0$ | hkl | d, Å | $I/I_0$ | hkl |
|---|---|---|---|---|---|---|---|---|
| 5.626 | 18 | | 3.178 | 83 | | 2.248 | 3 | |
| 5.498 | 17 | | 2.819 | 27 | | 2.138 | 24 | |
| 4.484 | 3 | | 2.751 | 12 | | 2.097 | 29 | |
| 3.951 | 100 | | 2.589 | 3 | | 2.080 | 32 | |
| 3.542 | 2 | | 2.504 | 1 | | 1.969 | 46 | |
| 3.477 | 2 | | 2.469 | 3 | | 1.951 | 24 | |
| 3.388 | 4 | | 2.362 | 32 | | | | |
| 3.255 | 49 | | 2.321 | 7 | | | | |

$KNbOF_4$
Tetragonal syngony, a = 15.43 Å, c = 7.757 Å (after Kuznezov et al. [139]).

| d, Å | $I/I_0$ | hkl | d, Å | $I/I_0$ | hkl | d, Å | $I/I_0$ | hkl |
|---|---|---|---|---|---|---|---|---|
| 7.73 | 10 | 200 | 2.874 | 10 | 501, 431 | 2.189 | 20 | 532, 550 |
| 5.46 | 80 | 220 | 2.735 | 7 | 440, 402 | 2.143 | 25 | 640 |
| 5.15 | 40 | 211 | 2.687 | 30 | 521 | 2.127 | 50 | 413, 701 |
| 4.87 | 20 | 310 | 2.655 | 60 | 332, 530 | 2.074 | 10 | 622 |
| 3.87 | 55 | 400, 002 | 2.575 | 10 | 600 | 2.048 | 15 | 721 |
| 3.64 | 100 | 330, 112 | 2.438 | 25 | 620 | 1.984 | 15 | 433, 503 |
| 3.46 | 95 | 420, 202 | 2.386 | 25 | 512 | 1.940 | 40 | 004, 800 |
| 3.37 | 100 | 411 | 2.232 | 5 | 442 | | | |
| 3.04 | 20 | 312, 510 | 2.209 | 15 | 323, 631 | | | |

$RbNbOF_4$
(after Agulyansky et al. [126]).

| d, Å | $I/I_0$ | hkl | d, Å | $I/I_0$ | hkl | d, Å | $I/I_0$ | hkl |
|---|---|---|---|---|---|---|---|---|
| 4.866 | 13 | 110 | 1.844 | 19 | 112 | 1.431 | 1 | 421 |
| 3.981 | 19 | 001 | 1.722 | 20 | 321, 202 | 1.377 | 5 | 322 |
| 3.446 | 100 | 101, 200 | 1.716 | 28 | 400 | 1.345 | 2 | 510 |
| 3.074 | 25 | 111 | 1.673 | 17 | 212 | 1.331 | 3 | 003 |
| 2.599 | 4 | 201 | 1.616 | 4 | 330 | 1.298 | 8 | 402, 501 |
| 2.429 | 22 | 220 | 1.575 | 1 | 401 | 1.283 | 7 | 113 |
| 2.167 | 45 | 310 | 1.534 | 31 | 420 | 1.280 | 5 | 511 |
| 1.993 | 90 | 002 | 1.503 | 3 | 302 | | | |
| 1.914 | 19 | 102 | 1.469 | 13 | 312 | | | |

$NH_4NbOF_4$
Tetragonal syngony, a = 8.04 Å, c = 3.95 Å (after Davidovich et al. [115]).

| d, Å | $I/I_0$ | hkl | d, Å | $I/I_0$ | hkl | d, Å | $I/I_0$ | hkl |
|---|---|---|---|---|---|---|---|---|
| 5.67 | 100 | 110 | 1.973 | 7 | 002 | 1.560 | 3 | 312 |
| 4.02 | 87 | 200 | 1.950 | 1 | 410 | 1.467 | 7 | 511 |
| 3.93 | 36 | 001 | 1.898 | 3 | 330 | 1.424 | 3 | 440 |
| 3.24 | 39 | 111 | 1.863 | 6 | 112 | 1.410 | 5 | 402 |
| 2.85 | 7 | 220 | 1.793 | 18 | 401 | 1.379 | 5 | 530 |
| 2.82 | 14 | 201 | 1.771 | 6 | 202 | 1.341 | 3 | 600 |
| 2.66 | 3 | 211 | 1.711 | 3 | 331 | 1.330 | 1 | 421 |
| 2.55 | 31 | 310 | 1.639 | 6 | 421 | 1.302 | 2 | 531 |
| 2.14 | 23 | 311 | 1.623 | 1 | 222 | | | |
| 2.01 | 28 | 400 | 1.581 | 9 | 510 | | | |

$(NH_4)_2NbOF_5$
Orthorhombic syngony, a = 14.34 Å, b = 7.20 Å, c = 5.96 Å
(after Davidovich et al. [115]).

| d, Å | $I/I_0$ | hkl | d, Å | $I/I_0$ | hkl | d, Å | $I/I_0$ | hkl |
|---|---|---|---|---|---|---|---|---|
| 7.17 | 3 | 200, 010 | 2.20 | 7 | 131 | 1.664 | 3 | 432 |
| 5.51 | 81 | 101 | 2.11 | 5 | 521 | 1.644 | 2 | 712 |
| 5.09 | 100 | 210 | 2.02 | 9 | 331 | 1.551 | 3 | 441, 821 |
| 4.60 | 63 | 201 | 1.999 | 3 | 430 | 1.542 | 4 | 901 |
| 3.74 | 11 | 301 | 1.975 | 2 | 710 | 1.525 | 2 | 540 |
| 3.60 | 44 | 400, 020 | 1.941 | 12 | 701 | 1.513 | 5 | 142 |
| 3.32 | 59 | 311 | 1.906 | 5 | 113 | 1.497 | 4 | 233 |
| 3.22 | 4 | 220, 410 | 1.883 | 12 | 621 | 1.479 | 9 | 541 |
| 3.01 | 28 | 121 | 1.814 | 19 | 232 | 1.462 | 3 | 204 |
| 2.60 | 10 | 321 | 1.785 | 6 | 140 | 1.439 | 3 | 050, 640 |
| 2.41 | 5 | 030 | 1.752 | 2 | 531 | 1.422 | 7 | 304 |
| 2.30 | 41 | 022 | 1.733 | 4 | 403, 123 | 1.411 | 2 | 250 |
| 2.28 | 21 | 402 | 1.711 | 3 | 141 | | | |

$(NH_4)_3NbOF_6$
Cubic syngony, a = 9.31 Å (after Davidovich et al. [115]).

| d, Å | $I/I_0$ | hkl | d, Å | $I/I_0$ | hkl | d, Å | $I/I_0$ | hkl |
|---|---|---|---|---|---|---|---|---|
| 5.37 | 100 | 111 | 1.901 | 14 | 422 | 1.404 | 2 | 622 |
| 4.65 | 50 | 200 | 1.793 | 13 | 511, 333 | 1.344 | 1 | 444 |
| 3.29 | 51 | 220 | 1.647 | 4 | 440 | 1.304 | 3 | 551, 711 |
| 2.81 | 16 | 311 | 1.574 | 7 | 531 | 1.291 | 1 | 640 |
| 2.33 | 20 | 400 | 1.551 | 5 | 600, 442 | 1.244 | 4 | 642 |
| 2.14 | 5 | 331 | 1.472 | 5 | 620 | 1.212 | 2 | 731, 553 |
| 2.08 | 11 | 420 | 1.420 | 3 | 533 | | | |

$Li_4NbO_4F$
Cubic syngony, a = 4.192 Å (after Agulyansky et al. [87]).

| d, Å | $I/I_0$ | hkl | d, Å | $I/I_0$ | hkl | d, Å | $I/I_0$ | hkl |
|---|---|---|---|---|---|---|---|---|
| 2.420 | 11 | 111 | 1.264 | 8 | 311 | 0.9617 | 3 | 331 |
| 2.096 | 100 | 200 | 1.210 | 27 | 222 | 0.9374 | 22 | 420 |
| 1.482 | 91 | 220 | 1.048 | 9 | 400 | 0.8557 | 16 | 422 |

$CoNbOF_5$
Tetragonal syngony, a = 7.81 Å, c = 9.02 Å (after Agulyansky et al. [129]).

| d, Å | $I/I_0$ | hkl | d, Å | $I/I_0$ | hkl | d, Å | $I/I_0$ | hkl |
|---|---|---|---|---|---|---|---|---|
| 4.52 | 10 | 002 | 1.948 | 88 | 400 | 1.500 | 2 | 423 |
| 3.90 | 100 | 200, 102 | 1.746 | 40 | 420 | 1.386 | 7 | 206 |
| 2.76 | 34 | 212 | 1.610 | 3 | 205 | 1.303 | 10 | 600 |
| 2.35 | 10 | 222 | 1.588 | 13 | 413 | | | |

## Tantalum-containing compounds

$K_2TaF_7$
Monoclinic syngony, a = 5.85 Å, b = 12.70, c = 8.52 Å, β = 90°
(after Davidovich et al. [115]).

| d, Å | $I/I_0$ | hkl | d, Å | $I/I_0$ | hkl | d, Å | $I/I_0$ | hkl |
|---|---|---|---|---|---|---|---|---|
| 5.30 | 7 | 110 | 2.32 | 12 | 231 | 1.632 | 4 | 054, 341 |
| 5.08 | 100 | 021 | 2.25 | 8 | 151, 222 | 1.621 | 4 | 115 |
| 4.51 | 57 | 111 | 2.19 | 5 | 052, 133 | 1.607 | 5 | 303 |
| 4.25 | 32 | 002, 030 | 2.15 | 5 | 240 | 1.590 | 5 | 235, 262 |
| 4.02 | 3 | 012 | 2.12 | 5 | 060, 043 | 1.582 | 6 | 035 |
| 3.84 | 4 | 121 | 2.10 | 21 | 014, 232 | 1.572 | 3 | 154 |
| 3.79 | 7 | 031 | 2.05 | 23 | 061 | 1.549 | 3 | 342 |
| 3.43 | 64 | 130, 102 | 2.00 | 5 | 104 | 1.523 | 3 | 351 |
| 3.32 | 55 | 112 | 1.995 | 5 | 143 | 1.513 | 10 | 244 |
| 3.18 | 58 | 040, 131 | 1.973 | 4 | 114 | 1.480 | 4 | 173 |
| 3.00 | 4 | 032 | 1.939 | 18 | 161, 223 | 1.469 | 7 | 263 |
| 2.93 | 20 | 200 | 1.921 | 16 | 250, 242 | 1.455 | 3 | 145, 164 |
| 2.79 | 3 | 140 | 1.839 | 4 | 233 | 1.434 | 3 | 360, 225 |
| 2.71 | 3 | 211 | 1.824 | 3 | 321 | 1.415 | 3 | 361, 055 |
| 2.67 | 10 | 132 | 1.802 | 5 | 153 | 1.393 | 2 | 091 |
| 2.59 | 9 | 023 | 1.769 | 8 | 330, 044 | 1.379 | 3 | 106 |
| 2.54 | 21 | 050, 042, 221 | 1.735 | 6 | 170, 331 | 1.374 | 3 | 116 |
| 2.50 | 16 | 113 | 1.720 | 4 | 204 | 1.356 | 3 | 273 |
| 2.41 | 10 | 202, 230 | 1.700 | 15 | 171 | 1.327 | 3 | 370, 065 |
| 2.37 | 3 | 123, 212 | 1.696 | 14 | 063 | 1.311 | 4 | 136, 371 |
| 2.33 | 11 | 150 | 1.684 | 10 | 261 | 1.294 | 2 | 413 |

$Rb_3TaOF_6$
Cubic syngony, a = 9.21 Å (after Davidovich et al. [115]).

| d, Å | $I/I_0$ | hkl | d, Å | $I/I_0$ | hkl | d, Å | $I/I_0$ | hkl |
|---|---|---|---|---|---|---|---|---|
| 5.30 | 43 | 111 | 2.06 | 3 | 420 | 1.536 | 2 | 600, 442 |
| 4.59 | 9 | 200 | 1.880 | 31 | 422 | 1.456 | 10 | 620 |
| 3.25 | 100 | 220 | 1.772 | 5 | 511, 333 | 1.330 | 4 | 444 |
| 2.77 | 3 | 311 | 1.629 | 16 | 440 | 1.290 | 1 | 711, 551 |
| 2.30 | 22 | 400 | 1.557 | 2 | 531 | 1.231 | 9 | 642 |

$K_2TaF_7$
High temperature modification, measured at 230°C
(after Agulyansky et al. [148]).

| d, Å | $I/I_0$ | hkl | d, Å | $I/I_0$ | hkl | d, Å | $I/I_0$ | hkl |
|---|---|---|---|---|---|---|---|---|
| 5.33 | 24 | | 3.271 | 26 | | 2.330 | 9 | |
| 5.167 | 87 | | 3.184 | 20 | | 2.275 | 30 | |
| 5.073 | 100 | | 3.100 | 50 | | 2.144 | 7 | |
| 4.885 | 26 | | 2.978 | 8 | | 2.074 | 10 | |
| 4.585 | 38 | | 2.883 | 42 | | 2.053 | 19 | |
| 3.801 | 19 | | 2.856 | 19 | | 2.034 | 46 | |
| 3.729 | 9 | | 2.756 | 14 | | 1.949 | 8 | |
| 3.562 | 60 | | 2.719 | 8 | | | | |
| 3.432 | 1 | | 2.504 | 14 | | | | |

$K_3TaOF_6$
Cubic syngony, a = 8.88 Å (after Davidovich et al. [115]).

| d, Å | $I/I_0$ | hkl | d, Å | $I/I_0$ | hkl | d, Å | $I/I_0$ | hkl |
|---|---|---|---|---|---|---|---|---|
| 5.12 | 80 | 111 | 1.985 | 17 | 420 | 1.355 | 5 | 533 |
| 4.43 | 44 | 200 | 1.813 | 37 | 422 | 1.339 | 2 | 622 |
| 3.13 | 100 | 220 | 1.709 | 14 | 511, 333 | 1.282 | 3 | 444 |
| 2.67 | 27 | 311 | 1.570 | 16 | 440 | 1.245 | 4 | 711, 551 |
| 2.56 | 2 | 222 | 1.501 | 10 | 531 | 1.187 | 9 | 642 |
| 2.22 | 36 | 400 | 1.480 | 8 | 600, 442 | 1.157 | 4 | 731, 553 |
| 2.04 | 10 | 331 | 1.405 | 12 | 620 | | | |

$Li_4TaO_4F$
Cubic syngony, a = 4.20 Å (after Agulyansky et al. [275]).

| d, Å | $I/I_0$ | hkl | d, Å | $I/I_0$ | hkl | d, Å | $I/I_0$ | hkl |
|---|---|---|---|---|---|---|---|---|
| 2.430 | 12 | 111 | 1.266 | 8 | 311 | 0.9635 | 4 | 331 |
| 2.090 | 100 | 200 | 1.212 | 27 | 222 | 0.9391 | 23 | 420 |
| 1.487 | 89 | 220 | 1.050 | 9 | 400 | 0.8573 | 12 | 422 |

$CaTaF_7$
(after Tsikaeva et al. [119]).

| d, Å | $I/I_0$ | hkl | d, Å | $I/I_0$ | hkl | d, Å | $I/I_0$ | hkl |
|---|---|---|---|---|---|---|---|---|
| 4.70 | 70 | | 2.33 | 8 | | 1.809 | 25 | |
| 4.04 | 100 | | 2.06 | 3 | | 1.660 | 7 | |
| 2.86 | 36 | | 2.02 | 21 | | 1.558 | 8 | |
| 2.44 | 25 | | 1.850 | 9 | | | | |

$SrTaF_7$
(after Tsikaeva et al. [119]).

| d, Å | $I/I_0$ | hkl | d, Å | $I/I_0$ | hkl | d, Å | $I/I_0$ | hkl |
|---|---|---|---|---|---|---|---|---|
| 4.86 | 7 | | 3.15 | 2 | | 1.990 | 4 | |
| 4.74 | 25 | | 2.88 | 36 | | 1.878 | 5 | |
| 4.09 | 100 | | 2.81 | 5 | | 1.827 | 12 | |
| 3.99 | 15 | | 2.47 | 6 | | 1.798 | 3 | |
| 3.65 | 5 | | 2.36 | 6 | | 1.743 | 2 | |
| 3.56 | 7 | | 2.15 | 2 | | 1.671 | 6 | |
| 3.34 | 7 | | 2.05 | 11 | | 1.574 | 4 | |

$BaTaF_7$
(after Tsikaeva et al. [119]).

| d, Å | $I/I_0$ | hkl | d, Å | $I/I_0$ | hkl | d, Å | $I/I_0$ | hkl |
|---|---|---|---|---|---|---|---|---|
| 4.99 | 4 | | 2.09 | 6 | | 1.569 | 14 | |
| 4.44 | 11 | | 2.06 | 6 | | 1.550 | 9 | |
| 4.09 | 3 | | 2.03 | 80 | | 1.533 | 3 | |
| 3.96 | 5 | | 1.984 | 9 | | 1.494 | 2 | |
| 3.77 | 50 | | 1.965 | 7 | | 1.480 | 5 | |
| 3.52 | 100 | | 1.843 | 8 | | 1.464 | 2 | |
| 3.37 | 25 | | 1.806 | 3 | | 1.433 | 4 | |
| 3.31 | 15 | | 1.753 | 13 | | 1.417 | 3 | |
| 2.92 | 4 | | 1.728 | 4 | | 1.403 | 2 | |
| 2.76 | 2 | | 1.681 | 2 | | 1.357 | 3 | |
| 2.48 | 20 | | 1.655 | 3 | | 1.328 | 12 | |
| 2.24 | 5 | | 1.632 | 3 | | | | |
| 2.17 | 14 | | 1.610 | 3 | | | | |

$Ba_3(TaF_8)_2$
(after Tsikaeva et al. [119]).

| d, Å | $I/I_0$ | hkl | d, Å | $I/I_0$ | hkl | d, Å | $I/I_0$ | hkl |
|---|---|---|---|---|---|---|---|---|
| 5.20 | 8 | | 3.76 | 40 | | 2.99 | 8 | |
| 5.10 | 11 | | 3.53 | 11 | | 2.87 | 2 | |
| 4.90 | 5 | | 3.39 | 22 | | 2.78 | 14 | |
| 4.76 | 10 | | 3.31 | 20 | | 2.64 | 5 | |
| 4.07 | 42 | | 3.19 | 55 | | 2.59 | 4 | |
| 3.91 | 20 | | 3.14 | 25 | | 2.54 | 3 | |
| 3.84 | 100 | | 3.07 | 16 | | 2.48 | 2 | |
| 3.82 | 74 | | 3.04 | 17 | | 2.45 | 2 | |

$LiTaF_6$
Trigonal syngony, a = 5.480 Å, α = 58°03′
(after Agulyansky et al. [159]).

| d, Å | $I/I_0$ | hkl | d, Å | $I/I_0$ | hkl | d, Å | $I/I_0$ | hkl |
|---|---|---|---|---|---|---|---|---|
| 4.53 | 72 | 003 | 1.791 | 21 | 107 | 1.4547 | 16 | 303 |
| 4.365 | 91 | 101 | 1.757 | 19 | 205 | 1.3759 | 4 | 126 |
| 3.811 | 100 | 102 | 1.740 | 19 | 120 | 1.3689 | 13 | 208 |
| 2.737 | 71 | 104 | 1.727 | 79 | 116 | 1.3301 | 8 | 220 |
| 2.660 | 40 | 110 | 1.687 | 46 | 122 | 1.3147 | 17 | 119 |
| 2.343 | 51 | 105 | 1.595 | 13 | 108 | 1.3053 | 8 | 222 |
| 2.292 | 81 | 113 | 1.550 | 18 | 124 | 1.2978 | 14 | 127 |
| 2.270 | 54 | 201 | 1.536 | 14 | 300 | 1.2728 | 24 | 311 |
| 2.183 | 13 | 202 | 1.486 | 12 | 207 | 1.2556 | 12 | 312 |
| 1.907 | 80 | 204 | 1.467 | 23 | 125 | | | |

$NaTaF_6$
Cubic, a = 8.273 Å,
(after Agulyansky et al. [159]).

| d, Å | $I/I_0$ | hkl | d, Å | $I/I_0$ | hkl | d, Å | $I/I_0$ | hkl |
|---|---|---|---|---|---|---|---|---|
| 4.77 | 96 | 111 | 1.399 | 10 | 531 | 1.010 | 1 | 733 |
| 4.135 | 100 | 200 | 1.379 | 10 | 600 | 1.003 | 3 | 820, 644 |
| 2.925 | 39 | 220 | 1.308 | 4 | 620 | 0.9750 | 2 | 822, 660 |
| 2.495 | 38 | 311 | 1.261 | 2 | 533 | 0.9559 | 2 | 751, 555 |
| 2.385 | 4 | 222 | 1.247 | 2 | 622 | 0.9498 | 1 | 662 |
| 2.067 | 34 | 400 | 1.194 | 1 | 444 | 0.9253 | 2 | 840 |
| 1.898 | 10 | 331 | 1.158 | 4 | 711, 551 | 0.9085 | 2 | 911, 753 |
| 1.850 | 36 | 420 | 1.148 | 3 | 640 | 0.9031 | 2 | 842 |
| 1.689 | 12 | 422 | 1.106 | 3 | 642 | 0.8818 | 0.5 | 664 |
| 1.592 | 15 | 511, 333 | 1.077 | 2 | 731, 553 | | | |
| 1.463 | 9 | 440 | 1.034 | 0.5 | 800 | | | |

$KTaF_6$
Tetragonal syngony, a = 5.186 Å, c = 10.04 Å
(after Agulyansky et al. [159]).

| d, Å | $I/I_0$ | hkl | d, Å | $I/I_0$ | hkl | d, Å | $I/I_0$ | hkl |
|---|---|---|---|---|---|---|---|---|
| 5.20 | 88 | 100 | 2.107 | 80 | 212 | 1.5211 | 5 | 116 |
| 5.04 | 59 | 002 | 2.072 | 39 | 114 | 1.4804 | 10 | 224 |
| 3.669 | 95 | 110 | 1.9092 | 2 | 213 | 1.4383 | 5 | 320 |
| 3.616 | 100 | 102 | 1.8351 | 20 | 220 | 1.4238 | 6 | 304 |
| 2.966 | 54 | 112 | 1.8038 | 26 | 221, 204 | 1.4041 | 3 | 206 |
| 2.598 | 14 | 200 | 1.7229 | 15 | 222, 300 | 1.3814 | 17 | 322 |
| 2.511 | 11 | 004 | 1.7089 | 21 | 214 | 1.3565 | 11 | 216 |
| 2.472 | 11 | 113 | 1.6374 | 21 | 310, 302 | 1.2558 | 4 | 008,410,324 |
| 2.315 | 18 | 210, 202 | 1.5926 | 12 | 106 | 1.2215 | 9 | 217, 330 |
| 2.260 | 14 | 211, 104 | 1.5593 | 8 | 312 | | | |

$RbTaF_6$
Trigonal syngony, a = 5.155 Å, α = 94°04′
(after Agulyansky et al. [159]).

| d, Å | $I/I_0$ | hkl | d, Å | $I/I_0$ | hkl | d, Å | $I/I_0$ | hkl |
|---|---|---|---|---|---|---|---|---|
| 5.079 | 41 | 101 | 1.9160 | 15 | 220 | 1.4224 | 7 | 232 |
| 3.834 | 100 | 110 | 1.8983 | 9 | 104 | 1.3482 | 4 | 314 |
| 3.404 | 79 | 102 | 1.7939 | 5 | 131 | 1.2753 | 4 | 330 |
| 3.058 | 13 | 201 | 1.7004 | 10 | 303, 204 | 1.2592 | 3 | 502 |
| 2.546 | 23 | 202 | 1.6717 | 12 | 312 | 1.2493 | 4 | 116 |
| 2.392 | 3 | 211 | 1.5559 | 14 | 214 | 1.2075 | 3 | 324 |
| 2.217 | 19 | 300 | 1.5316 | 7 | 402 | 1.1971 | 4 | 422 |
| 2.175 | 5 | 113 | 1.4957 | 2 | 321 | | | |
| 2.120 | 48 | 212 | 1.4491 | 10 | 410 | | | |

$CsTaF_6$
Trigonal syngony, a = 5.327 Å, α = 96°17′
(after Agulyansky et al. [159]).

| d, Å | $I/I_0$ | hkl | d, Å | $I/I_0$ | hkl | d, Å | $I/I_0$ | hkl |
|---|---|---|---|---|---|---|---|---|
| 5.261 | 13 | 101 | 1.975 | 21 | 220 | 1.379 | 2 | 606 |
| 3.948 | 100 | 110 | 1.768 | 9 | 303, 204 | 1.317 | 5 | 404 |
| 3.534 | 80 | 102 | 1.723 | 11 | 312 | 1.301 | 5 | 116 |
| 3.160 | 2 | 201 | 1.614 | 12 | 214 | 1.250 | 3 | 324 |
| 2.635 | 24 | 202 | 1.580 | 6 | 402 | 1.234 | 4 | 422 |
| 2.467 | 2 | 211 | 1.492 | 11 | 410, 205 | 1.178 | 3 | 512 |
| 2.278 | 20 | 300 | 1.467 | 7 | 322, 411 | | | |
| 2.192 | 45 | 212 | 1.396 | 5 | 314 | | | |

This Page Intentionally Left Blank

# REFERENCES

[1] C.E.D. Rowe, JOM 49 (1997) 26.
[2] B.I. Kogan, Rare metals. Status and perspectives, Nauka, Moscow, 1979 (in Russian).
[3] B. Egovska-Trshebyatovska, S. Kopach, T. Mikulsky, Rare elements, Mir, Moscow, 1979 (in Russian, translation from Polish).
[4] H. Stuart, International symposium on tantalum and niobium, October 2000, Proceedings, TIC, Brussels, 2000, p. 121.
[5] A.J. DeArdo, International symposium on tantalum and niobium, September 1995, Proceedings, TIC, Brussels, 1995, p. 113.
[6] G. Tither, International symposium on tantalum and niobium, September 1995, Proceedings, TIC, Brussels, 1995, p. 129.
[7] J. Eridon, International symposium on tantalum and niobium, October 2000, Proceedings, TIC, Brussels, 2000, p. 35.
[8] R. Henson, D. Holmes, International symposium on tantalum and niobium, October 2000, Proceedings, TIC, Brussels, 2000, p. 113.
[9] T. Carneiro, E.A.Loria, International symposium on tantalum and niobium, October 2000, Proceedings, TIC, Brussels, 2000, p. 235.
[10] K. Inoue, T. Takeuchi, Y.Iijima, A. Kikuchi, International symposium on tantalum and niobium, October 2000, Proceedings, TIC, Brussels, 2000, p. 189.
[11] R. Scanlan, International symposium on tantalum and niobium, October 2000, Proceedings, TIC, Brussels, 2000, p. 205.
[12] H.F. Morian, International symposium on tantalum and niobium, September 1995, Proceedings, TIC, Brussels, 1995, p. 341.
[13] T.T. Bakumenko, Catalytical properties of rare and rare-earth elements, AN USSR, Kiev, 1963 (in Russian).
[14] U.N. Venevtzev, E.D. Politova, S.A. Ivanov, Ferroelectrics and antiferroelectrics of barium titanate family, Khimiya, Moscow, 1985 (in Russian).

[15] Yu.S. Kuzminov, Niobate and tantalate of lithium, Nauka, Moscow, 1975 (in Russian).
[16] Yu. Xu, Ferroelectric materials and their applications, Elsevier Science Publishers B.V., North-Holland, Amsterdam, 1991.
[17] L.M. Shepard, Ceramic Bulletin 71 (1992) 85.
[18] T. Nishimura, S. Matsumura, International symposium on tantalum and niobium, September 1995, Proceedings, TIC, Brussels, 1995, p. 355.
[19] J. Gill, Passive component industry, May/June 2003, p. 22.
[20] C.E. Mosheim, TIC Bulletin (112) – December 2002, p. 2.
[21] I.M. Gibalo, Analytical chemistry of niobium and tantalum, Ann Arbor, London, 1970.
[22] J. Linden, International symposium on tantalum and niobium, September 1995, Proceedings, TIC, Brussels, 1995, p. 15.
[23] J. Linden, International symposium on tantalum and niobium, October 2000, Proceedings, TIC, Brussels, 2000, p. 19.
[24] Kirk-Othmer Encyclopedia of Chemical Technology, Fourth Edition, V.23, John Wiley & Sons, Inc. 1997, p. 658.
[25] C. Hatchett, Phil. Trans. (1802) 49.
[26] A.G. Ekeberg, Ann. Chim. 43 (1802) 276.
[27] M.C. Marignac, Ann. Chem. Phys. 8 (1866) 5.
[28] F. Fairbrother, The chemistry of niobium and tantalum, Elsevier Publishing Company, Amsterdam, 1967.
[29] Ya.G. Goroschenko, Chemistry of niobium and tantalum, Naukova Dumka, Kiev, 1965 (in Russian).
[30] W. Rockenbauer, Niobium – Proceedings, International Symposium, Metallurgical Sosiety of AIME, New York, 1984, p. 133.
[31] E.A. Brocchi, P.K. Jena, F.J. Moura, O. Barbosa-Filho, R.J. de Carvalho, Chloride metallurgy 2002: Practice and theory of chlorine/metal interaction, Annual Hydrometallurgy Meeting, Oct. 19-23, 2002, 1 (2002) 229.
[32] J. Eckert, International symposium on tantalum and niobium, September 1995, Proceedings, TIC, Brussels, 1995, p.51.
[33] K.B. Higbie, J.R.Werning, Separation of tantalum-columbium by solvent extraction, Bulletin No. 5239, U.S. Bureau of Mines, Washington, D.C., 1956.
[34] A.G. Babkin, B.G. Miorov, A.I. Nikolaev, Extraction of niobium tantalum and other elements from fluoride solutions, Nauka, Leningrad, 1988 (in Russian).
[35] V.I. Konstantinov, Electrochemical obtaining of tantalum, niobium and their alloys, Metallurgiya, Moscow, 1977 (in Russian).

[36] G.L. Miller, Tantalum and niobium, Butterworth Scientific Publishers, L., 1959.
[37] W.R. Barton, Niobium and tantalum, U.S. Bureau Mines Inform. Circ., 8120 (1959).
[38] L. Shekhter, L. Lanin, T. Tripp, H. Goldberg, K. Reichert, C. Schnitter and R. Wolf, International symposium on tantalum and niobium, October 2000, Proceedings, TIC, Brussels, 2000, p. 87.
[39] A.J. Adwards, Adv. Inorg. Chem. Radiochem. 27 (1982) 83.
[40] R.J. Hobson, Coord. Chem. Rev. 57 (1984) 279.
[41] R.W. Berg, Coord. Chem. Rev. 113 (1992) 1.
[42] I.S. Res, Properties of materials that are used in optoelectronic devices, Kirensky Institute of Physiscs, Moscow, 1975, p. 10.
[43] P. Hagenmuller, Inorganic solid fluorides, Acadimic Press, Inc., Orlando, 1985, p. 1.
[44] J. Raves, P. Hagenmuller, Ferroelectrics 14 (1976) 669.
[45] J. Raves, Rev. Chim. Miner. 23 (1986) 460.
[46] S.C. Abrahams, J. Ravez, Ferroelectrics 135 (1992) 21.
[47] J. Ravez, C. R. Acad. Sci. Paris 2 (Ser. II) (1999) 41.
[48] Y.A. Buslaev, R.L. Davidovich, V.A. Bochkareva, Inorg. Mater. 1 (1965) 483.
[49] A. Tressaud, F. Pintchovsky, L. Lazano, A. Wold, P. Hagenmuller, Mater. Res. Bull. 11 (1976) 689.
[50] C.E. Bamberger, Molten salts. Ed. G. Mamontov, New York – London, 1969, p. 177.
[51] E.G. Rakov, Fluorides of ammonium, Itogi nauki i techniki / ser. Neorg. Khim. VINITI, Moscow, 1983 (in Russian).
[52] E.G. Rakov, E.I. Melnichenko, Uspekhi chimii 53 (1984) 1463.
[53] G.S. Savchenko, I.V. Tananaev, Zh. Prikl. Khim. 20 (1947) 385.
[54] G.S. Savchenko, I.V. Tananaev, Zh. Prikl. Khim. 19 (1946) 1093.
[55] C.W. Balke, J. Amer. Chem. Soc. 27 (1905) 1140.
[56] C.W. Balke, E.F. Smith, J. Amer. Chem. Soc. 30 (1908) 1637.
[57] Y.A. Buslaev, E.G. Il'in, V.D. Kopanev, O.G. Gavrish, Izvestiya AN USSR Ser. Khim. 6 (1971) 1139.
[58] R. Stomberg, Acta Chem. Scand. A37 (1983) 453.
[59] R. Ritchie, G. Mitra, J. Fluor. Chem. 6 (1975) 291.
[60] D.V. Tsikaeva, S.D.Nikitina, A.I. Agulyansky, at al, Thesis of reports, XVI Chugaev's conference on chemistry of complex compounds, Krasnoyarsk, 1987 p. 296.
[61] D.V. Tsikaeva, A.I. Agulyansky, Y.I. Balabanov, V.Y. Kuznetsov, V.T. Kalinnikov, Zh. Neorg. Khim. 34 (1989) 3046.

[62] T.F. Levchishina, R.L. Davidovich, Complex fluorides of zirconium, hafnium, niobium and tantalum with cations of alkali earth metals, Dep. VINITI, No 3595-75 Dep 1975.
[63] R.L. Davidovich, T.F. Levchishina, T.A. Kaidalova, V.I. Sergienko, J. Less-Common metals 27 (1972) 35.
[64] T.A. O'Donnell, J. Fluor. Chem. 29 (1985) 12.
[65] F. Basolo, P. Pirson, Mechanism of inorganic interactions, (Translation from English to Russian), Mir, Moscow, 1971.
[66] E.G. Il'in, A.N. Zozulin, Yu.A. Buslaev, Dokl. AN USSR 296 (1987) 907.
[67] E.G. Il'in, A.N. Zozulin, Yu.A. Buslaev, Doklady Physical Chemistry (Translation of the physical chemistry section of Doklady Akademii Nauk) 384 (2002) 109.
[68] N.S. Nikolaev, D.D. Ikrami, Proceedings of III Symposium on chemistry of inorganic fluorides, Odessa (1972) 10.
[69] A.W. Lanbengayer, C.G. Polzer, J. Amer. Chem. Soc. 63 (1941) 3264.
[70] V. Gutmann, H.Y. Emeleus, J. Chem. Soc. (A) (1950) 1046.
[71] Main properties of inorganic fluorides. Handbook. Editor N.P. Galkin, Atomisdat, Moscow, 1976 (in Russian).
[72] V.A. Rabinovich, Z.Ya. Havin, Handbook on chemistry, Khimiya, Leningrad, 1978.
[73] D.S. Kopchihin, B.N. Sudarikov, E.G. Rakov, Physical chemistry and analytical chemistry, MKhTI , Moscow 62 (1969) 56.
[74] E.G. Rakov, D.S. Kopchihin, B.N. Sudarikov, Zh. Neorg. Khim. 18 (1973) 579.
[75] E.G. Rakov, D.S. Kopchihin, B.N. Sudarikov, B.V. Gromov, Atomic energy (Atomnaya Energiya) 31 (1971) 137.
[76] E.G Rakov, V.V. Mikulenok, S.V. Pevzov, Trudy MKhTI 97 (1977) 59.
[77] D. Bizot, M. Malek-Zadeh, Rev. Chim. Minerale 11 (1974) 710.
[78] D. Bizot, J. Fluor. Chem. 11 (1978) 497.
[79] E.G. Rakov, G.G. Feodorov, B.N. Sudarikov, Trudy III Symposium on chemistry of inorganic fluorides, Odessa, 1972, p. 98.
[80] G.G. Feodorov, E.G. Rakov, B.N. Sudarikov, V.A. Starobinsky, Trudy MKhTI 67 (1970) 89.
[81] J. Galy, S. Andersson, J. Portier, Acta Chem. Scand. 23 (1969) 2949.
[82] S. Andersson, A. Aström, Acta Chem. Scand. 19 (1965) 2136.
[83] V.I. Yampolsky, E.G. Rakov, V.A. Davidov at al, Zh. Neorg. Khim. 19 (1974) 2299.

[84] A.I. Agulyansky, Yu.I Balabanov, V.Ya. Kuznetzov, V.T. Kalinnikov, III conference on phys. – chem. Principals of technology ferroelectrics and related materials, Nauka, Moscow, 1983, p. 34.
[85] A.I. Agulyansky, D.V. Tsikaeva, N.F. Sklokina, R.A. Popova, V.T. Kalinnikov, Zh. Neorg. Khim. 29 (1984) 2877.
[86] A.I. Agulyansky, V.A. Bessonova, Zh. Neorg. Khim. 27 (1982) 1029.
[87] A.I. Agulyansky, V.A. Bessonova, V.Ya. Kuznetzov, V.T. Kalinnikov, Zh. Neorg. Khim. 29 (1984) 1066.
[88] F. Galasso, W. Darby, J. Phys. Chem. 66 (1962) 1318.
[89] V.Ya. Kuznetsov, D.L. Rogachov, G.G. Sadikov et al, Zh. Struct. Khim. 21 (1980) 142.
[90] A.I. Agulyansky, D.V. Tsikaeva, Zh. Neorg. Khim. 31 (1986) 3030.
[91] J.-P. Chaminad, M. Pouhard, P. Hagenmuller, Rew. Chim. Minerale 9 (1972) 381.
[92] M. Vlasse, A. Boukhari, J.-P. Chaminad, M. Pouchard, Mat. Res. Bull. 14 (1979) 101.
[93] L.A. Agulyansky, V.V. Belov, Z.I. Shapiro, A.I. Agulyansky, Vysokochistye Veschestva (High purity substances) 5 (1989) 153.
[94] A.I. Agulyansky, Yu.A. Serebryakov, L.S. Korobeinikov, Yu.I. Balabanov, L.A. Agulyansky, V.T. Kalinnikov, Zh. Obshch. Khim. 56 (1986) 734.
[95] R.P. Zivilev, S.A. Fedulov, N.F. Nezimaeva, Izv. Akad. Nauk SSSR, Neorg. Mater. 6 (1970) 1539.
[96] G.D. Yanson, I.S. Vinogradova, N.F. Zalezkite, S.E. Rozenzweig, Neorg. stekla, pokrytiya i materialy, RPI, Riga, No.6 (1989) 137.
[97] Sh. Shimada, K. Kodaira, T. Matsushita, Thermochimica Acta 23 (1978) 135.
[98] G.D. Yanson, Neorg. Stekla, pokrytiya i materialy, RPI, Riga, No1 (1974) 199.
[99] Z.I. Shapiro, A.I. Baliner, M.Z. Partashnikov, Trudy IREA No31 (1969) 56.
[100] A.I. Agulyansky, Yu.A. Serebryakov, M.N. Palatnikov, L.S. Korobeinikov, Yu.I. Balabanov, L.A. Agulyansky, V.T. Kallinikov, Izv. Akad. Nauk. SSSR, Neorg. Mater. 22 (1986) 471.
[101] A.I. Agulyansky, Yu.A. Serebryakov, M.N. Palatnikov, L.A. Agulyansky, Yu.I. Balabanov, Zh. Obshch. Khim. 55 (1985) 1923.
[102] A.I. Agulyansky, Yu.I. Balabanov, Yu.A. Serebryakov, L.A. Agulyansky, V.T. Kalinnikov, Tes. Dokladov II Vsesous. Konfer. (Actual problems of production and application of ferro- and piezoelectric materials) NIITEKhIM, Moscow, (1984) 469.

[103] E.K. Belyaev, V.I. Atroschenko, N.F. Kleschev, Isv. VUZov, Khimiya i Khim. Technol. 25 (1982) 838.
[104] Z.I. Shapiro, V.K. Trunov, V.V. Shishov, Methods of preparation of alkali metals niobates, NIITEKhIM, Moscow, 1978 (in Russian).
[105] A.I. Agulyansky, Isv. Akad. Nauk. SSSR, Neorg. Mater. 27 (1991) 376.
[106] D.D. Ikrami, M.E. Rahimov, A.S. Paramzim, S.Oripov, Zh. Neorg. Khim. 29 (1984) 1924.
[107] D.D. Ikrami, L.A. Olhovay, A.A. Luginina, Isv. Akad. Nauk SSSR, Neorg. Mater. 13 (1977) 1238.
[108] A.A. Luginina, L.A. Olhovay, D.D. Ikrami et al., Zh. Neorg. Khim. 26 (1981) 332.
[109] D.D. Ikrami, N.N. Levina, P. Okhunov, Isv. Akad. Nauk SSSR, Neorg. Mater. 19 (1983) 1549.
[110] E.I. Melnichenko, O.M. Gorbenko, E.G. Rakov, S.A. Polischuk, Zh. Neorg. Khim. 32 (1987) 76.
[111] U.R.K. Rao, K.S. Venkateswarlu, B.N. Wani, J. Fluor. Chem. 31 (1986) 29.
[112] Yu.A. Buslaev, E.G. Il'in, V.D. Kopanev, O.G. Gavrish, Isv. Akad. Nauk SSSR, ser. Khimicheskaya 6 (1971) 1139.
[113] V.T.Kallinikov, Yu.I. Balabanov, L.A. Agulyansky, A.I. Agulyansky, Yu.A. Serebryakov, Zh. Obschei Khim. 54 (1984) 1929.
[114] A.I. Agulyansky, Yu.I. Balabanov, V.Ya. Kuznetzov, L.A. Agulyansky, Proceedings of the second conference on phys. – chem. Fundamentals of ferroelectrics and related materials, Nauka, Moscow, 1983, p.85.
[115] R.L. Davidovich, T.A. Kaidalova, T.F. Levchishina, Atlas of infra-red absorption spectra and X-ray data of complex fluorides of IV and V groups, Nauka, Moscow, 1972 (in Russian).
[116] A.A. Opalovsky, T.D. Fedotova Hydrofluorides Nauka, Novosibirsk, 1979 (in Russian).
[117] A.I. Agulyansky, Yu.I. Balabanov, L.A. Agulyansky, V.T. Kalinnikov Koord. Khim. 10 (1984) 1512.
[118] V.T. Kalinnikov, Yu.I. Balabanov, A.I. Agulyansky Fifth European Meeting on Ferroelectricity (Abstracts), Benalmadena (Malaga), Spain 1983, p. 340.
[119] D.V. Tsikaeva, S.D. Nikitina, A.I. Agulyansky, V.T. Kalinnikov, Koord. Khim. 12 (1986) 929.
[120] J. Chassaing, C. Moteil, D. Bizot, J. Solid State Chem. 43 (1982) 327.
[121] Yu.I. Balabanov, A.I. Agulyansky, L.A. Agulyansky, Zh. Obschei Khim. 53 (1983) 2434.

[122] A.I. Agulyansky, Yu.I. Balabanov, V.A. Bessonova, A.G. Babkin, P.T. Stangrit, Isv. Akad. Nauk SSSR, Neorg. Mater. 21 (1985) 98.
[123] A.I. Agulyansky, Yu.I. Balabanov, V.A. Bessonova at al, Tesisy dokladov IV Vses. Sovecshaniya po phys.-khim. Analizu, Kiev – Moscow Nauka, 1983, p. 54.
[124] V.T. Kalinnikov, A.I.Agulyansky 11th Intern. Symp. On Fluor. Chem. (Abstracts) Berlin, 1985, p. 153.
[125] V.T. Kalinnikov, A.I. Agulyansky J. Fluor. Chem. 29 (1985) 61.
[126] A.I. Agulyansky, E.L. Tichomirova, V.Ya. Kuznetzov, V.T. Kalinnikov, Zh. Neorg. Khim. 33 (1988) 85.
[127] A.I. Agulyansky, E.L. Tichomirova, V.T. Kalinnikov, Tes. Dokladov VIII Vses. Symposium po khim. Neorg. Ftoridov (VIII Rus. Symposium on chem.. of inorg. Fluorides. Abstracts), Nauka, Polevskoy, 1987, p. 27.
[128] A.I. Agulyansky, V.A. Bessonova, V.Ya. Kuznetzov, Isv. Akad. Nauk SSSR, Neorg. Mater. 20 (1984) 1207.
[129] A.I. Agulyansky, E.L. Tikhomirova, V.T. Kalinnikov, Zh. Neorg. Khim. 32 (1987) 2079.
[130] R.L. Davidovich, Atlas of derivatographic patterns of complex fluorides of III –V groups metals Nauka, Moscow, 1976 (in Russian).
[131] A.I. Agulyansky, E.L. Tichomirova, V.A. Bessonova, V.Ya. Kuznetzov, VIII Rus. Symposium on Chem. of inorg. fluorides - Polevskoy (Abstracts), Nauka Moscow, 1987, p. 26.
[132] A.I. Agulyansky, Yu.A. Serebryakov, M.N. Palatnikov, L.A. Agulyansky, Yu.I. Balabanov, Zh. Obschei Khim. 55 (1985) 1923.
[133] A.I. Agulyansky, S.S. Pochivalov, V.M. Melnikova, Zh. Neorg. Khim. 34 (1989) 2740.
[134] M. O'Keeffe, B.G. Hyde, Nature 309 (1984) 411.
[135] G.B. Bokiy Introduction in crystal chemistry MGU, Moscow, 1954 (in Russian).
[136] J.L. Hoard, W.J. Martin, M.E. Smith, J.E. Whitney, J. Amer. Chem. Soc. 76 (1954) 3820.
[137] K. Nakamoto, Infrared spectra of inorganic and coordination compounds, Mir, Moscow, 1966 (translation to Russian).
[138] A.B. Lele, A.D. Tillu, K. Sathianadan, Indian J. Pure and Appl. Phys. 10 (1972) 864.
[139] V.Ya. Kuznetzov, L.A. Kamenskay, D.L. Rogachov, et al., Investigation of compounds of rare metals and their systems, Apatity, 1977, p. 37 (in Russian).

[140] T.A. Kaidalova, B.I. Pakhomov III Vses symp. po khim. Neorg. Ftoridov (III Russian Symposium on chemistry of inorganic fluorides), Odessa, 1972, p.139 (in Russian)
[141] J.L. Hoard, J. Amer. Chem. Soc. 61 (1939) 1252.
[142] J.M. Brown, L.A. Walker, Acta Cryst. 20 (1966) 220.
[143] R.B. English, A.M. Heyns, E.C. Reynhard, J. Phys. C. Solid State Phys. 16 (1983) 829.
[144] C.C. Torardi, L.H. Brixner, J. Solid State Chem. 67 (1987) 21.
[145] R.E. Eberts, F.X. Pink, J. Inorg. and Nucl. Chem. 30 (1968) 457.
[146] D. Bizot, J. Chassaing, Rev. Chim. Minerale 13 (1976) 139.
[147] C. Monteil, J. Chassaing, Rev. Chim. Minerale 16 (1979) 194.
[148] A.I. Agulyansky, V.A. Bessonova, V.Ya. Kuznetzov, N.F. Sklokina, Zh. Neorg. Khim. 27 (1982) 679.
[149] D. Bizot, J. Chassaing, A. Erb, J. Less-Common Metals 79 (1981) 39.
[150] M. Fouad, J. Ravez, J.-P. Chaminad, P. Hagenmuller, Rev. Chim. Minerale 24 (1987) 583.
[151] M.B. Williams, J.L. Hoard, J. Amer. Chem. Soc. 64 (1942) 1139.
[152] A.E. Baker, H.M. Haendler, Inorg. Chem. 1 (1962) 127.
[153] J.-P. Chaminad, M. Vlasse, M. Pouchard, P. Hagenmuller, Bull. Soc. Chim. France 9-10 (1974) 1791.
[154] V.I. Pakhomov, T.A. Kaidalova, R.L. Davidovich, Zh. Neorg. Khim. 19 (1974) 1823.
[155] O.L. Keller, A. Chetham-Strode, J. Inorg. Chem. 5 (1966) 367.
[156] T.A. Kaidalova X-Ray investigation of some complex oxyfluoroniobates – Abstract of dissertation, Moscow, 1974 (in Russian).
[157] G. Pausewand, R. Schmitt, K. Dehnicke, Z. anorg. allg. Chem. 408 (1974) 1.
[158] R.D.W. Kemmitt, D.R. Rassell, D.W.A. Sharp, J. Chem. Soc. 9 (1963) 4408.
[159] A.I. Agulyansky, V.Ya. Kuznetzov, L.A. Agulyansky, V.T. Kalinnikov, Koord. Khim. 10 (1984) 1512.
[160] J.H. Burns, Acta cryst. 15 (1962) 1098.
[161] J. Chassaaing, C. Monteil, D. Bizot, J. Solid State Chem. 43 (1982) 327.
[162] V. Delobbe, J. Chassaing, D. Bizot, et al., J. Magn. And Magn. Mater. 74 (1988) 165.
[163] B. Cox, J. Chem. Soc. (1956) 876.
[164] G. Teufer, Acta Cryst. 9 (1956) 539.
[165] H. Bode, H. Döhren, Acta Cryst. 11 (1958) 80.
[166] B.G. Muller, Angew. Chem. 99 (1987) 685.

[167] Anwendungen der schwingungsspectroskopie in der anorganischen chemie, von Dr. H. Siebert, Springer – Verlag, Berlin – Heidelberg – New York, 1966.
[168] H.H. Claasen, J. Chem. Phys. 30 (1959) 968.
[169] J.W. Linnet, C.J.S.M. Simpson, J. Inorg. Chem. (6) (1975) 535.
[170] R.D. Peacock, D.W.A. Sharp J. Chem. Soc. (London) Sept. – Oct. (1959) 2762.
[171] O.L. Keller, Inorg. Chem. 2 (1963) 783.
[172] V.I. Nefedov, Yu.V. Kokunov, Yu.A. Buslaev et al., Zh. Neorg. Khim. 18 (1973) 931.
[173] R. Stomberg, Acta Chemica Scandinavica A38 (1984) 603.
[174] G.Z. Pinsker, Kristallografiay (Crystallography) 11 (1966) 741.
[175] G. Pausewang, Z. Naturforsch. 266 (1971) 1218.
[176] G. Pausewang, Z. Naturforsch. 29 (1977) 49.
[177] Yu.E. Gorbunova Investigation of crystal structure of some carbonate containing hydroxocompounds of zirconium and oxyfluoroniobates – Abstract of dissertation, Moscow 1974 (in Russian).
[178] D. Gradjen, R. Weiss, Bull. Soc. Chim. France 8 (1967) 3040.
[179] D. Gradjen, R. Weiss, Bull. Soc. Chim. France 8 (1967) 3049.
[180] L.I. Baranova, Ya.K. Syrkin, R.L. Davidovich Zh. Struct. Khim. (7) (1966) 273.
[181] V.F. Chuvaev, R.L. Davidovich, Yu.A. Buslaev, Radiospectroscopy and quantum chemical methods in investigations of structure. Nauka, Moscow, 1967 p. 208 (in Russian).
[182] V.A. Skrin, V.Ya. Dudarev, L.E. Fykin et al. Dokl. Akad. Nauk. SSSR 236 (1977) 393.
[183] J.L. Hoard, W.J. Martin, J. Amer. Chem. Soc. 63 (1941) 11.
[184] V.I. Sergienko, M.A. Poray-Koshiz, T.S. Hadasheva, Zh. Srtruct. Khim. 13 (1972) 461.
[185] Yu.Ya. Kharitonov, Yu.A. Buslaev, Isv. Akad. Nauk. SSSR, Ser. Khim. (3) (1962) 893.
[186] Yu.Ya. Kharitonov, Yu.A. Buslaev, Isv. Akad. Nauk SSSR, Ser. Khim. (5) (1964) 808.
[187] L. Surandra, D.N. Sathyanarayana, G.V. Jeve J. Fluor. Chem. 23 (1983) 115.
[188] Yu.E. Gorbunova, V.I. Pakhomov, V.G. Kuznetzov, E.S. Kovaleva, Zh. Struct. Khim. 13 (1972) 165.
[189] H. Bode, E. Voss, Z. anorg. allg. Chem. 290 (1957) 1.
[190] E.G. Steward, H.P. Rockby, Acta Cryst. 6 (1953) 49.

[191] M. Fouad, J.-P. Chaminade, J. Ravez, P. Hagenmuller, Rev. Chim. Mineral 24 (1987) 1.
[192] J.-P. Chaminade, M. Pouhard, Ann. Chim. 10 (1975) 75.
[193] G. Pausewang, W. Rüdorff, Z. anorg. allg. Chem. 364 (1969) 69.
[194] M. Bolte, J.-P. Besse, C. r. Acad. SC. Paris. Serie C. 277 (1973) 1359.
[195] K. Dehnicke, G. Pausewang, W. Rüdorff, Z. anorg. allg. Chem. 366 (1969) 64.
[196] B. Anrivillius, Ark. Kemi. B5 (1953) 39.
[197] T.A. Kaidalova, V.I. Pakhomov, E.S. Panin, Koord. Khim. 2 (1976) 554.
[198] R.L. Davidovich, Yu.A. Buslaev, Chemical and physic-chemical methods of separations of compounds containing light and rare elements, SO AN SSSR, Vladivostok, 1968, p. 107 (in Russian).
[199] A.J. Edwards, J. Chem. Soc. 10 (1964) 3714.
[200] G.V. Romanov, V.P. Spiridonov, Vestnik Moskovskogo Universiteta (5) (1968) 7.
[201] J. Brunvoll, A.A. Ishchenko, I.N. Myakshin, G.V. Romanov, V.P. Spiridonov, T.G. Strand, V.F. Sukhoverkhov, Acta Chem. Scand. Sec. A. A34 (1980) 733.
[202] G.V. Girichev, V.N. Petrova, V.M. Petrov et al. Isv. Vusov, Khimiya I Khimicheskaya technologiya 24 (1981) 131.
[203] G.V. Girichev, V.N. Petrova, V.M. Petrov, K.S. Krasnov, Koord. Khim. 9 (1983) 799.
[204] V.I. Pakhomov, T.A. Kaidalova, Kristallographiya 19 (1974) 733.
[205] V.I. Pahomav, R.L. Davidovich, T.A. Kaidalova, T.F. Levchishina, Zh. Neorg. Khim. 18 (1973) 1240.
[206] V.T. Kalinnikov, A.I. Agulyansky, S.Yu. Stefanovich, Ferroelectrics 92 (1989) 77.
[207] R. Von Der Mühll, S. Andersson, J. Galy, Acta Cryst. B.27 (1971) 2345.
[208] R. Von Der Mühll, J. Ravez, Rev. Chim. Minerale 11 (1974) 652.
[209] A.I. Agulyansky, V.E. Zavodnik, V.Ya. Kuznetzov, et al. Neorg. Mater. 27 (1991) 1055.
[210] Yu.A. Buslaev, Yu.V. Kokunov, Isv. SO AN SSSR, Ser. Khim. Nauk (2) (1968) 50.
[211] A.I. Agulyansky, S.Yu. Stefanovich, D.V. Tsikaeva, V.T. Kalinnikov, Neorg. Mater. 27 (1991) 380.
[212] N.V. Sidorov, V.M. Mitrofanov, A.I. Agulyansky, Zh. Pricl. Spectr. 53 (1990) 94.
[213] G.P. Budova, I.K. Boskresenskaya, Zh. Neorg. Khim., 15 (1970) 859.
[214] Zui Bin-Sin, V.I. Konstantinov, N.P. Lujnaya, Zh. Neorg. Khim. 8 (1963) 396.

[215] D.L. Rogachev, V.Ya. Kuznetzov, A.N. Bogdanova et al., Zh. Struct. Khim. 17 (1976) 129.
[216] A.A. Lastochkina, I.A. Sheka, L.A. Malinko, Isv. Akad. Nauk SSSR, Neorg. Mater. 6 (1970) 897.
[217] J. Köhler, A. Simon, L. van Wüllen, S. Cordier, T. Roishel, M. Poulain, M. Somer, Z. Anorg. Allg. Chem. 628 (2002) 2683.
[218] M. Vlasse, J.-P. Chaminade, M. Pouchard, Mat. Res. Bull. 8 (1973) 117.
[219] S. Andersson, J. Galy, Rew. Chim. Minerale 25 (1969) 847.
[220] F. Galasso, W. Darby, J. Phys. Chem. 66 (1962) 1318.
[221] L.A. Kamenskaya Phys.-Chem. investigations of interactions between niobium and tantalum complex fluorides and oxyfluorides and potassium and sodium fluorides and chlorides in molten conditions. – Abstracts of Dissertation, Kiev, 1976 (in Russian).
[222] M. Lundberg, Ö. Sävborg, Chem. Scripta 13 (1978-79) 197.
[223] A. Garpy, P. Amestoy, J. Galy, C.r. Acad. Sc. Paris. 275 (1972) 833.
[224] M. Nanot, F. Queryroux, J.-C. Gilles, C. r. Acad. Sc. Paris. 277 (1973) 505.
[225] A. Boukhari, J.-P. Chaminade, M. Pouhard, M. Vlasse, Acta Cryst. B#2 (1980) 237.
[226] M. Vlasse, A. Boukhari, J.-P. Chaminade, M. Pouchard, Mat. Res. Bull 14 (1979) 101.
[227] A. Boukhari, J.-P. Chaminade, M. Vlasse, M. Pouchard, C. r. Acad. Sc. Paris 290 (Ser. C) (1980) 341.
[228] A. Boukhari, J.-P. Chaminade, M. Pouchard, M. Vlasse, Acta Cryst. B35 (1979) 2518.
[229] S. Andersson, Acta Chem. Scand. 21 (1967) 1777.
[230] J.-P. Chaminade, M. Vlasse, M. Pouchard, P. Hagenmuller, C. r. Acad. Sc. Paris. Ser. C. 277 (1973) 1141.
[231] A. Boukhari, J.-P. Chaminade, M. Vlasse, M. Pouchard, Acta Cryst. B35 (1979) 1983.
[232] V.Ya. Kuznetzov, D.L. Rogachov, G.G. Sadikov, et al. Zh. Struct. Khim. 21 (1980) 142.
[233] S. Andersson, A. Astrom, Acta Chem. Scand. 18 (1964) 2233.
[234] L.K. Frevel, H.W. Rinn, Acta Cryst. 9 (1956) 626.
[235] G. Ory, J.L. Fourget, C. Jacoboni, J.P. Mirandy, R. Pape, C. r. Acad. Sc. Paris C273 (1971) 747.
[236] D. Babel, G. Pausewang, W. Viebahn, Z. Natur-forsch. 22b (1967) 219.
[237] J.-L. Fourgnet, C. Jcoboni, R. De Pape, Acta Cryst. B35 (1979) 1570.
[238] J.-L. Fourgnet, F. Plet, R. Pape, C. r. Acad. Sc. Paris C283 (1976) 207.

[239] R. Masse, S. Aleonard, M.T. Averbuch-Rouchot, J. Solid State Chem. 53 (1984) 136.
[240] H. Arend, W. Peter, R. Schmidt, Mater. Res. Bull. 5 (1970) 753.
[241] A. Magneli, S. Nord, Acta Chem. Scand. 19 (1965) 1510.
[242] De-Yu Li, M. Lundbery, P.-E. Werner, M. Westdahl, Acta Chem. Scand. A38 (1984) 813.
[243] J.-P. Chaminade, M. Pouchard, P. Hagenmuller, C. r. Acad. Sc. Paris. C269 (1969) 1298.
[244] R. Pape, J.-L. Fourgnet, G. Gauthier, C. r. Acad. Sc. Paris 7 (1953) 315.
[245] A. Magneli, Acta Chem. Scand. 7 (1953) 315.
[246] J. Guelin, J. Ravez, P. Hagenmuller, J. Less-Common Metals 137 (1988) 75.
[247] W. Rudorff, D. Krug, Z. Anorg. Allg. Chem. b.329 (1964) 211.
[248] S. Andersson, Acta Chem. Scand. 18 (1964) 2339.
[249] W. Karl-Axel, L. Jahnberg, S Andersson, Acta Chem. Scand. 24 (1970) 1472.
[250] M. Vlasse, C. Moriliere, J.-P. Chaminade, M. Pouchard, Bull. Soc. Fr. Min. Cristallogr. 98 (1975) 325.
[251] B. Langenbach-Kuttert, R. Rob, R. Gruehu, Monatsh. Chem. b. (1985) 1275.
[252] M. Lundberg, Acta Chem. Scand. 18 (1964) 2339.
[253] M. Pouhard, J.-P. Chaminade, C. r. Acad. Sc. Paris 274 (1972) 1739.
[254] S. Andersson, Acta Chem. Scand. 19 (1965) 2285.
[255] P. Ndalamba Wa Llunda, Acta Chem. Scand. A38 (1984) 641.
[256] M. Lundberg, M. Sundberg, J. Less-Common Metals 137 (1988) 163.
[257] D.X. Li, J. Solid State Chem. 73 (1988) 1.
[258] Ö. Sävborg, Chem. Commun. #6 (1983) 1.
[259] A.I. Agulyansky, V.T. Kalinnikov, Zh. Neorg. Khim. 31 (1986) 63.
[260] V.T. Kalinnikov, A.I. Agulyansky, The sixth International Meeting on Ferroelectricity – Abstract Book – August 12-16, 1985 Kobe, Japan, p. 138.
[261] V.T. Kalinnikov, A.I. Agulyansky, Jap. J. Appl. Phys. 24 (1985) 628.
[262] J. Senegas, J. Galy, J. Inorg. Nucl. Chem. 38 (1976) 1807.
[263] J. Senegas, J. Galy, J. Solid State Chem. 5 (1972) 481.
[264] J. Senegas, J. Galy, C. r. Acad. Sc. Paris., Serie C 277 (1973) 1243.
[265] I. Naroi-Sabo Inorganic Crystal-chemistry, AN HPR, Budapest, 1969 (in Russian).
[266] L.A. Resnizky Vestn. Mosk. Universiteta, Seriya Khimiya 18 (1977) 427.
[267] G. Blasse, Z. anorg. allg. Chem. B.326 (1963) 44.

[268] N.F. Fedorov, O.V. Melnikova, L.E. Vladimirskaya, A.P. Pivovarova, Zh. Prikl. Khim. 56 (1983) 2735.
[269] G. Blasse, Z. anorg. allg. Chem. B.331 (1964) 44.
[270] M. Zocchi, M. Gatti, A. Santoro, R.S. Roth, US Dep. Commer. Nat. Bur. Stand. Techn. Note 1984 - # 1190: NB1 React: Sum. Activ., July 1982 – June 1983 p. 14.
[271] M. Zocchi, M. Gatti, A. Santoro, R.S. Roth, J. Solid State Chem. 48 (1983) 420.
[272] R. Hoffman, R. Hoppe, Z. anorg. allg. Chem. B.573 (1989) 157.
[273] R.S. Roth, J. Solid State Chem. 51 (1984) 403.
[274] A. Aragón-Piña, M.N. Villafuerte-Castrejón, R. Valenzuela, A.R. West, J. Mater. Sci. Lett. 3 (1984) 893.
[275] A.I. Agulyansky, V.A. Bessonova, V.Ya. Kuznetzov, V.T. Kallinikov, Zh. Neorg. Khim. 31 (1986) 2683.
[276] R.J. Hobson, Coord. Chem. Rev. 57 (1984) 279.
[277] D.E. Chirkst, Koord. Khim. 7 (1981) 3.
[278] V.Ya. Kuznetzov, D.L. Rogachev, A.I. Agulyansky, V.T. Kalinnikov, Zh. Strukt. Khim. 26 (1985) 85.
[279] L.A. Resnizky, Ya.I. Zelmanovich, Vestnik MGU Khimiya Moscow (1972) 10
[280] L.A. Resnizky, Vestnik Mosk. Univers. Khimiya 22 (1982) 60.
[281] L.A. Resnizky, Isv. AN SSSR, Neorg. Mater. 20 (1984) 855.
[282] A.I. Agulyansky, V.T. Kalinnikov, Actual problems of preparation and application of ferroelectric and piezoelectric materials. Abstracts of III Vses. Confer. Moscow NIITEChIM 1987 p. 15 (in Russian).
[283] L.E. Alexander, Inorg. Nucl. Chem. Letters 7 (1971) 1053.
[284] J.R. Beattie, K.M.S. Idwingston, G.A. Ozin, D.J. Reynolds, J. Chem. Soc. A (#6) (1969) 958.
[285] H. Selig, A. Reis, E.L. Gasner, J. Inorg. Nucl. Chem. 30 (1968) 2087.
[286] V.I. Yampolsky, E.G. Rakov, V.A. Davidov et al. Zh. Neorg. Khim. 19 (1974) 2299.
[287] I.M. Cheremisina, Zh. Strukt. Khim. 19 (1978) 336.
[288] N.S. Nikolaev, Yu.A. Buslaev, Zh. Neorg. Khim. 4 (1959) 205.
[289] J.A.S. Howell, K.C. Moss, J. Chem. Soc. A (1971) 2481.
[290] D.V. Tsikaeva, S.D. Nikitina, A.I. Agulyansky, V.T. Kalinnikov, X Vsesouznoe soveschanie. Primenenie koleb. spectrov v issledovanii neorg. i koord. soedinenii. Moscow, 1985 p. 129 (in Russian).
[291] D.V. Tsikaeva, S.D. Nikitina, A.I. Agulyansky, V.T. Kalinnikov, Zh. Obschei Khim. 57 (1987) 974.

[292] Yu.A. Buslaev, N.S. Nikolaev, Zh. Neorg. Khim. 4 (1959) 465.
[293] S.V. Volkov, V.F. Grischenko, Yu.K. Delimarsky, Koordinazionnaya khimiya solevykh rasplavov, Naukova dumka, Kiev, 1977.
[294] S.V. Volkov, K.B. Yazimirsky, Specrtoskopiya rasplavlennykh soley, Naukova dumka, Kiev, 1977.
[295] V.M. Amosov, Isv. Vusov, Zvetnaya metallurgiya #1 (1964) 110.
[296] V.M. Amosov, Isv. Vusov, Zvetnay metallurgiya #3 (1964) 123.
[297] A. Mukhtar, R. Winand, C. r. Acad. Sc. Paris, Ser. C, 260 (1965) 3674.
[298] F.X. McCawley, J.A. Barelay, J. Amer. Ceram. Soc. 51 (1971) 11.
[299] L.A. Kamenskaya, V.I. Konstantinov, Zh. Neorg. Khim. 16 (1971) 2003.
[300] L.A. Kamenskaya, V.I. Konstantinov, A.M. Matveev, Zh. Neorg. Khim. 17 (1972) 2567.
[301] L.A. Kamenskaya, V.I. Konstantinov, A.M. Matveev, Tesisy dokl. sovesch. po khimii, analisu i tekhnologii niobiya i tantala, Kiev, 1968, p. 22.
[302] L.A. Kamenskaya, V.I. Konstantinov, A.M. Matveev, Tesisy dokl. vsesousn. konferenzii po physiko-khimichskomu analizu, Rostov-na-Donu, 1972, p.161.
[303] L.A. Kamenskaya, V.I. Konstantinov, A.M. Matveev, Poluchenie chistykh poroshkov tugoplavkikh metallov metodom khlornoi metallurgii (Tesisy dokl.) Moscow, 1974 p. 23.
[304] V.F. Kovalev, V.M. Ioffe, V.E. Karzev, Zh. Neorg. Khim. 15 (1970) 1966.
[305] T. Iuchi, T. Matsuchima, K. Ono, Bull. Res. Mineral Dress. and Metall. Thoku Univ. 15 (1959) 87.
[306] Zui Bin-Sin, N.P. Lushnaya, V.I. Konstantinov, Zh. Neorg. Khim. 8 (1963) 389.
[307] I.D. Efros, M.F. Lantratov, About decomposition voltage of potassium fluorotantalate in molten salts solutions, Metallurgiya, Moscow, 1965 p. 284 (in Russian).
[308] I.D. Efros, M.F. Lantratov, Zh. Prikl. Khim. 36 (1963) 2659.
[309] F.V. Kovalev, V.E. Kartsev, V.M. Ioffe, M.E. Leonov, Zh. Neorg. Khim. 17 (1972) 3359.
[310] F.V. Kovalev, V.E. Kartsev, V.M. Ioffe, M.E. Leonov, Zh. Neorg. Khim. 18 (1973) 1352.
[311] Zui Bin-Sin, V.I. Konstantinov, N.P. Lushnaya, Zh. Neorg. Khim. 8 (1963) 396.
[312] Ya.V. Anosov, M.I. Ozerova, Yu.Ya. Fialkov, Fundamentals of physico-chemical analysis, Nauka, Moscow, 1976 (in Russian).

[313] Yu.Ya. Fialkov, Binary liquid systems, Technika, Kiev, 1969 (in Russian).
[314] B.F. Markov, V.D. Prisyagny, S.V. Volkov, Physical chemistry and electrochemistry of molten salts, Naukova dumka, Kiev, 1965, p. 70.
[315] B.F. Markov, L.A. Shumina, Dokl. AN SSSR, 110 (1956) 411.
[316] V.I. Konstantinov, S.A. Kuznetsov, P.T. Stangrit, Zh. Prikl. Khim. 53 (1980) 1029.
[317] S.A. Kuznetsov, P.T. Stangrit, Physicochemical investigations of rare elements and the processes of their separation from mineral raw material, Apatity, 1980, p. 25 (in Russian).
[318] S.A. Kuznetsov, E.G. Polyakov, Stangrit, Isv. Vuzov, Zvetnaya Metallurgiya #4 (1982) 76.
[319] F.V. Kovalev, V.M. Ioffe, N.S. Datlina, Trudy GIREDMET 42 (1972) 29.
[320] V.I. Konstantinov, V.A. Bessonova, O.A. Karpenko et al., Abstracts of reports on chemistry, analysis and technology of niobium and tantalum, Naukova dumka, Kiev, 1968 p. 21.
[321] V.A. Bessonova, V.I. Konstantinov, L.A. Stalyarova, E.G. Polyakov, Abstracts of reports on confer. Preparation of pure powders of refractive metals by method of chlorine metallurgy. IMet AN SSSR, Moscow, (1974) 22.
[322] A.I. Agulyansky, P.T. Stangrit, V.I. Konstantinov, Zh. Prikl. Khim. 51 (1978) 789.
[323] A.I. Agulyansky, P.T. Stangrit, Zh. Prikl. Khim. 50 (1977) 1201.
[324] A.I. Agulyansky, P.T. Stangrit, V.I. Konstantinov, Zh. Prikl. Khim. 51 (1978) 2720.
[325] I.N. Sheiko, Proceedings of Conference on physical chemistry of molten salts, Metallurgiya, Moscow, (1965) 79.
[326] F. Fairbrother, K.H. Grundy, A. Thompson, J. Chem. Soc. (Tan.) (1965) 761.
[327] Yu.V. Baimakov, M.M. Vetukov, Electrolysis of molten salts, Metallurgiya, Moscow 1966 (in Russian).
[328] A.I. Agulyansky, P.T. Stangrit, V.I. Konstantinov, II seminar on electrochemisty of refractory and rare metals (Abstracts), Apatity, 1979, Dep. BINITI (502-79) (1979) 26.
[329] W.B. Frank, L.M. Forster, J. Phys. Chem. 64 (1960) 95.
[330] K. Matiašovsky, M. Malinovsky, Coll. Chech. Chem. Commun. 36 (1971) 3746.
[331] A.I. Agulyansky, O.A. Khomchenko, Physicochemical investigations of compounds, metals and alloys, Apatity (1981) 46 (in Russian).

[332] V.I. Konstantinov, V.A. Bessonova, L.A. Stolyarova, Zvetnie metally, (2) (1973) 51.
[333] L.M. Toth, L.O. Gilpatrick, Inorg. Chem. 15 (1976) 243.
[334] I.E. Veneraky, O.E. Khlebnikov, V.I. Deshko, Pribory i technika experimenta (3) (1980) 244.
[335] S.V. Volkov, V.A. Sushko, Ukr. Khim. Zh. 39 (1973) 830.
[336] J.S. Fordyce, R.Z. Baum, J. Chem. Soc. (London) 44 (1966) 1159.
[337] J.S. Fordyce, R.Z. Baum, J. Chem. Phys. 44 (1966) 1166.
[338] J.S. Fordyce, R.Z. Baum, J. Phys. Chem. 69 (1965) 4335.
[339] T.R. Kozlowski, Appl. Opt. 7 (1968) 798.
[340] M.V. Smirnov, Yu.V. Yurinov, Yu.V. Nasonov, V.E. Komarov, Transactions of Electrochemical Institute Ural Scientific Center AN SSSR (20) (1973) 23.
[341] J.B. Bates, G.E. Boyd, Appl. Spectr. 27 (1973) 204.
[342] A.I. Agulyansky, Ya.A. Sakharov, Zh. Prikl. Spektr. 31 (1979) 288.
[343] D.H. Brown, K.P. Dixon, C.M. Livingston, R.H. Nuttall, D.W.A. Sharp, J. Chem. Soc. A (1) (1967) 100.
[344] N.A. Ereshko, A.A. Maltsev, Vibration spectra in inorganic chemistry, Nauka, Moskow, (1971) 93 (in Russian).
[345] P. Baraldy, G. Fabbri, Spectrochim Acta A39 (1983) 669.
[346] P. Baraldi, Spectrochim Acta A40 (1984) 81.
[347] C. Solomons, J.H.R. Clark, J.O'M. Bockris, J. Chem. Phys. 49 (1) (1968) 445.
[348] B. Gelbert, G. Mamontov, G.M. Begun, J. Chem. Phys. 62 (3) (1975) 950.
[349] M. Rolin, Rev. inst. hantes pempt. et refract. 13 (2) (1976) 83.
[350] B. Gilbert, G. Mamontov, G.M. Begun, Inorg. Nucl. Chem. Lett. 10 (12) (1974) 1123.
[351] A.S. Quist, J.B. Bates, G.E. Boyd, J. Phys. Chem. 76 (1972) 78.
[352] A.S. Quist, J.B. Bates, G.E. Boyd, J. Chem. Phys. 54 (1971) 4896.
[353] J.K. Wilmshurst, J. Chem. Phys. 39 (10) (1963) 2545.
[354] L.M. Toth, A.S. Quist, G.E. Boyd, J. Phys. Chem. 77 (11) (1973) 1384.
[355] L.M. Toth, G.E. Boyd, J. Phys. Chem. 77 (22) (1973) 2654.
[356] A.I. Agulyansky, S.A. Kirillov, V.D. Prisyagny, Ukrain. Khim. Zh. 46 (5) (1980) 457
[357] A.Z. Gadgiev, S.A. Kirillov, Zh. Prikl. Spektr. 21 (5) (1974) 929.
[358] A.I. Agulyansky, Zh. Neorg. Khim. 25 (11) (1980) 2998.
[359] E.N. Belen'kaya, S.A. Kirillov, A.I. Agulyansky, Theoretic and experimental chemistry 13 (4) (1977) 512.

[360] A.I. Agulyansky, B.M. Freidin, Investigations on physicochemical principals of refining technology of mineral raw material, Nauka, Leningrad, (1983) 19 (in Russian).
[361] R.V. Chernov, Physical chemistry and electrochemistry of molten salts, Naukova dumka, Kiev, 1965, 99.
[362] K.A. Valiev, Optics and spectroscopy 11 (4) (1961) 465.
[363] A.I. Agulyansky, V.A. Bessonova, Zh. Neorg. Khim. 29 (1) (1984) 79.
[364] L. Andrews, J.I. Raymond J. Chem. Phys. 55 (7) (1971) 3078.
[365] M. Moskoviz, G. Ozin, Cryochemistry Mir, Moscow, 1979 (in Russian).
[366] V.Ya. Rosolovsky, I.V. Nikitin, VINITI # 3865 – 71, Chernogolovka, 1971 (in Russian).
[367] A. Arkell, R.R. Reinhard, L.P. Larson, J. Amer. Chem. Soc. 87 (5) (1965) 1016.
[368] I.V. Fedorovich, Itogi nauki i tekhniki, Electrokhimiya, 14 (1979) 5.
[369] N.G. Bahkshiev Spectroscopy of intermolecular interactions, Nauka, Leningrad, 1972 (in Russian).
[370] A.Z. Gadgiev, S.A. Kirillov, Zh. Prikl. Spektr. 21 (5) (1974) 929.
[371] Yu.K. Delimarsky, S.A. Kirillov, Theoretical and experimental chemistry 10 (2) (1974) 201.
[372] V.A. Zasukha, S.V. Volkov, Ukrainian chemical journal 52 (4) (1986) 341.
[373] A.I. Agulyansky, O.A. Zalkind, V.A. Masloboev, Zh. Prikl. Spektr. 39 (6) (1986) 341.
[374] A. Pullet, J.-P. Matie Vibration spectra and symmetry of crystals (translation in to Russian) Mir, Moscow, 1974.
[375] V.I. Sergienko, L.N. Ignatieva, T.F. Levchishina, Koord. Khim. 3 (4) (1977) 480.
[376] V.I. Sergienko, L.N. Ignatieva,, A.G. Mirochnik, Specrtosc. Lett. 11 (11) (1978) 855.
[377] V.A. Zasukha, S.V. Volkov, Optika i spektroskopiya 50 (2) (1981) 391.
[378] A.I. Agulyansky, V.A. Bessonova, Zh. Prikl. Khim. 33 (5) (1983) 489.
[379] A.I. Agulyansky, E.L. Tichomirova, V.T. Kalinnikov, Zh. Neorg. Khim. 33 (5) (1988) 1155.
[380] Yu.I. Koltsov, Isv. AN SSSR, Neorg. Mater. 1 (6) (1965) 907.
[381] E.I. Krilov, I.V. Dmitriev, M.M. Strelina, Zh. Neorg. Khim. 7 (4) (1962) 803.
[382] A.A. Kazain, T.V. Afanasiev, V.F. Lomovtsev, Nauchnie trudy GIREDMET, Moscow, 74 (1977) 41.

[383] A.I. Agulyansky, V.M. Melnikova, E.L. Tichomirova, L.S. Korobeinikov, VIII Symposium on chemistry of inorganic fluorides – Abstracts, Polevskoy, Nauka, Moscow, 1987, p. 25.
[384] A.S. Alikhanian, K.N. Marushkin, E.G. Rakov, V.I. Gorgoraky, Zh. Neorg. Khim. 29 (9) (1984) 2184.
[385] G.A. Yagodin, A.A. Opalovsky, E.G. Rakov, A.S. Dudin, Dokl. Akad. Nauk SSSR, 252 (6) (1980) 1400.
[386] S. Deshman Principals of Vacuum Technique, Mir, Moscow, 1964 (translation to Russian).
[387] E.I. Krilov, I.V. Dmitriev, M.M. Strelina, Zh. Neorg. Khim. 7 (4) (1962) 803.
[388] G.A. Smolensky, V.A. Bokov, V.A. Isupov et al. Segnetoelectrics and antisegnetoelectrics, Nauka, Leningrad, 1971 (in Russian).
[389] S.C. Abrahams, E.T. Keve, Ferroelectrics 2 (2) (1971) 129.
[390] M.E. Lines, A.M. Glass Principals and application of ferroelectrics and related materials, Clarendon Press, Oxford, 1977.
[391] I.B. Bersuker, V.Z. Polynger, Vibronic interactions in molecules and crystals, Nauka, Moscow, 1983 (in Russian).
[392] P.N. D'yachkov, A.A. Levin, Vibronic theory of relative stability isomers in inorganic molecules and complexes, Itogy Nauki i tekhniki, ser. Stroenie molecul i khimicheskaya svyas, 11 (1987) (in Russian).
[393] J.P. Doumerc, M. Elaatmani, J. Ravez, M. Pouchard, P. Hagenmuller, Solid State Commun. 32 (1979) 111.
[394] J. Ravez, M. Elaatmani, J.-P. Chaminade, Solid State Commun. 32 (1979) 749.
[395] M. Elaamani, J. Ravez, G.P. Doumerc, P. Hagenmuller, Mater. Res. Bull. 16 (1981) 105.
[396] J.H. Ismailzade, J. Ravez, Ferroelectrics, 21 (1978) 423.
[397] J. Grannec, A. Yaciubi, J. Ravez, P. Hagenmuller, Solid State Commun. 62 (1987) 407.
[398] J.-p. Chaminade, M. Cervera-Marzal, J. Ravez, P. Hagenmuller, Mat. Res. Bull. 21 (1986) 1209.
[399] A. Yacoubi, J. Ravez, J. Grannec, Chem. Scripta 27 (1987) 429.
[400] J. Ravez, J. Phys. III France 7 (1997) 1129.
[401] S.P. Gabuda, S.G. Kozlova, Yu.G. Kriger, V.K. Goncharuk, Zh. Struct. Khim. 27 (2) (1986) 53.
[402] S.C. Abrahams, J. Raves, A. Simon, J.-P. Chaminade, J. Appl. Phys. 52 (7) (1981) 4740.
[403] J. Ravez, S.C. Abrahams, J.-P. Chaminade, A. Simon, J. Grannec, P. Hagenmuller, Ferroelectrics 38 (1981) 773.

[404] J. Ravez, A. Mogus-Milankovic, Jap. J. Appl. Phys. 24 (1985) 687.
[405] J. Guelin, J. Ravez, J. Grannec, P. Hagenmuller, Chem. Scripta 28 (1988) 137.
[406] J. Grannec, A. Yacoubi, J. Ravez, P. Hagenmuller, J. Solid State Chem. 75 (2) (1988) 263.
[407]. Zuo-Guang Ye, R. Von Der Mühll, J. Ravez, P. Hagenmuller, J. Mater. Res. 3 (1) (1988) 112.
[408] Zuo-Guang Ye, R. Von Der Mühll, J. Ravez, Materials Science and Engineering B5 (1989) 47.
[409] Zuo-Guang Ye, R. Von Der Mühll, J. Ravez, P. Hagenmuller, J. Phys. Chem. Solids 49 (10) (1988) 1153.
[410] Zuo-Guang Ye, R. Von Der Mühll, J. Ravez, Ferroelectrics 94 (1989) 265.
[411] Zuo-Guang Ye, R. Von Der Mühll, J. Ravez, Ferroelectrics 94 (1989) 261.
[412] Zuo-Guang Ye, R. Von Der Mühll, J. Ravez, J. Phys. Chem. Solids 50 (8) (1989) 809.
[413] A.A. Filimonov, V.S. Suvorov, I.S. Rez, Zh. exper. i teor. physiky (Journal of experimental and theoretic physics) 56 (5) (1969) 1519.
[414] S.Yu. Stefanovich, Yu.N. Venevtsev, Izv. AN SSSR, Ser. Phys. 41 (3) (1977) 537.
[415] S.K. Kurtz, J.P.Dougherty, Syst. Mater. Anal. 4 (1978) 269.
[416] A.P. Leonov, S.Yu. Stephanovich, Preparation and application of ferroelectric materials, Nauka, Moscow, 1984, p. 21 (in Russian).
[417] S.Yu. Stefanovich, A.P. Leonov, Yu.N. Venevtsev XIII International Congress on Crystallography, Hamburg, 1984, Collected Abstracts, p. 148 (N – 05.2 – 13)
[418] S.Yu. Stefanovich, B.A. Strukov, A.P. Leonov, A.I. Agulyansky, V.T. Kalinnikov, Abstract book of 6-th intern. Meeting on ferroelectrisity, Japan, Kobe, 1985, p. 138.
[419] S.Yu. Stefanovich, B.A. Strukov, A.P. Leonov, A.I. Agulyansky, V.T. Kalinnikov, Jap. J. Appl. Phys. 24 (1985) 630.
[420] A.P. Leonov, A.I. Agulyansky, XI USSR conference on physics of ferroelectrics (Chernovzy) – Abstracts Book, Kiev, 1 (1986) 134.
[421] M.N. Palatnikov, Yu.A. Serebryakov, A.Yu. Popovich, A.I. Agulyansky, XI USSR conference on physics of ferroelectrics (Chernovzy) – Abstracts Book, Kiev, 1 (1986) 286.
[422] V.U. Müller, Acta Crystallog. 1334 (3) (1978) 1044.
[423] S.C. Abrahams, P. Marsh, J. Ravez, J. Chem. Phys. 87 (10) (1987) 6012.
[424] R. Von der Mühll, C. r. Acad. Sc. 278 Ser. C, (1974) 713.

[425] V.T. Kalinnikov, A.I. Agulyansky, S.Yu. Stefanovich, Abstracts booklet 1-st European conference on application of polar dielectrics (Switzerland) Zurich, 1988, p. 40.
[426] V.T. Kalinnikov, A.I. Agulyansky, S.Yu. Stefanovich, Abstract book of III Russian conference on phys.-chem. bases of technology of ferroelectrics and related materials (Zvenigorod) Nauka, Moscow, 1988, p. 175.
[427] E.T. Keve, S.C. Abrahams, J.L. Berstein J. Chem. Phys. 58 (1970) 3279,
[428] J. Ravez, S.C. Abrahams, P. Marsh, S. Arguis, J.-P. Chaminade, Jap. J. Appl. Phys. 24 (1985) 232.
[429] S. Arguis, J. Ravez, J.-P. Chaminade, P. Hagenmuller, S.C. Abrahams, J. Albertsson, C. Svensson, J. Appl. Phys. 60 (1986) 357.
[430] S. Arguis, J. Ravez, S.C. Abrahams, J. Appl. Cryst. 19 (1986) 374.
[431] S.C. Abrahams, P. Marsh, J. Ravez, J. Appl. Phys. 87 (1987) 6012.
[432] J. Ravez, S. Arguis, J. Grannec, A. Simon, S.C. Abrahams, J. Appl. Phys. 62 (1987) 4299.
[433] S.C. Abrahams, J. Albertsson, C. Svensson, J. Ravez, Acta Cryst. B46 (1990) 497.
[434] J. Ravez, A. Simon, V. Andriamampianina, J. Grannec, P. Hagenmuller, S.C. Abrahams, J. Appl. Phys. 68 (1990) 3529.
[435] J. Ravez, V. Andriamampianina, A. Simon, J. Grannec, S.C. Abrahams, J. Appl. Phys. 70 (1991) 1331.
[436] V. Andriamampianina, J. Ravez, J. Ihringer, S.C. Abrahams, Ferroelectrics, 124 (1991) 287.
[437] V. Andriamampianina, J. Ravez, J.-P. Chaminade, S.C. Abrahams, Phys. Stat. Sol. 171 (1992) 111.
[438] A.I. Agulyansky, J. Ravez, J. Fluor. Chem. 67 (3) (1994) 225.
[439] N.V. Sidorov, V.M. Mitrofanov, S.Yu. Stefanovich, A.F. Gutzol, V.T. Kalinnikov, Neorg. Mater. 28 (1992) 1096.
[440] A.I. Agulyansky, J. Ravez, Eur. J. Solid State Inorg. Chem. 30 (1993) 673.
[441] A. Agulyansky, R. Cavagnat, M. Couzi, J. Ravez, Phys. Stat. Sol (a) 138 (1993) 327.
[442] A.I. Agulyansky, J. Ravez, R. Cavagnat, M. Couzi, Ferroelectrics 152 (1993) 373
[443] A. Agulyansky, J. Ravez, R. Von Der Mühll, A. Simon, Ferroelectrics 158 (1994) 139.
[444] I.I. Baram, Zh. Prikl. Khim. 38 (10) (1965) 2181.
[445] I.I. Baram, Izv. Vuzov, Zvetnaya Metallurgiya (4) (1969) 78.
[446] I.I. Baram, Izv. Vuzov, Zvetnaya Metallurgiya (1) (1970) 75.

[447] I.I. Baram, Izv. Vuzov, Zvetnaya Metallurgiya (3) (1970) 83.
[448] H. Majima, Y. Awakura, T. Yazaki, Y. Chikamori, Metall Trans. B 11B (1980) 209.
[449] H. Majima, Y. Awakura, T. Mishima, Metall. Trans. B 16B (1985) 23.
[450] H. Majima, Y. Awakura, Extraction Metallurgy '85, London, 50 (1985) 607.
[451] H. Majima, Y. Awakura, M. Mashima, T. Hirato, Metall. Trans. B 19B (1988) 355.
[452] V.V. Akimov, A.S. Chernyak,Zh. Prikl. Khim. 65 (7) (1992) 1453.
[453] N.J. Welham, Canadian Metallurgical Quarterly 40 (2) (2001) 143.
[454] N.H. Fletcher, N.J. Welham, J. American Institute of Chemical Engineers 46 (2000) 666.
[455] M. Kinoshita, S. Kuwahara, H. Watanabe, Japan patent # 2002241864.
[456] M. Kinoshita, S. Kuwahara, H. Watanabe, Japan patent # 2002241863.
[457] M. Kinoshita, S. Kuwahara, H. Watanabe, Japan patent # 2002327221.
[458] A.G. Babkin, V.G. Maiorov, A.I. Nikolaev, Extraction of niobium, tantalum and other elements from fluoride solutions, Nauka, Leningrad, 1988 (in Russian).
[459] A.I. Nikolaev, V.G. Maiorov, Solvent extraction of niobium and tantalum, Kola Science Center, Apatity, 1995 (in Russian).
[460] A.I. Nikolaev, E.G. Il'in, B.Ya. Spivakov, M.N. Shcherbakova, A.G. Babkin, Yu.A. Buslaev, Yu.A. Zolotov, Zh. Neorg. Khim. 20(1) (1975) 194.
[461] I.M. Kutyrev, E.S. Stoyanov, V.V. Bagreev, Yu.A. Zolotov, Zh. Neorg. Khim. 22(4) (1977) 1043.
[462] Yu.M. Golubkov, V.F. Travkin, E.G. Il'in, E.V. Karamushko, V.V. Kovalev, Zvetnaya Metallurgiya 10 (2001) 23.
[463] E.G. Il'in, A.N. Zozulin, Yu.A. Buslaev, Doklady RAN 296 (1987) 907.
[464] E.G. Il'in, A.N. Zozulin, Yu.A. Buslaev, Doklady RAN 335 (1994) 597.
[465] P.M. Brown, International Symposium on Tantalum and Niobium, September 24-28 1995 Goslar, Germany, TIC, Brussels, 1995, 65.
[466] J. He, Z. Zhang, Z. Xu et al. Tantalum – niobium International Study Center (TIC), Bulletin # 93 (1998) 1.
[467] V.G. Maiorov, A.I. Nikolaev, Hydrometallurgy 66 (2002) 77.
[468] V.G. Maiorov, A.I. Nikolaev, V.K. Kopkov, Russian Journal of Applied Chemistry (Translation of Zhurnal Prickadnoi Khimii) 75 (9) (2002) 1389.
[469] I.V. Baklanova, V.G. Maiorov, V.G. Kopkov, V.I. Baltsan, A.V. Mimonov, A.I. Nikolaev, Khimicheskaya Tekhnologiya (2) (2001) 28.

[470] V.G. Maiorov, A.I. Nikolaev, L.I. Sklokin, I.V. Baklanova, Russian Journal of Applied Chemistry (Translation of Zhurnal Prikladnoi Khimii) 74 (6) (2001) 945.
[471] V.F. Travkin, A.I. Agulyansky, Yu.M. Golubkov, E.V. Karamushko, Zvetnaya Metallurgiya (8-9) (1998) 18.
[472] V.F. Travkin, A.I. Agulyansky, Yu.M. Golubkov, E.V. Karamushko, Zvetnaya Metallurgiya (4) (1999) 19.
[473] A. Agulyansky, L. Agulyansky, V.F. Travkin, Chemical Engineering and Processing 43 (2004) 1231.
[474] R.K. Freier Aqueous solutions data for inorganic and organic components, Walter de Gruyter, Berlin – New York, 1976.
[475] Hadbook of chemistry and physics, David R. Lipe – editor-in-chief, 82nd Edition, 2001 – 2002.
[476] Solubilities of inorganic and organic compounds, Edited by Prof. H. Stephen and Dr. T. Stephen, Pergamon Press, Oxford – London – New York – Paris, 1963.
[477] V.G. Maiorov, A.I. Nikolaev, Russian Journal of Applied Chemistry (Translation of Zhurnal Prikladnoi Khimii) 76 (1) (2003) 153.
[478] N.S.K. Prasad, T.N. Ranganathan, M.S. Sastri, Ind. J. Technol. 4 (9) (1966) 268.
[479] Kim Yong Hyon, Li Gwi Song, Choe Chang Bong, Kw. Tongbo. (2) (1973) 36.
[480] V.G. Maiorov, A.I. Nikolaev, Tsvetnye Metally (7) (2002) 62.
[481] A.E. Childres, L.P. Greenland, Anal. Chim. Acta 116 (1) (1980) 185.
[482] A.I. Nikolaev, V.G. Maiorov, Tsvetnye Metally (3) (1995) 33.
[483] Y. Dai, H, Zhong, J. Li, Q. Li, Kuangchan Zonghe LIyong (1) (2002) 32.
[484] Y. Uchina, K. Azuma, Japanese patent # JP 2002316822.
[485] K. Azuma, M. Kinoshita, Japanese patent # JP 2001329321.
[486] Y. Uchino, K. Azuma, Japanese patent # JP 2002346596.
[487] R.E. Eberts, US patent # US 3653850.
[488] M.A. Zakharov, S.S. Korovin, V.M. Kluchnikov, I.A. Apraksin, Zh. Neorg. Khim. 18 (7) (1973) 1916.
[489] L.A. Reznichenko, O.M. Razumovskay, L.A. Shilkina et al. Izv. AN SSSR, Neorg. Mater. 24 (10) (1988) 1708.
[490] A.I. Vaicenberg, T.F. Zitkova, G.B. Lilyanova et al. Nauchnye trudy GIREDMet, Metallurgiya, Moscow, 20 (1968) 93.
[491] I.A. Sheka, A.A. Lastochkina, T.T. Mitureva, B.I. Danilzev, Khimicheskaya Tekhnologiya (1) (1975) 9.

[492] L.A. Agulyanskaya, Yu.I. Balabanov, V.A. Bessonova, V.Ya. Kuznezov, A.I. Agulyansky, VI Russian conference on phys.-chem. analysis, Kiev – 1983,Abstracts, Nauka, Moscow, 1983, p. 54 (in Russian).
[493] L.A. Agulyanskaya, Yu.I. Balabanov, A.I. Agulyansky, V.T. Kalinnikov, Abstracts – book, VIII Russian symposium on chemistry of inorganic fluorides (Polevskoy, 1987), Nauka, Moscow, 1987, p. 28.
[494] P.M. Brown, R.-C. Wu, R.C. Pedicone, M.G. Madara, US Patent # US 6338832 (Priority US 1995 -542286).
[495] W. Bludssus, E.R. Feuerhahn, H. Zimmermann, German patent # DE 4030707 (Priority application DE 1990 – 4030707).
[496] A.N. Zelikman, K.M. Rubailova, A.I. Borodina, Trudy GIREDMET Moscow, 13 (1964) 120.
[497] A.A. Titov, N.A. Shostenko, Zvetnie Metally, (7) (1985) 52.
[498] Y. Uchino, K. Azuma, Japanese patent # JP 2001213626.
[499] Yu.I. Balabanov, A.I. Agulyansky, L.A. Agulyanskya, Zh. Obsch. Khim. 53 (11) (1983) 2434.
[500] I.F. Mulyarchuk, G.V. Panchenko, Zh. Prikl. Khim. 45 (1982) 1154.
[501] V.V. Sakharov, N.E. Ivanova, S.S. Korovin, M.A. Zakharov, Zh. Neorg. Khim. 19 (1974) 579.
[502] A.V. Lapizki, Yu.P. Simanov, E.I. Yarembash, Zh. Phys. Khim. 26 (1952) 56.
[503] V.A. Titova, I.G. Slatinskaya, V.G. Pizuga, Zh. Neorg. Khim. 20 (1975) 2699.
[504] Y. Uchino, K. Azuma, Japanese patent # JP 2000-1660.
[505] A.A. Frolov, V.V. Pasichniy, Yu.I. Balabanov, A.I. Agulyansky, Abstract book of VIII Russian conference on optical methods of heating and high purity materials analysis, Gorikiy, 1988, p. 252.
[506] A.A. Frolov, V.V. Pasichniy, Yu.I. Balabanov, A.I. Agulyansky, Visokochistie Veschestva (High purity materials) (1) (1989) 102.
[507] L.A. Agulyanskaya, Yu.I. Balabanov, A.I. Agulyansky, Zh. Prikl. Khim. 62 (9) (1989) 2043.
[508] J. Kobayashi, J. Kawahara, M. Kinoshita, M. Sunahara, Japanese patent # JP 2002321917.
[509] Patent assigned by H.C. Starck, Patent # JP 08012333, DE 4422761, BR 9502973, CN 1128733 (priority application DE 1994 – 4422761).
[510] C.W. Balke, E.F. Smith, J. Am. Chem. Soc, 30 (1908) 1637.
[511] G.N. Latish, A.S. Chernyak, T.E. Serebrennikova, Zh. Neorg. Khim. 18 (4) (1973) 1014.
[512] V. Belov, L. Avdonina, A. Mikhlin, Ferroelectrics, 131 (1992) 63.
[513] A.K. Pikaev, Khimiya Visokikh Energii 21 (6) (1988) 483.

[514] S.N. Gaiz, A.P. Melnik, V.D. Parkhomenko, Plazma v khimicheskoi tekhnologii (Plasma in chemical technology) Tekhnika, Kiev, 1989 (in Russian).
[515] R.B. Bursel, Ispolsovanie plazmi v khimicheskikh processakh (Application of plasma in chemical processes) edited by L.S. Polak Mir, Moscow, 1970 (in Russian).
[516] Yu.N. Tumanov, Nizkotemperaturnaya plazma i bysokochastotnie elektromagnitnie polya v prozessakh polucheniya materialov dlya yadernoi energetiki (Low temperature plasma and high frequency fields in the processes of production materials for nuclei technique) Energoizdat, Moscow, 1989 (in Russian).
[517] Yu. I. Krasnokutsky, V.G. Verecshak, Poluchenie tugoplavkikh soedinenii v plazme (Preparation of refractory compounds in plasma) Vischa Schola, Kiev, 1987 (in Russian).
[518] V.D. Parkhomenko, P.I. Soroka, Yu.I. Krasnokutsky, P.N. Zibulev, V.G. Vereschak, A.I. Maksimov, A.L. Mosse, Plazmokhimicheskaya technologiya (Plasmochemical technology) 4 (1991) 392.
[519] B.A. Sakharov, Yu.A. Luk'yanichev, Zvetnie Metaly (4) (1990) 24.
[520] V.N. Troizky, B.M. Grebzov, I.A. Domashnev, S.V. Gurov, Plazmokhimicheskie reakzii i processi (Plasmochemical interactions and processes) Nauka, Moscow, 1977 (in Russian).
[521] G.K. Moiseev, N.A. Vatolin, S.K. Popov, Primenenie nizkotemperaturnoi plazmi v tekhnologii neorganicheskikh veschestv i poroshkovoi metallurgii (Application of low temperature plasma in technology of inorganic material and in powder metallurgy) Zinatne, Riga, 2 (1985) 3.
[522] I.V. Zalite, Ya.P. Grabis,G.L. Smishkalne, Primenenie nizkotemperaturnoi plazmi v tekhnologii neorganicheskikh veschestv i poroshkovoi metallurgii (Application of low temperature plasma in technology of inorganic material and in powder metallurgy) Zinatne, Riga, 2 (1985) 38.
[523] Yu.V. Zvetkov, S.A. Panfilov, Plazmennie processi v metallurgii i tekhnologii neorganicheskikh materiallov (Plasmic processes in metallurgy and technology of inorganic materials) Nauka, Moscow, 1973.
[524] A.I. Agulyansky, Yu.I. Balabanov, A.F. Gutsol, M.I. Sokolova, V.S. Voronina, N.A. Zirichev, V.I. Merkushkin, V.A. Ovchinnikov, Abstracts-book of IX symposium on chemistry of inorganic fluorides, Part I, Moscow, 1990 p. 24.

[525] A.I. Agulyansky, A.F. Gutsol, S.M. Masloboeva, L.I. Sklokin, Abstracts-book of IX symposium on chemistry of inorganic fluorides, Part I, Moscow, 1990 p. 26.
[526] A.I. Agulyansky, A.F. Gutsol, L.S. Corobeinikov, V.M. Melnikova, S.S. Pochivalov, Abstracts-book of IX symposium on chemistry of inorganic fluorides, Part I, Moscow, 1990 p. 25.
[527] A.I. Agulyansky, A.F. Gutsol, M.I. Sokolova, Abstracts-book of IX symposium on chemistry of inorganic fluorides, Part I, Moscow, 1990 p. 24.
[528] A. Gutsol, A. Agulyansky, 10-th Int. Symposium on Plasma Chemistry, Symp. proceedings, Bochum, Germany, August 2-6, 1991 1. 4-15, 1-6.
[529] A. Gutsol, A. Tikhonov, J. High Temp. Chem. Proc. 1 (1992) (3) 223.
[530] A.F. Gutsol, Zvetnie Metally, (1995) (3) 36.
[531] A.F. Gutsol, Khim. Visokikh Energiy 29 (1995) 373.
[532] A.F. Gutsol, V.T. Kalinnikov, Zh. Prikl. Khim. 68 (6) (1995) 885.
[533] E.G. Rakov, V.V. Teslenko, Pyrohydrolysis of inorganic fluorides, Energoizdat, Moscow 1987 (in Russian).
[534] M.E. Posin, Tekhologiya mineralnykh soley (Technology of mineral salts) Part II, Khimiya, Leningrad, 1970 (in Russian).
[535] M.J. Herak, M. Diksic, P. Strohal, Microchimica Acta, (1) (1971) 116.
[536] A. Agulyansky, J. Fluor. Chem. 123 (2003) 155.
[537] L. Shekhter, L. Lanin, T. Tripp, H. Goldberg, K. Reichert, C. Schnitter, R. Wolf, Proceedings of TIC symposium on tantalum and niobium, October 22nd – 25th 2000, San Francisco, California, USA, TIC Belgium, 2000, p. 87.
[538] D.K. Bose, C.K. Gupta, Min. Pro. Ext. Met. Rev. 22 (2001) 389.
[539] O. Toshiyuki, K. Satoshi, Japanese patent # JP 2003129115.
[540] C.W. Balke, Ind. Eng. Chem. 27 (1935) 1166.
[541] V.I. Konstantinov, V.M. Amosov, E.A. Holobes, Poroshkovaya Metallurgiya, (5) (1961) 42.
[542] C.C. Ma, Ind. Eng. Chem. 44 (1952) 342.
[543] A.J. Kolk, M.E. Silbert, M.A. Steinberg, Technology of Columbium (Niobium), Ed. by B.W. Gonser, E.M. Sherwood, N.S.L. 1958, p. 44.
[544] E.I. Gurovich, Zh. Neorg. Khim. 3 (1958) 450.
[545] A. Espinola, A.J.B. Durta, F.T. Silva, Analitica Chemica Acta 251 (1-2) (1991) 53.
[546] V.I. Konstantinov, E.G. Polyakov, P.T. Stangrit, Electrochimica Acta 23 (1978) 713.
[547] F. Lantelme, A. Barhoum, G. Li, J.-P. Besse, J. Electrochim. Soc. 139 (1992) 1249.

[548] L.P. Polyakova, E.G. Polyakov, E. Mattieesen, N.J. Bjerrum, J. Electrochem. Soc. 141 (11) (1994) 2982.
[549] P.R. Bandi, U. Stöhl, W. Freyland, Wiss. Abschlußber, 30 Intern. Seminar Univ. Karlsruhe, July 1995, (1995) 48 Universitaet Karlsruhe, Karsruhe, Germany.
[550] M. Chemla, V. Grinevitch, Bull. Soc. Chem. France (3) (1973) 853.
[551] Q. Zhiyu, P. Taxil, J. Appl. Electroch. 15 (1985) 259.
[552] A. Barhoun, Y. Berghoute, F. Lantelme, J. Alloys and Comp. 179 (1992) 241.
[553] F. Lanterme, Y. Berghoute, J.H. Von Barner, G.S. Picard, J. Electr. Soc. 142 (1995) 4097.
[554] C. Rosenkilde, A. Vik, T. Ostvold, E. Chistensen, N.J. Bjerrum, J. Electrochim. Soc. 147 (10) (2000) 3790.
[555] E.G. Polyakov, Rus. J. Appl. Chem. 71 (2) (1998) 187.
[556] N.J. Bjerrum, F, Matthiensen, E. Christensen, J.H. Von Barner, Int. Harald A. Oeye Symp. (1995) 15, Norw. Inst. Techn., Inst. Inorg. Chem., Trondheim, Norway, 1995.
[557] A.A. Kazain, T.V. Afanasiev, V.F. Lomovtsev, Nauchnye trudy GIREDMETA, Redkie Metally, 74 (1977) 41.
[558] V.V. Grinevitch, A.V. Arakcheeva, E.G. Polyakov, L.P. Polyakova, S.A. Kuznetsov, Electrochemical Soc. Proceedings (98-11 Molten Salts) (1998) 84.
[559] V.V. Grinevitch, S.A. Kuznetsov, E.G. Polyakov, L.M. Sevryukova, Metally (3) (1994) 18.
[560] S.V. Devyatkin, V.I. Taraneko, Kh.B. Kushkhov, V.I. Shapoval, Rasplavy (2) (1992) 71.
[561] A.V. Elyutin, V.E. Kartsev, F.V. Kovalev, Tsvetnye Metally (4) (1993) 37.
[562] A.V. Elyutin, V.E. Kartsev, V.F. Kovalev, Tsvetnye Metally (2) (1996) 47.
[563] A.V. Elyutin, V.E. Kartsev, F.V. Kovalev, Tsvetnye Metally (3) (1996) 48.
[564] A.V. Elyutin, V.E. Kartsev, F.V. Kovalev, Tsvetnye Metally (7) (1996) 45.
[565] P. Taxil, Zhi Yu Qiao, Proceedings – Electrochemical Soc. 86 – 1 (Molten salts) (1986) 485.
[566] V.N. Kolosov, E.S. Matychenko, V.Yu. Novichkov, Russian Journal of Electrochemistry (Translation of Elektrokhimiya) 32 (12) (1996) 1354.
[567] C. Decroly, A. Mukhtar, R. Winand, J. Electrochem. Soc 115 (9) (1968) 905.

[568] B.M. Freidin, L.A. Agulyanskaya, N.D. Sedelnikova, L.E. Freidina, Izv. VUZOV, Zvetnaya Metallurgiya (1) (1981) 112.
[569] Y. Hirabayshi, I. Nakagawa, Nagoya Kogyo Gijutsu Shikensho Hokoku 30 (3) (1981) 100.
[570] I. Nakagawa, Nagoya Kogyo Gijutsu Shikensho Hokoku 23 (9) (1974) 271.
[571] I. Nakagawa, T. Kirihara, Report of the Government Industrial Institute, Nagoya 23 (2) (1974) 56.
[572] N. Tumanova, O. Boyko, N. Buryak, S. Kochetova, NATO Science Series, II: Mathematics, Physiscs and Chemistry 92 (2003) 335.
[573] G.T. Cheek, P.C. Trulove, D.E. Clinton, P.L. Hagans, W.E. O'Grady, H.C. DeLong, R.A. Mantz, Proceedings of Symp. on Fundamental Aspects of Electrochem. Deposition and Dissolution Including Modeling, Pennington, NJ, USA, Electrochem. Soc. (1998) 204.
[574] J.J. Berzelius, Pogg. Ann. 4 (1825) 11.
[575] H. Rose, Pogg. Ann. 99 (1856) 69.
[576] T.B. Tripp, Tantalum – Proceeding of a Symposium held at the 125th TMS Annual Meeting and Exhibition, Anaheim, Calif. (February 5-8, 1996) Ed. E.S. Chen, Minerals, Metals & Materials Society, Warrendale, Pa, (1996) 23.
[577] O.P. Kolchin, M.A. Vol'dman, Izvestiya Akademii Nauk SSSR, Neorg. Mater. 3 (6) (1967) 1099.
[578] S.C. Jain, D.K. Bose, C.K. Gupta, Transactions of the Indian Institute of Metals, 24 (4) (1971) 1.
[579] M. Tamura, Japanese patent # JP 49034463.
[580] R. Haehn, D. Behrens, German patent # DE2517180.
[581] S. Takase, S. Hiratsuka, Y. Matsudaira, Japanese patent # JP 52150362.
[582] H. Miyazaki, M. Kuroki, K. Hosaka, S. Suzuki, Japanese patent # JP 02070028.
[583] J.S. Yoon, H.H. Oark, I.S. Bae, D.J. Yoon, B. Kim II, Han'guk Chaelyo Hakhoechi 11 (12) (2001) 1047.
[584] H. Lang, German patent # DE 815107.
[585] Y. Purushotham, T. Balaji, A. Kumar, T.L. Prakash, Transactions of the Indian Institute of Metals 55 (6) (2002) 525.
[586] W.H. Keller, J.P. Martin, USA patent # US 2927855.
[587] G.L. Martin, USA patent # US 2927854.
[588] H. Miyazaki, M. Kuroki, Japanese patent # JP 02070029.
[589] M. Gruner, H. Ibold, U. Naumann, German patent # DD 291580.
[590] E.G. Heller, G.L. Martin, USA patent # 2950185.
[591] S-L. Li, Xiyou Jinshu Yu Yingzhi Hejin (3) (2001) 10.

[592] H. Chang, USA patent # US 1990 – 525364.
[593] T. Izumi, Japanese patent # JP 60145304.
[594] X. He, J. Feng, Y. Yang, Xiyou Jinshu Yu Yingzhi Hejin 31 (2) (2003) 39.
[595] R. Hildreth, M. Shaw, T.B. Tripp, L.G. Gibbons, USA patent # US 5442978.
[596] V.N. Kolosov, V.M. Orlov, T.Yu. Prokhorova, A.T. Belyaevskii, Rasplavy (2) (2003) 57.
[597] C.F. Rerat, USA patent # US 874525.
[598] K.Yu. Belyaev, V.M. Orlov, T.Yu. Prokhorova, M.N. Miroshnichenko, Rasplavy, (5) (1998) 69.
[599] J.S. Yoon, H.H. Park, I.S. Bae, B.I. Kim, S.M. Jung, Han'guk Chaelyo Hakhoechi 12 (9) (2002) 706.
[600] J.S. Yoon, H.H. Park, I.S. Bae, S.B. Lee, B. I. Kim, Han'guk Chaelyo Hakhoechi 11 (12) (2001) 1052.
[601] B.I. Kim, H.H. Park, I.S. Bae, J.S. Yoon, Nippon Kinzoku Gakkaishi 66 (7) (2002) 735.
[602] L. Chai, H. Zhong, Transection of Nonferrous Metals Society of China 6 (3) (1996) 36.
[603] S.M. Jung, H.H. Park, Korean patent # WO 2001012867.
[604] L. Pan, A. Zheng, C. Zhu, F. Zeng, W. Shi, Z. Lu, Chinese patent # 1240688.
[605] K. Tierman, R.J. Millard, Proceedings Electronic Components Conference, IEEE Cat. # 83CH1902-2 (1983) 157.
[606] W.W. Albrecht, A. Hoppe, U. Papp, R. Wolf, USA patent # US 4537641.
[607] V.M. Orlov, T.Yu. Prokhorova, V.V. Sukhorukov, Metally (4) (2003) 19.
[608] T. Osaku, S. Komukai, Japanese patent # JP 2003129115.

# SUBJECT INDEX

This Page Intentionally Left Blank

# FORMULA INDEX